BACTERIOPHAGES ISOLATION FROM THE ENVIRONMENT AND THEIR ANTIMICROBIAL THERAPEUTIC POTENTIAL

EDITED BY: Krishna Khairnar, Robert Czajkowski, Sutthirat Sitthisak and Krishna Mohan Poluri

PUBLISHED IN: Frontiers in Microbiology

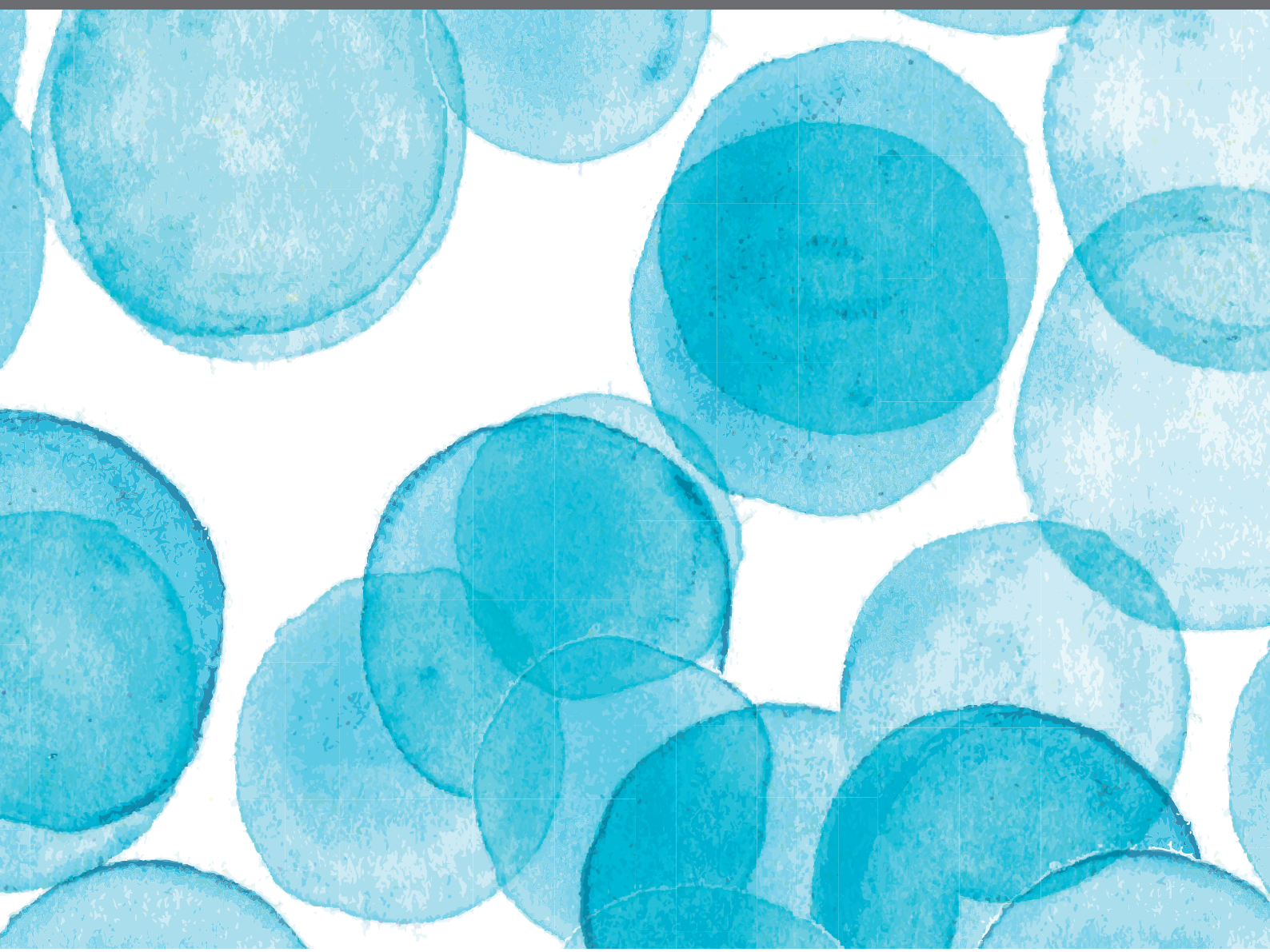

frontiers Research Topics

frontiers

Frontiers eBook Copyright Statement

The copyright in the text of individual articles in this eBook is the property of their respective authors or their respective institutions or funders. The copyright in graphics and images within each article may be subject to copyright of other parties. In both cases this is subject to a license granted to Frontiers.

The compilation of articles constituting this eBook is the property of Frontiers.

Each article within this eBook, and the eBook itself, are published under the most recent version of the Creative Commons CC-BY licence. The version current at the date of publication of this eBook is CC-BY 4.0. If the CC-BY licence is updated, the licence granted by Frontiers is automatically updated to the new version.

When exercising any right under the CC-BY licence, Frontiers must be attributed as the original publisher of the article or eBook, as applicable.

Authors have the responsibility of ensuring that any graphics or other materials which are the property of others may be included in the CC-BY licence, but this should be checked before relying on the CC-BY licence to reproduce those materials. Any copyright notices relating to those materials must be complied with.

Copyright and source acknowledgement notices may not be removed and must be displayed in any copy, derivative work or partial copy which includes the elements in question.

All copyright, and all rights therein, are protected by national and international copyright laws. The above represents a summary only. For further information please read Frontiers' Conditions for Website Use and Copyright Statement, and the applicable CC-BY licence.

ISSN 1664-8714
ISBN 978-2-88966-707-9
DOI 10.3389/978-2-88966-707-9

About Frontiers

Frontiers is more than just an open-access publisher of scholarly articles: it is a pioneering approach to the world of academia, radically improving the way scholarly research is managed. The grand vision of Frontiers is a world where all people have an equal opportunity to seek, share and generate knowledge. Frontiers provides immediate and permanent online open access to all its publications, but this alone is not enough to realize our grand goals.

Frontiers Journal Series

The Frontiers Journal Series is a multi-tier and interdisciplinary set of open-access, online journals, promising a paradigm shift from the current review, selection and dissemination processes in academic publishing. All Frontiers journals are driven by researchers for researchers; therefore, they constitute a service to the scholarly community. At the same time, the Frontiers Journal Series operates on a revolutionary invention, the tiered publishing system, initially addressing specific communities of scholars, and gradually climbing up to broader public understanding, thus serving the interests of the lay society, too.

Dedication to Quality

Each Frontiers article is a landmark of the highest quality, thanks to genuinely collaborative interactions between authors and review editors, who include some of the world's best academicians. Research must be certified by peers before entering a stream of knowledge that may eventually reach the public - and shape society; therefore, Frontiers only applies the most rigorous and unbiased reviews.
Frontiers revolutionizes research publishing by freely delivering the most outstanding research, evaluated with no bias from both the academic and social point of view. By applying the most advanced information technologies, Frontiers is catapulting scholarly publishing into a new generation.

What are Frontiers Research Topics?

Frontiers Research Topics are very popular trademarks of the Frontiers Journals Series: they are collections of at least ten articles, all centered on a particular subject. With their unique mix of varied contributions from Original Research to Review Articles, Frontiers Research Topics unify the most influential researchers, the latest key findings and historical advances in a hot research area! Find out more on how to host your own Frontiers Research Topic or contribute to one as an author by contacting the Frontiers Editorial Office: frontiersin.org/about/contact

BACTERIOPHAGES ISOLATION FROM THE ENVIRONMENT AND THEIR ANTIMICROBIAL THERAPEUTIC POTENTIAL

Topic Editors:
Krishna Khairnar, National Environmental Engineering Research Institute (CSIR), India
Robert Czajkowski, University of Gdansk, Poland
Sutthirat Sitthisak, Naresuan University, Thailand
Krishna Mohan Poluri, Indian Institute of Technology Roorkee, India

Citation: Khairnar, K., Czajkowski, R., Sitthisak, S., Poluri, K. M., eds. (2021). Bacteriophages Isolation From The Environment And Their Antimicrobial Therapeutic Potential. Lausanne: Frontiers Media SA.
doi: 10.3389/978-2-88966-707-9

Table of Contents

05 ***Editorial: Bacteriophages Isolation From the Environment and Their Antimicrobial Therapeutic Potential***
Krishna Mohan Poluri, Sutthirat Sitthisak, Krishna Khairnar and Robert Czajkowski

09 ***Genomic and Ecogenomic Characterization of* Proteus mirabilis *Bacteriophages***
Diana R. Alves, Jonathan Nzakizwanayo, Cinzia Dedi, Chara Olympiou, Aurélie Hanin, Witold Kot, Lars Hansen, Rene Lametsch, Cormac G. M. Gahan, Pascale Schellenberger, Lesley A. Ogilvie and Brian V. Jones

23 ***Isolation and Characterization of Specific Phages to Prepare a Cocktail Preventing* Vibrio *sp. Va-F3 Infections in Shrimp (*Litopenaeus vannamei*)***
Ling Chen, Jiqiang Fan, Tingwei Yan, Quan Liu, Shengjian Yuan, Haoran Zhang, Jinfang Yang, Deng Deng, Shuqiang Huang and Yingfei Ma

34 ***Biodiversity and Classification of Phages Infecting* Lactobacillus brevis**
Marine Feyereisen, Jennifer Mahony, Horst Neve, Charles M. A. P. Franz, Jean-Paul Noben, Tadhg O'Sullivan, Viktor Boer and Douwe van Sinderen

46 ***Natural Occurrence of* Escherichia coli*-Infecting Bacteriophages in Clinical Samples***
Cátia Pacífico, Miriam Hilbert, Dmitrij Sofka, Nora Dinhopl, Ildiko-Julia Pap, Christoph Aspöck, João André Carriço and Friederike Hilbert

64 ***vB_PaeM_MIJ3, a Novel Jumbo Phage Infecting* Pseudomonas aeruginosa*, Possesses Unusual Genomic Features***
Mohammed Imam, Bandar Alrashid, Faizal Patel, Ahmed S. A. Dowah, Nathan Brown, Andrew Millard, Martha R. J. Clokie and Edouard E. Galyov

79 ***The Novel* Enterococcus *Phage vB_EfaS_HEf13 Has Broad Lytic Activity Against Clinical Isolates of* Enterococcus faecalis**
Dongwook Lee, Jintaek Im, Hongjun Na, Sangryeol Ryu, Cheol-Heui Yun and Seung Hyun Han

93 ***Overexpression of AmpC Promotes Bacteriophage Lysis of Ampicillin-Resistant* Escherichia coli**
Shuang Wang, Bo Yin, Ling Yu, Mei Dang, Zhimin Guo, Guangmou Yan, Dongliang Hu, Jingmin Gu, Chongtao Du, Xin Feng, Wenyu Han, Yuren Yuan Adam, Changjiang Sun, Janine T. Bossé and Liancheng Lei

104 ***Morphologically Different* Pectobacterium brasiliense *Bacteriophages PP99 and PP101: Deacetylation of O-Polysaccharide by the Tail Spike Protein of Phage PP99 Accompanies the Infection***
Anna A. Lukianova, Mikhail M. Shneider, Peter V. Evseev, Anna M. Shpirt, Eugenia N. Bugaeva, Anastasia P. Kabanova, Ekaterina A. Obraztsova, Kirill K. Miroshnikov, Sofiya N. Senchenkova, Alexander S. Shashkov, Stepan V. Toschakov, Yuriy A. Knirel, Alexander N. Ignatov and Konstantin A. Miroshnikov

119 ***Novel Bacteriophages Capable of Disrupting Biofilms From Clinical Strains of* Aeromonas hydrophila**
Mwila Kabwe, Teagan Brown, Lachlan Speirs, Heng Ku, Michael Leach, Hiu Tat Chan, Steve Petrovski, Peter Lock and Joseph Tucci

132 *Isolation and Characterization of the Novel Phages vB_VpS_BA3 and vB_VpS_CA8 for Lysing* **Vibrio parahaemolyticus**
Meiyan Yang, Yongjian Liang, Shixuan Huang, Jumei Zhang, Jing Wang, Hanfang Chen, Yuanming Ye, Xiangyang Gao, Qingping Wu and Zhiyuan Tan

145 *The Yersinia Phage X1 Administered Orally Efficiently Protects a Murine Chronic Enteritis Model Against* **Yersinia enterocolitica** *Infection*
Yibing Xue, Shengjie Zhai, Zijing Wang, Yalu Ji, Gang Wang, Tianqi Wang, Xinwu Wang, Hengyu Xi, Ruopeng Cai, Rihong Zhao, Hao Zhang, Lanting Bi, Yuan Guan, Zhimin Guo, Wenyu Han and Jingmin Gu

155 *Impact of Frequent Administration of Bacteriophage on Therapeutic Efficacy in an A.* **baumannii** *Mouse Wound Infection Model*
Michael D. Rouse, Joshua Stanbro, Jessica A. Roman, Michelle A. Lipinski, Anna Jacobs, Biswaijt Biswas, James Regeimbal, Matthew Henry, Michael G. Stockelman and Mark P. Simons

168 *Genomic Analysis of Mic1 Reveals a Novel Freshwater Long-Tailed Cyanophage*
Feng Yang, Hua Jin, Xiao-Qian Wang, Qiong Li, Jun-Tao Zhang, Ning Cui, Yong-Liang Jiang, Yuxing Chen, Qing-Fa Wu, Cong-Zhao Zhou and Wei-Fang Li

180 *Deciphering the Role of Holin in Mycobacteriophage D29 Physiology*
Varun Rakeshbhai Bavda and Vikas Jain

189 *Isolation and Characterization of a New Phage Infecting* **Elizabethkingia anophelis** *and Evaluation of Its Therapeutic Efficacy* **in vitro** *and* **in vivo**
Shih-Yi Peng, Li-Kuang Chen, Wen-Jui Wu, Prajna Paramita, Po-Wei Yang, Yun-Zhong Li, Meng-Jiun Lai and Kai-Chih Chang

199 *Characterization and Genome Structure of Virulent Phage EspM4VN to Control* **Enterobacter** *sp. M4 Isolated From Plant Soft Rot*
Nguyen Cong Thanh, Yuko Nagayoshi, Yasuhiro Fujino, Kazuhiro Iiyama, Naruto Furuya, Yasuaki Hiromasa, Takeo Iwamoto and Katsumi Doi

214 *Separation of* **Mycobacterium smegmatis** *From a Mixed Culture Using the Cell Wall Binding Domain of D29 Mycobacteriophage Endolysin*
Gokul Nair and Vikas Jain

223 *Characterization of Novel Broad-Host-Range Bacteriophage DLP3 Specific to* **Stenotrophomonas maltophilia** *as a Potential Therapeutic Agent*
Danielle L. Peters, Jaclyn G. McCutcheon and Jonathan J. Dennis

244 *Isolation and Characterization of Novel Lytic Bacteriophages Infecting Epidemic Carbapenem-Resistant* **Klebsiella pneumoniae** *Strains*
Min Li, Min Guo, Long Chen, Chaowang Zhu, Yuyi Xiao, Pei Li, Hongxiong Guo, Liang Chen, Wei Zhang and Hong Du

256 *Identification of a Novel* **Acinetobacter baumannii** *Phage-Derived Depolymerase and Its Therapeutic Application in Mice*
Can Wang, Puyuan Li, Yang Zhu, Yong Huang, Mingming Gao, Xin Yuan, Wenkai Niu, Huiying Liu, Hang Fan, Yanhong Qin, Yigang Tong, Zhiqiang Mi and Changqing Bai

frontiers in Microbiology

EDITORIAL
published: 23 February 2021
doi: 10.3389/fmicb.2021.649334

Editorial: Bacteriophages Isolation From the Environment and Their Antimicrobial Therapeutic Potential

Krishna Mohan Poluri[1]*, *Sutthirat Sitthisak*[2]*, *Krishna Khairnar*[3]* and *Robert Czajkowski*[4]*

[1] Department of Biotechnology and Centre for Nanotechnology, Indian Institute of Technology Roorkee, Roorkee, India, [2] Department of Microbiology and Parasitology, Faculty of Medical Science, Naresuan University, Phitsanulok, Thailand, [3] Environmental Virology Cell (EVC), Council of Scientific & Industrial Research- National Environmental Engineering Research Institute (NEERI), Nagpur, India, [4] Division of Biologically Active Compounds, Intercollegiate Faculty of Biotechnology, University of Gdansk and Medical University of Gdansk, University of Gdansk, Gdańsk, Poland

Keywords: bacterial viruses, phage (bacteriophage), isolation, biological control, medicine, veterinary, agriculture

OPEN ACCESS

Edited by:
Karsten Becker, University Medicine Greifswald, Germany

Reviewed by:
Daniel De Vos, Queen Astrid Military Hospital, Belgium

***Correspondence:**
Krishna Mohan Poluri
mohanpmk@gmail.com; Krishna.poluri@bt.iitr.ac.in
Sutthirat Sitthisak
sutthirats@nu.ac.th
Krishna Khairnar
k_khairnar@neeri.res.in
Robert Czajkowski
robert.czajkowski@biotech.ug.edu.pl

Specialty section:
This article was submitted to Antimicrobials, Resistance and Chemotherapy, a section of the journal Frontiers in Microbiology

Received: *04 January 2021*
Accepted: *03 February 2021*
Published: *23 February 2021*

Citation:
Poluri KM, Sitthisak S, Khairnar K and Czajkowski R (2021) Editorial: Bacteriophages Isolation From the Environment and Their Antimicrobial Therapeutic Potential. Front. Microbiol. 12:649334. doi: 10.3389/fmicb.2021.649334

Editorial on the Research Topic

Bacteriophages Isolation From the Environment and Their Antimicrobial Therapeutic Potential

First bacterial viruses (named bacteriophages and/or phages—"eaters of bacteria") were discovered only as late as at the beginning of the twentieth century (Hadley, 1928; Abedon, 2014). Just after, since the early thirties of twentieth century, bacteriophages were widely used in the control and prevention of bacterial infections in humans (Van der Vlught and Verbeek, 2008). However, the discovery at the same time of the first natural antibiotics (i.e., penicillin) prevented the further development of therapies based on the use of phages in most Western European countries as well as in the rest of the world. Only recently, due to the worldwide appearance and spread of the multi-drug resistant bacterial infections in humans, bacteriophages have been rediscovered as potential antibacterial therapies and have started to be widely used again.

Despite the recent recognition of bacteriophages as potential "golden bullet" for treating infections caused by multi-drug resistant bacterial pathogens, only very little work has targeted this subject in detail. To boost this important research field, the Research Topic "*Bacteriophages isolation from the environment and their antimicrobial therapeutic potential*" was developed with the aim of underlining, among others, the potential new therapeutic roles of bacterial viruses in treatment of human, animal and crop plant infections.

Public health safety and economic concerns being the thematic megatrends define the societal development index. Bacteriophages can occur naturally and feed upon certain specific bacteria for their nutritional needs. Hence, they act as a natural antibacterial agent for particular organism. In the current thematic issue, several reports that include isolation of the bacteriophages from the natural niches are included. A diverse hotspot for the bacterial existence and their intuitive host (phages) is sewage sites. Yang M. et al. could isolate two lytic bacteriophages from the sewage collected in China. The phages were found to have *Vibrio parahaemolyticus* as their particular host, which implicatively destine these phages to be a potential control agent for multi-drug resistant *V. parahaemolyticus*. Morphological examination using electron microscopy enabled the authors to classify the virions in *Siphoviridae* family on the basis of typical features like icosahedral head and long non-contractile tail. Genetic annotations were used to tag major structural and functional genes involved in phage structure, packaging, host lysis, DNA metabolism etc. Similar to sewages, the outlets from the hospitals also attract fair amount of consideration with respect to phage isolation. Peng et al. isolated a phage named TCUEAP1 that has *Elizabethkingia anopheles*

as its host. The genome sequence analysis was performed to ascertain the exclusivity of phage. Additionally, in mice experiments, this phage showed high rescue rate after lethal bacteremia. Pacifico et al. studied and established the existence of coliphages in the blood, urine and tracheal aspirates of hospitalized patients. Upon classification, clinical isolates were found to belong to *Tunavirinae* sub family and to *Peduovirus* and *Tequintavirus* genera. These newly isolated phages were virulent with exception to some members belonging to *Peduovirus* that seem to reside as prophages. Imam et al. isolated and characterized so-called jumbo bacteriophage MIJ3 infecting *Pseudomonas aeruginosa*. The genome of the isolated virus contains genes coding for proteins of bacterial origin, not frequently present in bacteriophages *viz*. FtsH (ATP-dependent zinc metalloprotease)-like protein, and TilS–a putative lysidine synthase. The presence of bacterial genes in phage genomes may shed light on the bacteriophage-bacteria gene exchanges, spread of the bacterial genes in environment and size of the genetic pool that can be available for bacteria in nature.

Altered environmental conditions such as global warming have created substantial impact on environment. Due to significant change in the seasonal variation patterns, the opportunistic environmental bacteria have become more pathogenic. Kabwe et al. reported the isolation and characterization of lytic phage against *Aeromonas hydrophila*. This bacteria can survive in moist temperate environment, form biofilms, survive traditional disinfection methods and even disarm antibiotics; making it responsible for mortality rate as high as 46%. Another classical niche for the bacteria and the associated phages is the soil and forms the considerable ground for metagenomics study. Peters et al. isolated and characterized a phage from soil and found it specific to *Stenotrophomonas maltophilia*. This phage was named as DLP3 (second member in *Delepquintavirus* genus) and found to infect 22 out of 29 known strains of *S. maltophilia*. The authors also performed genome analysis thereby identifying the coding sequences, resistance modules and other important genomic aspects. The phage also exhibited lytic activity *in vivo*. Apart from the soil, water bodies also serve as an important ecosystem that show close knit association and companionship amongst microbes. Bio-accumulation of the nutrients in the water bodies lead to profuse growth of organism of lower strata. Cyanobacteria, lie at the base of the food chain operating in water and often present lethal threats to the aquatic life-forms as they lower the levels of dissolved oxygen. Yang F. et al. isolated a long-tailed cyanophage that can dwell on cyanobacteria from Lake Chaohu. The authors described the morphological features of this isolated phage Mic1 specific to *Microcystis aeruginosa* and performed genome and phylogenetic analyses. Common phylogenetic ancestry of DNA polymerase gene from Mic1 and mitochondria strikes a note common to ancestral relationships between cyanophages and their hosts.

Acquired antibiotic resistance due to horizontal gene transfer, during nosocomial infections, antibiotic misuse and frequent treatment prolapses, is a major concern in present scenario. Bacteriophages, viruses that can feed upon bacteria, are being tested for this purpose and yielding a better performance stats, worldwide. Several bacteriophages have been discovered are under testing to understand and cure the bacterial nuisances. Rising instances of antibiotic resistant *Acinetobacter baumannii* strains have created a worldwide alarming condition. Wang C. et al. once again characterized an already isolated phage (named vB_AbaM_IME285). Recombinant enzyme (Dp49), a product of depolymerase gene (ORF49) from this phage, showed significant antibiotic activity *in vitro*. Increased survival rate of the mice pre-infected with *A. baumannii* projects this phage to be suitable alternative to control multidrug-resistant *A. baumannii*. Likewise, Rouse et al. used a mouse model to assess the effectiveness of phage treatment against *A. baumannii* infections. In this proof-of-concept approach the authors demonstrated that the lytic bacterial viruses can be used with success as a potent and safe antibacterial agent against the pathogen and that exposure of animals to phages prior to infections with *A. baumannii* does not result in decrease of the observed antibacterial effects.

Another major clinical problem that can employ bacteriophage as an alternative antibacterial remedy is carbapenem-resistant *Klebsiella pneumoniae* (CRKP). By their formidable efforts, Li et al. could isolate 54 phages, corresponding to 54 clinical CRKP hosts. Interestingly, KPC-2 producing ST11 strain was the most abundant strain (88.9%) and a phage P545 from *Myoviridaes* was highly stable and inhibited the biofilm formation. Worldwide, *Yersinia enterolitica* is considered a troublesome food borne pathogen. Xue et al. isolated and tested Yersinia phage X1, which has broad host range covering almost half of the known strains. Exceptional ability of this phage to cross stomach and reach intestine with retained infectious ability, along with high stability and tolerance with respect to pH, temperature and enzymatic degradation; makes this phage a suitable candidate for oral administration. Intestinal histopathologic observations exhibited phenomenal improvement upon treatment with phage X1, and reduced the level of proinflammatory cytokines. Similarly, in another study, Wang S. et al. tested the phages to control ampicillin-resistant *Escherichia coli*. The authors demonstrated that overexpression of AmpC β-lactamase—an enzyme responsible for bacterial resistance to ampicillin, may promote infection of *E. coli* strains with phages that use an OmpA as a receptor for adsorption. Furthermore, this study demonstrated an interplay between phages and antibiotics in killing bacterial pathogens and may give important insights to the global effectiveness of therapies involving antimicrobials and bacterial viruses. An interesting example describing the study of phages infecting Gram-positive bacterial human pathogens is the work of Lee et al. who characterized a bacteriophage vB_EfaS_HEf13 expressing broad lytic activity against clinically-relevant antibiotic-resistant isolates of *Enterococcus faecalis*. The authors speculated that the mentioned bacteriophage may be potent as a dental therapeutic agent to treat periodontitis related to infections with *E. faecalis*. Furthermore, bacteriophages can be also used to prevent/reduce biofilm formation during catheterization of hospitalized patients. This approach has been exploited by Alves et al. who isolated lytic bacteriophages against *Proteus mirabilis*—a common causative agent of biofilm formation in catheters. The authors characterized in detail five phages able to infect *P. mirabilis*,

including these that shown to reduce formation of biofilm under experimental conditions. Such an approach may be of help in developing new therapies for hospitalized individuals who require (permanent) catheterization.

Tuberculosis, in last decade, has garnered extreme attention because of acquired drug resistance by *Mycobacterium tuberculosis*. *M. tuberculosis* poses a major global health threat and requires advancements related to better diagnostic approaches. Thus, Bavda and Jain scrutinized Mycobacteriophage D29, for its potential to infect and eliminate several mycobacterial species. In order to test the viability of the phage after removal of crucial holin protein, Bacteriophage Recombineering of Electroporated DNA (BRED) approach was applied to create D29 holin knockout (D291gp11). Retained functional ability of the phage after removal of holin suggests the protein is dispensable for this phage, in particular. Moving further, Nair and Jain designed a novel diagnostic approach using D29 mycobacteriophage LysA endolysin's C-terminal domain (CTD) construct. CTD possesses the ability to selectively bind to *M. tuberculosis* and *Mycobacterium smegmatis* peptidoglycan (PG). Exploring this specific interaction, Green fluorescent protein (GFP) and glutathione-S-transferase (GST) were tagged to CTD forming CTD-GFP and CTD-GST constructs. These constructs were used to separate the mixtures containing Gram-positive and Gram-negative bacteria. These innovative studies added positively to the diagnostic and treatment cohort against *M. tuberculosis*.

The use of bacteriophages in the biological control of bacterial infections in plants has never been so common in comparison with their use in prevention and treatment of infections in humans and animals or in a food industry. This is also reflected in this Research Topic, in which two publications have targeted bacteriophages infecting plant pathogens and their thereof use. Thanh et al. morphologically, phenotypically and genetically characterized a EspM4VN bacteriophage to be used to control soft rot disease in crops infected with *Enterobacter* spp. Likewise, Lukianova et al. analyzed in detail the attachment of two bacteriophages, viz. PP99 and PP101 to the surface of the plant pathogen *Pectobacterium brasiliense*. The authors revealed that PP99 and PP101 phages use a similar mechanism by which they interact with bacterial surface polysaccharides. As well, the authors described in detail the molecular basis of this mechanism governing interaction of phage tail spike proteins with bacterial O-polysaccharide. This in turn is an important insight into phage adsorption mechanisms used by viruses to infect soft rot plant pathogens.

An interesting approach of using bacteriophages in food industry to prevent spoilage is presented by Feyereisen et al. who evaluated lytic bacteriophages against *Lactobacillus brevis* responsible for beer decay. The authors discovered and characterized in detail intact prophages in the genomes of *L. brevis* that can be potentially used as antimicrobial agents. The idea was to combine prophage induction followed by host killing with sanitizers and/or UV treatment to remove the *L. brevis* bacteria from beer production environment. This innovative approach may be used to reduce the chemical input in beer production and provide a proof-of-concept data to evaluate this idea also in other food-related production systems.

Another innovative approach to prevent death of farmed shrimps caused by *Vibrio* sp. Va-F3 infections under aquacultural conditions was described in the work of Chen et al.. The authors implemented an integrated workflow designed to develop a cocktail containing lytic bacteriophages, and evaluated it. Application of bacteriophage cocktail significantly reduced the death of the treated shrimps in comparison with the untreated control proving that such antibiotic-less therapies may be used to protect farmed animals in aquacultures.

It is believed that the blooming of the phage research will continue. The rediscovery of bacteriophages and their role in medicine, veterinary, food microbiology and agriculture has transformed the research area of minor importance to a broad and scientifically significant topic of the twenty-first century.

Lastly, we would like to sincerely thank all the authors for their contribution to this thematic Research Topic, as well as acknowledge the excellent work of many reviewers for their critical assessments of the reviewed manuscripts.

AUTHOR CONTRIBUTIONS

All authors listed have made a substantial, direct and intellectual contribution to the work, and approved it for publication.

ACKNOWLEDGMENTS

KP acknowledge the support of Grants GKC-01/2016-17/212/NMCG-Research from NMCG-MoWR, and CRG/2018/001329 from SERB-DST, Government of India. SS acknowledges the receipt of Newton Fund Institutional Links (RDG61W0003) and an Institutional Links grant, ID 332371796, under the UK—Thailand Research and Innovation Partnership Fund. KK is thankful to Ministry of Jal Shakti, Department of Water Resources, River Development, and Ganga Rejuvenation, National Mission for Clean Ganga (NMCG), Government of India, New Delhi, India for financial assistance (GKC-01/2016-17/212, NMCG- Research), Director of CSIR-NEERI for infrastructure and support. RC acknowledges the grant support of NCN OPUS 13 (2017/25/B/NZ9/00036) from National Science Center, Poland (Narodowe Centrum Nauki, Polska). Authors thank Mr. Nipanshu Agarwal, IIT-Roorkee for the technical support during the preparation of the manuscript.

REFERENCES

Abedon, S.T. (2014). Phage therapy: eco-physiological pharmacology. *Scientifica* 2014:581639. doi: 10.1155/2014/581639

Hadley, P. (1928). The Twort-D'Herelle phenomenon: a critical review and presentation of a new conception (homogamic theory) of bacteriophage action. *J. Infect. Dis.* 42, 263–434.

Van der Vlught, R. A. A., and Verbeek, M. (2008). Bacteriophages: therapeuticals and alternative applications. Available online at:

http://www.cogem.net/index.cfm/en/publications/publicatie/bacteriophages-therapeuticals-and-alternative-applications COGEM Report.

Conflict of Interest: The authors declare that the research was conducted in the absence of any commercial or financial relationships that could be construed as a potential conflict of interest.

Copyright © 2021 Poluri, Sitthisak, Khairnar and Czajkowski. This is an open-access article distributed under the terms of the Creative Commons Attribution License (CC BY). The use, distribution or reproduction in other forums is permitted, provided the original author(s) and the copyright owner(s) are credited and that the original publication in this journal is cited, in accordance with accepted academic practice. No use, distribution or reproduction is permitted which does not comply with these terms.

frontiers in Microbiology

ORIGINAL RESEARCH
published: 06 August 2019
doi: 10.3389/fmicb.2019.01783

Genomic and Ecogenomic Characterization of *Proteus mirabilis* Bacteriophages

Diana R. Alves[1,2,3†], Jonathan Nzakizwanayo[1,4†], Cinzia Dedi[1†], Chara Olympiou[1,5], Aurélie Hanin[6], Witold Kot[7], Lars Hansen[7], Rene Lametsch[8], Cormac G. M. Gahan[6,9], Pascale Schellenberger[10], Lesley A. Ogilvie[1] and Brian V. Jones[1,3,4]**

[1] School of Pharmacy and Biomolecular Sciences, University of Brighton, Brighton, United Kingdom, [2] Blond McIndoe Research Foundation, Queen Victoria Hospital, East Grinstead, United Kingdom, [3] Queen Victoria Hospital NHS Foundation Trust, East Grinstead, United Kingdom, [4] Department of Biology and Biochemistry, University of Bath, Bath, United Kingdom, [5] School of Pharmacy, Queen's University, Belfast, United Kingdom, [6] APC Microbiome Ireland, University College Cork, Cork, Ireland, [7] Department of Plant and Environmental Sciences, University of Copenhagen, Copenhagen, Denmark, [8] Department of Food Science, University of Copenhagen, Copenhagen, Denmark, [9] School of Pharmacy, University College Cork, Cork, Ireland, [10] School of Life Sciences, University of Sussex, Brighton, United Kingdom

OPEN ACCESS

Edited by:
Robert Czajkowski,
University of Gdańsk, Poland

Reviewed by:
Yong Jiang,
Ocean University of China, China
Heejoon Myung,
Hankuk University of Foreign Studies, South Korea

***Correspondence:**
Lesley A. Ogilvie
ogilvie.lesley@googlemail.com
Brian V. Jones
B.V.Jones@bath.ac.uk

[†]These authors have contributed equally to this work

Specialty section:
This article was submitted to Virology, a section of the journal Frontiers in Microbiology

Received: 18 June 2019
Accepted: 18 July 2019
Published: 06 August 2019

Citation:
Alves DR, Nzakizwanayo J, Dedi C, Olympiou C, Hanin A, Kot W, Hansen L, Lametsch R, Gahan CGM, Schellenberger P, Ogilvie LA and Jones BV (2019) Genomic and Ecogenomic Characterization of Proteus mirabilis Bacteriophages. Front. Microbiol. 10:1783. doi: 10.3389/fmicb.2019.01783

Proteus mirabilis often complicates the care of catheterized patients through the formation of crystalline biofilms which block urine flow. Bacteriophage therapy has been highlighted as a promising approach to control this problem, but relatively few phages infecting *P. mirabilis* have been characterized. Here we characterize five phages capable of infecting *P. mirabilis*, including those shown to reduce biofilm formation, and provide insights regarding the wider ecological and evolutionary relationships of these phages. Transmission electron microscopy (TEM) imaging of phages vB_PmiP_RS1pmA, vB_PmiP_RS1pmB, vB_PmiP_RS3pmA, and vB_PmiP_RS8pmA showed that all share morphologies characteristic of the *Podoviridae* family. The genome sequences of vB_PmiP_RS1pmA, vB_PmiP_RS1pmB, and vB_PmiP_RS3pmA showed these are species of the same phage differing only by point mutations, and are closely related to vB_PmiP_RS8pmA. Podophages characterized in this study were also found to share similarity in genome architecture and composition to other previously described *P. mirabilis* podophages (PM16 and PM75). In contrast, vB_PimP_RS51pmB showed morphology characteristic of the *Myoviridae* family, with no notable similarity to other phage genomes examined. Ecogenomic profiling of all phages revealed no association with human urinary tract viromes, but sequences similar to vB_PimP_RS51pmB were found within human gut, and human oral microbiomes. Investigation of wider host-phage evolutionary relationships through tetranucleotide profiling of phage genomes and bacterial chromosomes, indicated vB_PimP_RS51pmB has a relatively recent association with *Morganella morganii* and other non-*Proteus* members of the *Morganellaceae* family. Subsequent host range assays confirmed vB_PimP_RS51pmB can infect *M. morganii*.

Keywords: phage therapy, ecogenomics, biofilms, catheters, bacteriophage

INTRODUCTION

The opportunistic pathogen *Proteus mirabilis* is a common cause of catheter-associated urinary tract infections (CAUTIs) and can significantly complicate the care of patients undergoing long-term urethral catheterization (Mobley, 1996; Stickler, 2008, 2014). *P. mirabilis* infection often leads to encrustation and blockage of catheters in these individuals, which if unnoticed, can result in the reflux of infected urine to the upper urinary tract and serious clinical symptoms including pyelonephritis, septicaemia, and shock (Mobley, 1996; Jacobsen et al., 2008; Stickler, 2008, 2014). Although blockage is usually not a problem in hospitalized patients, the majority of long-term catheterized individuals are cared for in the community where continual clinical surveillance is not possible, and blockage is often not detected until subsequent symptomatic complications arise (Stickler, 2014). As a result, catheter blockage is the underlying cause of a large proportion of emergency hospital referrals for individuals undergoing long-term catheterization (Kohler-Ockmore and Feneley, 1996; Stickler, 2014).

The blockage of catheters by *P. mirabilis* is derived from the ability of this organism to form dense biofilms on the surface of catheters, in conjunction with the production of a potent urease enzyme (Griffith et al., 1976; Jones and Mobley, 1987; Stickler et al., 1993; Jones et al., 2005). This highly active enzyme hydrolyses urea present in the urine and generates ammonia, which in turn elevates urinary pH (Hedelin et al., 1984; Cox and Hukins, 1989; Stickler et al., 1993; Holling et al., 2014a,b). Under these alkaline conditions, calcium and magnesium phosphates precipitate to form microcrystalline aggregates suspended in the urine (Stickler et al., 1993; Stickler, 2008). As the biofilm continues to develop, these crystals become trapped in the growing community, where the exopolymeric matrix further stabilizes and enhances their growth, eventually leading to the development of a mineralized crystalline biofilm structure that can block urine flow (Stickler et al., 1993; Stickler, 2008).

Although catheters designed to prevent CAUTIs and impede biofilm formation have been developed, they remain prone to encrustation and blockage by *P. mirabilis,* and are considered ineffective in long-term settings (Morris et al., 1997; Morgan et al., 2009; Stickler, 2014). This includes catheters approved for use within the United Kingdom National Health Service; for example, antimicrobial catheters coated with silver or nitrofurazone have been shown to have no significant impact on the incidence of CAUTI, even during short-term catheterization (Pickard et al., 2012). *P. mirabilis* also frequently causes chronic infection in long-term catheterized patients and can persist after catheter changes and multiple rounds of standard antibiotic treatment (Kunin, 1997). Therefore, there are currently no fully effective approaches to prevent or manage catheter blockage due to *P. mirabilis* CAUTI, and new strategies are required to deal with this persistent and growing clinical problem.

Previously, we have explored the use of bacteriophage (or phage) to combat *P. mirabilis* crystalline biofilm formation, and demonstrated the potential for this approach to control catheter encrustation (Nzakizwanayo et al., 2016). A combination of three phages that infect *P. mirabilis* were applied to *in vitro* models of the catheterized urinary tract. This cocktail was able to significantly inhibit crystalline biofilm formation in experiments simulating an established infection and completely eradicated *P. mirabilis* from models in experiments simulating the early stages of infection (Nzakizwanayo et al., 2016). Other *P. mirabilis* phages have also been characterized with therapeutic applications in mind, and include the podophages PM16, PM75 and vB_PmiP_5460 (Melo et al., 2016; Morozova et al., 2016, 2018), the Siphophage pPM_01 (Wirjon et al., 2016), and the Myophage vB_PmiP_5461 (Melo et al., 2016). Notably, phages vB_PmiP_5460 and vB_PmiP_5461 have also been demonstrated to reduce crystalline biofilm formation in models of CAUTI (Melo et al., 2016).

However, there is presently a general paucity of data regarding phages that infect *P. mirabilis*, and in order to fully explore the potential for phage therapy to control this pathogen, as well as to optimize the development of effective phage cocktails, a greater understanding of phages infecting this species is required. Here we describe the full genomic sequence and characterization of phages infecting *P. mirabilis*, including those previously shown to have potential utility in controlling crystalline biofilm formation (Nzakizwanayo et al., 2016). We demonstrate how genomic and ecogenomic profiling of these phages can identify broader affiliations with various microbial ecosystems and other bacterial host species. Collectively, these genomic and ecogenomic approaches will aid the development of phage cocktails for the control of *P. mirabilis* and other urinary tract pathogens.

MATERIALS AND METHODS

Bacterial Strains, Media, and Routine Culture

Clinical isolates of *P. mirabilis* used in this study were obtained from the Royal Sussex County Hospital (Brighton, United Kingdom), and all were isolated from urinary tract infection sites (**Supplementary Table S1**). All chemicals, reagents and growth media were obtained from either Thermo Fisher Scientific, United Kingdom, Oxoid, United Kingdom, or Sigma, United Kingdom, unless otherwise stated. Bacteria were routinely cultured in Luria-Bertani (LB) medium (5 g/L yeast extract, 10 g/L tryptone, 10 g/L sodium chloride) at 37°C with shaking, or on LB solidified by addition of 15 g/L Technical agar (LA). Soft agar overlays, used for phage enrichments, purification and enumeration, were derived from LB, and contained 6.5 g/L Technical agar (S-LA).

Phage Isolation and Purification

Phages were isolated from wastewater collected from treatment plants in the United Kingdom (Anglian Water, Milton Keynes, Luton, and Sharnbrook). Enrichments for phages active against *P. mirabilis* were performed by mixing 100 mL of wastewater with 387.5 mL of LB, and subsequent inoculation with 2.5 mL of an overnight culture of *P. mirabilis* (see **Supplementary Table S1** for host strains). This was incubated at 37°C overnight without

shaking. 10 mL aliquots were centrifuged (3000×*g* for 30 min), and supernatants filtered into fresh sterile tubes using 0.45 μm pore syringe filters (Sartorius, United Kingdom). 3 mL S-LA inoculated with 100 μL of an overnight *P. mirabilis* culture was mixed with 100 μL of filtered enrichment, swirled gently, and immediately poured over the surface of a LA plate. Plates were incubated at 37°C for 18–20 h, and phage with the ability to infect the host strain were identified by observing zones of lysis (plaques) in the agar. To isolate distinct phage, individual plaques were picked off using Pasteur pipettes and re-suspended in 300 μL suspension medium (SM) buffer (100 mM NaCl, 10 mM MgSO4.7H_2O, and 50 mM Tris–HCL pH 7.5, 0.01% gelatine). The resulting phage suspensions were serially diluted in SM Buffer, and the dilutions used to prepare agar overlays with overnight cultures of *P. mirabilis*, and plates incubated at 37°C overnight. To ensure phage purity, this process was repeated a further 5 times until bacterial lawns showed homogeneity of plaque morphology. An individual plaque was then picked off and re-suspended in SM buffer for use in subsequent experiments. Purified phage suspensions were stored at 4°C until required.

Preparation of High Titre Phage Stocks

To prepare high titre stocks of isolated phage (10^{10} pfu/ml), phages were propagated on their original host strain in LB broth (**Supplementary Table S1**), and 100 μL of the resulting phage lysate mixed with 100 μL of a fresh overnight culture of *P. mirabilis*. This was incubated for 5 min at room temperature without shaking, before being used to prepare soft agar overlays on LB agar plates, as described above. After an overnight incubation at 37°C, plates displaying confluent lysis were selected and flooded with 3 mL of SM buffer supplemented with 2% (v/v) chloroform, before incubation at 37°C for 4 h. The resulting phage suspension was removed from the plates, centrifuged (11,000 × *g* for 10 min) to remove cell debris, and filtered using 0.22 μm pore size syringe filters. In order to further concentrate the phage, one volume of 20% PEG-8000 solution supplemented with 1M NaCl (Sigma, United Kingdom) was added to the phage suspension and incubated at 4°C overnight, before centrifugation at 11,000 × *g* for 20 min. The resulting pellet was re-suspended in SM buffer and a 1/5 volume of chloroform was added, vortexed for 30 s to mix, followed by slow centrifugation (3,000 × *g* for 15 min at 4°C). The upper aqueous phase was removed and stored at 4°C until required.

Infection of Non-*Proteus* Species

The ability of phage to infect and replicate in alternate host species, was evaluated using spot tests of phage suspensions on agar overlays seeded with potential host bacteria. Isolates of species tested were obtained from DSMZ, and are described in **Supplementary Table S1**. For each bacterial species tested, 100 μL of an overnight culture was mixed with 3 mL of S-LA and poured onto a LA plate. Plates were left to dry for 20 min at 37°C. Phage lysates were standardized to a titre of 10^9 PFU/mL, and 10 μL of each lysate was spotted onto the bacterial lawns at concentrations ranging from 10^3 to 10^9 PFU/mL, and plates incubated overnight at 37°C. This assay was performed in triplicate, and evidence of phage replication taken as formation of plaques in the region of the spotted phage suspension.

Electron Microscopy

Purified phage particles at a concentration of 10^9 PFU/mL were deposited on 300 mesh carbon-coated copper grids (Agar Scientific, United Kingdom) and negatively stained with 1% uranyl acetate (pH 4) as follows: the surface of the copper grids were ionized for 2 min immediately prior to sample deposition. 5 μL of phage lysate were spotted on the surface of the grid and allowed to stand for 1 min. This was followed by 30 sec negative staining and subsequent air drying of the grid. Visualization was performed using a JEOL JEM-1400Plus TEM, operated at 120 kV (pixel size = 0.1 nm), equipped with a Gatan OneView 4K camera with automatic drift correction.

Phage DNA Sequencing, Assembly, and Inference of Physical Genome Structure

Phage genomic DNA was extracted through a direct plaque sequencing method described by Kot et al. (2014). DNA sequencing libraries were prepared using the Nextera XT DNA kit (Illumina, San Diego, CA, United States), according to the manufacturer's protocol. Individually tagged libraries were sequenced as part of a flow cell as 2 × 250 base paired-end reads using the Illumina MiSeq platform (Illumina, San Diego, CA, United States). Reads were analyzed, trimmed, and assembled using CLC Genomic Workbench version 6.5.1, as described previously (Kot et al., 2014).

Nanopore sequencing was conducted using multiplex barcoded sequencing of phage genomic libraries on the Oxford Nanopore Technologies (ONT) MinION sequencing platform. Genomic DNA was extracted from high titre phage stocks (10^{10} pfu/mL) using the Zinc precipitation method originally described by Santos (1991), with some minor modifications previously outlined in Ogilvie et al. (2012). The quantity and purity of the resulting DNA was tested using the Qubit 2.0 and the Nanodrop 2000, respectively. Sequencing libraries were prepared according to the ONT protocols for the Native Barcoding Kit (EXP-NBD103), and the Ligation sequencing Kit 1D (SQK-LSK108). For each phage, 1 μg of total genomic DNA was treated with the NEBNext End repair/dA-tailing Module (E7546; New England Biolabs), purified using 1× volume AMPure XP beads (Beckman Coulter), then eluted in nuclease – free water (25 μL). Next, 500 ng of each end – repaired adenylated DNA was ligated to one of the Native Barcodes (selected from NB01 to NB12; ONT) using the Blunt/TA Master Mix (M0367; New England Biolabs), cleaned using the AMPure XP beads, then eluted in nuclease – free water (26 μL). The barcoded samples were combined in equimolar amounts to produce a pooled sample of 700 ng in 50 μL nuclease-free water and Barcode Adapter ligation performed using T4 DNA ligase in the NEBNext Quick Ligation Module (E6056; New England Biolabs). The resulting library was eluted in the Nanopore Elution Buffer (15 μL) and amount of DNA quantified using the Qubit 2.0 to confirm total DNA recovery of ∼500 ng. The final library (12 μL) was mixed with Nanopore Running Buffer

with Fuel Mix (35 μL), Library Leading Beads (25.5 μL), and Nuclease-fee water (2.5 μL). This mixture was loaded onto a pre-primed single R9.4/FLO-MIN106 flow cell in a MinION Mk1B, and run for 48 h.

The resulting MinION reads were subject to basecalling using Albacore v2.3.1, and reads demultiplexed and trimmed using Porechop (v0.2.4 October 2018[1]). Nanopore reads with a minimum length of 500 nucleotides were subsequently assembled using CANU 1.17 (Koren et al., 2017) using default settings for assembly of raw nanopore reads, and assuming a maximum possible genome size of 50 or 100 kb. MinION assemblies were used to infer the physical structure and terminal repeat sequences of phage genomes through Mauve alignments v2.3.1 (Darling et al., 2004; implemented in Geneious 9.1.8), with initial Illumina assemblies. Terminal repeats in podophage genomes were detected using the Geneious 9.1.8 repeat finder tool as well as through comparison to the previously described podophage PM16 and PM75 (Morozova et al., 2016, 2018). Subsequently, Illumina assemblies were corrected manually to reflect the predicted physical genome structure of phage, and verified by comparison of predicted vs. actual restriction profiles of the phage genomes.

Restriction Digest of Phage Genomes

For restriction digest of phage genomes, phages were propagated on host strains and purified and harvested by filtration (0.22 μm pore size), followed by concentration using VIVASPIN® 15 10,000MWCO PES membranes (Sartorius). Concentrated phage lysate (1 mL) was treated with 10 μg DNAse I (Sigma-Aldrich) and 5 μg RNase A (Sigma-Aldrich) for 30 min at 37°C, prior to extraction of phage DNA using the QIAmp Min Elute Virus Spin kit (QIAGEN). Recovered phage DNA was digested using EcoRI and XbaI individually, according to manufacturer's instructions (Fermentas Fast Digest® enzymes), and restriction fragments separated using agarose gel electrophoresis.

Annotation and Analysis of Phage Genomes

Open reading frames (ORFs) were predicted from Illumina assemblies using Glimmer V3 (implemented in Geneious 9.1.8). The putative functions of the ORFs were predicted using translated ORF amino acid sequences in BlastP searches of the full non-redundant protein sequence database and NCBI CD-Search queries of the Conserved Domain Database (encompassing models from COG, Pfam, SMART, PRK, and TIGRFAM databases). Only BlastP hits with a minimum 20% identity and e-values of $1e^{-5}$, and Conserved Domain hits with e-values on $1e^{-2}$ were used to assigned putative functions to ORFs. Phage encoded ORFs were also used to search the Virulence Factor Database (October 2017) (Chen et al., 2005, 2016), and the MEGARes antibiotic resistance gene database (December 2016) (Lakin et al., 2017). In both cases, only hits generating a minimum of 20% identity and e-values of $1e^{-5}$ or lower were considered valid.

[1]https://github.com/rrwick/Porechop

Analysis of Proteins in Mature Phage Particles

The phage proteins were identified as previously described in Carstens et al. (2016). Briefly, 75 μL of the purified phage solution was mixed with 75 μL of 1% SDS and incubated for 30 min at 80°C followed by Trichloroacetic acid (TCA) precipitation. The proteins were re-solubilized in 8 M urea, 45 mM dithiothreitol (DTT), and 50 mM Tris, pH 8.0, reduced and alkylated. The proteins were trypsin digested and the resulting peptides analyzed using a Dionex 3000 rapid separation liquid chromotography (RSLC) ultra high performance LC (UHPLC) system (Thermo Fisher Scientific, Hvidovre, Denmark) with an Aeris PEPTIDE 1.7 μm XB-C18, 150 mm × 2.1 mm column (Phenomenex, Værløse, Denmark) coupled to a Q Exactive mass spectrometer (Thermo Fisher Scientific, Hvidovre, Denmark). The resulting data were analyzed with Proteome Discoverer software (version 1.4, Thermo Fisher Scientific, Hvidovre, Denmark), using an in house protein database based on the obtained DNA sequences. The search results were filtered using the integrated Target decoy peptide–spectrum matches (PSM) validator algorithm set to a q-value of <0.01, which ensures a peptide-spectrum match false discovery rate less than 0.01.

Analysis of Tetranucleotide Usage Profiles in Phage Genomes

Tetranucleotide usage profiles from phage genomes and bacterial chromosomes were calculated using the method of Teeling et al. (2004), adapted by Ogilvie et al. (2012, 2013). Sequences were extended by their reverse complement before usage profiles for all possible 256 tetranucleotide combinations were calculated over a 1 nt sliding window. The resulting counts for each tetranucleotide were converted to *Z*-scores and used for further analyses with the R packages Vegan and BioDist. For analysis of similarity (ANOSIM), *Z*-scores were utilized without further processing, whereas for non-metric multidimensional scaling (nMDS) *Z*-scores from each sequence were first used to construct Euclidian distance matrices using Vegan. The resulting matices were then used for nMDS ordination with 1000 random starts. Cladograms were constructed from Pearson dissimilarity matrices of *Z*-scores (generated using the BioDist package), using the neighbor-joining algorithm in Vegan (with 500 bootstrap replicates). The resulting cladograms were further analyzed to derive the majority consensus tree, and annotated using Dendroscope v3.5.7.

Representation of Phage-Encoded Sequences in Metagenomic Datasets

Ecogenomic analysis of sequences with similarity to ORFs encoded by *P. mirabilis* phage in metagenomic datasets was performed as previously described (Ogilvie et al., 2012, 2013). Datasets searched represent a range of different habitats within or on the human body, as well as range of habitats from marine and terrestrial environments. The details of metagenomic datasets searched can be found in **Supplementary Table S2**. Datasets were searched using tBlastn with amino acid sequences from each predicted phage ORF, and valid hits were considered to

be those generating ≥35% identity over ≥50% of the query sequence and an e-value of $\leq 1e^{-5}$. Valid hits were subsequently used to calculate the relative abundance of each phage-encoded ORF in each dataset (expressed as Hits/Mb of sequence data). The cumulative relative abundance of ORFs encoded by each phage was taken as the sum of all individual ORF relative abundances. Blast searches and calculation of relative abundance were automated using a custom PERL script as described in Ogilvie et al. (2018) (access and support is available on request to authors), which implemented BLAST v2.2.29 with default settings.

Statistical Analysis

All statistical analyses were performed using Prism 6.0c for Mac OS X (GraphPad Software, Inc., United States), or the R packages Vegan and BioDist (for nMDS, ANOSIM, and Cladograms). Significant differences in cumulative relative abundances between metagenomes were assessed using the Kruskal-Wallis test with Dunn's correction for multiple comparisons.

Phage Names and Accession Numbers

All phage sequences were named according to guidelines from the International Committee on Viral Taxonomy (Adriaenssens and Brister, 2017), and have been deposited in GenBank under the following accession numbers: Proteus_phage_vB_PmiP_RS1pmA (also representing RS1pmB and RS3pmA) – MG575418; Proteus_phage_vB_PmiP_RS8pmA – MG575419; Proteus_phage_vB_PmiM_RS51pmB – MG575421.

RESULTS

Phenotypic Characterization of *P. mirabilis* Phage

Phages capable of infecting *P. mirabilis* (designated Proteus_phage_vB_PmiP_RS8pmA, and Proteus_phage_vB_PmiM_RS51pmB) were isolated from sewage using clinical isolates of *P. mirabilis* recovered from urinary tract infections. Phages were initially characterized based on plaque and virion morphology and compared to previously isolated phages (Proteus_phage_vB_PmiP_RS1pmA, RS1pmB, and RS3pmA), which have been shown to reduce *P. mirabilis* crystalline biofilm formation when tested *in vitro* infection models (Nzakizwanayo et al., 2016). For simplicity, we refer to phage by their unique identifiers for the remainder of the manuscript: RS1pmA, RS1pmB, RS3pmA, RS8pmA, and RS51pmB.

Analysis of virion structure by TEM (**Figure 1**) showed that RS8pmA is likely a member of the *Podoviridae* family based on the short length of tails (∼10 nm in length), and similar to the previously isolated podophage RS1pmA, RS1pmB, and RS3pmA (Nzakizwanayo et al., 2016). RS8pmA was also observed to generate plaques with similar morphology to the previously isolated phages, including surrounding halos that are considered indicative of polysaccharide depolymerase (PD) activity (**Figure 1**; Sutherland et al., 2004). In contrast, TEM showed RS51pmB virion morphology aligned with membership of the *Myoviridae* family (**Figure 1**). RS51pmB generated small circular plaques of a consistent diameter, with no evidence of PD activity (**Figure 1**). All phages generated clear plaques with no indication of lysogenic replicaiton apparent.

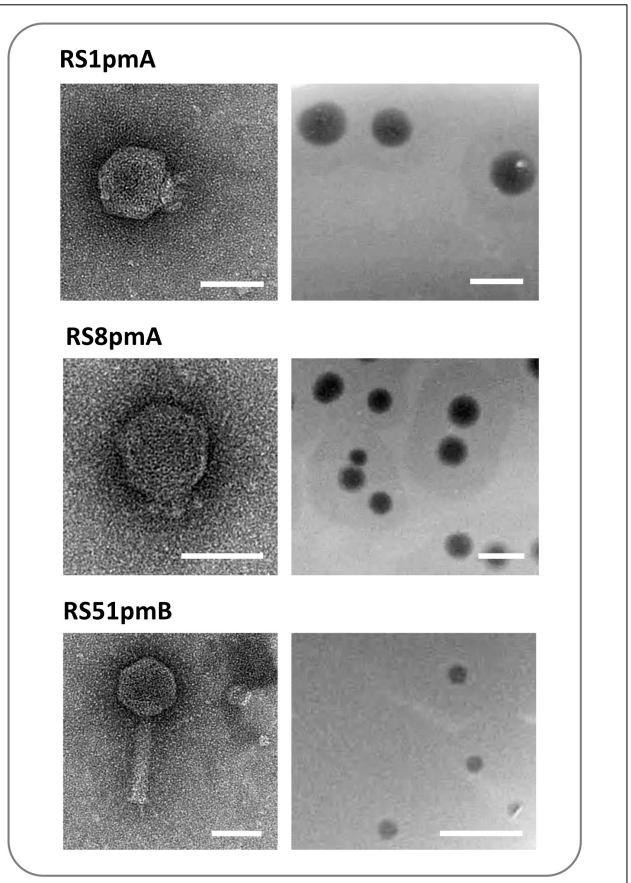

FIGURE 1 | Capsid and plaque morphology of *Proteus mirabilis* phages. Images show transmission electron microscopy (TEM) projections of negatively stained phage (left), and examples of plaques formed by each phage on lawns of host bacteria (right). Phage capsid structures were congruent with membership of the *Podoviridae* family (RS1pmA and RS8pmB), and the *Myoviridae* family (RS51pmB). RS1pmA is used to represent the previously described group of phages RS1pmA, RS1pmB and RS3pmA, which all have analogous capsid morphology (Nzakizwanayo et al., 2016). Scale bars show 50 nm on TEM images and 1 cm on images of plaques. TEM images shown are representative of at least 10 fields of view containing one or more virions.

Analysis of *P. mirabilis* Phage Genomes and Inference of Physical Structure

Phage genomes were initially generated using Illumina sequencing to an average depth of ∼181× coverage. However, the repeat sequences that are often present at the terminal ends of podophage genomes, and other terminally redundant features of phage genomes (arising from particular replication strategies), can lead to mis-assembly of short read data. To account for this we also generated phage genome assemblies from long-read nanopore sequencing methods, which were used in combination

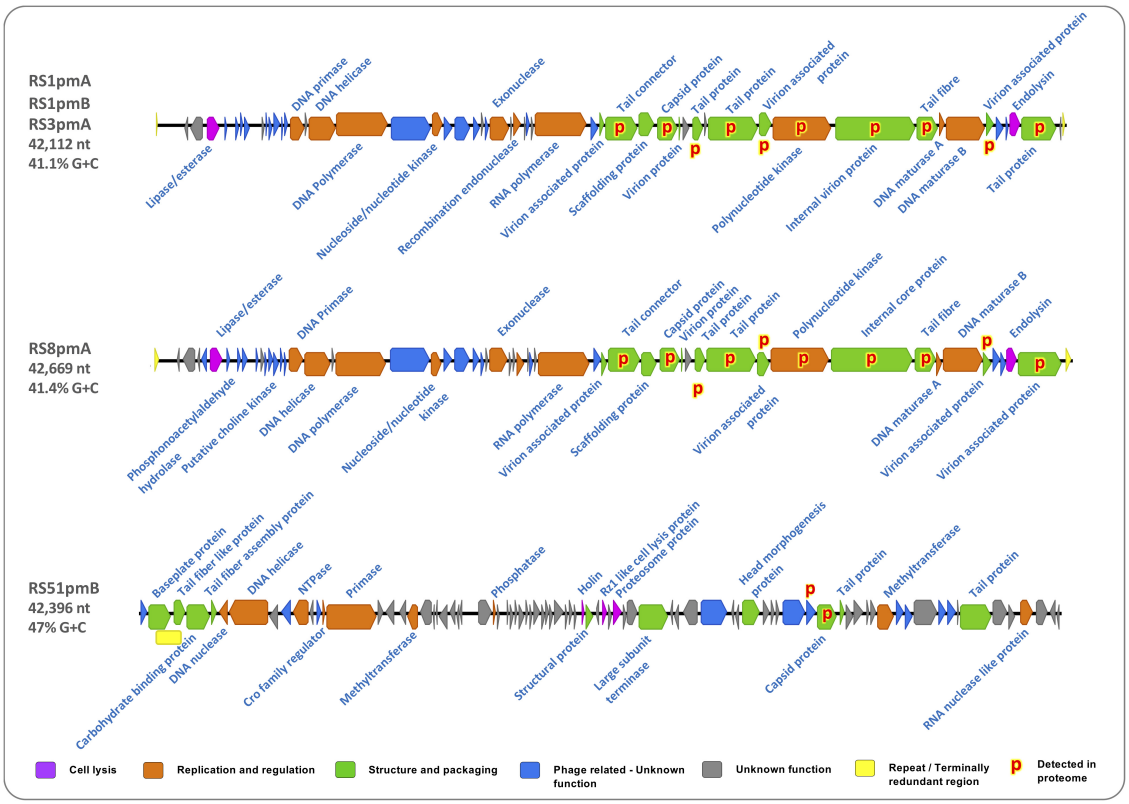

FIGURE 2 | Functional content and characteristics of *P. mirabilis* phage genomes. Maps show the physical gene architecture of *P. mirabilis* phages RS1pmA, RS51pmB, and RS8pmA. Block arrows represent positions of open reading frames (ORFs) with colors indicating affiliation to broad functional groups relevant to phage replication, as denoted by the associated key: Cell Lysis, predicted to encode for activities involved in lysis of host cells; Replication and Regulation, predicted to encode for activities involved in replication of phage genomes and regulation of this process; Structure and Packaging, predicted to encode components of the phage capsid or support packaging of new phage genomes during replication; Unknown Phage related, unknown function but homologous sequences identified in other phage genomes; Unknown, generated no valid hits in BlastP or Conserved Domain searches. Putative functions of each ORF were predicted using BlastP and conserved domains (CD) searches against the nr database (BlastP: minimum 20% identity, $1e^{-5}$ or lower; CD: $1e^{-2}$ or lower).

with restriction digests to infer the correct physical structure of phage genomes, identify terminal repeats, and correct Illumina assemblies (**Figure 2**).

This analysis indicated that the initial Illumina assemblies of phage genomes generated in this study (RS1pmA, RS1pmB, RS3pmA, RS8pmA, and RS51pmB) did not reflect the correct physical structure of phage genomes, most likely due to merging of terminal repeat regions during assembly. Restriction digest of phage genomes confirmed the nanopore-corrected Illumina assemblies provided a more accurate representation of the physical genome structure of these phages (**Supplementary Figures S1**, **S2**). In the case of RS51pmB, MinION data, and restriction digests also indicated this phage genome to be circularly permuted with terminal redundancies, indicative of the headful packaging mechanism observed in other members of the *Myoviridiae* (Schwudke et al., 2008; Casjens and Gilcrease, 2009; Yap and Rossmann, 2014). However, the packaging strategies used by these phages, the exact sequence and positions of repeats or regions of terminal redundancy, and the related molecular details of genome replication will require further detailed studies to confirm and elucidate.

Genome sequences of RS1pmA, RS1pmB, and RS3pmA revealed these to be species of the same phage, differing only by 7 point mutations at several locations in their genome sequences (**Figure 2** and **Supplementary Figure S3**). Five of these point mutations were predicted to lead to amino acid substitutions, and were predominantly associated with genes predicted to encode structural proteins in mature viral particles, including those likely to play a direct role in host attachment such as tail fiber proteins (**Supplementary Figure S2**). Due to the high level of identity between RS1pmA, RS1pmB and RS3pmA, subsequent analyses were conducted using RS1pmA as a representative of this group of phages. RS8pmA also exhibited notable similarities in genome sequence and gene synteny to the RS1 group of phages, in keeping with these phages all exhibiting similar virion morphology and belonging to the *Podoviridiae* family (**Figure 2**, **Supplementary Figure S4**, and **Supplementary Data S1**). In contrast, RS51pmB was found to encode distinct genome organization and gene contents from the other phages analyzed, congruent with differences in the virion morphology of this phage as compared to RS1pmA and RS8pmA (**Figure 2** and **Supplementary Data S1**).

When ORFs in each genome were assigned to broad categories based on putative function (as described in **Figure 2**), similar proportions of genes predicted to be involved in virion structure, aspects of regulation and replication, and host cell lysis, were observed in most phage genomes (**Figure 2**). As with many other phage genomes, a high proportion of ORFs with no identifiable function were also observed in all phage genomes. Although some of the ORFs with unknown function were found to also have homologs in other phage genomes, many showed no similarities to any sequences currently present in the NCBI non-redundant database (**Figure 2**). None of the phage genomes characterized here encoded identifiable genes for virulence factors or antibiotic resistance determinants.

Analysis of Mature Virion Proteomes

To support *in silico* predictions of virion-associated structural genes, the proteome in mature phage particles was also analyzed (**Figure 2** and **Supplementary Table S3**). In RS1pmA and RS8pmA this confirmed predictions of virion-associated genes based on BlastP and Conserved Domain homologies (**Figure 2** and **Supplementary Table S3**). However, for RS51pmB, proteomic analysis failed to detect the predicted products for most capsid-associated ORFs (**Figure 2** and **Supplementary Table S3**). There were also indications that proteins related to genes of unknown function (but with homologs in other phage genomes; RS51pmB), or ORFs predicted to encode polynucleotide kinase (RS1pmB and RS8pmA), are potentially present in mature virions (**Figure 2** and **Supplementary Table S3**). Alternatively, the detection of proteins assigned functions in replication and regulation could conceivably result from protein carry over in phage lysates, and the role, if any, of these proteins in the mature virion will require further investigation to confirm.

Representation of *P. mirabilis* Phage Genes in Other Phage Genomes

To evaluate similarities between the *P. mirabilis* phages isolated here and phage infecting other bacterial host species, we used all ORFs encoded by each *P. mirabilis* phage to search a collection of 715 publicly available phage genomes. This analysis demonstrated that the podophages RS1pmA and RS8pmA exhibit high levels of similarity to other available *Proteus* phage genomes, with 89–90% of ORFs encoded by these phages affiliated predominantly with PM16 (NC_027342), and PM75 (NC_027363) (Morozova et al., 2016, 2018; **Figure 3** and **Supplementary Data S1**). The similarity of RS1pmA and RS8pmA was explored further through pairwise alignments of these phage genomes with complete genomes of PM16 and PM75. This confirmed overall similarity and gene synteny between these phages (as well as providing further support for validity of the MinION-corrected genome structures), but also highlighted distinct variations across the genome sequences (**Supplementary Figure S5**). In contrast, RS51pmB did not exhibit any notable similarity to other *Proteus* phage genomes, and the majority of RS51pmB ORFs were not affiliated with any phage genomes searched using this approach (72.3%). The RS51pmB ORFs that could be affiliated with other phage genomes were associated with phage infecting a diverse array of Proteobacterial hosts, predominantly Gamma-proteobacteria, including *Salmonella, Klebsiella, Escherichia*, *Vibrio*, *Aggregatibacter* and *Actinobacillus* spp. (**Figure 3** and **Supplementary Data S1**).

Evaluation of Broader Evolutionary Host-Phage Relationships

To gain further insight into the potential broader evolutionary relationships of the *P. mirabilis* phages isolated in this study, we used alignment-free correlations of tetranucleotide usage patterns to discern potential associations between *Proteus* phage genomes characterized within the present study, and bacterial chromosomes from a range of species. This approach exploits similarities in global nucleotide usage patterns that develop between phage genomes and the chromosomes of long-term bacterial hosts (Pride et al., 2006; Ogilvie et al., 2012, 2013). The underlying hypothesis is that in phage which have recently become capable of infecting and replicating in a new host species, nucleotide usage profiles adapt more slowly and initially still reflect previous long-term hosts (Ogilvie et al., 2013, 2018).

Initial relationships were explored between the phages characterized in this study, other available *P. mirabilis* phages, and a collection of Gammaproteobacteria genomes representing genera to which other common urinary tract pathogens belong (Stickler, 2014). Initially, unsupervised ordination of phage and bacterial genomes by nMDS coupled with ANOSIM, was used to visualize potential relationships between *Proteus* phages and bacteria from different families (**Figures 4A,B**). This analysis indicated no detectable relationship between *Proteus* phages and members of the *Enterobacteriacea*, *Pseudomonadaceae*, and *Yersiniaceae* represented (**Figures 4A,B**). As expected, the *Morganellaceae* group, to which *Proteus* sp. belong, showed the closest association with *Proteus* phages (**Figures 4A,B**).

To explore these potential relationships in more detail, phage sequences and bacterial genomes were used to construct cladograms based on tetranucleotide profiles (**Figure 4C**). While this supported the nMDS and ANOSIM analyses and showed a general association of *Proteus* phages with bacterial genomes from species belonging to the *Morganellaceae*, this also revealed distinct differences between RS51pmB and other phages. RS51pmB did not cluster with other *Proteus* phages and was less closely associated with *P. mirabilis* genomes (**Figure 4C**). This separation was also observed directly in tetranuclotide usage profiles of RS1pmA and RS51pmB, when these were correlated with other *Proteus* phages and used to construct scatterplots (**Figure 4C** inset). To further test this observation, we also used Blast searches to affiliate each ORF encoded by RS51pmB with all bacterial genomes belonging to genera clustering with these phages in cladograms (*Proteus, Morganella, Providencia,* and *Serratia*) (**Figure 4D**). This also supported an association of RS51pmB with non-*Proteus* species, with the majority of assignable ORFs being affiliated to *Morganella* and *Providencia* sp. (**Figure 4D**).

Collectively, these analyses indicated the potential for RS51pmB to have a previous or ongoing evolutionary

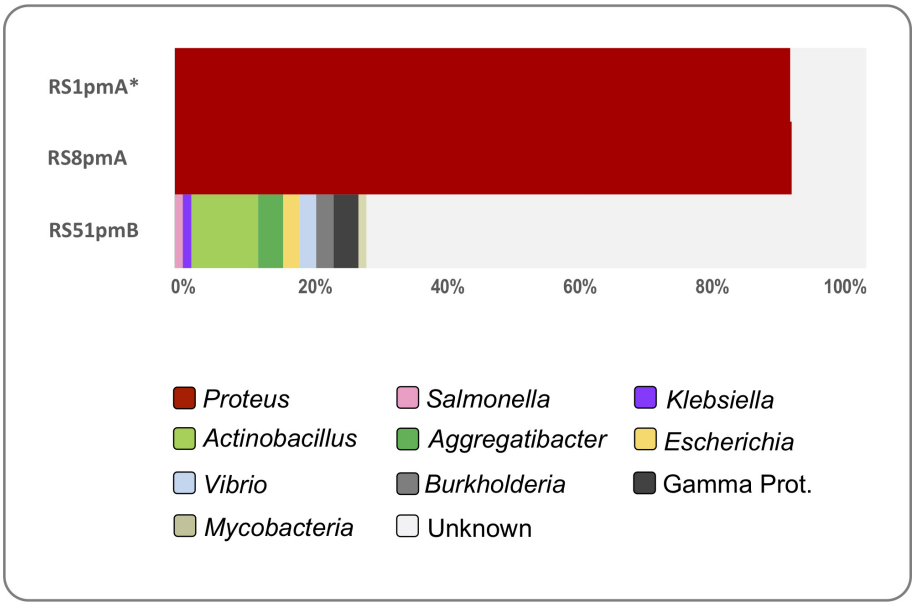

FIGURE 3 | Representation of *P. mirabilis* phage-encoded ORFs in other phage genomes. The representation of *P. mirabilis* ORF homologs in other phage genomes was explored using tBLASTn searches of 715 complete phage genomes. The proportion of ORFs affiliated to other phage genomes is based on top hit by bit score (min 35% identity, over ≥25 amino acids, $1e^{-5}$ or lower). Hits were categorized by genus of host bacterial species for phage genomes generating each hit. Legends associated with charts describe bacterial genera represented. The "Gamma Proteobacteria" group included *Hamiltonia* sp., *Listonella* sp., and *Pseudoalteromonas* sp., which were each represented by less than two hits across all phage genomes. RS51pmB also only generated a single hit to phage infecting *Mycobacterial* sp. ORFs generating no valid hits in tBlastn searches are designated as "Unknown." *RS1pmA is used to represent the previously described group of phages RS1pmA, RS1pmB, and RS3pmA (Nzakizwanayo et al., 2016), which were found to differ only by point mutations (see **Supplementary Figure S3**).

relationship with non-*Proteus* host species from these bacterial Genera. To explore this further, we tested the potential for RS1pmA, RS8pmA, and RS51pmB to replicate in potential alternate hosts represented in relevant clusters of the cladogram. Although it was not possible to use an exhaustive panel of species and strains, these experiments did demonstrate RS51pmB to be capable of infecting *Morganella morganii* (albeit inefficiently compared to *P. mirabilis*), supporting the inference of a relationship with non-*Proteus* hosts based on tetranucleotide usage profiles (**Figure 4E**). However, it should be noted that more extensive host-range assays will be required to determine how robust these relationships are, and fully understand the host range of these phages.

Ecogenomic Profiling of *P. mirabilis* Phage

To gain further insight into the broader ecological associations of these *P. mirabilis* phages, we also investigated the relative representation of sequences similar to *P. mirabilis* phage encoded ORFs in other bacterial ecosystems (**Figure 5**). No phage analyzed exhibited notable representation in metagenomes derived from human urinary tract viromes or environmental datasets, but associations with other human-derived habitats were observed (**Figure 5A**). As with the other analyses conducted here, RS1pmA and RS8pmA exhibited similar profiles, which were markedly different to those obtained for RS51pmB (**Figures 5A,B**). ORFs with similarity to those encoded by RS1pmA and RS8pmA were only poorly represented in the metagenomic datasets examined, with no statistically significant representation in any habitat, but with most homologs identified in datasets from the human oral cavity (**Figure 5B**).

In comparison, sequences similar to RS51pmB encoded ORFs showed significantly greater representation in metagenomic datasets than RS1pmA and RS8pmA, and a particular association with human-associated microbial or viral communities from the oral cavity, gastrointestinal tract and other body sites (**Figure 5**). In the case of RS51pmB, a wider range of ORFs was found to be generally well represented in the metagenomic datasets examined, with greatest representation in human oral microbiomes (ORFs 44 and 51), human gut microbiomes and viromes (ORFs 18, 44, 51, and 70), and human body associated datasets (ORF 51). These ORFs were predicted to encode a large terminase subunit (ORF 51); methyltransferases (ORFs 18 and 70) and a structural protein (ORF 44) (**Figure 5B** and **Supplementary Data S1**).

DISCUSSION

The potential for phages to control CAUTI, and in particular biofilm formation on urinary catheters, has previously been demonstrated using various models of infection (Curtin and Donlan, 2006; Carson et al., 2010; Fu et al., 2010; Lehman and Donlan, 2015; Melo et al., 2016; Nzakizwanayo et al., 2016). Phages offer a number of advantages over conventional

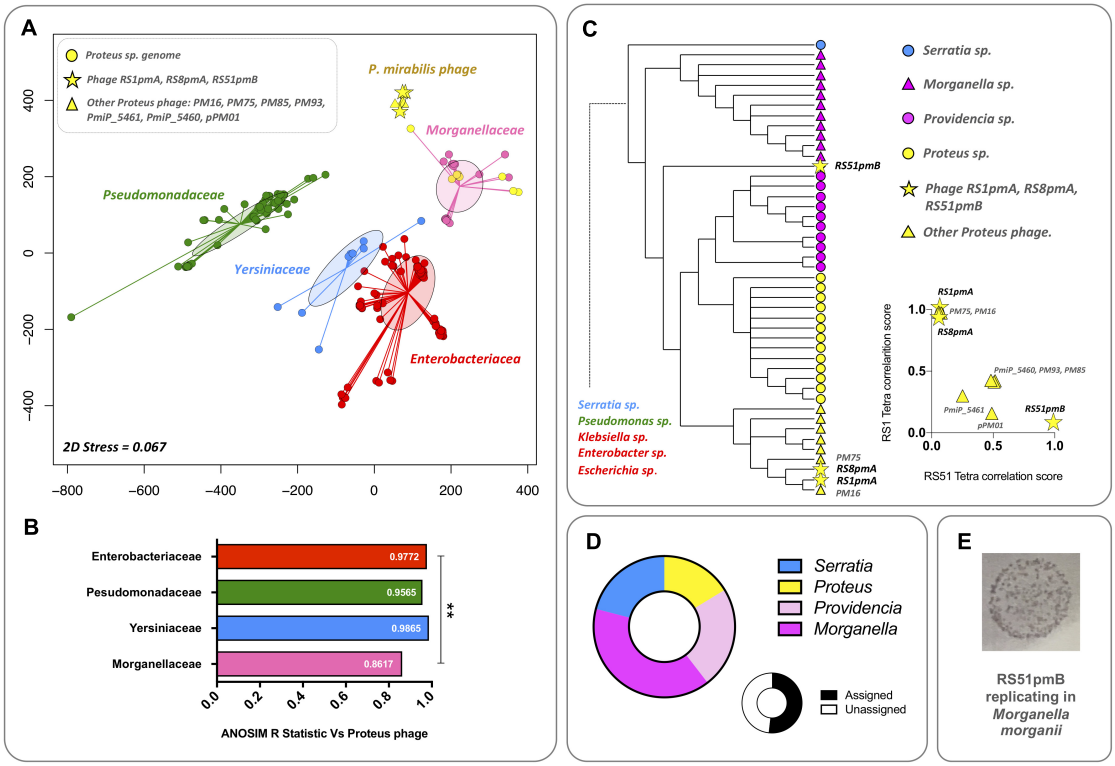

FIGURE 4 | Evaluation of broader evolutionary relationships and host affiliations. The potential for broader evolutionary relationships between *P. mirabilis* phages and other bacterial hosts were explored by comparing *P. mirabilis* phages with bacterial genomes belonging to genera containing the most common Gram-negative pathogens of the catheterized urinary tract (*Proteus, Providencia, Morganella, Pseudomonas, Escherichia, Klebsiella, Enterobacteria,* and *Serratia*) (Stickler, 2014). **(A)** Unsupervised ordination using nMDS was initially used to visualize relationships between all sequences based on tetranucleotide usage profiles (Ogilvie et al., 2012, 2013). Bacterial genomes were classified by family. For nMDS, points show position of individual genomes in the final ordination, with connecting lines indicating relationship to the group centroid. Filled ellipses show standard deviation of group dispersion relative to the group centroid. Ordination were based on an Euclidean distance matrix of tetranucleotide usage profiles from each sequence. nMDS analysis was conducted with 1000 random starts using the R package Vegan. **(B)** ANOSIM between groups of sequences represented in the nMDS ordination. Charts show the ANOSIM R Statistic for each group of bacterial genomes vs. the *P. mirabilis* phage group, where an increasing strength of separation between groups is indicated as the R Statistic approaches 1. **Denotes statistical significance of R Statistics between groups, $P \leq 0.001$ (calculated as part of the ANOSIM in the R Package Vegan). **(C)** Cladogram based on tetranucleotide usage profiles showing relationship between *P. mirabilis* phage sequences and genomes from *Morganellaceae* and *Yersiniaceae* groups represented in nMDS ordinations. The cladograms were constructed from a Pearson dissimilarity matrix of tetranucleotide profiles from all sequences used in nMDS analyses as majority consensus trees from 500 bootstrap replicates (as calculated by the R package BioDist). The cladogram presented shows a sub-region of the larger tree populated by *P. mirabilis* phages and the most closely related bacterial genomes by this analysis. *Chart Inset:* shows differences between *P. mirabilis* phage sequences, based on scatter plots of phage RS1pmA and RS51pmB tetranucleotide correlation scores with other phage sequences. **(D)** To further test relationships in phage RS51pmB indicated by tetranucleotide analyses, ORFs from this phage were searched against all sequences from genus level taxonomic groups represented in cladograms (*Proteus, Providencia, Morganella,* and *Serratia*) using BlastP, and hits used to assign a taxonomic affiliation. Only hits with a maximum e-value of $1e^{-3}$ were considered valid. Charts show the proportion of assignable ORFs affiliated to each genus, and the proportion of assigned and unassigned ORFs. **(E)** To test if the relationships with non-*Proteus* species indicated in tetranucleotide and Blast analyses were relevant to the host range of this phage, the ability of RS51pmB to replicate in species other than *P. mirabilis* was tested (**Supplementary Table S1**). The image presented demonstrates the ability of phage RS51pmB to use *M. morganii* as an alternate host species (**Supplementary Table S1**). Host range assays were performed in triplicate at phage titres ranging from ~10 to 10^7 PFU, with the image shown representative of *M. morganii* lawns exposed to 10^7 PFU of RS51pmB.

antimicrobials for the control of biofilm-associated infections, including mechanisms evolved to penetrate biofilms and access bacterial hosts normally protected by the matrix of extracellular polymeric substances (Sutherland et al., 2004; Lu and Collins, 2007). Phages are also not generally affected by a host species susceptibility to conventional antimicrobial agents, and may therefore also contribute to efforts to control antimicrobial resistance and address this global challenge.

This makes phages potentially well suited for controlling infections where biofilm formation is an important feature, and situations in which conventional antimicrobial agents often perform poorly (Sutherland et al., 2004; Lu and Collins, 2007; Stickler, 2014; Melo et al., 2016; Nzakizwanayo et al., 2016). There is also the potential to use phage in synergy with conventional antibiotic treatments, which may have considerable benefits in terms of enhanceing treatment efficacy, as well as curtailing the emergence of antibiotic resistant strains. It is also worth noting that phages isolated in this and our previous study were all recovered from sewage samples, using clinical isolates of *P. mirabilis* as the host species (Nzakizwanayo et al., 2016).

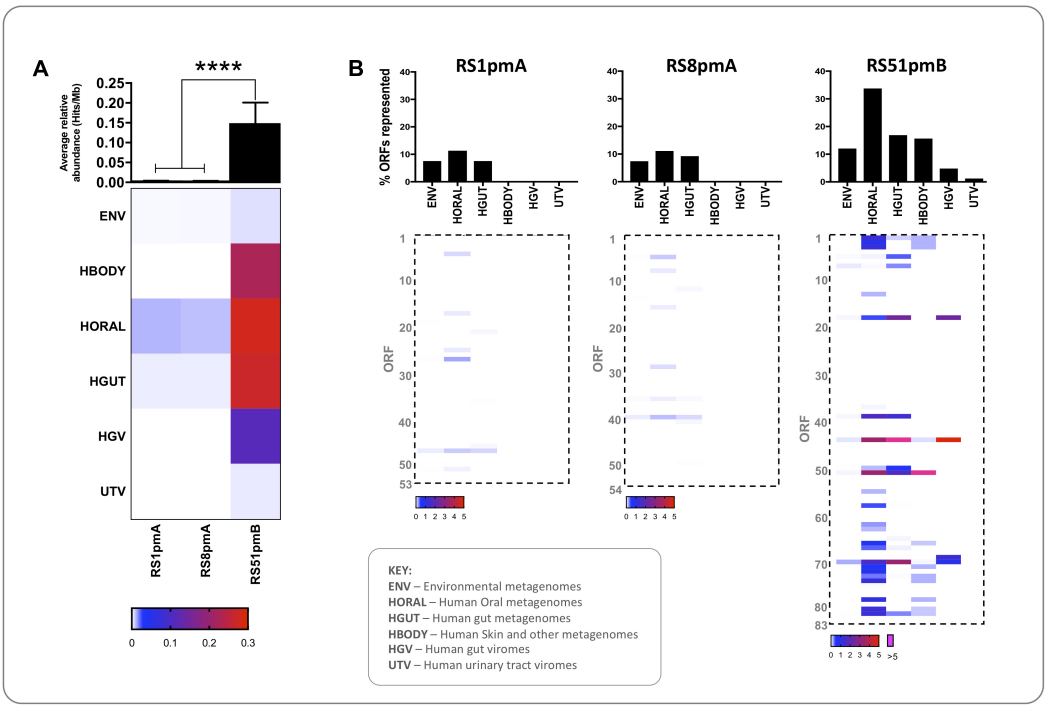

FIGURE 5 | Ecogenomic profiling of *P. mirabilis* phage encoded functions. The representation of functions encoded by *P. mirabilis* phages in a range of microbial habitats was investigated by calculating the relative abundance of similar sequences in 809 metagenomic data sets. Valid hits from tBlastn searches with *P. mirabilis* phage sequences (≥35% identity, ≥50% query coverage, ≤$1e^{-5}$) were used to calculate the average relative abundance of ORF homologs in each dataset (expressed as Hits/Mb). **(A)** The heatmap shows average relative abundance of ORFs from each phage in metagenomes or viromes from various habitats. Rows represent datasets grouped by habitat, and columns represent individual phage. The intensity of shading in cells indicate cumulative relative abundance of ORFs from a given phage in metagenomes from the corresponding habitat (according to the scale shown). The associated histogram shows average relative abundance of phage ORFs across all datasets. **(B)** Heatmaps show cumulative relative abundance of individual ORFs from each phage (Rows) in metagenomes from various habitats (Columns), and shading of cells indicates relative abundance according to the associated scale. Associated histograms show the proportion of ORFs in each phage with homologs detected in various habitats represented by metagenomes surveyed. ****$P < 0.0001$ (Kruskal-Wallis test with Dunn's correction), error bars show standard error of the mean. RS1pmA is used to represent the previously described group of phage RS1pmA, RS1pmB, and RS3pmA (Nzakizwanayo et al., 2016). ENV, whole community metagenomes with non-host associated environmental origin (n = 16); HGUT, HORAL, and HBODY, whole community metagenomes from the human gut microbiome, the human oral cavity, or various human body sites (primarily external) (n = 285, 295, and 181, respectively). HGV, viral metagenomes from the human gut (n = 12). UTV, viral metagenomes from the human urinary tract (n = 20). Details of datasets used can be found in **Supplementary Table S2**.

This further highlights that phages with potential therapeutic value can be easily recovered from such sources, and it is likely that sewage and a wastewater harbor diverse phage populations useful for a range of applications.

The majority of phages characterized in this study produced plaques with halos, as described previously for phages shown to be effective in controlling *P. mirabilis* crystalline biofilm formation (Nzakizwanayo et al., 2016). The most common explanation for plaques with halos is the presence of PD activity in phages. The expression of PD enzymes is believed to facilitate phage infection of host cells through degradation of exterior capsules, or by providing access to biofilm associated cells through the disruption of the encasing exopolymeric matrix (Sutherland et al., 2004; Lu and Collins, 2007). This feature appeared to be most apparent among the members of the *Podoviridae* family characterized in this study (RS1pmA, RS1pmB, RS3pmA, and RS8pmA), and these observations were congruent with characteristics of *P. mirabilis* phages PM16 and PM75 to which podophage examined in this study showed notable similarity in terms of gene content (Morozova et al., 2016, 2018). The potential importance of PD activity in the control of biofilm formation has perhaps been most clearly demonstrated by Lu and Collins, via the engineering of phage T7 (Lu and Collins, 2007). In this study, T7 phages augmented to express PD activity were significantly enhanced in their ability to disperse established biofilms as compared to wild-type counterparts (Lu and Collins, 2007).

However, no ORFs encoded by phages characterized in this study were identified as encoding potential PD activity (based on BlastP and Conserved Domain analyses); but it is possible that these phages encode novel PD enzymes not currently well represented in sequence databases. Alternatively, halos generated by these phages may be the result of other processes, such as lysis inhibition, where superinfection of cells leads to delays in cell lysis and a zone of partially lysed cells around plaques that can also manifest as a translucent halo (Hershey, 1946). Nevertheless,

the putative PD activity of these phages, and confirmation of the presence or absence of this activity, is likely to be important in further studies of their potential to disrupt *P. mirabilis* biofilms. PD activity may also have more direct pharmaceutical potential in its own right, in terms of developing novel anti-biofilm agents.

Other features of these phage genomes may also hold similar pharmaceutical potential in the context of developing novel antimicrobial agents, such as ORFs predicted to be involved in host cell lysis (Endersen et al., 2015; Czaplewski et al., 2016). Of particular interest are the putative endolysins encoded by RS1pmA and RS8pmA, which are involved in degradation of the host cell wall to facilitate phage release during the final stages of lytic replication. Although these enzymes have been found to be highly effective against Gram-positive bacteria when applied as exogenous preparations, the use of endolysins to control Gram-negative bacteria has been hampered by the presence of the outer lipopolysaccharide (LPS) membrane in these species, which prevents access to the peptidoglycan layer and blocks the anti-microbial action of these enzymes (Zimmer et al., 2002; Donovan et al., 2006; Doehn et al., 2013; Briers et al., 2014; Briers and Lavigne, 2015; Oliveira et al., 2016). The identification and characterization of putative endolysins from phages infecting Gram-negative bacteria may provide important insights and biological raw materials to address this challenge. There is already precedence for the identification of exogenously active Gram-negative endolysins from phages infecting *Acinetobacter baumanii*, and their potential use as alternatives to antibiotics (Lai et al., 2011; Lood et al., 2015; Oliveira et al., 2016), as well as for the engineering of these enzymes to improve spectrum of activity (Briers et al., 2014; Yang et al., 2014; Briers and Lavigne, 2015).

The genetic analysis of phages characterized here also provided further insight into their performance in previous evaluations of phage-mediated control of catheter blockage (Nzakizwanayo et al., 2016), and their suitability with regard to further development of phage therapy applications. We previously demonstrated that a cocktail of RS1pmA, RS1pmB, and RS3pmA could provide a significant increase in time taken for catheters to block during simulations of established CAUTI (Nzakizwanayo et al., 2016). When applied to models simulating early colonization of the catheterized urinary tract, these phages were able to eradicate infection and completely prevent catheter blockage, whereas under conditions simulating established infection they were only able to delay blockage (Nzakizwanayo et al., 2016).

Characterization of the corresponding phage genomes in this study now demonstrates these phages vary only by point mutations in their genomes. This supports the hypothesis that the eventual therapeutic failure during simulations of established infection may have been due to development of resistance (Nzakizwanayo et al., 2016), made possible by a lack of diversity in the cocktail used. This further highlights the utility of phage genome characterization in developing cocktails containing diverse and distinct phage types, to offset development of resistance in phage therapy applications. It should also be noted that the activity of phages we characterized here have been evaluated against only a small number of *P. mirabilis* isolates to date. Recent serotyping studies indicated a high diversity among UTI isolates with no predominant serotype (Kaca et al., 2011). Analysis of phage activity against a broader panel of well-defined *P. mirabilis* strains will also be important to the development of phage therapies, and *P. mirabilis* strain diversity may present additional challenges in this regard.

The characterization of phage genome sequences conducted here also highlighted how more expansive characterization can illuminate important facets of phage-host relations, and broader ecological affiliations that may be relevant to development of diverse, and effective combinations for phage therapy. Comparison of ORFs encoded by these phages, with ORFs in other phage genomes, showed most phages (RS1pmA, RS1pmB, RS3pmA, and RS8pmA) had a strong association with other available *P. mirabilis* phage genomes. This further highlighted the potential novelty of RS51pmB, in which most ORFS were not similar to those in any other phage genomes evaluated, and a clear divergence from other *P. mirabilis* phages was evident.

To further illuminate broader phage-host relationships relevant to the development of phage therapies, tetranucleotide usage profiling was employed, which highlighted the potential for extending host range to other problematic species involved in CAUTI. The hypothesis underlying the tetranucleotide approach is that co-evolution of host and phage leads to the development of tetranucleotide usage profiles in phage genomes that are similar to those found in the chromosomes of long-term bacterial hosts (Pride et al., 2006; Ogilvie et al., 2012, 2013). As such, phages that have more recently adapted to infect a particular host should theoretically exhibit less conformity in this genome-signature, and may exhibit tetranucleotide usage profiles more aligned to previous or alternative host species, providing insight into host-phage evolutionary relationships (Pride et al., 2006; Ogilvie et al., 2012, 2013).

This analysis revealed that RS51pmB was much less closely related to *P. mirabilis* than the other phages analyzed, and instead was most closely associated with a range of other members of the *Morganellaceae* family. The genome signature-based prediction was subsequently supported by host range assays which demonstrated the capacity for RS51pmB to infect and replicate within *M. morganii,* albeit relatively inefficiently compared with replication in *P. mirabilis* and only when used at high titres. Taken together, these data indicated that, in evolutionary terms, RS51pmB may have relatively recently adapted to infect and replicate within *P. mirabilis*, and the tetranucleotide genome signature of this phage has not yet acclimated to the *P. mirabilis* host.

Although a potential transition of this phage from *P. mirabilis* to *M. morganii* cannot be fully excluded, the clustering of RS51pmB with *M. morganii* based on the tetranucleotide genome signature, and the apparent ability to more readily replicate in *P. mirabilis*, is more compatible with a transition from *Morganella* to *Proteus*. This also raises the possibility of utilizing such phage as the basis to more directly develop derivatives with an extended spectrum of activity, for example using passage-based methods such as the Appelmans technique (Appelmans, 1921) and a wider range of *M. morganii* clinical isolates. This approach has already been utilized in the host range

extension of *P. mirabilis* phages for development of broad-spectrum cocktails (Lehman and Donlan, 2015). Nevertheless, it should also be noted that while tetranucleotide profiling has provided evidence that RS51pmB has a past relationship with *M. morganii*, the host-range assays undertaken in this study remain limited in scope overall. More expansive studies with a greater range of bacterial strains should now be undertaken to further evaluate the host-phage associations we observe based on genome-signatures, and test the robustness of the inferred evolutionary relationships. In particular, it will be important to understand how consistent and reliable such inferences are across different phage-host groups, datasets, and taxonomic scales.

Characterization of phage diversity, and the ecological success of different phages or phage encoded genes through ecogenomic profiling, also has the potential to provide insights into phages that are useful in biotechnological applications (Ogilvie et al., 2012, 2013, 2018). This information may help guide the selection of phages for inclusion in cocktails, or those with properties useful in other biotechnological applications, by facilitating identification of ecologically diverse phages and those that have particular associations with given habitats (Ogilvie et al., 2012, 2013, 2018). Notably, in the ecogenomic analyses conducted here, there was a lack of affiliation of any phage characterized with the human urinary viromes analyzed, despite the dominance of phage associated sequences in these datasets, and the diagnosis of UTI in 50% of the individuals from which they were derived (Santiago-Rodriguez et al., 2015). While this may initially seem contradictory, it is unlikely that *P. mirabilis* would constitute a member of the normal human urinary microbiome, and none of the culture-positive samples from which viromes were derived were found to contain *P. mirabilis* (Santiago-Rodriguez et al., 2015).

Conversely, ecogenomic profiling reinforced the novelty of RS51pmB observed in comparisons with other phage genomes, but also provided a greater understanding of the broader ecological associations of these phages. A distinct affiliation with the human alimentary microbiome (oral and gut) was observed for RS51pmB, and to a lesser extent RS1pmA and RS8pmA, in keeping with *P. mirabilis* being a common member of the human gut microbiome and the isolation of these phages from sewage. The human gut-associated ecogenomic profiles of RS51pmB may also highlight the possible value of this phage in other biotechnological applications, such as in the development of virome-based microbial source tracking tools for monitoring water quality (Adriaenssens and Brister, 2017; Ogilvie et al., 2018). The gene-by-gene nature of this analysis may also be relevant to bioprospecting studies seeking to exploit specific attributes or functions encoded by phages, where representation or activity within a particular habit may be desirable. In this context, the recovery of these phage from sewage reinforces the potential for wastewater treatment facilities to also provide access to a wealth of biological raw materials encoded by phages. However, it should also be noted that ecogenomic studies are currently restricted by the available metagenomic datasets, which represent only a relatively small sample size for many habitats, and leave many microbial ecosystems unrepresented (Ogilvie et al., 2012, 2013, 2018). Further research will be required to fully understand how phage ecological profiles may best be used to inform the development of phage therapy or exploit phage for other applications.

Overall, the genetic characterization of phages considered in this study, including evaluation of wider host-phage, ecological, and evolutionary relationships, highlight the potential for these broader genomic and ecogenomic assessments to assist in identifying phage with the most potential for pharmaceutical or biotechnological exploitation, or suitability for use in phage therapy. It is also clear that a range of easily accessible "waste" materials, such as sewage and wastewater, constitute useful sources of novel and biotechnologically relevant phages. Given the current rise in antimicrobial resistance and urgent need to address this global challenge, it seems likely that alternatives or supplements to conventional small molecule antimicrobials will become an important feature of strategies to address this problem (Zimmer et al., 2002). Phages are well suited to form an important part of this solution, particularly with regard to biofilm-associated infections, and approaches to help identify the most promising phages for pharmaceutical or biotechnological exploitation will be vital to the realization of more effective phage-based products.

Currently, the selection of phages to be used for the development of therapeutic applications is understandably driven by phenotypic characterization and activity against target pathogens, with genetic characterization often a secondary activity primarily used to screen for undesirable genes such as toxins. However, the generation of phage genome sequences is now accessible and affordable, and the increasing range of tools available for analyzing these data mean this aspect of phage characterization should now be viewed as a primary process in the selection of candidate phage for the development of therapeutic products, or other biotechnological applications. Although next generation sequencing technologies generating short reads (such as Illumina platform sequencing) can pose challenges in the correct assembly of some phage genomes, such approaches can still provide useful information regarding phage gene content and broader evolutionary relationships. However, technologies such as single molecule nanopore sequencing can potentially generate genome length reads, and we demonstrate here some of their potential to address many of the current limitations of next generation sequencing for phage genome analysis, related to read length. Furthermore, platforms such as the Oxford Nanopore MinION require no specialist genomics facilities or support to operate, offering the possibility for genome characterization of newly isolated phages to become a much more routine aspect of phage characterization.

DATA AVAILABILITY

The datasets generated for this study can be found in the GenBank under the accession numbers MG575418, MG575419, and MG575421.

AUTHOR CONTRIBUTIONS

BJ and DA conceived the study. All authors designed and conducted the experiments, analyzed the data, and edited the manuscript. BJ, LO, and JN wrote the manuscript.

FUNDING

This work was supported by funding from the Queen Victoria Hospital NHS Foundation Trust and the Queen Victoria Hospital Charitable Fund. JN was supported by funding from the Dunhill Medical Trust (R394/1114), the Medical Research Council (MR/N006496/1), and the Wellcome Trust (206854/Z/17/Z). The funders had no role in study design, data collection and analysis, decision to publish, or preparation of the manuscript.

SUPPLEMENTARY MATERIAL

The Supplementary Material for this article can be found online at: https://www.frontiersin.org/articles/10.3389/fmicb.2019.01783/full#supplementary-material

REFERENCES

Adriaenssens, E. M., and Brister, J. R. (2017). How to name and classify your phage: an informal guide. *Viruses* 9:E70. doi: 10.3390/v9040070

Appelmans, R. (1921). Le dosage du bactériophage. *Compt. Rend. Soc. Biol.* 85:1098.

Briers, Y., and Lavigne, R. (2015). Breaking barriers: expansion of the use of endolysins as novel antibacterials against gram-negative bacteria. *Future Microbiol.* 10, 377–390. doi: 10.2217/fmb.15.8

Briers, Y., Walmagh, M., Van Puyenbroeck, V., Cornelissen, A., Cenens, W., Aertsen, A., et al. (2014). Engineered endolysin-based "Artilysins" to combat multidrug-resistant gram-negative pathogens. *mBio* 5:e1379-14. doi: 10.1128/mBio.01379-14

Carson, L., Gorman, S. P., and Gilmore, B. F. (2010). The use of lytic bacteriophages in the prevention and eradication of biofilms of *Proteus mirabilis* and *Escherichia coli*. *FEMS Immunol. Med. Microbiol.* 59, 447–455. doi: 10.1111/j.1574-695X.2010.00696.x

Carstens, A. B., Kot, W., Lametsch, R., Neve, H., and Hansen, L. H. (2016). Characterisation of a novel enterobacteria phage, CAjan, isolated from rat faeces. *Arch. Virol.* 161, 2219–2226. doi: 10.1007/s00705-016-2901-0

Casjens, S. R., and Gilcrease, E. B. (2009). Determining DNA packaging strategy by analysis of the termini of the chromosomes in tailed-bacteriophage virions. *Methods Mol. Biol.* 502, 91–111. doi: 10.1007/978-1-60327-565-1_7

Chen, L. H., Yang, J., Yu, J., Yao, Z. J., Sun, L. L., Shen, Y., et al. (2005). VFDB: a reference database for bacterial virulence factors. *Nucleic Acids Res.* 33, D325–D328. doi: 10.1093/nar/gki008

Chen, L. H., Zheng, D. D., Liu, B., Yang, J., and Jin, Q. (2016). VFDB 2016: hierarchical and refined dataset for big data analysis - 10 years on. *Nucleic Acids Res.* 44, D694–D697. doi: 10.1093/nar/gkv1239

Cox, A. J., and Hukins, D. W. L. (1989). Morphology of mineral-deposits on encrusted urinary catheters investigated by scanning electron-microscopy. *J. Urol.* 142, 1347–1350. doi: 10.1016/s0022-5347(17)39095-x

Curtin, J. J., and Donlan, R. M. (2006). Using bacteriophages to reduce formation of catheter-associated biofilms by *Staphylococcus epidermidis*. *Antimicrob. Agents Chemother.* 50, 1268–1275. doi: 10.1128/AAC.50.4.1268-1275.2006

Czaplewski, L., Bax, R., Clokie, M., Dawson, M., Fairhead, H., Fischetti, V. A., et al. (2016). Alternatives to antibiotics—a pipeline portfolio review. *Lancet Infect. Dis.* 16, 239–251. doi: 10.1016/S1473-3099(15)00466-1

Darling, A. C., Mau, B., Blattner, F. R., and Perna, N. T. (2004). Mauve: multiple alignment of conserved genomic sequence with rearrangements. *Genome Res.* 14, 1394–1403. doi: 10.1101/gr.2289704

Doehn, J. M., Fischer, K., Reppe, K., Gutbier, B., Tschernig, T., Hocke, A. C., et al. (2013). Delivery of the endolysin Cpl-1 by inhalation rescues mice with fatal pneumococcal pneumonia. *J. Antimicrob. Chemother.* 68, 2111–2117. doi: 10.1093/jac/dkt131

Donovan, D. M., Lardeo, M., and Foster-Frey, J. (2006). Lysis of staphylococcal mastitis pathogens by bacteriophage w11 endolysin. *FEMS Microbiol. Lett.* 265, 133–139. doi: 10.1111/j.1574-6968.2006.00483.x

Endersen, L., Guinane, C. M., Johnston, C., Neve, H., Coffey, A., Ross, R. P., et al. (2015). Genome analysis of *Cronobacter* phage vB_CsaP_Ss1 reveals an endolysin with potential for biocontrol of gram-negative bacterial pathogens. *J. Gen. Virol.* 96, 463–477. doi: 10.1099/vir.0.068494-0

Fu, W., Forster, T., Mayer, O., Curtin, J. J., Lehman, S. M., and Donlan, R. M. (2010). Bacteriophage cocktail for the prevention of biofilm formation by *Pseudomonas aeruginosa* on catheters in an in vitro model system. *Antimicrob. Agents Chemother.* 54, 397–404. doi: 10.1128/AAC.00669-09

Griffith, D. P., Musher, D. M., and Itin, C. (1976). Urease, the primary cause of infection-induced urinary stones. *Invest. Urol.* 13, 346–350. doi: 10.1016/s0022-5347(17)53779-9

Hedelin, H., Eddeland, A., Larsson, L., Pettersson, S., and Ohman, S. (1984). The composition of catheter encrustations, including the effects of allopurinol treatment. *Br. J. Urol.* 56, 250–254. doi: 10.1111/j.1464-410x.1984.tb05382.x

Hershey, A. (1946). Mutation of bacteriophage with respect to type of plaques. *Genetics* 31, 620–640.

Holling, N., Dedi, C., Jones, C. E., Hawthorne, J. A., Hanlon, G. W., Salvage, J. P., et al. (2014a). Evaluation of environmental scanning electron microscopy for analysis of *Proteus mirabilis* crystalline biofilms in situ on urinary catheters. *FEMS Microbiol. Lett.* 355, 20–27. doi: 10.1111/1574-6968.12451

Holling, N., Lednor, D., Tsang, S., Bissell, A., Campbell, L., Nzakizwanayo, J., et al. (2014b). Elucidating the genetic basis of crystalline biofilm formation in *Proteus mirabilis*. *Infect. Immun.* 82, 1616–1626. doi: 10.1128/IAI.01652-13

Jacobsen, S. M., Stickler, D. J., Mobley, H. L. T., and Shirtliff, M. E. (2008). Complicated catheter-associated urinary tract infections due to *Escherichia coli* and *Proteus mirabilis*. *Clin. Microbiol. Rev.* 21, 26–59. doi: 10.1128/CMR.00019-07

Jones, B. D., and Mobley, H. L. (1987). Genetic and biochemical diversity of ureases of proteus, *Providencia*, and *Morganella* species isolated from urinary tract infection. *Infect. Immun.* 55, 2198–2203.

Jones, B. V., Mahenthiralingam, E., Sabbuba, N. A., and Stickler, D. J. (2005). Role of swarming in the formation of crystalline *Proteus mirabilis* biofilms on urinary catheters. *J. Med. Microbiol.* 4, 807–813. doi: 10.1099/jmm.0.46123-0

Kaca, W., Glenska, J., Lechowicz, L., Grabowski, S., Brauner, A., and Kwinkowski, M. (2011). Serotyping of *Proteus mirabilis* clinical strains based on lipopolysaccharide O-polysaccharide and core oligosaccharide structures. *Biochemistry* 76, 851-861. doi: 10.1134/S0006297911070169

Kohler-Ockmore, J., and Feneley, R. C. (1996). Long-term catheterization of the bladder: prevalence and morbidity. *Br. J. Urol.* 77, 347–351. doi: 10.1046/j.1464-410x.1996.09074.x

Koren, S., Walenz, B. P., Berlin, K., Miller, J. R., Bergman, N. H., and Phillippy, A. M. (2017). Canu: scalable and accurate long-read assembly via adaptive k-mer weighting and repeat separation. *Genome Res.* 27, 722–736. doi: 10.1101/gr.215087.116.

Kot, W., Vogensen, F. K., Sørensen, S. J., and Hansen, L. H. (2014). DPS - a rapid method for genome sequencing of DNA-containing bacteriophages directly from a single plaque. *J. Virol. Methods* 196, 152–156. doi: 10.1016/j.jviromet.2013.10.040

Kunin, C. M. (1997). *Urinary Tract Infections: Detection, Prevention and Management*, 5th edn. Baltimore, MD: Williams & Wilkins.

Lai, M. J., Lin, N. T., Hu, A., Soo, P. C., Chen, L. K., Chen, L. H., et al. (2011). Antibacterial activity of *Acinetobacter baumannii* phage ϕAB2 endolysin (LysAB2) against both gram-positive and gram-negative bacteria. *Appl. Microbiol. Biotechnol.* 90, 529–539. doi: 10.1007/s00253-011-3104-y

Lakin, S. M., Dean, C., Noyes, N. R., Dettenwanger, A., Ross, A. S., Doster, E., et al. (2017). MEGARes: an antimicrobial resistance database for high throughput sequencing. *Nucleic Acids Res.* 45, D574–D580. doi: 10.1093/nar/gkw1009

Lehman, S. M., and Donlan, R. M. (2015). Bacteriophage-mediated control of a two-species biofilm formed by microorganisms causing catheter- associated urinary tract infections in an in vitro urinary catheter model. *Antimicrob. Agents Chemother.* 59, 1127–1137. doi: 10.1128/AAC.03786-14

Lood, R., Winer, B. Y., Pelzek, A. J., Diez-Martinez, R., Thandar, M., Euler, C. W., et al. (2015). Novel phage lysin capable of killing the multidrug-resistant Gram-negative bacterium *Acinetobacter baumannii* in a mouse bacteremia model. *Antimicrob. Agents Chemother.* 59, 1983–1991. doi: 10.1128/AAC.04641-14

Lu, T. K., and Collins, J. J. (2007). Dispersing biofilms with engineered enzymatic bacteriophage. *Proc. Natl. Acad. Sci. U.S.A.* 104, 11197–11202. doi: 10.1073/pnas.0704624104

Melo, L. D. R., Veiga, P., Cerca, N., Kropinski, A. M., Almeida, C., Azeredo, J., et al. (2016). Development of a phage cocktail to control *Proteus mirabilis* catheter-associated urinary tract infections. *Front. Microbiol.* 7:1024

Mobley, H. L. T. (1996). "Virulence of *Proteus mirabilis*," in *Urinary Tract Infections: Molecular Pathogenesis and Clinical Management*. eds H. T. L, Mobley, and J. W. Warren. (Washington, DC: ASM Press), 245–265.

Morgan, S. D., Rigby, D., and Stickler, D. J. (2009). A study of the structure of the crystalline bacterial biofilms that can encrust and block silver foley catheters. *Urol. Res.* 37, 89–93. doi: 10.1007/s00240-009-0176-6

Morozova, V., Kozlova, Y., Shedko, E., Babkin, I., Kurilshikov, A., Bokovaya, O., et al. (2018). Isolation and characterization of a group of new Proteus bacteriophages. *Arch. Virol.* 163, 2189–2197. doi: 10.1007/s00705-018-3853-3

Morozova, V., Kozlova, Y., Shedko, E., Kurilshikov, A., Babkin, I., Tupikin, A., et al. (2016). Lytic bacteriophage PM16 specific for *Proteus mirabilis*: a novel member of the genus Phikmvvirus. *Arch. Virol.* 161, 2457–2472. doi: 10.1007/s00705-016-2944-2

Morris, N. S., Stickler, D. J., and Winters, C. (1997). Which indwelling urethral catheters resist encrustation by *Proteus mirabilis* biofilms? *Br. J. Urol.* 80, 58–63. doi: 10.1046/j.1464-410x.1997.00185.x

Nzakizwanayo, J., Hanin, A., Alves, D. R., McCutcheon, B., Dedi, C., Salvage, J., et al. (2016). Bacteriophage can prevent encrustation and blockage of urinary catheters by *Proteus mirabilis*. *Antimicrob. Agents Chemother.* 60, 1530–1536. doi: 10.1128/AAC.02685-15

Ogilvie, L. A., Caplin, J., Dedi, C., Diston, D., Cheek, E., Bowler, L., et al. (2012). Comparative (Meta)genomic analysis and ecological profiling of human gut-specific bacteriophage B124-14. *PLoS One* 7:e35053. doi: 10.1371/journal.pone.0035053

Ogilvie, L. A., Caplin, J., Dedi, C., Diston, D., Cheek, E., Bowler, L., et al. (2013). Genome signature-based dissection of metagenomic datasets to extract subliminal viral sequences. *Nat. Commun.* 4:2420. doi: 10.1038/ncomms3420

Ogilvie, L. A., Nzakizwanayo, J., Guppy, F. M., Dedi, C., Diston, D., Taylor, H., et al. (2018). Resolution of habitat-associated ecogenomic signatures in bacteriophage genomes and application to microbial source tracking. *ISME J.* 12, 942–958. doi: 10.1038/s41396-017-0015-7

Oliveira, H., Vilas Boas, D., Mesnage, S., Kluskens, L. D., Lavigne, R., Sillankorva, S., et al. (2016). Structural and enzymatic characterization of ABgp46, a novel phage endolysin with broad anti-gram-negative bacterial activity. *Front. Microbiol.* 7:208. doi: 10.3389/fmicb.2016.00208

Pickard, R., Lam, T., MacLennan, G., Starr, K., Kilonzo, M., McPherson, G., et al. (2012). Antimicrobial catheters for reduction of symptomatic urinary tract infection in adults requiring short-term catheterisation in hospital: a multicentre randomised controlled trial. *Lancet* 380, 1927–1935. doi: 10.1016/S0140-6736(12)61380-4

Pride, D. T., Wassenaar, T. M., Ghose, C., and Blaser, M. J. (2006). Evidence of host-virus co-evolution in tetranucleotide usage patterns of bacteriophages and eukaryotic viruses. *BMC Genomics* 7:8. doi: 10.1186/1471-2164-7-8

Santiago-Rodriguez, T. M., Ly, M., Bonilla, N., and Pride, D. T. (2015). The human urine virome in association with urinary tract infections. *Front. Microbiol.* 6:14. doi: 10.3389/fmicb.2015.00014

Santos, M. A. (1991). An improved method for the small scale preparation of bacteriophage DNA based on phage precipitation by zinc chloride. *Nucleic Acids Res.* 19:5442. doi: 10.1093/nar/19.19.5442

Schwudke, D., Ergin, A., Michael, K., Volkmar, S., Appel, B., Knabner, D., et al. (2008). Broad-host-range *Yersinia* phage PY100: genome sequence, proteome analysis of virions, and DNA packaging strategy. *J. Bacteriol.* 190, 332–342. doi: 10.1128/JB.01402-07

Stickler, D. J. (2008). Bacterial biofilms in patients with indwelling urinary catheters. *Nat. Clin. Pract. Urol.* 5, 598–608. doi: 10.1038/ncpuro1231

Stickler, D. J. (2014). Clinical complications of urinary catheters caused by crystalline biofilms: something needs to be done. *J. Intern. Med.* 276, 120–129. doi: 10.1111/joim.12220

Stickler, D. J., Ganderton, L., King, J., Nettleton, J., and Winters, C. (1993). *Proteus mirabilis* biofilms and the encrustation of urethral catheters. *Urol. Res.* 21, 407–411. doi: 10.1007/bf00300077

Sutherland, I. W., Hughes, K. A., Skillman, L. C., and Tait, K. (2004). The interaction of phage and biofilms. *FEMS Microbiol. Lett.* 232, 1–6. doi: 10.1016/S0378-1097(04)00041-2

Teeling, H., Waldmann, J., Lombardot, T., Bauer, M., and Glöckner, F. O. (2004). TETRA: a web-service and a stand-alone program for the analysis and comparison of tetranucleotide usage patterns in DNA sequences. *BMC Bioinform.* 5:163. doi: 10.1186/1471-2105-5-163

Wirjon, I. A., Lau, N.-S., and Arip, Y. M. (2016). Complete genome sequence of *Proteus mirabilis* phage pPM_01 isolated from raw sewage. *Interviology* 59, 243–253. doi: 10.1159/000468987

Yang, H., Yu, J., and Wei, H. (2014). Engineered bacteriophage lysins as novel anti-infectives. *Front. Microbiol.* 5:542. doi: 10.3389/fmicb.2014.00542

Yap, M. L., and Rossmann, M. G. (2014). Structure and function of bacteriophage T4. *Future Microbiol.* 9, 1319–1327. doi: 10.2217/fmb.14.91

Zimmer, M., Vukov, N., Scherer, S., and Loessner, M. J. (2002). The murein hydrolase of the bacteriophage 3626 dual lysis system is active against all tested *Clostridium perfringens* strains. *Appl. Environ. Microbiol.* 68, 5311–5317. doi: 10.1128/AEM.68.11.5311-5317.2002

Conflict of Interest Statement: The authors declare that the research was conducted in the absence of any commercial or financial relationships that could be construed as a potential conflict of interest.

Copyright © 2019 Alves, Nzakizwanayo, Dedi, Olympiou, Hanin, Kot, Hansen, Lametsch, Gahan, Schellenberger, Ogilvie and Jones. This is an open-access article distributed under the terms of the Creative Commons Attribution License (CC BY). The use, distribution or reproduction in other forums is permitted, provided the original author(s) and the copyright owner(s) are credited and that the original publication in this journal is cited, in accordance with accepted academic practice. No use, distribution or reproduction is permitted which does not comply with these terms.

frontiers in Microbiology

ORIGINAL RESEARCH
published: 11 October 2019
doi: 10.3389/fmicb.2019.02337

Isolation and Characterization of Specific Phages to Prepare a Cocktail Preventing *Vibrio* sp. Va-F3 Infections in Shrimp (*Litopenaeus vannamei*)

Ling Chen[1,2,3,4†], Jiqiang Fan[1,2,3†], Tingwei Yan[5], Quan Liu[6], Shengjian Yuan[1,2,4,7], Haoran Zhang[1,2], Jinfang Yang[8], Deng Deng[8], Shuqiang Huang[1,2,4] and Yingfei Ma[1,2,3,4*]*

[1]Institute of Synthetic Biology, Shenzhen Institutes of Advanced Technology, Chinese Academy of Sciences, Shenzhen, China, [2]Key Laboratory of Quantitative Engineering Biology, Chinese Academy of Sciences, Shenzhen, China, [3]Shenzhen Key Laboratory of Synthetic Genomics, Shenzhen Institutes of Advanced Technology, Chinese Academy of Sciences, Shenzhen, China, [4]Guangdong Provincial Key Laboratory of Genome Read and Write, Shenzhen Institutes of Advanced Technology, Chinese Academy of Sciences, Shenzhen, China, [5]College of Life Science and Technology, Jinan University, Guangzhou, China, [6]College of Life Science and Oceanography, Shenzhen University, Shenzhen, China, [7]University of Chinese Academy of Sciences, Beijing, China, [8]R&D Center, Shenzhen Alpha Feed Co., Ltd, Shenzhen, China

Vibrio is one of the most detrimental agents of shrimp premature death syndrome. Phage therapy for prevention and treatment of *Vibrio* infections has attracted increasing attentions due to the emergence of antibiotic-resistant bacterial variants. Here, we describe a workflow of preparing a phage cocktail against *Vibrio* infections for practical applications. Twenty *Vibrio* strains were isolated from the gut of diseased shrimp and aquaculture wastewater, and five of them were identified as pathogens causing shrimp vibriosis. Twenty-two lytic phages were then isolated using the above five pathogens as hosts, and five of them showed broad host ranges and high lytic capability against the *Vibrio* strains. Whole genomic sequencing and phylogenetic analysis of the five phages indicated that they are novel and belong to the *Siphoviridae* family. The phage cocktail consisting of these five phages showed higher efficiency in inhibiting the growth of pathogenic *Vibrio* sp. Va-F3 than any single phage *in vitro*. We then evaluated the performance of the phage cocktail in protecting shrimp against *Vibrio* sp. Va-F3 infections *in situ*. The results showed that shrimp survival rates could reach 91.4 and 91.6% in 7 days, for the cocktail-treated and the antibiotic-treated groups, respectively. By contrast, the shrimp survival rate of the group without any treatment was only 20.0%. Overall, this study describes a general workflow of how to prepare a phage cocktail and apply it in controlling bacterial infections in the shrimp aquaculture. Knowledge gained from this study will not only help fight against the shrimp vibriosis in practical but also facilitate the design of phage cocktails with a satisfying performance in controlling other animal diseases in aquaculture.

Keywords: vibriosis, phage therapy, *Vibrio*, phage cocktail, shrimp

OPEN ACCESS

Edited by:
Robert Czajkowski,
University of Gdańsk, Poland

Reviewed by:
Daniel Elias Castillo Bermudez,
University of Copenhagen, Denmark
Roberto Bastías,
Pontificia Universidad Católica de Valparaíso, Chile
Romilio T. Espejo,
University of Chile, Chile

***Correspondence:**
Shuqiang Huang
shuqiang.huang@siat.ac.cn
Yingfei Ma
yingfei.ma@siat.ac.cn

†These authors have contributed equally to this work

Specialty section:
This article was submitted to Virology, a section of the journal Frontiers in Microbiology

Received: *01 July 2019*
Accepted: *25 September 2019*
Published: *11 October 2019*

Citation:
Chen L, Fan J, Yan T, Liu Q, Yuan S, Zhang H, Yang J, Deng D, Huang S and Ma Y (2019) Isolation and Characterization of Specific Phages to Prepare a Cocktail Preventing Vibrio sp. Va-F3 Infections in Shrimp (Litopenaeus vannamei). Front. Microbiol. 10:2337. doi: 10.3389/fmicb.2019.02337

INTRODUCTION

Vibrio is a genus of Gram-negative, comma-shaped rod bacteria and grows preferentially in warm (>15°C) marine water (Bakeraustin et al., 2010) with low salinity (<25 ppt NaCl). In shrimp aquaculture, the severe infections of various *Vibrio* strains often cause the shrimp disease of vibriosis (Frans et al., 2011). Traditionally, various antibiotics (e.g., sulfonamides and tetracyclines) have been widely used in the treatments of the infections of *V. parahaemolyticus*, *V. harveyi*, *V. alginolyticus*, and other *Vibrio* strains in the shrimp aquaculture (Tendencia and de la Peña, 2001; Vinod et al., 2006; Al-Othrubi et al., 2014; Wang et al., 2015), consequently, causing the alarming emergence of multidrug-resistant pathogens. It is imperative to develop alternative strategies to prevent and treat the shrimp diseases caused by drug-resistant pathogenic bacteria infections (Miller and Miller, 2011; Young and Gill, 2015).

Bacteriophage was first discovered in 1915 by Twort (1972) and D'Herelle (2011). Since then, bacteriophage has been used to treat bacterial infections (commonly termed phage therapy). Nowadays, there has been a renewed interest in applying phage therapy to control bacterial pathogens due to the limited use of antibiotics (Golkar et al., 2014). So far, phage therapy has been applied in controlling the bacterial infections of plants, humans, domestic animals, and marine animals as well as a biological control for food productions (Chan et al., 2013; Doss et al., 2017; Kalatzis et al., 2018). The use of phage therapy has been proven to be medically safe and effective in several cases (Biswas et al., 2002; Karunasagar et al., 2007; Chhibber et al., 2009; Chadha et al., 2016; Wang et al., 2017).

To date, several phages against *V. alginolyticus* have been isolated and reported, including two myoviruses PVA1 (Zhang et al., 2014) and phi-A318 (Liu et al., 2014) and two podoviruses ValKK3 (Lal et al., 2016) and VEN (Kokkari et al., 2018). However, direct use of single phage for combating bacterial infections is quite limited because of low efficacy, narrow host range of single phage, and fast emergence of phage-resistant bacterial mutants (Pirnay et al., 2011; Chan et al., 2013; Letchumanan et al., 2016; Yen et al., 2017; Kilcher et al., 2018). Our study aims to explore the potential use of phage therapy as antibacterial tools in aquaculture against bacterial infections to combat the antibiotic crisis. Taking the disease of vibriosis as an example, here we describe an integrated workflow of how to develop an appropriate phage cocktail against the *Vibrio* pathogens and then determine the effectiveness of the cocktail in treating shrimp diseases caused by *Vibrio* sp. Va-F3 infections *in situ*.

MATERIALS AND METHODS

Animals and Conditions

Healthy two-month-old shrimp (*L. vannamei*; weight = 10.2 ± 0.6 g) and the commercial feeds for shrimp were provided by Aolong Seedling Plant of Shenzhen Alpha Feed Agriculture and Animal Husbandry Co., Ltd., Shanwei city, China (N: 22.782051, E: 115.541900). The shrimp were placed and cultured at Aolong Seedling Plant. The aquatic water temperature was maintained at 24 ± 1°C during the study.

Isolation and Identification of *Vibrio* Pathogens

Vibrio pathogenic strains used in this study were isolated from both the gut of the diseased shrimp collected from aquaculture pools where numerous shrimp died of vibriosis and the aquaculture wastewater samples collected from the drain exits of shrimp culturing pools (Nov. 2016, Aolong Seedling Plant, Shanwei city, China). The *Vibrio* strains were isolated by the selective medium containing thiosulfate citrate bile salt sucrose agar (TCBS agar, Haibo, China) and further incubated at 28°C in 2216E medium (5 g peptone and 2 g yeast extract per liter; Wang et al., 2015). Taxonomic assignment of these purified strains was performed based on the analysis of 16S rRNA gene sequences (Frank et al., 2008). Briefly, microbial DNA samples were used as the substrate for amplification of 16S rRNA gene fragments using the universal primers 27f and 1494r (Xu et al., 2018). The reaction mixture consists of 10 ng of template DNA, 10 pmol of each primer, 2.5 U of DNA polymerase, 5 μl of 10× PCR amplification buffer (100 mM Tris-HCl and 500 mM KCl), 200 μM dNTP, 1.5 mM $MgCl_2$, and 10 pmol of a primer. The above mixture was first denatured for 1 min at 98°C, followed by 30 typical PCR cycles of denaturation (10 s at 98°C), annealing (30 s at 56°C), and extension (40 s at 72°C). Finally, another extension was executed at 72°C for 2 min. The PCR products were sequenced by Sanger sequencing platform (BGI gene Co., Ltd., China). The 16S rRNA gene sequences have been submitted to the NCBI GenBank database with accession numbers (**Supplementary Table S1**).

The verified pathogenic strains were further typed based on the method described previously (Szczuka and Kaznowski, 2004). Briefly, ERIC-PCR (enterobacterial repetitive intergenic consensus sequence PCR) method with primers ERIC-R (5′-ATGTAAGCT CCTGGGGATTCAC-3′) and ERIC2 (5′-AAGTAAGTGACTGG GGTGAGCG-3′) (Versalovic et al., 1991) was employed to type the subspecies of the strains. The reaction mixture was denatured for 7 min at 95°C, then subjected to 30 cycles of denaturation for 30 s at 90°C, annealing for 1 min at 52°C, extension for 8 min at 65°C, and a final extension for 16 min at 65°C. The patterns of PCR products were visualized by 1.5% agarose gel (wt/vol) in 1× Tris-acetate buffer (40 mM Tris-acetate, 1 mM EDTA) running for 40 min under 80 V.

To determine the pathogenicity of the isolated *Vibrio* strains, healthy shrimp were challenged with the isolated *Vibrio* strains in April 2017. In total, 750 healthy shrimp were randomly divided into 25 groups, with 30 shrimp per group. For the control group, none of the *Vibrio* strains was included, whereas for the challenge groups, 500 ml of the bacterial suspension of each tested strain was added to the aquatic water at different concentrations (2.2×10^2, 2.2×10^4, and 2.2×10^6 CFU/ml). Each group of the shrimp was raised within a 20 L plastic bucket. The survival rate of the shrimp of each group was recorded after 6 days. Low survival rate of the shrimp suggests that the corresponding *Vibrio* strain used for challenge experiment is likely the pathogen of vibriosis.

Isolation and Purification of Bacteriophages

The verified pathogens from above experiment were then used as hosts to isolate their specific phages. The phages were isolated from the wastewater samples collected from sewage draining exits in the cities of Shenzhen, Zhanjiang, and Shanwei, China, respectively. The wastewater samples were collected in April-November 2017 and April-July 2018. For each sample, approximately 20–50 ml was collected into sterile homogeneous bags (500 ml, Hopebiol) and stored at 4°C. The samples were centrifuged at 8,000× *g* for 10 min, and the supernatants were filtered through a 0.22-μm pore-size membrane to remove the solid impurities and bacterial cells. The filtrates were then mixed with 1× 2216E medium and the pathogenic strain cultures for phage enrichment at 28°C overnight. Subsequently, the cultures were centrifuged again at 8,000× *g* for 10 min, and the supernatants were then filtered through the 0.22-μm pore-size membrane. The bacteriophage titer of the filtrate was determined using the double-layered method (Chen et al., 2018). Clear phage plaques were picked from the plates and placed into 1 ml of sterile 2216E medium. This separation procedure was repeated three times to ensure the purity of the isolated phages.

Determination of Phage Host Ranges

In total, 20 *Vibrio* strains (isolated from the above section of *isolation and identification of the bacterial pathogens*) were included to determine the host ranges of the isolated phages (**Supplementary Table S1**). Lytic capabilities of the isolated phages were evaluated using standard spot tests. Briefly, the bacterial strains were mixed with 0.7% 2216E medium top agar and overlaid on 1.5% 2216E medium plates, and then 10 μl of the purified phage suspension (10^8 PFU/ml) was dropped in the middle of each plate. The plates were examined in 12 h after incubation at 28°C. The bacterial hosts of a tested phage were confirmed if a clear phage lytic plague could be observed in the plate. This procedure was replicated three times for verification.

Transmission Electron Microscopy

Phage particles were precipitated with 10% polyethylene glycol 8,000 (PEG 8000) at 4°C overnight, centrifuged at 10,000× *g* for 15 min, and subsequently suspended in SM buffer (100 mM NaCl, 8 mM MgSO4, 50 mM Tris-HCl, and 0.01% gelatin). One drop of the concentrated phage particles was placed on copper grids with carbon-coated formvar films, followed by negative staining with 4 μl of 2% (wt/vol) phosphotungstic acid (pH 6.5). Then, the grids were dried and examined using a Tecnai G2 F20 S-Twin electron microscope (FEI, USA) operated at 120 kV of accelerating voltage.

Phage DNA Extraction, Genome Sequencing, and Assembly

The concentrated phage particles were treated using DNase I and RNase A (New England BioLab, England) to remove bacterial nucleic acids. Then, phage genomic DNA was extracted using the Lambda Bacteriophage Genomic DNA Rapid Extraction Kit (Aidlab, China) following the manufacturer's protocol. The purified phage DNA was sequenced using the Illumina HiSeq1500 sequencer platform (Annoroad gene technology Co. Ltd., China). The filtered reads were assembled using SOAP *de novo* by the default parameters (Luo et al., 2012). The complete genome of each phage was finished and then manually inspected.

Genome Analysis and Phylogenetic Analysis

Open reading frames (ORFs) encoded by the complete phage genomes were predicted by the program GeneMark.hmm (Besemer and Borodovsky, 2005). The ORFs were annotated using the BLASTP algorithm against the non-redundant (nr) protein database of the National Center for Biotechnology Information (NCBI; Song et al., 2009; Sharma et al., 2016) in January 2019. The putative promoter sequences and regions on the phage genomes were identified using promoter online analysis tools of Softberry (Shahmuradov et al., 2003) and Promoter Scan (Prestridge, 2000). We tried to detect virulent genes on the phage genomes using the Virulence Search program (Underwood et al., 2005). Rho-independent transcription terminators on the phage genomes were also predicted using the ARNold program (Naville et al., 2011). tRNAs carried by the phage genomes were detected using the protein analysis software of ARAGORN and tRNAscan-SE (Schattner et al., 2005). Comparative genome analysis of the isolated phages was conducted using EasyFig 2.1 (Rombouts et al., 2016). To determine the taxonomy of the isolated phages, phylogenetic analysis of the phages based on the protein sequences of large terminase subunits was carried out using the MEGA 5.02 software with the neighbor-joining method and 1,000 bootstrap replications (Tamura et al., 2011). Comparison of pairwise similarity of phage genomes based on their predicted proteins was performed using BLASTP and visualized using R (version 3.4.1) gplots package (Walter et al., 2015).

Inhibition of Pathogen by Phages *in vitro*

Vibrio sp. Va-F3 was selected as the host for phage inhibition test. Phages were selected for phage cocktail design based on the criteria: (1) the phages have broad and different host ranges; (2) the phages were isolated from the samples with different locations, and to the most degree, this warrants that the isolated phages are different without the knowledge of the genome sequences; and (3) the host ranges of the five phages cover the highest number of the tested bacteria (Crothers-Stomps et al., 2010; Chan et al., 2013). The phage cocktail was prepared by pooling equal volume of each purified phage solution at a concentration of 10^9 PFU/ml. Bacterium Va-F3 grew to the optical density at 600 nm (OD_{600}) of approximately 0.5, which was equal to approximately 10^8 CFU/ml. Each well of a 96-well plate was loaded with 100 μl bacterial culture and 100 μl of dilutions of the five phages and the cocktail (MOI, multiplicity of infection = 10). Three replications of each test were performed as well. Plate sterility, bacterial culture without any phage, and phage suspension without any bacterial cell were set up as controls. All the plates were incubated at 28°C for 36 h, and the value of OD_{600} of each plate was measured using the Bioscreen plate reader (Bioscreen C, Finland) at 30 min intervals.

Pathogenic Infections of Shrimp by *Vibrio* sp. Va-F3 and Phage Therapy *in situ*

To validate the therapeutic performance of the designed cocktail in controlling the pathogenic bacterial infections in practical applications, 540 healthy shrimp (weight = 10.2 ± 0.6 g) were equally divided into six groups for the experiment in November 2017. Each group contained 90 shrimp and was then divided equally into three parallel subgroups as replicates (30 shrimp per subgroup). Group I was supplemented with fresh 2,216 medium only. Group II was challenged with *Vibrio* sp. Va-F3 within a culturing bath at a concentration of 2×10^6 CFU/ml. Group III was treated with 10 mg/L kanamycin after a two-day challenge of Va-F3. Group IV was supplemented with the phage cocktail at a final concentration of 2×10^7 PFU/ml but without the challenge of Va-F3. Group V received the treatment of the phage cocktail at a final concentration of 2×10^7 PFU/ml after a two-day challenge of strain Va-F3 at 2×10^6 CFU/ml. The control group was set as the one without any treatment. The survival rate of the shrimp of each group was subsequently summarized after 7-day cultivation.

Nucleotide Sequence Accession Number and Phage Preservation

The phages were preserved in China Center for Type Culture Collection (Wuhan, China) with CCTCC Nos. M2107548 of ValLY-3, M2107549 of VspDsh-1, M2107547 of VpaJT-1, M2107552 of ValSw4-1, and M2107551 of VspSw-1. The complete genome sequences of the phages have been submitted to the NCBI GenBank database with accession numbers: MH925090 of ValLY-3, MH925091 of ValSw4-1, MH925092 of VpaJT-1, MH925093 of VspDsh-1, and MH925094 of VspSw-1.

RESULTS

Isolation and Characterization of *Vibrio* Pathogens

In this study, in total, 20 *Vibrio* strains were successfully identified, and the sequences of their 16S rRNA genes have been submitted to the NCBI GenBank database (**Supplementary Table S1**). According to the top hits of their 16S rRNA genes in NCBI nr database, 1 strain has top hit to *V. ovensii*, 8 to *V. parahaemolyticus*, 2 to *V. natriegens*, 2 to *V. metschnikovii*, 2 to *V. azureus*, and 5 to *V. alginolyticus*. These 20 *Vibrio* strains were then used to challenge the healthy shrimp to determine if they can cause shrimp vibriosis. Five *Vibrio* sp. strains Va-F4, Va-F2, Va-F3, Va-F10, and Val-3 are likely the pathogens of shrimp vibriosis because the mortality rates of the shrimp challenged by these strains reached from 16.7 to 73.4% after 6-day cultivation (**Figure 1; Supplementary Figure S1; Supplementary Table S1**). Meanwhile, we further typed the subspecies of the five *Vibrio* strains using ERIC-PCR primers, and the results indeed showed slightly different patterns of their PCR products (**Supplementary Figure S2**), suggesting that these five strains belong to different subtypes of the same species within the genus of *Vibrio*. Besides, among the five pathogenic strains, Va-F3 showed the highest pathogenic capability to the shrimp (73.4% mortality rate as shown in **Figure 1**). Therefore, Va-F3 was selected as the representative pathogen for the following studies.

Isolation of Lytic Bacteriophages Using Pathogenic *Vibrio* Strains as Hosts

Using the five pathogenic *Vibrio* strains as hosts, we successfully isolated 22 bacteriophages from the collected water samples. These phages can form clear plaques on their host strains following overnight incubation at 28°C, suggesting that all these phages are likely lytic phages against their hosts. The host ranges of the isolated phages were then determined using the 20 *Vibrio* strains isolated in this work (**Figure 2; Supplementary Table S1**). According to the results, five phages that were named ValLY-3, VspDsh-1, VspSw-1, VpaJT-1, and ValSw4-1 have broader host ranges against *Vibrio* strains, respectively (**Figure 2**). Notably, phage ValLY-3 appeared to be more effective against *Vibrio* sp. strains because it could lyse four of the five pathogenic *Vibrio* sp. strains and the top hits of their 16S rRNA genes in NCBI nr database all belong to *V. alginolyticus* (**Supplementary Table S1**). However, none of the isolated phages could individually infect all the five pathogens (Va-F4, Va-F2, Va-F3, Va-F10, and Val-3). Based on the observation that the host range of combining the five phages covers all the five pathogenic strains, it is likely that the cocktail consisting of these five phages can be applicable to effectively inhibit the growth of the *Vibrio* pathogens causing vibriosis *in situ*.

Morphology of the Lytic Bacteriophages

The morphologies of the isolated phages were observed using TEM, indicating that all the five phages exhibit hexagonal heads (diameter ranged from 55 to 90 nm) and non-contractile, flexible tails (length ranged from 100 to 200 nm), which are typical features of the phages belonging to the *Siphoviridae* family (**Figure 3**), although ValLY-3 and ValSw4-1 have a larger size in head with the diameters of 89.8 and 57.5 nm, respectively.

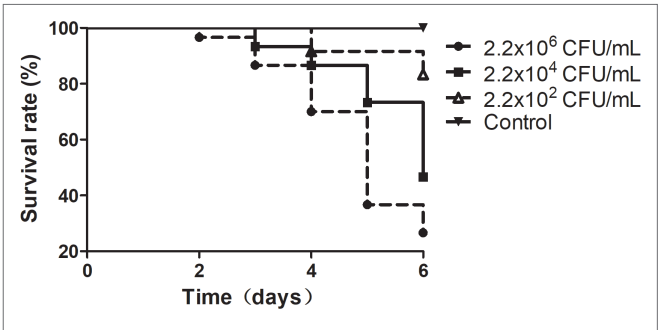

FIGURE 1 | Survival rates of the shrimp infected by *Vibrio* sp. Va-F3. Survival rates of the shrimp were calculated after cocultured with *Vibrio* strains for 1 week. The control group was set as no *Vibrio* strain included, and the experimental groups included 500 ml of bacterial suspension with three different bacterial concentrations, as 2.2×10^2, 2.2×10^4, and 2.2×10^6 CFU/ml.

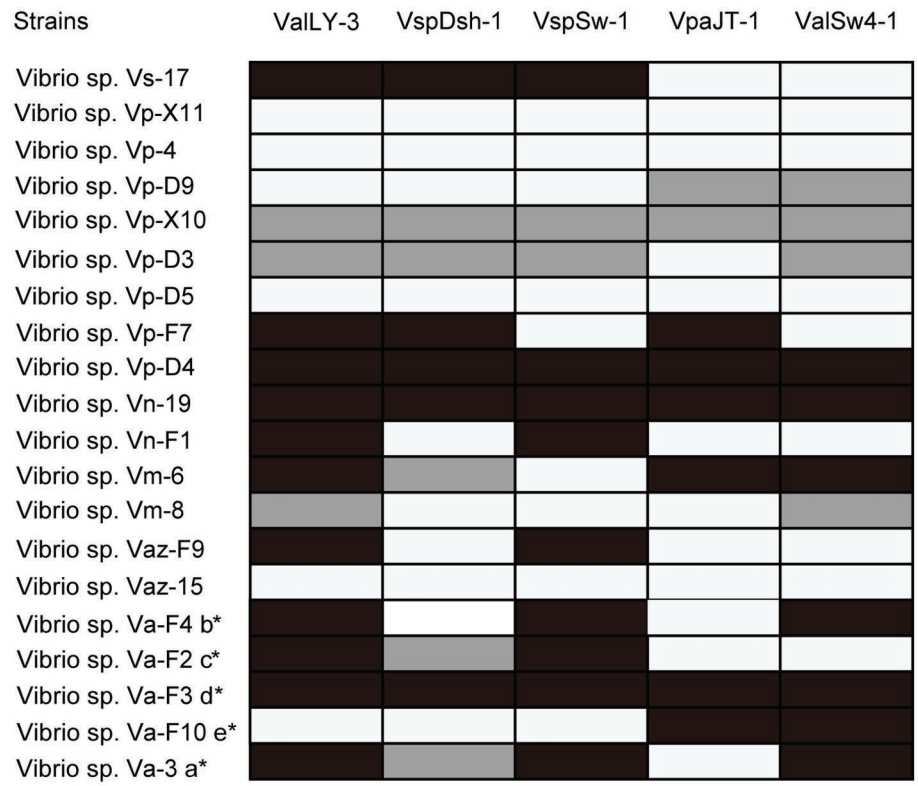

FIGURE 2 | Host ranges of phages ValLY-3, VspDsh-1, VspSw-1, VpaJT-1, and ValSw4-1. A total of 20 bacterial strains were used for determining the phage host ranges. The 16S rRNA gene sequences of all the strains have been sequenced and submitted to the NCBI with accession as attached above (more information referring to **Supplementary Table S1**). Black spots indicated clear plaque, gray for turbid plaque, and white for no phage plaque. a: The host strain used for VspDsh-1 isolation; b: VspSw-1 isolation; c: VpaJT-1 isolation; d: ValLY-3 isolation; e: ValSw4-1 isolation. *, Verified pathogenic strains in this study.

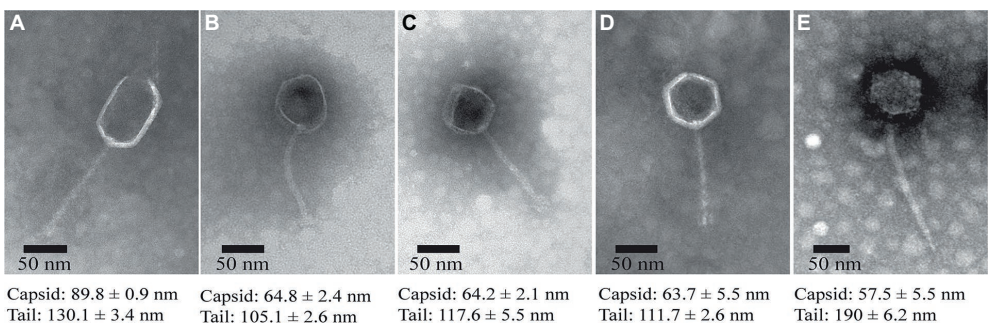

FIGURE 3 | TEM images of the isolated lytic phages. **(A)** ValLY-3, **(B)** VspDsh-1, **(C)** VpaJT-1, **(D)** ValSw4-1, and **(E)** VspSw-1. The phages were stained with 2% phosphotungstic acid and visualized at 120,000× magnification with transmission electron microscopy. Scale bars represent 20 nm.

Genome Sequencing and Annotation of the Phages

We further sequenced and characterized the whole genome sequences of the five phages. The features of the genomes were summarized in **Table 1**. The genomes range in size from 46.6 to 113.7 kb with GC contents of 43.8–49.2%. The GC contents of the five phages are lower than those of their *Vibrio* host genomes (averagely, 50%). Phage VspSw-1 encodes the highest number (n = 25) of tRNAs. By contrast, the other phages encode few tRNAs ($\leqq$2), indicating that they mainly depend on the host translation machinery. ORFs encoded by the phage genomes were predicted, and the corresponding functions were annotated by Blastp analysis against the NCBI nr database. About 66.2% (351/530) of ORFs share 26–100% identities of amino acid sequences with those deposited in the NCBI GenBank database. We identified the ORFs that were assigned to the basic phage-related functions (**Figure 4**), including DNA replication, DNA metabolism, DNA packaging,

TABLE 1 | Genomic features of the five phages.

		Phage name				
		VspDsh-1	**VpaJT-1**	**ValLY-3**	**ValSw4–1**	**VspSw-1**
Features	Genome length (bp)	46,692	60,177	76,310	79,545	113,778
	GC content (%)	46.7	49.2	48.8	45.7	43.8
	ORFs	60	96	104	112	158
	Terminators	25	29	57	58	68
	Promoters	110	134	179	190	271
	tRNAs	1	2	0	0	25
	Host	*Vibrio* sp. Va-F4	*Vibrio* sp. Va-F3	*Vibrio* sp. Val-3	*Vibrio* sp. Va-F3	*Vibrio* sp. Va-F2
	Accession ID	MH925093	MH925092	MH925090	MH925091	MH925094

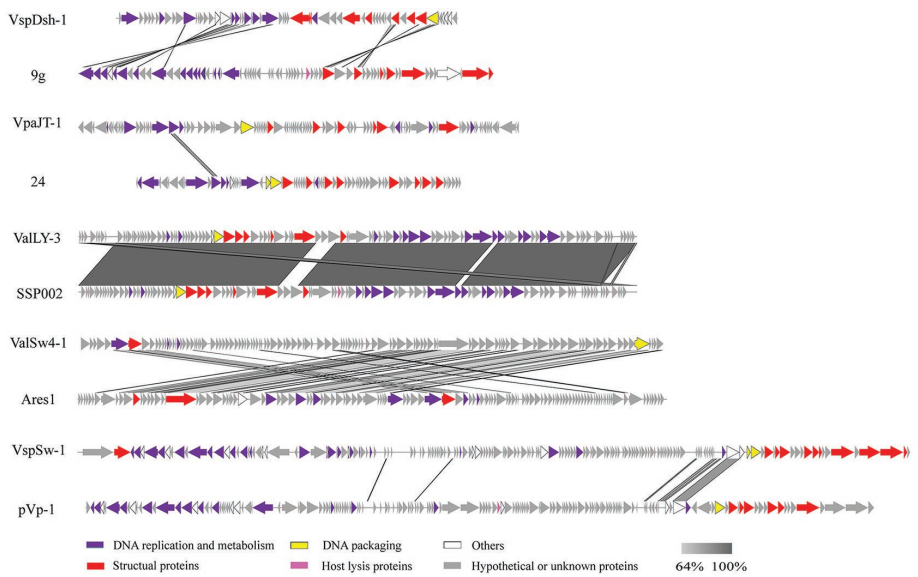

FIGURE 4 | Multiple sequence alignment of phage genomes. Whole genome sequences of the isolated phages (ValLY-3, VspDsh-1, VpaJT-1, ValSw4-1, and VspSw-1) and the highest similar reference phages were compared using Easyfig. The gray regions indicate high similarity among the genomic sequences. The predicted functional proteins are indicated by different colors. Blastn analyzes of the five phages' genomes show that the top hits in NCBI nr database of ValLY-3, VspDsh-1, VpaJT-1, ValSw4-1, and VspSw-1 are *Vibrio* phage SSP002 (JQ692107.1, with cover 95% and identity 99%), *Enterobacteria* phage 9 g (KJ419279.1, with cover 0% and identity 80%), vB_SenS_Sergei (KY002061.1, with cover 0% and identity 100%), *Vibrio* phage Ares1 (MG720309.1, with cover 31% and identity 67%), and *Vibrio* phage pVp-1 (JQ340389.1, with cover 2% and identity 79%), respectively.

structural proteins, and host lysis. Neither the genes responsible for toxins or virulence in the ARDB database (Liu and Pop, 2008) or the VFDB database (Chen et al., 2005), nor the known lysogenic-related genes (Oppenheim et al., 2005) were found within the genomes of the five phages. These genetic features ensure that these phages are suitable candidates for phage therapy.

Whole genomic sequence alignment also demonstrates the novelty of the five phages at the genomic levels. As shown in **Figure 4,** the phages have only few cross wires with those in the NCBI GenBank database, except for ValLY-3, whose genome highly resembles that of previously characterized *Vibrio* phages *SSP002* (JQ692107.1), with the identity of 95% (**Table 1**). Phylogenetic analysis was performed based on the large terminase subunits identified in ValLY-3, ValSw4-1, VpaJT-1, VspDsh-1, and VspSw-1, as well as other 21 classified phages ratified by ICTV (**Figure 5A**). The results indicated that the five phages belong to five different genera within the *Siphoviridae* family. VpaJT-1 and ValSw4-1 are members of two different unclassified genera within the *Siphoviridae* family, respectively, as they are grouped into different clades in the phylogenetic tree (**Figure 5A**). Moreover, we also conducted an *in silico* pairwise comparison of the proteomes of the phages used in the phylogenetic analysis. Eight different groups can be clustered, in line with the result of the phylogenetic analysis (**Figure 5B**). This analysis suggests that the five phages are different and likely employ different mechanisms to infect the *Vibrio* hosts.

Inhibition of Bacterial Growth by Phages *in vitro*

We then tested the infective capability of the five phages and the cocktail containing five phages against *Vibrio* sp. Va-F3 *in vitro*, respectively. Strain Va-F3 was verified to be the

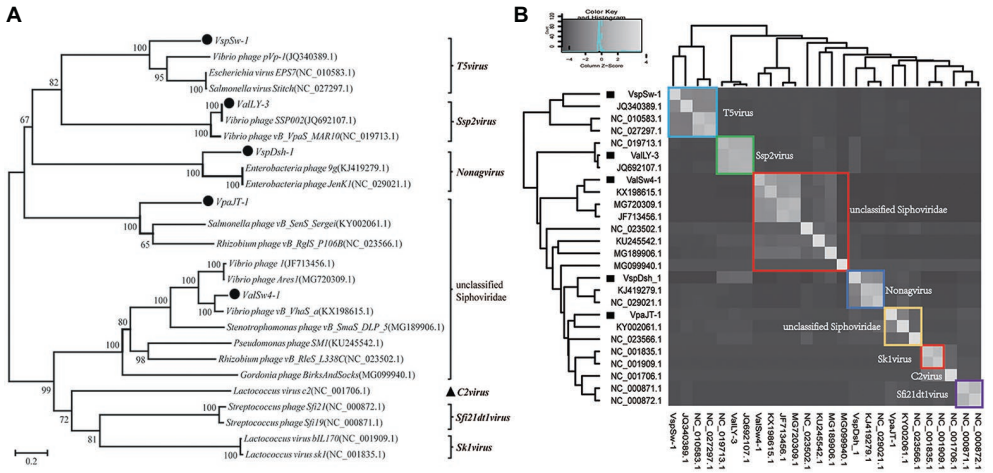

FIGURE 5 | Phylogenetic analysis of the five isolated bacteriophages. **(A)** Phylogenetic tree based on the sequences of the large subunits of terminases of the selected bacteriophages. The sequences of the large subunits of terminases were aligned using the Mega 5.05 program, and the phylogenetic tree was generated using the neighbor-joining method with 1,000 bootstrap replications. **(B)** Heat map showing percentage of the shared protein sequences among the bacteriophages.

pathogen with the highest mortality rate against the shrimp in our study (**Figure 1; Supplementary Figure S1**). As shown in **Figure 6**, all the five phages were found to be capable of inhibiting the growth of Va-F3, but the host growth recovery started in 2, 2, 6, 9, and 9 h when treated with phages VspDsh-1, ValLY-3, ValSw-1, VpaJT-1, and VspSw-1, respectively. This suggests different abilities of the five phages in inhibiting the growth of Va-F3. For the control group without phage treatment, the OD_{600} value of strain Va-F3 reached 0.45 after 2 h incubation, while the growth of Va-F3 was inhibited in all phage-treated groups within the first 2 h. By contrast, the inhibition effectiveness of the cocktail was higher than those of any single phage, as we can see that the growth inhibition of the host in the cocktail-treated group lasted for at least 24 h (**Figure 6**).

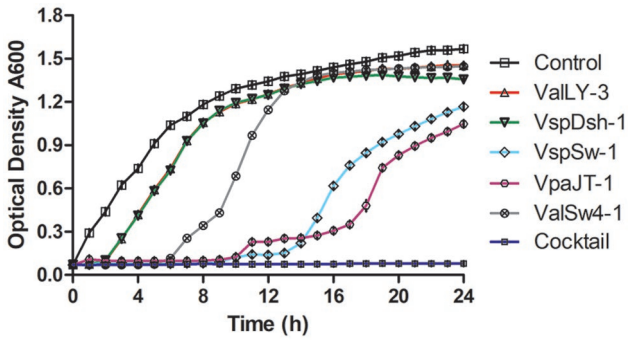

FIGURE 6 | Growth inhibition of *Vibrio* sp. Va-F3 by the five phages and the phage cocktail *in vitro*. The MOI was set as 10, the optical density of bacterial solution as approximately 0.5 (OD_{600}, 10^8 CFU/ml), and the concentrations of the phages (ValLY-3, VspDsh-1, VspSw-1, VpaJT-1, ValSw4-1, and their cocktail) as 2×10^9 PFU/ml. Each point represents the average result of three replicates, and error bars represent standard deviations. According to the curve, we can calculate the frequency of phage resistant bacteria in the population to a given phage. First, we calculated the number of the phage resistant bacterial cells starting to grow during the incubation using the formula: Nm = Nt(the number of bacterial cells at OD_{600} = 1)/$2^{[tOD600(\text{the time bacteria grow to OD600 = 1})/td(\text{bacterial cell doubling time})]}$, and then f(the frequency of phage resistant bacteria) = Nm(the number of bacterial mutant cells at beginning)/N0(the number of all bacterial cells at beginning). We determined N0 = 2×10^8 CFU/ml and td = 60 min; at OD_{600} = 1, tOD_{600} = 5 h for control, tOD_{600} = 8 h for ValLY-3 and VspDsh-1, tOD_{600} = 11 h for ValSw4-1, tOD_{600} = 20 h for VspSw-1, and tOD_{600} = 23 h for VpaJT-1; Nt = 10^9. Therefore, we calculated the f(ValLy-3 and VspDsh-1) = 0.20, f(ValSw4-1) = 0.002, f(VspSw-1) = 4.77E-06, f(VpaJT-1) = 5.96E-07. During the experiment in 24 h, we were not able to determine the growth of the bacterial cells when treated with the cocktail, suggesting the frequency of the cocktail resistant bacterial cells is extremely low.

Application of the Cocktail Against *Vibrio* sp. Va-F3 Infections of the Shrimp *in situ*

For practical application of phage therapy, we sought to validate the performance of the cocktail against the pathogenic infections of the shrimp *in situ*. In this experiment, we set up one control group and five experimental groups. The shrimp of group II were infected by the pathogen without any treatment, and the skin color of the shrimp became white and turbid and the intestine turned to be slightly red in 5 days. Meanwhile, the body of the infected shrimp was soft, the size of their hepatopancreas was enlarged, and the color was light yellow (**Supplementary Figures S3A–D**). The survival rate of the shrimp of group II reached only 20% in 7 days (**Figures 7A,B**). In comparison, the survival rate of the shrimp of group V treated by the cocktail reached 91.4%, which was quite comparable to that of group III treated by antibiotics (91.1%, **Figure 7A**). Furthermore, to eliminate the concern of potential phage toxicity, we included group IV where the shrimp got the cocktail treatment only, and the survival rate was similar to those of groups III and V, suggesting that no apparent side effects of the phages were detected.

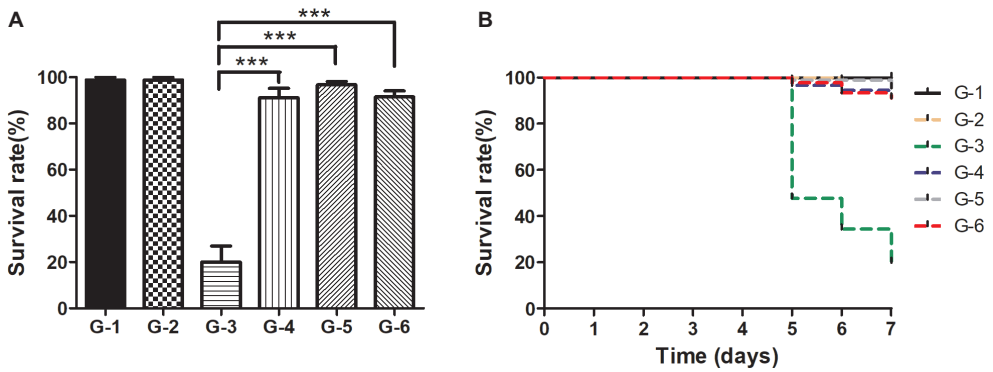

FIGURE 7 | Comparison of the survival rates of the shrimp in different treatment groups *in situ*. **(A)** Survival rates of the shrimp of each group after the 7-day treatment; **(B)** Survival rates of each group in the experiment duration. C: The control group was set up without any treatment. G-1: Group I was given fresh 2,216 medium only. G-2: Group II was challenged with *Vibrio* sp. Va-F3 at concentration of 2×10^6 CFU/ml. G-3: Group III was treated with 10 mg/l kanamycin after two-day challenge of Va-F3 at 2×10^6 CFU/ml. G-4: Group IV received treatment of the phage cocktail at the final concentration of 2×10^7 PFU/ml. G-5 Group V received treatment of the phage cocktail at the final concentration of 2×10^7 PFU/ml after two-day challenge of strain Va-F3 at 2×10^6 CFU/ml. Asterisks above the columns indicate significant differences at the $p < 0.01$ level (Wilcoxon-Mann-Whitney test).

DISCUSSION AND CONCLUSION

The concept of using phages as an agent for controlling pathogen infections has been widely accepted. There have been numerous studies describing the applications of phage therapy in controlling pathogen infections in aquaculture (Rao and Lalitha, 2014). However, the application of phage therapy in aquaculture as well as in clinics is still greatly limited. This can be attributed to the lack of a standard workflow of how to prepare a phage cocktail for controlling pathogen infections in practical applications. To our knowledge, for the first time, our study describes the integrated workflow starting from step (1) isolation and verification of the Vibrio pathogens from diseased animals; step (2) specific phage isolation, sequencing, and characterization; and step (3) phage cocktail preparation for the efficiency test *in vivo* and *in situ*. Each step of the workflow is necessary and will be the warrant of developing a safe and efficient phage cocktail in an application. Some studies directly used the pathogens provided by other studies for phage isolation and phage cocktail preparation (Higuera et al., 2013; Kalatzis et al., 2016). Thus, these bacterial strains may not be able to cause vibriosis *in situ*. Meanwhile, some studies failed to obtain the sequences of the phages used for phage cocktail (Higuera et al., 2013; Mateus et al., 2014; Zhang et al., 2015). This sequencing information of the phages could be quite helpful, and thus, we may exclude those phages carrying toxin genes for phage therapy based on the bioinformatics analysis of their gene sequences before phage cocktail preparation. More importantly, in our study, the *in situ* experiment showed that the administration of the resulted phage cocktail in treating the *Vibrio* infections of the shrimp promoted the survival rate of the shrimp as significantly as the antibiotic treatment (**Figure 7**).

Instead of using the *Vibrio* pathogens reported in other literature (Mechri et al., 2017; Rameshkumar et al., 2017; Lv et al., 2019) as hosts for lytic phage isolation, our study started with the isolation of *Vibrio* strains from the diseased shrimp within the shrimp-farmed pond. Furthermore, the pathogenicity of the five *Vibrio* sp. strains (Va-F4, Va-F2, Va-F3, Va-F10, and Val-3) was confirmed, respectively (**Figure 1; Supplementary Figure S1**). Other reported pathogenic *Vibrio* strains may not be able to cause the disease of vibriosis in shrimp in our study, because the shrimp hosts and other environmental factors are likely the key causative factors of vibriosis as well (Mahoney et al., 2010). We observed that strain Va-F3 showed different pathogenic capabilities in causing the shrimp vibriosis in the two challenge experiments (**Figures 1, 7**), which were performed in April and November 2017, respectively, highlighting that the environmental factors likely play important roles in the development of vibriosis in the shrimp. More importantly, due to the fact that phages usually are highly specific to infect their hosts (Schmelcher and Loessner, 2014; Kilcher et al., 2018), using the well-known *Vibrio* strains reported in other literature may probably lead to failure of phage therapy in practical applications.

The fast emergence of phage-resistant bacterial variants after treatment with single phage limited the therapeutic applications of phage therapy. Phage cocktail that can delay the appearance of resistant variants has been widely used in practical applications (Gu et al., 2012). Currently, no criteria have been developed to select phages for phage cocktail preparation due to the limited availability and the great diversity of phages. In our previous study, a phage cocktail containing only two phages with divergent genomes showed higher antimicrobial activity than other cocktails and any single phage (Chen et al., 2018). The divergent genomes of the selected phages imply that heterogeneous infection mechanisms against their hosts could be employed by the phages. Thus, the high performance of the phage cocktail can be explained by the fact that the heterogeneous mechanisms likely lead to phage synergy in killing the hosts.

Accordingly, in this study, three criteria (see in the section "Materials and Methods") were set up to select phages for phage cocktail preparation. These criteria warrant that the phages we selected are different in genome and infection mechanism. We selected five phages for cocktail preparation in terms of the observation that the five phages have broad host ranges against *Vibrio* strains (**Figure 2; Supplementary Table S1**). Our results indicate that the five phages have different host ranges, phylogenies, and divergent genome sequences. These observations suggest that the phages are likely to employ different mechanisms in infecting their hosts. Therefore, although it was shown that two phages (ValLY-3 and VpaJT-1) can infect all five tested pathogenic *Vibrio* strains, including Va-F4, Va-F2, Va-F3, Va-F10, and Val-3 (**Figure 2**), in our study, the main purpose of including five phages for phage cocktail preparation is to cover a high chance of emergence of phage resistant variants of the *Vibrio* strain during and before the treatment. As shown in **Figure 6**, bacterial variants emerged rapidly when treated with one single phage, while phage cocktail including the five phages can inhibit the growth of the strain for a long time. **Figure 6** also showed the frequencies of phage-resistant variants in *Vibrio* sp. strain Va-F3 when treated with single phage and cocktail. According to the growth curves of Va-F3 treated with different phages, the number of ValLY-3-resistant variants of Va-F3 is similar to that of VspDsh-1 but higher than those of VspSw-1, VpaJT-1, ValSw4-1, and the cocktail (the frequencies of ValLY-3 = VspDsh-1 > VspSw-1 > VpaJT-1 > ValSw4-1). Thus, in our study, the cocktail using the five phages that likely have different mechanisms to infect Va-F3 can kill not only the five isolated pathogenic *Vibrio* strains but also phage-resistant Va-F3 variants. This can be observed from **Figure 7** that a satisfying performance in controlling the pathogen growth was obtained in the practical application.

The concept of phage MOI describes the ratio of phages to their host bacteria (Abedon, 2016). The MOI value of 10 was directly used in our *in vitro* experiment. It is difficult to estimate the actual number of a specific bacterial pathogen in a given environment before the phage therapeutic application. Thus, we did not determine the optimal MOI of the phage cocktail for neither *in vitro* nor *in situ* experiments. We delivered the phage cocktail at the final phage concentration of 2×10^7 PFU/ml against pathogen Va-F3 in the 20 L bucket, resulting in a significantly high survival rate of the shrimp challenged by the pathogen *in situ* (**Figure 7**). A bacterial cell infected by a lytic phage may release up to several hundreds of progeny phage particles with infection activity for the next round infection (Guo et al., 2019). Thus, a lytic phage may generate enormous progeny phages in a given environment full of its host in a short time. This likely suggests that we do not have to use a large dose of phages in the prevention of shrimp vibriosis in practical applications.

The microbial compositions of the aquatic water, as well as the shrimp intestinal tract, are complex (Fan et al., 2019). We observed that the survival rate of the shrimp challenged by the pathogen increased significantly when the phage cocktail was administered as compared to that of the pathogen-challenged shrimp without any treatment. Nevertheless, we did not completely understand what happened to the microbial ecosystems of the aquatic water and the shrimp gut when the phages were administrated. In terms of the predator-prey relationship between phage and its bacterial host, both the environmental microbiota and the shrimp gut microbiota can be interfered by the phage treatment in the experiment *in situ*. We noticed that the intestine of the shrimp (group II) infected by Va-F3 turned to be slightly red, the body was soft, the size of the hepatopancreas was enlarged, and the color of the hepatopancreas was light yellow (**Supplementary Figures S3A–D**). However, the shrimp of group V with the treatment of the phage cocktail after *Vibrio* challenge did not show significant changes compared to those of group II. Further studies are needed to determine the interplays between phages, microbes, and the shrimp intestine throughout the whole process of phage therapeutic application using metagenomic sequencing, which will shed deep insights into the dynamics of shrimp gut microbiota, provide useful clues toward potential therapeutic applications of phages in aquaculture, and further warrant the success of applications in prevention and treatment of the bacterial infection diseases of the shrimp, and even for other animals.

In conclusion, our study describes a successful example of developing a phage cocktail and applying it in treating *Vibrio* sp. Va-F3 infection disease of the shrimp. Since the use of various antibiotics in aquaculture tends to be banned, the phage cocktail demonstrates the potential of being used as a therapeutic agent for controlling pathogenic bacterial infections, particularly, against vibriosis.

DATA AVAILABILITY STATEMENT

The datasets generated for this study can be found in the phages were preserved in China Center for Type Culture Collection (Wuhan, China) with CCTCC numbers. M2107548 of ValLY-3, M2107549 of VspDsh-1, M2107547 of VpaJT-1, M2107552 of ValSw4-1, and M2107551 of VspSw-1. The complete genome sequences of the phages have been submitted to the NCBI GenBank database with accession numbers: MH925090 of ValLY-3, MH925091 of ValSw4-1, MH925092 of VpaJT-1, MH925093 of VspDsh-1, and MH925094 of VspSw-1.

AUTHOR CONTRIBUTIONS

JF and YM conceived and designed the experiments. JF, LC, TY, QL, SY, HZ, JY, and DD performed the experiments. LC and JF analyzed the data. JY and DD contributed to sample materials. JF, LC, SH, and YM wrote the paper. YM, SH, JF, and LC managed the project.

FUNDING

This work received support from the Shenzhen Science and Technology Innovation Committee (JCYJ20170818155011625,

JCYJ20170413153329565). This work was also supported by the Shenzhen Peacock Team Project (KQTD2016112915000294), the National Natural Science Foundation of China (31570115, 31971350 and 31770111), and the Instrumental Project from the Chinese Academy of Sciences (YJKYYQ20170063).

SUPPLEMENTARY MATERIAL

The Supplementary Material for this article can be found online at: https://www.frontiersin.org/articles/10.3389/fmicb.2019.02337/full#supplementary-material

REFERENCES

Abedon, S. T. (2016). Phage therapy dosing: the problem(s) with multiplicity of infection (MOI). *Bacteriophage* 6:e1220348. doi: 10.1080/21597081.2016.1220348

Al-Othrubi, S. M. Y., Kqueen, C. Y., Mirhosseini, H., Radu, S., and Hadi, Y. A. (2014). Antibiotic resistance of *Vibrio parahaemolyticus* isolated from cockles and shrimp sea food marketed in Selangor, Malaysia. *Clin. Microbiol.* 3, 148–154. doi: 10.4172/2327-5073.1000148

Bakeraustin, C., Stockley, L., Rangdale, R., and Martinezurtaza, J. (2010). Environmental occurrence and clinical impact of *Vibrio vulnificus* and *Vibrio parahaemolyticus*: a European perspective. *Environ. Microbiol. Rep.* 2, 7–18. doi: 10.1111/j.1758-2229.2009.00096.x

Besemer, J., and Borodovsky, M. (2005). GeneMark: web software for gene finding in prokaryotes, eukaryotes and viruses. *Nucleic Acids Res.* 33, W451–W454. doi: 10.1093/nar/gki487

Biswas, B., Adhya, S., Washart, P., Paul, B., Trostel, A. N., Powell, B., et al. (2002). Bacteriophage therapy rescues mice bacteremic from a clinical isolate of vancomycin-resistant *Enterococcus faecium*. *Infect. Immun.* 70, 204–210. doi: 10.1128/IAI.70.1.204-210.2002

Chadha, P., Katare, O. P., and Chhibber, S. (2016). *In vivo* efficacy of single phage versus phage cocktail in resolving burn wound infection in BALB/c mice. *Microb. Pathog.* 99, 68–77. doi: 10.1016/j.micpath.2016.08.001

Chan, B. K., Abedon, S. T., and Loc-Carrillo, C. (2013). Phage cocktails and the future of phage therapy. *Future Microbiol.* 8, 769–783. doi: 10.2217/fmb.13.47

Chen, L., Yang, J., Yu, J., Yao, Z., Sun, L., Shen, Y., et al. (2005). VFDB: a reference database for bacterial virulence factors. *Nucleic Acids Res.* 33(Suppl. 1), D325–D328. doi: 10.1093/nar/gki008

Chen, L., Yuan, S., Liu, Q., Mai, G., Yang, J., Deng, D., et al. (2018). *In vitro* design and evaluation of phage cocktails against *Aeromonas salmonicida*. *Front. Microbiol.* 9:1476. doi: 10.3389/fmicb.2018.03308

Chhibber, S., Kaur, S., and Kumari, S. (2009). Therapeutic potential of bacteriophage in treating *Klebsiella pneumoniae* B5055-mediated lobar pneumonia in mice. *J. Med. Microbiol.* 57, 1508–1513. doi: 10.1099/jmm.0.2008/002873-0

Crothers-Stomps, C., Hoj, L., Bourne, D. G., Hall, M. R., and Owens, L. (2010). Isolation of lytic bacteriophage against *Vibrio harveyi*. *J. Appl. Microbiol.* 108, 1744–1750. doi: 10.1111/j.1365-2672.2009.04578.x

D'Herelle, F. (2011). On an invisible microbe antagonistic to dysentery bacilli. Note by M. F. d'Herelle, presented by M. Roux. Comptes Rendus Academie des Sciences 1917; 165:373–5. *Bacteriophage* 1, 3–5. doi: 10.4161/bact.1.1.14941

Doss, J., Culbertson, K., Hahn, D., Camacho, J., and Barekzi, N. (2017). A review of phage therapy against bacterial pathogens of aquatic and terrestrial organisms. *Viruses* 9:E50. doi: 10.3390/v9030050

Fan, J., Chen, L., Mai, G., Zhang, H., Yang, J., Deng, D., et al. (2019). Dynamics of the gut microbiota in developmental stages of *Litopenaeus vannamei* reveal its association with body weight. *Sci. Rep.* 9:734. doi: 10.1038/s41598-018-37042-3

Frank, J. A., Reich, C. I., Sharma, S., Weisbaum, J. S., Wilson, B. A., and Olsen, G. J. (2008). Critical evaluation of two primers commonly used for amplification of bacterial 16S rRNA genes. *Appl. Environ. Microbiol.* 74, 2461–2470. doi: 10.1128/AEM.02272-07

Frans, I., Michiels, C. W., Bossier, P., Willems, K. A., Lievens, B., and Rediers, H. (2011). Vibrio anguillarum as a fish pathogen: virulence factors, diagnosis and prevention. *J. Fish Dis.* 34, 643–661. doi: 10.1111/j.1365-2761.2011.01279.x

Golkar, Z., Bagasra, O., and Pace, D. G. (2014). Bacteriophage therapy: a potential solution for the antibiotic resistance crisis. *J. Infect. Dev. Ctries.* 8, 129–136. doi: 10.3855/jidc.3573

Gu, J., Liu, X., Li, Y., Han, W., Lei, L., Yang, Y., et al. (2012). A method for generation phage cocktail with great therapeutic potential. *PLoS One* 7:e31698. doi: 10.1371/journal.pone.0031698

Guo, Y., Chen, P., Lin, Z., and Wang, T. (2019). Characterization of two *Pseudomonas aeruginosa* viruses vB_PaeM_SCUT-S1 and vB_PaeM_SCUT-S2. *Viruses* 11:318. doi: 10.3390/v11040318

Higuera, G., Bastías, R., Tsertsvadze, G., Romero, J., and Espejo, R. T. (2013). Recently discovered vibrio anguillarum phages can protect against experimentally induced vibriosis in Atlantic salmon, *Salmo salar*. *Aquaculture* 392, 128–133. doi: 10.1016/j.aquaculture.2013.02.013

Kalatzis, P. G., Bastías, R., Kokkari, C., and Katharios, P. (2016). Isolation and characterization of two lytic bacteriophages, φSt2 and φGrn1; phage therapy application for biological control of *Vibrio alginolyticus* in aquaculture live feeds. *PLoS One* 11:e0151101. doi: 10.1371/journal.pone.0151101

Kalatzis, P. G., Castillo, D., Katharios, P., and Middelboe, M. (2018). Bacteriophage interactions with marine pathogenic Vibrios: implications for phage therapy. *Antibiotics* 7:1. doi: 10.3390/antibiotics7010015

Karunasagar, I., Shivu, M. M., Girisha, S. K., Krohne, G., and Karunasagar, I. (2007). Biocontrol of pathogens in shrimp hatcheries using bacteriophages. *Aquaculture* 268, 288–292. doi: 10.1016/j.aquaculture.2007.04.049

Kilcher, S., Studer, P., Muessner, C., Klumpp, J., and Loessner, M. J. (2018). Cross-genus rebooting of custom-made, synthetic bacteriophage genomes in L-form bacteria. *Proc. Natl. Acad. Sci. USA* 115, 567–572. doi: 10.1073/pnas.1714658115

Kokkari, C., Sarropoulou, E., Bastias, R., Mandalakis, M., and Katharios, P. (2018). Isolation and characterization of a novel bacteriophage infecting *Vibrio alginolyticus*. *Arch. Microbiol.* 200, 707–718. doi: 10.1007/s00203-018-1480-8

Lal, T. M., Sano, M., Hatai, K., and Ransangan, J. (2016). Complete genome sequence of a giant vibrio phage ValKK3 infecting vibrio alginolyticus. *Genom. Data* 8, 37–38. doi: 10.1016/j.gdata.2016.03.002

Letchumanan, V., Chan, K. G., Pusparajah, P., Saokaew, S., Duangjai, A., Goh, B. H., et al. (2016). Insights into bacteriophage application in controlling vibrio species. *Front. Microbiol.* 7:1114. doi: 10.3389/fmicb.2016.01114

Liu, W., Lin, Y.-R., Lu, M.-W., Sung, P.-J., Wang, W.-H., and Lin, C.-S. (2014). Genome sequences characterizing five mutations in RNA polymerase and major capsid of phages [greek small letter phi] A318 and [greek small letter phi] As51 of vibrio alginolyticus with different burst efficiencies. *BMC Genomics* 15:1. doi: 10.1186/1471-2164-15-505

Liu, B., and Pop, M. (2008). ARDB—antibiotic resistance genes database. *Nucleic Acids Res.* 37(Suppl. 1), D443–D447. doi: 10.1093/nar/gkn656

Luo, R., Liu, B., Xie, Y., Li, Z., Huang, W., Yuan, J., et al. (2012). SOAPdenovo2: an empirically improved memory-efficient short-read *de novo* assembler. *Gigascience* 1:18. doi: 10.1186/2047-217x-1-18

Lv, T., Song, T., Liu, H., Peng, R., Jiang, X., Zhang, W., et al. (2019). Isolation and characterization of a virulence related *Vibrio alginolyticus* strain Wz11 pathogenic to cuttlefish, *Sepia pharaonis*. *Microb. Pathog.* 126, 165–171. doi: 10.1016/j.micpath.2018.10.041

Mahoney, J. C., Gerding, M. J., Jones, S. H., and Whistler, C. A. (2010). Comparison of the pathogenic potentials of environmental and clinical *Vibrio parahaemolyticus* strains indicates a role for temperature regulation in virulence. *Appl. Environ. Microbiol.* 76, 7459–7465. doi: 10.1128/AEM.01450-10

Mateus, L., Costa, L., Silva, Y., Pereira, C., Cunha, A., and Almeida, A. (2014). Efficiency of phage cocktails in the inactivation of Vibrio in aquaculture. *Aquaculture* 424, 167–173. doi: 10.1016/j.aquaculture.2014.01.001

Mechri, B., Monastiri, A., Medhioub, A., Medhioub, M. N., and Aouni, M. (2017). Molecular characterization and phylogenetic analysis of highly pathogenic *Vibrio alginolyticus* strains isolated during mortality outbreaks in cultured *Ruditapes decussatus* juvenile. *Microb. Pathog.* 111, 487–496. doi: 10.1016/j.micpath.2017.09.020

Miller, A. A., and Miller, P. F. (2011). *Emerging trends in antibacterial discovery: Answering the call to arms*. United Kingdom: Horizon Scientific Press.

Naville, M., Ghuillot-Gaudeffroy, A., Marchais, A., and Gautheret, D. (2011). ARNold: a web tool for the prediction of rho-independent transcription terminators. *RNA Biol.* 8, 11–13. doi: 10.4161/rna.8.1.13346

Oppenheim, A. B., Kobiler, O., Stavans, J., Court, D. L., and Adhya, S. (2005). Switches in bacteriophage lambda development. *Annu. Rev. Genet.* 39, 409–429. doi: 10.1146/annurev.genet.39.073003.113656

Pirnay, J. P., De Vos, D., Verbeken, G., Merabishvili, M., Chanishvili, N., Vaneechoutte, M., et al. (2011). The phage therapy paradigm: pret-a-porter or sur-mesure? *Pharm. Res.* 28, 934–937. doi: 10.1007/s11095-010-0313-5

Prestridge, D. S. (2000). "Computer software of eukaryotic promoter analysis" in *Transcription factor protocols*. ed. M. J. Tymms (New York: Humana Press), 265–295.

Rameshkumar, P., Nazar, A. K. A., Pradeep, M. A., Kalidas, C., Jayakumar, R., Tamilmani, G., et al. (2017). Isolation and characterization of pathogenic *Vibrio alginolyticus* from sea cage cultured cobia (*Rachycentron canadum* (Linnaeus 1766)) in India. *Lett. Appl. Microbiol.* 65, 423–430. doi: 10.1111/lam.12800

Rao, B. M., and Lalitha, K. V. (2014). Bacteriophages for aquaculture: are they beneficial or inimical. *Aquaculture* 437, 146–154. doi: 10.1016/j.aquaculture.2014.11.039

Rombouts, S., Volckaert, A., Venneman, S., Declercq, B., Vandenheuvel, D., Allonsius, C. N., et al. (2016). Characterization of novel bacteriophages for biocontrol of bacterial blight in leek caused by *Pseudomonas syringae* pv. porri. *Front. Microbiol.* 7:279. doi: 10.3389/fmicb.2016.00279

Schattner, P., Brooks, A. N., and Lowe, T. M. (2005). The tRNAscan-SE, snoscan and snoGPS web servers for the detection of tRNAs and snoRNAs. *Nucleic Acids Res.* 33(Suppl. 2), W686–W689. doi: 10.1093/nar/gki366

Schmelcher, M., and Loessner, M. J. (2014). Application of bacteriophages for detection of foodborne pathogens. *Bacteriophage* 4:e28137. doi: 10.4161/bact.28137

Shahmuradov, I. A., Gammerman, A. J., Hancock, J. M., Bramley, P. M., and Solovyev, V. V. (2003). PlantProm: a database of plant promoter sequences. *Nucleic Acids Res.* 31, 114–117. doi: 10.1093/nar/gkg041

Sharma, A., Gilbert, J. A., and Lal, R. (2016). (Meta) genomic insights into the pathogenome of *Cellulosimicrobium cellulans*. *Sci. Rep.* 6:25527. doi: 10.1038/srep25527

Song, D., Yang, Y., Yu, B., Zheng, B., Deng, Z., Lu, B.-L., et al. (2009). Computational prediction of novel non-coding RNAs in *Arabidopsis thaliana*. *BMC Bioinf.* 10:S36. doi: 10.1186/1471-2105-10-S1-S36

Szczuka, E., and Kaznowski, A. (2004). Typing of clinical and environmental *Aeromonas sp.* strains by random amplified polymorphic DNA PCR, repetitive extragenic palindromic PCR, and enterobacterial repetitive intergenic consensus sequence PCR. *J. Clin. Microbiol.* 42, 220–228. doi: 10.1128/JCM.42.1.220-228.2004

Tamura, K., Peterson, D., Peterson, N., Stecher, G., Nei, M., and Kumar, S. (2011). MEGA5: molecular evolutionary genetics analysis using maximum likelihood, evolutionary distance, and maximum parsimony methods. *Mol. Biol. Evol.* 28, 2731–2739. doi: 10.1093/molbev/msr121

Tendencia, E. A., and de la Peña, L. D. (2001). Antibiotic resistance of bacteria from shrimp ponds. *Aquaculture* 195, 193–204. doi: 10.1016/S0044-8486(00)00570-6

Twort, F. W. (1972). An investigation on the nature of ultra-microscopic viruses: the lancet. *Acta Orthop. Belg.* 38, 566–578.

Underwood, A., Mulder, A., Gharbia, S., and Green, J. (2005). Virulence searcher: a tool for searching raw genome sequences from bacterial genomes for putative virulence factors. *Clin. Microbiol. Infect.* 11, 770–772. doi: 10.1111/j.1469-0691.2005.01210.x

Versalovic, J., Koeuth, T., and Lupski, J. R. (1991). Distribution of repetitive DNA sequences in eubacteria and application to fingerprinting of bacterial genomes. *Nucleic Acids Res.* 19, 6823–6831. doi: 10.1093/nar/19.24.6823

Vinod, M. G., Shivu, M. M., Umesha, K. R., Rajeeva, B. C., Krohne, G., Karunasagar, I., et al. (2006). Isolation of *Vibrio harveyi* bacteriophage with a potential for biocontrol of luminous vibriosis in hatchery environments. *Aquaculture* 255, 117–124. doi: 10.1016/j.aquaculture.2005.12.003

Walter, W., Sanchez-Cabo, F., and Ricote, M. (2015). GOplot: an R package for visually combining expression data with functional analysis. *Bioinformatics* 31, 2912–2914. doi: 10.1093/bioinformatics/btv300

Wang, Y., Barton, M., Elliott, L., Li, X., Abraham, S., O'Dea, M., et al. (2017). Bacteriophage therapy for the control of *Vibrio harveyi* in greenlip abalone (*Haliotis laevigata*). *Aquaculture* 473, 251–258. doi: 10.1016/j.aquaculture.2017.01.003

Wang, R. X., Wang, J. Y., Sun, Y. C., Yang, B. L., and Wang, A. L. (2015). Antibiotic resistance monitoring in *Vibrio spp.* isolated from rearing environment and intestines of abalone *Haliotis diversicolor*. *Mar. Pollut. Bull.* 101, 701–706. doi: 10.1016/j.marpolbul.2015.10.027

Xu, D., Ding, W., Ke, W., Li, F., Zhang, P., and Guo, X. (2018). Modulation of metabolome and bacterial community in whole crop corn silage by inoculating Homofermentative *Lactobacillus plantarum* and Heterofermentative *Lactobacillus buchneri*. *Front. Microbiol.* 9:3299. doi: 10.3389/fmicb.2018.03299

Yen, M., Cairns, L. S., and Camilli, A. (2017). A cocktail of three virulent bacteriophages prevents *Vibrio cholerae* infection in animal models. *Nat. Commun.* 8:14187. doi: 10.1038/ncomms14187

Young, R., and Gill, J. J. (2015). Phage therapy redux—what is to be done? *Science* 350, 1163–1164. doi: 10.1126/science.aad6791

Zhang, J., Cao, Z., Li, Z., Wang, L., Li, H., Wu, F., et al. (2015). Effect of bacteriophages on *Vibrio alginolyticus* infection in the sea cucumber, *Apostichopus japonicus* (Selenka). *J. World Aquacult. Soc.* 46, 149–158. doi: 10.1111/jwas.12177

Zhang, J., Cao, Z., Xu, Y., Li, X., Li, H., Wu, F., et al. (2014). Complete genomic sequence of the *Vibrio alginolyticus* lytic bacteriophage PVA1. *Arch. Virol.* 159, 3447–3451. doi: 10.1007/s00705-014-2207-z

Conflict of Interest: The authors declare that the research was conducted in the absence of any commercial or financial relationships that could be construed as a potential conflict of interest.

Copyright © 2019 Chen, Fan, Yan, Liu, Yuan, Zhang, Yang, Deng, Huang and Ma. This is an open-access article distributed under the terms of the Creative Commons Attribution License (CC BY). The use, distribution or reproduction in other forums is permitted, provided the original author(s) and the copyright owner(s) are credited and that the original publication in this journal is cited, in accordance with accepted academic practice. No use, distribution or reproduction is permitted which does not comply with these terms.

frontiers in Microbiology

ORIGINAL RESEARCH
published: 16 October 2019
doi: 10.3389/fmicb.2019.02396

Biodiversity and Classification of Phages Infecting *Lactobacillus brevis*

Marine Feyereisen[1], Jennifer Mahony[1,2], Horst Neve[3], Charles M. A. P. Franz[3], Jean-Paul Noben[4], Tadhg O'Sullivan[5], Viktor Boer[5] and Douwe van Sinderen[1,2]**

[1] School of Microbiology, University College Cork, Cork, Ireland, [2] APC Microbiome Ireland, University College Cork, Cork, Ireland, [3] Department Microbiology and Biotechnology, Federal Research Centre of Nutrition and Food, Max Rubner-Institut, Kiel, Germany, [4] Department Physiology Biochemistry and Immunology, Biomedical Research Institute, Hasselt University, Diepenbeek, Belgium, [5] HEINEKEN Global Innovation and Research, Heineken Supply Chain B.V, Zoeterwoude, Netherlands

Lactobacillus brevis is a lactic acid bacterium that is known as a food and beverage spoilage organism, and more specifically as a beer-spoiler. Phages of *L. brevis* have been described, but very limited data is available regarding temperate phages of *L. brevis*. Temperate phages may exert benefits to the host, while they may also be employed to combat beer spoilage. The current study reports on the incidence of prophage sequences present in nineteen distinct *L. brevis* genomes. Prophage induction was evaluated using mitomycin C exposure followed by genome targeted-PCR, electron microscopy and structural proteome analysis. The morphological and genome sequence analyses revealed significant diversity among *L. brevis* prophages, which appear to be dominated by members of the *Myoviridae* phage family. Based on this analysis, we propose a classification of *L. brevis* phages into five groups.

Keywords: lactic acid bacteria, beer spoilage, bacteriophage, lysogeny, prophage, genomic analysis, induction, *Myoviridae*

OPEN ACCESS

Edited by:
Robert Czajkowski, University of Gdańsk, Poland

Reviewed by:
Stefan Hertwig, Federal Institute for Risk Assessment (BfR), Germany
Simon J. Labrie, SyntBioLab Inc., Canada

****Correspondence:***
Marine Feyereisen
116221209@umail.ucc.ie
Douwe van Sinderen
d.vansinderen@ucc.ie

Specialty section:
This article was submitted to Virology, a section of the journal Frontiers in Microbiology

Received: *29 August 2019*
Accepted: *03 October 2019*
Published: *16 October 2019*

Citation:
Feyereisen M, Mahony J, Neve H, Franz CMAP, Noben J-P, O'Sullivan T, Boer V and van Sinderen D (2019) Biodiversity and Classification of Phages Infecting Lactobacillus brevis. Front. Microbiol. 10:2396. doi: 10.3389/fmicb.2019.02396

INTRODUCTION

The most prevalent spoilage bacteria associated with beer fermentations are members of the lactic acid bacteria (LAB), which account for approximately 70% of all microbial spoilage incidents (Vaughan et al., 2005; Bokulich and Bamforth, 2013; Garofalo et al., 2015). *Lactobacillus brevis* strains are frequently reported to be the cause of such spoilage events as they have developed mechanisms to survive and grow in beer (Suzuki et al., 2006). Strains of this species can be found on raw materials used in breweries and represent a major microbial contaminant during the production and storage of beer. Bacterial strains have acquired features throughout evolution allowing them to become more robust including resistance to virulent bacteriophages (Forde and Fitzgerald, 1999; Brüssow, 2001; Mahony et al., 2016b). Moreover, the chromosomes of the majority of LAB are known to harbor one or more prophage regions and their presence may benefit the host by providing resistance attributes to its environment (Canchaya et al., 2003). Upon induction, these phages enter the lytic cycle leading to bacterial cell death and formation of intact phage particles (Davidson et al., 1990), and therefore it is relevant to examine their presence and functionality (Kelleher et al., 2018). Prophages of LAB have been widely studied and particularly so in *Lactococcus lactis* (Kelleher et al., 2018) and *Streptococcus thermophilus* (Husson-Kao et al., 2000). Temperate phages of the genus *Lactobacillus* have been sequenced and are primarily classified as members of the *Siphoviridae* family (Villion and Moineau, 2009), being characterized by a non-contractile tail (Forsman, 1993). Successful induction of such prophages has been reported using UV, thermal

exposure or treatment with DNA damaging/antimicrobial compounds such as mitomycin C and bacteriocins (Chopin et al., 1989, 2001; Meijer et al., 1998; Madera et al., 2009).

While the presence of prophages in LAB genomes is widely described, only a small number of studies have investigated their integrity and inducibility within these strains (Mittler, 1996; Lunde et al., 2003). In the case of beer spoilage by *L. brevis,* prophage induction represents a beneficial attribute that could be harnessed as a natural alternative to chemical compounds in the eradication of spoilage bacteria. Indeed, induction of prophages is expected to cause bacterial cell lysis thus avoiding the development of spoilage organisms in the brewing industry. Although prophages represent a reservoir for adaptation, prophages of *L. brevis* are currently poorly described. To date, the genome of a single temperate phage of *L. brevis*, namely LBR48, has been sequenced and characterized. The prophage was induced from *L. brevis* strain C30 using mitomycin C. LBR48 is 48 Kb long containing 90 putative open reading frames (ORFs) and was classified as a member of the *Myoviridae* family. Interestingly, the LBR48 genome does not show protein sequence similarity with any other *Lactobacillus* phages (Jang et al., 2011).

Advances in genome sequencing technologies have considerably increased the number of available bacterial genome sequences, improving also the detection capability of prophage-encoded regions within these genomes. In the current study, nineteen publically available *L. brevis* genome sequences were used to identify prophage-encoding regions. Five of these strains were available for prophage induction trials, allowing the assessment of the ability of these temperate phages to form intact phage particles and cause host cell lysis. The diversity of *L. brevis* temperate phages was studied to establish relatedness between *L. brevis* phages (temperate and virulent), resulting in a proposed classification scheme of *L. brevis* phages based on morphology and genome sequence data.

MATERIALS AND METHODS

Bacterial Strains and Growth Conditions

Lactobacillus brevis strains used in this study are detailed in **Table 1**. Bacteria were cultured in MRS broth (Oxoid Ltd., Hampshire, United Kingdom) at 30°C.

Prophage Identification and Genome Annotation

PHAge search tool enhanced release (PHASTER) (Zhou et al., 2011; Arndt et al., 2016) was used to screen for prophage-specifying DNA regions within the genome of available *L. brevis* strains. Intact prophages were manually annotated to confirm the presence of all expected genes required to produce a fully functional phage particle including genes encoding proteins associated with replication functions (e.g., replisome and DNA-binding proteins) packaging (small and large terminases), morphogenesis (e.g., capsid and tail) and lysis (holin and lysin). Genes required for lysogeny maintenance (e.g., integrase and repressor) were also investigated (Kelleher et al., 2018). Integration sites of prophages (attL and attR) were recorded and are presented in **Supplementary Table S1**. Prophage genome sequences were retrieved and annotated as previously described (Kelleher et al., 2018). Briefly, ORF prediction was performed using the Prodigal prediction software (Hyatt et al., 2010) and confirmed using BLASTX alignments (Altschul et al., 1990). The automatic annotations were refined using Artemis v16.0.0 to allow visual inspection of ORF predictions (Rutherford et al., 2000). Moreover, BLASTP (Altschul et al., 1997) and HHPred (Söding et al., 2005) analyses were performed to assign functional annotations to the predicted ORFs. Transfer RNA (tRNA) genes were predicted using tRNA-scan-SE v2.0 (Schattner et al., 2005) and added manually using Artemis.

Phylogenetic Analysis

A proteomic tree was constructed using a concatenated amino acid sequence of all encoded proteins for each of the *L. brevis* phages sequenced to date. The concatenated amino acid sequence begins with the ORF encoding the small terminase subunit (TerS) (Casey et al., 2015). The concatenated sequences were aligned using ClustalW (Thompson et al., 2002). The phylogenetic tree was constructed using the neighbor-joining method and bootstrapped employing 1,000 replicates. The final tree was visualized using MEGA7 (Kumar et al., 2008).

Genome Characterization and Organization

Following phylogenetic analysis, genomes of representative temperate phages were selected for further analysis where overall genome content and organization were studied. The genome content and architecture were analyzed based on the observation of the modular organization of the genomes into the following modules: packaging, morphogenesis, lysis, lysogeny, and replication. Protein sequences of representative phages were compared using all-against-all, bi-directional BLAST alignments (Altschul et al., 1990). An alignment cut-off *E*-value of 0.0001, and a similarity cut-off level of at least 30% amino acid identity across 80% of the sequence length was applied. This analysis allowed the amino acid similarity assignment between temperate phage genomes and the study of the overall genome similarity/diversity among *L. brevis* phages.

Prophage Induction Trials

To assess the functionality of the identified prophage-encoding regions, prophage induction trials were performed using the DNA crosslinking agent mitomycin C (MitC). For this assay, five *L. brevis* strains were available for testing: ATCC367, SA-C12, UCCLB95, UCCLBBS124, and UCCLBBS449. 10 mL MRS broth was inoculated with 2% of a fresh overnight culture of the relevant bacterial strain. Cultures were incubated at 30°C until an OD_{600nm} of 0.1, 0.2, or 0.3 was reached at which point 0.1, 0.2, or 0.3 μg/mL MitC (final concentration) was added. A high concentration of 2 μg/mL MitC (final concentration) was applied when cells reached an OD_{600nm} of 0.2. This was performed to ascertain if cell lysis occurred due to prophage induction or lethal MitC toxicity. Indeed, MitC levels of between

TABLE 1 | *Lactobacillus brevis* strains used in this study and prophage regions predicted by PHASTER.

Strain name (isolation source)	Genbank accession	No. prophage regions detected by PHASTER			References
		Intact	Questionable	Incomplete	
100D8* (Silage)	CP015338	1	1	1	
ATCC 367 (Silage)	CP000416	1	0	0	Makarova et al., 2006
BDGP6* (*Drosophila*'s gut)	CP024635	4	1	2	
KB290* (Fermented vegetable)	AP012167	2	0	1	Fukao et al., 2013
NPS-QW-145* (Kimchi)	CP015398	0	1	2	Wu et al., 2015
NCTC13768* (Unknown)	LS483405	0	1	0	
SA-C12 (Silage)	CP031185	2	1	1	Feyereisen et al., 2019a
SRCM101106* (Food)	CP021674	3	0	1	
SRCM101174* (Food)	CP021479	3	0	1	
TMW 1.2108* (Beer)	CP019734	2	0	0	Fraunhofer et al., 2018
TMW 1.2111* (Beer)	CP019743	2	0	0	Fraunhofer et al., 2018
TMW 1.2112* (Beer)	CP016797	1	0	0	Fraunhofer et al., 2018
TMW 1.2113* (Brewery surface)	CP019750	2	0	0	Fraunhofer et al., 2018
UCCLB521 (Brewery surface)	CP031208	0	0	2	Feyereisen et al., 2019a
UCCLB556 (Brewery surface)	CP031174	0	1	0	Feyereisen et al., 2019a
UCCLB95 (Beer)	CP031182	1	0	2	Feyereisen et al., 2019a
UCCLBBS124 (Beer)	CP031169	1	0	1	Feyereisen et al., 2019a
UCCLBBS449 (Beer)	CP031198	1	0	3	Feyereisen et al., 2019a
ZLB004* (Pig's feces)	CP021456	1	0	0	

**These strains were not tested for prophage induction.*

0.1 and 0.3 μg/mL are relatively low and when induction occurs it would be considered genuine prophage-induction mediated cell lysis. Conversely, higher concentrations of MitC (e.g., 2 μg/mL MitC) are expected to cause growth arrest and cell death due to acute toxicity. Cultures were maintained at room temperature for 30 h during which the OD_{600nm} was recorded at 60 min time intervals for the first 8 h and then at 15, 20, 25, and 30 h.

Using the same protocol as MitC prophage induction, potential induction regimes using other stress-inducing chemicals (2% v/v NaOH, 2% v/v formic acid or 2% v/v acetic acid) or physical treatment (direct UV light exposure (254 nm) of 30 min at a distance of 5 cm on a 1 cm height culture suspension) that resemble circumstances in the brewing industry for cleaning and sanitizing purposes were also assessed (Schmidt, 1997; Loeffler, 2006).

Validation of Prophage Induction by DNA Sequencing and Electron Microscopy

To validate prophage induction from *L. brevis* strains cited above, the DNA derived from cell-free supernatants was extracted and sequenced. Phage DNA was isolated using a previously described phage DNA extraction protocol (Lavelle et al., 2018). Primers were designed based on prophage sequences in order to confirm the presence of induced prophages in the cell-free supernatants of MitC-treated cultures (**Table 2**).

To validate prophage induction using electron microscopy, MitC-treated cultures were harvested by centrifugation at 5000 × *g* for 10 min, after which the supernatant was filtered twice through a 0.45 μm filter prior to electron microscopy analysis. Transmission electron microscopy of the samples was performed as previously described (Casey et al., 2015). Negative staining was performed using 2% (w/v) uranyl acetate on freshly prepared ultrathin carbon films. Grids were analyzed in a Tecnai 10 transmission electron microscope (FEI Thermo Fisher Scientific, Eindhoven, Netherlands) at an acceleration voltage of 80 kV. Micrographs were taken with a MegaView G2 charge-coupled device camera (Emsis, Muenster, Germany).

Phage Structural Proteome and Mass-Spectrometry

An aliquot (30 μL) of CsCl-purified phage sample was mixed with 10 μL of SDS loading buffer containing 50 mM β-mercaptoethanol. The structural protein profile was generated by standard Tris-glycine sodium dodecyl sulfate (SDS)–12% polyacrylamide gel electrophoresis (PAGE). Gel slices were then excised, trypsinized, and analyzed using electrospray ionization tandem mass spectrometry (ESI-MS/MS), as previously described (Ceyssens et al., 2008; Holtappels et al., 2015).

Genome Accession Numbers

Lactobacillus brevis 100D8: CP015338, *L. brevis* ATCC 367: CP000416, *L. brevis* BDGP6: CP024635, *L. brevis* KB290: AP012167, *L. brevis* NCTC13768: LS483405, *L. brevis* NPS-QW-145: CP015398, *L. brevis* SA-C12: CP031185, *L. brevis* SRCM101106: CP021674, *L. brevis* SRCM101174: CP021479, *L. brevis* TMW 1.2108: CP019734, *L. brevis* TMW 1.2111: CP019743, *L. brevis* TMW 1.2112: CP016797, *L. brevis* TMW 1.2113: CP019750, *L. brevis* UCCLB521: CP031208, *L. brevis*

TABLE 2 | Primer sequences used to amplify specific regions of induced prophages.

Primer name	Sequence (5′ – 3′)	Target
TPMB095F	gaatcctggcgataactag	TMP region of TPMB095 prophage
TPMB095R	gtggcaccagcgtatcgaa	
TPMB449F	cttcaatcaccatctaag	TMP region of TPMB449 prophage
TPMB449R	gactatcagcaatcgcatt	
TPMB124F	ggttgccttctgcaagg	TMP region of TPMB124 prophage
TPMB124R	gttaaggaggtgtgactaa	
TPSAC12-1F	gtatggcaatcaagcacac	TMP region of TPSAC12-1 prophage
TPSAC12-1R	tgccatctcattggtgac	
TPSAC12-2F	gacttcataacagcaat	TMP region of TPSAC12-2 prophage
TPSAC12-2R	ggtccactaatggcgac	
TPATCC367F	ggaaccttgtcgttcata	TMP region of TPATCC367 prophage
TPATCC367R	gcagcttctctagcaccac	

UCCLB556: CP031174, *L. brevis* UCCLB95: CP031182, *L. brevis* UCCLBBS124: CP031169, *L. brevis* UCCLBBS449: CP031198, *L. brevis* ZLB004: CP021456, *L. brevis* phage 3-521: MK504444, *L. brevis* phage 521B: MK504443, *L. brevis* phage 3-SAC12: MK504442, *L. brevis* phage SAC12B: MK504446, *L. brevis* phage ATCCB: MK504445, *L. brevis* phage SA-C12: KU052488, and *L. brevis* phage LBR48: GU967410.

RESULTS AND DISCUSSION

Prophage Identification and Characterization

Lactobacillus brevis contamination of beer is a consistent threat for breweries as its survival and growth in beer cause spoilage thus leading to product withdrawal and economic loss. The food and beverage industries aim to apply more natural, environmentally friendly and safer food preservation methods. Phage bioremediation or sanitation may represent a potential method to prevent bacterial growth and spoilage. LAB strains are known to carry prophage regions which, upon induction, may cause phage particle release and bacterial cell death.

The genomes of nineteen completely sequenced *L. brevis* strains were screened for the presence of prophage-encoding regions using PHASTER (**Table 1**). Of the nineteen bacterial strains of *L. brevis*, twenty-seven intact prophage sequences were predicted ranging from one to four prophage regions per strain. Twenty-three partial (marked as questionable and incomplete according to PHASTER analysis (Zhou et al., 2011; Arndt et al., 2016)) prophage regions were also identified among these strains. Four *L. brevis* strains do not appear to harbor intact prophage regions in their sequences, yet are predicted to carry remnant prophage sequences. The high number of prophage regions (intact and partial) identified shows that prophages are a very common occurrence in *L. brevis* genomes. Predicted intact prophage regions were manually examined and extracted for further analysis (general genome features are detailed in **Table 3**). Among the fifteen *L. brevis* strains whose genomes contain predicted intact prophage regions, *L. brevis* BDGP6 presented the highest number with four such prophage regions ranging in size from 42 to 74 Kb (**Table 3**). Interestingly, *L. brevis* strains SRCM101106 and SRCM101174 harbor an identical prophage, designated TPSRCM101106-3 and TPSRCM101174-3, respectively (100% nucleotide similarity across the full length of their genomes), this can be explained by the similarity between the two *L. brevis* host strains which share 99.8% nt sequence identity across 94% of their genomes. Similarly, *L. brevis* TMW1.2108 harbors two prophage regions that are nearly identical to those present in the genome of TMW1.2111 (TPTMW1-4 and TPTMW1-6, and TPTMW1-5 and TPTMW1-7 bearing 99.99 and 100% nucleotide similarity, respectively) and in *L. brevis* TMW1.2112 and TMW1.2113 sharing a 99.99% nucleotide identical prophage

TABLE 3 | General genome features of *Lactobacillus brevis* intact prophage regions and virulent phages.

Strain name	Phages	Genome size (bp)	ORFs No	GC (%)
Lysogen	**Prophages**			
100D8*	TP100D8	41,993	62	44.6
ATCC 367	TPATCC367	56,030	78	43.4
BDGP6*	TPBDGP6-1	41,938	63	42.1
	TPBDGP6-2	74,412	100	43.6
	TPBDGP6-3	46,262	71	44.9
	TPBDGP6-4	44,732	59	40.8
KB290*	TPKB290-1	43,639	64	44.5
	TPKB290-2	47,873	70	44.3
SA-C12	TPSAC12-1	57,452	83	43.5
	TPSAC12-2	38,492	50	43.4
SRCM101106*	TPSRCM101106-1	48,237	71	43.8
	TPSRCM101106-2	69,528	92	44.2
	TPSRCM101106-3	49,505	74	43.7
SRCM101174*	TPSRCM101174-1	39,697	47	42.2
	TPSRCM101174-2	70,358	97	44.3
	TPSRCM101174-3	49,505	74	43.7
TMW 1.2108*	TPTMW1-4	49,253	74	43.8
	TPTMW1-5	40,616	60	41.5
TMW 1.2111*	TPTMW1-6	49,251	77	43.8
	TPTMW1-7	40,616	61	41.5
TMW 1.2112*	TPTMW1-1	51,644	72	43.6
TMW 1.2113*	TPTMW1-2	51,643	74	43.6
	TPTMW1-3	51,532	76	43.5
UCCLB95	TPMB095	66,077	80	44.1
UCCLBBS124	TPMB124	46,131	73	43.7
UCCLBBS449	TPMB449	50,224	72	43.8
ZLB004*	TPZLB004	68,360	92	43.3
Host	**Virulent phages**			
UCCLB521	3-521	140,816	155	36.9
UCCLB521	521B	136,442	188	32.3
SA-C12	SAC12B	136,608	191	32.4
SA-C12	3-SAC12	41,292	61	40.0
ATTC 367	ATCCB	80,538	96	30.8

**These strains were not tested for prophage induction.*

region (TPTMW1-1 and TPTMW1-2, respectively). These results are perhaps unsurprising as these *L. brevis* strains are more than 99% identical in their genome sequences but mostly differ in their plasmid content (Feyereisen et al., 2019a). The similarities observed in prophage content for some *L. brevis* strains might also be due to the common environment from which these strains have been isolated, i.e., food (South Korea) for *L. brevis* SRCM101106 and SRCM101174 and beer (Germany) for *L. brevis* TMW1.2108, TMW1.2111, TMW1.2112, and TMW1.2113. Integration sites (attL and attR sites) of prophages were identified and are presented in **Supplementary Table S1**. Diversity is observed among these integration sites; however, closely related prophages share the same sites, such as TPSRCM101106-3 and TPSRCM101174-3 or TPBDGP6-1 and TPSAC12-2. Several integration site sequences seem to be shared by certain prophages such as 5′-aaatcctgtactctcctt-3′ which was identified in five genomes. The presence of such sites acts as indicators of potential phage integration and movement, which is important in the context of phage and host evolution, fitness and adaptability in its ecological niche.

Temperate phages can be detrimental for the host if, for example, they switch to a lytic state but they can also be beneficial to the host by carrying genes that will help the strain survive in its environment. These genes may encode phage-resistance systems such as Abi system or Sie proteins as previously identified (Mahony et al., 2008). Abortive infection systems were shown to block phage multiplication leading to the release of few particles and the death of the infected cells allowing the survival of the bacterial overall population (Chopin et al., 2005). Superinfection proteins were identified in *Lactococcus lactis* strains where they were shown to prevent DNA injection of certain phages without affecting phage adsorption (Mahony et al., 2008). Of the 19 *L. brevis* strains studied, nine strains were predicted to carry potential prophage-encoded Sie systems. Meanwhile six were predicted to carry potential prophage-encoded Abi system such as observed in the prophages TPMB124 and TPSRCM101174-3 based on BlastN analysis. These two prophage regions harbor the same potential Abi system which show similarity to the AbiL system identified in *Lactococcus lactis* (Deng et al., 1999). The presence of these potential resistance systems is predicted to confer resistance to the host against phage infection thus increasing the overall host fitness. The absence of such systems in *L. brevis* UCCLB521 or SA-C12 may explain their higher sensitivity to lytic phage infection. Conversely, the presence of potential phage-resistance systems (i.e., Abi) in the prophage of the beer-spoiling *L. brevis* strain UCCLBBS124 could explain its resistance against lytic phage infection (Feyereisen et al., 2019b).

Prophage Inductions

Small scale prophage induction trials were performed for *L. brevis* strain UCCLBBS124. These trials were furthermore applied to ascertain the accuracy of the bioinformatic predictions of likely intact prophages within these genomes. MitC exposure was employed at sub-lethal (0.1–0.3 μg/mL) or lethal concentrations (2 μg/mL) to distinguish between genuine prophage induction-mediated cell lysis and cell death due to acute MitC toxicity. Prophage induction trials with *L. brevis* UCCLBBS124 generated different induction profiles (**Figure 1**), where both sub-lethal and lethal doses of MitC caused cell lysis, indicating that prophage induction may have occurred. Using the lowest concentration of MitC required for prophage induction in UCCLBBS124, phage inductions in other *L. brevis* strains were performed as described: cultures were grown and MitC was added at a sub-lethal concentration of 0.1 μg/mL MitC when the culture reached an OD_{600nm} of 0.1. *L. brevis* strains ATCC 367, SA-C12, UCCLB95, UCCLBBS124, and UCCLBBS449 exhibited lysis upon addition of 0.1 μg/mL MitC indicating prophage induction, cell lysis and phage particle release.

Prophage inductions using 2% v/v formic acid or UV light exposure for 30 min were successful as indicated by PCR validation after phage DNA isolation. However, no apparent prophage induction was observed when acetic acid (2% v/v) or sodium hydroxide (2% v/v) was used as a potential inducing agent (data not shown). While in some cases formic acid and UV treatment appeared to cause cell death, phage particles were not observed by electron microscopy despite positive PCR assay results. This may be due to the detection limit of the microscopy approach limiting the ability to visualize the particles or to the poor growth characteristics of certain cultures (which appear to lyse) thus representing bacteriostasis rather than lysis.

Validation of Prophage Induction

The five *L. brevis* strains that were available for testing showed lysis following induction using 0.1 μg/mL MitC. To further validate that the observed lysis corresponds to phage particle release, filtered cell free supernatants of the induced cultures were analyzed by (i) electron microscopy, (ii) DNA extraction to confirm the prophage sequence using a PCR-based technique, and (iii) structural proteome analysis using mass spectrometry. This was also performed to match a specific prophage sequence to virion morphology in cases where more than one intact prophage region was identified in a bacterial strain such as *L. brevis* SA-C12, which harbors two predicted prophage regions (**Table 3**).

Prophage induction attempts for five *L. brevis* strains, i.e., UCCLBBS124, ATCC 367, SA-C12, UCCLBBS449 and UCCLB95, resulted in the identification of intact virions which in one case was shown to bear morphological characteristics of *Siphoviridae* phages: TPSAC12-2 (induced from SA-C12) which is characterized by a long thin, non-contractile tail (**Figure 2** and **Table 3**), while in three cases *Myoviridae* phages were obtained: TPMB124 (induced from UCCLBBS124), TPATCC367 (induced from ATCC 367), TPMB449 (induced from UCCLBBS449) characterized by a decorated contractile-tailed phage (**Figure 2** and **Table 3**). No phage particles were visible following induction of strain UCCLB95, which indicates that the prophage may not be inducible (to produce detectable virions) under the tested conditions despite causing cell lysis highlighting the limitations of *in silico* analysis. Such predictions have previously been shown to require manual evaluation and assessment in lactococcal prophages thus necessitating induction trials employing various chemical agents and/or UV treatment (Kelleher et al., 2018).

In parallel, PCRs targeting the gene encoding the Tape Measure Protein (TMP) of the temperate phages (**Table 2**) as well as phage structural proteome analysis using mass spectrometry

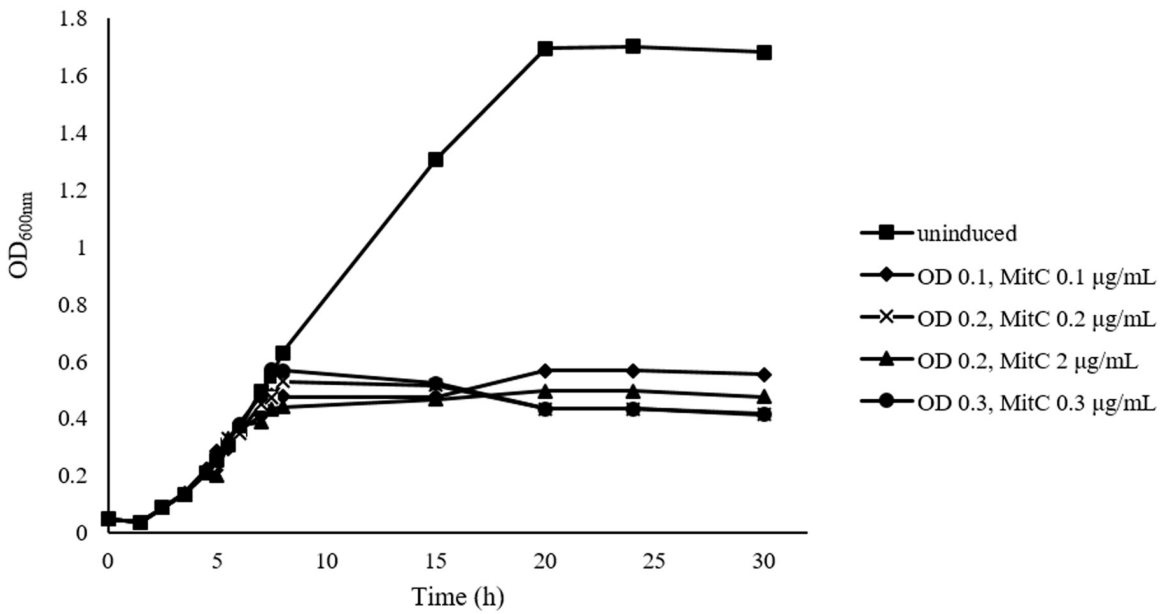

FIGURE 1 | MitC induction profiles of *Lactobacillus brevis* UCCLBBS124. Different concentrations of the inducing agent MitC: 0.1, 0.2, 2, and 0.3 µg/mL were added to the culture after growth of the bacterial strain at an OD_{600nm} of 0.1, 0.2, and 0.3, respectively. An uninduced culture was included as a control (indicated as "uninduced").

(**Table 4** and **Figure 4**) further validated the induction and prophage identification findings. Predicted proteins encoded within the morphogenesis module of the phage genomes of TPSAC12-2, TPMB124, TPATCC367, and TPMB449 were confirmed as structural proteins. Tail proteins, the major capsid protein and the portal protein were identified as structural proteins of the temperate phage TPSAC12-2 confirming the induction of this prophage from strain SA-C12 (no structural proteins matching those encoded by the prophage region TPSAC12-1 were identified, suggesting that this prophage was not induced upon MitC treatment) (**Table 4**). The minor capsid protein and three hypothetical proteins were confirmed as structural proteins of the prophage region TPMB124 (**Table 4**). More than ten proteins of TPATCC367 were identified as structural proteins among which the tape measure protein, the head protein and the major capsid protein (**Table 4**). Structural proteins of the temperate phage TPMB449 were identified by mass spectrometry including the capsid, head, and portal proteins. Some predicted structural proteins were not identified in the experimentally determined proteome, most likely due to their small size or their low relative abundance.

Morphology of *L. brevis* Phages

Electron microscopic analysis of *L. brevis* phages available to date were gathered, providing insights into the morphological diversity among *L. brevis* phages. From these analyses, three distinct morphologies were observed (**Figure 2**). Firstly, *Myoviridae* phages which exhibit imposing head structures and contractile tails ranging from 166 to 201.9 nm incorporating an organelle at the tail tip called a baseplate were termed *Myoviridae* Morphotype I phages (**Figure 2**). They are represented by the virulent phages 3-521, 521B, SAC12B (Feyereisen et al., 2019b), and SA-C12 (Deasy et al., 2011).

Secondly, *L. brevis* phages such as 3-SAC12, TPATCC367, TPMB124 and TPMB449 also belong to the *Myoviridae* family, although their common morphology differs from that of the virulent *Myoviridae* Morphotype I phages mentioned above (Feyereisen et al., 2019b). In this case, their morphology is represented by a small head structure and a decorated tail with a discrete baseplate, termed here as *Myoviridae* Morphotype II phages (**Figure 2**). This morphology is similar to the one observed for the prophage LBR48 (Jang et al., 2011) and interestingly, varying tail lengths were observed for phages of this morphotype (**Figure 2**).

Finally, some *L. brevis* phages were classified as members of the *Siphoviridae* family. Phages from this group, ATCCB and TPSAC12-2, are characterized as possessing a long non-contractile tail and an icosahedral head and were termed Morphotype III phages (**Figure 2**).

L. brevis Phage Phylogeny

In order to gain insight into the phylogeny of *L. brevis* prophages, a proteomic tree was constructed with all available sequences of *L. brevis* phages (virulent and temperate). Phylogenetic analysis resulted in the identification of five different groups (**Figure 3**) highlighting the apparent uniqueness of *L. brevis* phages. The virulent *Myoviridae* phages previously studied (Feyereisen et al., 2019b) were gathered in group I. Group II

TABLE 4 | Structural proteins extracted from purified phage particles by ESI-MS/MS.

Phage	ORF	Putative function	No. of peptides	Sequence coverage (%)
TPSAC12-2	SAC12_1335	Tail fiber protein	2	7.7
	SAC12_1361	Tail protein	5	30.2
	SAC12_1366	Major capsid protein	14	39.8
	SAC12_1368	Portal protein	4	19.8
TPMB124	UCCLBBS124_1395	Hypothetical protein	3	22.8
	UCCLBBS124_1396	Hypothetical protein	2	5.7
	UCCLBBS124_1402	Minor capsid protein	3	10.1
	UCCLBBS124_1457	Hypothetical protein	2	12.6
TPATCC367	LVIS_1073	Hypothetical protein	7	66.3
	LVIS_1080	Hypothetical protein	17	42.1
	LVIS_1081	Hypothetical protein	2	9.9
	LVIS_1084	Hypothetical protein	2	16.9
	LVIS_1085	Hypothetical protein	2	6.0
	LVIS_1087	Lysozyme	8	19.8
	LVIS_1088	Tape measure protein	24	13.2
	LVIS_1090	Hypothetical protein	6	38.9
	LVIS_1091	Hypothetical protein	7	49.4
	LVIS_1092	Hypothetical protein	12	56.4
	LVIS_1098	Major capsid protein	16	59.8
	LVIS_1099	Head protein	3	23.3
	LVIS_1102	Hypothetical protein	6	18.1
	LVIS_1128	Helicase	4	9.9
TPMB449	UCCLBBS449_1616	Hypothetical protein	5	10.6
	UCCLBBS449_1629	Hypothetical protein	3	33.3
	UCCLBBS449_1630	Structural protein	7	24.6
	UCCLBBS449_1636	Capsid protein	12	62.7
	UCCLBBS449_1638	Head protein	2	6.5
	UCCLBBS449_1641	Portal protein	3	6.2

A minimum of two independent unique peptides or 5% coverage were used as threshold values.

comprises twenty-one (one virulent and twenty temperate phages) *L. brevis* phages and phages of this group for which the family is known are all part of the *Myoviridae* family. Meanwhile group III gathers phages of the *Siphoviridae* family (when phage family is known). Groups IV and V each comprise of a single prophage sequence with distinct genetic composition and as yet unknown morphology (**Figure 3**). Interestingly, the majority of phages belong to the *Myoviridae* family, which is unusual among phages of LAB where *Siphoviridae* phages are more typically reported (Brüssow and Desiere, 2001; Casey et al., 2015; Kelleher et al., 2018).

Classification of *L. brevis* Phages

To date, limited studies of *L. brevis* phages have been undertaken despite the commercial relevance of this bacterial species and its associated bacteriophages (Deasy et al., 2011; Jang et al., 2011). Here, we propose a classification of *L. brevis* phages similar to what has previously been undertaken for *Leuconostoc* phages (Kot et al., 2014) based on morphology, phylogeny and genomic diversity. The classification suggested here, divides *L. brevis* phages into five groups, I to V, linking the phylogeny and morphology analyses as described above.

The group I observed on the proteomic tree (**Figure 3**), gathers virulent *Myoviridae* Morphotype I phages (**Figure 2**). They are further divided into three subgroups based on their genetic diversity level, phage 3-521 (Ia), phages 521B and SAC12B (Ib) sharing 97% nucleotide similarity (88% coverage) and finally SA-C12 (Ic). The previously described (Feyereisen et al., 2019b) phages 3-521, 521B and SAC12B are characterized by a large genome size (>136 Kb), probably in line with their imposing head structure, and a high degree of synteny throughout their genomes. Phage SA-C12 presents a similar morphology, yet harbors a smaller genome (79 Kb) (Deasy et al., 2011). The genome of SA-C12 is quite divergent and seems to be missing a certain number of genes encoding for hypothetical proteins and proteins involved in the replication process compared to other phages of this group.

Group II (**Figure 3**) is represented by *Myoviridae* Morphotype II phages (**Figure 2**), thereby encompassing over half of the *L. brevis* phages. Genomic and morphological analysis of representative isolates suggest that all members of this group belong to the *Myoviridae* family. Based on their genetic diversity, group II phages are divided here into four subgroups (**Figure 3**). The subgroup IIa is comprised of the virulent phage 3-SAC12 (40 Kb) which has previously been described

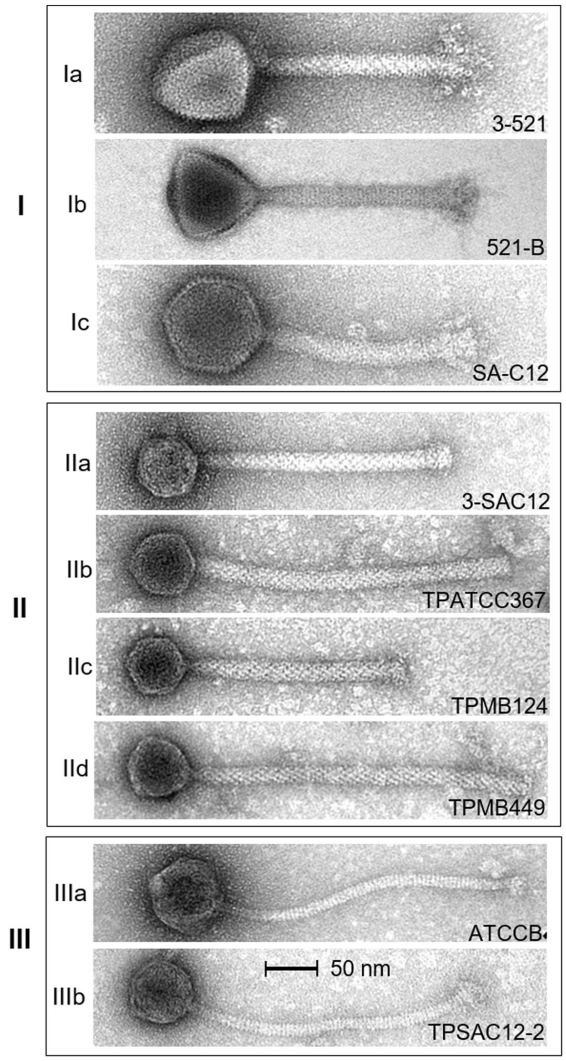

FIGURE 2 | Electron micrographs of *L. brevis* phages representing morphotypes I to III. Ia, virulent phage 3-521; Ib, virulent phage 521B (Feyereisen et al., 2019b); and Ic, virulent phage SA-C12 (Deasy et al., 2011). IIa, virulent phage 3-SAC12 (Feyereisen et al., 2019b); IIb, temperate phage TPATCC367 induced from the *L. brevis* strain ATCC 367; IIc, temperate phage TPMB124 induced from the *L. brevis* strain UCCLBBS124; and IId, temperate phage TPMB449 induced from the *L. brevis* strain UCCLBBS449. IIIa, virulent phage ATCCB (Feyereisen et al., 2019b) and IIIb, temperate phage TPSAC12-2 induced from the *L. brevis* strain SA-C12. Temperate phages were induced from *L. brevis* strains using 0.1 μg/mL MitC.

(Feyereisen et al., 2019b). Subgroup IIb is composed of six temperate phages, including TPATCC367 (**Figure 2**), which share around 90% nucleotide similarity (78% sequence coverage) and harbor a larger genome (average of 62 Kb) compared to other group II members. Subgroup IIc gathers temperate phages TPBDGP6-3 and TPMB124 with an average genome size of 46 Kb and sharing 92% nucleotide similarity (56% sequence coverage). The biggest subgroup, subgroup IId, comprises twelve temperate phages sharing at least 90% nucleotide similarity (55% sequence coverage) and harboring a genome with an average size of 49 Kb.

In depth comparative analysis highlighted the degree of amino acid similarity between these *Myoviridae* Morphotype II phages. Although divergence occurs within these phages, genomic synteny is observed and the genomes are organized into modules corresponding to DNA packaging, structure, lysis/lysogeny and replication (**Figure 4**). Different tail lengths were observed for phages belonging to the group II (**Figure 2**) and, as previously described, the length of the tail seems to be linked to the size of the TMP gene (Mahony et al., 2016a). Indeed, phages belonging to the group IIc and presenting the smallest tail (**Figure 2**), have on average a TMP-encoding gene of 4.82 Kb, while phages belonging to the group IIb and IId which present the longest tailed-phages (**Figure 2**) possess a TMP-encoding gene with an average size of 5.67 and 5.50 Kb, respectively (**Figure 4**). Proteins encoding holin and lysozyme (lysin) are highly conserved across the representative phages (more than 70% amino acid (aa) similarity). The virulent phage 3-SAC12 (IIa) and the temperate phages TPMB095 (IIb) and TPMB124 (IIc) revealed low levels of similarity (between 30 and 50% aa similarity) across their structural modules. Surprisingly, only temperate phage TPMB095 lacks sequence homology with other phages of this group in the region encoding the baseplate structure. The absence of such genes may be partly responsible for the inability of TPMB095 to form functional phage and thus was not inducible. Furthermore, the genome appears quite decayed with several transposase elements interjecting the genome and the overall genome appears to lack architectural conservation compared to many other phages of LAB. *L. brevis* prophages LBR48, TPMB449, and TPSAC12-1 (IId) share a high level of similarity (more than 70% aa similarity) across the entire packaging, structural and lysis module (**Figure 4**). They also share between 30 and 50% aa similarity between their predicted integrase proteins.

Group III (**Figure 3**) is represented by temperate and virulent phages, and gathers members of the *Siphoviridae* family (e.g., ATCCB and TPSAC12-2) characterized as Morphotype III (**Figure 2**). Other lysogenic bacteria carrying prophages of this group were not available for prophage induction, therefore their morphotype remains unknown. It is likely that they belong to the *Siphoviridae* family as they are most closely related to the siphophage TPSAC12-2. The group III is divided into two subgroups separating the virulent phage ATCCB (IIIa) with a genome size of approximately 80 Kb and five temperate phages (IIIb) harboring smaller genomes (size of around 40 Kb) and among which the siphophage TPSAC12-2 can be found (**Figure 3**). Representatives of group III for which electron microscopy images (where available) were chosen for further comparative analysis (**Figure 4**). Virulent phage ATCC-B and temperate phage TPSAC12-2 share synteny in terms of genome organization with the DNA packaging module followed by the structural module, the lysis/lysogeny module and the replication module. The two phages share a low level of similarity, yet synteny and aa similarity of around 30% across the DNA packaging and structural modules with proteins encoding terminase, capsid, and tail morphogenesis-associated

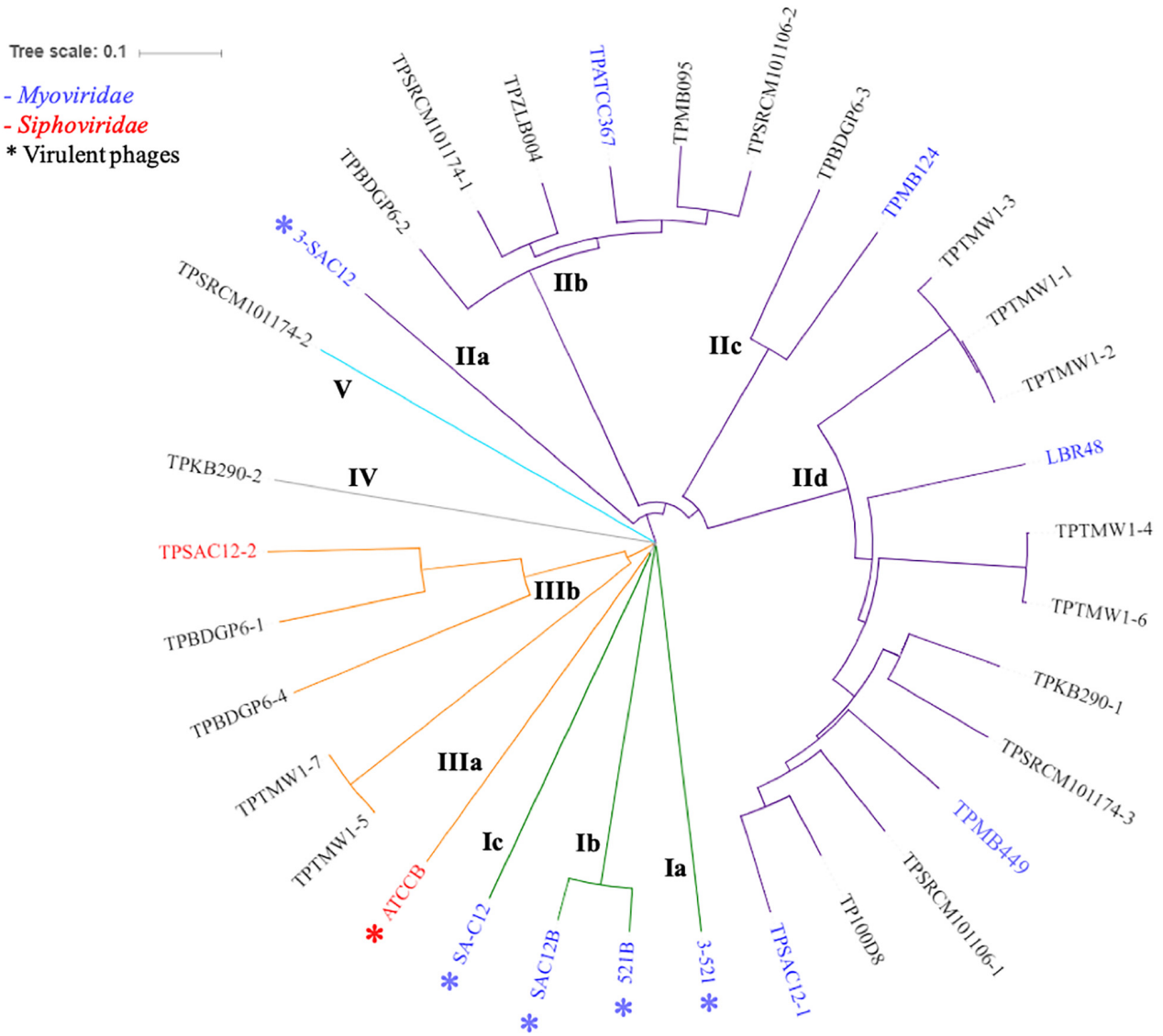

FIGURE 3 | Proteomic tree of *L. brevis* phages available so far: virulent (annotated with *) and temperate phages. The phylogenetic analysis revealed five distinct groups (I to V) highlighted by different colors on the tree (green I, purple II, orange III, gray IV, and light blue V). *Myoviridae* phages are labeled in blue, while *Siphoviridae* phages are labeled in red.

functions were observed. Temperate phage TPSAC12-2, unlike virulent phage ATCC-B, harbors ORFs encoding predicted lysogeny functions, such as a Cro/Cl repressor and an antirepressor (**Figure 4**).

Groups IV and V contain single members, i.e., prophages TPKB290-2 and TPSRCM101174-2, respectively, and do not share any significant sequence similarity to the other groups. The morphology of these phages is unknown and based on their genome analysis it is difficult to derive assumptions on the morphology/classification of TPSRCM101174-2. However, based on TPKB290-2 sequence data, a gene encoding a sheath protein is predicted suggesting that this phage is a *Myoviridae* member.

Induced temperate phages were tested for their potential ability to infect the seven *L. brevis* strains that were available in our collection (**Table 1**). However, these phages did not show any activity against the tested strains. Interestingly, the repressors encoded by prophages of *L. brevis* do not share widespread sequence homology indicating that homo-immunity based on the activity of repressors is not the basis of the observed phage-resistance. It is likely that the observed phage-resistance is due to the use of alternative receptors on the cell surface by different phage groups or through the activity of phage-resistance mechanisms such as abortive infection systems.

In order to evaluate the diversity of *L. brevis* phages in relation to other *Lactobacillus* phages, a proteomic tree was created gathering *L. brevis* phages described in this study as well as previously sequenced *Lactobacillus* phages (**Supplementary Figure S1**). The phylogenetic tree clearly shows the distinct grouping of *L. brevis* phages separately to other *Lactobacillus*

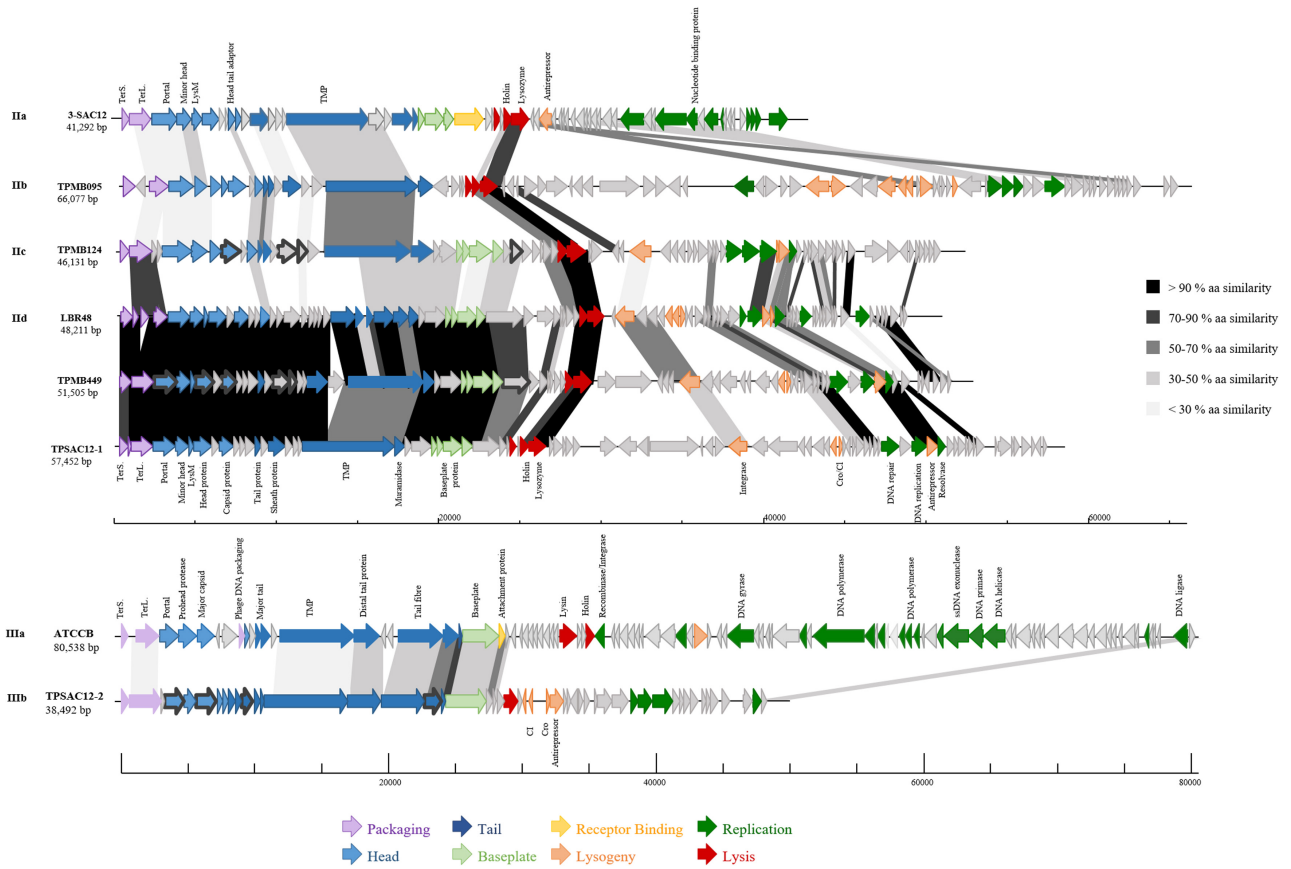

FIGURE 4 | Genomic organization of representatives of *L. brevis* phages belonging to group II (*Myoviridae* Morphotype II phages): (IIa) 3-SAC12, (IIb) TPMB095, (IIc) TPMB124, (IId) LBR48, TPMB449 and TPSAC12-1, and group III: (IIIa) ATCCB and (IIIb) TPSAC12-2. The scale at the bottom of genomes is in base pairs. Each arrow represents an ORF, with the color representing the putative function of the encoded protein. Shaded boxes match the percentage of amino acid similarity between ORFs (TerS, small terminase; TerL, large terminase; and TMP, tape measure protein). Confirmed structural protein-encoding genes from mass spectrometry analysis are also highlighted (dark gray bold outline).

phages. However, some *L. brevis* phages showed similarity with phages infecting other species such as observed for the *L. brevis* phage SA-C12 and the *Lb. plantarum* phage 8014-B2.

CONCLUSION

The genomes of nineteen bacterial strains of *L. brevis* analyzed in this study all harbor predicted prophage regions and twenty-seven intact prophage regions were identified. Only four *L. brevis* strains do not appear to contain intact prophage regions in their genomes. These numbers reveal the high incidence of prophages among *L. brevis* genomes with an average of 1.4 prophage region per strain. Of the five *L. brevis* strains available for prophage induction trials, four prophages were successfully induced and morphologically characterized by electron microscopy indicating a significant incidence of inducibility of these temperate phages. Electron microscopy observations, genome sequence analyses, and phylogeny allowed the classification of *L. brevis* phages into five groups, I to V. The results show substantial diversity among *L. brevis* phages and interestingly these entities are mostly represented by members of the *Myoviridae* family, unlike the majority of LAB phages.

The potential of prophages as antimicrobial agents in beer fermentation is a promising alternative to currently employed processes. Prophage induction in beer-spoiling *L. brevis* strain could be used during the cleaning process (such as coupled with sanitizers and/or UV treatment). However, this approach presents challenges and hurdles (i.e., scale-up for industrial settings and phage-encoded resistance mechanisms) that need to be addressed before their use in industry as bacterial spoilage control. To date, very few *L. brevis* phages have been characterized and the identification and characterization of additional phages will provide greater insights into *L. brevis* phage biodiversity and their potential application and role in food spoilage prevention.

DATA AVAILABILITY STATEMENT

All datasets generated for this study are included in the manuscript/**Supplementary Files**.

AUTHOR CONTRIBUTIONS

MF performed the experiments, annotation, genomic, and proteomic analysis. HN and CF carried out the electron microscopy analysis. J-PN carried out the mass spectrometry analysis. DS, JM, TO'S, and VB provided the materials and strains. MF, JM, TO'S, and DS were involved in project design and wrote the manuscript. All authors read and approved the final manuscript.

FUNDING

MF is the recipient of an Irish Research Council Enterprise Partnership Scheme postgraduate scholarship (Ref. No. EPSPG/2015/7). DS is supported by a Principal Investigator award (Ref. No. 450 13/IA/1953) through the Science Foundation Ireland (SFI). JM is in receipt of a Starting Investigator Research Grant (SIRG) (Ref. No. 15/SIRG/3430) funded by the Science Foundation Ireland (SFI).

ACKNOWLEDGMENTS

The authors acknowledge the technical help of Angela Back (Max Rubner-Institut, Kiel) in the electron microscopic analysis and Johan Mathijs for technical assistance in mass spectrometry.

SUPPLEMENTARY MATERIAL

The Supplementary Material for this article can be found online at: https://www.frontiersin.org/articles/10.3389/fmicb.2019.02396/full#supplementary-material

REFERENCES

Altschul, S., Gish, W., Miller, W., Myers, E., and Lipman, D. (1990). Basic local alignment search tool. *J. Mol. Biol.* 215, 403–410. doi: 10.1016/s0022-2836(05)80360-2

Altschul, S. F., Madden, T. L., Schaffer, A. A., Zhang, J., Zhang, Z., Miller, W., et al. (1997). Gapped BLAST and PSI-BLAST: a new generation of protein database search programs. *Nucleic Acids Res.* 25, 3389–3402. doi: 10.1093/nar/25.17.3389

Arndt, D., Grant, J. R., Marcu, A., Sajed, T., Pon, A., Liang, Y., et al. (2016). PHASTER: a better, faster version of the PHAST phage search tool. *Nucleic Acids Res.* 44, W16–W21. doi: 10.1093/nar/gkw387

Bokulich, N. A., and Bamforth, C. W. (2013). The microbiology of malting and brewing. *Microbiol. Mol. Biol. Rev.* 77, 157–172. doi: 10.1128/MMBR.00060-12

Brüssow, H. (2001). Phages of dairy bacteria. *Ann. Rev. Microbiol.* 55, 283–303. doi: 10.1146/annurev.micro.55.1.283

Brüssow, H., and Desiere, F. (2001). Comparative phage genomics and the evolution of *Siphoviridae*: insights from dairy phages. *Mol. Microbiol.* 39, 213–222.

Canchaya, C., Proux, C., Fournous, G., Bruttin, A., and Brüssow, H. (2003). Prophage genomics. *Microbiol. Mol. Biol. Rev.* 67, 238–276.

Casey, E., Mahony, J., Neve, H., Noben, J.-P., Dal Bello, F., and van Sinderen, D. (2015). Novel phage group infecting *Lactobacillus* delbrueckii subsp. lactis, as revealed by genomic and proteomic analysis of bacteriophage Ldl1. *Appl. Environ. Microbiol.* 81, 1319–1326. doi: 10.1128/aem.03413-14

Ceyssens, P.-J., Mesyanzhinov, V., Sykilinda, N., Briers, Y., Roucourt, B., Lavigne, R., et al. (2008). The genome and structural proteome of YuA, a new *Pseudomonas aeruginosa* phage resembling M6. *J. Bacteriol.* 190, 1429–1435. doi: 10.1128/jb.01441-07

Chopin, A., Bolotin, A., Sorokin, A., Ehrlich, S. D., and Chopin, M. C. (2001). Analysis of six prophages in *Lactococcus lactis* IL1403: different genetic structure of temperate and virulent phage populations. *Nucleic Acids Res.* 29, 644–651. doi: 10.1093/nar/29.3.644

Chopin, M.-C., Chopin, A., and Bidnenko, E. (2005). Phage abortive infection in lactococci: variations on a theme. *Curr. Opin. Microbiol.* 8, 473–479. doi: 10.1016/j.mib.2005.06.006

Chopin, M. C., Chopin, A., Rouault, A., and Galleron, N. (1989). Insertion and amplification of foreign genes in the *Lactococcus lactis* subsp. *lactis chromosome*. *Appl. Environ. Microbiol.* 55, 1769–1774.

Davidson, B. E., Powell, I. B., and Hillier, A. J. (1990). Temperate bacteriophages and lysogeny in lactic acid bacteria. *FEMS Microbiol. Lett.* 87, 79–90. doi: 10.1016/0378-1097(90)90698-p

Deasy, T., Mahony, J., Neve, H., Heller, K. J., and van Sinderen, D. (2011). Isolation of a virulent *Lactobacillus brevis* phage and its application in the control of beer spoilage. *J. Food Prot.* 74, 2157–2161. doi: 10.4315/0362-028x.jfp-11-262

Deng, Y.-M., Liu, C. Q., and Dunn, N. (1999). Genetic organization and functional analysis of a novel phage abortive infection system, AbiL, from *Lactococcus lactis*. *J. Biotechnol.* 67, 135–149. doi: 10.1016/S0168-1656(98)00175-8

Feyereisen, M., Mahony, J., Kelleher, P., Roberts, R. J., O'Sullivan, T., Geertman, J.-M. A., et al. (2019a). Comparative genome analysis of the *Lactobacillus brevis* species. *BMC Genomics* 20:416. doi: 10.1186/s12864-019-5783-1

Feyereisen, M., Mahony, J., Lugli, G. A., Ventura, M., Neve, H., Franz, C. M. A. P., et al. (2019b). Isolation and characterization of *Lactobacillus brevis* phages. *Viruses* 11:E393.

Forde, A., and Fitzgerald, G. F. (1999). Bacteriophage defence systems in lactic acid bacteria. *Antonie van Leeuwenhoek* 76, 89–113. doi: 10.1023/a:1002027321171

Forsman, P. (1993). Characterization of a prolate-headed bacteriophage of *Lactobacillus delbrueckii* subsp. lactis, and its DNA homology with isometric-headed phages. *Arch. Virol.* 132, 321–330. doi: 10.1007/bf01309542

Fraunhofer, M. E., Geissler, A. J., Wefers, D., Bunzel, M., Jakob, F., and Vogel, R. F. (2018). Characterization of β-glucan formation by *Lactobacillus brevis* TMW 1.*2112* isolated from slimy spoiled beer. *Int. J. Biol. Macromol.* 107, 874–881. doi: 10.1016/j.ijbiomac.2017.09.063

Fukao, M., Oshima, K., Morita, H., Toh, H., Suda, W., Kim, S. W., et al. (2013). Genomic analysis by deep sequencing of the probiotic *Lactobacillus brevis* KB290 harboring nine plasmids reveals genomic stability. *PLoS One* 8:e60521. doi: 10.1371/journal.pone.0060521

Garofalo, C., Osimani, A., Milanovic, V., Taccari, M., Aquilanti, L., and Clementi, F. (2015). The occurrence of beer spoilage lactic acid bacteria in craft beer production. *J. Food Sci.* 80, 2845–2852. doi: 10.1111/1750-3841.13112

Holtappels, M., Vrancken, K., Schoofs, H., Deckers, T., Remans, T., Noben, J. P., et al. (2015). A comparative proteome analysis reveals flagellin, chemotaxis regulated proteins and amylovoran to be involved in virulence differences between *Erwinia amylovora* strains. *J. Proteom.* 123, 54–69. doi: 10.1016/j.jprot.2015.03.036

Husson-Kao, C., Mengaud, J., Cesselin, B., van Sinderen, D., Benbadis, L., and Chapot-Chartier, M.-P. (2000). The *Streptococcus thermophilus* autolytic phenotype results from a leaky prophage. *Appl. Environ. Microbiol.* 66, 558–565. doi: 10.1128/aem.66.2.558-565.2000

Hyatt, D., Chen, G.-L., LoCascio, P. F., Land, M. L., Larimer, F. W., and Hauser, L. J. (2010). Prodigal: prokaryotic gene recognition and translation initiation site identification. *BMC Bioinformatics* 11:119. doi: 10.1186/1471-2105-11-119

Jang, S. H., Yoon, B. H., and Chang, H. I. (2011). Complete nucleotide sequence of the temperate bacteriophage LBR48, a new member of the family *Myoviridae*. *Arch. Virol.* 156, 319–322. doi: 10.1007/s00705-010-0841-7

Kelleher, P., Mahony, J., Schweinlin, K., Neve, H., Franz, C., and van Sinderen, D. (2018). Assessing the functionality and genetic diversity of lactococcal prophages. *Int. J. Food Microbiol.* 272, 29–40. doi: 10.1016/j.ijfoodmicro.2018.02.024

Kot, W., Neve, H., Heller, K. J., and Vogensen, F. K. (2014). Bacteriophages of *Leuconostoc, Oenococcus*, and *Weissella*. *Front. Microbiol.* 5:186. doi: 10.3389/fmicb.2014.00186

Kumar, S., Nei, M., Dudley, J., and Tamura, K. (2008). MEGA: a biologist-centric software for evolutionary analysis of DNA and protein sequences. *Brief. Bioinform.* 9, 299–306. doi: 10.1093/bib/bbn017

Lavelle, K., Murphy, J., Fitzgerald, B., Lugli, G. A., Zomer, A., Neve, H., et al. (2018). A decade of *Streptococcus thermophilus* phage evolution in an Irish dairy plant. *Appl. Environ. Microbiol.* 84:e02855-17. doi: 10.1128/aem.02855-17

Loeffler, D. (2006). "Modern brewery sanitation," in *Brewing New Technologies*, ed C. W. Bamforth (Sawston: Woodhead Publishing).

Lunde, M., Blatny, J. M., Lillehaug, D., Aastveit, A. H., and Nes, I. F. (2003). Use of real-time quantitative PCR for the analysis of φLC3 prophage stability in lactococci. *Appl. Environ. Microbiol.* 69, 41–48. doi: 10.1128/aem.69.1.41-48.2003

Madera, C., García, P., Rodríguez, A., Suárez, J. E., and Martínez, B. (2009). Prophage induction in *Lactococcus lactis* by the bacteriocin *Lactococcin* 972. *Int. J. Food Microbiol.* 129, 99–102. doi: 10.1016/j.ijfoodmicro.2008.11.004

Mahony, J., Alqarni, M., Stockdale, S., Spinelli, S., Feyereisen, M., Cambillau, C., et al. (2016a). Functional and structural dissection of the tape measure protein of *Lactococcal* phage TP901-1. *Sci. Rep.* 6:36667. doi: 10.1038/srep36667

Mahony, J., McDonnell, B., Casey, E., and van Sinderen, D. (2016b). Phage-host interactions of cheese-making lactic acid bacteria. *Ann. Rev. Food Sci. Technol.* 7, 267–285. doi: 10.1146/annurev-food-041715-0

Mahony, J., McGrath, S., Fitzgerald, G. F., and van Sinderen, D. (2008). Identification and characterization of lactococcal-prophage-carried superinfection exclusion genes. *Appl. Environ. Microbiol.* 74, 6206–6215. doi: 10.1128/aem.01053-08

Makarova, K., Slesarev, A., Wolf, Y., Sorokin, A., Mirkin, B., and Koonin, E. (2006). Comparative genomics of the lactic acid bacteria. *Proc. Natl. Acad. Sci. U.S.A.* 103, 15611–15616. doi: 10.1073/pnas.0607117103

Meijer, W., Dobbelaar, C., and Hugenholtz, J. (1998). Thermoinducible lysis in *Lactococcus lactis* subsp. *cremoris SK*110: implications for cheese ripening. *Int. Dairy J.* 8, 275–280. doi: 10.1016/S0958-6946(98)00052-1

Mittler, J. E. (1996). Evolution of the genetic switch in temperate bacteriophage. I. basic theory. *J. Theor. Biol.* 179, 161–172. doi: 10.1006/jtbi.1996.0056

Rutherford, K., Parkhill, J., Crook, J., Horsnell, T., Rice, P., Rajandream, M., et al. (2000). Artemis: sequence visualization and annotation. *Bioinformatics* 16, 944–945. doi: 10.1093/bioinformatics/16.10.944

Schattner, P., Brooks, A. N., and Lowe, T. M. (2005). The tRNAscan-SE, snoscan and snoGPS web servers for the detection of tRNAs and snoRNAs. *Nucleic Acids Res.* 33, W686–W689. doi: 10.1093/nar/gki366

Schmidt, R. H. (1997). *Basic Elements of Equipment Cleaning and Sanitizing in Food Processing and Handling Operations*. Florida: University of Florida.

Söding, J., Biegert, A., and Lupas, A. N. (2005). The HHpred interactive server for protein homology detection and structure prediction. *Nucleic Acids Res.* 33, W244–W248. doi: 10.1093/nar/gki408

Suzuki, K., Iijima, K., Sakamoto, K., Sami, M., and Yamashita, H. (2006). A review of hop resistance in beer spoilage lactic acid bacteria. *J. Inst. Brew.* 112, 173–191. doi: 10.1002/j.2050-0416.2006.tb00247.x

Thompson, J. D., Gibson, T. J., and Higgins, D. G. (2002). Multiple sequence alignment using ClustalW and ClustalX. *Curr. Protoc. Bioinform.* 2.3.1–2.3.22. doi: 10.1002/0471250953.bi0203s00

Vaughan, A., O'Sullivan, T., and van Sinderen, D. (2005). Enhancing the microbiological stability of malt and beer – a review. *J. Inst. Brew.* 111, 355–371. doi: 10.1002/j.2050-0416.2005.tb00221.x

Villion, M., and Moineau, S. (2009). Bacteriophages of *Lactobacillus*. *Front. Biosci.* 14, 1661–1683.

Wu, Q., Law, Y. S., and Shah, N. P. (2015). Dairy *Streptococcus thermophilus* improves cell viability of *Lactobacillus brevis* NPS-QW-145 and its γ-aminobutyric acid biosynthesis ability in milk. *Sci. Rep.* 5:12885. doi: 10.1038/srep12885

Zhou, Y., Liang, Y., Lynch, K. H., Dennis, J. J., and Wishart, D. S. (2011). PHAST: a fast phage search tool. *Nucleic Acids Res.* 39, 347–352. doi: 10.1093/nar/gkr485

Conflict of Interest: VB and TO'S are employees of Heineken.

The remaining authors declare that the research was conducted in the absence of any commercial or financial relationships that could be construed as a potential conflict of interest.

Copyright © 2019 Feyereisen, Mahony, Neve, Franz, Noben, O'Sullivan, Boer and van Sinderen. This is an open-access article distributed under the terms of the Creative Commons Attribution License (CC BY). The use, distribution or reproduction in other forums is permitted, provided the original author(s) and the copyright owner(s) are credited and that the original publication in this journal is cited, in accordance with accepted academic practice. No use, distribution or reproduction is permitted which does not comply with these terms.

frontiers in Microbiology

ORIGINAL RESEARCH
published: 31 October 2019
doi: 10.3389/fmicb.2019.02484

Natural Occurrence of *Escherichia coli*-Infecting Bacteriophages in Clinical Samples

*Cátia Pacífico[1,2], Miriam Hilbert[1,2], Dmitrij Sofka[1], Nora Dinhopl[3], Ildiko-Julia Pap[4], Christoph Aspöck[2,4], João André Carriço[5] and Friederike Hilbert[1]**

[1] Department of Farm Animals and Veterinary Public Health, Institute of Food Safety, Food Technology and Veterinary Public Health, University of Veterinary Medicine, Vienna, Austria, [2] Karl Landsteiner University of Health Sciences, Krems, Austria, [3] Department of Pathobiology, University of Veterinary Medicine, Vienna, Austria, [4] Institute of Hygiene and Microbiology, University Hospital St. Pölten, St. Pölten, Austria, [5] Faculty of Medicine, Instituto de Medicina Molecular, University of Lisbon, Lisbon, Portugal

The interaction between bacteriophages, bacteria and the human host as a tripartite system has recently captured attention. The taxonomic diversity of bacteriophages, as a natural parasite of bacteria, still remains obscure in human body biomes, representing a so-called "viral dark matter." Here, we isolated and characterized coliphages from blood, urine and tracheal aspirates samples collected at a tertiary care hospital in Austria. Phages were more often isolated from blood, followed by urine and tracheal aspirates. Phylogenetic analysis and genome comparisons allowed the identification of phages belonging to the *Tunavirinae* subfamily, and to the *Peduovirus* and *Tequintavirus* genera. *Tunavirinae* phages cluster together and are found in samples from 14 patients, suggesting their prevalence across a variety of human samples. When compared with other phage genomes, the highest similarity level was at 87.69% average nucleotide identity (ANI), which suggests that these are in fact a newly isolated phage species. *Tequintavirus* phages share a 95.90% with phage 3_29, challenging the ANI threshold currently accepted to differentiate phage species. The isolated phages appear to be virulent, with the exception of the *Peduovirus* members, which are integrative and seem to reside as prophages in bacterial genomes.

Keywords: bacteriophages, urine, tracheal aspirates, blood, *E. coli*, *Peduovirus*, *Tunavirinae*, *Tequintavirus*

OPEN ACCESS

Edited by:
Krishna Khairnar,
National Environmental Engineering Research Institute (CSIR), India

Reviewed by:
Mahesh Dharne,
National Chemical Laboratory (CSIR), India
Ahmed Askora,
Zagazig University, Egypt
Andrea Isabel Moreno Switt,
Universidad Andrés Bello, Chile

****Correspondence:***
Friederike Hilbert
friederike.hilbert@vetmeduni.ac.at

Specialty section:
This article was submitted to Virology, a section of the journal Frontiers in Microbiology

Received: *02 July 2019*
Accepted: *15 October 2019*
Published: *31 October 2019*

Citation:
Pacífico C, Hilbert M, Sofka D, Dinhopl N, Pap I-J, Aspöck C, Carriço JA and Hilbert F (2019) Natural Occurrence of Escherichia coli-Infecting Bacteriophages in Clinical Samples. Front. Microbiol. 10:2484. doi: 10.3389/fmicb.2019.02484

INTRODUCTION

E. coli, a bacterium that inhabits the gastrointestinal tract of humans and warm-blooded animals, is the most prevalent commensal bacteria. It represents the most frequent cause of infections in healthcare settings and in the community, and it is the reason for most bloodstream infections in Europe (Weinbauer, 2004). Additionally, it is involved in the development of bacterial diseases such as enteritis, neonatal meningitis, urinary tract infections, bloodstream infections and intra-abdominal infections (Allocati et al., 2013; European Centre for Disease Prevention and Control, 2016).

It had been previously demonstrated that phages have an impact on bacterial pathogenesis by carrying virulence factors, antimicrobial resistance genes, and host adaptation factors (Brussow et al., 2004). As important vehicles of horizontal gene transfer, phages contribute

significantly to the strain-to-strain differences observed within the same bacterial species (Desiere et al., 2001). They tend to infect specific isolates or groups of isolates of closely related species, particularly in the *Enterobacteriaceae* family, but some viruses can infect members of several genera (King et al., 2012). A predominant narrow host-range keeps the bacterial populations under control, retaining the balance of competitively dominant species or populations (Weinbauer, 2004).

Phages are typically found and transmitted in terrestrial and aqueous environments, even though they can be retrieved in any environment where their bacterial hosts are present (Weinbauer, 2004; McNair et al., 2012). Coliphages – bacteriophages that target specifically *Escherichia coli* strains – have been used as indicator for fecal coliforms and enteric viruses for water pollution (International Organization for Standardization, 2000). In this context, coliphages have been isolated in clinical settings from hospital effluents (Bibi et al., 2016; Latz et al., 2017; Peng and Yuan, 2018) and human body biomes such as the gastrointestinal tract, oral cavity, saliva, sputum, and urine (Górski and Weber-Dabrowska, 2005; Hyman and Abedon, 2012). The human body, as an ecosystem, consists of a significant amount of viral dark matter (Kowarsky et al., 2017; Thannesberger et al., 2017). This refers to the amount of unidentified phage sequences, estimated around 85% in the human gut while known prophages and temperate phages comprise the remaining part. In comparison to the high diversity in free-living bacterial communities, the number of phages per bacterial species in the human gut is reported to be quite reduced (Reyes et al., 2010). These phages are thought to be associated with the bacteria in the background microbial flora (Kowarsky et al., 2017). Metagenomics studies confirmed that phages appear to dominate the human body virome regardless of eukaryotic viruses (Reyes et al., 2010; Hyman and Abedon, 2012) and revealed that the predominant viral group of human fecal samples is siphoviruses (Breitbart et al., 2003), the most prevalent group in natural habitats (Weinbauer, 2004).

The occurrence of phages in the human body raises questions regarding their importance in physiology and pathology and in their interaction with the pre-existing microbial communities. In fact, prophages and phage-like sequences have been shown to contribute to 20% of the bacterial genomes (Wang et al., 2010). Given that a lot of uncultured viruses and metagenomic sequences lack morphological characterization, which is a key criteria for the classification by the International Committee on the Taxonomy of Viruses (ICTV), this study aimed to characterize the viral diversity underneath the viral dark matter that circulates in different human body habitats of clinical relevance.

MATERIALS AND METHODS

Sample Collection

The specimens included in this survey were anonymized leftovers from samples collected according to institutional standards for routine microbiological testing at an Austrian tertiary care hospital, and submitted to the local Institute of Hygiene and Microbiology. Between October 2017 and August 2018, a total of 111 human fluid samples (abdominal, lung, pleural, shoulder and knee effusions, transport fluid from nasal swabs and intravenous catheters, blood, tracheal aspirates and urine) were thus collected. After diagnostic routine, leftovers with a volume between 3 and 5 ml were placed in a sterile tube to be processed for further analysis preferably at the day of collection. Whenever this was not possible samples were stored at 4°C for a maximum of 1 day to avoid a decrease in phage viability. Priority was given to samples susceptive to the presence of *E. coli* or staphylococci. Trachea aspirates are collected for routine investigation of the respiratory fluids and urine samples were collected for testing of *Legionella* and pneumococci-antigen. The collection was done in four sampling rounds (I–IV) (**Table 1**). The samples were then further processed in a BSL-2 laboratory in our facilities. No personal data or any other information than the type of material, the date of collection and the result of routine microbiology analysis was associated with each specimen, inhibiting any correlation of these fully anonymized samples to the respective patients. Thus, according to national regulations and the institutional rules for Good Scientific Practice, the requirement for submission to an ethical committee and for obtaining patients' informed consent was waived.

Isolation of *Escherichia coli* Colonies

An aliquot of 50 μl of each sample was spread onto Coli-ID agar plates (bioMérieux, Marcy l'Etoile, France) and incubated at 37°C. Colony-forming units (CFUs) were counted at 24 and 48 h. Five colonies of each sample were further sub-cultured on Modified Scholtens' Agar (MSA) plates and incubated 24 h at 37°C. The isolates were stocked in 20% (wt/vol) glycerol (Sigma-Aldrich, St. Louis, MO, United States) at −80°C.

Bacterial Host, Culture Conditions, and Bacteriophage Isolation

Samples were filtered using a 0.22 μm filter to remove bacterial load and processed using the soft-agar overlay method according to standard ISO 10706-2:2000, as previously described (Shousha et al., 2015; Hilbert et al., 2017) but with slight modifications. Briefly, three milliliters of semi-solid Modified Scholtens' Agar (ssMSA) were preheated to 45°C and supplemented with 10 mM $CaCl_2$. An overnight culture of the indicator strain was used to inoculate a new culture and was grown to an optical density of 0.4 at 600 nm. One milliliter of host culture and 1 ml of sample were added to the preheated semi-solid MSB and the mixture was vortexed and overlaid on MSA at room temperature and after solidifying, incubated overnight at 37°C. *E. coli* DSM 12242 was used as indicator host strain for bacteriophage detection. The filtered sample was either plated directly with the host bacteria, or spotted in an overlay, or mixed with the host bacteria in a liquid culture with further plating of the resulting supernatant. Lysates of plaques (five per sample whenever possible) were prepared according to Groisman (Groisman, 1991) by individually picking plaques from the soft agar and suspending them in 1 ml MSB media. The solution was then incubated 30 min at 37°C and 250 rpm. After centrifugation at 10,000 *g* during 8 min, the lysates were filtered through a 0.22 μm-pore-size filter and stored at 4°C. Blood samples were pre-processed prior to filtration. These

TABLE 1 | Sampling scheme containing the type of biological fluid samples (urine, blood, respiratory tract fluids, and others) obtained during each of the four sampling rounds (I–IV), in a total of 111 samples analyzed.

Sampling round	Collection date	Type of sample (*n*)				
		Urine	Blood	Respiratory tract fluids	Others (e.g., abdominal, lung, pleural, shoulder and knee fluid, nasal swabs, IV catheter)	Total
I[a]	14/11/17	12	2	4	5	23
II	28/01/18	12	6	9	0	27
III	26/03/18	11	6	7	8	32
IV	22/08/18	9	7	13	0	29
Total		44	21	33	13	111

[a] *The samples collected during this sampling round were not tested for bacteria.*

samples were centrifuged at 10,000 rpm during 5 min and the upper layer was set aside, followed by a second centrifugation at the same conditions. The resulting supernatant was then filtered and used as described above.

Statistical Analysis

Statistical analysis was performed using Fisher's exact test to investigate the association between the absence/presence of *E. coli* in the body fluids analyzed and the absence/presence of lytic coliphages. The significance level was set to a level of $p < 0.05$.

Preparation of Concentrated Lysates

Bacteriophage suspensions were propagated by re-infection the indicator host in triplicate using the purified lysate and the soft agar overlay method. After overnight incubation at 37°C, the soft agar was shredded and 3 ml of media were added. The overlay was collected and centrifuged at 8,000 *g* during 5 min. The clear supernatant was filtered through a 0.22 μm-pore-size filter and kept at 4°C. Ten-fold serial dilutions (10^{-1} to 10^{-6}) were prepared by plating 10 μl of the diluted lysate with the indicator bacteria. After overnight incubation at 37°C, the plaques were counted and the titer was expressed as PFU/ml.

Transmission Electron Microscopy (TEM)

A droplet of the purified phage suspension (10^7–10^8 PFU/ml) was deposited on a copper grid (Science Services, Munich, Germany) with carbon-coated Formvar film for 10 min at room temperature and stained with 4% aqueous phosphotungstic acid (Merck, Darmstadt, Germany) at pH 7. The sample was air-dried overnight and analyzed with a Zeiss TEM 900 electron microscope (Carl Zeiss, Oberkochen, Germany) operated at 50 kV. The phage particles were visualized using the Image SP software and a CCD camera (TRS, Tröndle Restlichtverstärkersysteme, Moorenweis, Germany).

Host Range Analysis and Efficiency of Plating

The laboratory host bacteria *E. coli* DSM 12242, ATCC 11303, JM109, W3110, MC1061, and DH5α and other members of the *Enterobacteriaceae* family were used to assess the lytic spectra of the phages. Clinical isolates from our own bacterial collection and from the clinical samples analyzed in this study were included in the screening (**Table 2**). Ten microliters of concentrated phage lysates (10^8 PFU/ml) were spotted onto MSA plates previously overlaid with 100 μl of stationary phase cell suspensions mixed with 3 ml of Molten-soft agar supplemented with 10 mM $CaCl_2$. The plates were incubated overnight at 37°C. Whenever lysis was observed, the efficiency of plating (EOP) was calculated. EOP was defined as the ratio between PFU/ml on the sensitive bacteria and the PFU/ml on the indicator strain.

Tolerance to Disinfectants

Phage stability was determined in the presence of 0.25% commonly used hospital disinfectants TPH Protect and Hexaquart® plus. Phage preparations of 10^7 PFU/ml were incubated at RT and phage titer was determined at 0, 15, 30, and 60 min by serial dilutions tested on the indicator strain by means of the soft agar overlay method, as before (Salem and Skurnik, 2018). The phage particles were counted after overnight incubation at 37°C. Assays were performed in duplicate. All the tested conditions allowed the survival and normal growth of the host strain, not hindering the phage infection.

Bacteriophage DNA Extraction

DNA was isolated using a phenol-chloroform extraction method with some modifications. Concentrated phage suspensions were pretreated with DNase I (Quantabio, Beverly, MA, United States) and RNase A (Sigma-Aldrich, St. Louis, MO, United States) in 10 μg/ml final concentration and the mixture was inverted several times and incubated at 37°C during 30 min. Furthermore, 20 mg/ml proteinase K (40 μg) and a final concentration of 0.5% sodium dodecyl sulfate (SDS) were added and incubated at 65°C for 1 h. The suspension was cooled to RT and phenol:chloroform extraction was performed, followed by an ethanol precipitation. The precipitated DNA was dissolved in 200 μl ddH_2O. The DNA concentration was estimated based on the band intensity comparison to the 1 kb marker (peqGOLD 1 kb DNA-Ladder, PEQLAB Biotechnologie GmbH, Austria). Whenever the DNA concentration proved to be insufficient,

TABLE 2 | Bacterial strains used to characterize the lysis spectra of the phages and respective EOP.

Bacteria	Phage group			References
	Peduovirus **vB_EcoM-12474V**	***Tequintavirus*** **vB_EcoS-26175V**	***Tunavirinae*** **vB_EcoS-2004IV**	
Escherichia coli DSM 12242	1.000 ± 0.000	1.000 ± 0.000	1.000 ± 0.000	DSMZ
Escherichia coli ATCC 11303	–	0.228 ± 0.048	–	ATCC
Escherichia coli W3110 (ATCC 27325)	–	0.840 ± 0.260	0.812 ± 0.080	ATCC
Escherichia coli JM109 (DSM 3423)	–	0.011 ± 0.004	0.145 ± 0.030	DSMZ
Escherichia coli DH5α (DSM 6897)	–	0.195 ± 0.055	–	DSMZ
Escherichia coli MC1061 (ATCC 53338)	0.283 ± 0.150	0.541 ± 0.287	0.509 ± 0.034	ATCC
Klebsiella pneumoniae sub. pneumoniae ATCC 13883	–	–	–	ATCC
Yersinia enterocolitica sub. palearctica DSM 11502	–	–	–	DSMZ
Salmonella enterica sub. enterica ATCC 14028	–	–	–	ATCC
Salmonella typhimurium DT104 isolate H3380	–	–	–	Clinical (Briggs and Fratamico, 1999)
Escherichia coli isolated from samples (n = 18)	–	–	–	This study
Escherichia coli isolates (*n* = 20)	–	–	–	Clinical
Escherichia coli isolate *P3*	–	–	–	Clinical
Escherichia coli isolate *P4*	–	–	–	Clinical
Escherichia coli isolate *P5*	–	–	–	Clinical
Klebsiella pneumoniae isolate P6	–	–	–	Clinical
Klebsiella pneumoniae isolate P7	–	–	–	Clinical
Klebsiella pneumoniae isolate P8	–	–	–	Clinical
Klebsiella oxytoca isolate P10	–	–	–	Clinical

These consisted in E. coli laboratory strains used in phage enumeration and isolation, additional Enterobacteriaceae species, E. coli isolated from the biological fluid samples and other bacterial isolates collected from patients and outpatients in this clinical setting.

ethanol precipitation was repeated using ammonium acetate at a final concentration of 2.0–2.5 M. The DNA was restricted with enzyme *Pvu*II (Roche Diagnostics GmbH, Vienna, Austria) using manufacturer's protocol and separated on a 1% agarose gel as an attempt to distinguish different restriction profiles.

Whole Genome Sequencing (WGS)

All library preparation, DNA sequencing and sequence trimming were performed at MicrobesNG (Birmingham, United Kingdom). Genomic libraries were prepared using the Nextera XT Library Prep Kit (Illumina, San Diego, CA, United States) according to manufacturer's instructions with slight modifications. Libraries were sequenced on the Illumina HiSeq using 250 bp paired-ends approach. The trimmed reads were analyzed using the INNUca pipeline (Machado et al., 2016). Briefly, reads quality were improved using Trimmomatic v0.38 (Bolger et al., 2014) and assembly was performed using Pear v0.9.10 and SPAdes version 3.13 (Bankevich et al., 2012). Resulting assembly was corrected by Pilon v1.18 and contigs were annotated using Prokka 1.13.3 (Seemann, 2014). Hypothetical proteins were manually annotated by using blastp against viral databases (**Supplementary Data S2–S4**). Contigs having a coverage lower than 1/3 of the assembly and smaller than 200 bp were considered as putative artifacts/contaminations and therefore removed from the downstream analysis. Genomes yielding a coverage <15x were excluded from the analysis.

Bioinformatics and Comparative Genome Analysis

The taxonomic distribution was assessed using Kraken v1 (Wood and Salzberg, 2014). Phylogenetic analysis of the 43 bacteriophages was re-constructed using VICTOR[1] (Meier-Kolthoff et al., 2013) with recommended settings for prokaryotic viruses (Meier-Kolthoff and Göker, 2017). The presence of antimicrobial resistance determinants such as antibiotic resistance and virulence genes was investigated using the command-line tool ABRicate v0.8.10[2]. Genome maps were constructed using the web-based tool GenomeVx (Conant and Wolfe, 2008). Average nucleotide identity (ANI) was calculated using OrthoANI[3] (Ha et al., 2017). The amino acid sequences of the integrase (*Peduovirus*), the large subunit terminase protein (*Tunavirinae*) and the DNA polymerase (*Tequintavirus*) were used for phylogenetic analysis. Sequence alignment was determined using Clustal Omega (Sievers et al., 2011; Chojnacki et al., 2017) and trees were reconstructed applying a bootstrapped (500 replications) Maximum Likelihood (ML) analysis. Tree inference used a Nearest-Neighbor-Interchange (NNI) as a heuristic method and a Jones-Thaylor-Thornton (JTT) as substitution model. Bacteriophages were compared with complete phage genomes deposited in the NCBI Viruses database for *Peduovirus*, *Tequintavirus,* and subfamily *Tunavirinae* (April

[1]https://ggdc.dsmz.de/victor.php

[2]https://github.com/tseemann/abricate

[3]https://www.ezbiocloud.net/tools/ani

2019). Accession numbers and ANI% of the closest homologs according to MASH[4] are given in the **Supplementary Data S5**. Evolutionary analysis were carried out using MEGA X v10.0.5 (Kumar et al., 2018) and trees were visualized and edited with FigTree v1.4.4[5].

Sequence Accession Numbers

Raw sequence data were deposited in the ENA under project accession number PRJEB32459. Assembled genomes and annotations were directly submitted to NCBI (PRJNA541793). Accession numbers are given in the **Supplementary Data S1**.

RESULTS

Phage, Bacteria, and Prevalence in Clinical Samples

A total of 111 samples were screened for the presence of lytic bacteriophages infecting *E. coli* DSM 12242 (**Table 1**). Coliphages were detected in 16 samples, representing a prevalence of 14.4% in the body fluids analyzed. Phages were more commonly found in blood (23.8%), followed by urine (20.5%) and tracheal aspirates (6.1%). No coliphages were found in other samples analyzed (abdominal, lung, pleural, shoulder and knee fluid, nasal swabs, IV catheters). From 88 samples, 16 were positive for the presence of *E. coli*, with bacterial counts ranging between $1{,}65 \times 10^7$ and $3{,}45 \times 10^{12}$ CFU/ml. From these 16 samples, in 5 of them lytic phages were concomitantly isolated. In fact, a statistically significant association between the absence/presence of *E. coli* and the presence/absence of coliphages in the sample was determined ($p = 0.016$).

Bacteriophage Diversity

A total of 43 coliphages isolated from 16 human body fluid samples were purified, sequenced and analyzed (**Table 3**). Three distinct genetic groups of linear double-stranded DNA viruses were identified using both a Genome-BLAST Distance Phylogeny (GBDP) method and a MASH all-versus-all approach, where phage genomes were compared against each other and grouped based on sequence similarity (**Figure 1**). This genomic diversity was also in accordance with the output of Kraken, which evidenced the presence of three phage groups belonging to the "P2likevirus," "T5likevirus," and "Tunalikevirus." One representative phage of each genetic group was further selected for more in-depth analysis.

Basic Genome Characteristics and Phylogenetic Analysis

All assemblies generated one single contig, with the exception of vB_EcoS-26174I (**Table 3**). The genome of the four "P2likevirus" phages (vB_EcoM-12474II, III, IV, and V) is between 33,688 and 33,807 bp long, contains 44 protein-encoding CDS and no tRNA genes. The GC content is 50.9%. All four "P2likevirus" bacteriophages were isolated from the same blood sample and shared an ANI of 100%. From the 44 proteins predicted, 28 were initially deemed as hypothetical. After carefully inspecting each protein and using blastp searches, only two proteins were unique in our phages and had no homology in the NCBI viral database. The remaining proteins were annotated or designated as "hypothetical phage proteins" whenever homology in other phage sequences was found (**Figure 2**). Phage attachment sites, attL (CCCGCCCGCTTCATGGGTCGGTTTTAATG) and attR (CCCGCCCGCTTCATGGGTCGGTTTTAATG) were also detected in the sequence.

Five "T5likevirus" phages were isolated during this study from a urine sample, sharing a 99.93–100% nucleotide sequence homology among themselves. Phages vB_EcoS-26175 I, II, III, IV, and V have a genome length of 114,646–114,649 bp and between 39.9 and 40.0% GC content. These phages have 158 putative CDS and 31 tRNA genes. Eighty-seven phage-related hypothetical proteins were found and two have not been described in the databases used (**Figure 3**). The remaining 34 phages were classified as "Tunalikevirus" and had a genome of 44,219 bp, 64–68 CDS and 1 tRNA gene. From these, 38 were phage-related hypothetical proteins with homologs in other virus genomes in the database and two are unique to these sequences (**Figure 4**). The GC content was between 44.4 and 44.5%.

No bacterial antimicrobial resistance gene, toxin or virulence determinant were found in the phage genomes.

Peduovirus ("P2likevirus")

The greatest nucleotide similarity level identified with vB_EcoM-12474V were phages fiAA91-ss (NC_022750) and pro483 (NC_028943), both members of the *Peduovirus* genus. Similarity to bacteriophage P2 (NC_001895), representative of this genus, was 96.59%. The phylogeny of these phages was further investigated by comparison of the amino acid sequence of the integrase (367 amino acids) (**Figure 5**). The *Peduovirus* isolated in this study shares a 97.30% whole genome ANI with fiAA91-ss (NC_022750). These phages are closely associated with bacteriophage WPhi (NC_005056), L-413C (NC_004745), and P2 (NC_001895), all officially classified as *Peduovirus* by the ICTV. Whole-genome based phylogeny of all *Peduovirus* clearly corroborates this data (**Supplementary Figure S1**) and adds pro147 (NC_028896) and pro483 (NC_028943), also classified *Peduovirus*, as closest homologs. In fact, the ANI% of vB_EcoM-12474V is ≥95% with these seven phages, suggesting they are representatives of one of these species. An alignment of the P*eduovirus* genomes shows non-collinearization of phage genomes and almost no order conservation of the genetic blocks. Nonetheless the synteny seems to be maintained (**Supplementary Figure S2**).

Tequintavirus ("T5likevirus")

The *Tequintavirus* genus belongs to the *Siphoviridae* family. All the phages currently listed as part of this genus were extracted from Genbank. Greatest similarity to vB_EcoS-26175V was found to phage vB_Eco_mar003J3 (LR027389), S126 (MH370376), 3-29 (MK393882), A148 (MG065642), and 118970_sal2 (NC_031933), and Stitch (NC_027297) based on MASH identity. MASH identified at least 34 phages as closest homologs and from these, 27 having at least 93.11% ANI to

[4]https://github.com/marbl/Mash

[5]http://tree.bio.ed.ac.uk/software/figtree/

TABLE 3 | Description of the isolation source, morphology, and sequence characteristics of the 43 bacteriophages sequenced in the course of this study.

Phages analyzed	Sampling round	Isolation source	Clinical history and microbiological findings	Morphology	Genome characteristics			
					Size (Kb)	GC content (%)	CDS (n)	tRNAs (n)
vB_EcoS-2862I, vB_EcoS-2862II, vB_EcoS-2862III, vB_EcoS-2862IV, vB_EcoS-2862V	II	Tracheal aspirate	*Klebsiella variicola**	*Siphoviridae*	44.2	44.4–44.5	65–66	1
vB_EcoS-26020I, vB_EcoS-26020II, vB_EcoS-26020III, vB_EcoS-26020IV, vB_EcoS-26020V	I	Urine	**	*Siphoviridae*	44.2	44.4–44.5	65–67	1
vB_EcoS-12469II, vB_EcoS-12469III	III	Blood	Urinary tract infection (*E. coli, Bacteroides fragilis*)	*Siphoviridae*	44.2	44.4	66	1
vB_EcoS-12210I, vB_EcoS-12210III	III	Blood	Status febrilis (*S. aureus*)	*Siphoviridae*	44.2	44.4	64–65	1
vB_EcoS-2005III, vB_EcoS-2005IV	II	Urine	**	*Siphoviridae*	44.2	44.4	66	1
vB_EcoS-26046II, vB_EcoS-26046III, vB_EcoS-26046IV, vB_EcoS-26046V	I	Urine	**	*Siphoviridae*	44.2	44.4	66	1
vB_EcoS-2006III, vB_EcoS-2006IV, vB_EcoS-2006V	II	Urine	**	*Siphoviridae*	44.2	44.4	66	1
vB_EcoM-12474II, vB_EcoM-12474III, vB_EcoM-12474IV, vB_EcoM-12474V	III	Blood	Urinary tract infection (*E. coli*)	*Myoviridae*	33.7–33.8	50.9	44	0
vB_EcoS-2004III, vB_EcoS-2004IV	II	Urine	**	*Siphoviridae*	44.2	44.4	66	1
vB_EcoS-25988I, vB_EcoS-25988IV	I	Urine	**	*Siphoviridae*	44.2	44.4	65–66	1
vB_EcoS-26174I, vB_EcoS-26174II	I	Urine	**	*Siphoviridae*	44.2	44.4	65–66	1
vB_EcoS-26175I, vB_EcoS-26175II, vB_EcoS-26175III, vB_EcoS-26175IV, vB_EcoS-26175V	I	Urine	**	*Siphoviridae*	114.6	39.9–40.0	158	31
vB_EcoS-26047I, vB_EcoS-26047II	I	Urine	**	*Siphoviridae*	44.2	44.4	65–66	1
vB_EcoS-12397I, vB_EcoS-12397II, vB_EcoS-12397III, vB_EcoS-12397IV	III	Tracheal aspirate	Oropharyngeal flora and *Candida tropicalis* *	*Siphoviridae*	44.2	44.4	65–66	1

**routine investigation of respiratory tract fluids, clinical history most likely not because of infectious disease; ***all urine samples were not tested for bacterial culture but for Legionella or pneumococci-antigen only.*

our phages (**Supplementary Figure S3**). Nucleotide similarity to phage T5 (NC_005859) was only 82.79% and therefore it is not the same species (%ANI $\geq$ 95). ANI with 118970_sal2 and Stitch was 95.08 and 95.45% respectively, but the closest nucleotide identity was 95.90% with phage 3–29. The phylogeny of these phages was further investigated by comparison of the amino acid sequence of the DNA polymerase (1216 amino acids), as previously (Sváb et al., 2018; Michniewski et al., 2019; **Figure 6**). Phages S126 and S113 (MH370366) appear closer to 26175V. The phages were deposited under the name *Escherichia* phage vB_EcoS-26175I, vB_EcoS-26175II, vB_EcoS-26175III, vB_EcoS-26175IV, and vB_EcoS-26175V and their gene content was compared with the closest homologs (**Supplementary Figure S4**).

Tunavirinae

Thirty-four identical phages from 14 samples were identified in this study as putative "Tunalikevirus" according to Kraken, but whole-genome sequence analysis puts them closer to the members of the *Rtpvirus* genus (**Supplementary Figure S5**).

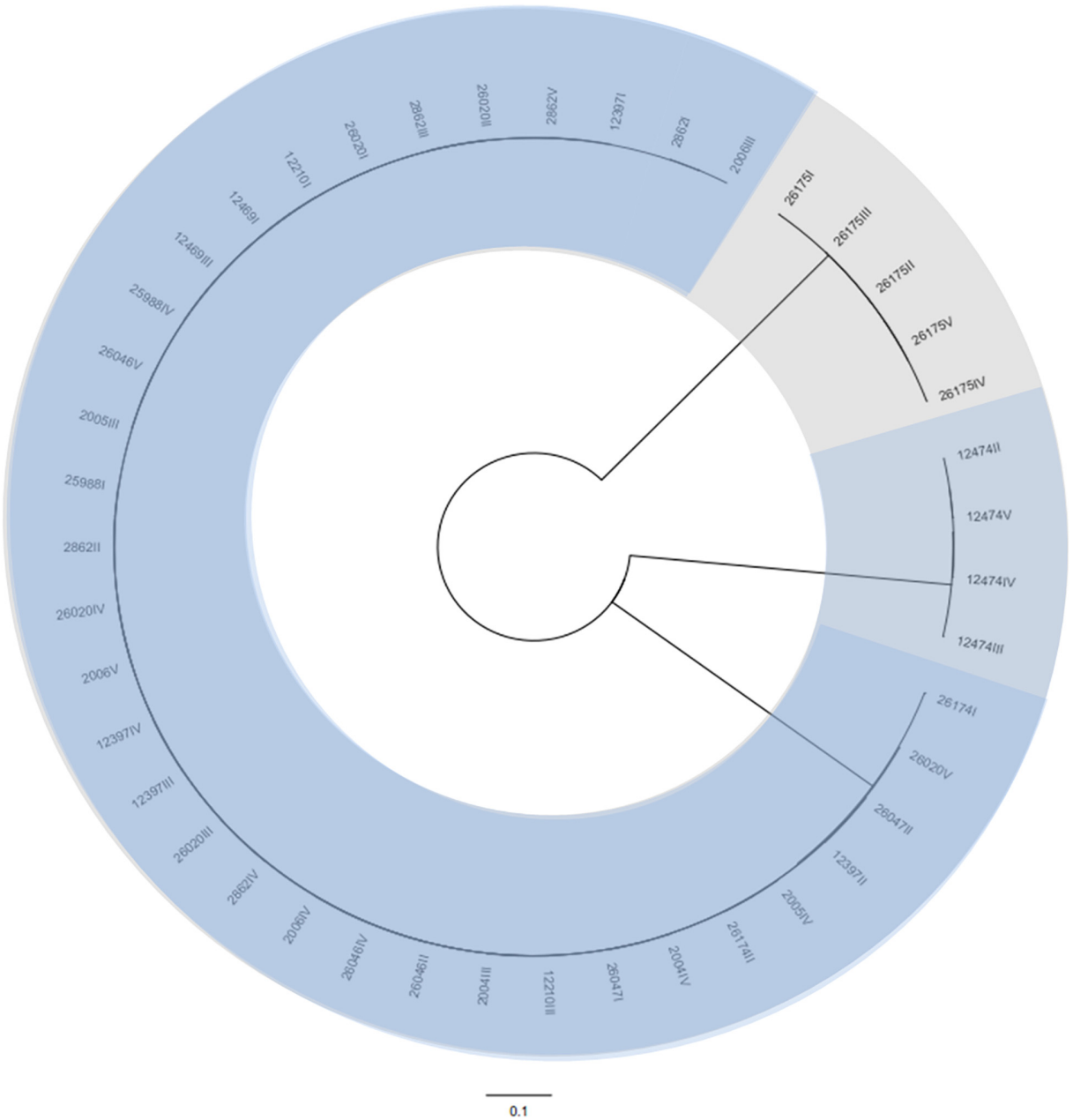

FIGURE 1 | Phylogenetic tree of the 43 bacteriophages isolated during this study using VICTOR (**Supplementary Data S1**). The scale represents homology % and yields an average support of 33%. The number of clusters determined were three, representing the genetic groups here described – *Peduovirus* (mild blue), *Tequintavirus* (gray) and *Tunavirinae* (blue).

To classify the phages identified in this study, the amino acid sequence of the large subunit terminase protein (534 amino acids) was chosen (Kropinski et al., 2015; Michniewski et al., 2019) and compared with the same sequence of 20 *Tunavirinae* members of both *Rtpvirus* and *Rogunavirus* genera identified as closest homologs using MASH, all having an ANI% $\geq$ 66.94 (**Figure 7**). According to the amino acid sequence of the terminase large subunit protein, both vB_EcoS_IME542 (MK372342) and the new *Tunavirinae* phages isolated in this study form a clade closer to the *Rogunavirus* genus. Phage vB_EcoS_IME542 is not classified by the ICTV but rather shows up in the NCBI database as an *Rtpvirus* member. In regards to ANI, the most similar phage genomes at the nucleotide level are the *Rtpvirus* phages A110b (MG065688), followed by the vB_Ecos_CEB_EC3a (KY398841), vB_EcoS-IME253 (KX130960), vB_EcoS_ACG-M12 (NC_019404), DTL (MG050172), RTP (NC_007603), and vB_EcoS_IME542. When looking at the amino acid sequence of the large subunit terminase,

FIGURE 2 | Genome map of the representative *Peduovirus* phage vB_EcoM-12474V (MK907239) isolated during this study.

both vB_EcoS_IME542 and the newly isolated phage vB_EcoS-2004IV are closer to *Rogunavirus*. Both share a 96.37% amino acid identity at the level of the large subunit terminase. Whole genome analysis and ANI% places them both closer to the *Rtpvirus*. The most similar phage is A110b, a non-classified phage also closer to the *Rtpvirus* genus according to whole-genome phylogeny reconstruction, with an 87.69% ANI in common with the new phages, the highest value obtained when scanning the database (**Supplementary Figure S6**).

Bacteriophage Characterization

Phylogenetic analysis corroborates that three groups of phages where identified in this study. Transmission electron micrographs from phages vB_EcoM-12474V, vB_EcoS-26175V, and vB_EcoS-2004IV show phages with icosaheadral heads and long tails (**Figure 8**). Phage vB_EcoM-12474V belongs to the *Myoviridae* family and has a head of about 62 nm and a 155 nm contractile tail. Phages vB_EcoS-2004IV and vB_EcoS-26175V are both siphoviruses and have long non-contractile tails of 232 and 186 nm, respectively. Phage heads have an approximate diameter of 100 and 85 nm.

The lytic capacity of phages from the different groups was investigated using enterobacterial collection strains, clinical isolates and *E. coli* isolated from the samples (**Table 2**). *Peduovirus* vB_EcoM-12474V, *Tequintavirus* vB_EcoS-26175V, and *Tunavirinae* vB_EcoS-2004IV showed different lysis patterns. None of the isolated phages lysed the bacteria isolated from the blood, urine and tracheal aspirates samples or other

vB_EcoS−26175V
114646 bp
0.00kb
18.33kb
36.67kb
55.00kb
73.33kb
91.67kb
hypothetical phage proteins
serine/threonine protein phosphatase
Serine/threonineprotein phosphatase
thioredoxin
hypothetical phage protein
Holin
ATP-dependent Clp protease proteolytic subunit
Deoxynucleoside-5-monophosphate kinase
tRNA-Met
tRNA-Ile
tRNA-Thr
tRNA-Gly
tRNA-Gln
tRNA-Arg
tRNA-His
tRNA-Ser
tRNA-Leu
tRNA-Ala
tRNA-Val
tRNA-Lys
tRNA-Met
tRNA-Pro
tRNA-Gly
tRNA-Asp
tRNA-Asn
tRNA-Cys
tRNA-Phe
tRNA-Trp
tRNA-Glu
tRNA-Tyr
tRNA-Leu
tRNA-Met
tRNA-Ser
H-N-H endonuclease FTflVI
nicotinamide mononucleotide transporter
nicotinamidenucleotide adenylyltransferase
hypothetical phage protein
putative membrane protein
tRNA-Arg
hypothetical phage protein
tRNA-Sec
recombination related exonuclease
spore cortex-lytic enzyme precursor
hypothetical phage protein
hypothetical phage protein
hypothetical phage protein
putative metallopeptidase
hypothetical phage proteins
ribonuclease H
hypothetical phage protein
hypothetical phage protein
Thymidylate synthase
Dihydrofolate reductase
aerobic ribonucleoside diphosphate reductase small
putative H-N-H endonuclease PTflVIII
Ribonucleosidediphosphate reductase large subunit
hypothetical phage protein
phosphate starvation inducible protein
Anaerobic ribonucleosidetriphosphate reductase
hypothetical phage protein
NADdependent deacetylase of SIR2 family
hypothetical phage protein
hypothetical phage protein
hypothetical phage protein

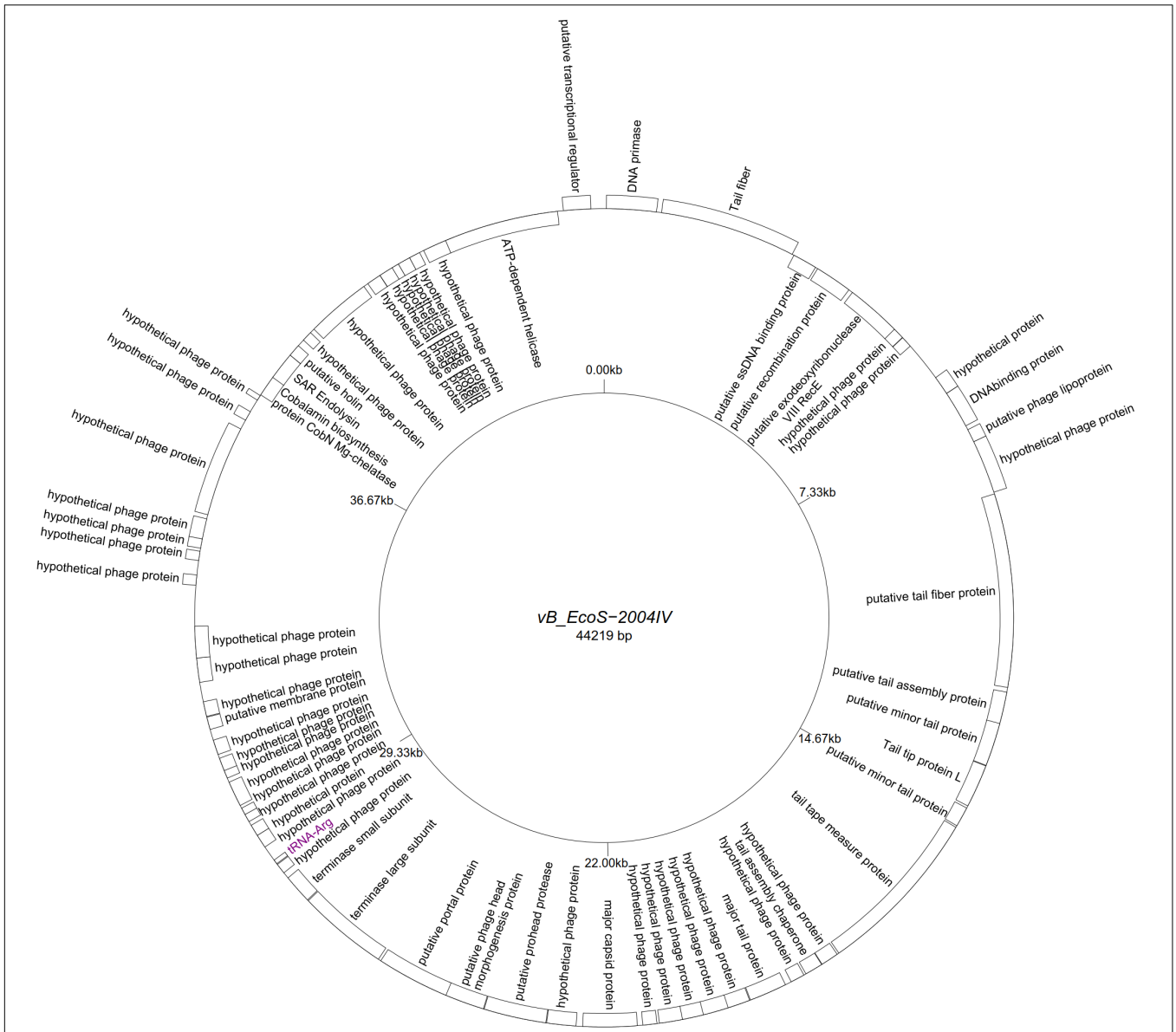

FIGURE 4 | Genome map of the representative *Tunavirinae* phage vB_EcoS-2004IV (MK907241) isolated during this study.

STEC O145:H28 strain RM12581 (CP007136), STEC O145:H28 strain RM13514 (CP006027), STEC O145:H28 strain 2015C-3125 (CP027763), and STEC O145 strain RM9872 (CP028379). *Tequintavirus* vB_EcoS-26175V and *Tunavirinae* phage vB_EcoS-2004IV were not detected in previously sequenced bacteria deposited in the database. The phage stability in the presence of the disinfectants TPH Protect and Hexaquart® plus was investigated (**Figure 9**). A concentration as low as 0.25% TPH Protect was sufficient to inactivate all phage particles of the three phage groups described, after 15 min. After incubation with Hexaquart® plus for 60 min *Peduovirus* vB_EcoM-12474V and *Tequintavirus* vB_EcoS-26175V virions could still be isolated. *Tunavirinae* vB_EcoS-2004IV could no longer be detected after 30 min.

DISCUSSION

In this study, we were able to successfully isolate natural-occurring phages from different human sources and further characterize the phage community found not only at the morphological level, but also at the nucleotide level. Coliphages that were able to infect the host strain *E. coli* DSM 12242 were present in 14.4% of the samples analyzed in this study. This prevalence is below what was reported in a previous study that surveyed the presence of phages, mainly siphoviruses in human blood, ascitic fluid, urine, cerebrospinal fluid, and serum (>45% of abdominal fluid and urine) (Brown-Jaque et al., 2016). The successful isolation of virions from clinical samples mostly relies on the use of large volumes of human body fluid samples. Despite

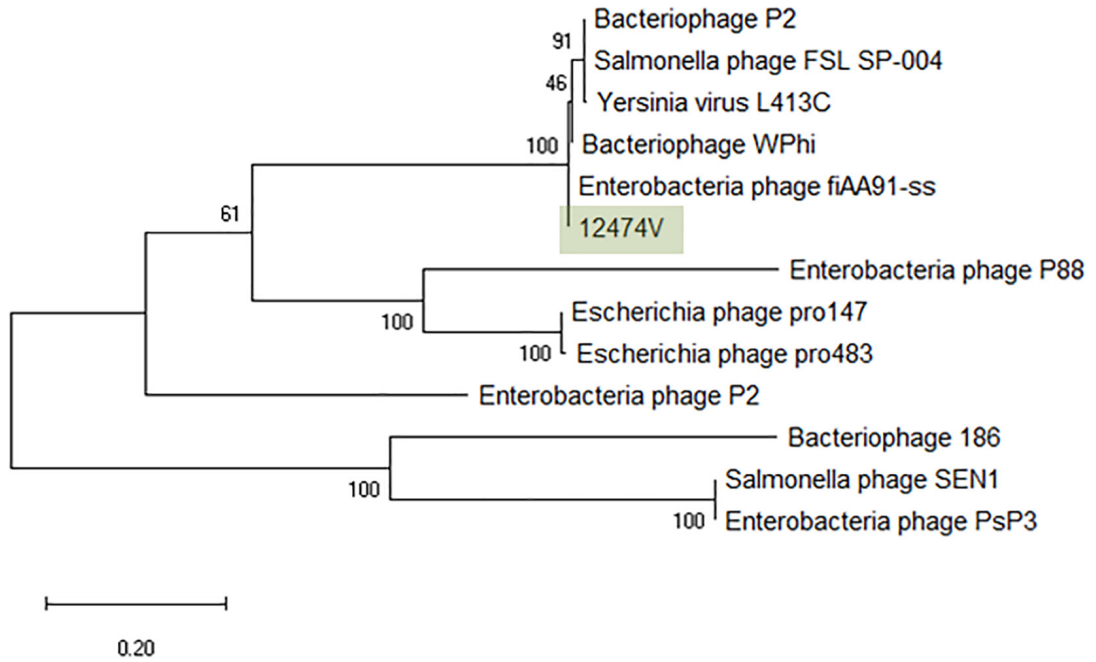

FIGURE 5 | Phylogenetic tree of *Peduovirus* phage based on the Clustal Omega alignment of the integrase protein sequence of the representative phage vB_EcoM-12474V (MK907239). The percentage of trees in which the associated taxa clustered together is shown next to the branches. The list of genomes included and GenBank accession numbers are described in **Supplementary Data S5**.

the high level of sensitivity of *E. coli* DSM 12242 to detect bacteriophages, as previously shown (International Organization for Standardization, 2000; Shousha et al., 2015; Hilbert et al., 2017), we assume that some of the coliphages present in the samples analyzed might have been missed due to a narrow host range (e.g., strain specific) and to the low phage densities despite the use of liquid cultures as an enrichment method. Additionally, some of the phages that are able to infect the strain used may have reduced plating efficiency during the first passage (Weinbauer, 2004).

Human body sites are not as sterile as previously thought and data from phage diversity studies showed that this diversity tends to be very different between ecological niches. The amount of uncharacterized, unknown, and abundant phage populations described in the late years in metagenomics studies highlighted the emergent need to characterize bacteriophages and disclose their role in human health and disease (Hyman and Abedon, 2012). Previous work conducted in our lab highlighted the important role of phages in the transfer of antimicrobial resistance genes through transduction mechanisms in other environments (Shousha et al., 2015; Hilbert et al., 2017). We chose a culture-based method in order to be able to study transduction instead of a metagenomics approach that would only provide information about genes but not the mechanism and ability of transfer. Moreover, the majority of the metagenomics studies cannot classify phages due to lack of homolog sequences in the databases and the so-called "viral dark matter" remains in obscure (Breitbart et al., 2003; Willner et al., 2009; Pride et al., 2012; Dinakaran et al., 2014; Dutilh et al., 2014; Ma et al., 2018).

Studies on the phage distribution in the human body are quite scarce, especially in a clinical context (Brown-Jaque et al., 2016; Navarro and Muniesa, 2017). The vast majority of studies available are mainly focused on the human gut (Górski and Weber-Dabrowska, 2005; Górski et al., 2006; Manrique et al., 2017; Ma et al., 2018) and feces (Havelaar et al., 1986; Cornax et al., 1994; Furuse et al., 2019), with other studies describing phage colonization of the mouth (Ly et al., 2014; Naidu et al., 2014) and respiratory tract (Willner et al., 2009; Willner and Furlan, 2010).

Phages were previously expected to be found everywhere their bacterial host is present, but recent studies suggest that bacterial abundance does not necessarily predict the relative abundance of their phages (Ly et al., 2014; Naidu et al., 2014; Brown-Jaque et al., 2016). The observation of phages at body sites where the bacterial host was not detected gives strength to the possibility of phage translocation through the human body (Górski et al., 2006; Brown-Jaque et al., 2016; Tetz and Tetz, 2018). As a matter of fact, in this study coliphages and *E. coli* were only found concomitantly in five samples. In 11 other samples, phages were found despite the non-detection of the bacterial host.

Phage genomes are characterized by a rapid evolutionary rate, horizontal gene transfer events and recombination between different viral genes, which makes the inference of phylogenetic relationships more reliable when considering individual genes or modules instead of whole genomes (Zois et al., 2011). This work relied on whole-genome analysis (VICTOR), gene content (multi-sequence alignment) and single-gene analysis (signature genes with no signs of recombination) to better disclose the

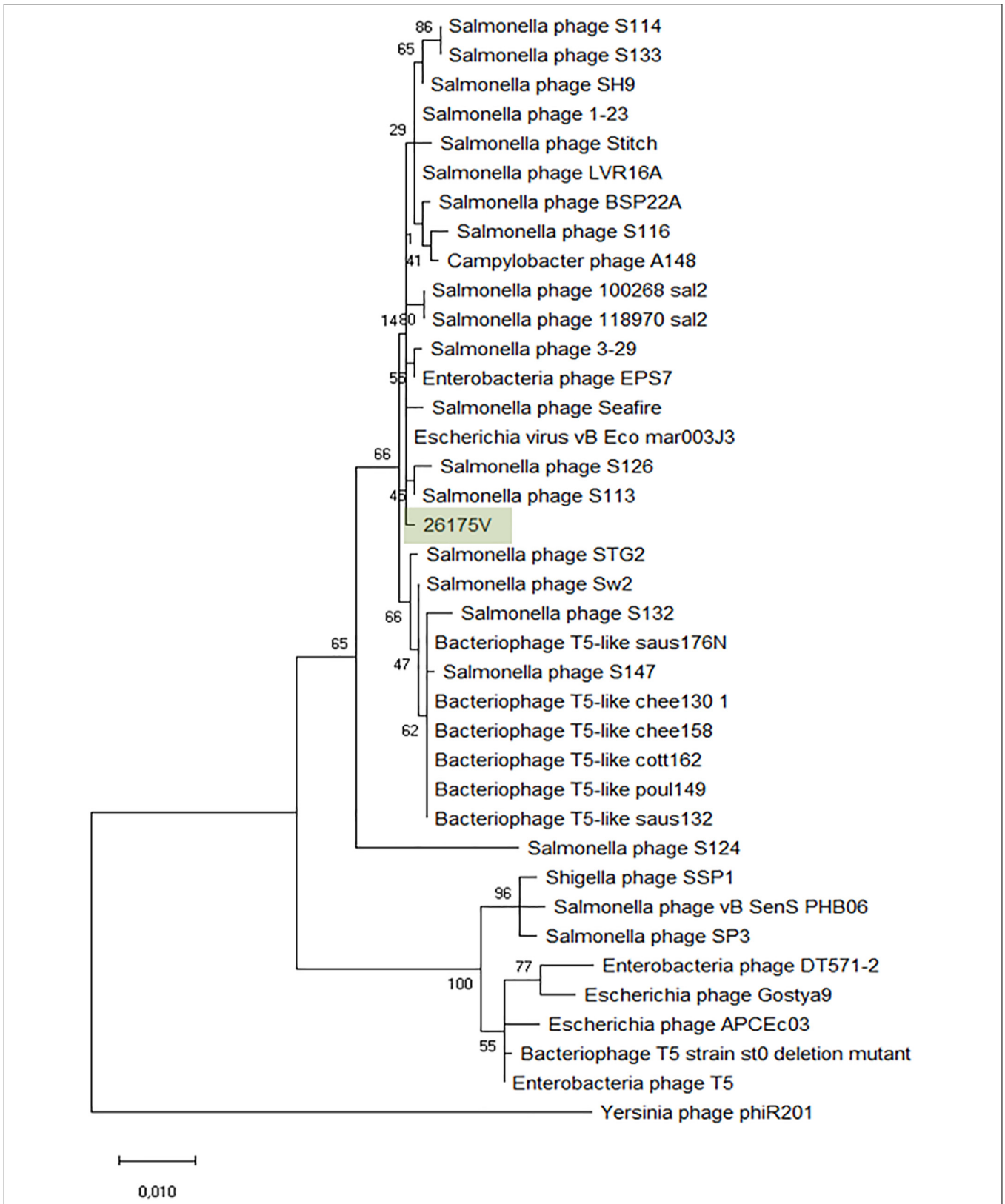

FIGURE 6 | Phylogenetic tree of *Tequintavirus* phage based on the Clustal Omega alignment of the DNA polymerase I protein sequence of the representative phage vB_EcoS-26175V (MK907271). The percentage of trees in which the associated taxa clustered together is shown next to the branches. The list of genomes included and GenBank accession numbers are described in **Supplementary Data S5**.

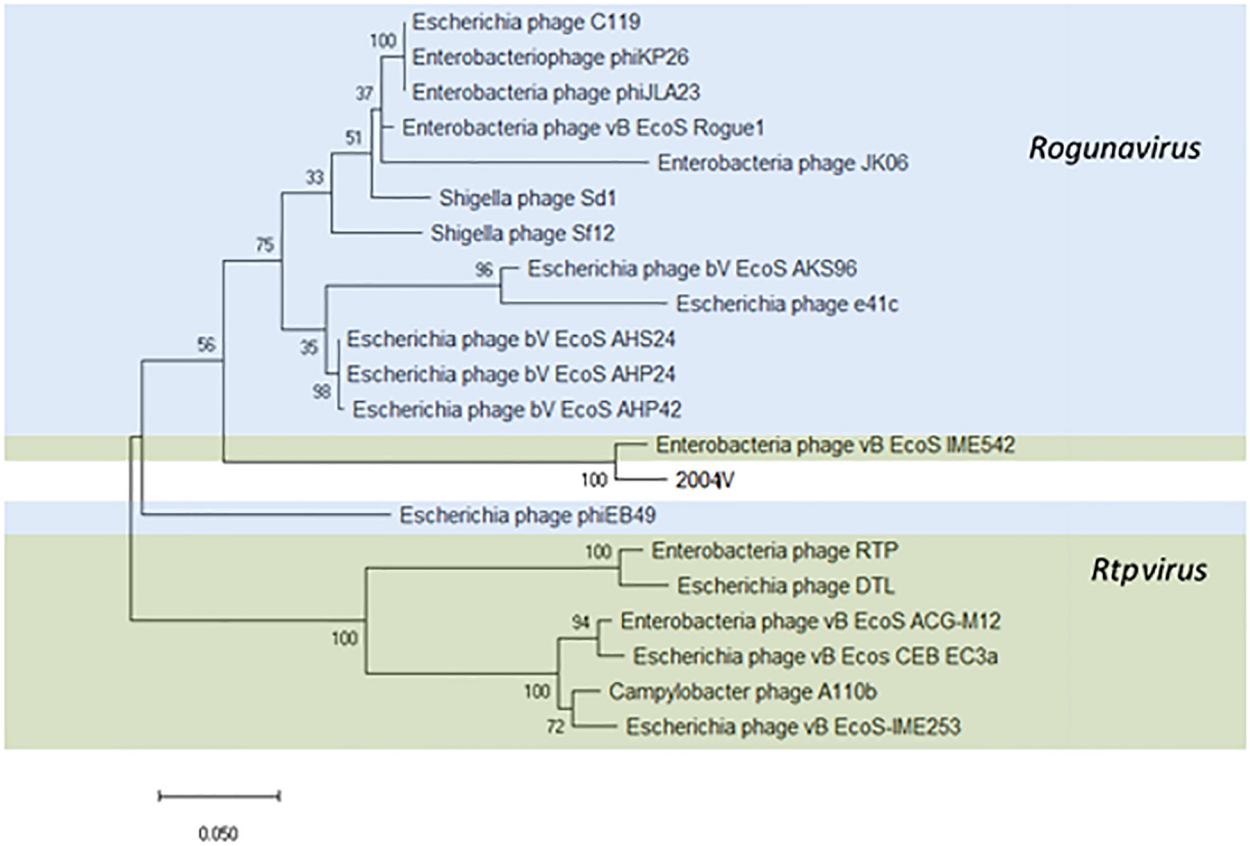

FIGURE 7 | Phylogenetic tree of *Tunavirinae* phage based on the Clustal Omega alignment of the terminase large subunit protein sequence of the representative phage vB_EcoS-2004IV (MK907241). Phages currently classified as Rogunavirus and as Rtpvirus are highlighted in blue and green, respectively. The percentage of trees in which the associated taxa clustered together is shown next to the branches. The list of genomes included and GenBank accession numbers are described in **Supplementary Data S5**.

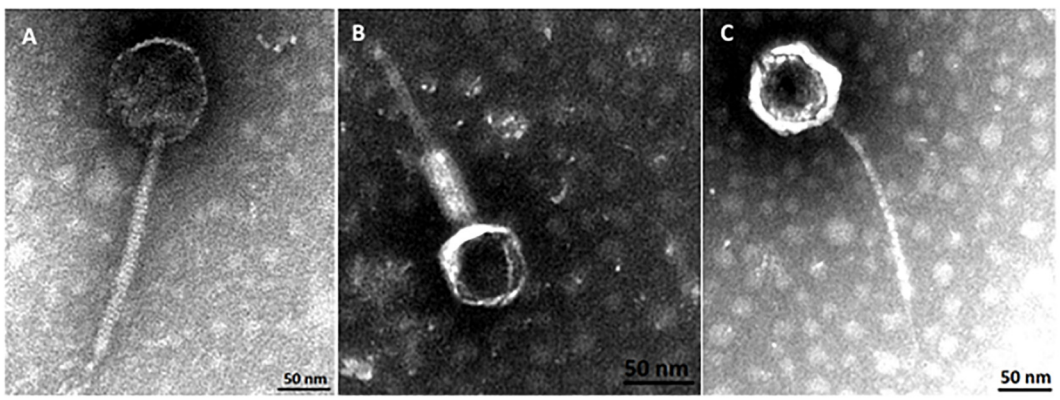

FIGURE 8 | Virion morphology of phages, **(A)** vB_EcoS-2004IV (*Siphoviridae*), **(B)** vB_EcoM-12474V (*Myoviridae*), and **(C)** vB_EcoS-26175V (*Siphoviridae*).

phylogenetic relationship between these phages and other phages from the viral databases. We were able to successfully isolate and characterize 43 phages belonging to three different species (**Figure 2**). There was a surprising low level of diversity observed, regarding the taxonomical distribution of phages isolated in our study. Phages belonging to the *Peduovirus*, *Tequintavirus,* and *Tunavirinae* subfamily were present in 16 samples. Interestingly, *Peduovirus* and *Tequintavirus* were isolated from a single sample, whilst the *Tunavirinae* were found across several samples. All of the phages were very similar, reflecting a low level of intra-sample

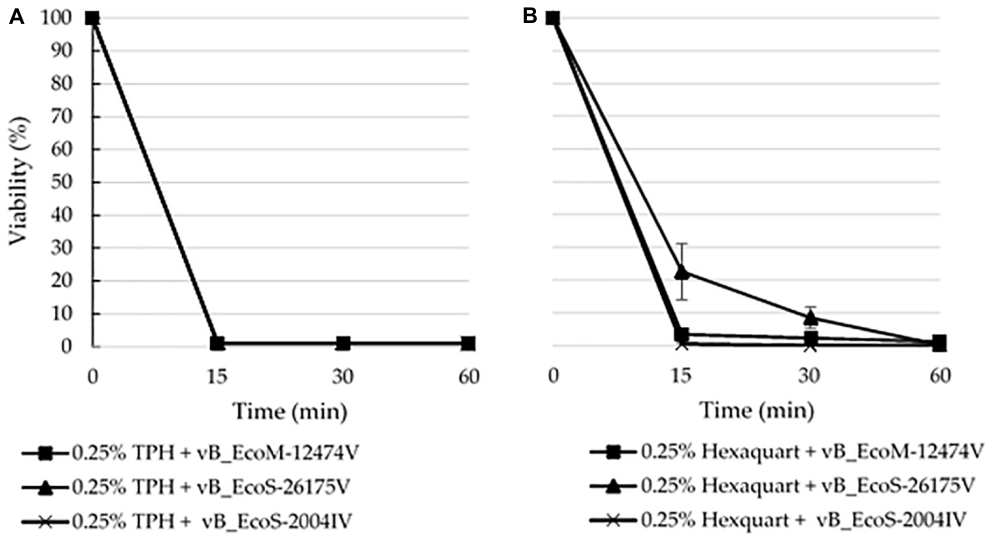

FIGURE 9 | Disinfectant stability of the phages vB_EcoM-12474V (MK907239), vB_EcoS-26175V (MK907271) and vB_EcoS-2004IV (MK907241) in the presence of 0.25% **(A)** TPH Protect and **(B)** Hexaquart© plus.

diversity. The same can be said about the inter-sample diversity observed for the *Tunavirinae*, which was in fact unexpected. This low level of diversity might be mainly due to the ability of specific phages to survive and multiply in the biological materials tested given the challenges that they present to the phage stability, such as e.g., high and/or low pH conditions (Weinbauer, 2004). Moreover, enteric bacteria and coliphage in pure urine were found to be rapidly inactivated in stored urine, being highly dependent on its pH (Chandran and Pradhan, 2009). The most similar phage genomes in the NCBI Viruses database was compared with the representative of each phage genome sequenced in this study (**Supplementary Figures S2**, **S4**, **S6**). Annotation of the features of the phage nucleotide sequences showed that these are conserved throughout the genomes, with only some genomic rearrangements occurring, according to the different modules that characterize each species analyzed. The vast majority of the phage sequences were structural proteins, with a part of hypothetical proteins, which were further investigated using blastp searches in the viral database for homology in other phage species. This strategy allowed the association of the majority of the hypothetical proteins as phage-related. Moreover, no features associated with antibiotic resistance or virulence were identified in any of the genomes.

When testing these phages for the host range, they could only infect *E. coli* laboratory strains DSM 12242, ATCC 11303, JM109, W3110, MC1061, and DH5α, having no activity against other *Enterobacteriaceae* or other *E. coli* clinical isolates tested (**Table 2**). These observations highlight the importance of using an adequate host strain for phage isolation, as the use of different *E. coli* strains to analyze the same set of samples has previously shown to yield different *Siphoviridae* coliphages (Chibani-Chennoufi et al., 2004).

The genus *Peduovirus*, together with *Hpunavirus*, compose the *Peduovirinae* subfamily, family *Myoviridae* according to the ICTV. *Peduovirus* vB_EcoM-12474V shared a 97.30% ANI with phage fiAA91-ss, a recognized member of the *Peduovirus* genus previously isolated from an *E. coli* O157:H7 strain from urban raw wastewater (Allué-Guardia et al., 2013). The sequence characteristics are also in accordance with the phage genomes already described for members of this genus, which range between 29.5 and 40.6 Kb and have 40–60 CDS. The classification of these phages as members of the *Peduovirus* genus is also supported by the presence of signature genes as the regulatory region containing the integrase gene *int*, the lytic-lysogenic transcriptional switch genes *cox* (lytic repressor gene) and *C* (immunity repressor gene), and the P2 type of late genes – capsid scaffold gene *O*, major capsid precursor gene *N*, small terminase subunit gene *M* and capsid completion gene *L* (**Supplementary Data S2**). These genes control the central mechanism of integration/excision in the host genome and the life cycle after infection. The major difference between the vB_EcoM-12474 phages and fiAA91-ss relies on the absence of the cytolethal toxin genes (Allué-Guardia et al., 2013). Altogether, this suggests that the four phages are indeed part of the *Peduovirus* genus, within a previously existing species. Previous works attempted to detect the presence of natural phages in human or animal blood without success (Gaidelyte et al., 2007; Brown-Jaque et al., 2016; Navarro and Muniesa, 2017). They are thought to be inherently absent in the blood of healthy individuals and are not expected to occur naturally. In fact, to the best of our knowledge, the only report describing virulent phage isolation from native blood was in septicemic patients (Gaidelyte et al., 2007). The associated bacterial host DNA is usually co-detected, which may suggest the translocation of bacteria harboring phage particles or lysogenized prophages into the bloodstream (Huh et al., 2019). Phage titers were also previously shown to increase with the severity of the symptoms. In patients with leukemic diseases, an increase in coliphage titer

and virulent phages (including T-phages) was previously reported (Furuse et al., 2019). In the case of the *Peduoviruses* isolated in this study, the temperate lifestyle and the co-detection of bacteria suggests a case of lysogenized prophages released by the *E. coli* found in the bloodstream. Moreover, these phages can be found as prophage sequences of Shiga toxin-producing *E. coli* (STEC) strains when searching the NCBI bacterial database. Typically, *Peduovirus* are temperate phage-infecting members of the γ-proteobacteria and tend to be similar when infecting the same host (Zois et al., 2011). The absence of bacteriophages in the blood of healthy individuals was also observed when compared with the virome of patients with HIV/AIDS (Li et al., 2012). Other two blood samples contained siphoviruses, with an apparent lytic lifestyle, which might have reached the bloodstream through translocation from other body sites. No evidence of lysogeny was found in the phage genomes, suggesting that these are lytic phages.

Data on the presence of bacteriophages in human urine is scarce (Caldwell, 1928; Thannesberger et al., 2017; Santiago-Rodriguez, 2018). It was for long assumed as sterile until the urethra level and the presence of microorganisms was normally associated with disease. This idea changed with the use of NGS that strongly support the presence of bacterial communities also in healthy individuals. The urine viral community was previously shown to be quite robust, comprising of about 10^7 virus-like particles (VLPs), both in healthy subjects and patients harboring an urinary tract infection (Santiago-Rodriguez et al., 2015). These urinary viral communities are mainly composed by phages and Human Papillomaviruses (HPV). Phages in human urine are thought to be mostly lysogenic, infecting bacteria from a wide range of phyla, such as Proteobacteria, Bacteroidetes, Firmicutes and Verrucomicrobia (Santiago-Rodriguez et al., 2015; Santiago-Rodriguez, 2018). This same idea of sterility was assumed for the respiratory tract. The respiratory tract of healthy people is believed to be poorly colonized by microorganisms, thus suggesting that no significant phage population is established. However, samples from the sputum of cystic fibrosis patients revealed a core of cystic fibrosis-associated phage, encoding a plethora of virulence factors as adhesins, biofilm-formation and quorum-sensing genes. In contrast, phages collected from the sputum of healthy individuals were highly diverse and most likely resembled environmental communities (Willner et al., 2009; Willner and Furlan, 2010). All the phages detected in urine and sputum during this study show a lack of integrative elements and seem to have a lytic lifestyle.

Dominant phages that persist at an increased number in individuals through an extended period of time showed no significant genome divergence or mutation, suggesting indeed a high genome stability of phage genomes, maybe due to the absence of substantial selective pressure acting on either bacteria or phages (Reyes et al., 2010). Possibly, this might explain why almost no inter-sample variability was found, and why the *Tunavirinae* group described here was widespread in almost all patients. The subfamily *Tunavirinae* belongs to the *Siphoviridae* family and has currently 8 genera classified: *Eclunavirus, Hanrivervirus*, *Rogunavirus*, *Rtpvirus*, *Sertoctavirus*, *Tlsvirus*, *Tunavirus,* and *Webervirus* [plus a non-classified species *Cronobacter* virus Esp2949-1 (NC_019509)]. Members of this subfamily are between 45 and 52 kb and have between 45 and 94 CDS. The highly abundant *Tunavirinae* isolated across our samples are confidently part of this subfamily, and highest homology was found within the *Rtpvirus*. However, analysis of the large subunit terminase suggests that they are closer to the *Rogunavirus.* The closest related phages were all phages isolated in other *Enterobacteriaceae* such as *Yersinia* sp. and *Salmonella* sp. However, the *Tunavirinae* phage vB_EcoS-2004IV appears to be very similar to a campylobacter phage, which unfortunately is still deemed as unverified, which would suggest an unusual level of promiscuity between phages that infect different host families. The closest homolog shares an 87.69% ANI, which is not enough to place the phages within a pre-existent genus, but enough to classify it as a member of the *Tunavirinae* family. Currently the ANI for the demarcation of a new species is at 95% according to the ICTV criteria. Nonetheless, recent studies suggest that a 97% would provide better accuracy for *Tequintavirus*, *Rb69virus* and *Seuratvirus* (Sazinas et al., 2018; Michniewski et al., 2019). In this case, the ANI criteria set to 97% would mean that also the *Tequintavirus* phage isolated in our study would also be a new species within this genus. Phage vB_EcoS-26175V, despite containing a vast abundance of structural proteins, also contained proteins associated with RNA metabolism (JOHFDMOO_00089) and protein degradation (JOHFDMOO_00009).

By surviving disinfection, these phages could be widespread around the clinical setting and in close proximity with the environment of the patients. The survival of phages in this environment might have deleterious consequences on the outcome of infectious diseases, by mediating the acquisition and dissemination of antimicrobial resistance, as observed in other settings (Colomer-Lluch et al., 2011, 2014; Fard et al., 2011; Shousha et al., 2015; Hilbert et al., 2017). The phage stability in the presence of the disinfectants TPH Protect and Hexaquart® plus was investigated, given their common use as hospital disinfectants. In particular, TPH Protect is the disinfectant used in the hospital where the samples were collected, and is used in a final concentration of 0.5% (v/v). None of the phages survived contact with half that concentration. However, upon exposure to 0.25% (v/v) Hexaquart® plus, *Peduovirus* vB_EcoM-12474V and *Tequintavirus* vB_EcoS-26175V could still be detected after 60 min (**Figure 9**).

The phages isolated during the course of this study and genome comparison analysis provided new insights regarding the phages that inhabit and colonize human body surfaces and revealed the presence of at least one new taxonomic group. *Peduovirus* vB_EcoM-12474V is a pre-existent species, *Tequintavirus* vB_EcoS-26175V might be a new species (depending on the ANI cut-off considered) and *Tunavirinae* vB_EcoS-2004IV represents a novel species. TEM also provided morphological evidence that supports the inclusion of the phages of this study in the above mentioned taxonomic groups (**Figure 9**). Instead of characterizing the whole population

through metagenomics, this approach allowed the isolation and purification of bacteriophages. This work is a very important contribution and a meaningful attempt in the disclosure of the key players behind the viral dark matter observed, their interaction with bacteria found on site and their possible involvement in the health status of the individuals.

DATA AVAILABILITY STATEMENT

The datasets generated for this study were deposited under the accession numbers PRJEB32459 and PRJNA541793.

AUTHOR CONTRIBUTIONS

FH acquired the funding and administered the project. FH and CP conceived and designed the experiments. I-JP, CA, and CP provided the data and collected the samples. CP, MH, and DS performed the experiments. FH, CP, MH, ND, I-JP, CA, JC, and DS contributed with reagents, materials, and analysis tools. ND and MH performed transmission electronic microscopy analysis. CP prepared the original draft and wrote the manuscript. FH, CA, I-JP, JC, and CP reviewed and edited the manuscript.

FUNDING

This work was in part supported by the NFB (Niederoesterreichische Forschungs- und Bildungsgesellschaft) Grant No. LS14-006.

ACKNOWLEDGMENTS

We are thankful to the bioinformatics staff of the Molecular Microbiology and Infection Unit at the Instituto de Medicina Molecular of the University of Lisbon for the assistance provided and to João Costa-Nunes (Sechenova University, Moscow) and João Viana da Silva for critically reviewing and correcting the manuscript. We are very grateful to Franz Trautinger for his expert opinion as chair of the ethics commission of the Karl Landsteiner University on the sampling procedure.

SUPPLEMENTARY MATERIAL

The Supplementary Material for this article can be found online at: https://www.frontiersin.org/articles/10.3389/fmicb.2019.02484/full#supplementary-material

REFERENCES

Allocati, N., Masulli, M., Alexeyev, M. F., and Di Ilio, C. (2013). *Escherichia coli* in Europe: an overview. *Int. J. Environ. Res. Public Health* 10, 6235–6254. doi: 10.3390/ijerph10126235

Allué-Guardia, A., Imamovic, L., and Muniesa, M. (2013). Evolution of a self-inducible cytolethal distending toxin type V- encoding bacteriophage from *Escherichia coli* O157:H7 to *Shigella sonnei*. *J. Virol.* 87, 13665–13675. doi: 10.1128/JVI.02860-2813

Bankevich, A., Nurk, S., Antipov, D., Gurevich, A. A., Dvorkin, M., Kulikov, A. S., et al. (2012). SPAdes: a new genome assembly algorithm and its applications to single-cell sequencing. *J. Comput. Biol.* 19, 455–477. doi: 10.1089/cmb.2012.0021

Bibi, Z., Abbas, Z., and Rehman, S. (2016). The phage P. *E*1 isolated from hospital sewage reduces the growth of *Escherichia coli*. *Biocontrol Sci. Technol.* 26, 181–188. doi: 10.1080/09583157.2015.1086311

Bolger, A. M., Lohse, M., and Usadel, B. (2014). Trimmomatic: a flexible trimmer for illumina sequence data. *Bioinformatics* 30, 2114–2120. doi: 10.1093/bioinformatics/btu170

Breitbart, M., Hewson, I., Felts, B., Mahaffy, J. M., Nulton, J., Salamon, P., et al. (2003). Metagenomic analyses of an uncultured viral community from human feces. *J. Bacteriol.* 185, 6220–6223. doi: 10.1128/JB.185.20.6220

Briggs, C. E., and Fratamico, P. M. (1999). Molecular characterization of an antibiotic resistance gene cluster of *Salmonella* typhimurium DT104. *Antimicrob. Agents Chemother.* 43, 846–849.

Brown-Jaque, M., Muniesa, M., and Navarro, F. (2016). Bacteriophages in clinical samples can interfere with microbiological diagnostic tools. *Sci. Rep.* 6:33000. doi: 10.1038/srep33000

Brussow, H., Canchaya, C., and Hardt, W.-D. (2004). Phages and the evolution of bacterial pathogens: from genomic rearrangements to lysogenic conversion. *Microbiol. Mol. Biol. Rev.* 68, 560–602. doi: 10.1128/MMBR.68.3.560

Caldwell, J. A. (1928). Bacteriologic and bacteriophagic infected urines. *J. Infect. Dis.* 43, 353–362. doi: 10.1093/infdis/43.4.353

Chandran, A., and Pradhan, S. K. (2009). Survival of enteric bacteria and coliphage MS2 in pure human urine. *J. Appl. Microbiol.* 107, 1651–1657. doi: 10.1111/j.1365-2672.2009.04353.x

Chibani-Chennoufi, S., Sidoti, J., Bruttin, A., Dillmann, M. L., Kutter, E., Qadri, F., et al. (2004). Isolation of *Escherichia coli* bacteriophages from the stool of pediatric diarrhea patients in Bangladesh. *J. Bacteriol.* 186, 8287–8294. doi: 10.1128/JB.186.24.8287-8294.2004

Chojnacki, S., Cowley, A., Lee, J., Foix, A., and Lopez, R. (2017). Programmatic access to bioinformatics tools from EMBL-EBI update: 2017. *Nucleic Acids Res.* 45, 550–553. doi: 10.1093/nar/gkx273

Colomer-Lluch, M., Jofre, J., and Muniesa, M. (2011). Antibiotic resistance genes in the bacteriophage DNA fraction of environmental samples. *PLoS One* 6:e17549. doi: 10.1371/journal.pone.0017549

Colomer-Lluch, M., Jofre, J., and Muniesa, M. (2014). Quinolone resistance genes (qnrA and qnrS) in bacteriophage particles from wastewater samples and the effect of inducing agents on packaged antibiotic resistance genes. *J. Antimicrob. Chemother.* 69, 1265–1274. doi: 10.1093/jac/dkt528

Conant, G. C., and Wolfe, K. H. (2008). GenomeVx: simple web-based creation of editable circular chromosome maps. *Bioinformatics* 24, 861–862. doi: 10.1093/bioinformatics/btm598

Cornax, R., Morinigo, M. A., Gonzalez-jaen, F., Alonso, M. C., and Borrego, J. J. (1994). Bacteriophages presence in human faeces of healthy subjects and patients with gastrointestinal disturbances. *Zentralbl Bakteriol* 224, 214–224. doi: 10.1016/S0934-8840(11)80572-80574

Desiere, F., Mcshan, W. M., Sinderen, D., Van, Ferretti, J. J., and Brüssow, H. (2001). Comparative genomics reveals close genetic relationships between phages from dairy bacteria and pathogenic streptococci: evolutionary implications for prophage-host interactions. *Virology* 341, 325–341. doi: 10.1006/viro.2001.1085

Dinakaran, V., Rathinavel, A., and Pushpanathan, M. (2014). Elevated levels of circulating DNA in cardiovascular disease patients: metagenomic profiling of microbiome in the circulation. *PLoS One* 9:e0105221. doi: 10.1371/journal.pone.0105221

Dutilh, B. E., Cassman, N., Mcnair, K., Sanchez, S. E., Silva, G. G. Z., Boling, L., et al. (2014). A highly abundant bacteriophage discovered in the unknown sequences of human faecal metagenomes. *Nat. Commun.* 5, 1–11. doi: 10.1038/ncomms5498

European Centre for Disease Prevention and Control (2016). Surveillance of antimicrobial resistance in Europe 2016. Annual Report of the European

Antimicrobial Resistance Surveillance Network (EARS-Net), European Centre for Disease Prevention and Control, Solna Municipality. doi: 10.2900/296939

Fard, R. M., Barton, M. D., and Heuzenroeder, M. W. (2011). Bacteriophage-mediated transduction of antibiotic resistance in enterococci. *Lett. Appl. Microbiol.* 52, 559–564. doi: 10.1111/j.1472-765X.2011.03043.x

Furuse, K., Osawa, S., Kawashiro, J., Tanaka, R., Ozawa, A., Sawamura, S., et al. (2019). Bacteriophage distribution in human faeces: continuous survey of healthy subjects and patients with internal and leukaemic diseases. *J. Gen. Virol.* 64, 2039–2043. doi: 10.1099/0022-1317-64-9-2039

Gaidelyte, A., Vaara, M., and Bamford, D. H. (2007). Bacteria, phages and septicemia. *PLoS One* 2:e1145. doi: 10.1371/journal.pone.0001145

Górski, A., Wazna, E., Dabrowska, B., Dabrowska, K., Switała-Jeleń, K., and Miedzybrodzki, R. (2006). Bacteriophage translocation. *FEMS Immunol. Med. Microbiol.* 46, 313–319. doi: 10.1111/j.1574-695X.2006.00044.x

Górski, A., and Weber-Dabrowska, B. (2005). The potential role of endogenous bacteriophages in controlling invading pathogens. *Cell. Mol. Life Sci.* 62, 511–519. doi: 10.1007/s00018-004-4403-4406

Groisman, E. A. (1991). "In vivo genetic engineering with bacteriophage Mu," in *Methods in Enzymology*, eds J. Abelson, M. Simon, G. Verdine, and A. Pyle (Cambridge, MA: Academic Press), 180–212. doi: 10.1016/0076-6879(91)04010-L

Ha, S. Y. S., Lim, J., Kwon, S., and Chun, J. (2017). A large-scale evaluation of algorithms to calculate average nucleotide identity. *Antonie Van Leeuwenhoek* 110, 1281–1286. doi: 10.1007/s10482-017-0844-844

Havelaar, A., Furuse, K., and Hogeboom, V. (1986). Bacteriophages and indicator bacteria in human and animal faeces. *J. Appl. Bacteriol.* 60, 255–262. doi: 10.1111/j.1365-2672.1986.tb01081.x

Hilbert, M., Csadek, I., Auer, U., and Hilbert, F. (2017). Antimicrobial resistance-transducing bacteriophages isolated from surfaces of equine surgery clinics - a pilot study. *Eur. J. Microbiol. Immunol.* 7, 296–302. doi: 10.1556/1886.2017.00032

Huh, H., Wong, S., Jean, J. S., and Slavcev, R. (2019). Bacteriophage interactions with mammalian tissue: therapeutic applications. *Adv. Drug Deliv. Rev.* doi: 10.1016/j.addr.2019.01.003 [Epub ahead of print].

Hyman, P., and Abedon, S. T. (2012). *Bacteriophages in Health and Disease*, 1st Edn. Oxfordshire: CAB International.

International Organization for Standardization (2000). *Water Quality— Detection and Enumeration of Bacteriophages. Part 2. Enumeration of Somatic Coliphages. ISO 10705-2:2000*. Geneva: ISO.

King, A., Adams, M., Carstens, E., and Lefkowitz, E. (2012). "Order - Caudovirales," in *Virus Taxonomy: Ninth Report of the International Committee on Taxonomy of Viruses*, eds A. M. Q. King, E. Lefkowitz, M. J. Adams, and E. B. Carstens (Amsterdam: Elsevier), 39–45. doi: 10.1016/B978-0-12-384684-6.00001-X

Kowarsky, M., Camunas-soler, J., Kertesz, M., Vlaminck, I., De, Koh, W., et al. (2017). Numerous uncharacterized and highly divergent microbes which colonize humans are revealed by circulating cell-free DNA. *Proc. Natl. Acad. Sci. U.S.A.* 114, 9623–9628. doi: 10.1073/pnas.1707009114

Kropinski, A. M., Niu, D., and Adriaenssens, E. M. (2015). *Proposal2015.019a-abB Tunavirinae. ICTV Propos.*, 1–26. Available at: https://talk.ictvonline.org/ICTV/proposals/2015.019a-abB.A.v3.Tunavirinae.pdf (accessed April 2019).

Kumar, S., Stecher, G., Li, M., Knyaz, C., and Tamura, K. (2018). MEGA X: molecular evolutionary genetics analysis across computing platforms. *Mol. Biol. Evol.* 35, 1547–1549. doi: 10.1093/molbev/msy096

Latz, S., Krüttgen, A., Häfner, H., Buhl, E. M., and Horz, H. (2017). Differential effect of newly isolated phages viruses against multi-drug resistant *Pseudomonas aeruginosa* under varying growth conditions. *Viruses* 9:E315. doi: 10.3390/v9110315

Li, S., Leung, R. K., Guo, H., Wei, J., Wang, J., Kwong, K., et al. (2012). Detection and identification of plasma bacterial and viral elements in HIV/AIDS patients in comparison to healthy adults. *Clin. Microbiol. Infect.* 18, 1126–1133. doi: 10.1111/j.1469-0691.2011.03690.x

Ly, M., Abeles, S. R., Boehm, T. K., Robles-sikisaka, R., Naidu, M., Santiago-rodriguez, T., et al. (2014). Altered oral viral ecology in association with periodontal disease. *mBio* 5:e01133-1114. doi: 10.1128/mBio.01133-1114

Ma, Y., You, X., Mai, G., Tokuyasu, T., and Liu, C. (2018). A human gut phage catalog correlates the gut phageome with type 2 diabetes. *Microbiome* 6, 1–12. doi: 10.1186/s40168-018-0410-y

Machado, M. P., Halkilahti, J., Jaakkonen, A., Silva, D. N., Mendes, I., Nalbantoglu, Y., et al. (2016). *INNUca GitHub*. Available at: https://github.com/B-UMMI/INNUca (accessed April 2019).

Manrique, P., Dills, M., and Young, M. J. (2017). The human gut phage community and its implications for health and disease. *Viruses* 9:E141. doi: 10.3390/v9060141

McNair, K., Bailey, B. A., and Edwards, R. A. (2012). PHACTS, a computational approach to classifying the lifestyle of phages. *Bioinformatics* 28, 614–618. doi: 10.1093/bioinformatics/bts014

Meier-Kolthoff, J. P., Auch, A. F., Klenk, H. P., and Göker, M. (2013). Genome sequence-based species delimitation with confidence intervals and improved distance functions. *BMC Bioinformatics* 14:60. doi: 10.1186/1471-2105-14-60

Meier-Kolthoff, J. P., and Göker, M. (2017). VICTOR: genome-based phylogeny and classification of prokaryotic viruses. *Bioinformatics* 33, 3396–3404. doi: 10.1093/bioinformatics/btx440

Michniewski, S., Redgwell, T., Grigonyte, A., Rihtman, B., Aguilo-ferretjans, M., Christie-oleza, J., et al. (2019). Riding the wave of genomics to investigate aquatic coliphage diversity and activity. *Environ. Microbiol.* 21, 2112–2128. doi: 10.1111/1462-2920.14590

Naidu, M., Robles-sikisaka, R., Abeles, S. R., Boehm, T. K., and Pride, D. T. (2014). Characterization of bacteriophage communities and CRISPR profiles from dental plaque. *BMC Microbiol.* 14:1–13. doi: 10.1186/1471-2180-14-175

Navarro, F., and Muniesa, M. (2017). Phages in the human body. *Front. Microbiol.* 8:1–7. doi: 10.3389/fmicb.2017.00566

Peng, Q., and Yuan, Y. (2018). Characterization of a newly isolated phage infecting pathogenic *Escherichia coli* and analysis of its mosaic structural genes. *Sci. Rep.* 8:8086. doi: 10.1038/s41598-018-26004-26004

Pride, D. T., Salzman, J., Haynes, M., Rohwer, F., Davis-long, C., White, R. A. III, et al. (2012). Evidence of a robust resident bacteriophage population revealed through analysis of the human salivary virome. *ISME J.* 6, 915–926. doi: 10.1038/ismej.2011.169

Reyes, A., Haynes, M., Hanson, N., Angly, F. E., Heath, A. C., Rohwer, F., et al. (2010). Viruses in the faecal microbiota of monozygotic twins and their mothers. *Nature* 466, 334–338. doi: 10.1038/nature09199

Salem, M., and Skurnik, M. (2018). Genomic characterization of sixteen yersinia enterocolitica-infecting podoviruses of pig origin. *Viruses* 10:E174. doi: 10.3390/v10040174

Santiago-Rodriguez, T. M. (2018). "Identification and quantification of DNA viral populations in human urine using next-generation sequencing approaches," in *The Human Virome: Methods and Protocols*, eds A. Moya, and V. Pérez Brocal (Berlin: Springer Science+Business Media), 191–200. doi: 10.1007/978-1-4939-8682-8_14

Santiago-Rodriguez, T. M., Ly, M., Bonilla, N., and Pride, D. T. (2015). The human urine virome in association with urinary tract infections. *Front. Microbiol.* 6:14. doi: 10.3389/fmicb.2015.00014

Sazinas, P., Redgwell, T., Rihtman, B., Grigonyte, A., Michniewski, S., Scanlan, D. J., et al. (2018). Comparative genomics of bacteriophage of the genus seuratvirus. *Genome Biol. Evol.* 10, 72–76. doi: 10.1093/gbe/evx275

Seemann, T. (2014). Prokka: rapid prokaryotic genome annotation. *Bioinformatics* 30, 2068–2069. doi: 10.1093/bioinformatics/btu153

Shousha, A., Awaiwanont, N., Sofka, D., Smulders, F. J. M., Paulsen, P., Szostak, M. P., et al. (2015). bacteriophages isolated from chicken meat and the horizontal transfer of antimicrobial resistance genes. *Appl. Environ. Microbiol.* 81, 4600–4606. doi: 10.1128/AEM.00872-815

Sievers, F., Wilm, A., Dineen, D., Gibson, T. J., Karplus, K., Li, W., et al. (2011). Fast, scalable generation of high-quality protein multiple sequence alignments using clustal omega. *Mol. Syst. Biol.* 7:539. doi: 10.1038/msb.2011.75

Sváb, D., Falgenhauer, L., Rohde, M., and Szabó, J. (2018). Identification and characterization of T5-Like bacteriophages representing two novel subgroups from food products. *Front. Microbiol.* 9:202. doi: 10.3389/fmicb.2018.00202

Tetz, G., and Tetz, V. (2018). Bacteriophages as new human viral pathogens. *Microorganisms* 6:E54. doi: 10.3390/microorganisms6020054

Thannesberger, J., Hellinger, H., Klymiuk, I., Kastner, M., Rieder, F. J. J., Schneider, M., et al. (2017). Viruses comprise an extensive pool of mobile genetic elements

in eukaryote cell cultures and human clinical samples. *FASEB J.* 31, 1987–2000. doi: 10.1096/fj.201601168R

Wang, X., Kim, Y., Ma, Q., Hong, S. H., Pokusaeva, K., Sturino, J. M., et al. (2010). Cryptic prophages help bacteria cope with adverse environments. *Nat. Commun.* 1:1146. doi: 10.1038/ncomms1146

Weinbauer, M. G. (2004). Ecology of prokaryotic viruses. *FEMS Microbiol. Rev.* 28, 127–181. doi: 10.1016/j.femsre.2003.08.001

Willner, D., and Furlan, M. (2010). Deciphering the role of phage in the cystic fibrosis airway. *Virulence* 1, 309–313. doi: 10.4161/viru.1.4.12071

Willner, D., Furlan, M., Haynes, M., Schmieder, R., Angly, F. E., Silva, J., et al. (2009). Metagenomic analysis of respiratory tract DNA Viral communities in cystic fibrosis and non-cystic fibrosis individuals. *PLoS One* 4:e7370. doi: 10.1371/journal.pone.0007370

Wood, D. E., and Salzberg, S. L. (2014). Kraken: ultrafast metagenomic sequence classification using exact alignments. *Genome Biol.* 15:R46. doi: 10.1186/gb-2014-15-3-r46

Zois, C. E., Giatromanolaki, A., Sivridis, E., Papaiakovou, M., Kainulainen, H., and Koukourakis, M. I. (2011). Phylogenetic structure and evolution of regulatory genes and integrases of P2-like phages. *Autophagy* 7, 1371–1378. doi: 10.4161/bact.1.4.18470

Conflict of Interest: The authors declare that the research was conducted in the absence of any commercial or financial relationships that could be construed as a potential conflict of interest.

Copyright © 2019 Pacífico, Hilbert, Sofka, Dinhopl, Pap, Aspöck, Carriço and Hilbert. This is an open-access article distributed under the terms of the Creative Commons Attribution License (CC BY). The use, distribution or reproduction in other forums is permitted, provided the original author(s) and the copyright owner(s) are credited and that the original publication in this journal is cited, in accordance with accepted academic practice. No use, distribution or reproduction is permitted which does not comply with these terms.

frontiers in Microbiology

ORIGINAL RESEARCH
published: 28 November 2019
doi: 10.3389/fmicb.2019.02772

vB_PaeM_MIJ3, a Novel Jumbo Phage Infecting *Pseudomonas aeruginosa*, Possesses Unusual Genomic Features

*Mohammed Imam[1,2], Bandar Alrashid[3,4], Faizal Patel[3], Ahmed S. A. Dowah[3], Nathan Brown[3], Andrew Millard[3], Martha R. J. Clokie[3] and Edouard E. Galyov[3]**

[1] Department of Respiratory Sciences, College of Life Sciences, University of Leicester, Leicester, United Kingdom, [2] Laboratory Department, University Medical Center, Umm Al-Qura University, Mecca, Saudi Arabia, [3] Department of Genetics and Genome Biology, College of Life Sciences, University of Leicester, Leicester, United Kingdom, [4] King Faisal Specialist Hospital and Research Centre, Riyadh, Saudi Arabia

Phages are the most abundant biological entity on Earth. There are many variants in phage virion sizes, morphology, and genome sizes. Large virion sized phages, with genome sizes greater than 200 kbp have been identified and termed as Jumbo phages. These phages exhibit certain characteristics that have not been reported in phages with smaller genomes. In this work, a jumbo phage named MIJ3 (vB_PaeM_MIJ3) that infects *Pseudomonas aeruginosa* PAO1 was isolated from an equine livery yard in Leicestershire, United Kingdom. The genome and biological characteristics of this phage have been investigated. MIJ3 is a Myovirus with multiple long tail fibers. Assessment of the host range of MIJ3 revealed that it has the ability to infect many clinical isolates of *P. aeruginosa.* Bioinformatics analysis of the phage genome indicated that MIJ3 is closely related to the *Pseudomonas* phage, PA5oct. MIJ3 possesses several unusual features that are either rarely present in other phages or have not yet been reported. In particular, MIJ3 encodes a FtsH-like protein, and a putative lysidine synthase, TilS. These two proteins have not been reported in phages. MIJ3 also possesses a split DNA polymerase B with a novel intein. Of particular interest, unlike other jumbo phages infecting *Pseudomonas* spp., MIJ3 lacks the genetic elements required for the formation of the phage nucleus, which was believed to be conserved across jumbo *Pseudomonas* phages.

Keywords: bacteriophages, *Pseudomonas aeruginosa*, jumbo phages, intein, host range analysis, antibiotic resistance, phylogenetic analysis

OPEN ACCESS

Edited by:
Robert Czajkowski, University of Gdańsk, Poland

Reviewed by:
Adelaide Almeida, University of Aveiro, Portugal
Shuai Le, Army Medical University, China

***Correspondence:**
Edouard E. Galyov
eg98@leicester.ac.uk

Specialty section:
This article was submitted to Virology, a section of the journal Frontiers in Microbiology

Received: *13 September 2019*
Accepted: *13 November 2019*
Published: *28 November 2019*

Citation:
Imam M, Alrashid B, Patel F, Dowah ASA, Brown N, Millard A, Clokie MRJ and Galyov EE (2019) vB_PaeM_MIJ3, a Novel Jumbo Phage Infecting Pseudomonas aeruginosa, Possesses Unusual Genomic Features. Front. Microbiol. 10:2772. doi: 10.3389/fmicb.2019.02772

INTRODUCTION

Pseudomonas aeruginosa is a widespread Gram-negative bacterium. It is an opportunistic pathogen and is the major cause of nosocomial infection with significant mortality rates. *P. aeruginosa* causes a wide variety of infections, ranging from self-limiting skin infections to life-threatening pneumonia and septicemia. Between January 2018 and January 2019, a total of 4,543 septicemia cases caused by *P. aeruginosa* were reported in England alone (Public Health England, 2019). The severity of *P. aeruginosa* infections is particularly high and problematic in immunocompromised

patients with conditions such as cystic fibrosis (CF) and chronic obstructive pulmonary disease (COPD) (Gonçalves-de-Albuquerque et al., 2016). In fact, chronic pulmonary infections with *P. aeruginosa* is a major cause of death in CF patients (Ashish et al., 2012). With increasing rates of multiple-drug resistance (MDR) *P. aeruginosa* infections, phages are suggested as an alternative treatment solution, or to be combined with antibiotic, to treat bacterial infections (Krylov et al., 2015).

Bacterial viruses, bacteriophages (or phages), are the most abundant microorganisms in the environment (Suttle, 2005). Strikingly, it is estimated that almost half of the bacterial cells present in the environment are killed by phages every day (Potera, 2013). Phages are generally found in abundance where their hosts are found, and as such they are commonly found and isolated from environments such as freshwater, seawater, and animal manure (Clokie et al., 2011; Chaturongakul and Ounjai, 2015). The most common habitats for *P. aeruginosa* are water, soil, plants, and animals (Chatterjee et al., 2017). These sources are natural environments from which *Pseudomonas*-specific phages can be isolated, as phages coexist with their host cells (Shaburova et al., 2006; Krylov, 2014). There is strong evidence supporting the effectiveness of phage therapy in the treatment of lung infections associated with *P. aeruginosa* (Waters et al., 2017). Recent work by Cafora et al. (2019) shows the effectivity of phages against *P. aeruginosa* infection in a model of zebrafish with CF.

Phages vary in their size, morphology, and genomes. Examples of common and well-studied phages are the T4 Myovirus, which has a genome size of 168,903 bp, the T7 Podovirus which has a genome size of 39,937 bp, and the T5 Siphovirus which has a genome size of 121,752 bp. Phages with larger genome sizes are grouped as either jumbo or mega phages.

Phages with genome sizes over 500 kb are grouped collectively as megaphages (Devoto et al., 2019). To date, only 15 megaphages have been found, all of which infect bacteria from the *Prevotella* genus (Devoto et al., 2019). All of the megaphages were identified genomically from the analysis of viral metagenomics data; these phages have not been physically isolated yet. On the other hand, phages with genome sizes >200 kb, but <500 kb, have been termed jumbo phages (Yuan and Gao, 2017). Over 150 jumbo phage genomes have been deposited into the EBI and NCBI databases. The majority of them infect different Gram-negative bacteria, of which includes species from *Escherichia*, *Aeromonas*, *Caulobacter*, *Erwinia*, *Pseudomonas*, *Vibrio*, and *Salmonella*. Only six jumbo phages infecting Gram-positive bacteria have been characterized; all of which infect *Bacillus* species. A full list of megaphages and jumbo phages described to date, can be found in **Supplementary Table 1**.

At the time of this manuscript's submission, the largest jumbo phages described are: *Bacillus* virus G with a genome size of 497,513 bp (Donelli et al., 1975), *Agrobacterium* phage Atu_ph07 with a genome size of 490,380 bp (Attai et al., 2018), and *Salicola* phage SCTP-2 with a genome size of 440,001 bp. According to the latest review on jumbo phages, the largest *Pseudomonas* phage is the *P. chlororaphis* phage 201φ2-1, with a 316,674 bp genome size (Thomas et al., 2008). All reported *Pseudomonas* jumbo phages are listed in **Table 1**.

TABLE 1 | A full list of jumbo phages infecting *Pseudomonas* species, including phage MIJ3 (red).

	Accession	Phage name	Classification	Genome length (bp)
1	NC_010821	201phi2-1	Phikzvirus	316,674
2	HQ630627	PhiPA3	Phikzvirus	309,208
3	MF042360	Phabio	Phikzvirus	309,157
4	LR588166	MIJ3	Unclassified	288,170
5	MK797984	PA5oct	Unclassified	287,182
6	JN627160	OBP	Unclassified	284,757
7	NC_017972	Lu11	Unclassified	280,538
8	AF399011	phiKZ	Phikzvirus	280,334
9	MF805716	SL2	Phikzvirus	279,696
10	KU521356	KTN4	Phikzvirus	279,593
11	AP019418	PA02	Phikzvirus	279,095
12	MF063068	Noxifer	Noxifervirus	278,136
13	JX233784	PA7	Phikzvirus	266,743
14	KF147891	PaBG	Unclassified	258,139
15	AJ697969	EL	Elvirus	211,215

Because of their large genome size, jumbo phages encode many hypothetical proteins with unknown functions, in addition to encoding homologs of bacterial proteins, which might be an indication for phage–bacterial evolutionary events. Unlike other well-studied phages such as T4, jumbo phages lack recognizable modular genome characteristics that help to classify this group of phages. Phylogenetic analysis of the essential phage elements such as the major capsid proteins, terminases, and other proteins, revealed the presence of a new and phylogenetically related group within the jumbo phages, these have been termed the "Rak2-like viruses" (Šimoliūnas et al., 2013). This group encompasses eight phages: CBB, vB_CsaM_GAP32, BF, vB_KleM-Rak2, K64-1, 121Q, vB_Eco_slurp01, PBECO4, and Atu_ph07 (Attai et al., 2018). Most of the other characterized jumbo phages belong to different taxonomic families and orders, making it a challenging task to determine the similarities between them. Therefore, the terms "megaphages" and "jumbo phages" are umbrella terms which refer to the size of phages rather than an inherent set of qualities.

Jumbo phages exhibit characteristics that are rarely, or not at all observed in phages with smaller genomes. However, most *Pseudomonas* jumbo phages share some lifestyle features. In particular, it has been shown by Chaikeeratisak et al. (2017a) that the genomes of *Pseudomonas* jumbo phages (201phi2-1, phiKZ, and phiPA3) encode conserved proteins responsible for the formation of the phage nucleus, and tubulin spindle in the host bacterium during phage replication. A nucleus-like structure is formed in the cytoplasm of infected bacteria after phage DNA injection. It surrounds the phage DNA and separates it from the host cytoplasm, allowing the replication and transcription of phage DNA to occur inside the "phage nucleus" (Chaikeeratisak et al., 2017b). It has been suggested that the presence of such a nucleus-like structure is a conserved characteristic feature of all jumbo phages infecting *Pseudomonas* species (Chaikeeratisak et al., 2017a).

In this article, we report the isolation and characterization of a novel *P. aeruginosa* jumbo phage designated MIJ3 (vB_PaeM_MIJ3) with a genome size of 288,170 bp. We describe the MIJ3 phage morphology, pattern of infectivity, genomics characteristics, and proteomic identification of some of the major structural components. We also discuss how phage MIJ3 is a unique phage representing a novel phage species and genus.

MATERIALS AND METHODS

Bacterial Strains and Culture Conditions

Pseudomonas aeruginosa strain PAO1 was used for phage isolation and propagation. Cells were cultivated in LB (Luria-Bertani) broth at 37°C with shaking at 120 RPM. The bacterial strains used for the phage MIJ3 host range analysis were 44 Liverpool Epidemic Strains (LES) (Winstanley et al., 2009), 12 strains isolated from patients with ventilator-associated pneumonia (VSP) at the Leicester Royal Infirmary (Freestone et al., 2012), a strain isolated from a COPD patient (Source: Dr. Christopher Turkington) and 2 lab strains *P. aeruginosa* PAO1 and PA14 (**Table 2**).

Isolation of Phage MIJ3

Phage MIJ3 was isolated from a manure run-off in an equine livery yard, on which sheep are also kept, in Leicestershire. Due to the nature of the sample, a series of filtration steps were performed, starting initially with a 25 mm filter, down to filters with 0.22 μm pore sizes, this in order to remove bacteria. The filtered sample was screened for the presence of culturable phages using the plaque assay technique (Bonilla et al., 2016). Briefly, a mixture containing 300 μl of mid-log bacterial culture, 100 μl of the filtered sample, and 7 ml of LB top agar (0.7%) was poured on to a LB base plate and incubated overnight at 37°C to allow for the formation of phage plaques.

Plaque Purification and Phage Propagation

A single plaque was picked and resuspended in 500 μl of SM buffer (5.8 g NaCl, 2.0 g $MgSO_4 \cdot 7H_2O$, 50 ml 1 M Tris–HCl, pH 7.4, in 1 L of dH_2O). After incubating for 60 min at 37°C, the solution was centrifuged, and the supernatant was filtered through 0.22 μm pore size filters. To produce a homogenous phage stock, seven rounds of single plaque purification were performed. Thereafter, the propagation of the phage was performed by preparing a plate lysate. The lysate was centrifuged, and the supernatant was filtered through a 0.22 μm pore size filter to remove bacterial cells (Bonilla et al., 2016). The titer of propagated phage was measured by the spot test as described in Mazzocco et al. (2009) with modifications. Briefly, phage lysate was serially diluted (12-fold) in SM buffer, and 10 μl of each dilution was spotted on a double-layer LB plate. The bottom layer contains 1% (w/v) LB agar and the top layer is composed of 0.5% (w/v) LB agar mixed with 100 μl of exponentially growing *P. aeruginosa* culture. The plates were all dried for 25 min in a laminar flow hood (ASTEC, MicroFlow) before it was incubated at 37°C for 18 h. The plaque forming unit (pfu/ml) was measured by counting the plaques in the dilution that have 3–30 countable plaques using the following calculation: Average number of plaque × 100 × reciprocal of dilution = pfu/ml.

TABLE 2 | A summary list of *P. aeruginosa* strains used in this study (a full detailed list of strains is presented in **Supplementary Table 2**).

Strain	Source	References
PAO1	Lab strain	Lab strain
PA14	Lab strain	Lab strain
LES strains 1–40	Cystic fibrosis patients	Winstanley et al., 2009
LES400	Cystic fibrosis patient	
LES431	Cystic fibrosis patient	
LESB58	Cystic fibrosis patient	
LESB65	Cystic fibrosis patient	
LRI strains 1–12	Ventilator-associated pneumonia patients	Freestone et al., 2012
COPD	COPD patient	Dr. Christopher Turkington

Transmission Electron Microscopy

Transmission electron microscopy analysis was performed according to the protocol of Ackermann (2009). Phage MIJ3 was negatively stained using 2% uranyl acetate on a carbon-coated grid, and visualized using the JEM 1400 transmission electron microscope (JEOL Co., Japan) with an accelerating voltage of 80 kV (Leicester, United Kingdom). Phage particle dimensions were measured using ImageJ version 1.49o[1] in relation with the scale bar generated from the microscope.

Adsorption Assay

To determine the time required for phage MIJ3 to attach to its host *P. aeruginosa* PAO1, an adsorption assay was performed according to the protocol mentioned by Kropinski (2009). Briefly, 0.95 ml of LB broth, and three drops of chloroform were added to 12 labeled tubes and placed on ice to chill for 10 min. A mid-log phase bacterial culture was diluted to 10 ml to an OD_{600} of 0.2. Two flasks (A and C) were filled with 9 ml of bacterial culture and LB broth, respectively, and placed in a shaking water bath (60 rpm) at 37°C. At 0 min, 1 ml of the warmed phage being tested at a titer of 1×10^5 pfu/ml was added. Immediately, 1 ml of phage was added to the control flask (C). Aliquots of 0.05 ml from flask (A) were removed to the chilled labeled tubes every 1 min and mixed vigorously. Plaque assays were performed using test tubes containing 0.1 ml of chloroform in order to measure the phage titration.

One-Step Growth Curve

To define the latent period and the average burst size of MIJ3, the one-step growth experiment was performed as described previously (Hyman and Abedon, 2009). Briefly, 9 ml of bacterial culture at an OD_{600} of 0.2, and 90 μl of phage MIJ3 at a concentration of 10^8 (MOI of 0.01) were mixed and incubated

[1]https://imagej.nih.gov/ij/

for 6 min at 37°C. The mixture was centrifuged at 4,500 rpm for 5 min at 4°C to pellet the cells. The resultant pellet was washed with 5 ml of fresh LB broth and centrifuged again. The pellet was re-suspended in 10 ml of LB broth, and the mixture was incubated at 37°C. Aliquots of 1 ml of the mixture were collected at 15-min intervals for 2 h. Phages at each time points, including time point 0, were diluted and enumerated via the plaque assay. The pfu/ml was calculated and plotted against time. The period of latency was observed, and phage burst size was calculated from the plotted curve.

Killing Assay

To assess the killing activity of phage MIJ3 on the host, *P. aeruginosa* PAO1 growing in LB was infected with MIJ3 in different MOIs as described in Chen et al. (2018). Briefly, 30 μl of phage at concentrations of 10^{10}, 10^{9}, and 10^{8} PFU/ml were mixed separately with 270 μl of mid-log bacteria at concentration of 10^{8} CFU/ml to make MOIs of 10, 1, and 0.1, respectively. The mixtures were incubated at 37°C and the bacterial growth was then monitored by measuring optical densities at OD_{600} for 3 h. Bacterial culture without phages was used as a control. The data were obtained from three independent experiments.

Thermal and pH Stability of Phage MIJ3

The stability of phage MIJ3 in different temperatures was investigated. Aliquots of phage MIJ3 were incubated at 40, 50, 60, 70, 80, 90, and 100°C for 1 h before enumerating the surviving phages by spot test. Phage stability under different pH conditions was carried out according to Ahmadi et al. (2016). SM buffer was prepared with different pH values, ranging from 1 to 10 using either 1 M HCL or 1 M NaOH. MIJ3 at a concentration of 10^{11} was added to each pH solution, and the solutions were incubated for an hour before quantifying the number of phages in each solution.

Host Range Analysis

To determine the host range of MIJ3, 10 μl of phage lysate was spotted on to a lawn of each of the tested *P. aeruginosa* strains isolated from patients with CF or COPD. The appearance of the spot was observed after an overnight incubation of the plates at 37°C, and scored as (1) for complete lysis, (2) for turbid and weak lysis, and (3) for no lysis. Strains marked as 1 or 2 were analyzed further by spot testing to confirm any plaque formation.

Phage DNA Extraction

The DNA from phage MIJ3 was extracted by using the phenol–chloroform–isoamyl alcohol method as described in Nale et al. (2015). Phage lysate was treated with DNase and RNase to remove free DNA. To degrade the phage capsid, EDTA, proteinase K, and SDS were added to the lysate, and the mixture was incubated for an hour at 55°C. Phenol–chloroform–isoamyl alcohol (25:24:1) was added to the mixture at a 1:1 ratio and vortexed. The resulting sample was centrifuged at 21,000 × *g* for 15 min. The top aqueous layer was collected and treated with 1 volume of 3 M sodium acetate, and 2 volumes of ice-cold absolute ethanol, and then incubated for 3 h at −20°C and, centrifuged at 21,000 × *g* for 15 min. The DNA pellet was washed with 75% ethanol and re-suspended in upH_2O. The DNA concentration was measured using the Qubit fluorometer (Thermo Scientific).

Sequencing and Bioinformatics Analysis

Genomic libraries of phage MIJ3 DNA were prepared using Illumina's TruSeq® DNA Library Prep Kit (300 bp, FC-121-2003, Illumina), and whole genome sequencing was carried out using the MiSeq® FGx system (Illumina). The resulting FASTQ files were assembled with Megahit version 1.2.1 (Li et al., 2015, 2016). The genome was sequenced to an average coverage depth of 35.38×. The resultant single phage contig was annotated with Prokka version 1.12, using the protein model databases HAMAP, VOG and Bacteria Viruses. In addition to this, manual gene prediction using all of the complete viral genomes available within the NCBI database and the European Nucleotide Archive (ENA) was performed (Seemann, 2014). Another method of annotation was performed using the Rapid Annotation using Subsystem Technology (RAST) pipeline as described previously (McNair et al., 2018).

An MIJ3 genome map was generated and visualized using Artemis version 17.0.1 (Carver et al., 2011). For phylogenetic analysis, amino acid sequences of phage core proteins such as the major capsid and terminase were checked for similarities in the NCBI database using BLASTp tool. Moreover, phages with homology to the amino acid sequences of these MIJ3 proteins were selected to generate phylogenetic trees using the MEGA7 software (Molecular Evolutionary Genetics Analysis) version 7.0 (Kumar et al., 2016). Selected amino acid sequences of phage proteins (major capsid protein and terminase) were aligned using ClustalW, and the resulting alignment file was used to create phylogenetic trees by the neighbor-joining method (Saitou and Nei, 1987). Genome comparison was analyzed using EasyFig version 2.2.3 (Sullivan et al., 2011).

To determine genome-to-genome distance of phage MIJ3 and other phages in the databases, VICTOR online tool was used[2]. All pairwise comparisons of the amino acid sequences were conducted using the Genome-BLAST Distance Phylogeny (GBDP) method (Meier-Kolthoff et al., 2013) under settings recommended for prokaryotic viruses (Meier-Kolthoff and Göker, 2017). The resulting intergenomic distances were used to infer a balanced minimum evolution tree with branch support via FASTME including SPR post-processing (Lefort et al., 2015). Branch support was inferred from 100 pseudo-bootstrap replicates each. Trees were rooted at the midpoint (Farris, 1972). Taxon boundaries at the species, genus, and family level were estimated with the OPTSIL program (Göker et al., 2009), the recommended clustering thresholds (Meier-Kolthoff and Göker, 2017), and an *F*-value (fraction of links required for cluster fusion) of 0.5 (Meier-Kolthoff et al., 2014).

[2]https://ggdc.dsmz.de/victor.php

Accession Numbers

Reads for phage MIJ3 were deposited to the ENA at the European Bioinformatics Institute (EBI) under project accession number PRJEB32093. The taxon ID of MIJ3 is 2567864, and the phage genome was submitted under accession number LR588166.

Phage Purification Using CIM® Monoliths

Phage MIJ3 was purified using an anion-exchange chromatography column as described in Vandenheuvel et al. (2018) with some modifications. Briefly, 5 ml of the phage lysate (1.5×10^{11} pfu/ml) was dialyzed overnight at 4°C against a loading buffer (4 g $MgSO_4 \cdot 6H_2O$, 50 ml of 1 M Tris–HCl, pH 7.5, ultra-pure H_2O up to 1 L). The CIMmultus™ QA-1 Advanced Composite Column was attached to the AKTA™ FPLC™ system before washing with the loading buffer. The elution buffer [116.9 g (2 M) NaCl, 4 g $MgSO_4 \cdot 6H_2O$, 50 ml of 1 M Tris–HCl, pH 7.5, ultra-pure H_2O up to 1 L] was added to the phage lysate, and the mixture was loaded on to the column. The fractions were analyzed using the UNICORN™ and GraphPad Prism software. Phage titers in each fraction were determined by spot tests (**Supplementary Figure 1**).

Proteomics Analysis

An aliquot of 25 μl purified phage was suspended in SDS loading buffer and heated for 5 min at 95°C. Then, proteins were separated using 12% SDS-PAGE gel, and stained using Coomassie stain. The major bands were extracted from the gel and analyzed by mass spectrometry (LC–MS/MS) at the Protein Nucleic Acid Chemistry Laboratory (PNACL, University of Leicester, United Kingdom), in accordance with Lavigne et al. (2009).

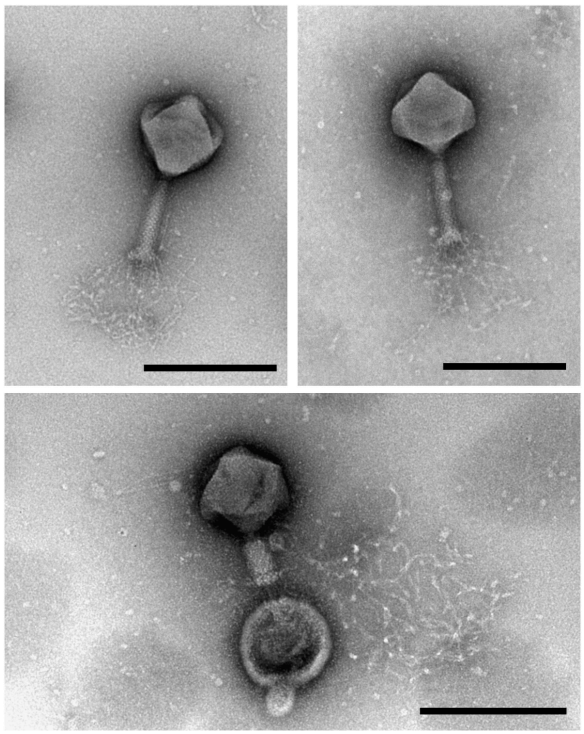

FIGURE 1 | Transmission electron microscopy analysis of the purified phage MIJ3 revealed that MIJ3 belongs to the *Myoviridae* family and has an overall length of 258 nm. Phage MIJ3 possesses long tail fibers attached to the baseplate. Contracted tail can be observed upon interaction of MIJ3 with an outer membrane vesicle of *P. aeruginosa* (scale bar = 200 nm).

RESULTS

Isolation of Phage MIJ3

In an attempt to isolate novel phages capable of infecting *P. aeruginosa*, we sampled water from mixed animal manure (horse and sheep) from an equine yard. A sample of the manure runoff water was collected and analyzed for the presence of phages capable of infecting *P. aeruginosa* using spot tests. Several phage plaques were observed on the *P. aeruginosa* PAO1 lawn. Plaques with distinct morphologies were selected for further studies. A small distinct plaque (approx. 0.5 mm in diameter) was purified via several rounds of plaque assays. The isolated phage was designated as vB_PaeM_MIJ3 (referred to herein as MIJ3), according to the phage naming criteria suggested by Adriaenssens and Brister (2017).

Morphological Characteristics of Phage MIJ3

Transmission electron microscopy analysis of purified MIJ3 revealed that the phage belongs to the *Myoviridae* family. The average overall length of the phage from the top of the capsid to the base plate is 258 nm, with an average head height of 130 nm and 118 nm width. The phage tail has a height of 140 nm and length of 28 nm (n = 10 phages) (**Figure 1**). MIJ3 has the characteristic morphological features of a Myovirus morphotype A1: a classical phage head, a contractile tail with a collar, and a spiky baseplate attached to thin long kinked fibers (**Figure 1**).

Adsorption Assay and One-Step Growth Curve

An adsorption assay was performed to identify the rate at which phage MIJ3 adsorbs to the surface of *P. aeruginosa* PAO1. The resulted graph (**Figure 2A**) revealed that around 50% of the phages attach to the host cells within 6 min, and 90% of the phages were adsorbed to host cells in 20 min. Phage growth parameters were determined by analyzing the phage growth cycle using the one-step growth curve experiment. The latent period of MIJ3 is between 45 and 50 min, and the burst size of one lytic cycle is approx. 68 pfu per infected cell (**Figure 2B**).

Killing Assay

To assess the killing activity of the phage on the host strain, *P. aeruginosa* PAO1 was grown in LB broth and infected with MIJ3 using different MOI values (10, 1, and 0.1), and the bacterial growth was monitored by measuring optical densities at OD_{600}. In each case, the phage infection resulted in the inhibition of bacterial growth, which was progressively more prominent with an increase in the MOI. The lysis kinetics of MIJ3 was determined on strain PAO1. The optical density of the culture decreased at

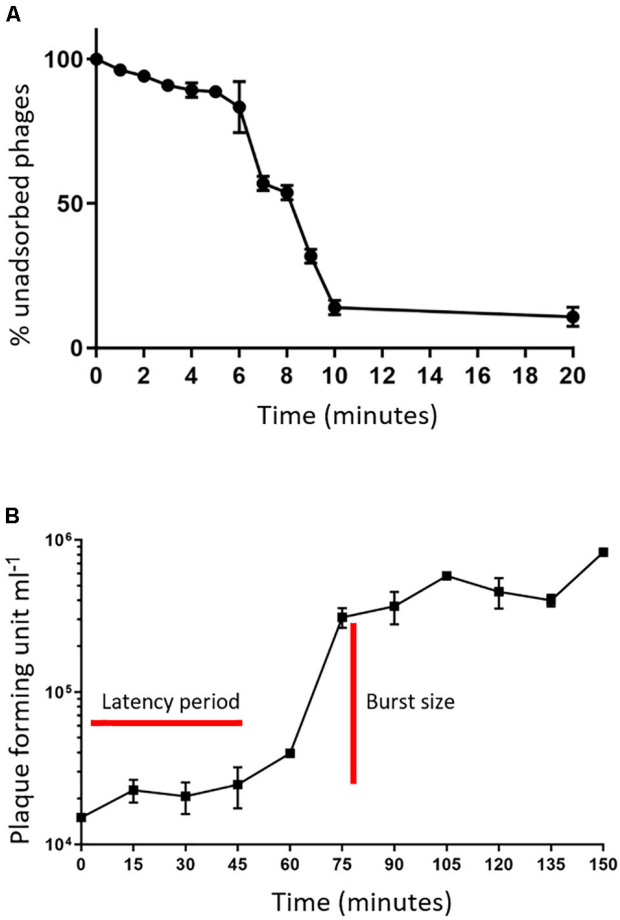

FIGURE 2 | (A) Adsorption assay of phage MIJ3 on *P. aeruginosa*. **(B)** Growth parameters of MIJ3. The latent period of MIJ3 is between 45 and 50 min, and the burst size of one lytic cycle is 68 pfu per infected cell. Three biological replicates performed.

approximately 80 min post-infection with all three MOI values. At a high phage titer (MOI of 10), the bacterial growth rate was reduced because of phage infection. When an equal ratio of phage to bacteria was used (MOI of 1), bacterial growth showed a slight increase after 90 min. At a lower phage titer (MOI of 0.1), bacterial growth was higher than that observed with the cells infected at an MOI of 1 and 10, but still lower than the non-infected cells. The non-infected sample was used as a control, showing the growth of *P. aeruginosa* without adding any phage (**Figure 3**).

Thermal and pH Stability of Phage MIJ3

Assessing the stability of phages provides essential information for storage, transfer, and downstream experiments with the phage. Phage MIJ3 shows high stability at temperatures of 40, 50, and 60°C, as phage titers were similar to the control (4°C). After incubation for an hour at 70°C, there was a 4-log reduction in the phage MIJ3 titer, indicating that only 1 in 10,000 phages have survived under such conditions. Very few, if any, MIJ3 phage particles were able to survive at 80, 90, and 100°C (**Figure 4A**). Phage MIJ3 appears to be stable at pH values from 3 to 10. However, MIJ3 is not able to survive highly acidic pH values, as no phages survived testing against pH values of 2 and 1 (**Figure 4B**).

Host Range of Phage MIJ3

The host range and lytic activity of MIJ3 on different clinical strains of *P. aeruginosa* was assessed by using spot test assays. Zones of lysis were observed and scored as (1) for complete lysis, (2) for turbid and weak lysis, and (3) for no lysis. For strains that were marked as (1) or (2), the phage stock was diluted and spotted on the bacterial lawn to show that the phage was forming single plaques, and the clearing was not due to lysis from without. The results reveal that MIJ3 is able to infect, and form plaques on,

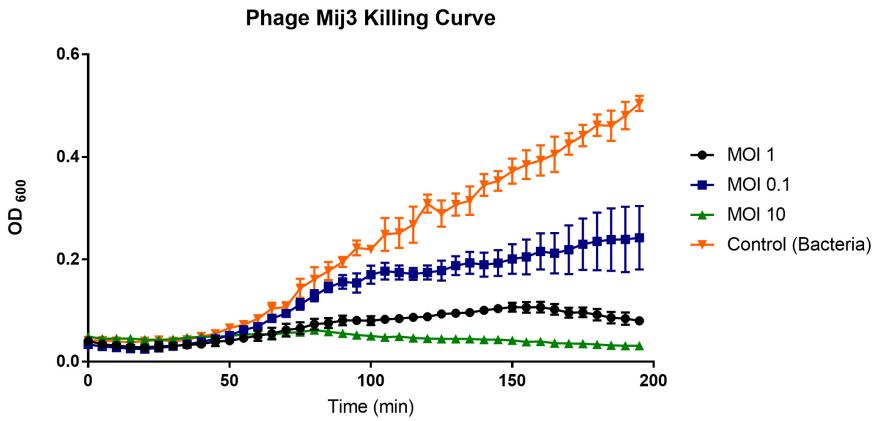

FIGURE 3 | A graph showing the ability of phage MIJ3 to lyse *P. aeruginosa* PAO1 at different multiplicity of infections (0.1, 1, and 10) in LB medium at 37°C. At a high phage titer (MOI 10), bacterial growth was inhibited because of the phage infection (green). When an equal ratio of phage/bacteria was used (MOI 1), bacterial growth showed a slight increase after 90 min (black). At lower phage titer (MOI 0.1), bacteria were growing at higher levels but less than the non-infected cells (blue). The non-infected sample was used as a control (orange). Each experiment was done in triplicate, and OD_{600} values were measured, averaged, and plotted. Error bars represent SEM for three replicates.

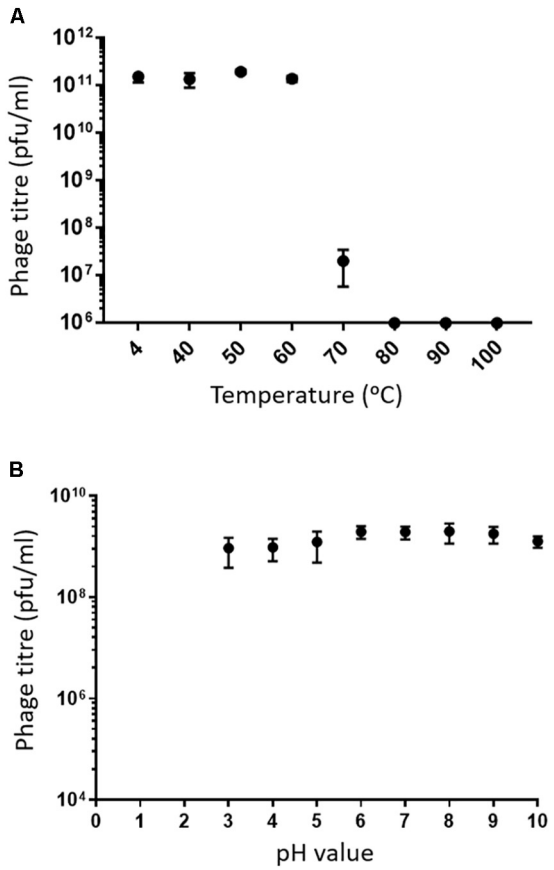

FIGURE 4 | (A) Thermal stability of MIJ3: the phage was incubated in LB medium at different temperatures for 60 min. The phages survived at temperatures of 40, 50, and 60°C. At 70°C, phage concentration showed a 4-log drop. MIJ3 was not able to survive at 80, 90, and 100°C. Error bars represent SEM for three replicates. **(B)** pH stability of MIJ3. The phage is highly stable at pH values from 3 to 10; however, no survival was observed when phages at a pH of 2 and 1.

multiple clinical strains of *P. aeruginosa* isolated from patients with CF or VSP (as detailed in **Supplementary Table 2**).

MIJ3 Genome and Phylogeny Analysis

The genome of phage MIJ3 was sequenced using the MiSeq platform, and the sequence was annotated by Prokka and RAST as described previously (Seemann, 2014; McNair et al., 2018). The phage was found to possess a large genome of 288,170 bp and was thus classified as a jumbo phage. The average G + C content of the genome of MIJ3 is 33.3%, which is in striking contrast to that of the bacterial host (66%). Blastn comparison of the MIJ3 sequence against the NCBI non-redundant database revealed that MIJ3 has significant similarity with one phage, a *Pseudomonas* phage vB_PaeM_PA5oct (98.72% identity). This was a surprising finding as the genome size of PA5oct was previously reported to be 375 kbp (Drulis-Kawa et al., 2014). However, the sequence deposited in the NCBI database revealed that the actual genome size of PA5oct is 287,182 bp (accession number: MK797984).

The annotation of the phage MIJ3 sequence revealed the presence of 405 predicted open-reading frames (ORFs) and 12 tRNAs (**Supplementary Table 3** and **Figure 5**). There are 21 ORFs encoding structural components, including 5 capsid proteins (gp41, gp406, gp409, gp410, and gp411) and 6 predicted tail proteins (gp1, gp4, gp36, gp142, gp144, and gp386). In addition, 24 proteins involved in DNA replication, recombination, repair, and transcription were identified. The majority of predicted genes (328 ORFs) encode hypothetical proteins with unknown functions. The MIJ3 genome encodes 12 tRNAs located between gp228 and gp246 and arranged as tRNA-Met, tRNA-Leu, tRNA-Asn, tRNA-Thr, tRNA-Met, tRNA-Leu, tRNA-Arg, tRNA-Met, tRNA-Pro, tRNA-Gly, tRNA-Ser, and tRNA-Ser.

Phages MIJ3 and PA5oct have <10% ANI when compared with other phage sequences in the current databases, suggesting that they are a new species which belong to a new genus of phages that are not closely related to other phage groups. To find the location of MIJ3 in the phage continuum context, phylogenetic trees were generated for some of the predicted essential phage proteins, including the major capsid protein (**Figure 6**) and the terminase large subunit (**Figure 7**). From the assessment of phylogenetic trees, it seems that phage MIJ3 is not related to any other specific group of phages. The trees show the cluster of the newly identified group of jumbo phages called the Rak2-like phages family, which contains *Xanthomonas* phage XacN1 (Yoshikawa et al., 2018), *Agrobacterium* phage Atu_ph07 (Attai et al., 2018), *Serratia* phage BF (Casey et al., 2017), *Enterobacteria* phage vB_PcaM_CBB (Buttimer et al., 2017), *Cronobacter* phage vB_CsaM_GAP32 (Abbasifar et al., 2014), *Klebsiella* phage K64-1 (Pan et al., 2017), *Escherichia* phage 121Q (Ackermann and Nguyen, 1983), and *Klebsiella* phage vB_KleM-RaK2 (Šimoliūnas et al., 2013). Although the terminase of phage MIJ3 has similarities with RaK2-like phages, it is not considered as Rak2-like since all of these phages are over 300,000 bp, and due to the wide distance between the sequence of the major capsid protein sequence of phage MIJ3 and the Rak2-like phages. Furthermore, phylogenetic analysis of the major capsid protein tree shows that other *Pseudomonas* jumbo phages form an outgroup according to this protein sequence and are not closely related to MIJ3.

Like other jumbo phages described to date, in addition to ORFs encoding "typical" phage proteins, the MIJ3 genome encodes for several proteins showing sequence similarity to bacterial host proteins. Several such "host-like" proteins found to be encoded in the MIJ3 genome are rare in phages, of which, two proteins not been found in any phages to date. These two proteins are homologs of the FtsH protein (ATP-dependent zinc metalloprotease) and TilS [tRNA(Ile)-lysidine synthase]. FtsH and TilS are widely conserved proteins in bacteria. FtsH, formerly known as HflB, plays an important role in maintaining membrane integrity, cell division, and in the heat shock response (Bieniossek et al., 2006). TilS is a tRNA modification enzyme and is essential for bacterial viability (Suzuki and Miyauchi, 2010). To analyze the evolutionary relationship of the unique phage borne FtsH in phage MIJ3, and to track down the origin of this protease, a phylogenetic tree of FtsH was created as described

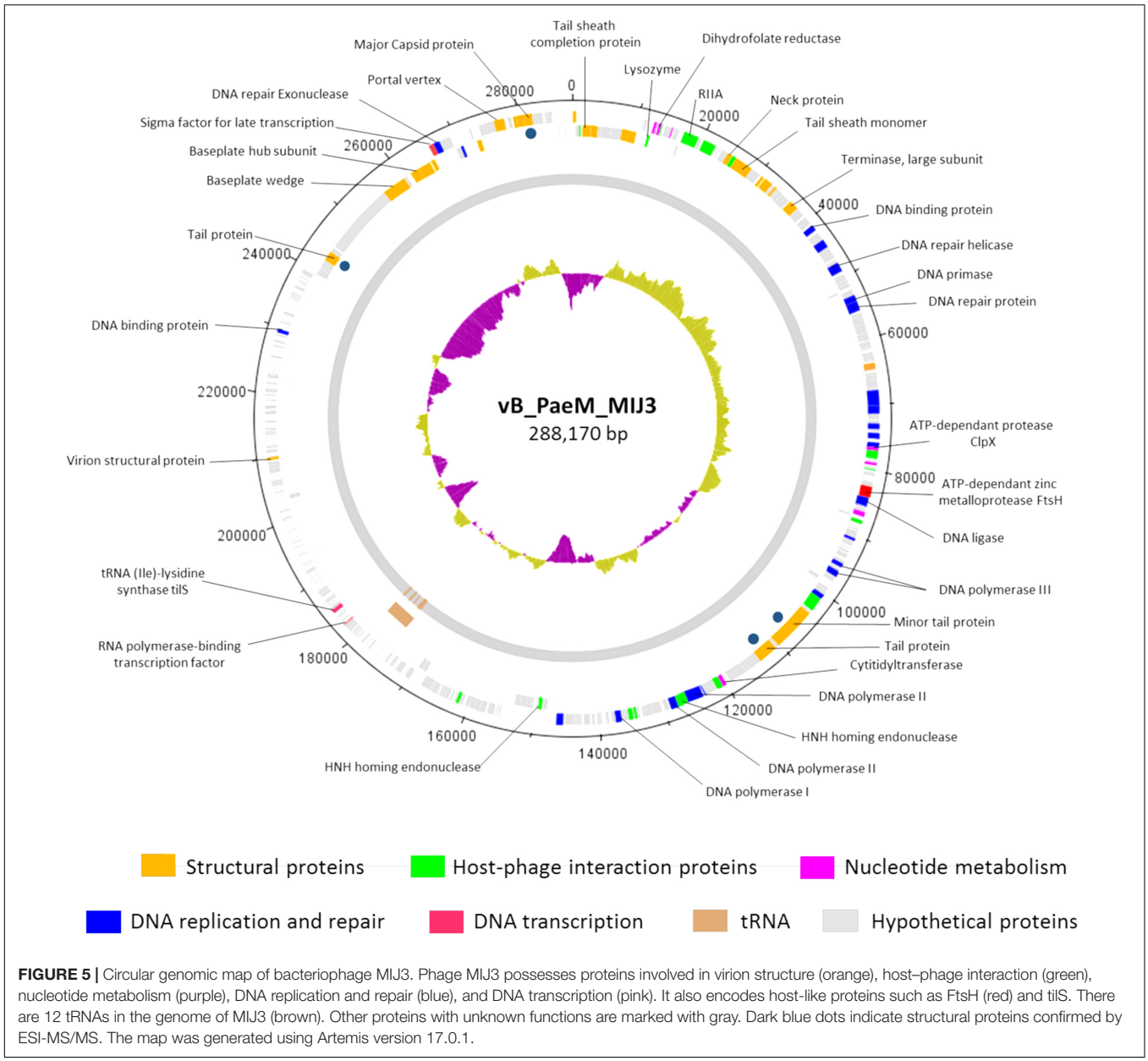

FIGURE 5 | Circular genomic map of bacteriophage MIJ3. Phage MIJ3 possesses proteins involved in virion structure (orange), host–phage interaction (green), nucleotide metabolism (purple), DNA replication and repair (blue), and DNA transcription (pink). It also encodes host-like proteins such as FtsH (red) and tilS. There are 12 tRNAs in the genome of MIJ3 (brown). Other proteins with unknown functions are marked with gray. Dark blue dots indicate structural proteins confirmed by ESI-MS/MS. The map was generated using Artemis version 17.0.1.

previously (**Figure 8**). The analysis shows that the bacterial FtsH proteins are grouped separately from viral FtsH. The FtsH of phage MIJ3 has a closer relationship to the bacterial FtsH, rather than the viral FtsH.

For the same purpose, a phylogenetic tree for the TilS protein was constructed using the neighbor-joining method shows that TilS MIJ3 amino acid sequence is identical to the sequence of the uncharacterized protein in phage PA5oct. Similar to the findings from the FtsH phylogeny analysis, the TilS sequence of phage MIJ3 is a closer relative to the bacterial TilS protein rather than the viral TilS. Although the genome of *P. aeruginosa* PAO1, the bacterial host of MIJ3, encodes TilS protein, the Tils protein of MIJ3 is distantly related to the host Tils (**Figure 9**).

Further analysis of the annotated MIJ3's genomic data revealed another unusual feature: a putative split intein with an HNH homing endonuclease family (orf154) within the genes encoding the DNA polymerase B (orfs153 and 155) (**Figure 10**). Inteins are mobile self-splicing elements intervening the host protein sequence, and they are excised post-translation through a process known as protein splicing (Perler, 2005). They are often associated with the homing endonuclease domain to mediate this genetic transfer (Dassa et al., 2009). Intein motifs can be identified by conserved residues that are involved in protein splicing (Pietrokovski, 1994; Perler et al., 1997). In phage MIJ3, the intein motif blocks were identified in the N-terminal splicing region: block A (SVDGSTILNTSL), block N2 (TIEELFNV), block B (NKVIVTEDHSIMV), and block N4

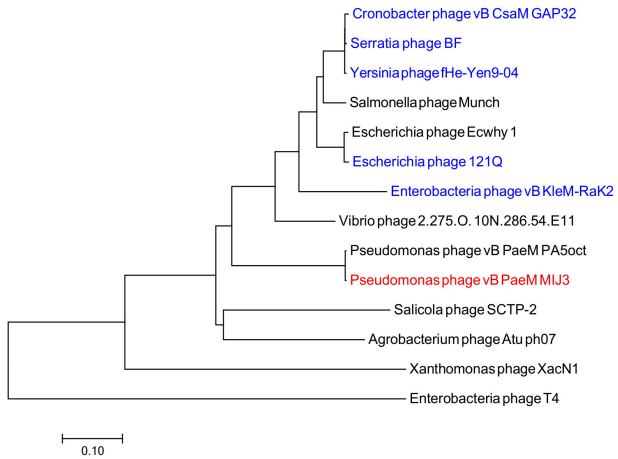

FIGURE 6 | Phylogenetic tree comparing the major capsid protein of phage MIJ3 (red) with its corresponding in other jumbo phages, including Rak2-like phages (blue). Phages were selected as they share homology with the amino acid sequences of the major capsid using Blastp. Phage T4 was selected as an outgroup phage that is not closely related to the corresponding sequence of MIJ3. The evolutionary history was inferred using the neighbor-joining method and the tree was constructed using MEGA7.

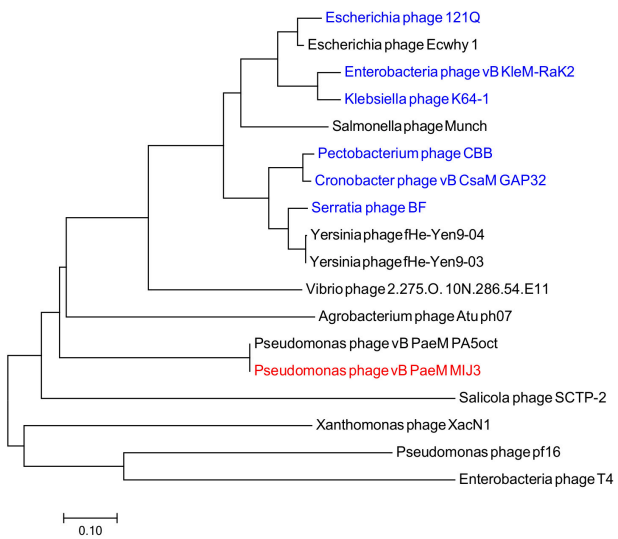

FIGURE 7 | Phylogenetic tree comparing the terminase, large subunit of phage MIJ3 (red) with its corresponding in other jumbo phages, including Rak2-like phages (blue). Phages were selected as they share homology with the amino acid sequences of the terminase using Blastp. Phage T4 was selected as an outgroup phage that is not closely related to the corresponding sequence of MIJ3. The evolutionary history was inferred using the neighbor-joining method and the tree was constructed using MEGA7.

(LLEVKPTDLTDSDIIL); and in the C-terminal splicing region: block F (VYDIGMKNPDNPYFF) and block G (GNNILVHNS). Bioinformatic analysis of the protein-splicing sequence element of the phage revealed that the putative MIJ3 split intein shares a similarity with the mini-intein present in the gene encoding PolB in another jumbo phage, the *Salicola* phage SCTP-2 (**Figure 10**).

Phage Purification Using CIM® Monoliths and Proteomics Analysis

Phage MIJ3 was purified by using an anion-exchange chromatography column as previously described in the section "Materials and Methods" (**Figure 11A**). Eluted fragments under the phage peak were pooled, and the phage titers were calculated using spot tests. The purified MIJ3 titer was 4×10^{10} pfu/ml, indicating that the phage titer decreased by 1 log, compared to the titer of the non-purified phage, which was 1.2×10^{11} pfu/ml. The purified MIJ3 virions were separated by SDS-PAGE, and several major protein bands were analyzed by MS. Four structural proteins were identified by LC–MS/MS, including the major (gp144) and the minor tail proteins (gp142), a tail fiber protein (gp386), and the major capsid protein (gp411) (**Figure 11B**). These proteins were confirmed by the genome annotation of the phage in relation to the sizes of their amino acid sequences in the gel and in the annotation information.

DISCUSSION

Phages are abundant in different environments but very large phages are not commonly isolated. They could be removed during the filtration process due to their large virion sizes, or because of their limited mobility on semi-solid plates (Serwer et al., 2007). Genomes of jumbo phages and megaphages encode a number of hypothetical proteins with unknown functions, and their biological features are understudied and not found in small phages. Jumbo phages have more genes encoding DNA replication and metabolism such as DNA polymerase and RNA polymerase in addition to genes responsible for translation (Yuan and Gao, 2017). Abundance of these genes indicates less dependency on the host in addition to wider host ranges. More studies are expected to be conducted to reveal more features of these phages.

Phage MIJ3, described here, is an interesting representative of jumbo phages for numerous reasons. The phage is effective against clinical strains of *P. aeruginosa* that were isolated from patients with CF or COPD. This suggests that MIJ3 can potentially be used for further phage therapy trials, especially for infections with multi-drug resistant *P. aeruginosa*. It can also be added to the existing phage cocktails for more effective outcomes. There is the need to test phage MIJ3 with other *P. aeruginosa* phages against more strains to expand the therapeutic applicability of jumbo phages. Other jumbo phages such as phiPA3, PA5oct, phiKZ, SL2, KTN4, PA02, PA7, and PaBG also have the ability to infect a wide range of clinical isolates of *P. aeruginosa* (Mesyanzhinov et al., 2002; Monson et al., 2011; Sykilinda et al., 2014; Latz et al., 2017). These phages were isolated from different sources all of which are, respectively, different to each other, examples include sewage, mudflat, lake water, and manure, indicating the diversity of available sources of phages with promising therapeutic potential.

Pseudomonas aeruginosa strains are associated with mucus formations and are able to surround themselves with exopolysaccharides, which are alginic acids, providing resistance

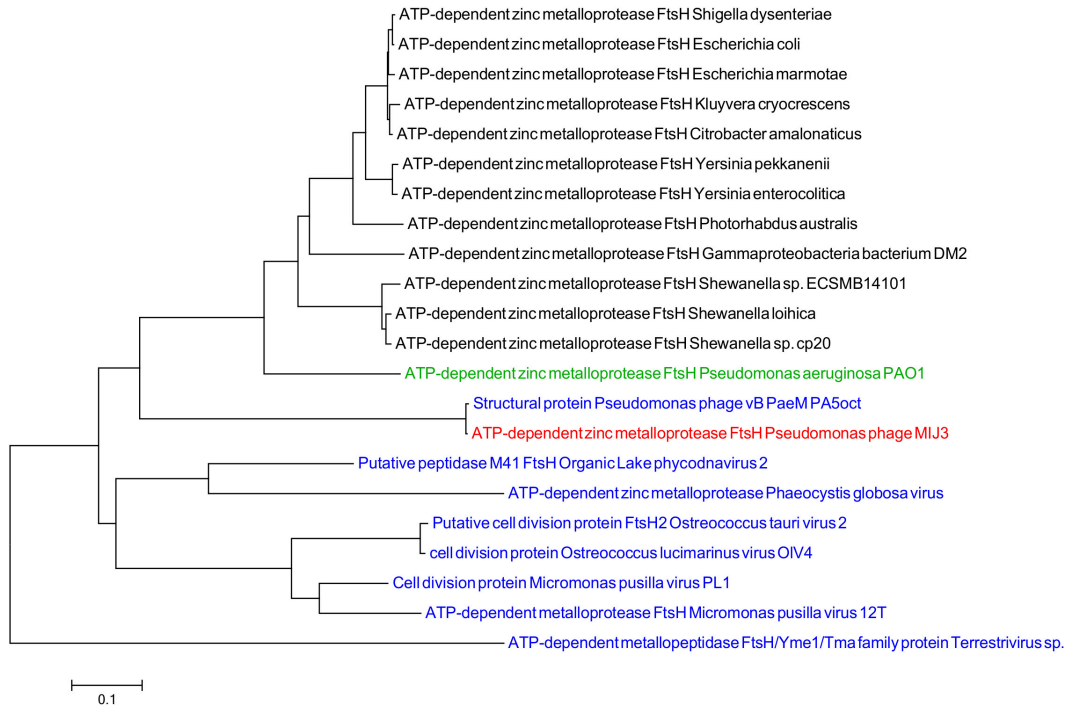

FIGURE 8 | Phylogenetic tree of FtsH based on the amino acid sequence of phage MIJ3 and the most similar sequences in the database. It shows the FtsH of MIJ3 (red), the most similar amino acid sequences in viruses (blue), and bacteria (black) including *P. aeruginosa* PAOI, the bacterial host of MIJ3 (green).

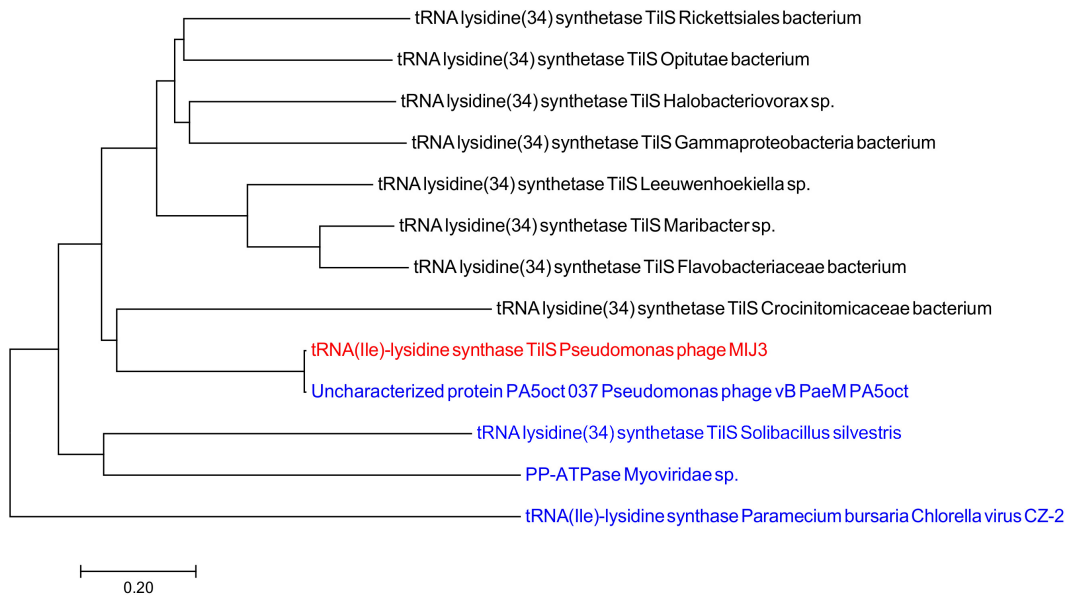

FIGURE 9 | Phylogenetic tree of TilS based on the amino acid sequence of phage MIJ3 and the most similar sequences in the database. It shows the TilS of MIJ3 (red), the most similar TilS amino acid sequences in viruses (blue), and bacteria (black).

to antibiotics and immune cells, especially in CF patients (Glonti et al., 2010; Morello et al., 2011). Phages have showed promising effects in treating infections caused by multi-drug resistant *P. aeruginosa* isolated from patients with CF *in vivo* and *in vitro* (Furfaro et al., 2018). Therefore, phage MIJ3 can potentially be used in phage therapy against *Pseudomonas* infections. In addition, phage endolysins and peptidoglycan-degrading enzymes from phages phiKZ and EL have been previously

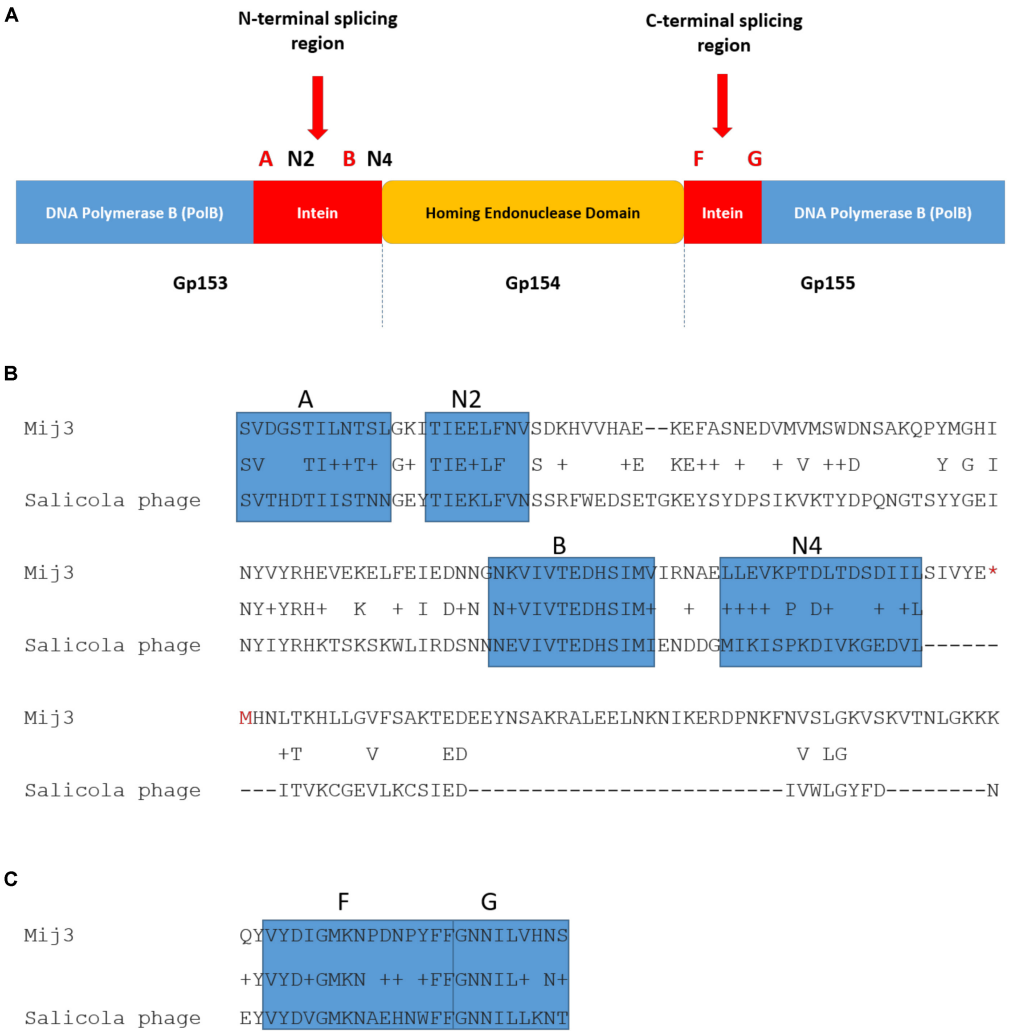

FIGURE 10 | The presence of intein in MIJ3. **(A)** A diagram illustrating the location of the intein and its conserved motifs in the genome of MIJ3 jumbo phage. **(B)** N-terminal splicing region sequence alignment between inteins inserted in the PolB of MIJ3 and the *Salicola* phage SCTP-2 with the identified intein motifs highlighted as blocks A, N2, B, and N4. **(C)** C-terminal splicing region sequence alignment of the intein in both phages with the identified intein motifs are highlighted as blocks F and G.

tested as potential antibacterial agents against *Pseudomonas* infections (Briers et al., 2007). Similar proteins from MIJ3 could be investigated and used for the same purpose.

The physical and chemical stability of phage MIJ3 was determined to provide more information with regards to phage storage, transport, and potential applications. MIJ3 is stable at temperatures ranging from 4 to 60°C; however, only approximately 1 in 10,000 phage particles survived when incubated at 70°C for 1 h, and it was inactivated when incubated at 80, 90, and 100°C. More than 90% of MIJ3 phage survived at pH values ranging from pH 10 to 3 but, couldn't survive at pH 1 and 2. It has been suggested that tailed phages are more resistant to adverse conditions such as temperature change and pH (Ackermann et al., 2004). For therapeutic purposes, phages are required to maintain stability in a wide range of temperatures and pH, to resist changes in environmental and ambient condition, and MIJ3 appears to satisfy these criteria. The ability to withstand the aforementioned conditions provides valuable information as to whether MIJ3 would be able to survive downstream processing steps such as encapsulation or spray drying, especially if MIJ3 was to be used for therapeutic purposes.

The genomic sequence of MIJ3 and PA5oct have greater than 95% suggesting that they represent a new phage species according to the main species demarcation criterion (Adriaenssens and Brister, 2017). These phages are unique as their genome sequences share ANI of < 1% with other phages in the database. Members of the same genus share a high degree of nucleic acid similarity (>50%) with others, along with factors such as genome length, average and percentage of coding sequencing, number of tRNA, and the presence of certain signature genes in member viruses (Adriaenssens and Brister, 2017).

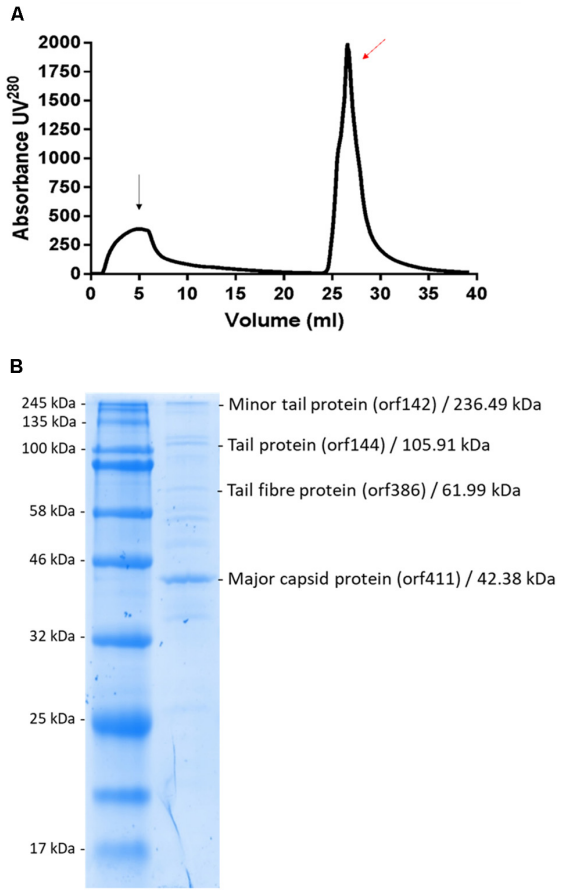

FIGURE 11 | (A) Linear gradient of MIJ3 purification using a DEAE column. The black arrow indicates the flow-through and the red arrow indicates the peak that corresponds with the presence of phage MIJ3. **(B)** Proteomic analysis of phage MIJ3 particles. Proteins of purified phage particles **(B)** were separated in 12% (wt/vol) polyacrylamide gel by SDS-PAGE and stained with Coomassie brilliant blue. The protein bands were subjected to LC–MS/MS analysis. On the right are the descriptions of the genes, their deduced molecular sizes based on the ORF sequences, and their possible functions. Positions of size markers are shown on the left **(A)**.

Analysis of the genome-to-genome phylogeny of phage MIJ3 and other phages (**Figure 12**), and the phylogenetic trees of the major capsid protein and terminase (large subunit) (**Figures 6**, **7**), shows that MIJ3 has a distant relation with other phages including GAP32, K64-1, Rak2, PBECO 4, and 121Q. According to the ICTV database, these phages are classified into different genera. Phages K64-1 and Rak2 are members of the *Alcyoneusvirus* genus, phages 121Q and PBECO4 belong to the *Asteriusvirus* genus, and phage GAP32 belongs to the *Mimasvirus* genus. In addition to VICTOR analysis, this suggests that MIJ3 and PA5oct represent a new genus.

The phage MIJ3 genome encodes proteins that have not yet been reported in phages, including the ATP-dependent zinc metalloprotease, FtsH (gp107), and the tRNA (Ile)-lysidine synthase, TilS (gp263). The functions of these proteins in MIJ3 are unknown. In bacteria, both FtsH and TilS play important roles and are essential to the viability of the cell (Shotland et al., 2000; Soma et al., 2003; Lin et al., 2013). Therefore, it is tempting to speculate that their role in MIJ3 could be to maintain the host viability during phage replication. This can be examined by constructing FtsH and or TilS mutants and comparing the infectivity of these mutants with the wild-type phage. The amino acid sequences of *ftsH* and *tilS* in MIJ3 are homologous to gp342 and gp37, respectively, of phage PA5oct, which were annotated as a structural protein and an uncharacterized protein, respectively. Further research is needed to confirm the nature and the function of these unique phage genes and proteins in MIJ3 and PA5oct.

The MIJ3 jumbo phage has several unusual genomic features, such as the GC content being drastically different from the host genome, or the presence of rare phage genes. However, MIJ3 is also unusual due to the absence of some features that were believed to be conserved across all *Pseudomonas* jumbo phages, such as the phage nucleus and phage spindle (Chaikeeratisak et al., 2017a). During the replication step, *Pseudomonas* phages 201phi2-1, phiPA3, and phiKZ can form a proteinaceous nucleus, or shell inside the host. This nucleus encloses viral DNA and enzymes involved in the DNA replication and transcription. Unlike these *Pseudomonas* jumbo phages, phage MIJ3 does not appear to encode the PhuZ bipolar tubulin spindle, as genome

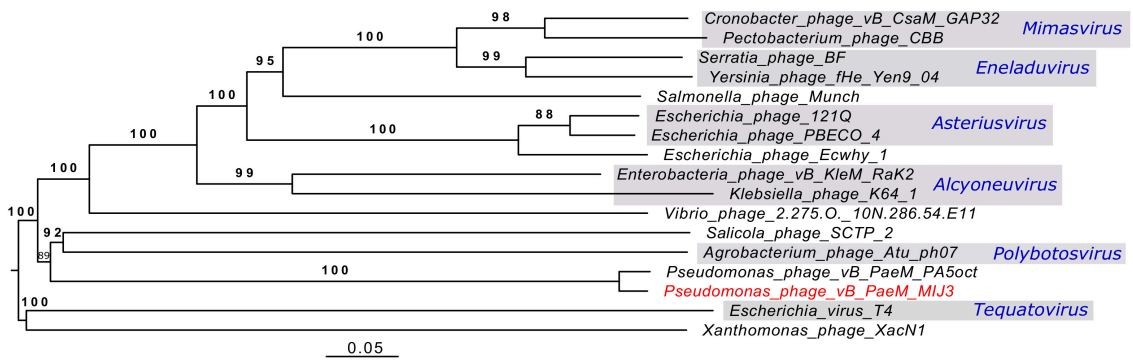

FIGURE 12 | A phylogenetic tree of phage MIJ3 and the closest phages. It shows the phylogenomic GBDP tree yielding average support of 97%. The numbers above branches are GBDP pseudo-bootstrap support values from 100 replications. The branch lengths of the resulting VICTOR trees are scaled in terms of the respective distance formula used. Phage MIJ3 is marked in red color, and genus of classified phages is marked in blue. The tree was generated using the VICTOR server.

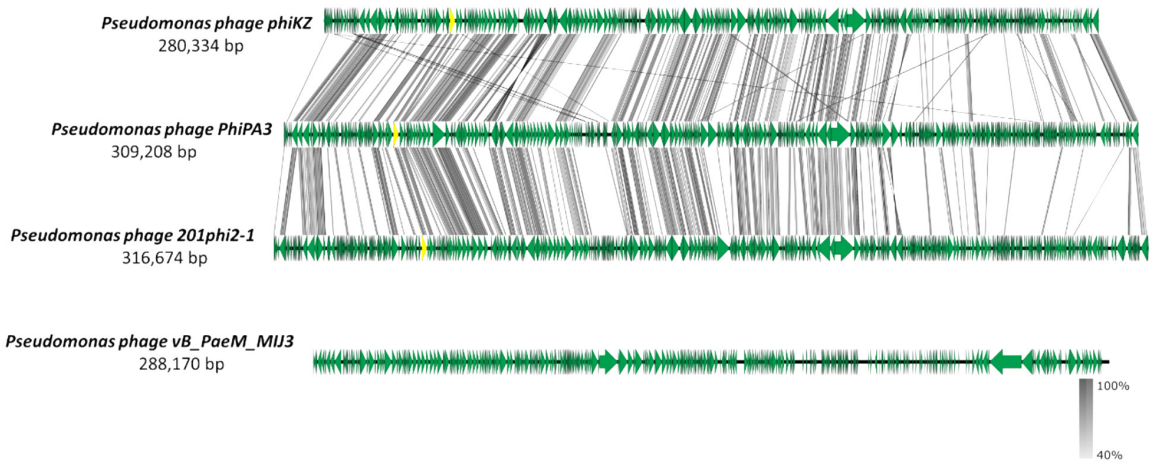

FIGURE 13 | Comparative analysis of phage MIJ3 genome with the genomes of other jumbo *Pseudomonas* phages phiKZ, PhiPA3, and 201phi2-1. Phage MIJ3 shows no homology to the other three phages. The yellow areas indicate the conserved genes encoding the phage nucleus and spindle tubulin in phages phiKZ, PhiPA3, and 201phi2-1, of which is absent in phage MIJ3.

comparison between MIJ3 and phages 201φ2-1, phiPA3, and φKZ revealed that there is no gene encoding a protein with recognizable sequence similarity to PhuZ in the sequence of phage MIJ3 (**Figure 13**).

MIJ3 DNA sequence is highly similar to that of another *Pseudomonas* phage, PA5oct (Accession Number MK797984). An earlier publication describing PA5oct suggests that its genome size is approximately 375 kb (Drulis-Kawa et al., 2014). However, the genomic sequence of phage PA5oct was released in April 2019, and is in fact 287,182 bp. It is intriguing that two highly related phages were independently isolated from two geographically distant locations: phage MIJ3 (described here) was isolated from a manure sample of a domestic farm near Leicester, United Kingdom, while phage PA5oct was isolated from a sewage sample from an irrigated field near Wrocław, Poland (Drulis-Kawa et al., 2014). These findings not only suggest a wide distribution of MIJ3/PA5oct phages, but also indicate their high genomic stability.

CONCLUSION

In conclusion, this study presents analyses of the biological and genomic features of MIJ3, suggesting that phage MIJ3 and the previously identified phage PA5oct should be grouped together into a novel phage genus. In addition, phage MIJ3 has antimicrobial activity against clinical *P. aeruginosa* isolates, suggesting the potential use of this phage as a therapeutic agent.

DATA AVAILABILITY STATEMENT

Whole genome sequencing datasets generated for this study can be found in the ENA, LR588166.

AUTHOR CONTRIBUTIONS

MI carried out the main body of research, performed the bioinformatics analysis, and wrote the manuscript. BA contributed to the phage growth experiments. FP contributed to the pH stability and adsorption assay experiments. AD contributed to the AKTA purification work. NB contributed to the sequencing. AM edited the manuscript and contributed in bioinformatics analysis. MC edited the manuscript and collected the sample for phage isolation. EG supervised the work progress and edited the manuscript.

FUNDING

This work was funded by the Ministry of Education in Saudi Arabia as a Ph.D. sponsorship to MI (UMU554), the MRC Consortium grant for Medical Microbial Bioinformatics (MR/L015080/1), and EVAL-FARMS grant: Evaluating the Threat of Antimicrobial Resistance in Agricultural Manures and Slurries (NE/N019881/1).

ACKNOWLEDGMENTS

The authors thank Natalie Allcock and Anna Straatman-Iwanowska for their assistance with the TEM. The authors also thank Peter Hickenbotham for his technical assistance throughout the project.

SUPPLEMENTARY MATERIAL

The Supplementary Material for this article can be found online at: https://www.frontiersin.org/articles/10.3389/fmicb.2019.02772/full#supplementary-material

REFERENCES

Abbasifar, R., Griffiths, M. W., Sabour, P. M., Ackermann, H. W., Vandersteegen, K., Lavigne, R., et al. (2014). Supersize me: *Cronobacter sakazakii* phage GAP32. *Virology* 460, 138–146. doi: 10.1016/j.virol.2014.05.003

Ackermann, H., Tremblay, D., and Moineau, S. (2004). Long-term bacteriophage preservation. *WFCC Newslett.* 38, 35–40.

Ackermann, H. W. (2009). Basic phage electron microscopy. *Methods Mol. Biol.* 501, 113–126. doi: 10.1007/978-1-60327-164-6_12

Ackermann, H. W., and Nguyen, T. M. (1983). Sewage coliphages studied by electron microscopy. *Appl. Environ. Microbiol.* 45, 1049–1059.

Adriaenssens, E., and Brister, J. R. (2017). How to name and classify your phage: an informal guide. *Viruses* 9:E70. doi: 10.3390/v9040070

Ahmadi, M., Karimi Torshizi, M. A., Rahimi, S., and Dennehy, J. J. (2016). Prophylactic bacteriophage administration more effective than post-infection administration in reducing *Salmonella enterica* serovar Enteritidis shedding in quail. *Front. Microbiol.* 7:1253. doi: 10.3389/fmicb.2016.01253

Ashish, A., Shaw, M., Winstanley, C., Ledson, M. J., and Walshaw, M. J. (2012). Increasing resistance of the Liverpool Epidemic Strain (LES) of *Pseudomonas aeruginosa* (Psa) to antibiotics in cystic fibrosis (CF)-a cause for concern? *J. Cyst. Fibros.* 11, 173–179. doi: 10.1016/j.jcf.2011.11.004

Attai, H., Boon, M., Phillips, K., Noben, J., Lavigne, R., and Brown, P. J. (2018). Larger than life: isolation and genomic characterization of a jumbo phage that infects the bacterial plant pathogen, *Agrobacterium tumefaciens*. *Front. Microbiol.* 9:1861. doi: 10.3389/fmicb.2018.01861

Bieniossek, C., Schalch, T., Bumann, M., Meister, M., Meier, R., and Baumann, U. (2006). The molecular architecture of the metalloprotease FtsH. *Proc. Natl. Acad. Sci. U.S.A.* 103, 3066–3071. doi: 10.1073/pnas.0600031103

Bonilla, N., Rojas, M. I., Cruz, G. N. F., Hung, S., Rohwer, F., and Barr, J. J. (2016). Phage on tap–a quick and efficient protocol for the preparation of bacteriophage laboratory stocks. *PeerJ* 4:e2261. doi: 10.7717/peerj.2261

Briers, Y., Volckaert, G., Cornelissen, A., Lagaert, S., Michiels, C. W., Hertveldt, K., et al. (2007). Muralytic activity and modular structure of the endolysins of *Pseudomonas aeruginosa* bacteriophages φKZ and EL. *Mol. Microbiol.* 65, 1334–1344. doi: 10.1111/j.1365-2958.2007.05870.x

Buttimer, C., Hendrix, H., Oliveira, H., Casey, A., Neve, H., McAuliffe, O., et al. (2017). Things are getting hairy: enterobacteria bacteriophage vB_PcaM_CBB. *Front. Microbiol.* 8:44. doi: 10.3389/fmicb.2017.00044

Cafora, M., Deflorian, G., Forti, F., Ferrari, L., Binelli, G., Briani, F., et al. (2019). Phage therapy against *Pseudomonas aeruginosa* infections in a cystic fibrosis zebrafish model. *Sci. Rep.* 9:1527. doi: 10.1038/s41598-018-37636-x

Carver, T., Harris, S. R., Berriman, M., Parkhill, J., and McQuillan, J. A. (2011). Artemis: an integrated platform for visualization and analysis of high-throughput sequence-based experimental data. *Bioinformatics* 28, 464–469. doi: 10.1093/bioinformatics/btr703

Casey, E., Fitzgerald, B., Mahony, J., Lugli, G. A., Ventura, M., and van Sinderen, D. (2017). Genome sequence of *Serratia marcescens* phage BF. *Genom. Announc.* 5:e00211-17. doi: 10.1128/genomeA.00211-217

Chaikeeratisak, V., Nguyen, K., Egan, M. E., Erb, M. L., Vavilina, A., and Pogliano, J. (2017a). The phage nucleus and tubulin spindle are conserved among large *pseudomonas* phages. *Cell Rep.* 20, 1563–1571. doi: 10.1016/j.celrep.2017.07.064

Chaikeeratisak, V., Nguyen, K., Khanna, K., Brilot, A. F., Erb, M. L., Coker, J. K., et al. (2017b). Assembly of a nucleus-like structure during viral replication in bacteria. *Science* 355, 194–197. doi: 10.1126/science.aal2130

Chatterjee, P., Davis, E., Yu, F., James, S., Wildschutte, J. H., Wiegmann, D. D., et al. (2017). Environmental *Pseudomonads* inhibit cystic fibrosis patient-derived *Pseudomonas aeruginosa*. *Appl. Environ. Microbiol.* 83, e2701–e2716. doi: 10.1128/AEM.02701-2716

Chaturongakul, S., and Ounjai, P. (2015). Phage–host interplay: examples from tailed phages and gram-negative bacterial pathogens. *Front. Microbiol.* 5:442. doi: 10.3389/fmicb.2014.00442

Chen, L., Yuan, S., Quan, L., Mai, G., Yang, J., Deng, D., et al. (2018). In vitro design and evaluation of phage cocktails against *Aeromonas salmonicida*. *Front. Microbiol.* 9:1476. doi: 10.3389/fmicb.2018.01476

Clokie, M. R., Millard, A. D., Letarov, A. V., and Heaphy, S. (2011). Phages in nature. *Bacteriophage* 1, 31–45. doi: 10.4161/bact.1.1.14942

Dassa, B., London, N., Stoddard, B. L., Schueler-Furman, O., and Pietrokovski, S. (2009). Fractured genes: a novel genomic arrangement involving new split inteins and a new homing endonuclease family. *Nucleic Acids Res.* 37, 2560–2573. doi: 10.1093/nar/gkp095

Devoto, A. E., Santini, J. M., Olm, M. R., Anantharaman, K., Munk, P., Tung, J., et al. (2019). Megaphages infect prevotella and variants are widespread in gut microbiomes. *Nat. Microbiol.* 4, 693–700. doi: 10.1038/s41564-018-0338-339

Donelli, G., Dore, E., Frontali, C., and Grandolfo, M. (1975). Structure and physico-chemical properties of bacteriophage G: III. A homogeneous DNA of molecular weight 5× 108. *J. Mol. Biol.* 94, 555–565. doi: 10.1016/0022-2836(75)90321-90326

Drulis-Kawa, Z., Olszak, T., Danis, K., Majkowska-Skrobek, G., and Ackermann, H. W. (2014). A giant *Pseudomonas* phage from Poland. *Arch. Virol.* 159, 567–572. doi: 10.1007/s00705-013-1844-y

Farris, J. S. (1972). Estimating phylogenetic trees from distance matrices. *Am. Nat.* 106, 645–668. doi: 10.1086/282802

Freestone, P. P., Hirst, R. A., Sandrini, S. M., Sharaff, F., Fry, H., Hyman, S., et al. (2012). *Pseudomonas aeruginosa*-catecholamine inotrope interactions: a contributory factor in the development of ventilator-associated pneumonia? *Chest* 142, 1200–1210. doi: 10.1378/chest.11-2614

Furfaro, L. L., Payne, M. S., and Chang, B. J. (2018). Bacteriophage therapy: clinical trials and regulatory hurdles. *Front. Cell. Infect. Microbiol.* 8:376. doi: 10.3389/fcimb.2018.00376

Glonti, T., Chanishvili, N., and Taylor, P. (2010). Bacteriophage-derived enzyme that depolymerizes the alginic acid capsule associated with cystic fibrosis isolates of *Pseudomonas aeruginosa*. *J. Appl. Microbiol.* 108, 695–702. doi: 10.1111/j.1365-2672.2009.04469.x

Göker, M., García-Blázquez, G., Voglmayr, H., Tellería, M. T., and Martín, M. P. (2009). Molecular taxonomy of phytopathogenic fungi: a case study in *Peronospora*. *PLoS One* 4:e6319. doi: 10.1371/journal.pone.0006319

Gonçalves-de-Albuquerque, C. F., Silva, A. R., Burth, P., Rocco, P. R. M., Castro-Faria, M. V., and Castro-Faria-Neto, H. C. (2016). Possible mechanisms of *Pseudomonas aeruginosa*-associated lung disease. *Int. J. Med. Microbiol.* 306, 20–28. doi: 10.1016/j.ijmm.2015.11.001

Hyman, P., and Abedon, S. T. (2009). Practical methods for determining phage growth parameters. *Methods Mol. Biol.* 501, 175–202. doi: 10.1007/978-1-60327-164-6_18

Kropinski, A. M. (2009). Measurement of the rate of attachment of bacteriophage to cells. *Methods Mol. Biol.* 501, 151–155. doi: 10.1007/978-1-60327-164-6_15

Krylov, V. N. (2014). Bacteriophages of *Pseudomonas aeruginosa*: long-term prospects for use in phage therapy. *Adv. Virus Res.* 88, 227–278. doi: 10.1016/B978-0-12-800098-4.00005-2

Krylov, V., Shaburova, O., Pleteneva, E., Krylov, S., Kaplan, A., Burkaltseva, M., et al. (2015). Selection of phages and conditions for the safe phage therapy against *Pseudomonas aeruginosa* infections. *Virol. Sin.* 30, 33–44. doi: 10.1007/s12250-014-3546-3543

Kumar, S., Stecher, G., and Tamura, K. (2016). MEGA7: molecular evolutionary genetics analysis version 7.0 for bigger datasets. *Mol. Biol. Evol.* 33, 1870–1874. doi: 10.1093/molbev/msw054

Latz, S., Krüttgen, A., Häfner, H., Buhl, E., Ritter, K., and Horz, H. (2017). Differential effect of newly isolated phages belonging to PB1-Like, phiKZ-Like and LUZ24-Like Viruses against Multi-Drug Resistant *Pseudomonas aeruginosa* under varying growth conditions. *Viruses* 9:315. doi: 10.3390/v9110315

Lavigne, R., Ceyssens, P., and Robben, J. (2009). Phage proteomics: applications of mass spectrometry. *Methods Mol. Biol.* 502, 239–251. doi: 10.1007/978-1-60327-565-1_14

Lefort, V., Desper, R., and Gascuel, O. (2015). FastME 2.0: a comprehensive, accurate, and fast distance-based phylogeny inference program. *Mol. Biol. Evol.* 32, 2798–2800. doi: 10.1093/molbev/msv150

Li, D., Liu, C., Luo, R., Sadakane, K., and Lam, T. (2015). MEGAHIT: an ultra-fast single-node solution for large and complex metagenomics assembly via succinct de Bruijn graph. *Bioinformatics* 31, 1674–1676. doi: 10.1093/bioinformatics/btv033

Li, D., Luo, R., Liu, C., Leung, C., Ting, H., Sadakane, K., et al. (2016). MEGAHIT v1. 0: a fast and scalable metagenome assembler driven by advanced methodologies and community practices. *Methods* 102, 3–11. doi: 10.1016/j.ymeth.2016.02.020

Lin, T., Hu, Y., and Shaw, G. (2013). Two enzymes, TilS and HprT, can form a complex to function as a transcriptional activator for the cell division protease gene ftsH in Bacillus subtilis. *J. Biochem.* 155, 5–16. doi: 10.1093/jb/mvt081

Mazzocco, A., Waddell, T. E., Lingohr, E., and Johnson, R. P. (2009). Enumeration of bacteriophages using the small drop plaque assay system. *Methods Mol. Biol.* 501, 81–85. doi: 10.1007/978-1-60327-164-6_9

McNair, K., Aziz, R. K., Pusch, G. D., Overbeek, R., Dutilh, B. E., and Edwards, R. (2018). Phage genome annotation using the RAST pipeline. *Methods Mol. Biol.* 1681, 231–238. doi: 10.1007/978-1-4939-7343-9-17

Meier-Kolthoff, J. P., Auch, A. F., Klenk, H. P., and Göker, M. (2013). Genome sequence-based species delimitation with confidence intervals and improved distance functions. *BMC Bioinformatics* 14:60. doi: 10.1186/1471-2105-14-60

Meier-Kolthoff, J. P., and Göker, M. (2017). VICTOR: genome-based phylogeny and classification of prokaryotic viruses. *Bioinformatics* 33, 3396–3404. doi: 10.1093/bioinformatics/btx440

Meier-Kolthoff, J. P., Hahnke, R. L., Petersen, J., Scheuner, C., Michael, V., Fiebig, et al. (2014). Complete genome sequence of DSM 30083 T, the type strain (U5/41 T) of *Escherichia coli*, and a proposal for delineating subspecies in microbial taxonomy. *Stand. Genom. Sci.* 9:2. doi: 10.1186/1944-3277-9-2

Mesyanzhinov, V. V., Robben, J., Grymonprez, B., Kostyuchenko, V. A., Bourkaltseva, M. V., Sykilinda, N. N., et al. (2002). The genome of bacteriophage φKZ of *Pseudomonas aeruginosa*. *J. Mol. Biol.* 317, 1–19. doi: 10.1006/jmbi.2001.5396

Monson, R., Foulds, I., Foweraker, J., Welch, M., and Salmond, G. P. (2011). The *Pseudomonas aeruginosa* generalized transducing phage φPA3 is a new member of the φKZ-like group of 'jumbo'phages, and infects model laboratory strains and clinical isolates from cystic fibrosis patients. *Microbiology* 157, 859–867. doi: 10.1099/mic.0.044701-44700

Morello, E., Saussereau, E., Maura, D., Huerre, M., Touqui, L., and Debarbieux, L. (2011). Pulmonary bacteriophage therapy on *Pseudomonas aeruginosa* cystic fibrosis strains: first steps towards treatment and prevention. *PLoS One* 6:e16963. doi: 10.1371/journal.pone.0016963

Nale, J. Y., Spencer, J., Hargreaves, K. R., Buckley, A. M., Trzepinski, P., Douce, G. R., et al. (2015). Bacteriophage combinations significantly reduce clostridium difficile growth in vitro and proliferation in vivo. *Antimicrob. Agents Chemother.* 60, 968–981. doi: 10.1128/AAC.01774-15

Pan, Y. J., Lin, T. L., Chen, C. C., Tsai, Y. T., Cheng, Y. H., Chen, Y. Y., et al. (2017). Klebsiella phage ΦK64-1 encodes multiple depolymerases for multiple host capsular types. *J. Virol.* 91:e2457-16. doi: 10.1128/JVI.02457-2416

Perler, F. B. (2005). Protein splicing mechanisms and applications. *IUBMB Life* 57, 469–476. doi: 10.1080/15216540500531739

Perler, F. B., Olsen, G. J., and Adam, E. (1997). Compilation and analysis of intein sequences. *Nucleic Acids Res.* 25, 1087–1093. doi: 10.1093/nar/25.6.1087

Pietrokovski, S. (1994). Conserved sequence features of inteins (protein introns) and their use in identifying new inteins and related proteins. *Protein Sci.* 3, 2340–2350. doi: 10.1002/pro.5560031218

Potera, C. (2013). Phage renaissance: new hope against antibiotic resistance. *Environ. Health Perspect.* 121, a48–a53. doi: 10.1289/ehp.121-a48

Public Health England (2019). *Table 15: P. Aeruginosa Bacteraemia: Monthly Counts Split by Location of Onset by NHS Trust, from January 2018 to January 2019. GOV.UK*. London: Public Health England.

Saitou, N., and Nei, M. (1987). The neighbor-joining method: a new method for reconstructing phylogenetic trees. *Mol. Biol. Evol.* 4, 406–425. doi: 10.1093/oxfordjournals.molbev.a040454

Seemann, T. (2014). Prokka: rapid prokaryotic genome annotation. *Bioinformatics* 30, 2068–2069. doi: 10.1093/bioinformatics/btu153

Serwer, P., Hayes, S. J., Thomas, J. A., and Hardies, S. C. (2007). Propagating the missing bacteriophages: a large bacteriophage in a new class. *Virol. J.* 4:21. doi: 10.1186/1743-422X-4-21

Shaburova, O. V., Hertveldt, K., Krylov, S. V., Pleteneva, E. A., Burkaltseva, M. V., Lavigne, R., et al. (2006). Comparison of new giant bacteriophages OBP and Lu11 of soil pseudomonads with bacteriophages of phiKZ-supergroup of *Pseudomonas aeruginosa*. *Genetika* 42, 1065–1074.

Shotland, Y., Shifrin, A., Ziv, T., Teff, D., Koby, S., Kobiler, O., et al. (2000). Proteolysis of bacteriophage lambda CII by *Escherichia coli* FtsH (HflB). *J. Bacteriol.* 182, 3111–3116. doi: 10.1128/jb.182.11.3111-3116.2000

Šimoliūnas, E., Kaliniene, L., Truncaitė, L., Zajančkauskaitė, A., Staniulis, J., Kaupinis, et al. (2013). Klebsiella phage vB_KleM-RaK2-A giant singleton virus of the family myoviridae. *PLoS One* 8:e60717. doi: 10.1371/journal.pone.0060717

Soma, A., Ikeuchi, Y., Kanemasa, S., Kobayashi, K., Ogasawara, N., Ote, T., et al. (2003). An RNA-modifying enzyme that governs both the codon and amino acid specificities of isoleucine tRNA. *Mol. Cell.* 12, 689–698. doi: 10.1016/s1097-2765(03)00346-0

Sullivan, M. J., Petty, N. K., and Beatson, S. A. (2011). Easyfig: a genome comparison visualizer. *Bioinformatics* 27, 1009–1010. doi: 10.1093/bioinformatics/btr039

Suttle, C. A. (2005). Viruses in the sea. *Nature* 437:356. doi: 10.1038/nature04160

Suzuki, T., and Miyauchi, K. (2010). Discovery and characterization of tRNAIle lysidine synthetase (TilS). *FEBS Lett.* 584, 272–277. doi: 10.1016/j.febslet.2009.11.085

Sykilinda, N. N., Bondar, A. A., Gorshkova, A. S., Kurochkina, L. P., Kulikov, E. E., Shneider, M. M., et al. (2014). Complete genome sequence of the novel giant *Pseudomonas* phage PaBG. *Genome Announc.* 2:e929-13. doi: 10.1128/genomeA.00929-913

Thomas, J. A., Rolando, M. R., Carroll, C. A., Shen, P. S., Belnap, D. M., Weintraub, S. T., et al. (2008). Characterization of *Pseudomonas* chlororaphis myovirus 201ϕ2-1 via genomic sequencing, mass spectrometry, and electron microscopy. *Virology* 376, 330–338. doi: 10.1016/j.virol.2008.04.004

Vandenheuvel, D., Rombouts, S., and Adriaenssens, E. M. (2018). Purification of bacteriophages using anion-exchange chromatography. *Methods Mol. Biol.* 1681, 59–69. doi: 10.1007/978-1-4939-7343-9_5

Waters, E. M., Neill, D. R., Kaman, B., Sahota, J. S., Clokie, M. R. J., Winstanley, C., et al. (2017). Phage therapy is highly effective against chronic lung infections with *Pseudomonas aeruginosa*. *Thorax* 72, 666–667. doi: 10.1136/thoraxjnl-2016-209265

Winstanley, C., Langille, M. G., Fothergill, J. L., Kukavica-Ibrulj, I., Paradis-Bleau, C., Sanschagrin, F., et al. (2009). Newly introduced genomic prophage islands are critical determinants of in vivo competitiveness in the Liverpool Epidemic Strain of *Pseudomonas aeruginosa*. *Genome Res.* 19, 12–23. doi: 10.1101/gr.086082.108

Yoshikawa, G., Askora, A., Blanc-Mathieu, R., Kawasaki, T., Li, Y., Nakano, M., et al. (2018). *Xanthomonas citri* jumbo phage XacN1 exhibits a wide host range and high complement of tRNA genes. *Sci. Rep.* 8:4486. doi: 10.1038/s41598-018-22239-3

Yuan, Y., and Gao, M. (2017). Jumbo bacteriophages: an overview. *Front. Microbiol.* 8:403. doi: 10.3389/fmicb.2017.00403

Conflict of Interest: The authors declare that the research was conducted in the absence of any commercial or financial relationships that could be construed as a potential conflict of interest.

Copyright © 2019 Imam, Alrashid, Patel, Dowah, Brown, Millard, Clokie and Galyov. This is an open-access article distributed under the terms of the Creative Commons Attribution License (CC BY). The use, distribution or reproduction in other forums is permitted, provided the original author(s) and the copyright owner(s) are credited and that the original publication in this journal is cited, in accordance with accepted academic practice. No use, distribution or reproduction is permitted which does not comply with these terms.

frontiers in Microbiology

ORIGINAL RESEARCH
published: 17 December 2019
doi: 10.3389/fmicb.2019.02877

The Novel *Enterococcus* Phage vB_EfaS_HEf13 Has Broad Lytic Activity Against Clinical Isolates of *Enterococcus faecalis*

Dongwook Lee[1], Jintaek Im[1], Hongjun Na[2], Sangryeol Ryu[2], Cheol-Heui Yun[2] and Seung Hyun Han[1]*

[1] Department of Oral Microbiology and Immunology, DRI, and BK21 Plus Program, School of Dentistry, Seoul National University, Seoul, South Korea, [2] Department of Agricultural Biotechnology, Research Institute for Agriculture and Life Sciences, Center for Food and Bioconvergence, Seoul National University, Seoul, South Korea

Enterococcus faecalis is a Gram-positive, facultative anaerobic bacterium frequently found in the gastrointestinal tract, oral cavity, and periodontal tissue. Although it is considered a commensal, it can cause bacteremia, endocarditis, endodontic infections, and urinary tract infections. Because antibiotics are cytotoxic not only to pathogens, but also to health-beneficial commensals, phage therapy has emerged as an alternative strategy to specifically control pathogenic bacteria with minimal damage to the normal flora. In this study, we isolated a novel phage, *Enterococcus* phage vB_EfaS_HEf13 (phage HEf13), with broad lytic activity against 12 strains of *E. faecalis* among the three laboratory strains and 14 clinical isolates of *E. faecalis* evaluated. Transmission electron microscopy showed that phage HEf13 has morphological characteristics of the family *Siphoviridae*. Phage HEf13 was stable at a wide range of temperature (4–60°C) and showed tolerance to acid or alkaline (pH 3–12) growth conditions. Phage HEf13 had a short latent period (25 min) with a large burst size (approximately 352 virions per infected cell). The lytic activity of phage HEf13 at various multiplicities of infection consistently inhibited the growth of diverse clinical isolates of *E. faecalis* without any lysogenic process. Moreover, phage HEf13 showed an effective lytic activity against *E. faecalis* on human dentin *ex vivo* infection model. Whole genome analysis demonstrated that the phage HEf13 genome contains 57,811 bp of double-stranded DNA with a GC content of 40.1% and 95 predicted open reading frames (ORFs). Annotated functional ORFs were mainly classified into four groups: DNA replication/packaging/regulation, phage structure, host cell lysis, and additional functions such as RNA transcription. Comparative genomic analysis demonstrated that phage HEf13 is a novel phage that belongs to the *Sap6virus* lineage. Furthermore, the results of multiple sequence alignment showed that polymorphism of phage infection protein of *E. faecalis* (PIP_{EF}) contributes to determine the host specificity of phage HEf13 against various *E. faecalis* strains. Collectively, these results suggest that phage HEf13 has characteristics of a lytic phage, and is a potential therapeutic agent for treatment or prevention of *E. faecalis*-associated infectious diseases.

Keywords: phage, *Enterococcus* phage HEf13, *Enterococcus faecalis*, phage infection protein of *Enterococcus faecalis*, whole genome analysis, human dentin

OPEN ACCESS

Edited by:
Robert Czajkowski,
University of Gdańsk, Poland

Reviewed by:
Ahmed Askora,
Zagazig University, Egypt
Jean-Christophe Giard,
University of Caen Normandy, France

***Correspondence:**
Seung Hyun Han
shhan-mi@snu.ac.kr

Specialty section:
This article was submitted to Virology, a section of the journal Frontiers in Microbiology

Received: *10 September 2019*
Accepted: *28 November 2019*
Published: *17 December 2019*

Citation:
Lee D, Im J, Na H, Ryu S, Yun C-H and Han SH (2019) The Novel Enterococcus Phage vB_EfaS_HEf13 Has Broad Lytic Activity Against Clinical Isolates of Enterococcus faecalis. Front. Microbiol. 10:2877. doi: 10.3389/fmicb.2019.02877

INTRODUCTION

Enterococcus is a genus of Gram-positive, non-spore-forming bacteria that are frequently found in the oral cavity, gastrointestinal tract, and vagina (Jett et al., 1994). Although most *Enterococcus* species are considered to be commensal in humans and animals (Gu et al., 2018), *Enterococcus faecalis* can act as an opportunistic pathogen causing bacteremia, meningitis, endocarditis, or urinary tract- and wound-related infections (Arias et al., 2010; Weiner et al., 2016). In humans, *E. faecalis* has been predominantly detected in the root canals of patients with post-treatment apical periodontitis or refractory apical periodontitis, suggesting an etiological role in progression of these diseases (Souto and Colombo, 2008; Vidana et al., 2011).

Antibiotics are widely used to treat and prevent diseases caused by various pathogenic bacteria. However, the emergence of antibiotic resistant *E. faecalis*, such as vancomycin-resistant *E. faecalis* (VRE), has diminished the clinical usefulness of antibiotics (O'Driscoll and Crank, 2015). On the one hand, because most strains of *E. faecalis* isolated from root canal and periodontal infections show a high level of resistance to antibiotics including tetracycline and erythromycin used in dental procedures, antibiotic options for endodontic treatment are limited (Pinheiro and Mayer, 2014). On the other hand, indiscriminate use of antibiotics can result in disruption of normal gut microflora, and can negatively affect human health by promoting the evolution of antibiotic resistance in the microbiome and compromising immune homeostasis (Cho and Blaser, 2012; Francino, 2015).

There is currently renewed interest in phage therapy using lytic phages, also called viruses, as a potential alternative strategy to control pathogenic bacteria as this strategy overcomes the limitations of antibiotics (Golkar et al., 2014). Unlike antibiotics, phages are highly specific for their target pathogen and thus do not damage the normal flora (Moelling et al., 2018). Phages have many other advantages, including ease of isolation and better efficacy than antibiotics at destroying bacteria in biofilms (Khalifa et al., 2016). Moreover, many clinical trials have shown that the use of phages is safe without side-effects in both humans and animals (Burrowes et al., 2011).

Based on previously published studies, a total of 22 lytic phages targeting *E. faecalis* (14 *Siphoviridae*, 6 *Myoviridae*, and 2 *Podoviridae* phages) have been isolated from various sources, including sewage, animal farmyard effluents, and human feces (Bonilla et al., 2010; Bolocan et al., 2019; Lossouarn et al., 2019). Although previous studies have demonstrated the therapeutic potency of newly isolated phages for targeting *E. faecalis*, practical use of these phages has been limited by their relatively narrow host range against clinically isolated *E. faecalis* strains (Rigvava et al., 2013; Zhang et al., 2013; Ladero et al., 2016; Cheng et al., 2017; Rahmat Ullah et al., 2017; Wang et al., 2018). In addition, despite the importance of *E. faecalis* in the pathogenesis of recurrent and incurable periodontitis, curative efficiency of *E. faecalis* phages has not been evaluated against *E. faecalis* strains isolated from the oral cavity. Therefore, we focused on isolation, characterization, and genomic analysis of a novel *E. faecalis* lytic phage against clinically isolated *E. faecalis* strains from the oral cavity.

MATERIALS AND METHODS

Bacterial Strains and Culture Conditions

A total of 17 strains of *E. faecalis*, including 14 clinical isolates and three laboratory strains, were used to determine the host range of phage HEf13. As shown in **Table 1**, three laboratory strains of *E. faecalis* and two laboratory strains of *E. faecium* were obtained from the Korean Agricultural Culture Collection (KACC, Wanju, Republic of Korea) and 14 clinically isolated *E. faecalis* strains, recovered from blood, dental plaques, mucormycosis, pus, urine (VRE), and the vagina were provided by the Korean Collection

TABLE 1 | Information of *E. faecalis* strains and the host specificity of phage HEf13.

Enterococcus	Plaque formation[a]	Source[b]
Enterococcus faecalis		
KACC 11304	T	KACC, type strain
KACC 11859	–	KACC, type strain
KACC 13807	–	KACC, type strain
KCOM 1083	C	KCOM, clinical isolate (dental plaque)
KCOM 1161	C	KCOM, clinical isolate (dental plaque)
KCOM 1162	C	KCOM, clinical isolate (dental plaque)
KCOM 2816	T	KCOM, clinical isolate (mucormycosis)
KCOM 2823	T	KCOM, clinical isolate (mucormycosis)
KCTC 5291	C	KCTC, clinical isolate (dental plaque)
KCTC 5292	C	KCTC, clinical isolate (dental plaque)
NCCP 14623	C	NCCP, clinical isolate (pus)
NCCP 14624	–	NCCP, clinical isolate (blood)
NCCP 14673	C	NCCP, clinical isolate (vagina)
NCCP 15611	–	NCCP, clinical isolate (blood)
NCCP 16130	T	NCCP, clinical isolate (VRE, urine)
NCCP 16131	–	NCCP, clinical isolate (VRE, urine)
NCCP 16132	T	NCCP, clinical isolate (VRE, urine)
Enterococcus faecium		
KACC 10782	–	KACC, type strain
KACC 11954	–	KACC, type strain

[a]*C, clear-plaques; T, turbid-plaques; –, no plaques and susceptibility.* [b]*KACC, Korean Agricultural Culture Collection; KCOM, Korean Collection for Oral Microbiology; KCTC, Korean Collection for Type Cultures; NCCP, National Culture Collection of Pathogens.*

for Oral Microbiology (KCOM, Gwangju, Republic of Korea), Korean Collection for Type Cultures (KCTC, Jeongeup, Republic of Korea), or the National Culture Collection of Pathogens (NCCP, Chungju, Republic of Korea). All strains of *E. faecalis* were grown in brain heart infusion broth (BHI broth, Difco Laboratories Inc., Franklin Lakes, NJ, United States) at 37°C with shaking under aerobic conditions.

Phage Isolation

Raw sewage water was collected from a local sewerage system (Seoul, Republic of Korea) and used as a source of *E. faecalis* phages. Phage isolation was performed as previously described (Lee et al., 2016). Briefly, sewage sample (10 mL) was homogenized with 40 mL sodium chloride–magnesium sulfate buffer [SM buffer; 100 mM NaCl, 10 mM $MgSO_4 \cdot 7H_2O$, and 50 mM Tris–HCl (pH 7.5)] containing 1% chloroform. After centrifugation at 10,000 × *g* and 4°C for 10 min, supernatants were collected and then filtered through 0.22 μm pore-size membrane filters (Corning Inc., Corning, NY, United States). Supernatants (10 mL) were mixed with an equal volume of 2× concentrated BHI broth and incubated with 1% of overnight culture of 12 *E. faecalis* strains mixture with shaking at 37°C for 12 h. The suspension was harvested by centrifugation at 10,000 × *g* at 4°C for 10 min and filtered to remove bacterial debris. Then, supernatants diluted 10–1,000 times with BHI broth were spotted on molten 0.4% BHI soft agar containing 1×10^8 CFU/mL of *E. faecalis*. The next day, clear phage plaques were picked from the BHI agar plates and the phages were resuspended in SM buffer. These phage plaque isolation and phage resuspension steps were repeated three times to obtain individual phages with high purity.

Phage Propagation, Purification, and Titration

Propagation and purification of the phages were performed as described previously with minor modifications (Sambrook and Russell, 2001). For phage propagation, early log phase cultures of *E. faecalis* KCOM 1162 (OD_{600} = 0.35) were infected with phage and incubated with vigorous shaking at 37°C for 5 h. After centrifugation at 12,000 × *g* at 4°C for 10 min, supernatants containing phages were filtered using bottle-top vacuum filters with a 0.22-μm pore-size membrane (Merck Millipore, Burlington, MA, United States). Following the propagation step, filtrates were mixed with 1 M NaCl containing 10% polyethylene glycol 6000 (Junsei Chemical Co., Tokyo, Japan) and incubated overnight at 4°C. Precipitated phages were then harvested by centrifugation at 12,000 × *g* for 20 min at 4°C and resuspended in 2 mL SM buffer. Resuspended phages were subjected to density gradient ultracentrifugation (CP100NX, Hitachi, Tokyo, Japan) with different cesium chloride steps (density for each step = 1.3, 1.45, 1.5, and 1.7 g/mL) at 111,000 × *g* at 4°C for 2 h. Finally, purified phages were collected from the band corresponding to viral particles and dialyzed in standard dialysis buffer [10 mM NaCl, 10 mM $MgCl_2$, 50 mM Tris–HCl (pH 8.0)] at 4°C for 2 h. To titrate the purified phages, serially diluted phages (10^{-1}–10^{-9} folds) were dropped on an *E. faecalis* KCOM 1162 (1×10^9 CFU/mL) lawn. Plaques were examined the next day and plaque-forming units (PFUs) were calculated based on the minimal dilution rate of phages generating plaques.

Determination of Host Range

The host range of purified phages was determined by spotting assay (Kropinski et al., 2009) against the 17 strains of *E. faecalis* (**Table 1**). Briefly, 100 μL of each freshly cultured *E. faecalis* strain was mixed with 6 mL of warm 0.4% BHI soft agar and overlaid on previously prepared 1.5% BHI agar plates. After agar hardening, a 10 μL aliquot of purified phages at 1×10^9 PFU/mL was spotted on each agar plate and the plates were incubated at 37°C overnight. The next day, bacterial sensitivity to phages was estimated by the clarity of plaques on each plate.

Bacterial Challenge Assay

Among the 17 strains of *E. faecalis* tested in the host range assay, 12 strains sensitive to the purified phages based on the results of host range analysis were chosen for the bacterial challenge assay (Xie et al., 2018). One percent of an overnight culture of each *E. faecalis* strain was inoculated in triplicate on a 96-well plate and the plate was cultured at 37°C with shaking until the optical density at 600 nm (OD_{600}) reached 0.2 (∼1×10^8 CFU/mL). Bacteria were infected with the purified phages at various multiplicities of infection (MOI) ranging from 0.01 to 1, and incubated at 37°C with shaking for 0–12 h. Bacterial growth was assessed by measuring OD_{600} using a spectrophotometer every 2 h for up to 12 h. *E. faecalis* strains not infected with phages were used as controls for this assay. To determine whether phage HEf13 is a temperate or lytic phage, *E. faecalis* KCOM 2816 strain (1×10^8 CFU/mL) at early mid log phase was infected with phage HEf13 (MOI 1) for 16 h. The infected bacteria were inoculated on 96-well plate by 1% (w/v) and incubated at 37°C for an additional 2 h. After the incubation, cultured bacteria were reinfected with phage HEf13 (MOI 0.1 and 1) in the presence or absence of mitomycin C (MMC) at 5 μg/mL (Sigma–Aldrich, St. Louis, MO, United States) (Stevens et al., 2009). Bacterial growth was measured every 2 h for up to 12 h using a spectrophotometer.

Preparation of Human Dentin Slices

Experiments using human dentin slices were approved by the Institutional Review Board of Seoul National University Dental Hospital, Seoul, Republic of Korea (CRI 17010). Extracted human single-rooted pre-molars were sonicated in 0.5% sodium azide with an ultrasonic scaler (SH-2140; Saehan-Sonic, Seoul, Republic of Korea). The roots were sliced into a size of 500 μm with an Isomet precision saw (Buehler, Lake Bluff, IL, United States). The slices were sequentially treated with 17% EDTA (Sigma–Aldrich) for 5 min, 2.5% sodium hypochlorite (Sigma–Aldrich) for 5 min, and 5% sodium thiosulfate (Sigma–Aldrich) for 5 min, followed by autoclave-sterilization for 15 min at 121°C.

Ex vivo Analysis of Phage Lytic Activity

The lytic activity of phage HEf13 against *E. faecalis* on human dentin slice was examined by scanning electron microscope

(SEM) analysis as previously described (Kim et al., 2019). Briefly, *E. faecalis* (1×10^8 CFU/mL) was grown on dentin slices in the presence or absence of phage HEf13 (MOI 0.1) in BHI medium at 37°C for 12 h. Attached bacteria on dentin slice were rinsed with phosphate-buffered saline (PBS) and prefixed with a 2.5% glutaraldehyde and 2% paraformaldehyde (pH 7) at 4°C overnight. After washing with PBS, the dentin slices were fixed with 1% osmium tetroxide for 90 min, then washed with distilled water, and subsequently dehydrated by gradual increase of ethanol concentrations (70–100% for 15 min). After drying with hexamethyldisilazane and coating with gold sputter, samples were visualized by SEM (S-4700, Hitachi, Tokyo, Japan).

Morphological Analysis by Electron Microscopy

Morphology of the purified phages was examined by transmission electron microscopy (TEM) analysis. The glow-discharge step to prepare Formvar/carbon-coated copper grids was performed at 15 mA and 0.26 mBar for 30 s using a glow discharge cleaning system (PELCO easiGlow; Ted Pella Inc., Redding, CA, United States). Purified phage stock (approximately 3×10^7 PFU) was dropped onto the prepared Formvar/carbon-coated copper grids and incubated at room temperature for 1 min. *E. faecalis* KCOM 1162 (1×10^8 CFU/mL) incubated with phages (1×10^{10} PFU/mL) at room temperature for 10 min was collected by centrifugation and resuspended in SM buffer. Bacteria were also dropped onto the prepared Formvar/carbon-coated copper grids and after a 1 min incubation, the grids were negatively stained with 2% uranyl acetate and electron micrographs of phages were obtained by TEM (Libra 120 model; Zeiss, Oberkochen, Germany operated at an accelerating voltage of 80 kV). Identification and classification of phages was conducted according to the guidelines of the International Committee on the Taxonomy of Viruses (ICTVs).

One-Step Growth Curve Analysis

One-step growth experiments were conducted as described previously with a slight modification (Parasion et al., 2012). When the culture of *E. faecalis* KCOM 1162 reached early log phase (OD_{600} = 0.35), bacteria were harvested by centrifugation at 10,000 × *g* at 4°C for 10 min and resuspended in fresh BHI broth. Bacteria were infected with purified phages at a MOI of 0.01 and incubated at room temperature for 5 min. After centrifugation and removal of the supernatant containing unbound phages, pellets were resuspended in 50 mL fresh BHI medium and incubated at 37°C with shaking for up to 90 min. Samples were taken every 5 min, serially diluted, and plated on *E. faecalis* KCOM 1162 lawn for phage titration. Burst sizes of phages were calculated as the ratio of the average phage titer value at plateau phase to that at latent phase (Svab et al., 2018).

Thermal and pH Stability

Stability of the phages to temperature and pH was assessed by phage titration after incubation in SM buffer at different temperature or pH values (Park et al., 2017). Briefly, 1.5 mL tubes containing the same amount of the purified phages (1×10^8 PFU/mL) were incubated at various temperatures ranging from 4 to 70°C, or under different pH conditions (SM buffer at pH 2–12 adjusted by NaOH or HCl) at 37°C for 12 h. After incubation, phage titers were determined using *E. faecalis* KCOM 1162 as described above.

Whole Genome Sequencing and Bioinformatic Analysis

Genomic DNA from purified phages was extracted using the Norgen phage DNA isolation kit (Norgen Biotek Corp., ON, Canada) according to the manufacturer's instruction. Sequencing libraries with single index were prepared using the TruSeq Nano DNA library prep kit (Illumina, San Diego, CA, United States) and then sequenced on the Illumina MiSeq sequencing platform (Illumina, San Diego, CA, United States) with paired-end 300 nucleotide reads. Raw reads were trimmed and *de novo* assembled using the CLC Genomic Workbench program (Version 10.0.1; QIAGEN Inc., Hilden, Germany). Annotation of the specific function of ORFs was conducted using rapid annotations of subsystems technology (RAST) and the BLASTP database (Altschul et al., 1997; Aziz et al., 2008). Artemis (version 16; Sanger Institute, Cambridge, United Kingdom) was used to visualize and browse the genome and annotate ORFs (Carver et al., 2008). The presence of tRNA-encoding genes was determined using the tRNAscan-SE database (Lowe and Chan, 2016). A circular representation of the genome of phage HEf13 was visualized using the CGView server database (Stothard and Wishart, 2005). Phage virulence factor analysis was conducted using the Virulence Searcher database (Underwood et al., 2005). Comparative analysis of genome sequences and visualization of the genomes of phage HEf13 and other *Enterococcus* phages was performed using BLASTN and BLASTP databases and the EasyFig program (Version 2.2; Beatson Microbial Genomic Lab, Brisbane, Australia) (Sullivan et al., 2011).

Comparative Phylogenetic Analysis

Full length amino acid (aa) sequences of the phage portal protein (511 aa), tail fiber protein (1,330 aa), and DNA methyltransferase (150 aa) of phage HEf13 were aligned with those of nine *Enterococcus* phages in the *Sap6virus* genus and *Listeria* phages showing high similarity using the ClustalW Multiple sequence alignment (MSA) module in the BioEdit Sequence Alignment Editor program (Ibis Therapeutics, Carlsbad, CA, United States) (Larkin et al., 2007). After alignment, phylogenetic trees for each of the three phage proteins were generated by the Neighbor-joining method using Molecular Evolutionary Genetics Analysis 7 (MEGA7) software (Pennsylvania State University, State College, PA, United States) (Tamura et al., 2013) and groupings were estimated by bootstrap analysis (1,000 replication).

Analysis of Phage Infection Protein of *E. faecalis* (PIP_{EF}) Polymorphism

Polymorphism of the variable region of PIP_{EF} for *E. faecalis* strains used in the current study was analyzed to examine correlation between the host specificity of phage HEf13

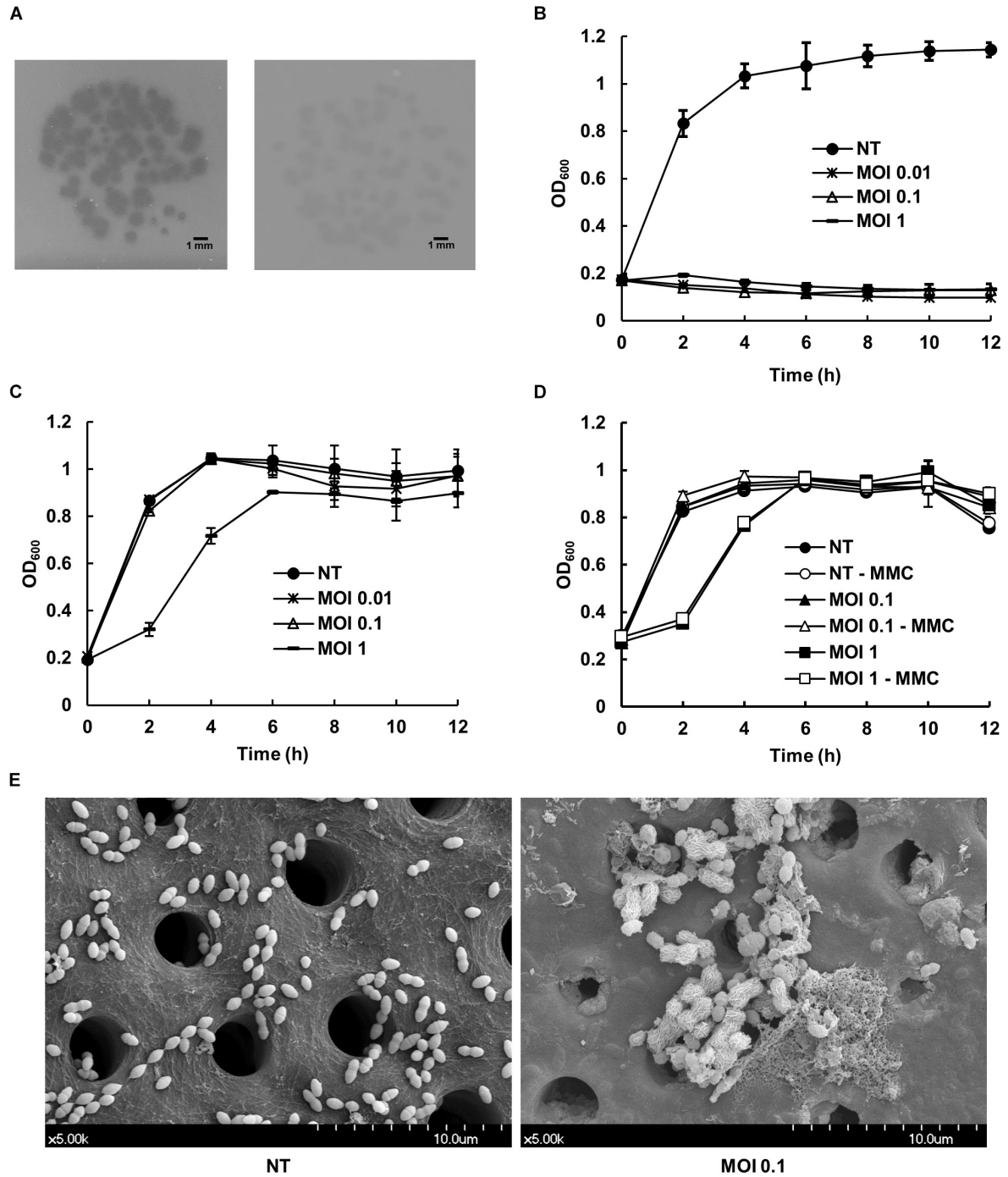

FIGURE 1 | Effect of newly isolated *Enterococcus* phage vB_EfaS_HEf13 (phage HEf13) on the growth of *E. faecalis*. **(A)** Phage HEf13 suspension (1×10^4 PFU/mL) was spotted on *E. faecalis* KCOM 1162 (clear-plaque, left) or KACC 11304 (turbid-plaque, right) lawn and incubated at 37°C overnight. Plaque formation by phage HEf13 was photographed. Scale bar indicates 1 mm. **(B,C)** Representative *E. faecalis* strains showing clear- (**B**; KCOM 1162) or turbid-plaque formation (**C**; KCOM 2816) by phage HEf13 were chosen for the bacterial challenge assay. Each *E. faecalis* strain was infected with phage HEf13 at various MOI (0.01–1) and incubated at 37°C for 0–12 h. **(D)** Turbid-plaque-forming *E. faecalis* strain (KCOM 2816) was infected with phage HEf13 (MOI 1) for 16 h and the infected bacteria were then grown to early mid-log phase. After the culture, the infected bacteria were cultured in the presence or absence of phage HEf13 (MOI 0.1 or 1) and MMC at 5 μg/mL. Bacterial growth at each indicated time point was measured by spectrophotometer at 600 nm. Values are means ± standard deviations from triplicates of each treatment. **(E)** Dental isolate of *E. faecalis* strain (KCOM 1162) was inoculated on human dentin slices in the presence or absence of phage HEf13 (MOI 0.1) for 12 h. Then, the dentin slices were fixed and images were obtained by SEM (magnification: 5,000×). Scale bar indicates 10 μm with 1 μm ticks. MMC, mitomycin C; MOI, multiplicity of infection; NT, non-treatment.

and PIP_{EF} as previously described (Duerkop et al., 2016). Briefly, genomic DNA was extracted from 17 strains of *E. faecalis* using a commercially available kit according to the manufacturer's instruction (iNtRON Biotechnology, Seongnam, Republic of Korea). The genomic DNAs were amplified by PCR under the following conditions: denaturation at 95°C for 30 s and amplification via 28 cycles of 50°C for 3 min and 72°C for 3 min. PCR products were purified using a PCR/Gel purification kit (Bioneer, Daejeon, Republic of Korea) and sequenced at Cosmo Genetech (Seoul, Republic of Korea). MSAs of homologs were analyzed using Geneious 6.0.5. software (Biomatters Ltd., Auckland, New Zealand). Phylogenetic tree of PIP_{EF} homologs was constructed by Neighbor-Joining method (1,000 bootstrap) (Tamura et al., 2013).

RESULTS

Isolation, Host Range Determination, and Lytic Activity of Phage HEf13

E. faecalis phage vB_EfaS_HEf13 (phage HEf13) was newly isolated from sewage water of a local sewerage system in Seoul, Republic of Korea. The host range of phage HEf13 was assessed using a spotting assay against a total 17 strains of *E. faecalis* (three laboratory strains and 14 clinically isolated strains including three VRE strains), and two laboratory strains of *E. faecium*. Phage HEf13 formed clear- or turbid-plaques in 12 *E. faecalis* strains, including all dental isolates of *E. faecalis* (**Figure 1A** and **Table 1**). However, phage HEf13 cannot recognize and lyse *E. faecium*, suggesting that phage HEf13 is specific only to *E. faecalis*, but not to other *Enterococcus* species. To examine the lytic activity of phage HEf13, *E. faecalis* strains where clear- or turbid-plaques were observed in the spotting assay were subjected to bacterial challenge assays at various MOI for up to 12 h. Similar to the pattern of host range determination, phage HEf13 showed strong lytic activity against *E. faecalis* where clear-plaque formation was observed in the previous spotting assay, but not the strains where turbid-plaque formation was observed (**Figures 1B,C** and **Supplementary Figures S1A–J**). However, the results showed a possibility that turbid-plaque formation by phage HEf13 may result from its lysogenic property. Therefore, in order to determine whether the phage is lytic or lysogenic, we examined the growth of *E. faecalis* infected with phage HEf13 in the presence of MMC, which is a lysogenic phage inducer (Stevens et al., 2009). As shown in **Figure 1D**. *E. faecalis* infected with phage HEf13 was not affected by MMC treatment, implying that the turbid-plaque formation by phage HEf13 was not due to a lysogenic process of phage HEf13. Furthermore, we evaluated the effect of phage HEf13 against *E. faecalis* using an *ex vivo* human dentin infection model. When *E. faecalis* on dentin slice infected with phage HEf13 was visualized using a SEM, *E. faecalis* was completely eradicated (**Figure 1E**). These results suggest that phage HEf13 is a potential therapeutic agent to treat diseases associated with *E. faecalis* infection such as refractory apical periodontitis.

Morphology of Phage HEf13

Morphological analysis of phage HEf13 and its adsorption to *E. faecalis* was examined by TEM. Phage HEf13 has a prolate head with a long non-contractile tail (**Figures 2A–C**). Head diameter is 38.4 ± 2.4 nm with a length of 95.6 ± 1.7 nm, and tail length is 135.2 ± 4.7 nm (**Figures 2A–C**). TEM images of *E. faecalis* KCOM 1162 infected with phage HEf13 demonstrated adsorption of phages to the surface of *E. faecalis* as marked by the arrows in **Figure 2D**. Taken together, these results indicate that phage HEf13 belongs to the *Siphoviridae* family in the order *Caudovirales* according to the ICTV guidelines (Fauquet et al., 2005).

Latent Period and Burst Size of Phage HEf13

The latent period and burst size of phage HEf13 were measured by one-step growth curve analysis against *E. faecalis* KCOM 1162. The latent period of phage HEf13, calculated as the time interval between adsorption and the beginning of the first burst, was approximately 25 min (**Figure 3**). The rise period of phage HEf13 was about 30 min and mean burst size, defined as the mean phage titer value at plateau phase divided by that of the latent phase, was approximately 352 virions per infected cell. These results indicate that phage HEf13 has a short latent period and long rise period with

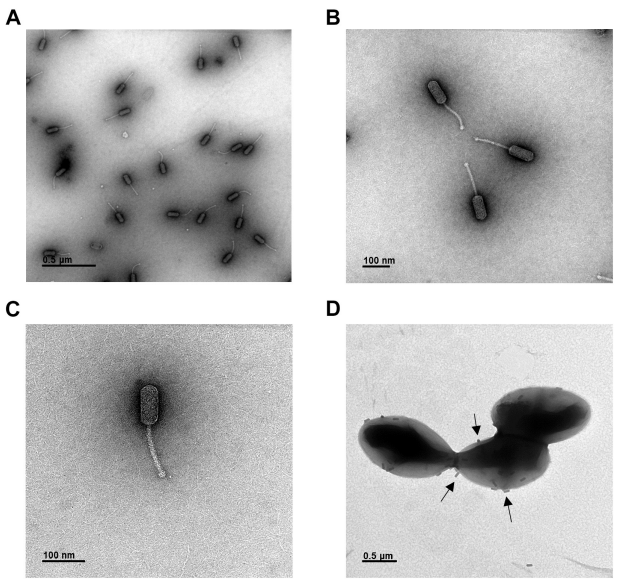

FIGURE 2 | Phage HEf13 belongs to the *Siphoviridae* family. **(A–C)** Phage HEf13 (1×10^8 PFU) was dropped onto a Formvar/carbon-coated copper grid and then negatively stained with 2% uranyl acetate. **(D)** *E. faecalis* KCOM 1162 (1×10^8 CFU/mL) incubated with phage HEf13 (1×10^{10} PFU/mL) was dropped onto copper grids and stained with 2% uranyl acetate. Electron micrographs of phage HEf13 were obtained by TEM at **(A)** 35,000×, **(B,C)** 100,000×, and **(D)** 35,000× magnification. Identification and classification of phages was conducted according to ICTV guidelines. Scale bar indicates 100 nm **(B,C)** or 0.5 μm **(A,D)**. Arrows in panel **(D)** show phage HEf13 binding to the cell wall membrane of *E. faecalis* KCOM 1162.

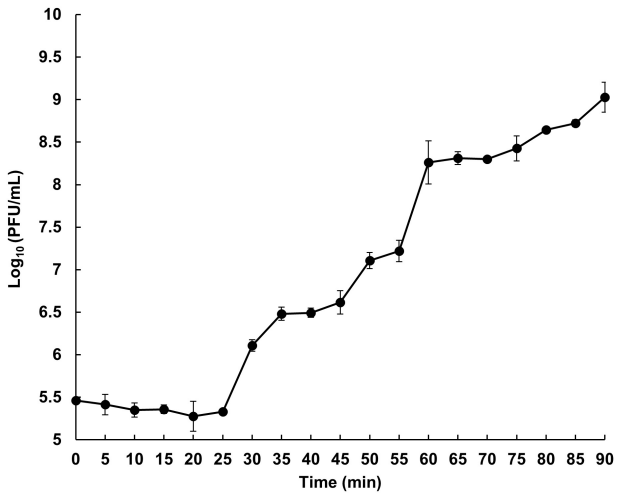

FIGURE 3 | Phage HEf13 has a relatively short latent period and enhanced large burst size against *E. faecalis*. *E. faecalis* KCOM 1162 was infected with Phage HEf13 at an MOI of 0.01 and incubated for 5 min. After removing unbound phages by centrifugation, bacteria were incubated at 37°C up to 90 min. Samples were taken every 5 min and subjected to phage titration by spotting assay as described in the section "Materials and Methods." Values are means ± standard deviations from triplicates of each time point.

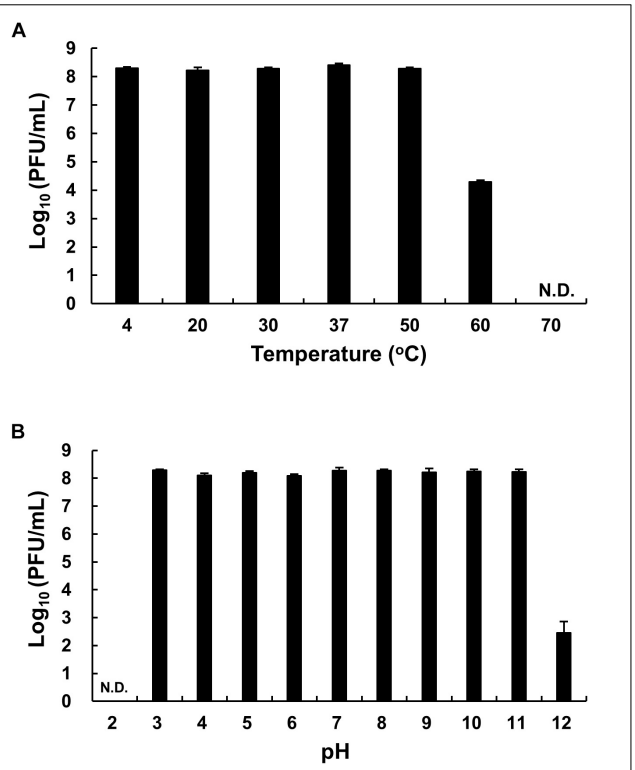

FIGURE 4 | Phage HEf13 is stable over a broad range of temperature and pH values. **(A)** Phage HEf13 (1×10^8 PFU/mL) was incubated at various temperatures ranging from 4 to 70°C for 12 h. **(B)** Phage HEf13 (1×10^8 PFU/mL) was also incubated at different pH values ranging from 2 to 12 at 37°C for 12 h. Then, phage titers were determined by spotting assay as described in the section "Materials and Methods." Values are presented as log values of the ratio of phage titers in each treatment to that of the initial phage titer. Values are means ± standard deviations from triplicates of each treatment. N.D., not detected.

a large burst size, accounting for its strong lytic activity against *E. faecalis*.

Stability of Phage HEf13 to Different Temperature and pH Conditions

The thermal stability of phage HEf13 was evaluated by phage titration assay after phage incubation at various temperatures ranging from 4 to 70°C for 12 h. While no loss was observed in phage titers at temperatures ranging from 4 to 50°C, a phage titer of <60% was observed at 60°C. Furthermore, no phage titer was detected when phage HEf13 was incubated at 70°C (**Figure 4A**). Phage HEf13 tolerated a broad range of pH values from 3 to 12. However, no phage activity was noted under extremely acidic conditions (pH 2) (**Figure 4B**). These data show that phage HEf13 can tolerate a broad range of temperature and pH values.

Genomic Characterization of Phage HEf13

Whole genome sequence analysis showed that the genome of phage HEf13 (GenBank Accession Number: MH618488) is 57,811 bp in length with 95 predicted ORFs and one tRNA gene, a GC content of 40.03%, and the following nucleotide composition: G (10,737 bp, 18.57%), C (12,405 bp, 21.45%), A (15,765 bp, 27.26%), and T (18,904 bp, 32.69%) (**Figure 5**). Average gene length was 532 bp, with a range of 116–3,992 nucleotides, and gene coding percentage was 87.4%. Among the 95 putative ORFs, 15 ORFs were on the positive strand while the other 80 ORFs were on the negative strand. Only 30 ORFs (31.5%) were predicted to be functional proteins, whereas 65 ORFs (68.4%) were annotated as hypothetical proteins (**Supplementary Table S1**). Annotation of the function of the 30 ORFs predicted as functional proteins by RAST and BLASTP analyses revealed four major functional groups: DNA replication/packaging/regulation, phage structure, host cell lysis, and additional function. The DNA replication/packaging/regulation module comprised 16 genes, suggesting that phage HEf13 has a host-independent DNA replication/packaging/regulation system with the following components: DNA replication proteins (DNA polymerase I, DNA primase, DNA replication protein, and replicative DNA helicase), packaging proteins (glutaredoxin-like protein, phage portal protein, phage terminase large subunit, and phage terminase small subunit), and regulation proteins (crossover junction endodeoxyribonuclease RuvC, cytidine deaminase, deoxynucleoside monophosphate kinase, DNA binding protein, DNA methyltransferase, HNH endonuclease, and HNH homing endonuclease). The phage structural module comprised seven genes required for host recognition and phage structural assembly: tail-associated proteins (phage tail protein, phage tail tube protein, tail fiber, and tail tape measure protein) and head-associated proteins (head morphogenesis protein, head-tail connector family protein, and major capsid protein). The host cell lysis gene module encoded cell-wall binding and cell lysis

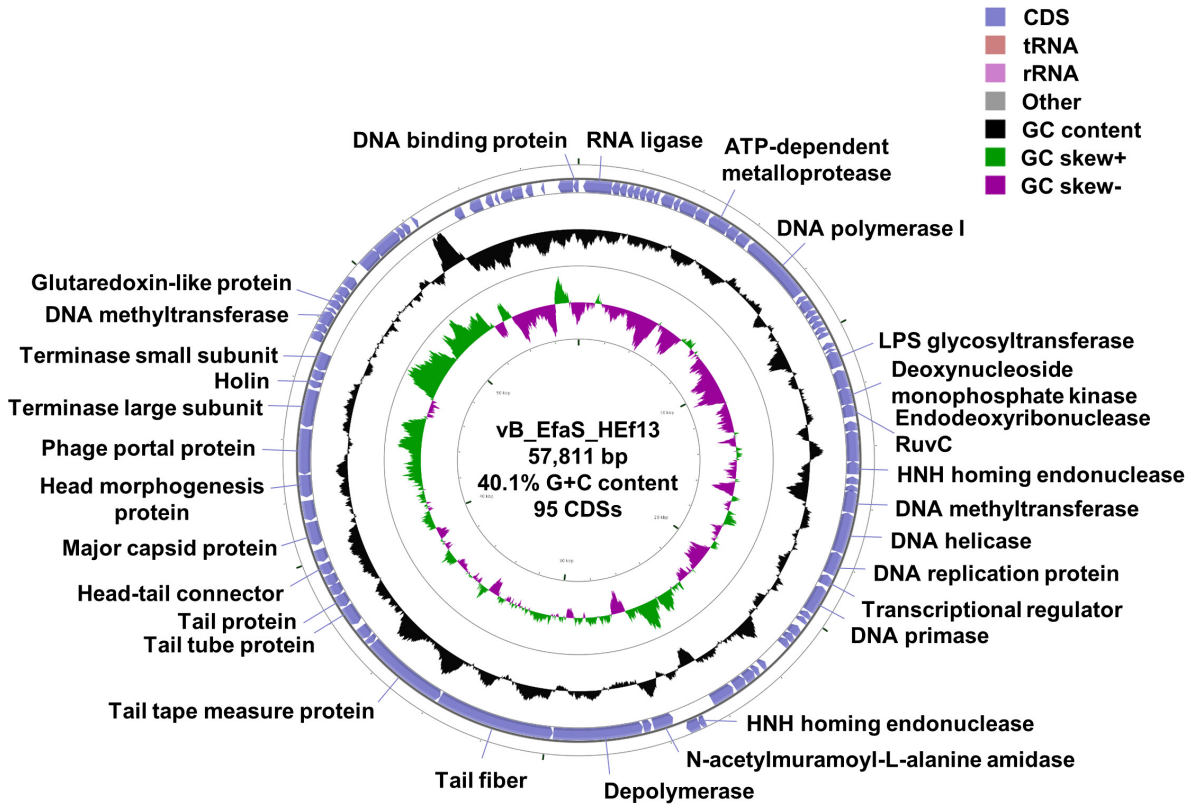

FIGURE 5 | Genome map of phage HEf13 and its genetic characteristics. The whole genome sequence of phage HEf13 was determined using the Illumina Miseq platform and circular genome visualization of phage HEf13 was performed using the CGView server database. Annotation of the specific function of ORFs was conducted using RAST and the BLASTP database, and the complete genome sequence and annotation of ORFs were handled using the Artemis program. The second inner circle with the green and purple histogram shows the GC skew +/–, while the fourth inner circle with the black histogram indicates the GC content. The outer circle indicates the predicted ORFs of phage HEf13 together with their putative functions.

proteins (depolymerase, endolysin, and holin). In addition, four functional proteins had annotations of RNA transcription (RNA ligase and transcriptional regulator) or unidentified function (ATP-dependent metalloprotease and LPS glycosyltransferase). No lysogenic genes such as lytic repressor proteins, recombinases, excisionases, or integrases were identified, suggesting that phage HEf13 might be an obligate lytic phage only with a lytic cycle. Furthermore, virulence factor analysis of the phage HEf13 genome using the Virulence Searcher database revealed that none of the ORFs encode any functional proteins that can act as human virulence factors. Thus, our results suggest that phage HEf13 does not contain any possible pathogenic factors, and is therefore safe to use to treat *E. faecalis*-associated diseases.

Comparative Genome Analysis of Phage HEf13 and Other *Enterococcus* Phages

Comparison of the nucleotide sequence of phage HEf13 with that of other *E. faecalis* phages using the BLASTN database revealed an average similarity of 95% between vB_EfaS_IME198 and phage EF-P29 (84–85% sequence coverage) belonging to the *Sap6virus* genus (**Supplementary Table S1**). To further analyze similarities and differences between phage HEf13 and other *Sap6virus* phages, we visualized comparative genome maps to assess similarities and differences in ORF organization. Most of the genes from phage HEf13 and other relative *Sap6virus* phages had a similar gene arrangement and were highly homologous. However, some genetic differences were observed in genes in the DNA replication/packing/regulation module (indicated in purple in **Figure 6**). Based on comparison of amino acid sequences using BLASTP, 77 of 95 ORFs in phage HEf13 shared 90–100% identity with ORFs of the other compared phages, but 18 ORFs, including the four unidentified ORFs, shared 0–89% identity (**Supplementary Table S2**). Interestingly, the four unidentified ORFs had no significant homology with any other sequences in *E. faecalis* phages. To determine the taxonomic affinity of phage HEf13, phylogenetic analysis using previously published genome sequences of eight other phages belonging to the *Sap6virus* genus was conducted. Phylogenetic trees constructed based on the amino acid sequences of phage portal protein, tail fiber protein, and DNA methyltransferase demonstrated that phage HEf13 clustered within the *Sap6virus* genus together with phages EF-P29, VD13, BC-611, SAP6, IME-EF1, vB_EfaS_IME198, SPQ-S1, and EF-P10 (**Figures 7A–C**). Collectively, the results of the phylogenetic analysis together with results of morphological – and comparative genome – analyses indicate that phage HEf13

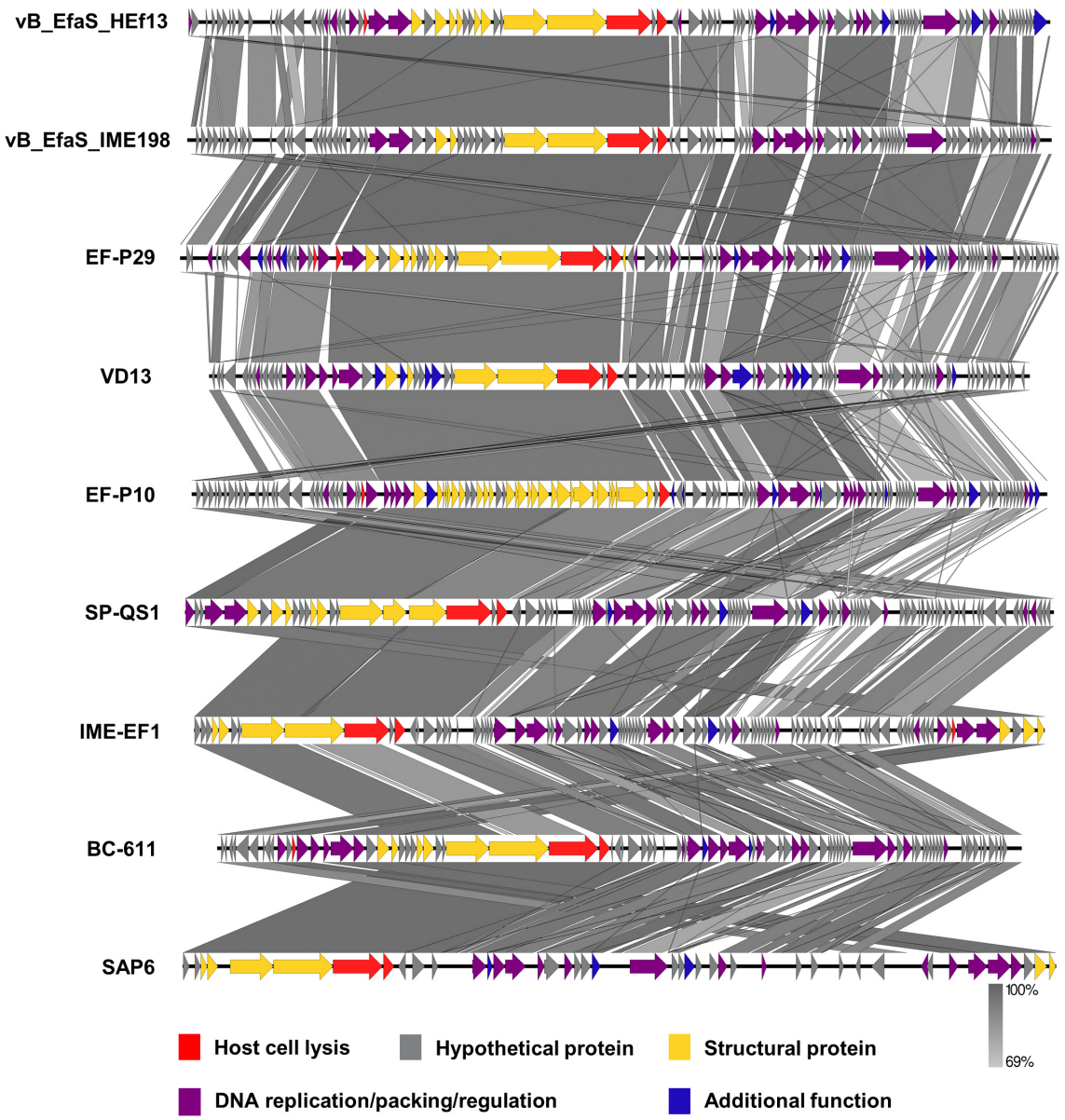

FIGURE 6 | Phage HEf13 has high homology with phages in the *Sap6virus* genus of *Enterococcus* phages. Comparative genome analysis of phage HEf13 and eight other *Enterococcus* phages was performed using the EasyFig program. ORFs of phages were color-coded according to their predicted functions: host cell lysis (red), hypothetical protein (gray), structural protein (yellow), DNA replication/packing/regulation (purple), and additional function (blue). Genetic similarity profiles between phage HEf13 and other phages are presented in grayscale (percent homology).

belongs to the genus *Sap6virus* in the family *Siphoviridae*, order *Caudovirales*.

Analysis of Polymorphism in the Potential Phage Receptor PIP_{EF}

To understand the host specificity of phage HEf13, we investigated host cell receptors for phage HEf13. Among various bacterial cell wall membrane proteins, the PIP_{EF} has recently been identified as a specific host cell receptor of *E. faecalis Siphoviridae* phages. Moreover, it has been reported that polymorphism in the variable region (covering amino acids 342–494) of PIP_{EF} affects the binding affinity of phages to the host bacteria, subsequently determining the host range of the phage (Duerkop et al., 2016). Therefore, we examined polymorphism in the variable region of PIP_{EF} by MSA for all *E. faecalis* strains used in the current study. As shown in **Figure 8A**, all of clear-plaque-forming strains have the same amino acid sequence in the variable region of PIP_{EF}. However, most of turbid-plaque-forming strains and phage-resistant strains (7 of 10 strains), except for one turbid-plaque-forming strain and two phage-resistant strains, showed different sequences with those of clear-plaque-forming strains.

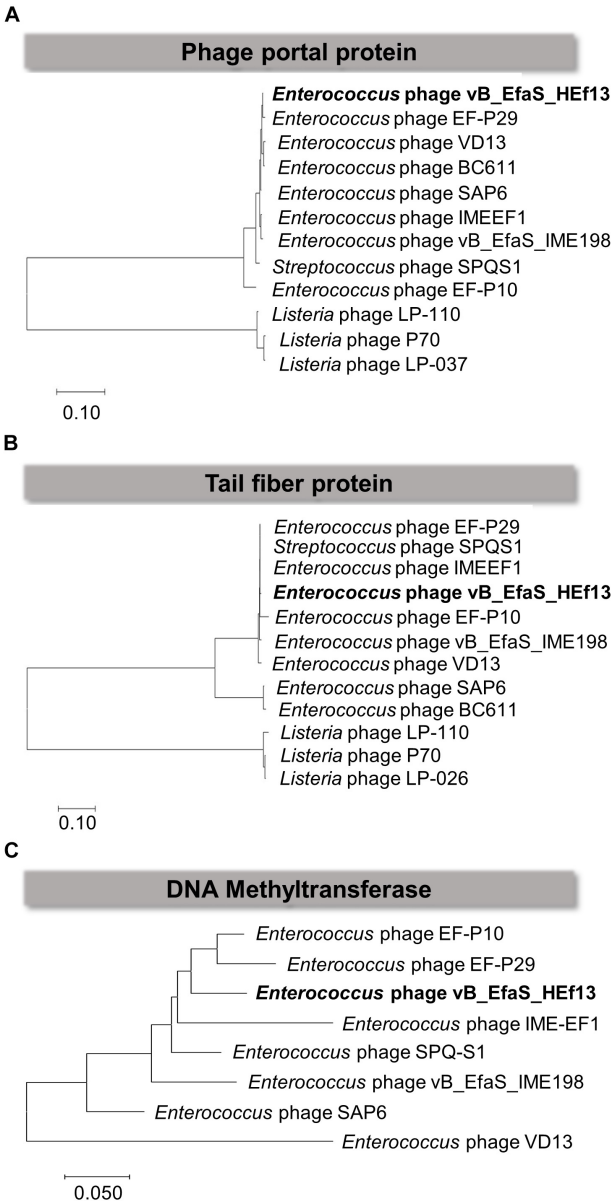

FIGURE 7 | Phage HEf13 was classified as the *Sap6virus* lineage. The amino acid sequences of the phage portal protein, tail fiber protein, and DNA methyltransferase of phage HEf13 were compared with those of other phages using the BioEdit Sequence Alignment Editor program. A phylogenetic tree for each phage protein was generated using MEGA7 software. Scale bars represent a 10 **(A,B)** or 5% **(C)** difference in sequence similarity between phages.

Furthermore, phylogenetic tree of PIP_{EF} based on the results of MSA showed that cluster of clear-plaque-forming strains were clearly distinguished from that of turbid-plaque-forming strains and phage-resistant strains, except for three strains (NCCP 15611, 16131, and 16132) (**Figure 8B**). These results demonstrated that polymorphism of PIP_{EF} might be closely related with the host specificity of phage HEf13 to *E. faecalis*.

DISCUSSION

Antibiotic-resistant *E. faecalis* strains have decreased the utility of antibiotics in clinical settings, making the phage therapy a highly attractive alternative therapeutic strategy. In this study, we isolated a novel lytic *E. faecalis* phage belonging to the genus *Sap6virus* in the family *Siphoviridae*. Our results demonstrated that phage HEf13 has a relatively broader host spectrum than previously isolated *E. faecalis* lytic phages. Notably, the host range of phage HEf13 was 70.5% against all tested *E. faecalis* strains (12 out of 17 tested strains), which is broader than other *E. faecalis* lytic phages with the host range from 7.6 to 42.5% (Rigvava et al., 2013; Zhang et al., 2013; Ladero et al., 2016; Cheng et al., 2017; Rahmat Ullah et al., 2017; Wang et al., 2018).

Regarding burst size, whereas the average burst size of *E. faecalis* phages reported previously was typically 36–122 PFU/infected bacteria, phage HEf13 has an approximately threefold higher burst size of 352 PFU/infected bacteria (Rigvava et al., 2013; Cheng et al., 2017; Wang et al., 2018). Moreover, phage HEf13 has an average latent time of 25 min after infection, which is shorter than those of other *E. faecalis* phages (30–50 min) (Uchiyama et al., 2008; Cheng et al., 2017; Wang et al., 2018). In addition, phage HEf13 showed strong lytic activities against all tested dental clinical isolates of *E. faecalis* at a broad range of MOI from 0.01 to 1 (**Figure 1B** and **Supplementary Figures S1A,B,E,F**). Earlier *E. faecalis* phage studies tested the lytic activity of phages against laboratory strains or clinically isolated antibiotic resistant strains recovered from various clinical specimens, but not against clinical isolates from oral specimens (Parasion et al., 2012; Rigvava et al., 2013; Zhang et al., 2013; Cheng et al., 2017; Wang et al., 2018). Thus, to the best of our knowledge, this is the first study to demonstrate the potential utility of *E. faecalis* phages as dental therapeutic reagents for post-treatment apical or refractory apical periodontitis, which are conditions closely related to *E. faecalis* infection.

Phage HEf13 appeared to be highly stable to a broad range of temperatures (4–60°C) and pH values (3–12). While phage HEf13 maintained over 50% of its titer for a long-term incubation period (after 12 h) at 60°C (**Figure 4A**), other previously isolated *E. faecalis* phages maintained about 40% of their titer for a short-term incubation period (even after 1 h) at 45–60°C (Rigvava et al., 2013; Rahmat Ullah et al., 2017). Since little is known about the pH stability of *E. faecalis* phages, we compared the pH stability of phage HEf13 with those of other Gram-positive bacteria phages. Phage HEf13 titers were not affected by incubation at pH 11 and remained at around 30% at pH 12 (**Figure 4B**), whereas reported titers of other phages were almost completely abolished at pH 11 (Li and Zhang, 2014; Chen et al., 2016; Phothichaisri et al., 2018). These comparisons demonstrated that phage HEf13 is relatively more stable to high temperatures and strongly basic conditions than other phages. Furthermore, these findings suggest that phage HEf13 may be highly potent in clinical settings considering that *E. faecalis* can survive and grow under harsh environments such as a pH of 11 and temperature of 45°C (McHugh et al., 2004; Foulquie Moreno et al., 2006). These characteristics of phage HEf13 make it potentially ideal to use in combinatory treatment with alkaline disinfectants such as calcium hydroxide

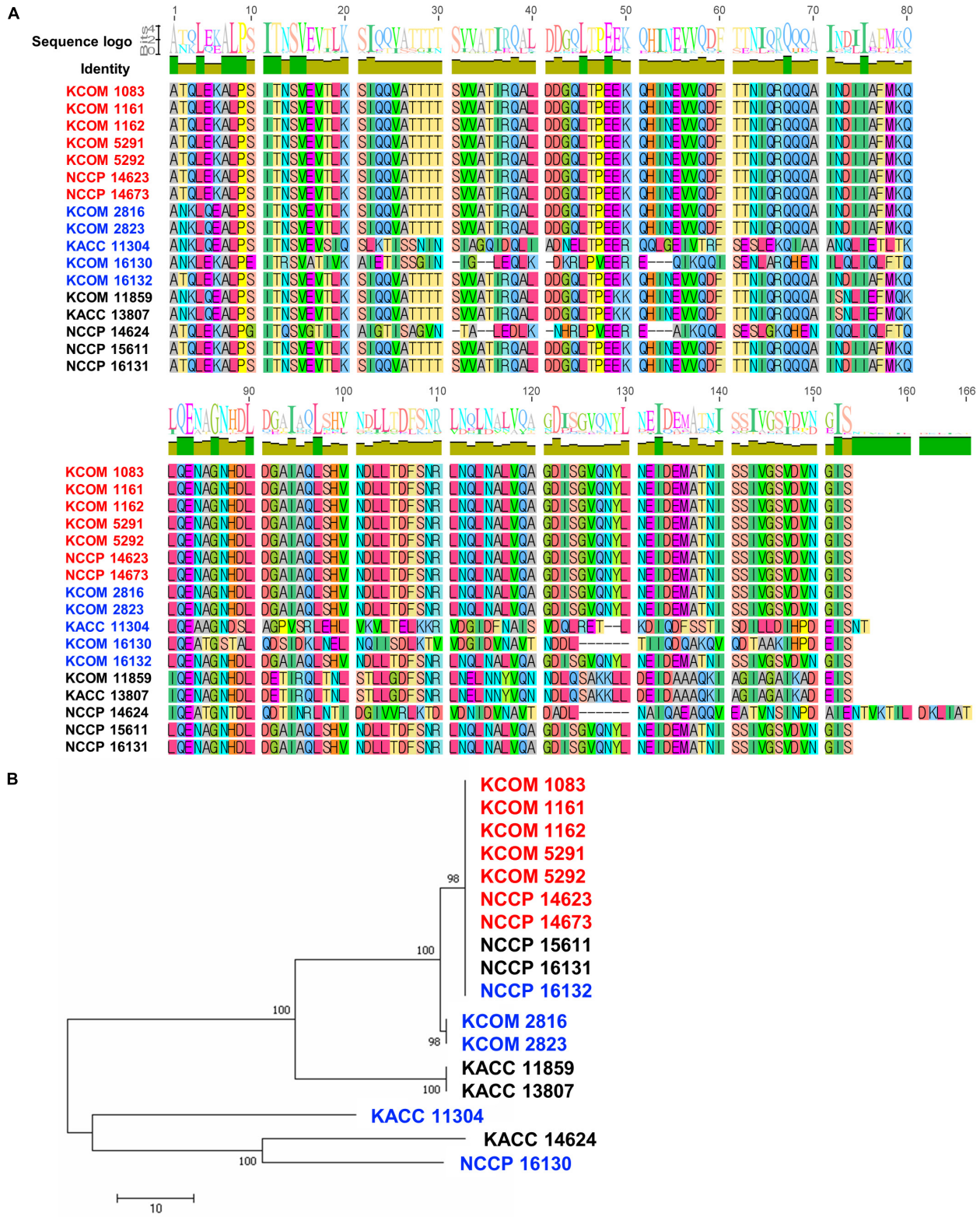

FIGURE 8 | Polymorphism in the variable region of PIP_{EF} in *E. faecalis* strains is related with phage HEf13 host specificity. **(A)** Multiple amino acid sequence alignment of the PIP_{EF} variable region in 17 strains of *E. faecalis* was generated by Geneious 6.0.5 software. Difference in amino acid sequence of *E. faecalis* strains is presented in different colors. **(B)** Phylogenetic tree of PIP_{EF} homologs was constructed by Neighbor-joining method with 1,000 replicates. Scale bar represents a 10% difference in sequence similarity between homologs. Strains are indicated by color as follows: clear-plaque-forming strain (red), turbid-plaque-forming strains (blue), and phage-resistant strains (black).

and sodium hypochlorite, which are commonly used to treat endodontic infection.

Comparative genome analysis revealed that the genome sequence of phage HEf13 is highly conserved with those of other tested *Sap6virus* phages. Among 77 ORFs that showed high similarity to the ORFs of other phages in this genus, we found two ORFs of phage HEf13 that may generate different host specificity and phage protection based on differences in amino acid sequence. While the receptor binding protein (RBP) in the phage tail apparatus of phage HEf13 (ORF55) has a negatively charged amino acid (443D), the other eight *Sap6virus* phages evaluated have an uncharged amino acid at same position (443N). Because RBP plays an important role in phage adsorption to host bacteria, this may result in a different host specificity of phage HEf13 to other phages in same genus. In fact, a recent study using point-mutated phages demonstrated that point mutation of an amino acid in the RBP (K653N) generated significant differences in host specificity (Le et al., 2013). Additionally, the sequence of DNA methyltransferase (ORF75), which protects phages from bacterial restriction modification system, differed by 8–16% between phage HEf13 and the other *Sap6virus* phages evaluated, suggesting differences in phage protection.

The host specificity of HEf13 against *E. faecalis* appears to be associated with the PIP_{EF} in light of the fact that all of the clear-plaque-forming strains possess the same amino acids sequence in the variable region of PIP_{EF} even though turbid-plaque-forming strains and phage-resistant strains were not differentially clustered in the phylogenetic tree. Remarkably, three strains belonging to turbid-plaque-forming strain (NCCP 16132) or phage-resistant strains (NCCP 15611 and 16131) were also clustered in the same clade with clear-plaque-forming strains (**Figure 8B**). Although further study is needed, it can be explained by two potential mechanisms based on the previous studies. First, Gram-positive bacterial cell-wall components, such as capsular polysaccharides, wall-teichoic acids, and lipoteichoic acids, could hide the phage receptor by masking them, subsequently making phages inaccessible to its receptor (Munsch-Alatossava and Alatossava, 2013; Ozaki et al., 2017). Second, the aforementioned bacterial cell wall components could also compete with the receptors for phage adsorption, thereby interfering with a successful phage infection (Seed, 2015).

So far, a total of 22 *E. faecalis* lytic phages have been isolated and their stability and efficacy against various clinical and non-clinical strains have been evaluated. The phages identified previously, however, have a relatively narrow host spectrum and low stability to broad temperature and pH ranges, limiting their practical usefulness. Here, we characterized a newly isolated phage, HEf13, and demonstrated that this phage is highly potent against various *E. faecalis* strains and has high lytic ability and stability. Furthermore, the high lytic activity of phage HEf13 against dental clinical isolates suggests that phage HEf13 may be effective as a dental therapeutic agent to treat recurrent or refractory apical periodontitis related to *E. faecalis* infection.

DATA AVAILABILITY STATEMENT

The raw datasets generated in this study can be found in GenBank, Accession Number: MH618488.

AUTHOR CONTRIBUTIONS

DL and SH designed the research. DL and HN carried out the experiments. DL, JI, and SH analyzed and interpreted the data. DL, JI, SR, C-HY, and SH prepared and reviewed the manuscript. All authors have read and accepted the final manuscript.

FUNDING

This work was supported by grants from the National Research Foundation of Korea, which is funded by the Korean Government (NRF-2019R1A2C2007041 and NRF-2018R1A5A2024418).

ACKNOWLEDGMENTS

We thank the National Culture Collection for Pathogens for providing the pathogen resources (NCCP 14623, 14624, 14673, 15611, 16130, 16131, and 16132) of this study. We also thank the Korean Agricultural Culture Collection, Korean Collection for Oral Microbiology, and Korean Collection for Type Cultures for kindly providing *E. faecalis* strains.

SUPPLEMENTARY MATERIAL

The Supplementary Material for this article can be found online at: https://www.frontiersin.org/articles/10.3389/fmicb.2019.02877/full#supplementary-material

REFERENCES

Altschul, S. F., Madden, T. L., Schaffer, A. A., Zhang, J., Zhang, Z., Miller, W., et al. (1997). Gapped BLAST and PSI-BLAST: a new generation of protein database search programs. *Nucleic Acids Res.* 25, 3389–3402. doi: 10.1093/nar/25.17.3389

Arias, C. A., Contreras, G. A., and Murray, B. E. (2010). Management of multidrug-resistant enterococcal infections. *Clin. Microbiol. Infect.* 16, 555–562. doi: 10.1111/j.1198-743X.2010.03214.x

Aziz, R. K., Bartels, D., Best, A. A., DeJongh, M., Disz, T., Edwards, R. A., et al. (2008). The RAST Server: rapid annotations using subsystems technology. *BMC Genomics* 9:75. doi: 10.1186/1471-2164-9-75

Bolocan, A. S., Upadrasta, A., Bettio, P. H. A., Clooney, A. G., Draper, L. A., Ross, R. P., et al. (2019). Evaluation of phage therapy in the context of *Enterococcus faecalis* and its associated diseases. *Viruses* 11:E366. doi: 10.3390/v11040366

Bonilla, N., Santiago, T., Marcos, P., Urdaneta, M., Domingo, J. S., and Toranzos, G. A. (2010). Enterophages, a group of phages infecting *Enterococcus faecalis*, and their potential as alternate indicators of human faecal contamination. *Water Sci. Technol.* 61, 293–300. doi: 10.2166/wst.2010.815

Burrowes, B., Harper, D. R., Anderson, J., McConville, M., and Enright, M. C. (2011). Bacteriophage therapy: potential uses in the control of antibiotic-resistant pathogens. *Expert Rev. Anti. Infect. Ther.* 9, 775–785. doi: 10.1586/eri.11.90

Carver, T., Berriman, M., Tivey, A., Patel, C., Bohme, U., Barrell, B. G., et al. (2008). Artemis and ACT: viewing, annotating and comparing sequences stored in a relational database. *Bioinformatics* 24, 2672–2676. doi: 10.1093/bioinformatics/btn529

Chen, X., Xi, Y., Zhang, H., Wang, Z., Fan, M., Liu, Y., et al. (2016). Characterization and adsorption of *Lactobacillus* virulent phage P1. *J. Dairy Sci.* 99, 6995–7001. doi: 10.3168/jds.2016-11332

Cheng, M., Liang, J., Zhang, Y., Hu, L., Gong, P., Cai, R., et al. (2017). The Bacteriophage EF-P29 efficiently protects against lethal vancomycin-resistant *Enterococcus faecalis* and alleviates gut microbiota imbalance in a murine bacteremia model. *Front. Microbiol.* 8:837. doi: 10.3389/fmicb.2017.00837

Cho, I., and Blaser, M. J. (2012). The human microbiome: at the interface of health and disease. *Nat. Rev. Genet.* 13, 260–270. doi: 10.1038/nrg3182

Duerkop, B. A., Huo, W., Bhardwaj, P., Palmer, K. L., and Hooper, L. V. (2016). Molecular basis for lytic bacteriophage resistance in enterococci. *mBio* 7:e01304–16. doi: 10.1128/mBio.01304-1316

Fauquet, C., Mayo, M. A., Maniloff, J., Desselberger, U., and Ball, L. A. (2005). *Virus Taxonomy: Classification and Nomenclature of Viruses: Eighth Report of the International Committee on Taxonomy of Viruses*. Cambridge, MA: Elsevier/Academic Press.

Foulquie Moreno, M. R., Sarantinopoulos, P., Tsakalidou, E., and De Vuyst, L. (2006). The role and application of enterococci in food and health. *Int. J. Food Microbiol.* 106, 1–24. doi: 10.1016/j.ijfoodmicro.2005.06.026

Francino, M. P. (2015). Antibiotics and the human gut microbiome: dysbioses and accumulation of resistances. *Front. Microbiol.* 6:1543. doi: 10.3389/fmicb.2015.01543

Golkar, Z., Bagasra, O., and Pace, D. G. (2014). Bacteriophage therapy: a potential solution for the antibiotic resistance crisis. *J. Infect. Dev. Ctries* 8, 129–136. doi: 10.3855/jidc.3573

Gu, Y. H., Yamasita, T., and Kang, K. M. (2018). Subchronic oral dose toxicity study of *Enterococcus faecalis* 2001 (EF 2001) in mice. *Toxicol. Res.* 34, 55–63. doi: 10.5487/TR.2018.34.1.055

Jett, B. D., Huycke, M. M., and Gilmore, M. S. (1994). Virulence of enterococci. *Clin. Microbiol. Rev.* 7, 462–478. doi: 10.1128/cmr.7.4.462

Khalifa, L., Shlezinger, M., Beyth, S., Houri-Haddad, Y., Coppenhagen-Glazer, S., Beyth, N., et al. (2016). Phage therapy against *Enterococcus faecalis* in dental root canals. *J. Oral Microbiol.* 8:32157. doi: 10.3402/jom.v8.32157

Kim, A. R., Ahn, K. B., Yun, C. H., Park, O. J., Perinpanayagam, H., Yoo, Y. J., et al. (2019). *Lactobacillus plantarum* lipoteichoic acid inhibits oral multispecies biofilm. *J. Endod.* 45, 310–315. doi: 10.1016/j.joen.2018.12.007

Kropinski, A. M., Mazzocco, A., Waddell, T. E., Lingohr, E., and Johnson, R. P. (2009). Enumeration of bacteriophages by double agar overlay plaque assay. *Methods Mol. Biol.* 501, 69–76. doi: 10.1007/978-1-60327-164-6_7

Ladero, V., Gomez-Sordo, C., Sanchez-Llana, E., Del Rio, B., Redruello, B., Fernandez, M., et al. (2016). Q69 (an *E. faecalis*-infecting bacteriophage) as a biocontrol agent for reducing tyramine in dairy products. *Front. Microbiol.* 7:445. doi: 10.3389/fmicb.2016.00445

Larkin, M. A., Blackshields, G., Brown, N. P., Chenna, R., McGettigan, P. A., McWilliam, H., et al. (2007). Clustal W and Clustal X version 2.0. *Bioinformatics* 23, 2947–2948. doi: 10.1093/bioinformatics/btm404

Le, S., He, X., Tan, Y., Huang, G., Zhang, L., Lux, R., et al. (2013). Mapping the tail fiber as the receptor binding protein responsible for differential host specificity of *Pseudomonas aeruginosa* bacteriophages PaP1 and JG004. *PLoS One* 8:e68562. doi: 10.1371/journal.pone.0068562

Lee, J. H., Bai, J., Shin, H., Kim, Y., Park, B., Heu, S., et al. (2016). A novel bacteriophage targeting *Cronobacter sakazakii* is a potential biocontrol agent in foods. *Appl. Environ. Microbiol.* 82, 192–201. doi: 10.1128/AEM.01827-1815

Li, L., and Zhang, Z. (2014). Isolation and characterization of a virulent bacteriophage SPW specific for *Staphylococcus aureus* isolated from bovine mastitis of lactating dairy cattle. *Mol. Biol. Rep.* 41, 5829–5838. doi: 10.1007/s11033-014-3457-3452

Lossouarn, J., Briet, A., Moncaut, E., Furlan, S., Bouteau, A., Son, O., et al. (2019). *Enterococcus faecalis* countermeasures defeat a virulent picovirinae bacteriophage. *Viruses* 11:48. doi: 10.3390/v11010048

Lowe, T. M., and Chan, P. P. (2016). tRNAscan-SE On-line: integrating search and context for analysis of transfer RNA genes. *Nucleic Acids Res.* 44, W54–W57. doi: 10.1093/nar/gkw413

McHugh, C. P., Zhang, P., Michalek, S., and Eleazer, P. D. (2004). pH required to kill *Enterococcus faecalis* in vitro. *J. Endod.* 30, 218–219. doi: 10.1097/00004770-200404000-200404008

Moelling, K., Broecker, F., and Willy, C. (2018). A wake-up call: we need phage therapy now. *Viruses* 10:E688. doi: 10.3390/v10120688

Munsch-Alatossava, P., and Alatossava, T. (2013). The extracellular phage-host interactions involved in the bacteriophage LL-H infection of Lactobacillus delbrueckii ssp. *lactis ATCC* 15808. *Front. Microbiol.* 4:408. doi: 10.3389/fmicb.2013.00408

O'Driscoll, T., and Crank, C. W. (2015). Vancomycin-resistant enterococcal infections: epidemiology, clinical manifestations, and optimal management. *Infect. Drug Resist.* 8, 217–230. doi: 10.2147/IDR.S54125

Ozaki, T., Abe, N., Kimura, K., Suzuki, A., and Kaneko, J. (2017). Genomic analysis of *Bacillus subtilis* lytic bacteriophage varphiNIT1 capable of obstructing natto fermentation carrying genes for the capsule-lytic soluble enzymes poly-gamma-glutamate hydrolase and levanase. *Biosci. Biotechnol. Biochem.* 81, 135–146. doi: 10.1080/09168451.2016.1232153

Parasion, S., Kwiatek, M., Mizak, L., Gryko, R., Bartoszcze, M., and Kocik, J. (2012). Isolation and characterization of a novel bacteriophage phi4D lytic against *Enterococcus faecalis* strains. *Curr. Microbiol.* 65, 284–289. doi: 10.1007/s00284-012-0158-158

Park, E. A., Kim, Y. T., Cho, J. H., Ryu, S., and Lee, J. H. (2017). Characterization and genome analysis of novel bacteriophages infecting the opportunistic human pathogens *Klebsiella oxytoca* and *K. pneumoniae*. *Arch. Virol.* 162, 1129–1139. doi: 10.1007/s00705-016-3202-3203

Phothichaisri, W., Ounjai, P., Phetruen, T., Janvilisri, T., Khunrae, P., Singhakaew, S., et al. (2018). Characterization of bacteriophages infecting clinical isolates of *Clostridium difficile*. *Front. Microbiol.* 9:1701. doi: 10.3389/fmicb.2018.01701

Pinheiro, E. T., and Mayer, M. P. M. (2014). *Enterococcus faecalis* in oral infections. *JBR J. Interdiscipl. Med. Dent. Sci.* 3:160. doi: 10.4172/2376-032X.1000160

Rahmat Ullah, S., Andleeb, S., Raza, T., Jamal, M., and Mehmood, K. (2017). Effectiveness of a lytic phage SRG1 against vancomycin-resistant *Enterococcus faecalis* in compost and soil. *Biomed. Res. Int.* 2017:9351017. doi: 10.1155/2017/9351017

Rigvava, S., Tchgkonia, I., Jgenti, D., Dvalidze, T., Carpino, J., and Goderdzishvili, M. (2013). Comparative analysis of the biological and physical properties of *Enterococcus faecalis* bacteriophage vB_EfaS_GEC-EfS_3 and *Streptococcus mitis* bacteriophage vB_SmM_GEC-SmitisM_2. *Can. J. Microbiol.* 59, 18–21. doi: 10.1139/cjm-2012-2385

Sambrook, J., and Russell, D. W. (eds). (2001). "Bacteriophage lambda and its vectors," in *Molecular Cloning: A Laboratory Manual*, 3rd edn (New York: Cold, Spring Harbor Laboratory Press), 2.1–2.117.

Seed, K. D. (2015). Battling phages: how bacteria defend against viral attack. *PLoS Pathog.* 11:e1004847. doi: 10.1371/journal.ppat.1004847

Souto, R., and Colombo, A. P. (2008). Prevalence of *Enterococcus faecalis* in subgingival biofilm and saliva of subjects with chronic periodontal infection. *Arch. Oral. Biol.* 53, 155–160. doi: 10.1016/j.archoralbio.2007.08.004

Stevens, R. H., Porras, O. D., and Delisle, A. L. (2009). Bacteriophages induced from lysogenic root canal isolates of *Enterococcus faecalis*. *Oral Microbiol. Immunol.* 24, 278–284. doi: 10.1111/j.1399-302X.2009.00506.x

Stothard, P., and Wishart, D. S. (2005). Circular genome visualization and exploration using CGView. *Bioinformatics* 21, 537–539. doi: 10.1093/bioinformatics/bti054

Sullivan, M. J., Petty, N. K., and Beatson, S. A. (2011). Easyfig: a genome comparison visualizer. *Bioinformatics* 27, 1009–1010. doi: 10.1093/bioinformatics/btr039

Svab, D., Falgenhauer, L., Rohde, M., Szabo, J., Chakraborty, T., and Toth, I. (2018). Identification and characterization of T5-Like bacteriophages representing two novel subgroups from food products. *Front. Microbiol.* 9:202. doi: 10.3389/fmicb.2018.00202

Tamura, K., Stecher, G., Peterson, D., Filipski, A., and Kumar, S. (2013). MEGA6: molecular evolutionary genetics analysis version 6.0. *Mol. Biol. Evol.* 30, 2725–2729. doi: 10.1093/molbev/mst197

Uchiyama, J., Rashel, M., Maeda, Y., Takemura, I., Sugihara, S., Akechi, K., et al. (2008). Isolation and characterization of a novel *Enterococcus faecalis* bacteriophage phiEF24C as a therapeutic candidate. *FEMS Microbiol. Lett.* 278, 200–206. doi: 10.1111/j.1574-6968.2007.00996.x

Underwood, A. P., Mulder, A., Gharbia, S., and Green, J. (2005). Virulence searcher: a tool for searching raw genome sequences from bacterial genomes for putative virulence factors. *Clin. Microbiol. Infect.* 11, 770–772. doi: 10.1111/j.1469-0691.2005.01210.x

Vidana, R., Sullivan, A., Billstrom, H., Ahlquist, M., and Lund, B. (2011). *Enterococcus faecalis* infection in root canals - host-derived or exogenous source? *Lett. Appl. Microbiol.* 52, 109–115. doi: 10.1111/j.1472-765X.2010.02972.x

Wang, R., Xing, S., Zhao, F., Li, P., Mi, Z., Shi, T., et al. (2018). Characterization and genome analysis of novel phage vB_EfaP_IME195 infecting *Enterococcus faecalis*. *Virus Genes* 54, 804–811. doi: 10.1007/s11262-018-1608-1606

Weiner, L. M., Webb, A. K., Limbago, B., Dudeck, M. A., Patel, J., Kallen, A. J., et al. (2016). Antimicrobial-Resistant pathogens associated with healthcare-associated infections: summary of data reported to the national healthcare safety network at the centers for disease control and prevention, 2011-2014. *Infect. Control Hosp. Epidemiol.* 37, 1288–1301. doi: 10.1017/ice.2016.174

Xie, Y., Wahab, L., and Gill, J. J. (2018). Development and validation of a microtiter plate-based assay for determination of bacteriophage host range and virulence. *Viruses* 10:E189. doi: 10.3390/v10040189

Zhang, W., Mi, Z., Yin, X., Fan, H., An, X., Zhang, Z., et al. (2013). Characterization of *Enterococcus faecalis* phage IME-EF1 and its endolysin. *PLoS One* 8:e80435. doi: 10.1371/journal.pone.0080435

Conflict of Interest: The authors declare that the research was conducted in the absence of any commercial or financial relationships that could be construed as a potential conflict of interest.

Copyright © 2019 Lee, Im, Na, Ryu, Yun and Han. This is an open-access article distributed under the terms of the Creative Commons Attribution License (CC BY). The use, distribution or reproduction in other forums is permitted, provided the original author(s) and the copyright owner(s) are credited and that the original publication in this journal is cited, in accordance with accepted academic practice. No use, distribution or reproduction is permitted which does not comply with these terms.

frontiers in Microbiology

ORIGINAL RESEARCH
published: 08 January 2020
doi: 10.3389/fmicb.2019.02973

Overexpression of AmpC Promotes Bacteriophage Lysis of Ampicillin-Resistant *Escherichia coli*

*Shuang Wang[1], Bo Yin[2], Ling Yu[1], Mei Dang[2], Zhimin Guo[3], Guangmou Yan[1], Dongliang Hu[1,4], Jingmin Gu[1], Chongtao Du[1], Xin Feng[1], Wenyu Han[1], Yuren Yuan Adam[2], Changjiang Sun[1], Janine T. Bossé[5] and Liancheng Lei[1,6]**

[1] College of Veterinary Medicine, Jilin University, Changchun, China, [2] Center for Bioengineering and Biomedical Sciences, National University of Singapore (Suzhou) Research Institute, Jiangsu, China, [3] Department of Respiratory Medicine, The Second Hospital of Jilin University, Changchun, China, [4] Department of Zoonoses, Kitasato University School of Veterinary Medicine, Towada, Japan, [5] Department of Infectious Disease, Imperial College London, London, United Kingdom, [6] College of Animal Science, Yangtze University, Jingzhou, China

Infections caused by antibiotic-resistant *Escherichia coli* are a threat to human and animal health globally. Phage therapy has made great progress for the treatment of drug-resistant infections, but it is still unclear whether *E. coli* resistance to antibiotics could change the lysis ability of phages. In this study, we demonstrate that over expression of AmpC, an important β-lactamase for ampicillin resistance, promotes lysis of *E. coli* by phage utilizing OmpA as a receptor. *E. coli* strains expressing more AmpC showed higher levels of OmpA, an *E. coli* outer membrane protein known to serve as a receptor for T-even phages, which resulted in increased adsorption and lysis by the phage tested in this study. These data demonstrate that increased ampicillin resistance can increase the sensitivity of *E. coli* to some lytic phage, which provides evidence for the feasibility of synergistic application of phage and antibiotics.

Keywords: bacteriophage, antibiotic resistance, ampicillin, *E. coli*, AmpC

OPEN ACCESS

Edited by:
Robert Czajkowski, University of Gdańsk, Poland

Reviewed by:
Cristobal Chaidez, Centro de Investigación en Alimentación y Desarrollo (CIAD), Mexico
Daniel Elias Castillo Bermudez, University of Copenhagen, Denmark
Josefina Leon-Felix, Centro de Investigación en Alimentación y Desarrollo (CIAD), Mexico
William Calero-Cáceres, Technical University of Ambato, Ecuador
Sílvio B. Santos, University of Minho, Portugal

***Correspondence:**
Liancheng Lei
leiliancheng@163.com

Specialty section:
This article was submitted to Antimicrobials, Resistance and Chemotherapy, a section of the journal Frontiers in Microbiology

Received: *26 September 2019*
Accepted: *10 December 2019*
Published: *08 January 2020*

Citation:
Wang S, Yin B, Yu L, Dang M, Guo Z, Yan G, Hu D, Gu J, Du C, Feng X, Han W, Adam YY, Sun C, Bossé JT and Lei L (2020) Overexpression of AmpC Promotes Bacteriophage Lysis of Ampicillin-Resistant Escherichia coli. Front. Microbiol. 10:2973. doi: 10.3389/fmicb.2019.02973

INTRODUCTION

Escherichia coli is an important foodborne opportunistic pathogen, and acquired antibiotic resistance is increasing the global threat. The World Health Organization has listed 12 drug-resistant pathogens of greatest concern for human health, the most important of which are *Acinetobacter baumannii*, *Pseudomonas aeruginosa*, and *Enterobacteriaceae* (Tacconelli et al., 2017). Antibiotic resistance accounts for 700,000 deaths every year, and is estimated to reach 10 million by 2050 if there is no reduction in antimicrobial resistance or development of new antibiotics (Willyard, 2017). There is now an increased focus on alternative biotherapies (Thiel, 2004; Kelly et al., 2016).

Bacteriophages are regarded as potential biotherapeutic agents in the fight against resistant bacteria (Matsuzaki et al., 2014). Phage therapy has many advantages over the current use of antibiotics, such as reducing the incidence of recurrence after cessation of treatment, protecting the host from excessive intestinal growth of other pathogens, and diminished resistance to metronidazole or vancomycin (Ramesh et al., 1999). Furthermore, phage-lysed bacteria release less endotoxin than antibiotic-treated bacteria (Dufour et al., 2017). Phage replication at the site

of infection enhances efficacy; a single intraperitoneal injection of phage ENB6 rescued 100% of mice with vancomycin-resistant enterococci bacteremia (Biswas et al., 2002). Since long-term use of phage is not known to produce any side effects, it can be used for the treatment of chronic infectious diseases (Drilling et al., 2017). Selection for phage-resistant isolates may occur, but this is limited to the target bacterial species of the phage used for treatment. In contrast, prolonged antibiotic treatment may select for increased resistance amongst all exposed bacteria (pathogens and commensals) not only for the antimicrobial agent used, but also any other agents for which the resistance genes are co-selected (Murray et al., 2018). Whether bacteriophages can effectively lyse antibiotic-resistant bacteria remains unclear.

β-Lactam drugs play an important role in fighting infections caused by Gram-negative bacteria. However, the spread of β-lactamases (in particular those with broad spectrum of activity) in pathogenic bacteria has become a serious problem, increasingly leading to treatment failures (Bai et al., 2017). Chromosomally encoded AmpC is present in many *Enterobacteriaceae* species and confers resistance to multiple β-lactam antibiotics (Fisher et al., 2005; Jacoby, 2009). In some species, the release of cell wall degradation products upon exposure to β-lactams contributes to a complex regulatory pathway involving numerous proteins, culminating in high level expression of *ampC* following displacement of the repressor, AmpR (Jacoby, 2009; Pérez-Gallego et al., 2016). Inducible expression of chromosomal *ampC* does not occur in *E. coli*, which lacks AmpR (Jacoby, 2009). However, hyperproduction of AmpC in *E. coli* has been associated with mutations in the promoter and/or attenuator regions upstream of *ampC*, as well as with the presence of extra copies of the gene, either in the chromosome or on acquired plasmids (Nelson and Elisha, 1999; Peter-Getzlaff et al., 2011).

Resistance to β-lactams is also affected by alterations in the bacterial outer membrane which affect uptake of antibiotics, in particular, changes in expression profiles of the major porins. Some β-lactam resistant clinical isolates of *E. coli* have been found to lack OmpF in addition to hyperproducing AmpC (Martinez-Martinez et al., 2000). Recently, Choi and Lee (2019) constructed mutants of all porins in *E. coli* and confirmed that OmpF is the main porin associated with uptake of antibiotics, especially β-lactams, with OmpC contributing to a lesser extent. In contrast, loss of OmpA was associated with increased sensitivity to antibiotics (Choi and Lee, 2019). It is not yet known if antibiotic-induced changes in outer membrane profiles of Gram-negative bacteria affect their sensitivity to phage.

In previous studies, we have identified and characterized two related phage, vB_EcoM-ep3 and vB_EcoM_ECOO78, both *Myoviridae* capable of infecting a number of multiple-drug resistant *E. coli* clinical isolates (Lv et al., 2015; Guo et al., 2017). In this study, we show that hyper-production of AmpC is directly related to decreased OmpF, and increased OmpA, expression in *E. coli* and that these changes are associated with increased adsorption and lysis by these phages. Our findings provide a viable basis for the use of phage therapy for bacterial infections, in particular for treatment of β-lactam resistant bacterial infections.

MATERIALS AND METHODS

Bacterial Strains, Bacteriophages, and Growth Condition

Escherichia coli strains and their sources are listed in **Table 1**. Phage vB_EcoM-ep3 and vB_EcoM_ECOO78 were isolated previously in our laboratory (Lv et al., 2015; Guo et al., 2017); all other phages were isolated from hospital or domestic sewage, or water from rivers and lakes around Changchun, either as part of this or a previous study in our laboratory. Except for phage vB_EcoM-ep3 and vB_EcoM_ECOO78, the remaining phages were not characterized in depth. Phages and their host spectra are listed in **Supplementary Table S1**. Unless otherwise stated, *E. coli* was grown in 3 mL LB broth (1% [wt/vol] tryptone, 0.5% [wt/vol] yeast extract, 1% [wt/vol] NaCl) at 37°C. In order to proliferate phage, 100 μL of fresh logarithmic host bacteria were inoculated into LB broth, and a single phage plaque was scraped from a double-layer plate, prepared as previously described (Barrow et al., 1998), using a sterile loop and inoculated into the above medium. The culture was incubated at 37°C, with shaking (180 rpm), until the host bacteria were completely lysed to make the medium clear (about 2–6 h but varies for different phages).

Minimum Inhibitory Concentration (MIC) Assay

Minimum inhibitory concentration of ampicillin were determined by standard methods (Wiegand et al., 2008) for all *E. coli* strains used in this study. A single colony of each *E. coli* strain was inoculated into fresh LB medium and cultured to logarithmic growth phase; 2 μL of the bacterial culture were inoculated into 200 μL CAMHB medium containing ampicillin at final concentration of 800, 400, 200, 100, 50, 25, 12.5, or 6.25 mg/L and cultured at 35°C for 18 h, after which the bacterial growth was observed.

Host Range Determination

The 81 phages shown in **Table 1** were tested, using double-layer plate assay, for their ability to lyse the 29 clinical *E. coli* isolates (from human or animal sources), as well as strains obtained from culture collections, i.e., ATCC25922 (antibiotic sensitive serotype O6 reference strain), BL21(DE3) and K12 MG1655 (both antibiotic-sensitive rough strains, lacking O polysaccharide chains), and CVCC1418 (an antibiotic-sensitive O78-type *E. coli* strain). In addition, a spontaneous mutant of the latter strain, CVCC1418AmpR, with high resistance to ampicillin was selected following serial passage in LB broth containing increasing concentrations of ampicillin (from 1 to 1024 mg/L). This mutant strain was also tested for lysis with the panel of phages. For the double-layer agar plate test (Barrow et al., 1998), the phage dilution and the tested *E. coli* strain were added to the melted semi-solid medium (45°C) and immediately mixed, then poured onto LB agar plates and cultured at 37°C for 10 h. The formation of plaques was observed following over-night incubation of the plates at 37°C.

TABLE 1 | Information of *E. coli* strains and number of corresponding phages.

E. coli strains	MIC (ampicillin mg/L)	Number of corresponding phages	*E. coli* strains	MIC (ampicillin mg/L)	Number of corresponding phages
E. coli HXM[a]	>800	1	*E. coli* TSQ[a]	>800	1
E. coli LSZ[a]	>800	1	*E. coli* ZDY[a]	>800	1
E. coli CZ [a]	>800	3	*E. coli* O78-3[b]	>800	4
E. coli ZLH[a]	>800	3	*E. coli* O78-6[b]	>800	5
E. coli WZ[a]	>800	4	*E. coli* CC11[b]	>800	6
E. coli SGF[a]	>800	1	*E. coli* GYP[a]	>800	2
E. coli O78-5[b]	>800	2	*E. coli* S-F23[c]	>800	4
E. coli CVCC1418AmpR	>800	4	*E. coli* ATCC25922[d]	25	3
E. coli CVCC1418[e]	25	3	*E. coli* K12 MG1655[f]	25	2
E coli ZDZ[a]	25	3	*E. coli* MYL[a]	25	2
E. coli LHY[a]	25	1	*E. coli* ZZJ[a]	25	2
E. coli 84[a]	25	1	*E. coli* BDY[a]	25	1
E. coli YFX[a]	25	1	*E. coli* PJ[a]	25	4
E. coli TC[a]	12.5	2	*E. coli* YXM[a]	12.5	1
E. coli MLD[a]	12.5	2	*E. coli* ZX[a]	12.5	1
E. coli DQQ[a]	12.5	3	*E. coli* WHL[a]	<6.25	3
E. coli SWD[a]	<6.25	2	*E. coli* BL21(DE3)[g]	<6.25	2

[a]Isolated from patients at the First Hospital of Jilin University (Changchun, China); [b]Isolated from chicken of Feng Xin chicken farm in Chuangchun; [c]Isolated from swine lung from Changchun farm; [d]Purchased from the ATCC; [e]Purchased from the China veterinary culture collection center; [f]Purchased from China biovector plasmid vector bacterial cellular protein antibody gene collection center. [g]Purchased from Tiangen Biotech (Beijing), Co., Ltd.

Bacterial Lysis Assay

A bacterial lysis assay was performed following a published procedure (Ronayne et al., 2016) with some modifications. Briefly, logarithmic phase cultures of *E. coli* were diluted 1:100 in fresh LB and grown at 37°C to an optical density at 600 nm (OD_{600}) of at least 0.55. Within each experiment, cultures were adjusted to an equal OD_{600} (0.5 to 1.2) and phage was added at a multiplicity of infection (MOI) of 10. Control cultures were left uninfected. Every 20 min, over a 2 h period, 200 μL aliquots were removed to measure the OD_{600} using BioPhotometer plus (Eppendorf). Phage lysis rate was calculated as [1-(the OD_{600} of phage treated group/the OD_{600} of control group)] × 100% after phage treatment for 80 min. Three biological replicates were performed, and the data is represented as mean with standard deviation.

Adsorption Rate Assay

Phage absorption was assessed as described previously (Park et al., 2017), with some modifications: mid-exponential phase recipient *E. coli* strains were mixed with phage lysate in phage buffer (50 mM Tris-HCl pH 7.5, 100 mM NaCl, 10 mM $CaCl_2$) at a MOI of 10 and incubated for 20 min at 37°C. Phage bound to bacterial cells were removed by microcentrifugation of 1 mL of the infected culture at 13,000 × *g* for 15 min at 4°C. The plaque-forming units (PFUs) of the supernatant containing the unbound phage was determined by the double-layer agar plate test. The phage absorption (% input) was calculated as [1 - (the number PFU of unbound phage/input PFU)] × 100%. Each absorption assay was repeated at least three times.

Genetic Manipulations

Bacterial genomic DNA was extracted using the Bacterial DNA Kit (Omega, Norcross, GA, United States), and phage DNA extracted using Viral DNA Kit (Omega, Norcross, GA, United States). Plasmids were isolated using 96 Well Plasmid DNA Mini-Preps Kit (Sangon Biotec, China). Restriction endonucleases and T4 DNA ligase were purchased from Thermo Scientific and used according to manufacturers' instructions. Premix Taq™ (Ex Taq™ Version 2.0) (TAKARA, # RR003Q, Japan) was used to amplify AmpC, OmpA, and Dpo41. Primers used are listed in **Supplementary Table S2**. Sequence analysis was performed by Genewiz[1].

pET-23a-*ampC* Construction for Over-Expression of AmpC and Complementation

The coding sequence of *ampC* was amplified from *E. coli* strain K12 MG1655 genomic DNA using primers AmpCF/AmpCR. Sequence was digested with *Bam*HI and *Eco*RI and inserted downstream of the T7 promoter in the plasmid pET-23a to produce pET-23a-*ampC*, and the resulting plasmid was transformed into *E. coli* DH5α by electroporation. Clones were selected on LB with kanamycin (34 mg/L) and insertions were confirmed by sequencing using primers AmpCF/AmpCR.

For overexpression of AmpC, the plasmid pET-23a-*ampC* was introduced into *E. coli* strain CVCC1418, where it was stably maintained. The bacterial culture was harvested by

[1]https://www.genewiz.com.cn/

centrifugation and re-suspended in ice-cold lysis buffer (25 mM Tris pH 7.4, 25 mM KH_2PO_4, 500 mM NaCl, 10% glycerol and 1 mM dithiothreitol). Cell suspensions were disrupted using an EmulsiFlex-C3 high-pressure homogenizer (Avestin) four times and centrifuged at 13,000 × *g* for 1 h at 4°C to remove cell debris. The soluble cytoplasmic proteins in the resulting supernatant were identified by SDS-PAGE.

The same plasmid, pET-23a-*ampC*, was used to complement the *ampC* deletion mutant of *E. coli* strain K12 MG1655, described in the next section. The original plasmid pET-23a was used as a complementation control. Plasmids propagated in *E. coli* strain DH5α were transformed into *E. coli* strain K12 MG1655Δ*ampC*.

Strain K12 MG1655Δ*ampC* Construction

Gene knockout was performed as described previously (Jiang et al., 2015). Following unsuccessful attempts to delete *ampC* in strain CVCC1418, CRISPR/Cas9 was used to knock out *ampC* in *E. coli* strain K12 MG1655. In this two-plasmid system, the cas9 gene and the sgRNA directing it to the targeted region were separated into pCas (Addgene: #62225) and pTargetT-Δ*ampC*. The latter plasmid was constructed by inserting the donor DNA used as the genome editing template into pTargetF (Addgene: #62226), followed by N20 sequence mutation via inverse PCR using the KOD-plus-neo polymerase (TOYOBO, Osaka) with primers pAmpC01/pAmpC02. The genome editing template was concatenated by a 550-bp sequence homologous to each side of the *ampC* gene through overlap PCR of the two fragments amplified from K12 MG1655 using primers pUAmpC1/pDAmpC1 to form the upstream, and pUAmpC2/pDAmpC2 to form the downstream, region. Strain K12 MG1655 competent cells harboring pCas were prepared and the plasmid pTargetT-Δ*ampC* was then introduced both by electroporation (2.5 kV), as described previously (Jiang et al., 2015). Cells were recovered at 30°C for 2 h before being spread onto LB agar containing kanamycin (34 μg/mL), spectinomycin (50 μg/mL), and arabinose (10 mM) and incubated 16 h at 30°C. Colonies harboring both pCas and pTargetT-Δ*ampC* were picked randomly and inoculated into 5 mL LB medium with the addition of kanamycin (34 μg/mL) and isopropyl β-D-thiogalactoside (IPTG) (0.8 mM). After 24 h cultivation, the culture was diluted and spread onto LB agar plates containing kanamycin (34 μg/mL) and IPTG (0.8 mM). The colonies were confirmed as cured by determining their sensitivity to spectinomycin (50 μg/mL). The colonies cured of the TargetT-Δ*ampC* were used for extraction of genomic DNA, and they were validated by PCR using primers pUAmpC1/pDAmpC2 and DNA sequencing. For the curing of pCas, an edited colony harboring pCas was inoculated into LB medium at 37°C non-selectively.

Western Blot Analysis of AmpC Expression

Western blotting was performed as described previously (Ballesteros-Plaza et al., 2013) with some modifications: *E. coli* cells were sonicated. *E. coli* cell (1×10^8 CFU) lysates were boiled in 5× loading buffer [0.25M Tris-HCL (pH 6.8); 10% (w/v) sodium dodecyl sulfate; 0.5% (w/v) bromophenol blue; 50% (v/v) glycerol; 5% (w/v) β-mercaptoethanol], and proteins were separated by SDS-PAGE and transferred to polyvinylidene difluoride membranes using eBlot Protein Transfer Device (Genscript), according to manufacturer's instructions. Membranes were probed with anti-*E. coli* AmpC Ab (mouse polyclonal antiserum; for details of preparation, see **Supplementary Data**) and anti-GAPDH Ab (1:1000 in PBS, rabbit polyclonal, #E-AB-20059, from Elabscience) followed by horseradish peroxidase (HRP)-conjugated goat anti-mouse Antibody (1:5000 in PBS, #bsm-0294M-HRP, Bioss, China). Chemiluminescence was developed using an Immobilon Western chemiluminescent HRP substrate (Millipore) and documented using a Tanon 5200 milti (Biotanon). Densitometry was performed using ImageJ software (Ver 1.4.3.67) and was normalized to GapA (probed by anti-GAPDH Ab) (Wu et al., 2012).

iTRAQ Proteomics

iTRAQ analysis was performed at Beijing Qinglian Bio Biotechnology, Co., Ltd. (BQB, Beijing, China). The protocol was as follows, *E. coli* strain CVCC1418 and CVCC1418AmpR were cultured to logarithmic phase. After centrifugation at 3000 × *g* for 5 min at room temperature, cells were washed three times with a sterile PBS solution, cells and collected after removing the PBS solution. Samples (wet weight is 400 μg) were resuspended in 700 μL of lysis buffer (7M urea, 2M thiourea, 0.1% CHAPS) and mixed by vortex. Sample was sonicated using an ultrasonic cell disruptor (0.2 s bursts every 2 s for 60 s, at an amplitude of 22%, Nanjing Atpio, Cat No: XO) and incubated at room temperature for 30 min, followed by centrifugation at 13,000 × *g* for 4 min at 4°C. The protein concentration of the supernatant was determined by Bradford Assay (Bradford, 1976). Enzymatic hydrolysis and labeling was performed using the iTRAQ kit (AB Sciex, PN: 4381664), according to manufacturer's instructions. Primary separation of digested peptides and LC-MS/MS analysis (Thermo Q-Exactive mass spectrometer) were performed after that, using default parameters. Proteins with a difference of ≥1.2, or a difference of ≤0.833, were analyzed. Gene Ontology (GO) functional annotation (Dessimoz and Škunca, 2017), functional enrichment analysis, and localization analysis were performed on the identified proteins using the bioinformatics analysis tool DAVID (Huang et al., 2007). *P*-value calculation formula for the significant enrichment of the differential protein in a certain GO functional category is as follows:

$$\text{pValue} = 1 - \sum_{k=0}^{n-1} \frac{\binom{n-k}{N-M}\binom{k}{M}}{\binom{n}{N}} \quad (1)$$

In the formula (1), N is the total number of proteins annotated by GO; M is the number of proteins belonging to a certain GO subclass; n is the number of protein sets subjected to

GO enrichment analysis; and k is the number of proteins belonging to M in n.

Phage Receptor Binding Protein (RBP) Identification

To identify the RBP of phage vB_EcoM-ep3, we used a previously published method (Simpson et al., 2016). Briefly, extracted phage genomic DNA was broken using ultrasound waves into random fragments of 150 to 2500 bp. Following end-filling using Quick Blunting™ Kit (NEB, #E1201L) and phosphorylation using Alkaline Phosphatase (NEB, #M0290S), the purified random phage DNA fragments were ligated into *Eco*RV-digested pET-30a vector and transformed into BL21 (DE3) competent cells, with positive clones selected on LB plates containing kanamycin (34 μg/mL). Phage protein fragments expressed by the resulting positive clones capable of binding to *E. coli* O78-6 were recognized as encoding RBPs.

Phage Blocking Experiment

For the phage blocking assay, 1×10^9 PFU of phage vB_EcoM-ep3 were pretreated with 10 μL anti-Dpo41 serum or GST-OmpA (1 mg/mL) for overnight at 4°C, culture of *E. coli* strain O78-6 in logarithmic growth phase was added (MOI of 10). The calculation of the adsorption rate and the lyse rate were as described above.

Co-immunoprecipitation (Co-IP)

The Co-IP experiments were performed using a Pierce™ Classic Magnetic IP/Co-IP Kit (Thermo Fisher, #88804) following the manufacturer's instructions. Briefly, His-Dpo41 and GST-OmpA (for details of preparation, see **Supplementary Data**), 0.5 mM for each protein, were incubated with IP antibody (Anti-GST antibody; Sungene biotech, # KM8005, China) overnight at 4°C to form antigen-antibody complex, following which complexes were bound to Protein A/G magnetic beads for 1 h at room temperature. Beads were washed twice with IP Lysis/Wash Buffer and once with purified water. The antigen/antibody complexes were eluted and collected and analyzed by western blot using Anti-GST antibody and Anti-His antibody.

Reveres Transcription-Polymerase Chain Reaction

Bacteria were cultured to logarithmic growth phase, and the cells were collected by centrifugation at 3000 × *g* for 5 min. RNA was extracted using Bacterial RNA extraction Kit (Omega, #R6950-01). An aliquot of total RNA (0.5 μg) was reverse transcribed to cDNA using PrimeScript™ RT reagent with gDNA eraser (Perfect Real Time) kit (TAKARA, #RR047A, Japan), following the manufacturer's instructions. Diluted cDNA was subjected to real-time PCR using TB greenTM premix Ex taq II (Tli RNaseH plus) (TAKARA, #RR820A, Japan) and the RT-PCR–specific primers listed in **Supplementary Table S2**: *E. coli* 16S rRNA (*E. coli* 16SF and *E. coli* 16SR), *ompA* (OmpA-RTF and OmpA-RTR). Data is represented after normalization with 16S rRNA.

Statistical Analysis

All data analysis was performed using SPSS version 19.0 (SPSS, Inc., Chicago, IL, United States). One-way analysis of variance (ANOVA) was performed on the normal distribution data. Qualitative data were analyzed using chi-square test and two-sided Fisher's exact test. *P*-values < 0.05 were considered statistically significant.

RESULTS

Increased Resistance of *E. coli* Strains to Ampicillin Is Associated With Higher Susceptibility to Phage Lysis

To study the association between ampicillin resistance and phage lysis, 34 strains of *E. coli* were used in the isolation of, and host-range determination for, a total of 81 phages (**Table 1** and **Supplementary Table S1**). The MICs of ampicillin for these *E. coli* strains, and the lysis rates obtained using their associated phages, were determined. Bacterial strains were divided into low-resistance ($\leq$25 mg/L) comprising of 19 strains which were able to host a total of 36, and high-resistance ($\geq$800 mg/L) group comprising of 15 strains which were able to host a total of 42, of the tested phage. Furthermore, the high-resistance group showed a significantly higher phage sensitivity ($P = 0.026$) (**Figure 1**). These results suggested that increased ampicillin resistance may be associated with increased susceptibility of *E. coli* to phage.

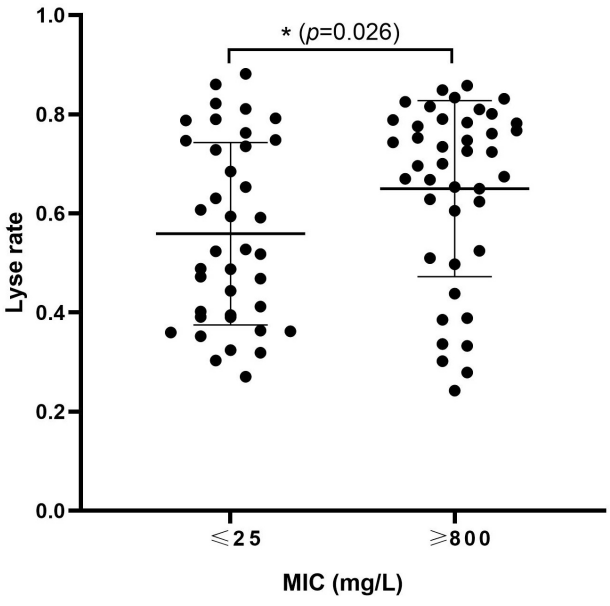

FIGURE 1 | High levels of ampicillin resistance are associated with increased susceptibility of *Escherichia coli* to phage. Thirty-four *E. coli* strains and 81 phages isolated with these strains were used to investigate the relationship between ampicillin MIC and phage sensitivity of *E. coli*. Each dot: the lyse rate for a phage on its host. *$0.01 < p < 0.05$.

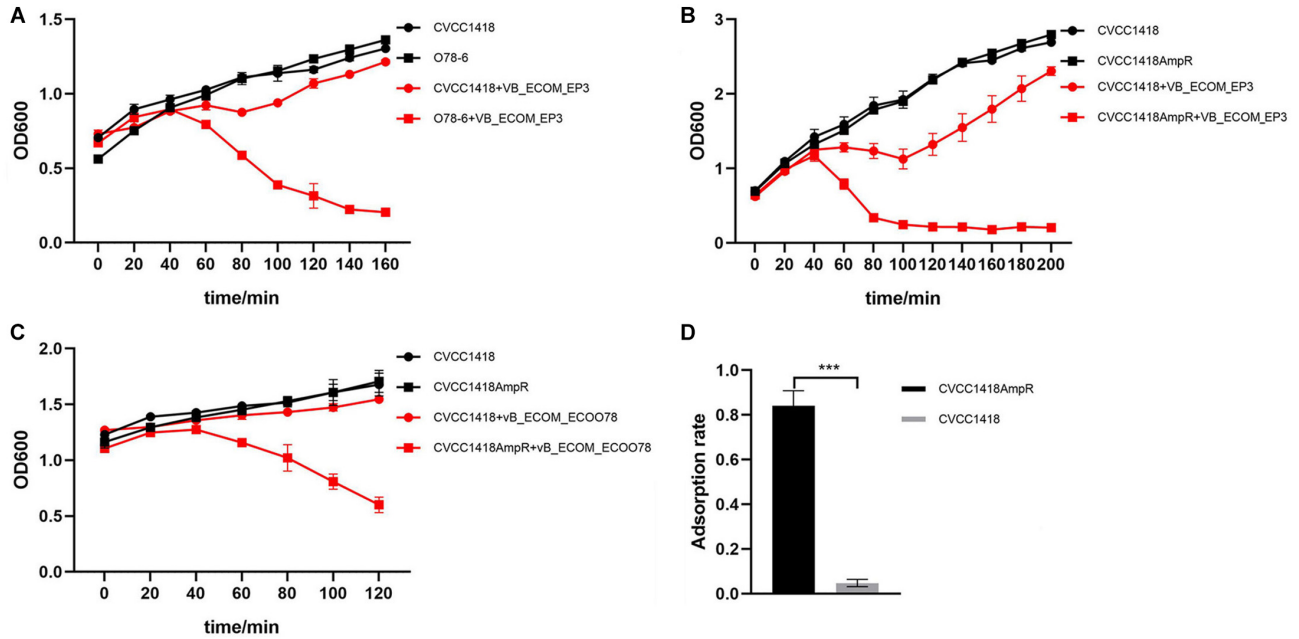

FIGURE 2 | Comparison of lysis rates between serotype O78 *E. coli* isolates with high or low resistance to ampicillin. **(A)** Phage vB_EcoM-ep3 showed greater lysis of isolate O78-6 (MIC ≥ 800 mg/L) than isolate CVCC1418 (MIC ≤ 25 mg/L). **(B)** Phage vB_EcoM-ep3 showed greater lysis of CVCC1418AmpR (MIC ≥ 800 mg/L) than CVCC1418 (MIC ≤ 25 mg/L). **(C)** The related *Myoviridae* phage, vB_EcoM_ECOO78, also showed greater lysis of CVCC1418AmpR than CVCC1418. **(D)** The adsorption rate of phage vB_EcoM-ep3 onto CVCC1418AmpR was significantly higher than onto CVCC1418. ***$p < 0.01$.

Four of the clinical isolates from chicken farms with high MICs of ampicillin (>800 mg/L) belong to serotype O78 and were used to isolate a total of 17 of the tested phage, including previously characterized members of the *Myoviridae* family, vB_EcoM-ep3 and vB_EcoM_ECOO78 (Lv et al., 2015; Guo et al., 2017). Full host range determination further revealed that these four strains were able to host a total of 27 phages amongst them, with individual strains hosting up to 13 different phages (**Supplementary Table S1**). Strain CVCC1418, also serotype O78 but with a low MIC of ampicillin (<25 mg/L), was initially used in the isolation of three phage and was further able to host vB_EcoM-ep3 and vB_EcoM_ECOO78 and four other phages, mostly those isolated using other O78 strains (**Supplementary Table S1**). Comparing strain O78-6 (the strain able to host the most phages) with CVCC1418 for sensitivity to lysis by phage vB_EcoM-ep3, showed that although strain CVCC1418 could host this phage, it was much less sensitive to lysis by it than the O78-6 strain (**Figure 2A**).

To further investigate the relationship between levels of ampicillin resistance and phage susceptibility, we generated a spontaneous mutant, CVCC1418AmpR, with higher ampicillin resistance compared to CVCC1418 and found that the mutant was much more sensitive to lysis by phage vB_EcoM-ep3 than parental strain (**Figure 2B**). In addition, CVCC1418AmpR was also much more sensitive than the parental strain to lysis by the related phage vB_EcoM_ECOO78 (**Figure 2C**). Further study found that the adsorption rate of phage vB_EcoM-ep3 was higher on strain CVCC1418AmpR than on CVCC1418 (**Figure 2D**). Taken together, these results demonstrate that increasing ampicillin resistance made *E. coli* strain CVCC1418 more vulnerable to the tested phage.

Increased Ampicillin Resistance Is Associated With Differential Expression of a Number of Proteins Including AmpC and Some Outer Membrane Proteins

To better understand how the increased ampicillin resistance in strain CVCC1418AmpR is related to greater susceptibility to the *Myoviridae* phages vB_EcoM-ep3 and vB_EcoM_ECOO78, we compared the protein profiles of this mutant and its parental strain by iTRAQ. We identified 54 proteins that were differentially expressed, including the chromosomally encoded AmpC, which showed increased expression in the CVCC1418AmpR mutant (**Figure 3**). In addition, six of the differentially expressed proteins were indicated by Gene Ontology analysis to be located in the bacterial outer membrane (**Supplementary Figure S1**), including the porin proteins ChiP and OmpA, which were upregulated, and OmpF, which was down-regulated, in the CVCC1418AmpR mutant.

Increased AmpC Promotes Expression of the Phage Receptor Protein OmpA

Increased AmpC expression in CVCC1418AmpR compared to the parental strain CVCC1418 was confirmed by Western blot analysis (**Supplementary Figures S2A,B**). However, as the CVC1418AmpR mutant was generated spontaneously by exposure to increasing concentrations of ampicillin, and

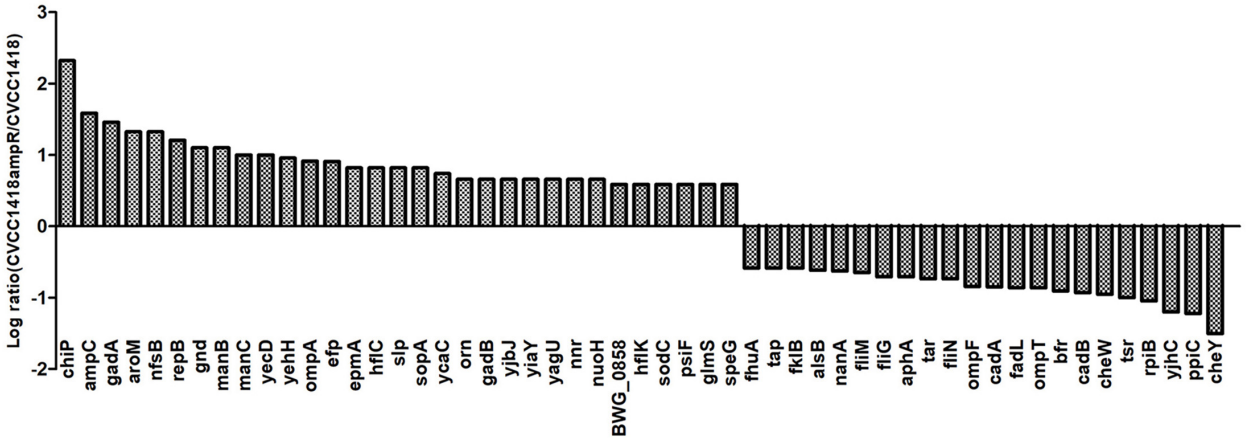

FIGURE 3 | Differential protein expression in CVCC1418AmpR compared to CVCC1418. Experiments were carried out three times.

proteomic analysis showed differential expression of numerous proteins in comparison to the parental strain, we sought to confirm the association between AmpC expression and phage sensitivity using genetically defined mutants.

Strain CVCC1418pAmpC, generated by introduction of cloned *ampC* gene on plasmid pET-23a-*ampC* (**Supplementary Figure S3A**), showed greater lysis by vB_EcoM-ep3, and greater adsorption of this phage, compared to the control strain containing empty vector (**Figures 4A,B**). As attempts to generate an *ampC* deletion mutant in strain CVCC1418 were unsuccessful, we used strain K12 MG1655 (K12) to generate an *E. coli* mutant (K12Δ*ampC*) lacking *ampC* and complemented this mutation using the pET-23a-*ampC* plasmid (**Supplementary Figures S3B,C**). Using phage PK12, which specifically targets strain K12 MG1655, we demonstrated that deletion of *ampC* in K12Δ*ampC* reduced lysis and adsorption by this phage compared to the parental and complemented strains, whereas introduction of the empty control vector did not restore wild-type levels of lysis or adsorption (**Figures 4C,D**).

The association of over-expression of the periplasmic AmpC protein with an increased phage adsorption, along the with results of iTRAQ analysis above, suggest concomitant changes in expression of phage receptor(s) located on the surface of the bacteria. In order to identify specific outer membrane receptor(s) for phage vB_EcoM-ep3, we first identified two putative PRBs of phage vB_EcoM-ep3; phage major capsid protein (ep3_0031) and putative tail fiber protein (ep3_0041) (**Supplementary Table S3**). BLASTx analysis of ep3_0041 revealed 99% identity with the reported tail protein-depolymerase, Dpo42 (Gene ID:40076521), of phage vB_EcoM_ECOO78. It is, therefore, speculated that ep3_0041 is also a tail-protein depolymerase, so we named it Dpo41. Since RBPs for phage are usually tail proteins, we hypothesized that Dpo41 may be the main RBP for phage vB_EcoM-ep3.

In order to confirm the role of Dpo41 as a RBP, we cloned, over-expressed and purified the His-tagged protein (from *E. coli* BL21-pDpo41), which was then used to generate a polyclonal rabbit antiserum (**Supplementary Figure S4**). Blocking Dpo41 using this antiserum significantly reduced the adsorption rate of vB_EcoM-ep3 to strain O78-6 (**Figure 5A**) and the lysis of this strain by the phage (**Figure 5B**), supporting the role of Dpo41 as RBP of phage vB_EcoM-ep3.

Co-immunoprecipitation using the His-tagged Dpo41 protein incubated with a cell lysate of strain O78-6 identified a number of different proteins, visualized on silver stained SDS-polyacrylamide gels (**Figure 6A**), which were sent for mass spectrometry. The identified putative receptors were Lpp, OmpA, and Eno (**Supplementary Table S4**). As OmpA has previously been reported as a receptor for other *E. coli Myoviridae* (T-even) phages, we expressed a GST-OmpA fusion in *E. coli* strain BL21 (DE3) and purified this for co-immunoprecipitation analysis with His-Dpo41. The results showed that Dpo41 bound to OmpA (**Figure 6B**) and GST-OmpA pre-treatment prevented phage vB_EcoM-ep3 adsorption to strain O78-6 (**Figure 6C**). These results indicate that OmpA is a receptor for vB_EcoM-ep3.

Deletion of *ampC* significantly reduced the transcription of OmpA in *E. coli* strain K12 MG1655, whereas over-expression of AmpC in strains CVCC1418AmpR and CVCC1418pAmpC was associated with increased OmpA expression compared with strain CVCC1418 (**Figure 6D**). In summary, increased expression of AmpC appears to promote the production of OmpA, which in turn increases adsorption of, and lysis by, *E. coli* by phage for which OmpA is a receptor.

DISCUSSION

During isolation of phages using clinical isolates of *E. coli* from human and animal sources in the Changchun region of China, we noticed that those isolates with high MICs of ampicillin appeared to host a larger number of phages (**Supplementary Table S1**). Although only a few of the *E. coli* isolates used in this study were serotyped, we also noticed that the largest number of phages were hosted by *E. coli* originating from chicken farms belonging to serotype O78, suggesting that the common LPS in these isolates contributed to binding of a related set of phages. However, not

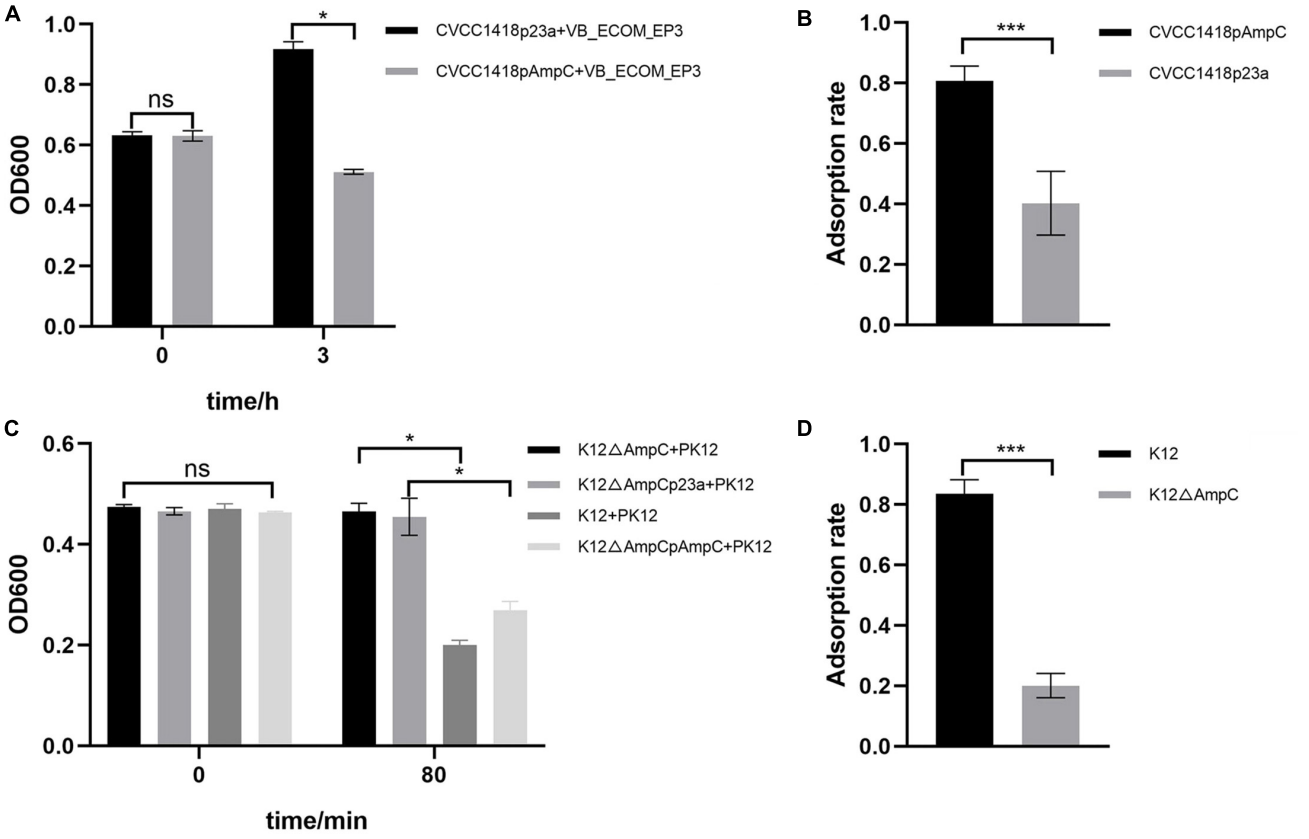

FIGURE 4 | Expression of AmpC associated with increased phage adsorption and lysis. **(A)** The rate of lysis of CVCC1418pAmpC by vB_EcoM-ep3 was significantly higher than that of CVCC1418. **(B)** The adsorption rate of phage vB_EcoM-ep3 on CVCC1418pAmpC was higher than that on CVCC1418p23a. **(C)** The rate of lysis of K12△*ampC* by phage PK12 was significantly lower than that of K12 MG1655 and K12△*ampC*pAmpC while no significant difference was seen for K12△ampCp23a. **(D)** The adsorption rate of PK12 was significantly lower on K12△*ampC* than on K12 MG1655. *$0.01 < p < 0.05$; ***$p < 0.01$.

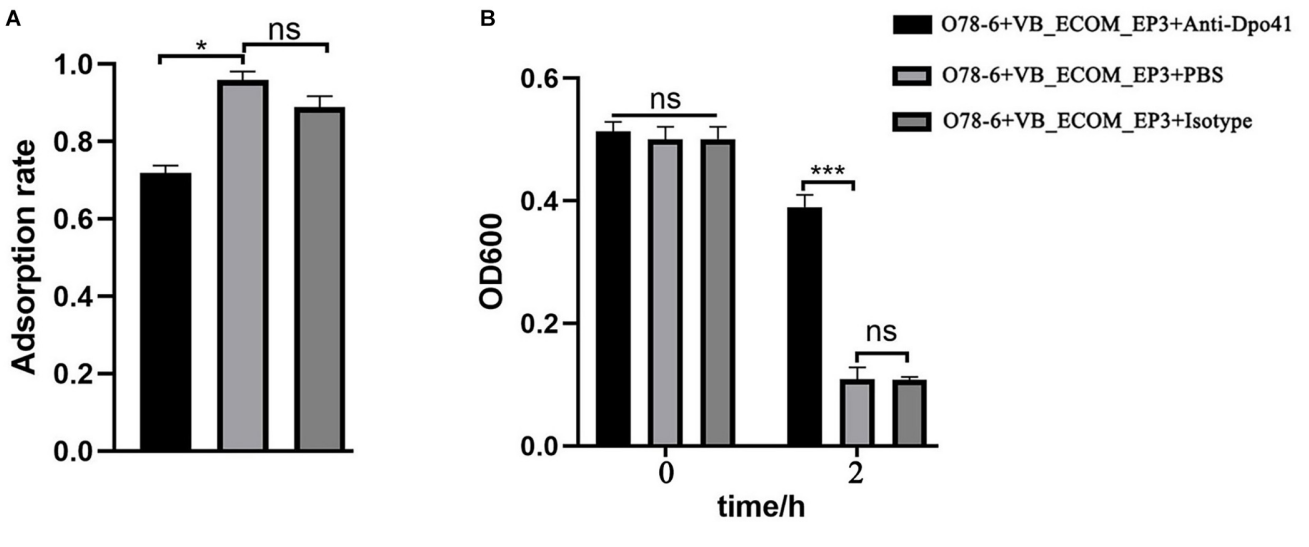

FIGURE 5 | vB_EcoM-ep3 protein Dpo41 is critical for lysis of *E. coli* O78-6. Tail fiber protein Dpo41 blocked by polyclonal antibody decreased the phage adsorption efficiency **(A)** and bacteria lysis **(B)**. Anti-Dpo41: IgG obtained by immunizing rabbits with purified Dpo41, isotype: IgG obtained by immunizing rabbits with PBS. *$0.01 < p < 0.05$; ***$p < 0.01$.

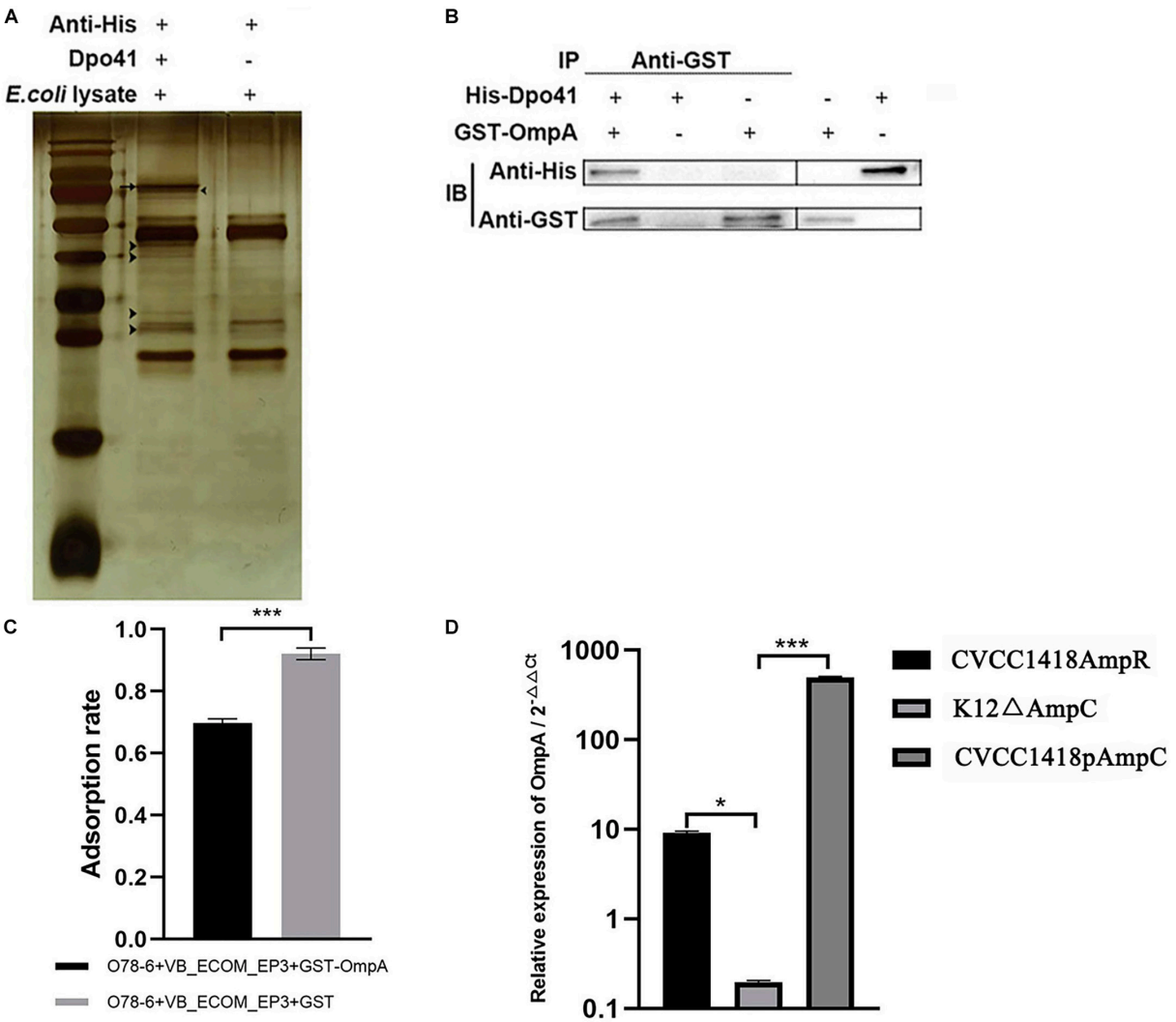

FIGURE 6 | vB_EcoM-ep3 protein Dpo41 interacts with *E. coli* strain O78-6 OmpA during adsorption phase. **(A)** Identification of receptor for Dpo41 using Co-IP. Arrow: band of Dpo41, arrow head: bands for mass spectrometry. **(B)** Dpo41 bound to OmpA. The purified protein His-Dpo41 (or PBS) was incubated with purified GST-OmpA (or PBS) in the presence of Anti-GST antibody. The obtained immune complexes were subjected to CO-IP assay (see section "Materials and Methods") and analyzed by Western blot using anti-His and Anti-GST antibodies. **(C)** OmpA pre-treatment prevented phage vB_EcoM-ep3 binding to *E. coli* strain O78-6. Phage vB_EcoM-ep3 was incubated with GST-OmpA (0.1 mg/mL) for 3 h before adsorption rate assay, the control group was treated with GST with the same amount. **(D)** Overexpression of AmpC increased the production of OmpA. The relative expression of OmpA of CVCC1418AmpR, K12Δ*ampC*, CVCC1418pAmpC were compared with that of CVCC1418, K12, CVCC1418p23a, respectively. $^{*}0.01 < p < 0.05$; $^{***}p < 0.01$.

all O78-derived phages were able to infect all of the O78 type strains, suggesting other phage receptor(s) are likely involved that differ in expression and/or accessibility amongst these isolates. That might be the reason why the difference between the two groups didn't seem that significant (**Figure 1**). Furthermore, strain CVCC1418 (also serotype O78, but with a low MIC of ampicillin) hosted fewer of the O78-derived phages than the other *E. coli* of this serotype and was less susceptible to lysis by the previously characterized *Myoviridae* phages, vB_EcoM-ep3 and vB_EcoM_ECOO78 (**Figure 2**) (Lv et al., 2015; Guo et al., 2017). These results suggested that differences in the level of ampicillin resistance amongst O78 serotype strains may affect susceptibility to their specific phage. The 24 *E. coli* isolates that were from human sources likely belong to other serotypes, as suggested by comparatively little if any infection by O78-derived phage (**Supplementary Table S1**), and we did not explore the nature of the receptors bound by their associated phage in this study. These phages may bind receptors that are not affected by the level of ampicillin resistance, as suggested by some of the highly resistant isolates with lower lysis rates and the more even distribution of lysis rates for *E. coli* with low resistance (**Figure 1**).

We have shown that increased expression of AmpC, either via spontaneous mutation (likely in the promoter/attenuator region of the chromosomal copy of *ampC*) or by over-expression of

the *ampC* gene on a plasmid, promoted decreased expression of OmpF and increased expression of OmpA in *E. coli* strain CVCC1418 (**Figure 3**). Lack of OmpF has previously been associated with β-lactam-resistant clinical isolates of *E. coli* hyperproducing AmpC (Martinez-Martinez et al., 2000), and loss of OmpA has previously been reported to increased sensitivity to antibiotics (Choi and Lee, 2019). Here, we have shown that the increased production of OmpA associated with increased expression of AmpC promotes the adsorption of, and lysis by, tested *Myoviridae* phages (**Figures 4**, **6D**). We demonstrated that OmpA functions as a receptor for the tail fiber protein, Dpo41, of phage vB_EcoM-ep3, which is homologous to the tail fiber protein, Dpo42, of phage vB_EcoM_ECOO78 (Guo et al., 2017).

Our results confirm the feasibility of using phage to treat β-lactam-resistant *E. coli* infections. A previous report indicated that *Shigella flexneri* phage Sf6 uses OmpA and OmpC on the bacterial surface as receptors (Parent et al., 2014), so the phenomenon observed in this study may also be present in other Gram-negative species, which we plan to further investigate. It is possible that enhanced resistance to other antibiotics which lead to changes in expression of bacterial surface antigens, may also promote, rather than reduce, phage lysis efficiency, and these resistant bacteria can be used to screen for more efficient phages for use as biotherapeutic agents.

Our results support the combined use of phage and antibiotics to provide synergistic efficacy in treating bacterial infections, as reported by others (Oechslin et al., 2016; Ronayne et al., 2016; Wang et al., 2017). The combination of phage and antibiotics can also act synergistically to reduce bacterial density in biofilms (Akturk et al., 2019). A recent study reported that while the phage had a small effect on pathogen density on its own, it considerably increased the sensitivity of *Ralstonia solanacearum* to antibiotics produced by *Bacillus amyloliquefaciens* (Wang et al., 2017). In that study, they showed that the fitness cost of bacterial adaptation (reduced growth) was highest when the pathogen had evolved in the presence of both the phage and the competitor (Wang et al., 2017). However, the mechanism of synergism between phage and antibiotics was not fully elucidated. Another study showed that Ref endonuclease encoded by bacteriophage P1 renders *E. coli* more sensitive to the DNA-damaging antibiotic ciprofloxacin (Ronayne et al., 2016), indicating that in this case, synergy involved a mechanism other than increased phage adsorption.

CONCLUSION

We investigated the mechanism by which increased AmpC expression promoted lysis of the O78 *E. coli* strain CVCC1418 by the tested phages, and identified increased production of OmpA, which we confirmed as a receptor for the *Myoviridae* phage, vB_EcoM-ep3. We further identified differential expression of other proteins following increased expression of AmpC that were not investigated as part of this study. It is possible that some of these proteins could promote lysis by other phages, as suggested by the reduced lysis of the *E. coli* K12 MG1655Δ*ampC* by phage PK12 (which does not appear to be related to the *Myoviridae* in this study), but this has yet to be explored. In general, the process of bacteria acquiring resistance to antibiotics is bound to bring about changes in expression of multiple proteins that affect bacterial metabolism and fitness, and further research is required to determine if these changes can be exploited for identification of biotherapeutic phages which can be used in combined therapies to treat bacterial infections.

DATA AVAILABILITY STATEMENT

The raw data supporting the conclusions of this article will be made available by the authors, without undue reservation, to any qualified researcher.

ETHICS STATEMENT

New Zealand white rabbits (female, 1.3–1.6 kg) were purchased from Changchun Yisi Experimental Animal Technology, Co., Ltd. (Changchun, China). All animal managements and experiments were strictly abided by the Regulations for the Administration of Affairs Concerning Experimental Animals approved by the State Council of the People's Republic of China (1.11.1988) and approved by the Animal Welfare and Research Ethics Committee at Jilin University.

AUTHOR CONTRIBUTIONS

SW, JB, BY, and LY drafted the main manuscript. MD performed the data analysis. SW, BY, LY, and ZG planned and performed the experiments. SW, JG, CD, XF, WH, YA, CS, and LL were responsible for experimental design. SW, GY, DH, and LL were responsible for guiding and supporting the experiments and manuscript revisions.

FUNDING

This study was supported by funds from the National Key R&D Program of China (2017YFD0500204), National Key Research and Development Plan (2016YFD0501307), Research Grants from the Natural Science Foundation in Jiangsu Province (BK20160373), and Project 2017169 supported by the Graduate Innovation Fund of Jilin University. JB was supported by grants from the Biotechnology and Biological Sciences Research Council (BBSRC, grants BB/S019901/1 and BB/S002103/1). The funders had no role in study design, data collection and analysis, decision to publish, or preparation of the manuscript.

SUPPLEMENTARY MATERIAL

The Supplementary Material for this article can be found online at: https://www.frontiersin.org/articles/10.3389/fmicb.2019.02973/full#supplementary-material

REFERENCES

Akturk, E., Oliveira, H., Santos, S. B., Costa, S., Kuyumcu, S., Melo, L. D. R., et al. (2019). Synergistic action of phage and antibiotics: parameters to enhance the killing efficacy against mono and dual-species biofilms. *Antibiotics* 8:E103. doi: 10.3390/antibiotics8030103

Bai, L., Wang, L., Yang, X., Wang, J., Gan, X., Wang, W., et al. (2017). Prevalence and molecular characteristics of extended-spectrum β-Lactamase Genes in *Escherichia coli* isolated from diarrheic patients in China. *Front. Microbiol.* 8:144. doi: 10.3389/fmicb.2017.00144

Ballesteros-Plaza, D., Holguera, I., Scheffers, D. J., Salas, M., and Munoz-Espin, D. (2013). Phage 29 protein p1 promotes replication by associating with the FtsZ ring of the divisome in *Bacillus* subtilis. *Proc. Natl. Acad. Sci.U.S.A.* 110, 12313–12318. doi: 10.1073/pnas.1311524110

Barrow, P., Lovell, M. jr., and Berchieri, A. (1998). Use of Lytic bacteriophage for control of experimental *Escherichia coli* septicemia and meningitis in chickens and calves. *Clin. Diagn. Lab. Immunol.* 5, 294–298.

Biswas, B., Adhya, S., Washart, P., Paul, B., Trostel, A. N., Powell, B., et al. (2002). Bacteriophage therapy rescues mice bacteremic from a clinical isolate of vancomycin-resistant *Enterococcus faecium*. *Infect. Immun.* 70, 204–210. doi: 10.1128/IAI.70.1.204

Bradford, M. M. (1976). A rapid and sensitive method for the quantitation of microgram quantities of protein utilizing the principle of protein-dye binding. *Anal. Biochem.* 72, 248–254. doi: 10.1016/0003-2697(76)90527-3

Choi, U., and Lee, C. (2019). Distinct roles of outer membrane porins in antibiotic resistance and membrane integrity in *Escherichia coli*. *Front. Microbiol.* 10:953. doi: 10.3389/fmicb.2019.00953

Dessimoz, C., and Škunca, N. (2017). *The Gene Ontology Handbook*. New York, NY: Humana Press.

Drilling, A. J., Ooi, M. L., Miljkovic, D., James, C., Speck, P., Vreugde, S., et al. (2017). Long-term safety of topical bacteriophage application to the frontal sinus region. *Front. Cell Infect. Microbiol.* 7:49. doi: 10.3389/fcimb.2017.00049

Dufour, N., Delattre, R., Ricard, J., and Debarbieux, L. (2017). The lysis of pathogenic *Escherichia coli* by bacteriophages releases less endotoxin than by β-Lactams. *Clin. Infect. Dis.* 64, 1582–1588. doi: 10.1093/cid/cix184

Fisher, J. F., Meroueh, S. O., and Mobashery, S. (2005). Bacterial resistance to β-Lactam antibiotics: compelling opportunism. Compelling Opportunity. *Chem. Rev.* 105, 395–424. doi: 10.1021/cr030102i

Guo, Z., Huang, J., Yan, G., Lei, L., Wang, S., Yu, L., et al. (2017). Identification and characterization of Dpo42, a novel depolymerase derived from the *Escherichia coli* Phage vB_EcoM_ECOO78. *Front. Microbiol.* 8:1460. doi: 10.3389/fmicb.2017.01460

Huang, D. W., Sherman, B. T., Tan, Q., Collins, J. R., Alvord, W. G., Roayaei, J., et al. (2007). The DAVID gene functional classification tool: a novel biological module-centric algorithm to functionally analyze large gene lists. *Genome Biol.* 8:R183. doi: 10.1186/gb-2007-8-9-r183

Jacoby, G. A. (2009). AmpC β-Lactamases. *Clin. Microbiol. Rev.* 22, 161–182. doi: 10.1128/CMR.00036-08

Jiang, Y., Chen, B., Duan, C., Sun, B., Yang, J., and Yang, S. (2015). Multigene editing in the *Escherichia coli* genome via the CRISPR-Cas9 system. *Appl. Environ. Microbiol.* 81, 2506–2514. doi: 10.1128/AEM.04023-14

Kelly, R., Zoubiane, G., Walsh, D., Ward, R., and Goossens, H. (2016). Public funding for research on antibacterial resistance in the JPIAMR countries, the European Commission, and related European Union agencies: a systematic observational analysis. *Lancet Infect. Dis.* 16, 431–440. doi: 10.1016/S1473-3099(15)00350-3

Lv, M., Wang, S., Yan, G., Sun, C., Feng, X., Gu, J., et al. (2015). Genome sequencing and analysis of an *Escherichia coli* phage vB_EcoM-ep3 with a novel lysin. *Lysep3. Virus Genes* 50, 487–497. doi: 10.1007/s11262-015-1195-8

Martinez-Martinez, L., Conejo, M. C., Pascual, A., Hernandez-Alles, S., Ballesta, S., Ramirez, D. A. E., et al. (2000). Activities of imipenem and cephalosporins against clonally related strains of *Escherichia coli* hyperproducing chromosomal beta-lactamase and showing altered porin profiles. *Antimicrob. Agents Chemother.* 44, 2534–2536. doi: 10.1128/aac.44.9.2534-2536.2000

Matsuzaki, S., Uchiyama, J., Takemura-Uchiyama, I., and Daibata, M. (2014). Perspective: the age of the phage. *Nature* 509:S9. doi: 10.1038/509S9a

Murray, A. K., Zhang, L., Yin, X., Zhang, T., Buckling, A., Snape, J., et al. (2018). Novel insights into selection for antibiotic resistance in complex microbial communities. *Mbio* 9, e918–e969. doi: 10.1128/mBio.00969-18

Nelson, E. C., and Elisha, B. G. (1999). Molecular Basis of AmpC Hyperproduction in Clinical Isolates of *Escherichia coli*. *Antimicrob. Agents Ch.* 43, 957–959. doi: 10.1128/AAC.43.4.957

Oechslin, F., Piccardi, P., Mancini, S., Gabard, J., Moreillon, P., Entenza, J. M., et al. (2016). Synergistic interaction between phage therapy and antibiotics clears *Pseudomonas aeruginosa* infection in endocarditis and reduces virulence. *J. Infect. Dis.* 215, 703–712. doi: 10.1093/infdis/jiw632

Parent, K. N., Erb, M. L., Cardone, G., Nguyen, K., Gilcrease, E. B., Porcek, N. B., et al. (2014). OmpA and OmpC are critical host factors for bacteriophage Sf6 entry inShigella. *Mol. Microbiol.* 92, 47–60. doi: 10.1111/mmi.12536

Park, J. Y., Moon, B. Y., Park, J. W., Thornton, J. A., Park, Y. H., and Seo, K. S. (2017). Genetic engineering of a temperate phage-based delivery system for CRISPR/Cas9 antimicrobials against Staphylococcus aureus. *Sci. Rep.* 7:44929. doi: 10.1038/srep44929

Pérez-Gallego, M., Torrens, G., Castillo-Vera, J., Moya, B., Zamorano, L., Cabot, G., et al. (2016). Impact of AmpC derepression on fitness and virulence: the mechanism or the pathway? *Mbio* 7, e1716–e1783. doi: 10.1128/mBio.01783-16

Peter-Getzlaff, S., Polsfuss, S., Poledica, M., Hombach, M., Giger, J., Bottger, E. C., et al. (2011). Detection of AmpC Beta-Lactamase in *Escherichia coli*: comparison of three phenotypic confirmation assays and genetic analysis. *J. Clin. Microbiol.* 49, 2924–2932. doi: 10.1128/JCM.00091-11

Ramesh, V., Fralick, J. A., and Rolfe, R. D. (1999). Prevention of clostridium difficile-induced ileocecitis with Bacteriophage. *Anaerobe* 5, 69–78. doi: 10.1006/anae.1999.0192

Ronayne, E. A., Wan, Y. C. S., Boudreau, B. A., Landick, R., and Cox, M. M. (2016). P1 ref endonuclease: a molecular mechanism for phage-enhanced antibiotic lethality. *Plos Genet.* 12:e1005797. doi: 10.1371/journal.pgen.1005797

Simpson, D., Sacher, J., and Szymanski, C. (2016). Development of an assay for the identification of receptor binding proteins from bacteriophages. *Viruses* 8:17. doi: 10.3390/v8010017

Tacconelli, E., Carmeli, Y., Harbarth, S., Kahlmeter, G., Kluytmans, J., Mendelson, M., et al. (2017). *Global Priority List of Antibiotic-Resistant Bacteria to Guide Research, Discovery, and Development of New Antibiotics*, Chap. Geneva. WHO.

Thiel, K. (2004). Old dogma, new tricks-21st century phage therapy. *Nat. Biotechnol.* 22, 31–36. doi: 10.1038/nbt0104-31

Wang, X., Wei, Z., Li, M., Wang, X., and Shan, A. (2017). Parasites and competitors suppress bacterial pathogen synergistically due to evolutionary trade-offs. *Evolution* 71, 733–746. doi: 10.1111/evo.13143

Wiegand, I., Hilpert, K., and Hancock, R. E. (2008). Agar and broth dilution methods to determine the minimal inhibitory concentration (MIC) of antimicrobial substances. *Nat. Protoc.* 3, 163–175. doi: 10.1038/nprot.2007.521

Willyard, C. (2017). Drug-resistant bacteria ranked. *Nature* 543:15.

Wu, Y., Wu, M., He, G., Zhang, X., Li, W., Gao, Y., et al. (2012). Glyceraldehyde-3-phosphate dehydrogenase: a universal internal control for western blots in prokaryotic and eukaryotic cells. *Anal. Biochem.* 423, 15–22. doi: 10.1016/j.ab.2012.01.012

Conflict of Interest: The authors declare that the research was conducted in the absence of any commercial or financial relationships that could be construed as a potential conflict of interest.

Copyright © 2020 Wang, Yin, Yu, Dang, Guo, Yan, Hu, Gu, Du, Feng, Han, Adam, Sun, Bossé and Lei. This is an open-access article distributed under the terms of the Creative Commons Attribution License (CC BY). The use, distribution or reproduction in other forums is permitted, provided the original author(s) and the copyright owner(s) are credited and that the original publication in this journal is cited, in accordance with accepted academic practice. No use, distribution or reproduction is permitted which does not comply with these terms.

frontiers in Microbiology

ORIGINAL RESEARCH
published: 23 January 2020
doi: 10.3389/fmicb.2019.03147

Morphologically Different *Pectobacterium brasiliense* Bacteriophages PP99 and PP101: Deacetylation of O-Polysaccharide by the Tail Spike Protein of Phage PP99 Accompanies the Infection

*Anna A. Lukianova[1,2], Mikhail M. Shneider[1], Peter V. Evseev[1], Anna M. Shpirt[3], Eugenia N. Bugaeva[4], Anastasia P. Kabanova[1,4], Ekaterina A. Obraztsova[1], Kirill K. Miroshnikov[5], Sofiya N. Senchenkova[3], Alexander S. Shashkov[3], Stepan V. Toschakov[5], Yuriy A. Knirel[3], Alexander N. Ignatov[4] and Konstantin A. Miroshnikov[1]**

[1] Shemyakin-Ovchinnikov Institute of Bioorganic Chemistry, Russian Academy of Sciences, Moscow, Russia, [2] Department of Biology, Lomonosov Moscow State University, Moscow, Russia, [3] Zelinsky Institute of Organic Chemistry, Russian Academy of Sciences, Moscow, Russia, [4] Research Center "PhytoEngineering" Ltd., Rogachevo, Moscow, Russia, [5] Winogradsky Institute of Microbiology, Federal Research Center "Fundamentals of Biotechnology", Russian Academy of Sciences, Moscow, Russia

OPEN ACCESS

Edited by:
Robert Czajkowski,
University of Gdansk, Poland

Reviewed by:
Grazyna Majkowska-Skrobek,
University of Wrocław, Poland
Jens Andre Hammerl,
Federal Institute for Risk Assessment (BfR), Germany
Shuguang Lu,
Third Military Medical University, China

***Correspondence:**
Konstantin A. Miroshnikov
kmi@ibch.ru

Specialty section:
This article was submitted to Virology, a section of the journal Frontiers in Microbiology

Received: 30 September 2019
Accepted: 29 December 2019
Published: 23 January 2020

Citation:
Lukianova AA, Shneider MM, Evseev PV, Shpirt AM, Bugaeva EN, Kabanova AP, Obraztsova EA, Miroshnikov KK, Senchenkova SN, Shashkov AS, Toschakov SV, Knirel YA, Ignatov AN and Miroshnikov KA (2020) Morphologically Different Pectobacterium brasiliense Bacteriophages PP99 and PP101: Deacetylation of O-Polysaccharide by the Tail Spike Protein of Phage PP99 Accompanies the Infection. Front. Microbiol. 10:3147. doi: 10.3389/fmicb.2019.03147

Soft rot caused by numerous species of *Pectobacterium* and *Dickeya* is a serious threat to the world production of potatoes. The application of bacteriophages to combat bacterial infections in medicine, agriculture, and the food industry requires the selection of comprehensively studied lytic phages and the knowledge of their infection mechanism for more rational composition of therapeutic cocktails. We present the study of two bacteriophages, infective for the *Pectobacterium brasiliense* strain F152. *Podoviridae* PP99 is a representative of the genus *Zindervirus*, and *Myoviridae* PP101 belongs to the still unclassified genomic group. The structure of O-polysaccharide of F152 was established by sugar analysis and 1D and 2D NMR spectroscopy:

→ 4)-α-D-Man*p*6Ac-(1→ 2)-α-D-Man*p*-(1→ 3)-β-D-Gal*p*-(1→
3
↑
1
α-l-6dTal*p*Ac$_{0-2}$

The recombinant tail spike protein of phage PP99, gp55, was shown to deacetylate the side chain talose residue of bacterial O-polysaccharide, thus providing the selective attachment of the phage to the cell surface. Both phages demonstrate lytic behavior, thus being prospective for therapeutic purposes.

Keywords: bacteriophage, *Pectobacterium brasiliense*, lipopolysaccharide, O-specific polysaccharide, 6-Deoxy-l-talose, random sugar O-acetylation, tail spike, deacetylase

INTRODUCTION

Pectobacterium brasiliense (Pbr) is a member of the soft rot *Pectobacteriaceae* (SRP) (Adeolu et al., 2016). The representatives of *Pectobacterium* and *Dickeya* genera comprising this family are important pathogens of many crops and ornamental plants worldwide (Ma et al., 2007). Pbr was first identified as a strain group within *Pectobacterium carotovorum,* causing severe black leg disease of potatoes in Brazil (Duarte et al., 2004). This group of strains shared some physiological properties with *P. atrosepticum* (Pat), and was able to grow in a broader range of environmental temperatures. Since then, similar strains were identified as causative agents of black leg and soft rot of potatoes in many countries, including Russia (Malko et al., 2019; Voronina et al., 2019b). Following the taxonomic reassessment of phytopathogenic pectobacteria, Pbr was rated as a subspecies of the *P. carotovorum* (Nabhan et al., 2012), and was recently elevated to the species rank (Portier et al., 2019).

One of the currently applied promising strategies for plant and crop preservations is treating seeds and harvested tubers with bacteriophage preparations. This approach is friendly to the environment and offers a good protection degree against plant bacterial pathogens (Frampton et al., 2012; Svircev et al., 2018). One of the pathogen groups that were studied in this context are pectolytic bacteria *Pectobacterium* and *Dickeya*, where good results of phage application have been reported. Most trials in phage control were applied either to the most widespread or most virulent pathogens–*P. carotovorum* (Lim et al., 2013; Muturi et al., 2019), *P. atrosepticum* (Carstens et al., 2019) and *Dickeya solani* (Adriaenssens et al., 2012; Czajkowski et al., 2017). Most phages suitable for the control of these phytopathogens are members of subfamilies *Autographivirinae*, *Aglimvirinae*, and lytic phages belonging to the less characterized genera. Usually, such phages are stable and infective in a broad pH range and ionic strength, at temperatures up to 50°C, resistant to chloroform, but are rapidly inactivated by UV irradiation (Gupta et al., 1995; Czajkowski et al., 2015, 2017). Up to now, no bacteriophages specifically infectious to Pbr are reported, to our knowledge. Some phages isolated against *Pectobacterium carotovorum* subsp. *carotovorum* have been shown to infect several strains of Pbr (Lim et al., 2015, 2017; Kim et al., 2019). Information on the factors explaining the host range of particular SRP phages is also limited. Present study is focused on an investigation of Pbr–specific bacteriophages isolated in Russia, and the details of their interaction with the bacterial host on molecular level.

MATERIALS AND METHODS

Bacterial Strain

Pectobacterium brasiliense strain F152 (PB29) was isolated in 2014 in a Moscow region from a potato tuber with soft rot symptoms. The strain was analyzed using commercial Biolog GN2 Microplate System (Biolog, Inc.) and API 20E system (bioMérieux). The Biolog GN2 Microplate System and the API 20E system were used in parallel twice, independently. The bacteria were incubated on LB agar (10 g of tryptone, 5 g of yeast extract, and 10 g of NaCl in 1 l, pH 7.2) at 28°C for 24 h prior to analysis. The optical density of the suspension was adjusted as recommended by the manufacturer, and the further procedure was held according to the system instructions. Control for repeatability was held by second round of testing.

Isolation and Purification of Phages PP99 and PP101

Bacteriophage PP99 and PP101 were isolated in May, 2015, from the same sample of sewage water in a warehouse containing potatoes (Moscow region, Russia). Phages were propagated on a Pbr strain F152 (PB29) in LB at 28°C using a published protocol (Clokie and Kropinski, 2009). The lysate was treated with chloroform, centrifuged to clear the cell debris (8,000 g, 20 min), sterilized by filtering through a 0.22 μm pore size membrane filter (Millipore), and treated with DNase I (0.5 mg/mL, 60 min). Phage particles were pelleted in the ultracentrifuge (100,000 g, 60 min, 4°C, Beckman Type 45 rotor) and further purified by CsCl step gradient (0.5–1.7 g/ml density range) ultracentrifugation (22,000 g, 120 min, 4°C, Beckman SW28 rotor). The resulting suspensions of PP99 and PP101 were dialyzed overnight against suspension medium SM (10 mM Tris HCl, pH 7.4, 10 mM $MgSO_4$) to remove CsCl. Purified phages were stored at 4°C in SM buffer as a transparent liquid showing no signs of aggregation.

Electron Microscopy

Purified phage particles were applied to nitrocellulose/carbon film-coated TEM grids and stained with a 1% uranyl acetate aqueous solution (Ackermann, 2009). The specimens were visualized in a Zeiss Libra 120 electron microscope at 100 kV accelerating voltage. The dimensions of phage virions were averaged from the reads of at least 20 particles.

Host Range and General Characterization of Phages PP99 and PP101

The host range of phages was tested by standard plaque formation assay using phage serial dilutions and by direct spotting phage suspensions (10^6 pfu/ml) onto a bacterial lawn. Bacterial strains listed in **Table S1** were cultivated on LB agar at 28°C. In phage adsorption experiments, the host strains were grown to an OD_{600} ∼0.4 and infected with individual phages at a multiplicity of infection of 0.1, or a mixture of PP99 and PP101 at MOI 0.05 each. Every 1 min after infection, 100 μl aliquots of phage-host mixture were taken and transferred into an 800 μl LB medium supplied with 50 μl of chloroform. After bacterial lysis the mixtures were centrifuged and the supernatant was assayed to determine the amount of non-adsorbed or reversibly bound phages. Phage stability was studied by incubating a 10^7 pfu/ml phage suspension at different temperatures or in a range of buffer solutions (20 mM Tris HCl/20 mM Na citrate/20 mM Na phosphate), adjusted with NaOH to pH range 4–9. One-step-growth assays were performed according to Adriaenssens et al. (2012). To assay a lytic activity of phages an exponentially growing culture of host bacteria (10^6 cfu/ml) was mixed with PP99 or PP101 (MOI of 0.1). The mixture was then incubated with shaking at 28°C. Every 10 min, aliquots were taken, chilled, centrifuged, and the appropriate dilutions of the supernatant containing unbound phages were spread on LB agar plates

and incubated overnight at 28°C. The next day, colonies were counted. All experiments were performed independently 3–4 times, and the results were averaged.

Genome Sequencing and Annotation

Bacterial and phage DNA was phenol extracted and fragmented with a Bioruptor Sonicator (Diagenode). Paired-end libraries were constructed using a Nebnext Ultra DNA library prep kit (New England Biolabs) and sequenced on the Illumina MiSeq™ platform (Illumina), using paired 150 bp reads. After filtering with a CLC Genomics Workbench 8.5 (Qiagen), overlapping paired-end library reads were merged with the SeqPrep tool (https://github.com/jstjohn/SeqPrep). Reads from bacteriophages PP99 and PP101 were assembled on a CLC Genomic workbench v. 7.5; reads from a F152 (PB29) bacterial strain were assembled using SPADES 3.6.1 (Bankevich et al., 2012).

The bacterial genome was annotated with the online RAST automated pipeline (http://rast.nmpdr.org/) (Aziz et al., 2008). Phage genomes were annotated by predicting and validating open reading frames (ORFs) using Prodigal 2.6.1 (Hyatt et al., 2010), GeneMarkS 4.3 (Besemer et al., 2001), and Glimmer 3.02 (Delcher et al., 1999). Found ORFs were manually curated to ensure fidelity. Functions were assigned to ORFs using a BLAST search on NCBI databases (http://blast.ncbi.nlm.nih.gov), InterProScan (Mitchell et al., 2015), HHpred (https://toolkit.tuebingen.mpg.de/#/tools/hhpred) (Söding et al., 2005), using databases PDB, SCOP, Pfam, NCBI_CONSERVED. tRNA coding regions were identified with tRNAscan-SE (Schattner et al., 2005) and ARAGORN (Laslett and Canback, 2004). Putative phage promoters were predicted by PHIRE (Lavigne et al., 2004) and phiSITE (Klucar et al., 2009). Resulting genomes were visualized in Geneious Prime, version 2019.2.1 (https://www.geneious.com).

Genome Comparison and Taxonomy

Bacterial and phage reference genomes were downloaded from NCBI Genbank (ftp://ftp.ncbi.nlm.nih.gov/genbank). The phylogenetic tree of *Pectobacterium brasiliense* was generated by means of a UBCG pipeline, using 92 core genes (Na et al., 2018). To conduct bootstrap analysis phylogeny, we have aligned concatenated sequences of 92 core genes made by UBCG with MAFFT (FFT-NS-x1000, 200 PAM/k = 2), and constructed bootstrap trees with an RAxML program (Stamatakis, 2014) (GTR Gamma I DNA substitution model). The robustness of the trees was assessed by fast bootstrapping (1000).

Genes of phage DNA polymerase, a major capsid protein, RNA polymerase and a terminase large subunit were extracted from downloaded Genbank annotated genomes. Gene products in genomes annotated as "hypothetical protein CDS" were considered as known genes if their pairwise identity with known homologous was more than 50%. Phylograms were generated based on the amino acid sequences of proteins and their concatenated alignments, using Geneious Prime and applying Clustal Omega for sequence alignment with auto settings. Trees were constructed using the maximum likelihood (ML) method with an RAxML program (Stamatakis, 2014) with a GAMMA I BLOSUM62 protein model and the robustness of the trees was assessed by fast bootstrapping (1000). Average nucleotide identity (ANI) was computed using Jspecies (Richter and Rossello-Mora, 2009) (blast algorithm ANIb, 500 bp fragment length for phages and 1020 bp for bacteria). Distance matrix was computed using an Enveomics server (http://enve-omics.ce.gatech.edu) (Konstantinidis and Tiedje, 2005). Digital DNA-DNA hybridization (dDDH) was estimated using a GGDC calculator (https://ggdc.dsmz.de/ggdc.php) (Meier-Kolthoff et al., 2013).

Tail Spike Protein Cloning, Expression, and Purification

ORF55 of phage PP99 (42,368–44,020 bp range) was PCR-amplified using primers 5′-TATTTCCAGGGCAGCGGAT CCGGTTATAGTACAAAGCCAAAAAGA (forward) and 5′-GCTCGAGTGCGGCCGCAAGCTTACAGGTTTGCTGTT ACAGAATA (reverse) with generated BamHI and HindIII cloning sites, respectively. The amplified ORF was cloned to vector pTSL (Taylor et al., 2016), using a NEBuilder HiFi DNA Assembly kit (New England Biolabs). Clones carrying the insert were screened by PCR using the same primers, endonuclease hydrolysis, and verified by Sanger sequencing. Protein synthesis was performed in *E. coli* B834(DE3) inducing the expression with 1 mM IPTG at 16°C overnight. Cells were centrifuged at 4,000 g, resuspended in a 20 mM Tris-HCl (pH 8.0), 200 mM NaCl buffer, lysed by ultrasonic treatment (Virsonic, VirTis) and the debris and unbroken cells were removed by centrifugation at 13,000 g. The protein product (PP99 gp55) was purified on a Ni-NTA Sepharose column (GE Healthcare, 5 mL) by 0–200 mM imidazole step gradient in 20 mM TrisHCl (pH 8.0), 200 mM NaCl. The resulting eluate containing the purified protein was dialyzed against 20 mM TrisHCl (pH 8.0) to remove imidazole, and 6× His-tag was removed by TEV protease (12 h at 20°C incubation). The target protein was finally purified on a 5 mL SourceQ 15 (GE Healthcare) using a linear gradient of 0–600 mM NaCl in 20 mM TrisHCl (pH 8.0). Protein concentration was determined spectrophotometrically at 280 nm, using a calculated molar extinction coefficient of 56,435 M^{-1} cm^{-1}. The PP99 gp55 oligomeric state was assessed by gel-filtration on a calibrated Superdex 200 10 × 300 column (GE Healthcare).

Isolation and O-Deacetylation of the O-Polysaccharides

Bacterial lipopolysaccharide (LPS) was isolated in a yield of 8.4% from bacterial cells by the phenol-water method (Westphal and Jann, 1965) and purified by precipitation of nucleic acids and proteins with aq 50% CCl_3CO_2H as described (Zych et al., 2001). Then the LPS sample (84 mg) was degraded with aq 2% HOAc for 1.5 h at 100°C. Lipids were removed by centrifugation (13,000 g, 20 min), and the supernatant was applied to the gel-filtration column 70 × 3.0 cm, Sephadex G-50 Superfine (GE Healthcare), using 0.05 M pyridinium acetate pH 4.5 as eluent and monitoring with a differential refractometer (Knauer). A high-molecular mass polysaccharide was obtained in a yield of ∼25% of the lipopolysaccharide weight.

Total O-Deacetylation was performed by treatment of an O-polysaccharide sample (21 mg), with 12% aq ammonia (0.6 mL) at 37°C for 16 h. After ammonia evaporation the remaining solution was lyophilized, and an O-deacetylated polysaccharide (DPS) sample was obtained in a yield of 46% of the O-polysaccharide weight.

The effect of the phage PP99 tail spike protein was studied by an addition of a 300 μg aliquote of PP99 gp55 to the O-polysaccharide sample (20 mg), and incubation for 2 h at room temperature. The product was isolated by gel-permeation chromatography, as described above.

Sugar Analysis

Hydrolysis of the O-polysaccharide was performed with 2 M CF_3CO_2H (120°C, 2 h), and the monosaccharides were analyzed by GLC as the alditol acetates (Sawabdekeb et al., 1965) on a Maestro (Agilent 7820) chromatograph (Interlab) equipped with an HP-5ms column (0.32 mm × 30 m), using a temperature program of 160°C (1 min) to 290°C at 7°C min^{-1}.

NMR Spectroscopy

Samples were deuterium-exchanged by freeze-drying from 99.9% D_2O. NMR spectra were recorded for solutions in 99.95% D_2O at 30°C on a Bruker Avance II 600 MHz spectrometer with a 5-mm broadband inverse probe head. Sodium 3-(trimethylsilyl) propanoate-2,2,3,3-d_4 (δ_H 0, δ_C −1.6) was used as an internal reference for calibration. Two-dimensional NMR spectra were obtained using standard Bruker software, and a Bruker TopSpin 2.1 program was used to acquire and process the NMR data. A spin-lock time of 60 ms and a mixing time of 200 ms were used in two-dimensional TOCSY and ROESY experiments, respectively. A two-dimensional ^1H, ^{13}C HMBC experiment was performed with a 60-ms delay for evolution of long-range couplings in order to optimize the spectrum for coupling constant $J_{H,C}$ 8 Hz.

RESULTS

Properties and Genomics of Strain F152 (PB29)

Pectobacterium brasiliense strain F152 (PB29) was isolated in 2014, and initially was attributed as *P. c.* subsp. *carotovorum*. Further complete genome sequencing identified this strain as a Pbr. Variability in physiology, plant host range, virulence, and genomics of strains representing *P. carotovorum* have promoted the first rough distribution of this genus to separate the subspecies *carotovorum*, *brasiliense* and *odoriferum* (Nabhan et al., 2012). Later, a number of further separations of *P. carotovorum* subsp. *carotovorum* were offered, forming new species, *polaris* (Dees et al., 2017), *maceratum/versatile* (Shirshikov et al., 2018; Portier et al., 2019), *peruviense* (Waleron et al., 2018), and *aquaticum* (Pédron et al., 2019), based on genomic analysis of available MLST markers, draft and complete genomes in databases. Recently, a substantial redistribution of pectobacterial taxonomy was processed, elevating a number of *P. carotovorum* subspecies to the species level, including Pbr (Portier et al., 2019). Strain F152 follows the general biochemical and physiological properties typical for Pbr species (Nabhan et al., 2012; Portier et al., 2019). Bacterial cells of strain F152 are gram-negative, facultative anaerobes, negative for oxidase, urease, indol production, and gelatin liquefaction. They were negative for acid production from D-arabitol, dulicitol, and sorbitol, and were unable to utilize malonate and citrate. Cells are catalase positive, produce acid from lactose, rhamnose, and trehalose, resistant to 6% NaCl and grow at both 28 and 37°C. Strain F152 induces a hypersensitive reaction in tobacco leaves and causes severe black leg symptoms on green plants and soft rot symptoms on potato tuber disks compared to the characterized strains of *P. polaris, P. aquaticum*, *P. versatile*, and *P. atrosepticum* in a temperature range from 20 to 28°C. The same properties were observed for other Pbr strains previously isolated in Russia, F126 and F157 (Voronina et al., 2019b). However, the genome sequences of Pbr strains deposited to the NCBI GenBank demonstrate pronounced diversity, forming several branches of the phylogenomic clade (Zhang et al., 2016; Li et al., 2018). Phylogenetic analysis using concatenated sequences of 92 core genes resulted in a similar tree (**Figure 1**), where the genomes of F126 (RRYQ00000000), F152 (PJDM00000000), and F157 (PJDL00000000) are located in a branch diverged from the Pbr type strain LMG 21371 (=PBR1692). Measurements of ANI and dDDH also demonstrate a genetic difference between two clades of Pbr (**Figure 1**, **Figure S1**). Therefore, the properties of strain F152, including phage susceptibility, cannot be directly extrapolated to all strains representing Pbr.

Phage PP99 and PP101—Biology, Host Range, Morphology

Bacteriophages PP99 and PP101 were isolated using Pbr strain F152 previously found in the same location as a host. Both phages form small (1–3 mm in diameter) plaques, normally indistinguishable from each other. Host ranges of PP99 and PP101 are nearly identical to each other. Both phages infect all strains of Pbr isolated in Central European Russia in 2000–2015, as well as nine of 26 *Pectobacterium* strains available in our collection (**Table S1**). Besides Pbr, all *Pectobacterium* strains susceptible to PP99 and PP101 belong to the newly formed species *P. versatile* (Pve) (Portier et al., 2019). The only strain that is infected by PP101 but is resistant to PP99 is F100, attributed as Pve by 16S RNA gene sequencing and genomic fingerprinting. Other tested strains belonging to *P. atrosepticum*, *P. polaris*, *P. parmentieri*, *P. carotovorum*, *P. aquaticum*, some strains of *P. versatile*, and all strains of genus *Dickeya,* were resistant to phages PP99 and PP101.

The morphology of bacteriophages PP99 and PP101 was assessed using transmission electron microscopy. Phage PP101 belongs to the family *Myoviridae* in the order *Caudovirales*, morphotype A1 (**Figure 2B**). The tail length is ∼132 ± 5 nm, and the head diameter is ∼62 ± 3 nm. PP99 shows typical *Podoviridae* morphology (morphotype C1) with an icosahedric capsid of ∼54 ± 3 nm in diameter and a short (∼10 nm) tail (**Figure 2A**). According to the proposed unified phage naming (Kropinski

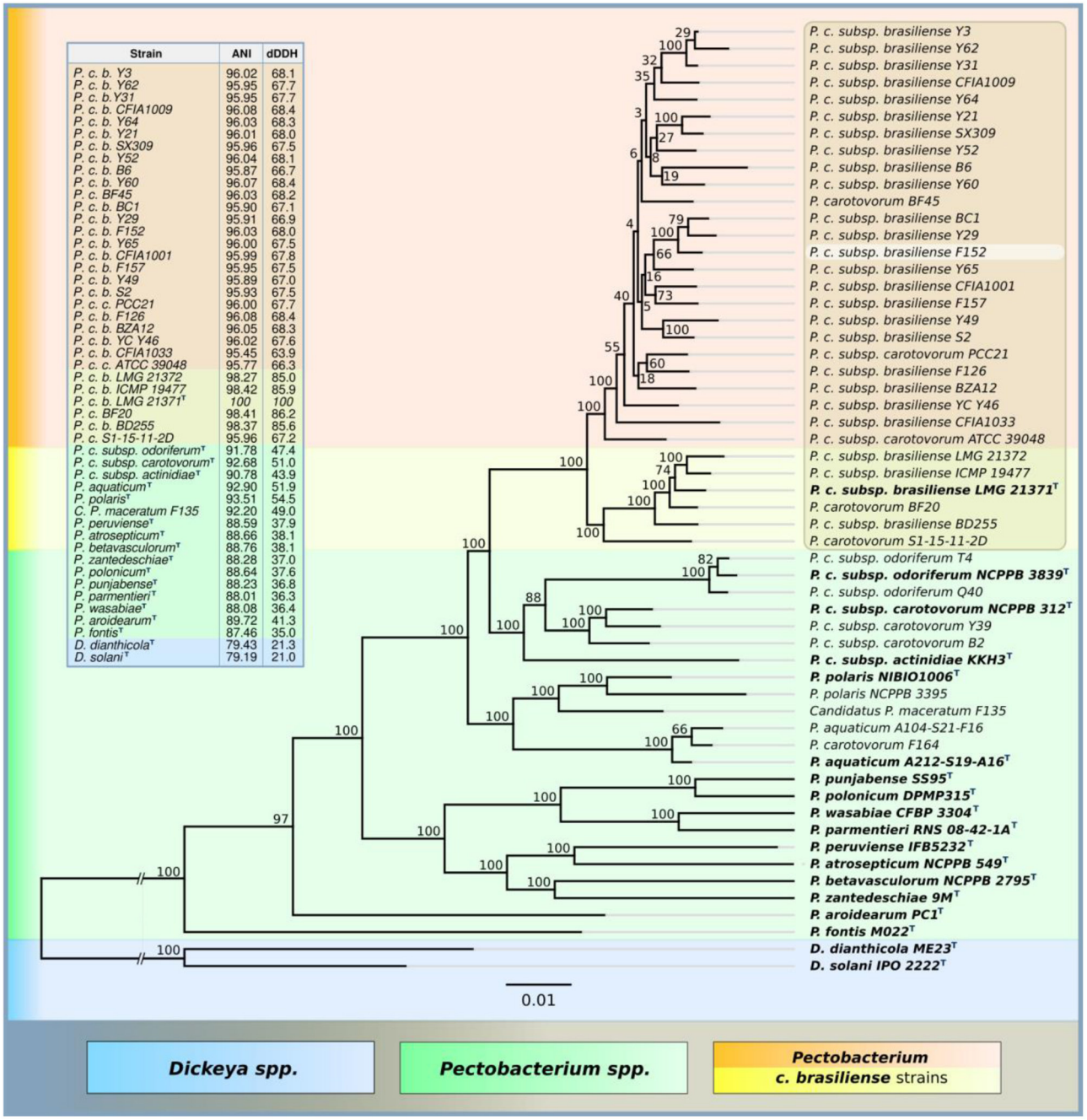

FIGURE 1 | Phylogenetic tree of nucleotide sequences of UBCG proteins of *Pectobacterium* spp. NCBI genomes (RAxML,GAMMA I BLOSSUM62 protein model, with 1,000 bootstrap replicates), ANI and dDDH are compared to *P. brasiliense* LMG 21371 type strain.

et al., 2009), the phages should be referred to as vB_PbrP_PP99 and vB_PbrM_PP101, respectively.

Both phages demonstrate biological properties close to each other and other studied pectobacterial phages, retaining infectional activity at temperatures below 50°C, and in the pH range 3–8. With respect to their isolation host, Pbr strain F152, phages PP99 and PP101 demonstrate similar infection kinetics adsorbing to bacteria in 4–6 min, with a latent period of 30–35 min and a burst size of 100–150 progeny phages/cell at 28°C (**Figure 3**). The combined action of PP99 and PP101 did not change the overall shape of the single-step growth curve (**Figure 3**) in short-term observations. Within a 2 h interval, the concentration of unadsorbed or progeny phages never changed substantially compared to a single-action mode of PP99 or PP101. This indicates an absence of synergistic or antagonistic character of two phages (Schmerer et al., 2014). It may mean that phages

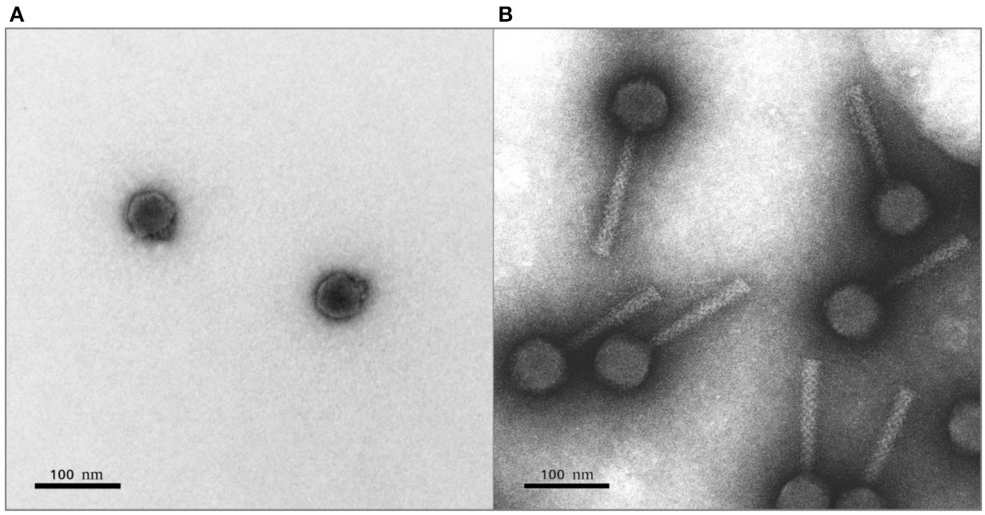

FIGURE 2 | Transmission electron micrograph of bacteriophages PP99 **(A)** and PP101 **(B)**. Staining with 1% uranyl acetate. The scale bar is 100 nm.

PP99 and PP101 independently use the same receptor molecule on the bacterial surface for adsorption, and none of them shows dominant affinity to this receptor; additionally, both phages can overcome the protective systems of Pbr F152 equally effectively.

Bacteriophage PP99 Genome Features

The genome of bacteriophage PP99 (read in 1006× coverage) consists of 46,609 bp with a GC content of 45.54%. The only bacteriophage with noticeable homology in the genome sequence is the *Escherichia* phage ECBP5 (KJ749827), genetically assessed as a mosaic composition between various *Autographivirinae* phages (Lee et al., 2015; **Figure 4A**). Phylogenetic trees generated using concatenated alignments of amino acid sequences of DNA polymerase, a major capsid protein and a terminase large subunit show the relationship between PP99 and *Salmonella* phage SP6 (NCBI accession number AY370673) (Dobbins et al., 2004), *Pectobacterium* phage PP1 (NC_019542) (Lee et al., 2012), *Vibrio* phage φA318 (KF322026) (Liu et al., 2014), and a number of other Podoviruses infecting a broad range of bacteria (**Figures S2**, **S3**). Thus, PP99 can be assigned as a member of the genus *SP6virus.* This genus is currently named *Zindervirus,* after Norman D. Zinder (1928–2012), who discovered the phage-driven gene transfer. A total of 56 unidirectional ORFs and no tRNA genes were predicted. The functions of 26 ORFs can be predicted as members of transcription/translation, DNA replication/modification and nucleotide metabolism, phage morphogenesis, and host lysis modules. We were able to predict 10 phage-specific promotors (**Figure 4A**). Twenty-five ORFs were characterized as hypothetical proteins (**Table S2**). Only three small ORFs can be considered as unique to the PP99 genome. No genes responsible for lysogeny and toxin production were identified. The overall genome layout of PP99 follows the general features of SP6-like phages, including the presence of a pronounced set of early genes preceding the gene-encoding phage RNA polymerase, several apparently non-coding regions, and a holin/muramidase lysis module. Many SP6-like phages, including PP99, share a unified two-component structure of a tail spike (Gebhart et al., 2017; Tu et al., 2017). The gene encoding an adaptor protein providing an attachment of the spike to the tail is separated from the gene encoding the spike in the genome. The C-terminal part of the tail spike protein encoded by PP99 (ORF 55), optimized for an attachment to the surface of the Pbr host, differs from those of other SP6-like phages. The highest (though moderate) sequence similarity is observed with the tail spike protein of phage PP1 infecting a similar pectobacterial host. Sequence analysis of PP99 ORF55 using HHPred predicts a structure resembling (*E*-value 3.3 e^{-19}) the tail spike of *Escherichia* phage G7C (*Podovididae*, *Gamaleyavirus*) with the proposed polysaccharide-modifying enzyme activity (Prokhorov et al., 2017). However, according to the genome analysis, tail spikes of PP99 are not branched as in G7C, so we suggest that PP99 gp55 interacts with the single receptor of Pbr.

Bacteriophage PP101 Genome Features

Phage PP101 (vB_PbrM-PP101) contains a dsDNA genome (read in 1,458× coverage) of 53,333 bp, with a GC content of 44.94%. We were unable to verify the exact location and size of terminal repeats in the PP101 genome experimentally. However, according to the annotations of similar phages, we consider it as terminally redundant linear with the headful DNA-packing mechanism (Born et al., 2011). Comparative analysis of complete genomes shows noticeable identity (above 80%) of PP101 with *Pectobacterium carotovorum* phage PM1 (NCBI accession number NC_023865) (Lim et al., 2014), *Escherichia* phages ST32 (MF044458) (Liu et al., 2018), phiEcoM-GJ1 (NC_010106) (Jamalludeen et al., 2008), *Erwinia* phages vB_EamM-Y2 (NC_019504) (Born et al., 2011), and Faunus (MH191398) (**Table S3**). This group of phages forms a separate phylogenetic clade not yet assigned as a taxonomic genus (**Figure 4B**, **Figures S2**, **S3**). Compared to these phages, the genome of phage PP101 has the same unidirectional transcription orientation, and a similar number of identified ORFs organized in functional

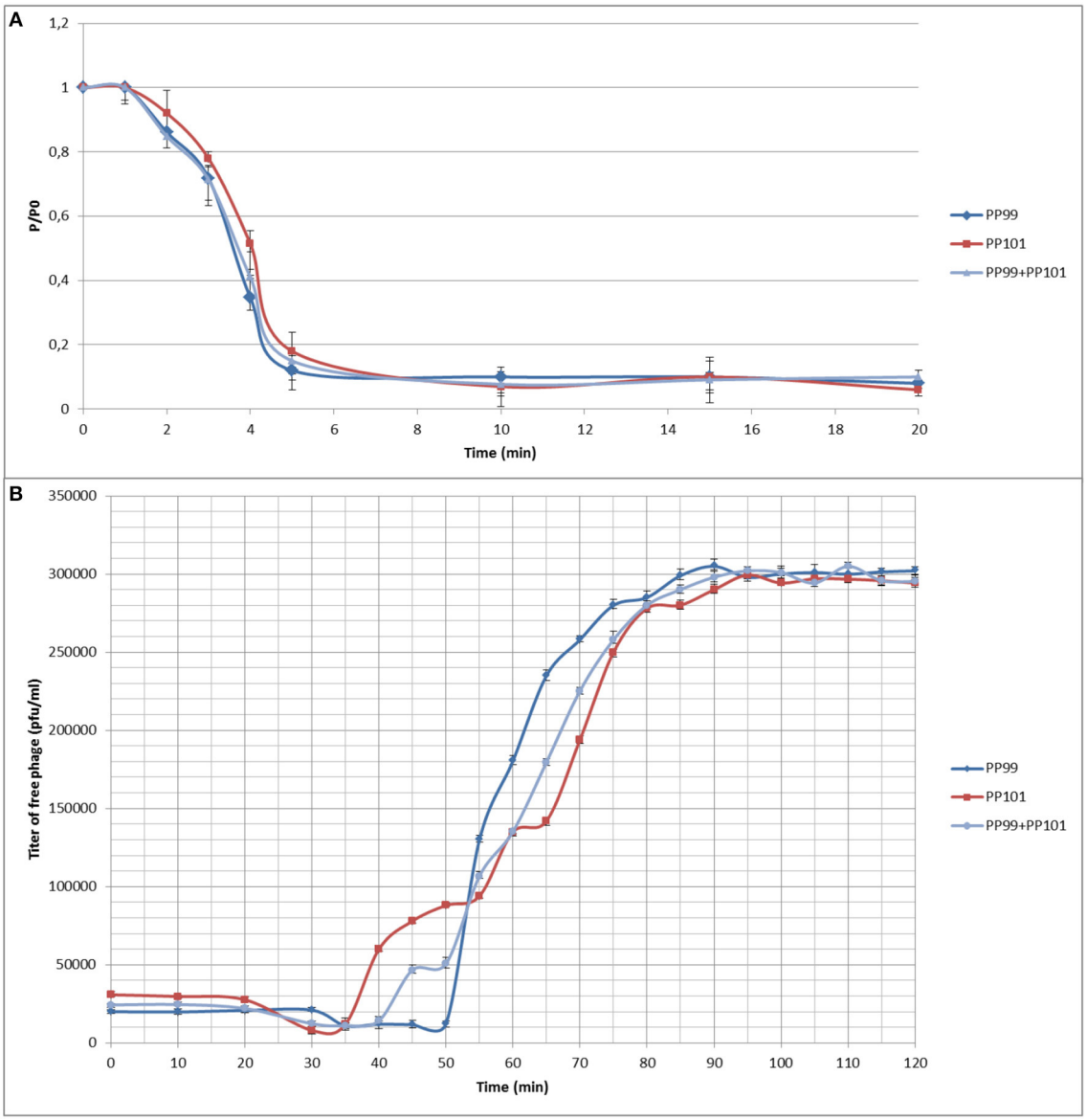

FIGURE 3 | (A) Adsorption of phages on the surface of host strain F152: PP99 (blue) and PP101 (red) in MOI = 0.1 separately, and a mixture of PP99 and PP101 (gray) in MOI = 0.05 each. P/Po—ratio of titers of unadsorbed phages to the phage amount initially added; **(B)** One-step growth curves of phages PP99 (blue) and PP101 (red) in MOI = 0.1 separately, and a mixture of PP99 and PP101 (gray) in MOI = 0.05 each.

clusters (**Figure 4B**). The functions of 36 ORFs could be predicted. Only six ORFs (07, 18, 20, 26, 35, 36), encoding small hypothetical proteins, are unique for PP101. The comprehensive genomic comparison of this group of lytic phages (with the emphasis to *Escherichia* phages) has been presented previously (Liu et al., 2018). We would like to outline a few features of this group of *Enterobacterial* phages, including PP101, that are essential for the realization of the inflectional cycle. First, all phages of this group possess the early gene encoding a single-subunit RNA polymerase, similar to T7-like *Autographivirinae* Podoviruses, and a similar arrangement of transcription-related ORFs. Therefore, we were able to hypothesize the existence of eight consensus promotor sequences throughout the genome that regulates the transcription of gene cascades and key structural genes. The sequence and the proposed positions of phage RNA-polymerase-specific promotors are shown in **Figure 4B**, and this arrangement provides effective multiplication of the phage in a broad range of conditions and host strains. Second, all the phages of this group contain the two-gene lysis module "holin-SAR endolysin" (ORF 80 and 81 in case of PP101) (**Table S3**). The third feature is the complex composition of the adsorption apparatus. Three proteins are predicted to form tail fibers of PP101, and these proteins have orthologs in other phages of the group (**Table 1**). We suggest the presence of the multicomponent

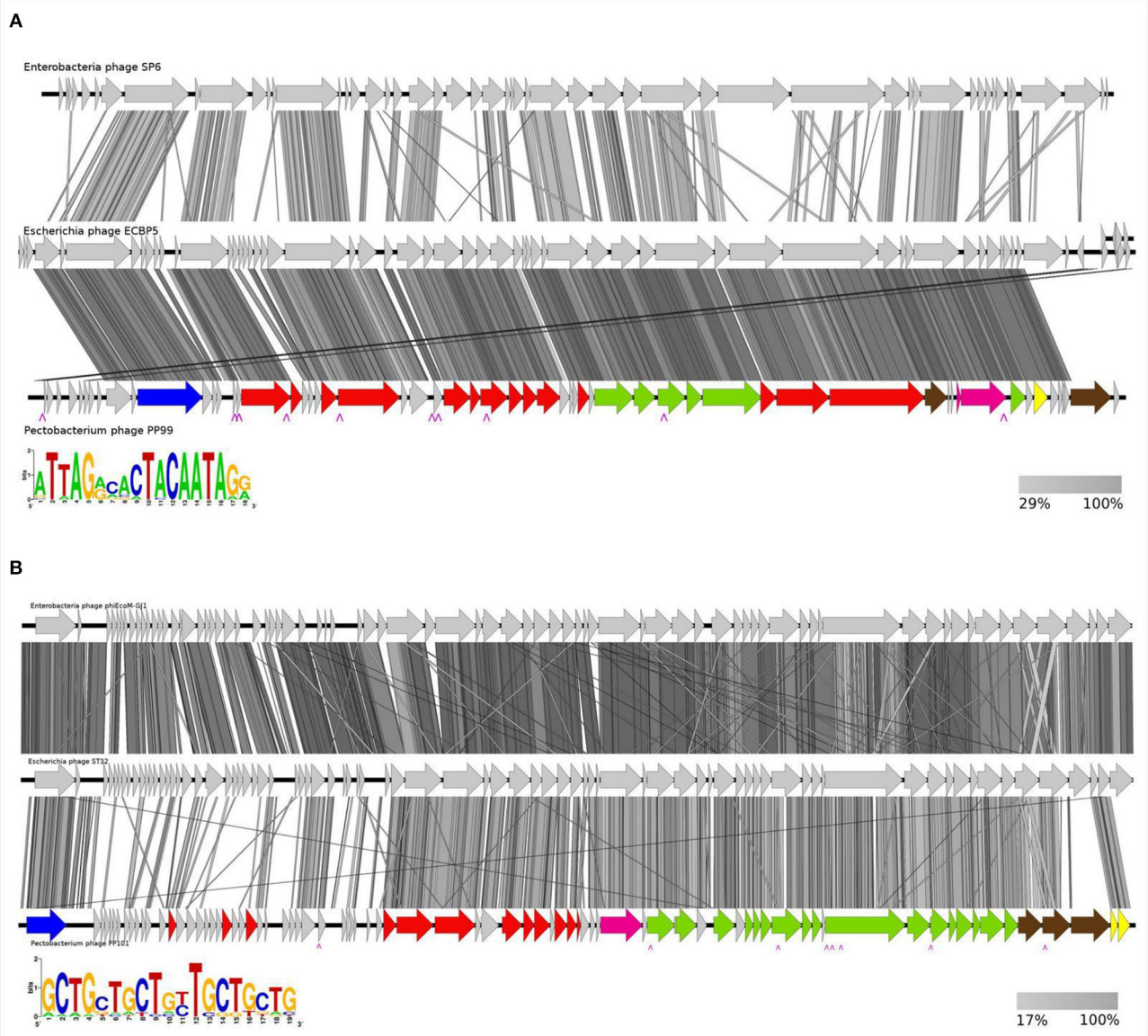

FIGURE 4 | Genome map of bacteriophages. **(A)** PP99, and comparison with phages ECBP5 and SP6; **(B)** PP101, and comparison with PM1 and ST32. Arrows indicate predicted open reading frames presumably responsible for replication and metabolism (red), assembly and packaging (green). ORFs of discussed functions are marked blue (RNA polymerase), magenda (terminase), brown (tail spikes and fibers), and yellow (host lysis). Hypothetical proteins are indicated by tan arrows. The positions of predicted phage promotors are marked. The amino acid sequence similarities between the phages are indicated by gray shading (right insert). The left insert indicates the consensus sequence of the phage promoter.

tail fibers resembling those of phage T4 (Hyman and van Raaij, 2018) in PP101. PP101 ORF 77 and ORF78 have a high degree of identity with corresponding ORFs of PM1/ST32/phiEcoM-GJ1/vB_EamM-Y2/Faunus, presumably forming the proximal part of the fiber and the knee-knob. A high-resolution EM image of the *Erwinia* phage vB_EamM-Y2 (Born et al., 2011) reveals bicomponent fibers with a globular junction. This observation supports our hypothesis about the structure of PP101 tail fibers involving distal and proximal fibrous parts, and the globular intermediate. HHPred analysis of PP101gp78 shows a number of structural homologs with a β-structural domain responsible for carbohydrate-binding activity (5HON, *E*-value 9.1e-10; 4XJW, 3.9e-9). Being a part of the fiber, this protein may provide irreversible binding to the carbohydrates of the cell surface. The third putative tail fiber component, ORF79, has no homology with any protein of the above phages, except for PM1 infecting *P. carotovorum*. However, genes encoding putative prophage proteins with distantly close (30–40% identity) sequences can be found in the genomes of *Pectobacterium* spp. Therefore, we could propose that the receptor recognized by a similar protein is

TABLE 1 | Genomic features of *Myoviridae* phages similar to PP101.

Phage	NCBI #	Host	ANI, %	Genome size, bp	# ORFs	Tail fiber 1	Tail fiber 2	Tail fiber 3
PP101	KY087898	*Pectobacterium*	100	53,333	81	77	78	79
PM1	NC023865	*Pectobacterium*	93.96	55,098	63	59	60	61
phiEcoM-GJ1	NC010106	*Escherichia*	69.21	52,975	75	70	71	72
ST32	MF044458	*Escherichia*	68.89	53,072	79	74	75	76
Faunus	MH191398	*Erwinia*	68.49	54,065	78	72	73	74
EamM-Y2	HQ728264	*Erwinia*	66.95	56,621	92	82	84	85

conservative in *Pectobacteria,* and it was used for host attachment by various phages in an evolutionally long period.

Composition of F152 O-Polysaccharide

Sugar analysis of F152 O-polysaccharide (OPS) revealed 6-deoxytalose (6dTalp), mannose, and galactose in the ratios 1–2.2: 1.3 (GLC detector response), respectively. The ^{1}H NMR and ^{13}C NMR (**Figure 5**, middle) spectra showed significant structural heterogeneity of the OPS due to non-stoichiometric O-acetylation (there were multiple signals for O-acetyl groups at δ_H 2.10–2.23 and δ_C 21.5–21.8). The OPS was O-deacetylated with aqueous ammonia to give a regular polymer (DPS). Its ^{13}C NMR spectrum (**Figure 5**, top) contained, inter alia, signals for four anomeric carbons at δ 95.9–103.7, one CH_3-C group at δ 16.6 (C-6 of 6dTalp), and three $HOCH_2$-C groups at δ 61.6–62.9 (C-6 of Man and Gal). Accordingly, the ^{1}H NMR spectrum of the DPS displayed signals for four anomeric protons at δ 4.44–5.27 and one CH_3-C group at δ 1.26 (3H, d, $J_{5,6}$ 6.3, H-6 of 6dTal). These data demonstrated that DPS has a tetrasaccharide repeating unit, containing two residues of D-Man and one residue each of D-Gal and L-6dTal.

The D configuration of Man and Gal and the L configuration 6dTalp were established by known regularities in glycosylation effects on ^{13}C NMR chemical shifts (Shashkov et al., 1988), combined with calculation of the specific optical rotation of the DPS by Klyne's rule ($\alpha_{calc} = 18.9°$, $\alpha_{exp} = 15.6°$).

Linkage and Sequence Analyses

The ^{1}H NMR and ^{13}C NMR spectra of the DPS were assigned (**Table S4**) using one-dimensional ^{1}H,^{1}H TOCSY, two-dimensional ^{1}H,^{1}H COSY, TOCSY, ROESY, ^{1}H,^{13}C HSQC, HMBC, HSQC-NOESY, and HSQC-TOCSY experiments. The configurations of the glycosidic linkages were established by ^{13}C NMR chemical shifts of C-5, compared with published data of the corresponding α- and β-pyranosides (Lipkind et al., 1988; Knirel et al., 1992). The β configuration of the Gal residue (unit **A**) was confirmed by a relatively large coupling constant $J_{1,2}$ 7.3 Hz and H-1/H-3 and H-1/H-5 correlations in the ^{1}H,^{1}H ROESY spectrum of the DPS. The α configuration of the Man and 6dTal residues (units **B**–**D**) was confirmed by H-1/H-2 correlations in the ^{1}H,^{1}H ROESY spectrum, with no H-1/H-3 and H-1/H-5 correlations.

The two-dimensional ^{1}H,^{1}H ROESY spectrum showed inter-residue correlations between the following anomeric protons and protons at the linkage carbons: Gal **A** H-1/Man **B** H-4,

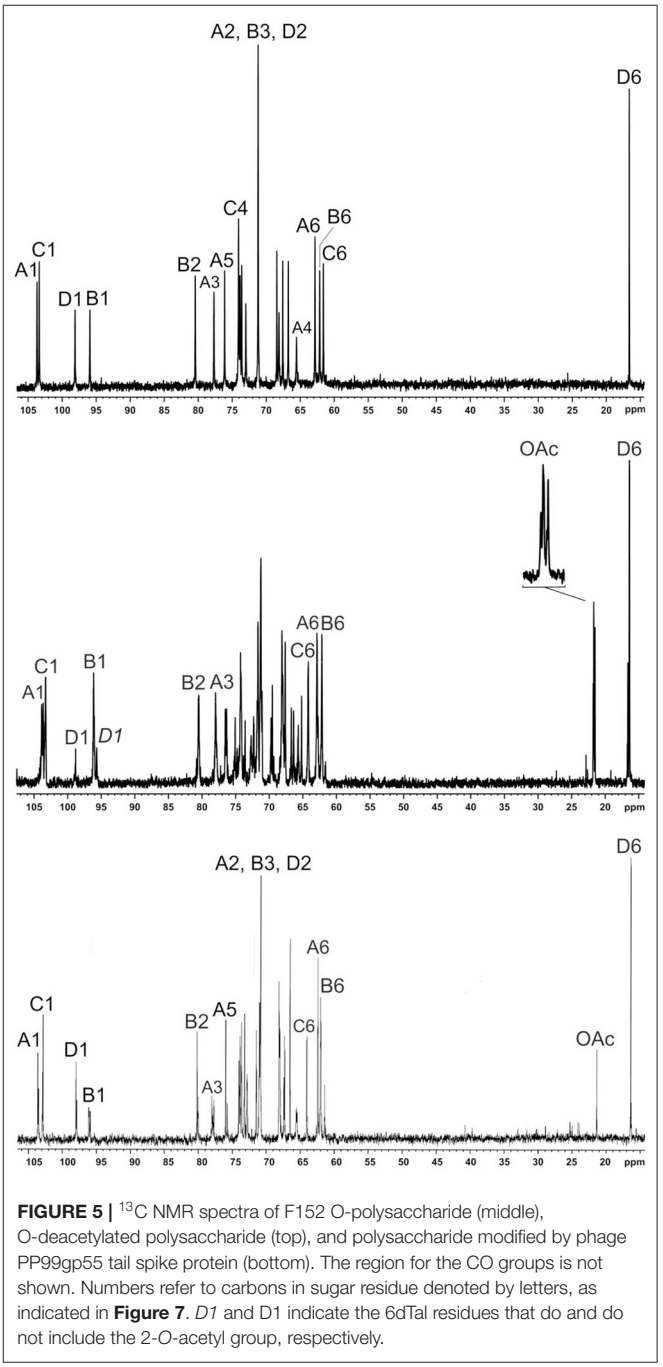

FIGURE 5 | ^{13}C NMR spectra of F152 O-polysaccharide (middle), O-deacetylated polysaccharide (top), and polysaccharide modified by phage PP99gp55 tail spike protein (bottom). The region for the CO groups is not shown. Numbers refer to carbons in sugar residue denoted by letters, as indicated in **Figure 7**. *D1* and D1 indicate the 6dTal residues that do and do not include the 2-*O*-acetyl group, respectively.

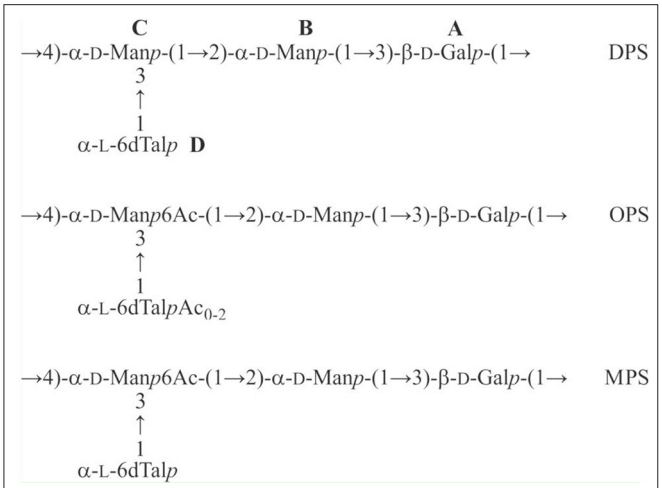

FIGURE 6 | Structures of the O-polysaccharide (OPS), O-deacetylated polysaccharide (DPS), and modified polysaccharide (MPS) of *Pectobacterium brasiliense* strain F152.

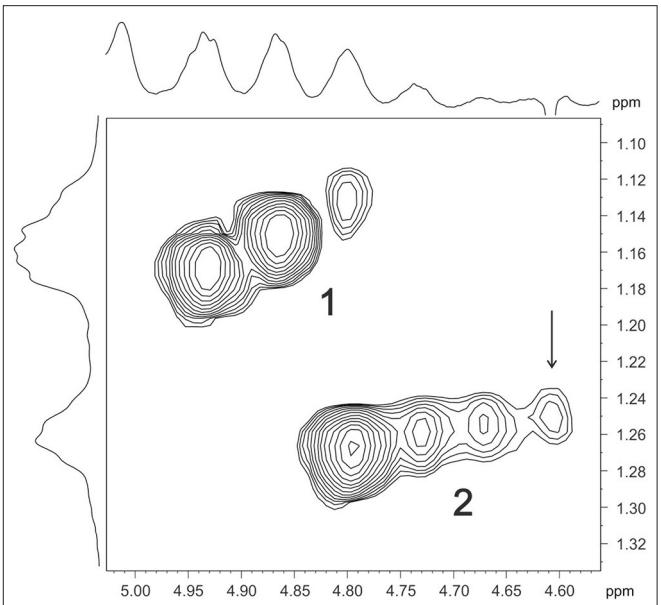

FIGURE 7 | Part of a 600-MHz two-dimensional COSY spectrum of F152 O-polysaccharide, displaying 6dTal H-5/H-6 correlations. Two series of cross-peaks (1 and 2) were assigned to the O-acetylated forms of 6dTal that do and do not include the 4-*O*-acetyl group, respectively. Arrow points to the H-5/H-6 cross-peak of a non-acetylated 6dTal residue.

Man **C** H-1/Man **B** H-2, Man **B** H-1/Gal **A** H-3, and 6dTal **D** H-1/Man **C** H-3 at δ 4.44/3.94, 5.08/4.04, 5.27/3.75, and 5.07/4.02, respectively. These findings were supported by the ^{1}H,^{13}C HMBC and HSQC-NOESY experiments.

The glycosylation pattern of the monosaccharides was confirmed by low-field positions of the linkage carbons C-3 of unit **A**, C-2 of unit **B**, and C-3 and C-4 of unit **C** at δ 77.7, 80.4, 73.1, and 74.1 in the ^{13}C NMR spectrum of the DPS, as compared with their positions at δ 74.1, 72.0, 71.5, and 68.2 in the corresponding non-substituted monosaccharides (Lipkind et al., 1988). The ^{1}H and ^{13}C NMR chemical shifts of 6dTalp were essentially identical to those for the O-polysaccharide of *Aeromonas hydrophila* O:34, in which this monosaccharide terminated a side chain (Knirel et al., 2002).

Based on the data obtained, we conclude that the DPS has the structure shown in **Figure 6**, middle.

O-Acetylation Pattern of the O-Polysaccharide

A comparison of the 1D and 2D NMR spectra of the initial OPS and DPS showed that the signals for units **A** and **B** have almost the same ^{1}H and ^{13}C NMR chemical shifts in both samples, and hence, they are not O-acetylated in the OPS. In the ^{1}H, ^{13}C HSQC spectrum of the OPS, a major part of the H-6/C-6 cross-peak of D-Man **C** shifted downfield to δ_H/δ_C 4.35, 4.53/64.2 from its position at δ_H/δ_C 3.81, 3.96/61.6 in the spectrum of DPS. Accordingly, the signal for C-5 of D-Man **C** shifted upfield from δ 73.1 in the DPS to δ 71.9 in the OPS (a β-effect of O-acetylation). As judged by the ratio of integral intensities of the signals for the O-acetylated and non-acetylated forms of Man **C**, the degree of O-acetylation of this sugar residue at position 6 is ∼75%.

The 6dTal residue showed multiple signals in the NMR spectra of the OPS, due to the presence of various O-acetylated forms. Particularly, in the 2D ^{1}H, ^{1}H COSY spectrum, there were seven H-5/H-6 cross-peaks for 6dTalp, which formed two series, 1 and 2 (**Figure 7**). Such an O-acetylation pattern is similar to that reported for the O-polysaccharide of *Aeromonas hydrophila* O:34 (Knirel et al., 2002). Series 1 of four cross-peaks contained the H-5/H-6 cross-peak for the non-acetylated form at δ 4.61/1.25 (in **Figure 5**, this cross-peak is indicated by an arrow; compare with the 6dTalp H-5/H-6 cross-peak at δ 4.62/1.26 in the COSY spectrum of the DPS). As the H-5 and H-6 chemical shift are influenced mostly by an acetyl group at O-4, the three other peaks of Series 1 were assigned to the O-acetylated forms that do not include the 4-O-acetyl group, namely to the 2-O-acetylated, 3-O-acetylated, and 2,3-di-O-acetylated forms (Knirel et al., 2002). Correspondingly, the three cross-peaks of series 2 were assigned to the 4-O-acetylated, 2,4-di-O-acetylated and 3,4-di-O-acetylated forms of 6dTal. Therefore, the O-polysaccharide of Pbr F152 has the structure shown in **Figure 6**, top.

Properties of Recombinant PP99 Tail Spike Protein Gp55, and Modification of the O-Polysaccharide

Highly copious moieties such as cell surface polysaccharides, including the O-antigens of lipopolysaccharides (LPS), are good candidates for receptor interaction with phages (Steinbacher et al., 1996). Tail spikes contain processive enzymatic domains (Leiman and Molineux, 2008) that depolymerize (Barbirz et al., 2008) or deacetylate (Prokhorov et al., 2017) OPS to allow a phage to attach to the cell surface. Recombinant tail spike proteins of phages were shown to feature mostly uniform trimeric β-helical architecture (Fokine and Rossmann, 2014). The enzymatically

active domains located either on the surface of the resulting trimeric prism, or within the secondary structure elements such as loops protruding from the prism (Leiman and Molineux, 2008). Recombinant PP99 gp55 tail spike protein forms trimeric complexes spontaneously (**Figure S4**), and is easily purified to homogeneous state. The protein tends to aggregate at high concentrations, so the structural research is hindered. In a dilute solution (<2 mg/mL), PP99 gp55 is stable for a few weeks at 4°C. Treatment of the O-polysaccharide with a PP99 tail spike protein resulted in a modified polysaccharide (MPS), which was studied by NMR spectroscopy, as described above for the initial polysaccharide (for the 13C NMR spectrum of the MPS, see **Figure 5**, bottom). The H-6/C-6 and H-5/C-5 cross-peaks of the 6-O-acetylated D-Man **C** residue in the $^{1}H,^{13}C$ HSQC spectrum of the MPS were found at the same positions as in the OPS. In contrast, signals of the variously O-acetylated L-6dTal **D** residues were absent from the MPS, and the cross-peaks of α-L-6dTal were at the same positions as in the DPS. Therefore, the MPS has the structure shown in **Figure 6**, bottom.

DISCUSSION

Soft rot and black leg caused by *Pectobacterium* and *Dickeya* spp. are responsible for considerable damage to the potatoes, both during the vegetation season and post-harvest storage (Pérombelon, 2002). No effective control methods currently exist to combat these diseases. Considering the limitations in using pesticides and antibacterial compounds, especially post-harvest, there exists a noticeable demand for new safe and environmentally friendly alternative approaches to pathogen control. The use of bacteriophages to combat plant pathogenic bacteria is one of such promising methods. Phages naturally occur in the environment and are easily biodegradable, which make them suitable for organic agriculture (Frampton et al., 2012; Buttimer et al., 2017; Svircev et al., 2018). Successful applications of phages to protect potatoes from SRP are reported in simulated conditions (Czajkowski et al., 2017; Carstens et al., 2019) and field trials (Adriaenssens et al., 2012; Voronina et al., 2019a). However, these experiments employed a limited number of phages and/or model strains of pathogen initially known to be susceptible to the phage used. An implication of phage control to real horticulture needs to consider many additional factors, including the diversity of pathogens (Svircev et al., 2018).

In this paper we investigate two different phages, isolated using *Pectobacterium brasiliense* as a major host. Pbr has been shown to play an important role in potato soft rot pathogenesis in many countries worldwide in recent years. However, phages specifically infecting this bacterium are understudied, as are the details of their interaction with the host. Both studied phages, PP99 (vB_PbrP_PP99) and PP101 (vB_PbrM_PP101), are lytic phages suitable for phage control. These phages demonstrate different morphology, and can be phylogenetically assigned. PP99 belongs to the genus *Zindervirus* of the *Autographivirinae* subfamily, and PP101 is a member of a clade of unclassified *Myoviridae* phages infecting *Enterobacteria* (Jamalludeen et al., 2008; Lim et al., 2014; Liu et al., 2018) that can be potentially assigned as a new genus of bacteriophages (**Table 1**, **Figure 8**). It is worth noting that despite the morphologic difference of PP99 and PP101, their genomes share some features common for "T7-like phages": unidirectional assignment of ORFs, clear distribution of ORFs to separate gene cascades, early position of the gene encoding the single-subunit RNA polymerase, and a similar arrangement of promotors presumably specific to this polymerase. Some of such features were noticed earlier for phages similar to PP101 (Jamalludeen et al., 2008; Liu et al., 2018). Some evolutionary relationship between phages PP99 and PP101 may be traced based on the phylogeny of DNA polymerase, the terminase large subunit, and, to a lesser extent, major capsid protein genes (**Figure 8**, **Figures S2, S3**).

Phages PP99 and PP101 demonstrate similar infection parameters with respect to their type host, Pbr strain F152 (PB29). Host range of tailed phages is largely defined by interaction of their baseplate structures (tail fibers and tail spikes) with molecules on the bacterial surface (Fokine and Rossmann, 2014), as earlier papers suggest. Many bacteriophages use tail spike/fiber proteins for primary contact with bacterial surface polysaccharides. A recognition mechanism involving lipopolysaccharides (LPS) and capsule polysaccharides was suggested as common for SPR phages (Evans et al., 2010) and was experimentally shown for *Dickeya* phage PP35 (Kabanova et al., 2019) and *Pectobacterium carotovorum* subsp. *carotovorum* phage POP72 (Kim et al., 2019). Therefore, our further investigation was directed to reveal the molecular details of phage-host interaction. We have determined the structure of O-polysaccharide of F152, which has no direct analogs in the bacterial world, especially in its acetylation pattern, with ∼75% repeating units of D-mannose residues in the main chain O-acetylated at position 6, and ∼90% side-chain 6-deoxy-L-talose residues is randomly mono- or di-O-acetylated at any position (**Figure 6**). This unique composition of F152 O-polysaccharide requires very specific arrangement of amino acid residues on the surface of the proteins of phage recognition apparatus to provide selective contact with the bacterial host. The adsorption system of phage PP101 involves three putative tail fiber proteins (ORF 77–79). This composition is conserved in all phages similar to PP101 (**Table 1**), and the product of ORF79 is believed to be responsible for the contact with the receptor. However, we were unable to obtain functionally active PP101gp79, therefore this hypothesis still requires experimental proof.

Unlike tail fibers, the structural architecture of phage tail spike proteins performing the contact with the receptor and often bearing the enzyme domain degrading or modifying bacterial polysaccharide is relatively unified (Leiman et al., 2007; Leiman and Molineux, 2008). The genome of phage PP99 contains the gene encoding such tail spike proteins. The recombinant product of this gene, PP99gp55, forms a trimeric biologically active protein that deacetylates the carbohydrate chain of Pbr OPS. The removal of the acetyl group occurs at the side chain of 6-deoxytalose residue, but the acetylated mannose residue of the main chain remains unchanged. We could suggest that the removal of the acetyl provides the spatial flexibility

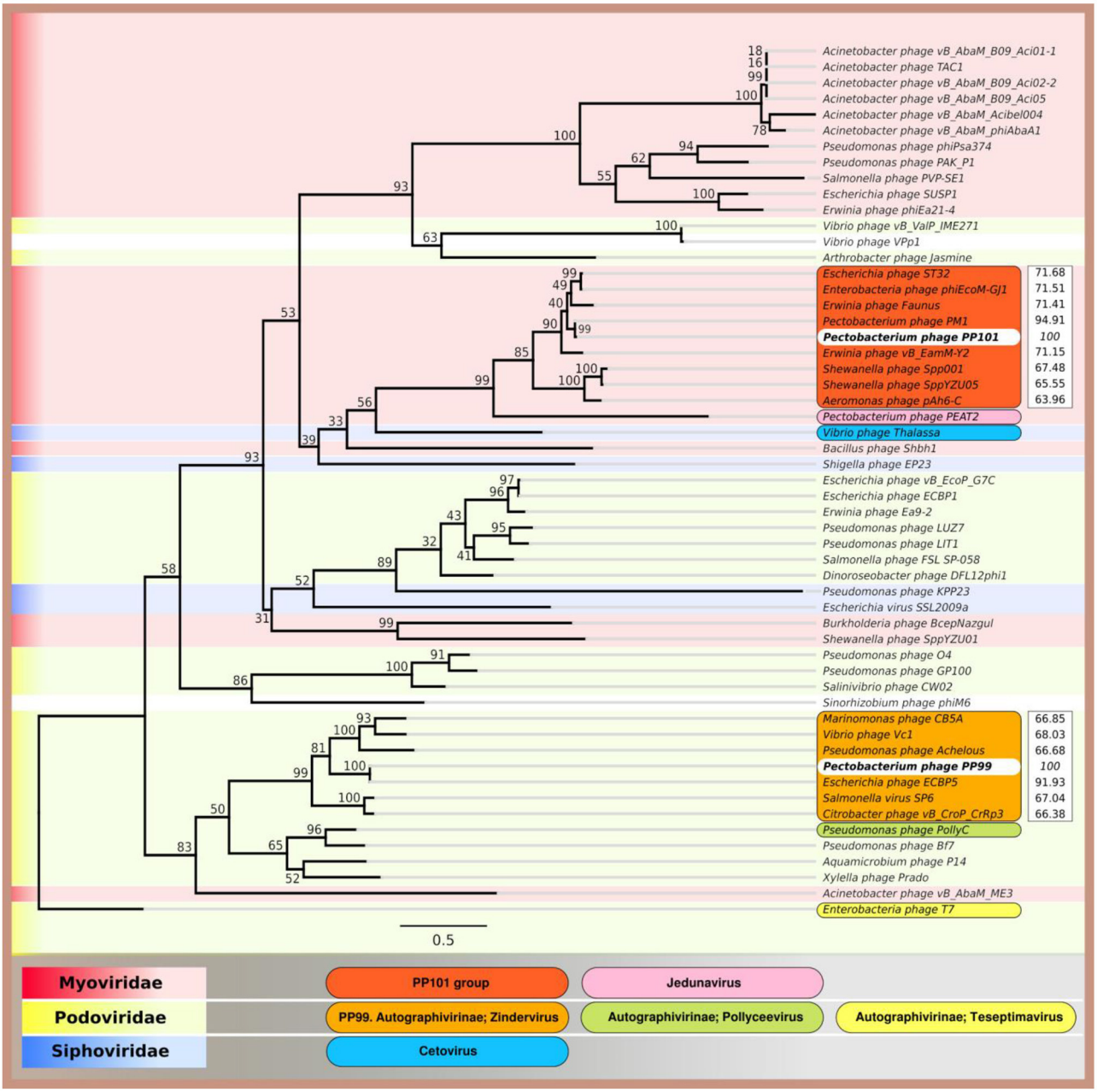

FIGURE 8 | Phylogenetic tree of amino acid sequences of the major capsid proteins of *Pectobacterium brasiliense* phage PP99, *Pectobacterium brasiliense* phage PP101, and 53 phages using RAxML (GAMMA I BLOSSUM62 protein model with 1,000 bootstrap replicates), and ANI compared to PP99 and PP101 calculated with Jspecies.

of sugar chains sufficient for the penetration of the tail spike protein to the cell surface. Similar dependence of phage specificity upon the modification pattern of bacterial OPS was previously observed for *Escherichia* phages (Bertozzi Silva et al., 2016; Letarov and Kulikov, 2017).

The knowledge of phage adsorption mechanism and cell receptors used in the course of phage infection is beneficial for the construction of phage cocktails to combat bacterial infections in medicine, agriculture, and the food industry. The use of phages employing different cell receptors of the same bacterial host usually expands an efficacy of antibacterial action, and reduces the possibility of the evolution of phage-resistant mutants. In the studied case, *Pectobacterium brasiliense* phages PP99 and PP101 provide no advantage for combined use, but either of them can be potentially included in phage preparations to control the soft rot of potatoes.

DATA AVAILABILITY STATEMENT

The complete genome sequences of phages PP99 and PP101 have been deposited in the NCBI database under the GenBank accession numbers KY250034 and KY087898, correspondingly. Draft genome assembly of strain F152 (PB29) and related information can be found in the NCBI database under the GenBank Accession number PJDM00000000.1.

AUTHOR CONTRIBUTIONS

MS, AI, and KAM designed the experiment. AL, MS, AMS, EB, AK, EO, SS, and ASS planned and performed experiments. AL, PE, KKM, ST, AI, YK, and KAM performed data analysis. AL, AI, and KAM wrote the manuscript.

FUNDING

This research was supported by a Russian Science foundation grant #16-16-00073.

SUPPLEMENTARY MATERIAL

The Supplementary Material for this article can be found online at: https://www.frontiersin.org/articles/10.3389/fmicb.2019.03147/full#supplementary-material

REFERENCES

Ackermann, H. W. (2009). Basic phage electron microscopy. *Methods Mol. Biol.* 501, 113–126. doi: 10.1007/978-1-60327-164-6_12

Adeolu, M., Alnajar, S., Naushad, S., and Gupta, R. S. (2016). Genome-based phylogeny and taxonomy of the 'Enterobacteriales': proposal for *Enterobacterales* ord. nov. divided into the families *Enterobacteriaceae*, *Erwiniaceae* fam. nov., *Pectobacteriaceae* fam. nov., *Yersiniaceae* fam. nov., *Hafniaceae* fam. nov., *Morganellaceae* fam. nov., and *Budviciaceae* fam. nov. *Int. J. Syst. Evol. Microbiol.* 66, 5575–5599. doi: 10.1099/ijsem.0.001485

Adriaenssens, E. M., van Vaerenbergh, J., Vandenheuvel, D., Dunon, V., Ceyssens, P. J., de Proft, M., et al. (2012). T4-related bacteriophage LIMEstone isolates for the control of soft rot on potato caused by "Dickeya solani." *PLoS ONE* 7:e33227. doi: 10.1371/journal.pone.0033227

Aziz, R. K., Bartels, D., Best, A. A., DeJongh, M., Disz, T., Edwards, R. A., et al. (2008). The RAST Server: rapid annotations using subsystems technology. *BMC Genomics* 9:75. doi: 10.1186/1471-2164-9-75

Bankevich, A., Nurk, S., Antipov, D., Gurevich, A. A., Dvorkin, M., Kulikov, A. S., et al. (2012). SPAdes: a new genome assembly algorithm and its applications to single-cell sequencing. *J. Comput. Biol.* 19, 455–477. doi: 10.1089/cmb.2012.0021

Barbirz, S., Müller, J. J., Uetrecht, C., Clark, A. J., Heinemann, U., and Seckler, R., (2008). Crystal structure of *Escherichia coli* phage HK620 tailspike: podoviral tailspike endoglycosidase modules are evolutionarily related. *Mol. Microbiol.* 69, 303–316. doi: 10.1111/j.1365-2958.2008.06311.x

Bertozzi Silva, J., Storms, Z., and Sauvageau, D. (2016). Host receptors for bacteriophage adsorption. *FEMS Microbiol. Lett.* 363:fmw002. doi: 10.1093/femsle/fnw002

Besemer, J., Lomsadze, A., and Borodovsky, M. (2001). GeneMarkS: a self-training method for prediction of gene starts in microbial genomes. Implications for finding sequence motifs in regulatory regions. *Nucleic Acids Res.* 29, 2607–2618. doi: 10.1093/nar/29.12.2607

Born, Y., Fieseler, L., Marazzi, J., Lurz, R., Duffy, B., and Loessner, M. J. (2011). Novel virulent and broad-host-range Erwinia amylovora bacteriophages reveal a high degree of mosaicism and a relationship to *Enterobacteriaceae* phages. *Appl. Environ. Microbiol.* 77, 5945–5954. doi: 10.1128/AEM.03022-10

Buttimer, C., McAuliffe, O., Ross, R. P., Hill, C., O'Mahony, J., and Coffey, A. (2017). Bacteriophages and bacterial plant diseases. *Front. Microbiol.* 8:34. doi: 10.3389/fmicb.2017.00034

Carstens, A. B., Djurhuus, A. M., Kot, W., and Hansen, L. H. (2019). A novel six-phage cocktail reduces *Pectobacterium* atrosepticum soft rot infection in potato tubers under simulated storage conditions. *FEMS Microbiol. Lett.* 366:fnz101. doi: 10.1093/femsle/fnz101

Clokie, M. R. J., and Kropinski, A. M. (2009). *Bacteriophages: Methods and Protocols Volume 1: Isolation, Characterization, and Interactions*, Vol. 502. New York, NY: Humana Press.

Czajkowski, R., Ozymko, Z., de Jager, V., Siwinska, J., Smolarska, A., Ossowicki, A., et al. (2015). Genomic, proteomic and morphological characterization of two novel broad host lytic bacteriophages *Φ*PD10.3 and *Φ*PD23.1 infecting pectinolytic *Pectobacterium* spp. and *Dickeya* spp. *PLoS ONE* 10:e0119812. doi: 10.1371/journal.pone.0119812

Czajkowski, R., Smolarska, A., and Ozymko, Z. (2017). The viability of lytic bacteriophage ΦD5 in potato-associated environments and its effect on *Dickeya* solani in potato (*Solanum tuberosum* L.) plants. *PLoS ONE* 12:e0183200. doi: 10.1371/journal.pone.0183200

Dees, M. W., Lysøe, E., Rossmann, S., Perminow, J., and Brurberg, M. B. (2017). *Pectobacterium polaris* sp. nov., isolated from potato (*Solanum tuberosum*). *Int. J. Syst. Evol. Microbiol.* 67, 5222–5229. doi: 10.1099/ijsem.0.002448

Delcher, A. L., Harmon, D., Kasif, S., White, O., and Salzberg, S. L. (1999). Improved microbial gene identification with GLIMMER. *Nucleic Acids Res.* 27, 4636–4641. doi: 10.1093/nar/27.23.4636

Dobbins, A. T., George, M., Basham, D. A., Ford, M. E., Houtz, J. M., Pedulla, M. L., et al. (2004). Complete genomic sequence of the virulent salmonella bacteriophage SP6. *J. Bacteriol.* 186, 1933–1944. doi: 10.1128/jb.186.7.1933-1944.2004

Duarte, V., De Boer, S. H., Ward, L. J., and De Oliveira, A. M. R. (2004). Characterization of atypical Erwinia carotovora strains causing blackleg of potato in Brazil. *J. Appl. Microbiol.* 96, 535–545. doi: 10.1111/j.1365-2672.2004.02173.x

Evans, T. J., Ind, A., Komitopoulou, E., and Salmond, G. P. C. (2010). Phage-selected lipopolysaccharide mutants of *Pectobacterium* atrosepticum exhibit different impacts on virulence. *J. Appl. Microbiol.* 109, 505–514. doi: 10.1111/j.1365-2672.2010.04669.x

Fokine, A., and Rossmann, M. G. (2014). Molecular architecture of tailed double-stranded DNA phages. *Bacteriophage* 4:e28281. doi: 10.4161/bact.28281

Frampton, R. A., Pitman, A. R., and Fineran, P. C. (2012). Advances in bacteriophage-mediated control of plant pathogens. *Int. J. Microbiol.* 2012, 326452. doi: 10.1155/2012/326452

Gebhart, D., Williams, S. R., and Scholl, D. (2017). Bacteriophage SP6 encodes a second tailspike protein that recognizes Salmonella enterica serogroups C_2 and C_3. *Virology*. 507, 233–236. doi: 10.1016/j.virol.2017.02.025

Gupta, K., Lee, Y., and Yin, J. (1995). Extremo-phage: *in vitro* selection of tolerance to a hostile environment. *J. Mol. Evol.* 41, 113–114. doi: 10.1007/BF00170661

Hyatt, D., Chen, G. L., Locascio, P. F., Land, M. L., Larimer, F. W., and Hauser, L. J. (2010). Prodigal: prokaryotic gene recognition and translation initiation site identification. *BMC Bioinformatics* 11:119. doi: 10.1186/1471-2105-11-119

Hyman, P., and van Raaij, M. (2018). Bacteriophage T4 long tail fiber domains. *Biophys. Rev.* 10, 463–471. doi: 10.1007/s12551-017-0348-5

Jamalludeen, N., Kropinski, A. M., Johnson, R. P., Lingohr, E., Harel, J., and Gyles, C. L. (2008). Complete genomic sequence of bacteriophage phiEcoM-GJ1, a novel phage that has myovirus morphology and a podovirus-like RNA polymerase. *Appl. Environ. Microbiol.* 74, 516–525. doi: 10.1128/AEM.00990-07

Kabanova, A. P., Shneider, M. M., Korzhenkov, A. A., Bugaeva, E. N., Miroshnikov, K. K., Zdorovenko, E. L., et al. (2019). Host specificity of the *Dickeya* bacteriophage PP35 is directed by a tail spike interaction with bacterial O-antigen, enabling the infection of alternative non-pathogenic bacterial host. *Front. Microbiol.* 9:3288. doi: 10.3389/fmicb.2018.03288

Kim, H., Kim, M., Bai, J., Lim, J. A., Heu, S., and Ryu, S. (2019). Colanic acid is a novel phage receptor of *Pectobacterium carotovorum* subsp. carotovorum Phage POP72. *Front. Microbiol.* 10:143. doi: 10.3389/fmicb.2019.00143

Klucar, L., Stano, M., and Hajduk, M. (2009). PhiSITE: database of gene regulation in bacteriophages. *Nucleic Acids Res.* 38, D366–D370. doi: 10.1093/nar/gkp911

Knirel, Y. A., Paramonov, N. A., Shashkov, A. S., Kochetkov, N. K., Yarullin, R. G., Farber, S. M., et al. (1992). Structure of the polysaccharide chains of Pseudomonas pseudomallei lipopolysaccharides. *Carbohydr. Res.* 233, 185–193. doi: 10.1016/S0008-6215(00)90930-3

Knirel, Y. A., Shashkov, A. S., Senchenkova, S. N., Merino, S., and Tomás, J. M. (2002). Structure of the O-polysaccharide of Aeromonas hydrophila O:34; a case of random O-acetylation of 6-deoxy-L-talose. *Carbohydr. Res.* 337, 1381–1386. doi: 10.1016/s0008-6215(02)00136-2

Konstantinidis, K. T., and Tiedje, J. M. (2005). Genomic insights that advance the species definition for prokaryotes. *Proc. Natl. Acad. Sci. U.S.A.* 102, 2567–2572. doi: 10.1073/pnas.0409727102

Kropinski, A. M., Prangishvili, D., and Lavigne, R. (2009). Position paper: the creation of a rational scheme for the nomenclature of viruses of *Bacteria* and *Archaea*. *Environ. Microbiol.* 11, 2775–2777. doi: 10.1111/j.1462-2920.2009.01970.x

Laslett, D., and Canback, B. (2004). ARAGORN, a program to detect tRNA genes and tmRNA genes in nucleotide sequences. *Nucleic Acids Res.* 32, 11–16. doi: 10.1093/nar/gkh152

Lavigne, R., Sun, W. D., and Volckaert, G. (2004). PHIRE, a deterministic approach to reveal regulatory elements in bacteriophage genomes. *Bioinformatics* 20, 629–635. doi: 10.1093/bioinformatics/btg456

Lee, J. H., Shin, H., Ji, S., Malhotra, S., Kumar, M., Ryu, S., et al. (2012). Complete genome sequence of phytopathogenic *Pectobacterium carotovorum* subsp. carotovorum bacteriophage PP1. *J. Virol.* 86, 8899–8900. doi: 10.1128/JVI.01283-12

Lee, J. S., Jang, H. B., Kim, K. S., Kim, T. H., Im, S. P., Kim, S. W., et al. (2015). Complete genomic and lysis-cassette characterization of the novel phage, KBNP1315, which infects Avian Pathogenic *Escherichia coli* (APEC). *PLoS ONE* 10:e0142504. doi: 10.1371/journal.pone.0142504

Leiman, P. G., Battisti, A. J., Bowman, V. D., Stummeyer, K., Mühlenhoff, M., Gerardy-Schahn, R., et al. (2007). The structures of bacteriophages K1E and K1-5 explain processive degradation of polysaccharide capsules and evolution of new host specificities. *J. Mol. Biol.* 371, 836–849. doi: 10.1016/j.jmb.2007.05.083

Leiman, P. G., and Molineux, I. J. (2008). Evolution of a new enzyme activity from the same motif fold. *Mol. Microbiol.* 69, 287–290. doi: 10.1111/j.1365-2958.2008.06241.x

Letarov, A. V., and Kulikov, E. E. (2017). Adsorption of bacteriophages on bacterial cells. *Biochemistry* 82, 1632–1658. doi: 10.1134/S0006297917130053

Li, X., Ma, Y., Liang, S., Tian, Y., Yin, S., Xie, S., et al. (2018). Comparative genomics of 84 *Pectobacterium* genomes reveals the variations related to a pathogenic lifestyle. *BMC Genomics* 19:889. doi: 10.1186/s12864-018-5269-6

Lim, J.-A., Heu, S., Park, J., and Roh, E. (2017). Genomic characterization of bacteriophage vB_PcaP_PP2 infecting *Pectobacterium carotovorum* subsp. carotovorum, a new member of a proposed genus in the subfamily Autographivirinae. *Arch. Virol.* 162, 2441–2444. doi: 10.1007/s00705-017-3349-6

Lim, J.-A., Lee, D. H., and Heu, S. (2015). Isolation and genomic characterization of the T4-like bacteriophage PM2 infecting *Pectobacterium carotovorum* subsp. carotovorum. *Plant Pathol. J.* 31, 83–89. doi: 10.5423/PPJ.NT.09.2014.0099

Lim, J.-A., Shin, H., Lee, D. H., Han, S.-W., Lee, J.-H., Ryu, S., et al. (2014). Complete genome sequence of the *Pectobacterium carotovorum* subsp. carotovorum virulent bacteriophage PM1. *Arch. Virol.* 159, 2185–2187. doi: 10.1007/s00705-014-2005-7

Lim, J. A., Jee, S., Lee, D. H., Roh, E., Jung, K., Oh, C., et al. (2013). Biocontrol of *Pectobacterium carotovorum* subsp. carotovorum using bacteriophage PP1. *J. Microbiol. Biotechnol.* 23, 1147–1153. doi: 10.4014/jmb.1304.04001

Lipkind, G. M., Shashkov, A. S., Knirel, Y. A., Vinogradov, E. V., and Kochetkov, N. K. (1988). A computer-assisted structural analysis of regular polysaccharides on the basis of 13C-n.m.r. data. *Carbohydr. Res.* 175, 59–75. doi: 10.1016/0008-6215(88)80156-3

Liu, H., Geagea, H., Rousseau, G., Labrie, S., Tremblay, D., Liu, X., et al. (2018). Characterization of the *Escherichia coli* virulent myophage ST32. *Viruses* 10:E616. doi: 10.3390/v10110616

Liu, W., Lin, Y. R., Lu, M. W., Sung, P. J., Wang, W. H., and Lin, C. S. (2014). Genome sequences characterizing five mutations in RNA polymerase and major capsid of phages ϕA318 and ϕAs51 of Vibrio alginolyticus with different burst efficiencies. *BMC Genomics* 15:505. doi: 10.1186/1471-2164-15-505

Ma, B., Hibbing, M. E., Kim, H.-S., Reedy, R. M., Yedidia, I., Breuer, J. J., et al. (2007). Host range and molecular phylogenies of the soft rot enterobacterial genera *Pectobacterium* and *Dickeya*. *Phytopathology* 97, 1150–1163. doi: 10.1094/PHYTO-97-9-1150

Malko, A., Frantsuzov, P., Nikitin, M., Statsyuk, N., Dzhavakhiya, V., Golikov, A., et al. (2019). Potato pathogens in Russia's regions: an instrumental survey with the use of real-time PCR/RT-PCR in matrix format. *Pathogens* 8:E18. doi: 10.3390/pathogens8010018

Meier-Kolthoff, J. P., Auch, A. F., Klenk, H.-P. P., and Göker, M. (2013). Genome sequence-based species delimitation with confidence intervals and improved distance functions. *BMC Bioinformatics* 14:60. doi: 10.1186/1471-2105-14-60

Mitchell, A., Chang, H. Y., Daugherty, L., Fraser, M., Hunter, S., Lopez, R., et al. (2015). The InterPro protein families database: the classification resource after 15 years. *Nucleic Acids Res.* 43, D213–221. doi: 10.1093/nar/gku1243

Muturi, P., Yu, J., Maina, A. N., Kariuki, S., Mwaura, F. B., and Wei, H. (2019). Bacteriophages isolated in China for the control of *Pectobacterium carotovorum* causing potato soft rot in Kenya. *Virol. Sin.* 34, 287–294. doi: 10.1007/s12250-019-00091-7

Na, S. I., Kim, Y. O., Yoon, S. H., Ha, S-m, Baek, I., and Chun, J. (2018). UBCG: Up-to-date bacterial core gene set and pipeline for phylogenomic tree reconstruction. *J. Microbiol.* 56, 280–285. doi: 10.1007/s12275-018-8014-6

Nabhan, S., De Boer, S. H., Maiss, E., and Wydra, K. (2012). Taxonomic relatedness between *Pectobacterium carotovorum* subsp. carotovorum, *Pectobacterium carotovorum* subsp. *Odoriferum and Pectobacterium carotovorum* subsp. *brasiliense* subsp. nov. *J. Appl. Microbiol.* 113, 904–913. doi: 10.1111/j.1365-2672.2012.05383.x

Pédron, J., Bertrand, C., Taghouti, G., Portier, P., and Barny, M.-A. (2019). *Pectobacterium aquaticum* sp. nov., isolated from waterways. *Int. J. Syst. Evol. Microbiol.* 69, 745–751. doi: 10.1099/ijsem.0.003229

Pérombelon, M. C. M. (2002). Potato diseases caused by soft rot erwinias: an overview of pathogenesis. *Plant Pathol.* 51, 1–12. doi: 10.1046/j.0032-0862.2001.Short title.doc.x

Portier, P., Pédron, J., Taghouti, G., Fischer-Le Saux, M., Caullireau, E., Bertrand, C., et al. (2019). Elevation of *Pectobacterium carotovorum* subsp. odoriferum to species level as *Pectobacterium odoriferum* sp. nov., proposal of *Pectobacterium brasiliense* sp. nov. and *Pectobacterium actinidiae* sp. nov., emended description of *Pectobacterium carotovorum* and description of *Pectobacterium versatile* sp. nov., isolated from streams and symptoms on diverse plants. *Int. J. Syst. Evol. Microbiol.* 69, 3207–3216. doi: 10.1099/ijsem.0.003611

Prokhorov, N. S., Riccio, C., Zdorovenko, E. L., Shneider, M. M., Browning, C., Knirel, Y. A., et al. (2017). Function of bacteriophage G7C esterase tailspike in host cell adsorption. *Mol. Microbiol.* 105, 385–398. doi: 10.1111/mmi.13710

Richter, M., and Rossello-Mora, R. (2009). Shifting the genomic gold standard for the prokaryotic species definition. *Proc. Natl. Acad. Sci. U.S.A.* 106, 19126–19131. doi: 10.1073/pnas.0906412106

Sawabdekeb, J. S., Sloneker, J. H., and Jeanes, A. (1965). Quantitative determination of monosaccharides as their alditol acetates by gas liquid chromatography. *Anal. Chem.* 37, 1602–1604. doi: 10.1021/ac60231a048

Schattner, P., Brooks, A. N., and Lowe, T. M. (2005). The tRNAscan-SE, snoscan and snoGPS web servers for the detection of tRNAs and snoRNAs. *Nucleic Acids Res.* 33, W686–689. doi: 10.1093/nar/gki366

Schmerer, M., Molineux, I. J., and Bull, J. J. (2014). Synergy as a rationale for phage therapy using phage cocktails. *PeerJ* 2:e590. doi: 10.7717/peerj.590

Shashkov, A. S., Lipkind, G. M., Knirel, Y. A., and Kochetkov, N. K. (1988). Stereochemical factors determining the effects of glycosylation on the 13C chemical shifts in carbohydrates. *Magn. Reson. Chem.* 26, 735–747. doi: 10.1002/mrc.1260260904

Shirshikov, F. V., Korzhenkov, A. A., Miroshnikov, K. K., Kabanova, A. P., Barannik, A. P., Ignatov, A. N., et al. (2018). Draft genome sequences of new genomospecies "*Candidatus Pectobacterium maceratum*" strains, which cause soft rot in plants. *Genome Announc.* 6:e00260-18. doi: 10.1128/genomeA.00260-18

Söding, J., Biegert, A., and Lupas, A. N. (2005). The HHpred interactive server for protein homology detection and structure prediction. *Nucleic Acids Res.* 33, W244–248. doi: 10.1093/nar/gki408

Stamatakis, A. (2014). RAxML version 8: A tool for phylogenetic analysis and post-analysis of large phylogenies. *Bioinformatics* 30, 1312–1313. doi: 10.1093/bioinformatics/btu033

Steinbacher, S., Baxa, U., Miller, S., Weintraub, A., Seckler, R., and Huber, R. (1996). Crystal structure of phage P22 tailspike protein complexed with *Salmonella* sp. O-antigen receptors. *Proc. Natl. Acad. Sci U.S.A.* 93, 10584–10588. doi: 10.1073/pnas.93.20.10584

Svircev, A., Roach, D., and Castle, A. (2018). Framing the future with bacteriophages in agriculture. *Viruses* 10:E218. doi: 10.3390/v10050218

Taylor, N. M. I., Prokhorov, N. S., Guerrero-Ferreira, R. C., Shneider, M. M., Browning, C., Goldie, K. N., et al. (2016). Structure of the T4 baseplate and its function in triggering sheath contraction. *Nature* 533, 346–352. doi: 10.1038/nature17971

Tu, J., Park, T., Morado, D. R., Hughes, K. T., Molineux, I. J., and Liu, J. (2017). Dual host specificity of phage SP6 is facilitated by tailspike rotation. *Virology* 507, 206–215. doi: 10.1016/j.virol.2017.04.017

Voronina, M. V., Bugaeva, E. N., Vasiliev, D. N., Kabanova, A. P., Barannik, A. P., Shneider, M. M., et al. (2019a). Characterization of *Pectobacterium carotovorum* subsp. carotovorum bacteriophage PP16 prospective for biocontrol of potato soft rot. *Microbiology.* 13, 458–469. doi: 10.1134/S0026261719040118

Voronina, M. V., Kabanova, A. P., Shneider, M. M., Korzhenkov, A. A., Toschakov, S. V., Miroshnikov, K. K., et al. (2019b). First report of *Pectobacterium carotovorum* subsp. brasiliense causing blackleg and stem rot disease of potato in Russia. *Plant Dis.* 103, 364–364. doi: 10.1094/PDIS-03-18-0456-PDN

Waleron, M., Misztak, A., Waleron, M., Franczuk, M., Wielgomas, B., and Waleron, K. (2018). Transfer of *Pectobacterium carotovorum* subsp. carotovorum strains isolated from potatoes grown at high altitudes to *Pectobacterium peruviense* sp. nov. *Syst. Appl. Microbiol.* 41, 85–93. doi: 10.1016/j.syapm.2017.11.005

Westphal, O., and Jann, K. (1965). Bacterial lipopolysaccharides extraction with phenol-water and further applications of procedure. *Methods Carbohydr. Chem.* 5, 83–91.

Zhang, Y., Fan, Q., and Loria, R. (2016). A re-evaluation of the taxonomy of phytopathogenic genera *Dickeya* and *Pectobacterium* using whole-genome sequencing data. *Syst. Appl. Microbiol.* 39, 252–259. doi: 10.1016/j.syapm.2016.04.001

Zych, K., Toukach, F. V., Arbatsky, N. P., Kołodziejska, K., Senchenkova, S. N., Shashkov, A. S., et al. (2001). Structure of the O-specific polysaccharide of proteus mirabilis D52 and typing of this strain to Proteus serogroup O33. *Eur. J. Biochem.* 268, 4346–4351. doi: 10.1046/j.1432-1327.2001.02356.x

Conflict of Interest: EB, AK, and AI are employed by Research Center "PhytoEngineering" Ltd.

The remaining authors declare that the research was conducted in the absence of any commercial or financial relationships that could be construed as a potential conflict of interest.

Copyright © 2020 Lukianova, Shneider, Evseev, Shpirt, Bugaeva, Kabanova, Obraztsova, Miroshnikov, Senchenkova, Shashkov, Toschakov, Knirel, Ignatov and Miroshnikov. This is an open-access article distributed under the terms of the Creative Commons Attribution License (CC BY). The use, distribution or reproduction in other forums is permitted, provided the original author(s) and the copyright owner(s) are credited and that the original publication in this journal is cited, in accordance with accepted academic practice. No use, distribution or reproduction is permitted which does not comply with these terms.

frontiers in Microbiology

ORIGINAL RESEARCH
published: 14 February 2020
doi: 10.3389/fmicb.2020.00194

Novel Bacteriophages Capable of Disrupting Biofilms From Clinical Strains of *Aeromonas hydrophila*

Mwila Kabwe[1], Teagan Brown[1], Lachlan Speirs[1], Heng Ku[1], Michael Leach[2], Hiu Tat Chan[3], Steve Petrovski[4], Peter Lock[5] and Joseph Tucci[1]**

[1] Department of Pharmacy and Biomedical Science, La Trobe Institute for Molecular Science, La Trobe University, Melbourne, VIC, Australia, [2] School of Rural Health, Monash University, Bendigo, VIC, Australia, [3] Department of Microbiology, The Royal Melbourne Hospital, Melbourne, VIC, Australia, [4] Department of Physiology, Anatomy and Microbiology, La Trobe University, Melbourne, VIC, Australia, [5] La Trobe Institute for Molecular Science, La Trobe University, Melbourne, VIC, Australia

OPEN ACCESS

Edited by:
Krishna Mohan Poluri,
Indian Institute of Technology Roorkee, India

Reviewed by:
Xiangmin Lin,
Fujian Agriculture and Forestry University, China
Maria José Saavedra,
Universidade de Trás-os-Montes e Alto Douro, Portugal

***Correspondence:**
Mwila Kabwe
M.Kabwe@latrobe.edu.au
Joseph Tucci
j.tucci@latrobe.edu.au

Specialty section:
This article was submitted to Antimicrobials, Resistance and Chemotherapy, a section of the journal Frontiers in Microbiology

Received: 22 November 2019
Accepted: 28 January 2020
Published: 14 February 2020

Citation:
Kabwe M, Brown T, Speirs L, Ku H, Leach M, Chan HT, Petrovski S, Lock P and Tucci J (2020) Novel Bacteriophages Capable of Disrupting Biofilms From Clinical Strains of Aeromonas hydrophila. Front. Microbiol. 11:194. doi: 10.3389/fmicb.2020.00194

The increase in global warming has favored growth of a range of opportunistic environmental bacteria and allowed some of these to become more pathogenic to humans. *Aeromonas hydrophila* is one such organism. Surviving in moist conditions in temperate climates, these bacteria have been associated with a range of diseases in humans, and in systemic infections can cause mortality in up to 46% of cases. Their capacity to form biofilms, carry antibiotic resistance mechanisms, and survive disinfection, has meant that they are not easily treated with traditional methods. Bacteriophage offer a possible alternative approach for controlling their growth. This study is the first to report the isolation and characterization of bacteriophages lytic against clinical strains of *A. hydrophila* which carry intrinsic antibiotic resistance genes. Functionally, these novel bacteriophages were shown to be capable of disrupting biofilms caused by clinical isolates of *A. hydrophila*. The potential exists for these to be tested in clinical and environmental settings.

Keywords: *Aeromonas hydrophila*, bacteriophage, genomics, biofilm, antimicrobial resistance

INTRODUCTION

Aeromonas hydrophila is a Gram-negative rod found in fresh water, brackish water, and mud in temperate climates (Batra et al., 2016). They are an established fish pathogen causing septicemia and ulcerative diseases (Chowdhury et al., 1990). *Aeromonas* spp. were first reported as infective agents in humans in 1951, and from that time have been seen as important human pathogens (Janda and Abbott, 2010). *A. hydrophila* implicated in human infections is usually mesophilic and grows optimally between 35 and 37°C (Janda and Abbott, 2010). Clinical infections may be a result of direct skin invasion from muddy water (Vally et al., 2004) or drinking contaminated water leading to local (gastritis, skin necrotizing infection) or systemic (peritonitis, sepsis, meningitis, respiratory, and hepatic) infections (Janda and Abbott, 2010; Igbinosa et al., 2012). Mortality in systemic infections may be as high as 46% (Dryden and Munro, 1989).

The incidence of *A. hydrophila* has been correlated to warmer summer periods when the prevalence of this bacterium is increased in harvested rain water (Picard and Goullet, 1987) and in chlorinated or unchlorinated metropolitan water supplies (Burke et al., 1984a,b).

Global climate change and population increases are expected to put greater pressures on water resources (DeNicola et al., 2015) and lead to increased investment in alternative sources such as rain harvesting (Ahmed et al., 2008). This is certainly the case in countries such as Australia, that is experiencing harsher summers and where use of recycled water for human consumption is not in vogue. *A. hydrophila* is estimated to be present in up to 33% of rain harvested water in Australia's major cities (Chubaka et al., 2018) and they are known to survive in chlorinated water by forming biofilms (Igbinosa et al., 2012). Biofilms provide bacterial cell-to-cell contact allowing for the transfer of genetic material that enhances the niche and increases resistance to stress and antibiotics (Talagrand-Reboul et al., 2017). Therefore, water originating from rain harvested tanks, municipal supplies, recreational settings such as swimming pools, and in the natural environment may serve as potential sources of infection.

Aeromonas spp. play a major role in the transfer of antibiotic resistance, making these organisms particularly problematic. They have been implicated as mediators of the transfer of antibiotic resistance markers between hospital and environmental strains (Varela et al., 2016), and are associated with innate multi-antibiotic resistance due to efflux pumps, inducible cephalosporinases, and inducible metallo beta lactamases (Azzopardi et al., 2011; Sinclair et al., 2016). Controlling *A. hydrophila* infection is therefore paramount as this organism threatens food security (by causing fish diseases and increasing their mortality) (Talagrand-Reboul et al., 2017) and human health (Neyts et al., 2000). Since the World Health Organization declaration that antibiotic resistance was a global emergency (World Health Organisation [WHO], 2014), alternatives for antibiotics have been actively researched (Czaplewski et al., 2016).

Bacteriophages, although discovered before antibiotics, have recently emerged as adjuncts and alternatives to antibiotics (Golkar et al., 2014). While temperate (Beilstein and Dreiseikelmann, 2008; Dziewit and Radlinska, 2016) and lytic (Chow and Rouf, 1983; Merino et al., 1990a,b; Shen et al., 2012; Jun et al., 2013; Anand et al., 2016; Wang et al., 2016; Le et al., 2018; Yuan et al., 2018) bacteriophages against *A. hydrophila* have been previously reported, these were isolated using environmental and fish pathogenic isolates of *A. hydrophila*. In the instances where host range was tested, their activity did not extend to clinical strains of *A. hydrophila* (Wang et al., 2016), that is, strains which were isolated from hospital patients suffering from *A. hydrophila* infections. Clinical strains of *A. hydrophila* have been shown to differ from environmental strains including those pathogenic in fish, in their production of virulence factors (Janda and Abbott, 2010), as well as other features. For instance, clinical strains are reported to restrict production of protease activity in favor of cytotoxicity and hemolysin production when temperatures increase from 30 to 37°C (Yu et al., 2007; Rasmussen-Ivey et al., 2016). Further, environmental strains can survive at temperatures as low as 4°C where clinical strain growth is inhibited (Mateos et al., 1993; Rasmussen-Ivey et al., 2016). To date there have been no lytic bacteriophages isolated that have demonstrated killing of clinical strains of *A. hydrophila*. This study screened for lytic bacteriophages against clinical strains of *A. hydrophila* associated with various human diseases. The isolated bacteriophages were characterized phenotypically and genomically, and functionally assessed for their capacity to degrade *A. hydrophila* biofilms.

MATERIALS AND METHODS

Ethics Statement

All methods were performed in accordance with the La Trobe University Ethics, Biosafety, and Integrity guidelines and regulations. Clinical isolates of *A. hydrophila* were obtained from specimen cultures as part of routine care. Informed consent was obtained from participants for their involvement and use of samples in this study. The study protocols were approved by the La Trobe University Ethics Committee, reference number: S17–111.

Bacterial Growth and Strain Identification

Aeromonas hydrophila bacteria was isolated from a deep wound infection (Strain AHB0117), a polymicrobial liver abscess on a background of cholangiocarcinoma (Strain AHB0148), a polymicrobial surgical site of infection (Strain AHB0116), diarrhea fecal samples (Strain AHB0139), and a scalp abscess due to trauma (Strain AHB0147), all de-identified. All strains were cultured in nutrient broth or agar (Oxoid, Australia) at 37°C aerobically. The bacterial strains were initially identified by Matrix Assisted Laser Desorption/Ionization – Time of Flight (MALDI-TOF; Bruker Daltonik, Germany). Conclusive identification was achieved by sequencing of the 16S rRNA region (see **Table 1** for PCR conditions), as well as screening for intrinsic antibiotic resistance markers endogenous to *A. hydrophila* (see below). The 16s rRNA amplicons were purified using QIAquick® PCR purification kits (Qiagen, Australia) and Sanger sequenced by the Australian Genome Research Facility (AGRF) in Queensland, Australia. The strains that were identified as *A. hydrophila* were used for subsequent bacteriophage screening.

Antibiotic Sensitivity, Intrinsic Antibiotic Resistance, and CRISPR Characterization

Antibiotic sensitivity of the *A. hydrophila* clinical strains used in this study was assessed using the VITEK® 2 analyzer (bioMérieux, Australia), according to the manufacturer's instructions. Whole genome sequences of *A. hydrophila* strains published in the GenBank NCBI database were imported into CARD (Comprehensive Antibiotic Resistance Database) (Jia et al., 2017) and analyzed for genes coding antibiotic resistance. These genomes were also screened for CRISPR coded sequences using CRISPRFinder (Grissa et al., 2007). Identified sequences from (version 9.5.4) multiple strains were aligned in CLC genomic workbench and PCR primers designed from their conserved regions. The primer sequences and their PCR conditions are listed in **Table 1** and amplicons were confirmed by sequencing (AGRF, Australia). Bacteriophage whole genome sequences were

TABLE 1 | Primers and PCR reaction conditions for bacteria and antibiotic resistance characterization.

Oligo name	Sequence (5′ – 3′)	Cycling conditions
16S rRNA	U27F: AGAGTTTGATCMTGGCTCAG U492R: AAGGAGGTGWTCCARCC	Hold: 95°C, 3 min 32 cycles of 95°C, 30 s; 60°C, 30 s; 72°C, 90 s
CphA beta-lactamase class B	FP: ACTCCATGGTCTATTTCGGG RP: GTCTTGATCGGCAGCTTCAT	Hold: 95°C, 10 min 35 cycles of 95°C, 30 s; 54°C, 30 s; 72°C, 45 s; 72°C, 10 min
FOX/MOX beta lactamase class C	FP: TACTATCGCCAGTGGACGCC RP: TCCGCCGAGCTGGTCTTGAT	Hold: 95°C, 10 min 35 cycles of 95°C, 30 s; 54°C, 30 s; 72°C, 45 s; 72°C, 10 min
OXA-12 beta lactamase class D	FP: TTTCTCTATGCCGACGGCAA RP: GTTGCCGTAGTCAAAACGGT	Hold: 95°C, 10 min 35 cycles of 95°C, 30 s; 54°C, 30 s; 72°C, 45 s; 72°C, 10 min
Chloramphenicol resistance	FP: ATCACCTGGTTCCTGTTCAG RP: TACCGACGATGACCGCATAA	Hold: 95°C, 10 min 35 cycles of 95°C, 30 s; 54°C, 30 s; 72°C, 45 s; 72°C, 10 min
MFS transporter	FP: TTCTTCGTGGTGATGCCCAT RP: GAAGATCAGCATCACCTGGA	Hold: 95°C, 10 min 35 cycles of 95°C, 30 s; 53°C, 30 s; 72°C, 45 s; 72°C, 10 min
Type I-E CRISPR-associate protein Cas5/casD	FP: AACCCTACCTGCTACTATGG RP: ATTCTGGTGACAACGGGCAA	Hold: 95°C, 10 min 35 cycles of 95°C, 30 s; 51°C, 30 s; 72°C, 45 s; 72°C, 10 min

also screened for antimicrobial resistance genes (ARGs) and CRISPR as above.

Bacteriophage Isolation and Host Range

Wastewater and fishpond samples from Victoria, Australia, were screened for bacteriophages by enriching the samples with *A. hydrophila*. In brief, 100 μL of log phase *A. hydrophila* was added to 10 mL of broth with 1 mL of filtered sample (0.2 μm cellulose acetate; Advantec, Australia). This enrichment was incubated for 4 days before filtration, and 10 μL of this filtrate was then spotted onto a bacterial lawn of *A. hydrophila* on agar to screen for the presence of plaques. Host range testing was performed on five clinical strains of *A. hydrophila*.

One-Step Growth Analysis

Aeromonas hydrophila strains in exponential growth phase, collected by centrifugation at 12,000 × *g* for 10 min and resuspended in fresh nutrient broth at a concentration of 0.6U (OD_{600}), were used for the one step growth experiments (Wang et al., 2016). The strain AHB0147 was used for one-step growth experiments involving LAh1–LAh5 bacteriophages while LAh6–LAh10 bacteriophage one-step growth experiments were performed using the strain AHB0116. One hundred microliters of bacteriophage were added to 900 μL of each *A. hydrophila* strain at a MOI of 0.01 and incubated at 4°C for 30 min to allow for adsorption. Adsorbed bacteriophage were collected by centrifugation at 12,000 × *g* for 10 min and pellet resuspended in 50 mL of fresh nutrient broth. The mixture was incubated aerobically at 37°C and bacteriophages assayed using aliquots collected every 5 min by centrifugation at 12,000 × *g* for 2 min at 4°C.

Transmission Electron Microscopy

Bacteriophage particles were visualized by Transmission Electron Microscopy using a JEOL JEM-2100 transmission electron microscope (TEM) at 200 kV. Bacteriophage lysate was adsorbed onto 400-mesh formvar and carbon coated copper grids (ProSciTech, Australia) for 1 min. Grids were rinsed with milli-Q water and adsorbed phage particles were negatively stained twice using 2% (W/V) uranyl acetate (Sigma-Aldrich®, Australia) for 20 s. Excess stain was removed using filter paper and grids air dried for 30 min. Images were captured on a Gatan Orius SC200D 1 wide-angle camera using the Gatan Microscopy Suite and Digital Micrograph Imaging software (version 2.3.2.888.0). The images obtained were further analyzed using ImageJ (version 1.8.0_112).

Bacteriophage DNA Extraction

All chemicals were purchased from Sigma-Aldrich® (Australia), unless stated otherwise. Concentrated bacteriophage stock (approximately 10^{11} PFU mL^{-1}) was treated with 5 mmol L^{-1} of $MgCl_2$ as well as RNase A and DNase I (Promega, Australia) to a final concentration of 10 μg mL^{-1}. The digest was incubated at room temperature for 30 min before polyethylene glycol precipitation at 4°C using PEG-8000 at 10% (w/v) and sodium chloride (1 gL^{-1}). Precipitated virions were recovered by centrifugation at 12,000 × *g* for 5 min to obtain a pellet which was then resuspended in 50 μL nuclease free water (Promega, Australia). Viral proteins were digested with 50 μg mL^{-1} of proteinase K, 20 mmol L^{-1} EDTA and 0.5% (v/v) of sodium dodecyl sulfate for 1 h at 55°C to release phage DNA. Bacteriophage DNA was separated from proteins by addition of an equal volume of phenol-chloroform-isoamyl alcohol (29:28:1) and carefully collecting the aqueous phase after centrifugation at 12,000 × *g* for 10 min. An equal volume of isopropanol and overnight incubation at −20°C was used to precipitate bacteriophage DNA. Bacteriophage DNA was then collected by centrifugation (12,000 × *g* for 5 min) before washing in 70% ethanol, air-drying, and re-suspending in 30 μL of nuclease free water (Promega, Australia).

Bacteriophage Whole Genome Sequencing and *in silico* Analysis

Nextera® XT DNA sample preparations kits were used to prepare phage DNA for sequencing according to the manufacturer's instructions. Whole genome sequencing of the prepared libraries

was performed on an Illumina MiSeq® using a MiSeq® V2 300 cycle reagent kit. Sequence reads were imported into CLC genomics workbench (version 9.5.4) and assembled *de novo*. Open reading frames (ORFs) were predicted and translated using CLC genomics workbench (version 9.5.4). Translated ORFs were analyzed using BLASTP (Mount, 2007) and tRNAs and tmRNAs predicted using ARAGORN (Laslett and Canback, 2004) and tRNAscan-SE 2.0 (Lowe and Chan, 2016). Bacteriophage genomes were also analyzed for CRISPR sequences using the CRISPR database (Grissa et al., 2007). Whole genome alignments of isolated bacteriophages and those against other *Aeromonas* spp. (sourced from GenBank) were conducted and a phylogenetic tree constructed by neighbor joining method with 1000 bootstrap replicates in CLC genomics workbench (version 9.5.4). The bacteriophage genomes were also assessed by MAUVE plugin (Darling et al., 2004) in Geneious (version 11.0.5)[1].

Biofilm Degradation Assays

The capacity to disrupt *A. hydrophila* biofilms was determined by growing *A. hydrophila* mono-biofilms in a 96 well polystyrene plate (Greiner bio-one, Australia). The 96 well plates were inoculated with 100 μL of 10^8 CFU mL^{-1} log phase *A. hydrophila* in broth culture and a further 100 μL of sterile broth added. The cultures were then incubated aerobically at 37°C, shaking, for 4 days. Ten microliters of bacteriophage at a concentration of 10^8 PFU mL^{-1} was added to the established biofilms and for each experiment, heat inactivated (autoclaved) bacteriophage was used as a control to confirm that the effects on biofilm were the result of bacteriophage particles, rather than chemical residues or other matter in the preparation. Bacterial attachment was assayed according to Merritt et al. (2005). Briefly, plates were submerged in water to wash cells for 5 min before staining with 200 μL of 0.1% crystal violet for 10 min. The excess crystal violet was removed by submerging the plates in water for 5 min. The stained adherent cells were then solubilized in 70% ethanol and the absorbance in each well determined (at a wavelength of 550 nm) using a FlexStation 3 plate reader (Molecular devices, United States). Bacteriophages LAh7, LAh9, and LAh10 were tested on *A. hydrophila* strain AHB0116 biofilm whilst LAh1 was tested on biofilm formed by AHB0147.

Viability of Biofilm

Aeromonas hydrophila biofilms grown on glass slides were stained with 100 μL of SYBR® gold (Eugene, OR, United States; 1 mg mL^{-1}) diluted in dimethyl sulfoxide (Sigma-Aldrich®, Australia) and 3 μL of 1 mg mL^{-1} propidium iodide (PI) in nuclease free water (Promega, Australia) for 30 min in the dark. The live/dead stained cells were mounted with 10 μL Vectorshield® (Burlingame, CA, United States) on coverslips. The stained slides were visualized with an Olympus Fluoview Fv10i-confocal laser-scanning microscope (Olympus Life Science, Australia). PI stained DNA of membrane-compromised cells red while SYBR Gold® stained DNA from both intact and membrane-compromised cells green.

[1]http://www.geneious.com/

Statistical Analysis

Statistical tests were used to assess the capacity of bacteriophages to break down biofilms from clinical strains of *A. hydrophila*. Firstly, the Shapiro–Wilk test was used to assess whether, for each individual bacteriophage, biofilm absorbance at OD_{550nm} was normally distributed. As these data were found to be non-normally distributed, biofilm absorbance at OD_{550nm} for each phage was summarized in terms of the median rather than the mean, with the full five-number summaries presented in side-by-side boxplots. The interquartile range (IQR) was also calculated. Due to the non-normality of the data, the biofilm absorbance at OD_{550nm} for each bacteriophage was compared with that for every other phage using a non-parametric test – the Wilcoxon signed-rank test. *p*-values less than 0.05 were considered to be statistically significant. All statistical tests were performed in SPSS version 24 (SPSS Inc., United States).

RESULTS

Antibiotic Resistance in *Aeromonas hydrophila*

Five clinical isolates identified as *A. hydrophila* were screened for ARGs by PCR amplification, revealing intrinsic multi-antibiotic resistance. These included genes coding for chloramphenicol resistance (5/5), major facilitator superfamily efflux transporter (5/5), CphA class B beta lactamase (5/5), FOX/MOX class C beta lactamase (4/5), and OXA-12 class D beta lactamases (5/5) (**Figure 1**). All strains used in this study were susceptible to ciprofloxacin, cotrimoxazole, and gentamicin.

Isolation of Novel Bacteriophages Against Clinical Strains of *Aeromonas hydrophila*

Wastewater and pond samples collected from the cities of Bendigo and Melbourne, Victoria, Australia were screened for bacteriophages. Ten bacteriophages against five clinical strains of *A. hydrophila* were isolated. Of these, eight were *Podoviridae* (comprising five icosahedral and three elongated *Podoviridae*), one was a *Siphoviridae* and one was a *Myoviridae* virus. The novel bacteriophages were labeled LAh1–LAh10, with LAh1–LAh5 representing the icosahedral *Podoviridae*, LAh6, LAh8, and LAh9 representing the elongated version of the *Podoviridae*, while LAh7 and LAh10 were *Siphoviridae* and *Myoviridae* bacteriophages respectively (**Figure 2**). The elongated *Podoviridae* bacteriophages had capsid length ≈ 172 ± 10 nm, width ≈ 35 ± 2 nm and tail length ≈ 18 ± 1 nm while the icosahedral *Podoviridae* had capsid diameter ≈ 82 ± 4 nm and tail ≈ 8 ± 1 nm. The *Siphoviridae* bacteriophages had capsid length and tail length of ≈ 44 ± 3 nm and ≈232 ± 13 nm, respectively. *Myoviridae* bacteriophages had capsid diameter of ≈ 116 ± 13 nm and tail length ≈ 183 ± 5 nm (**Figure 2**). Specific features of the bacteriophages and their characteristics are summarized in **Table 2** while their respective one-step growth curves are shown in **Figure 3**.

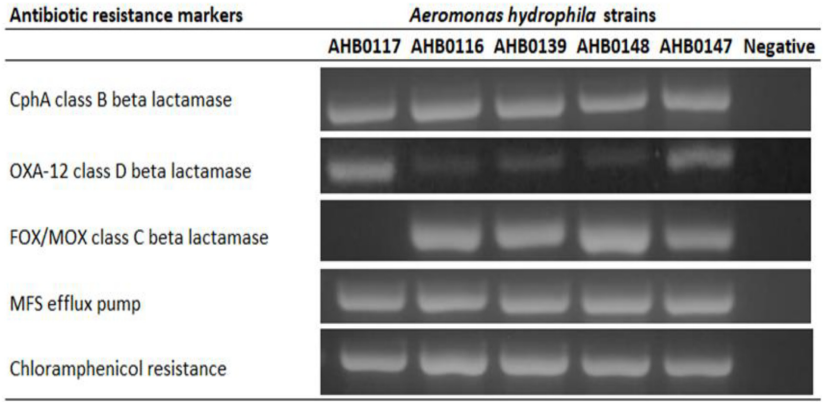

FIGURE 1 | PCR detection of antibiotic resistance markers in clinical strains of *A. hydrophila* used in this study. All resistance genes were present in all clinical strains except class C beta lactamase in AHB0117. The images presented here are taken from two separate gels, which are displayed in **Supplementary Figures S1, S2**. The white space between these images delineates sections that were cropped from different regions of the gels in **Supplementary Figures S1, S2**.

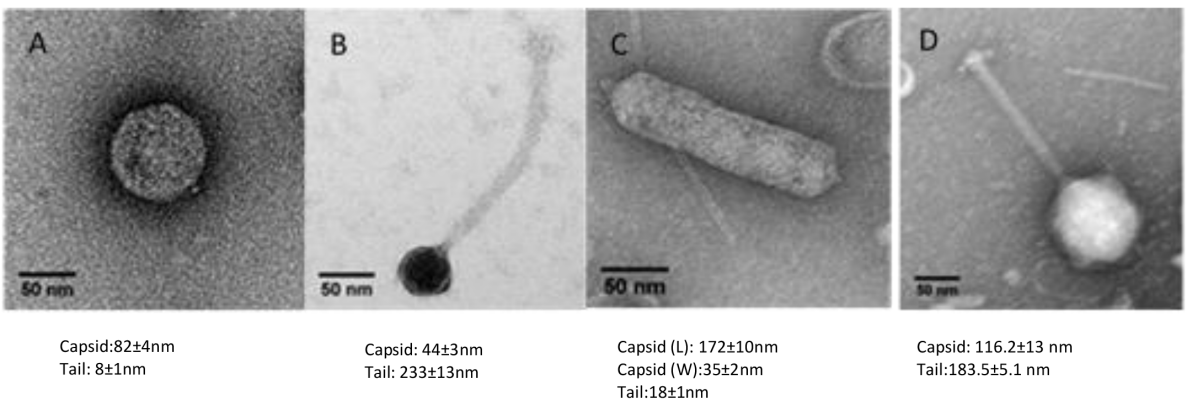

FIGURE 2 | Transmission electron microscopy of representative bacteriophages from LAh1–LAh10. **(A)** Typical morphology of LAh1–LAh5 (icosahedral *Podoviridae*); **(B)** LAh7 (*Siphoviridae*); **(C)** typical morphology of LAh6, LAh8, and LAh9 (elongated *Podoviridae*); and **(D)** LAh10 (*Myoviridae*). All scale bar at 50 nm.

TABLE 2 | LAh1–LAh10 genotypic and phenotypic characteristics.

Phage name	Source	EM morphology	Genome size (bp)	ORFs	GC%	Host range (bacterial strain)					Number of tRNAs	GenBank accession
						AHB0148	AHB0147	AHB0139	AHB0117	AHB0116		
LAh1	Wastewater	*Podoviridae*	42002	45	59.30	No	Yes	No	No	No	0	MK838107
LAh2	Wastewater	*Podoviridae*	42008	45	59.30	No	Yes	No	No	No	0	MK838108
LAh3	Wastewater	*Podoviridae*	42002	50	59.30	No	Yes	No	No	No	0	MK838109
LAh4	Wastewater	*Podoviridae*	42002	52	59.30	No	Yes	No	No	No	0	MK838110
LAh5	Wastewater	*Podoviridae*	41985	53	59.30	No	Yes	No	No	No	0	MK838111
LAh6	Fish pond	*Podoviridae*	101437	165	42.30	Yes	No	Yes	No	Yes	21	MK838112
LAh7	Wastewater	*Siphoviridae*	61426	75	61.90	No	No	Yes	Yes	Yes	0	MK838113
LAh8	Wastewater	*Podoviridae*	97408	143	42.20	Yes	No	Yes	No	Yes	21	MK838114
LAh9	Wastewater	*Podoviridae*	97988	147	42.40	Yes	No	No	No	Yes	18	MK838115
LAh10	Wastewater	*Myoviridae*	260310	227	47.50	No	No	Yes	No	Yes	4	MK838116

Whole Genome Sequencing of Bacteriophages LAh1–LAh10

Illumina sequencing revealed novel and diverse genomes with several displaying a similar size of approximately 42,000 bp (LAh1–LAh5). While the genomes of LAh1–LAh5 were the most similar to each other, specific differences were seen, and these resulted in non-synonymous amino acid changes (differences in their genomes and amino acid sequences are highlighted in

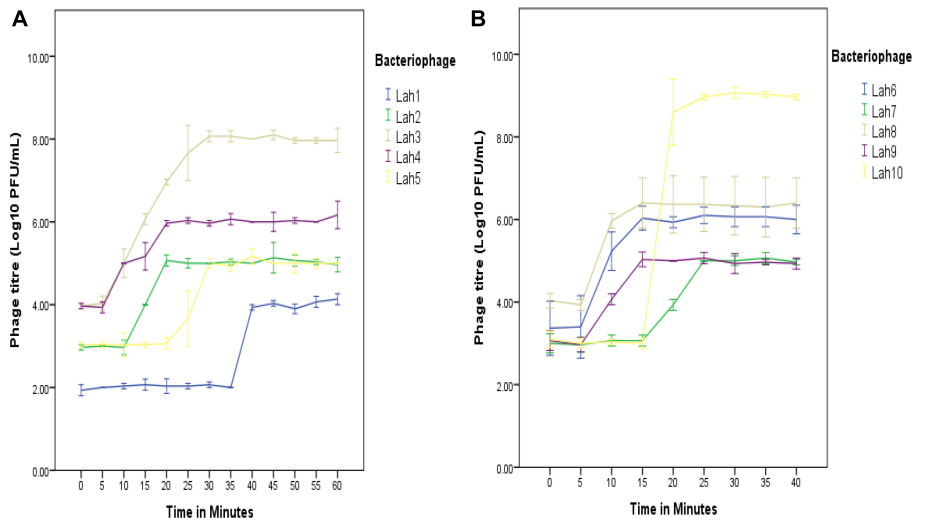

FIGURE 3 | One-step growth curves for *A. hydrophila* bacteriophages LAh1–LAh10 on two separate bacterial strains (depending on host range specificity). On the same host (*A. hydrophila* AHB0147), replication kinetics were different for LAh1–LAh5 **(A)**. LAh6–LAh10 differed in their growth kinetics when grown on *A. hydrophila* strain AHB0116 **(B)**. The standard errors of the mean are calculated from three independent experiments.

Table 3). Larger genomes were found in LAh7 (61,426 bp), LAh8 (97,408 bp), LAh9 (97,988 bp), and LAh6 (101,437 bp). LAh10 had the largest genome (260,310 bp) which is the also the largest reported to date against *A. hydrophila*. The genomes for LAh1–LAh10 were annotated and submitted to GenBank with accession numbers shown in **Table 2**. All bacteriophages had their genomes in a linear topology except LAh6 which had a circularly permuted genome. The number of ORFs varied with the genome size and ranged from 45 to 227 (**Table 2**). The GC% content ranged from 42.2% in LAh8 to 61.9% in LAh7. While no bacteriophage showed presence of tmRNA in their genomes, tRNAs were present in 4/10 of the bacteriophages (**Table 2**). The number or type of tRNAs were not associated with genome size. LAh6 and LAh8 had the highest number of tRNAs at 21 each, followed by LAh9 with 18 tRNAs and LAh10 with 4 tRNAs. Therefore, the bacteriophages with a lower GC% content had a higher number of tRNAs (**Table 2**). Bacteriophages LAh1–LAh5, and LAh7 did not have any tRNAs in their genomes. None of the bacteriophages isolated in this study had genes coding for putative CRISPR sequences, ARGs, toxins or chromosome integration genes in their genomes.

Bacteriophage Phylogeny and Host Specificity

Prior to this study there were 30 reported bacteriophages against *Aeromonas* spp. including eight against *A. hydrophila* which have had their genome completely sequenced. The 10 bacteriophages reported here are the first lytic bacteriophages to be isolated against clinical strains of *A. hydrophila*. The complete genome sequences of the previously isolated bacteriophages against *Aeromonas* spp. sourced from GenBank and those from this study were compared. **Figure 4** reveals the clustering of bacteriophages against clinical strains of *A. hydrophila* forming two clusters among other bacteriophages isolated using *A. hydrophila* strains from the environment but further away from those against other *Aeromonas* species.

These differences among the isolated bacteriophage genomes were further analyzed by Mauve whole genome alignment of LAh1–LAh10 (**Figure 5**). The differences in the bacteriophage cluster of LAh1–LAh5 is detailed in **Table 3** to highlight functional differences between these bacteriophages. For the cluster of bacteriophages LAh6, LAh8, and LAh9, the Mauve alignment showed the presence of a genetic segment (Blue colored colinear block in **Figure 5**) in the region of the putative tail fiber genes of bacteriophages that possibly contributed to their differences in host range. While similar in their genomes, LAh6 and LAh8 are able to lyse *A. hydrophila* strain AHB0139 that LAh9 is not (**Table 2**). The genome alignments show close homology between LAh1 and LAh5, and a diversity of nucleotide sequence between genomes of LAh7 and LAh10.

Capacity of LAh1–LAh10 to Disrupt *Aeromonas hydrophila* Biofilms *in vitro*

The capacity to disrupt *A. hydrophila* biofilms was analyzed quantitatively by evaluating the biofilm mass remaining after bacteriophage treatment and estimating the viability of the remnant biofilm. A representative bacteriophage from each morphological group was analyzed for capacity to disrupt biofilm. LAh1 was used as an example of icosahedral *Podoviridae*, LAh9 for the elongated *Podoviridae*, LAh7, a *Siphoviridae*, and LAh10 a *Myoviridae*. All biofilm experiments were performed using *A. hydrophila* bacterial strain AHB0116 that was lysed by all bacteriophages isolated here except for LAh1, in which case the host AHB0147 was used. In all cases, the biofilm mass was significantly reduced in bacteriophage treated compared to non-treated groups ($p < 0.001$). The untreated biofilm had a median (IQR)

TABLE 3 | Differences in the genomes of bacteriophages LAh2–LAh5 compared to LAh1.

Bacteriophage	Nucleotide change	Position	Non-synonymous amino acid change	Putative protein
LAh2; LAh4	C > A	1939	Z > K	Scaffolding protein
LAh5	A > G	8203	R > G	Hypothetical
LAh5	G > C	8205	R > G	Hypothetical
LAh5	Deletion (18 bp)	8207..8224	R; P; S; R; TGA (STOP); S	Hypothetical
LAh4	G > A	14009	A > T	Tail fiber
LAh2; LAh4	A > G	15068	N > D	Tail fiber
LAh3; LAh5	A > G	15075	C > Y	Tail fiber
LAh2	Insertion 4 bp	33001..33006	I and M (START)	DNA polymerase

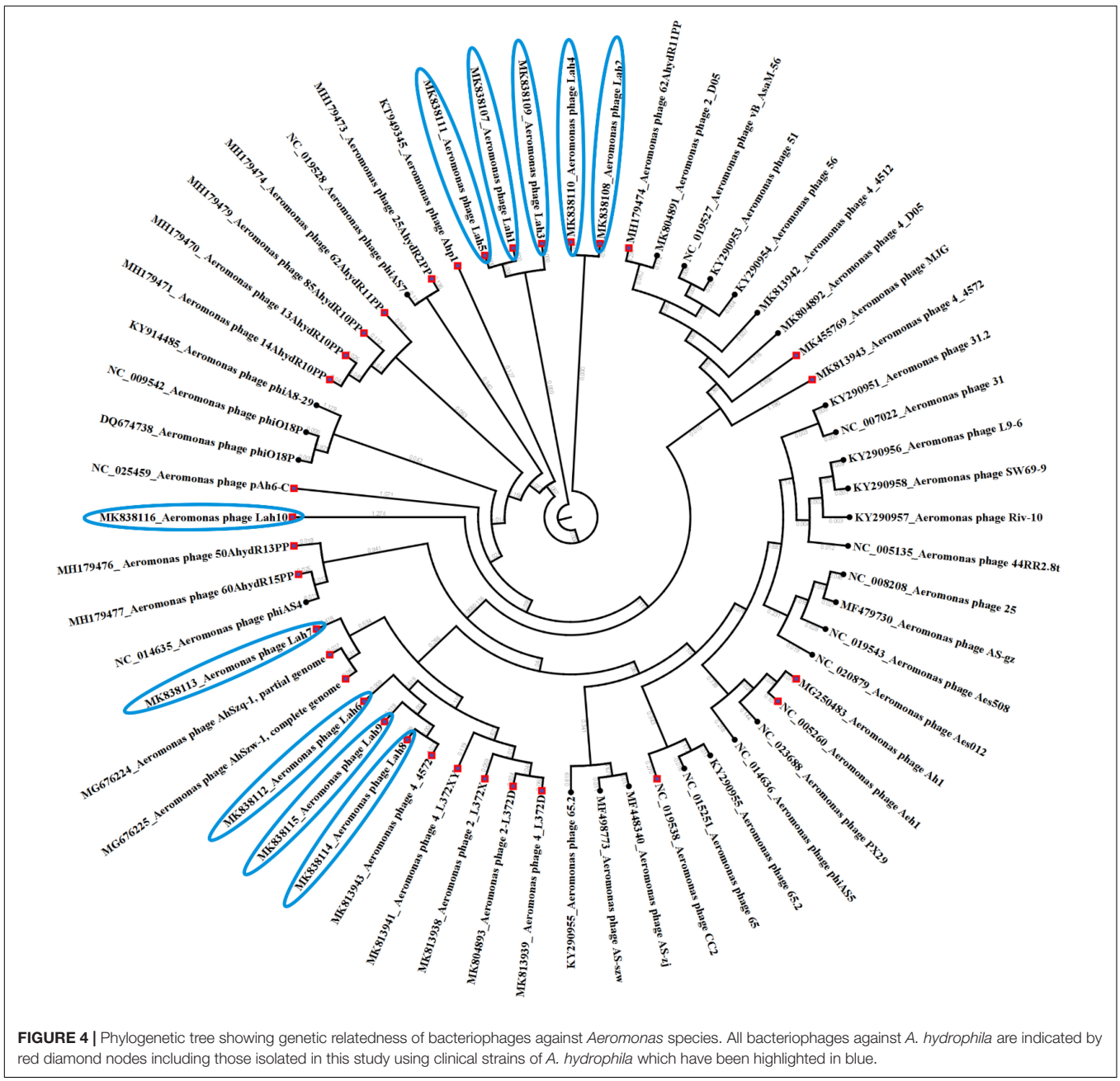

FIGURE 4 | Phylogenetic tree showing genetic relatedness of bacteriophages against *Aeromonas* species. All bacteriophages against *A. hydrophila* are indicated by red diamond nodes including those isolated in this study using clinical strains of *A. hydrophila* which have been highlighted in blue.

FIGURE 5 | Whole genome alignment of LAh1–LAh10 from top to bottom showing similarities and differences between genomes. Each colored colinear block represents a conserved region across the genomes, and these are connected by colored matching lines to trace homology between genomes. Colinear blocks that are offset represent regions that are expressed in the opposite orientation. The uncolored gaps between and within the colinear blocks represent differences between genomes or differences within conserved regions across genomes. The origin of individual ORFs is represented by vertical black lines below the colinear blocks (detailed annotation and putative functionality of each ORF can be accessed through GenBank with accession numbers provided in **Table 2**). LAh1–LAh5 share all their conserved regions (represented by green, yellow, and red blocks) with differences indicated by nicks and gaps within those blocks. Two of the three colinear blocks from LAh1–LAh5 are shared with LAh7 (green and yellow) and one (red) with all the other bacteriophage genomes (LAh6, LAh8, LAh9, and LAh10). LAh6, LAh8, and LAh9 share homology in three blocks (red, pink, and purple), while LAh6 and LAh9 share a fourth region (blue) which is also found in LAh10 but not LAh8. The purple block is conserved between LAh6, LAh8, LAh9, and LAh10.

absorbance at OD_{550nm} of 1.73 (0.86) whilst the largest value for the remnant biofilm after bacteriophage treatment was 1.20 (0.27), $p < 0.001$ (following treatment with LAh9). Treatment with LAh1 resulted in the lowest absorbance for the remnant biofilm [median (IQR) at OD_{550nm} of 0.35 (0.04)], significantly lower ($p < 0.001$) than those treated with all the other bacteriophages. LAh7 and LAh10 had statistically similar ($p = 0.58$) remaining biofilm with absorbance of median (IQR) at OD_{550nm} of 0.43 (0.29) and 0.48 (0.13), respectively (**Figure 6**). Of the bacteriophages tested on the *A. hydrophila* biofilms, those with higher GC% content and lower numbers of tRNAs [LAh1 (59.30%; 0), LAh7 (61.90%; 0), and LAh10 (47.50%; 4)] showed significantly greater capacity to degrade biofilms ($p < 0.001$) than that with lower GC% content and higher numbers of tRNAs [LAh9 (42.40%; 18)] (**Figure 6**).

Viability of Biofilm Treated With Bacteriophages

The viability of the biofilm mass was investigated using SYBR Gold® and PI live/dead staining. **Figure 7** shows cells fluorescing green (whole population of cells making up the biofilm) and red (dead, membrane-compromised cells). The icosahedral *Podoviridae* Bacteriophage LAh1 on host strain AHB0147 was used in the biofilm viability experiments. **Figure 7** shows untreated biofilm with a sparse population of membrane-compromised cells (**Figure 7B1**)

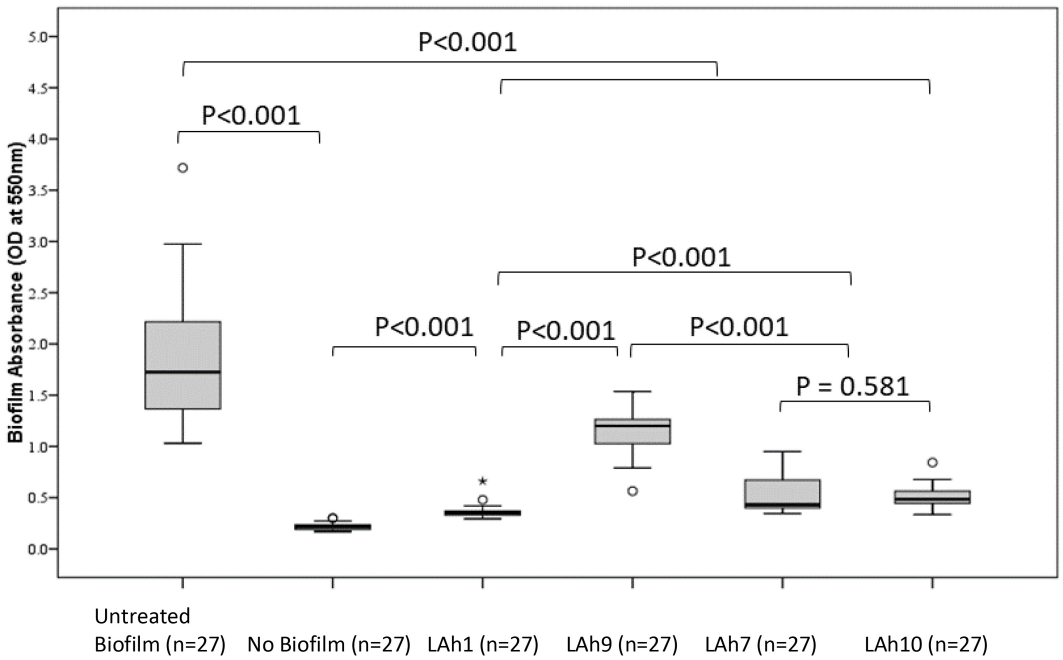

FIGURE 6 | *Aeromonas hydrophila* biofilm absorbance measurements after treatment with bacteriophages LAh1, LAh7, LAh9, and LAh10. Bacteriophages LAh7, LAh9, and LAh10 were tested on *A. hydrophila* strain AHB0116 biofilm whilst LAh1 was tested on biofilm formed by AHB0147. Bacteriophages with higher GC% content and lower numbers of tRNAs [LAh1 (59.30%; 0), LAh7 (61.90%; 0), and LAh10 (47.50%; 4)] showed significantly greater capacity to degrade biofilms ($p < 0.001$) than that with lower GC% content and higher numbers of tRNAs [LAh9 (42.40%; 18)]. * Is an extreme outlier.

compared to a dense total population (**Figure 7B2**). This indicated that cell population in the untreated biofilm was comprised of mostly membrane-intact cells. This was in contrast to the biofilms treated with bacteriophage (**Figures 7A1,A2**) in which the density was comparable between total population and membrane-compromised cells implying the cell population was mostly dead. In the bacteriophage treated biofilm, the total population and dead cells were both sparse. Treatment with heat inactivated (autoclaved) bacteriophage did not affect biofilm growth, indicating that *Aeromonas* biofilm disruption was the result of bacteriophage particles, and not other material in the preparation.

DISCUSSION

Increasing global temperatures have allowed a number of micro-organisms to emerge as potential causes of disease (Aguirre and Tabor, 2008). *A. hydrophila* is one bacterial species benefiting from global warming with more clinical strains emerging (Azzopardi et al., 2011). These bacteria are usually resistant to first and second line antibiotic therapy involving beta-lactam drugs and third generation cephalosporins via mechanisms such as resistance genes and biofilm formation (Janda and Abbott, 2010). Bacteriophages, which have been suggested as an alternative to antibiotics, have been isolated against environmental and fish pathogen strains of *A. hydrophila* (Chow and Rouf, 1983; Merino et al., 1990a,b; Gibb and Edgell, 2007; Shen et al., 2012; Jun et al., 2013; Anand et al., 2016; Wang et al., 2016; Le et al., 2018; Yuan et al., 2018; Bai et al., 2019; Cao et al., 2019; Kazimierczak et al., 2019). The host range of these bacteriophages, however, was not reported to extend to clinical strains. The current study is the first to report the isolation and characterization of bacteriophages lytic against clinical strains of *A. hydrophila*, all of which carry intrinsic antibiotic resistance markers. These bacteriophages (LAh1–LAh10) displayed diversity in their morphology and genomic composition. The genomes of LAh1–LAh5 were the most similar to each other, yet specific differences were seen, and these resulted in non-synonymous amino acid changes. These changes may have contributed to the differences in growth kinetics observed between LAh1 and LAh5. Phylogenetic comparison between LAh1 and LAh10 and other *Aeromonas* bacteriophages revealed that LAh1–LAh10 clustered separately to those lytic for environmental strains of *A. hydrophila* and to bacteriophages against other species of *Aeromonas*.

Aeromonas hydrophila has been shown to thrive in water storage tanks and swimming pools as biofilms (Julia Manresa et al., 2009; Chubaka et al., 2018). The persistence of *A. hydrophila* in such environments has been implicated in several diseases such as diarrhea, sepsis and necrotizing fasciitis (Janda and Abbott, 2010). Bacteria growing in biofilm communities are more difficult to control than planktonic ones and *A. hydrophila* in particular is resistant to treatment with antibiotics and disinfectants such as chlorine (Donlan and Costerton, 2002; Janda and Abbott, 2010). Bacteriophages, which have been shown to be safe in clinical applications (Malik et al., 2017; Dedrick et al., 2019;

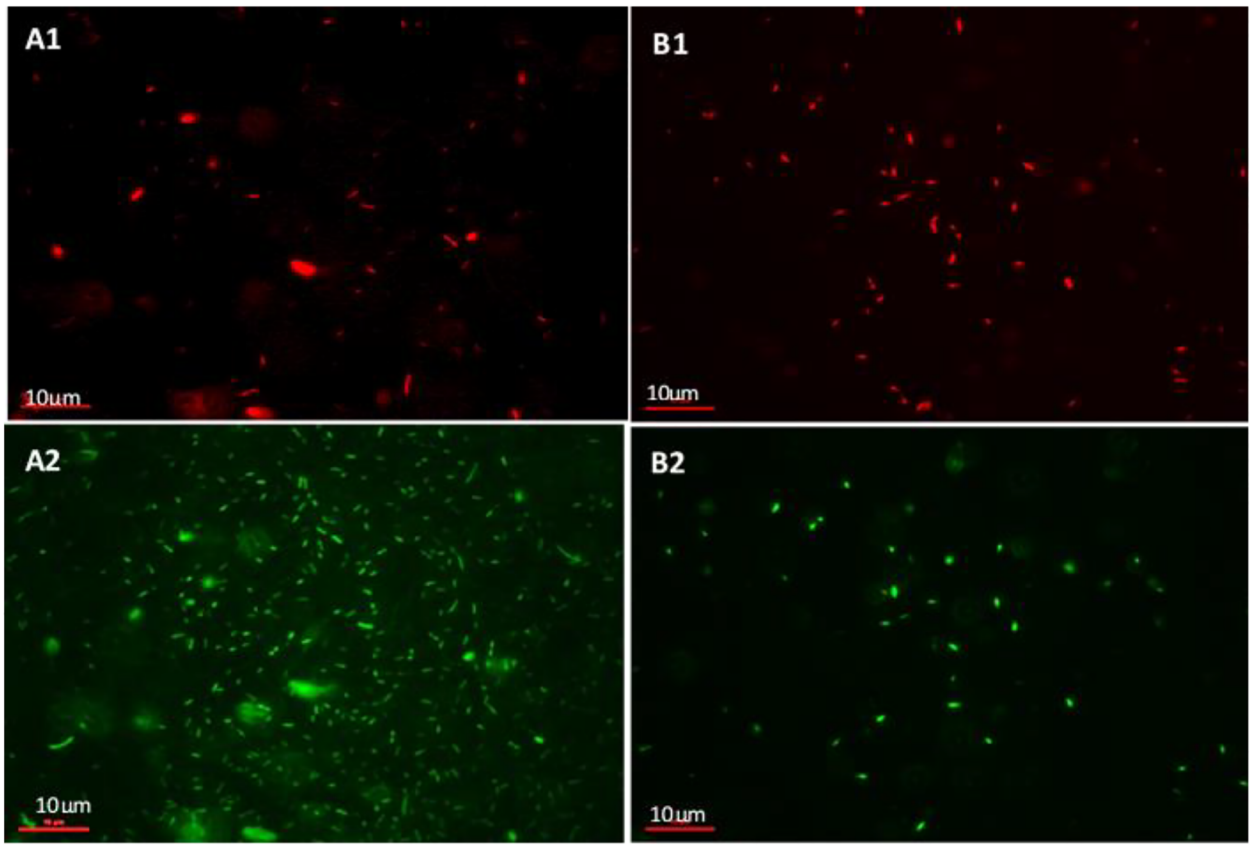

FIGURE 7 | Live/dead staining of *A. hydrophila* biofilm using propidium Iodide (PI) and SYBR gold®. **(A1,A2)** show untreated *A. hydrophila* biofilm on a glass slide. **(A1)** PI stained (dead) cells and **(A2)** cells stained with SYBR gold® (total population of cells). **(B1,B2)** *A. hydrophila* biofilm on a glass slide treated with bacteriophage LAh1 for 60 min. **(B1)** PI stained (dead) cells and **(B2)** cells stained with SYBR gold® (total population of cells).

Nir-Paz et al., 2019; Schmidt, 2019) may provide a useful solution to controlling this bacterium in a changing climate. The bacteriophages isolated and tested in this study were able to significantly reduce the *A. hydrophila* biofilm mass after 24 h of treatment. While these bacteriophages as well as others are active against biofilms (Hansen et al., 2019; Saha and Mukherjee, 2019), the factors associated with their efficacy have not been fully elucidated. The bacteriophages isolated in this study were diverse in morphology, genome content and organization. Their *Podoviridae*, *Siphoviridae*, or *Myoviridae* morphology was not associated with their capacity to disrupt a biofilm. The size of the genome and physical size of the bacteriophages was also not associated with their biofilm disruptive capabilities. However, bacteriophages in this study with a low GC% content and with a higher number of tRNAs had a lower biofilm disruptive efficacy. While we did not assess the GC% content of the *A. hydrophila* strains used for the biofilm assays here, the GC% of *A. hydrophila* published genomes ranged from 60.2 to 61.3% (Chan et al., 2015; Tan et al., 2015a,b; Forn-Cuni et al., 2016a,b; Moura et al., 2017). Assuming our bacterial strains had similar content, then it would appear that bacteriophages in our study which matched more closely the GC% of the bacteria were significantly more successful in degrading biofilms. Bacteria growing in biofilms will slow down their metabolism (Donlan and Costerton, 2002), and this factor may have a greater impact on those bacteriophages that carry their own tRNAs. It is important, however, to highlight that the sample of bacteriophages we assayed in our study was small, and the number of those with and without tRNAs was even smaller. Therefore, more concrete experimental data and extensive sampling is required before definitive conclusions can be drawn from such observations.

While others report that bacteriophage GC% content was related to GC% content of host bacteria (Xia and Yuen, 2005) and that presence of tRNAs was characteristic of more virulent bacteriophages (Bailly-Bechet et al., 2007), in our study there was no apparent relationship between host range and GC% content or number of tRNAs present in bacteriophage genomes. In the bacteriophages isolated here, those with lower GC% content had higher numbers of tRNAs, similar to findings in a study of bacteriophages against *Aeromonas salmonicida* subsp. *Salmonicida* (Vincent et al., 2017). This may not be surprising if we assume that the genomes of *A. hydrophila* used here have a similar GC% content to those previously published [60.2–61.3% (Chan et al., 2015; Tan et al., 2015a,b; Forn-Cuni et al., 2016a,b; Moura et al., 2017)] and that while bacteriophage genomes evolve to match the GC% of their hosts (Xia and Yuen, 2005), those

whose GC content is lower may require tRNAs to complement their biochemical requirements. Finally, certain bacteriophages may code for and transfer ARGs in bacteria through transduction (Gunathilaka et al., 2017; Brown-Jaque et al., 2018; Larranaga et al., 2018; Wang et al., 2018). None of the bacteriophages isolated here were found to code for these, which may be a favorable feature if they were to be used in environmental or clinical settings.

CONCLUSION

We report here a diverse range of novel bacteriophages, LAh1–LAh10, which are the first shown to be active against clinical strains of *A. hydrophila*. While these bacteria may survive decontaminating efforts in water by quorum sensing and forming biofilms, bacteriophages offer the potential of an alternative to control their growth in the environment, as well as following human infection. Functionally, the bacteriophages tested here were capable of *A. hydrophila* biofilm disruption.

DATA AVAILABILITY STATEMENT

The complete genome sequences have been submitted to NCBI GenBank with accession numbers: MK838107, MK838108, MK838109, MK838110, MK838111, MK838112, MK838113, MK838114, MK838115, and MK838116.

AUTHOR CONTRIBUTIONS

JT, HC, and MK: conceptualization. MK, HK, and HC: data collection. MK and TB: genomics. MK, LS, and PL: electron microscope imaging and biofilm. MK, ML, and JT: data analysis. JT, HC, and SP: supervision. MK and JT: writing – original draft. MK, TB, HC, and JT: writing – review and editing.

ACKNOWLEDGMENTS

The authors would like to acknowledge the La Trobe University Bio-imaging Facility (La Trobe Institute for Molecular Science) for the TEM images.

SUPPLEMENTARY MATERIAL

The Supplementary Material for this article can be found online at: https://www.frontiersin.org/articles/10.3389/fmicb.2020.00194/full#supplementary-material

REFERENCES

Aguirre, A. A., and Tabor, G. M. (2008). Global factors driving emerging infectious diseases. *Ann. N. Y. Acad. Sci.* 1149, 1–3. doi: 10.1196/annals.1428.052

Ahmed, W., Huygens, F., Goonetilleke, A., and Gardner, T. (2008). Real-time Pcr detection of pathogenic microorganisms in roof-harvested rainwater in Southeast Queensland, Australia. *Appl. Environ. Microbiol.* 74, 5490–5496. doi: 10.1128/AEM.00331-08

Anand, T., Vaid, R. K., Bera, B., Singh, J., Barua, S., Virmani, N., et al. (2016). Isolation of a lytic bacteriophage against virulent Aeromonas hydrophila from an organized equine farm. *J. Basic Microbiol.* 56, 432–437. doi: 10.1002/jobm.201500318

Azzopardi, E. A., Azzopardi, S. M., Boyce, D. E., and Dickson, W. A. (2011). Emerging gram-negative infections in burn wounds. *J. Burn. Care Res.* 32, 570–576. doi: 10.1097/BCR.0b013e31822ac7e6

Bai, M., Cheng, Y. H., Sun, X. Q., Wang, Z. Y., Wang, Y. X., Cui, X. L., et al. (2019). Nine novel phages from a plateau lake in southwest china: insights into aeromonas phage diversity. *Viruses* 11:E615. doi: 10.3390/v11070615

Bailly-Bechet, M., Vergassola, M., and Rocha, E. (2007). Causes for the intriguing presence of trnas in phages. *Genome Res.* 17, 1486–1495. doi: 10.1101/gr.6649807

Batra, P., Mathur, P., and Misra, M. C. (2016). *Aeromonas* spp.: an emerging nosocomial pathogen. *J. Lab. Physicians* 8, 1–4. doi: 10.4103/0974-2727.176234

Beilstein, F., and Dreiseikelmann, B. (2008). Temperate bacteriophage PhiO18P from an Aeromonas media isolate: characterization and complete genome sequence. *Virology* 373, 25–29. doi: 10.1016/j.virol.2007.11.016

Brown-Jaque, M., Calero-Caceres, W., Espinal, P., Rodriguez-Navarro, J., Miro, E., Gonzalez-Lopez, J. J., et al. (2018). Antibiotic resistance genes in phage particles isolated from human faeces and induced from clinical bacterial isolates. *Int. J. Antimicrob. Agents* 51, 434–442. doi: 10.1016/j.ijantimicag.2017.11.014

Burke, V., Robinson, J., Gracey, M., Peterson, D., Meyer, N., and Haley, V. (1984a). Isolation of *Aeromonas* spp. from an unchlorinated domestic water supply. *Appl. Environ. Microbiol.* 48, 367–370. doi: 10.1128/aem.48.2.367-370.1984

Burke, V., Robinson, J., Gracey, M., Peterson, D., and Partridge, K. (1984b). Isolation of *Aeromonas hydrophila* from a metropolitan water supply: seasonal correlation with clinical isolates. *Appl. Environ. Microbiol.* 48, 361–366. doi: 10.1128/aem.48.2.361-366.1984

Cao, Y., Li, S., Wang, D., Zhao, J., Xu, L., Liu, H., et al. (2019). Genomic characterization of a novel virulent phage infecting the Aeromonas hydrophila isolated from rainbow trout (*Oncorhynchus mykiss*). *Virus Res.* 273:197764. doi: 10.1016/j.virusres.2019.197764

Chan, K. G., Tan, W. S., Chang, C. Y., Yin, W. F., and Mumahad Yunos, N. Y. (2015). Genome sequence analysis reveals evidence of quorum-sensing genes present in aeromonas hydrophila strain M062, Isolated from Freshwater. *Genome Announc.* 3:e00100-15. doi: 10.1128/genomeA.00100-15

Chow, M. S., and Rouf, M. A. (1983). Isolation and partial characterization of two *Aeromonas hydrophila* bacteriophages. *Appl. Environ. Microbiol.* 45, 1670–1676. doi: 10.1128/aem.45.5.1670-1676.1983

Chowdhury, M. A., Yamanaka, H., Miyoshi, S., and Shinoda, S. (1990). Ecology of mesophilic *Aeromonas* spp. in aquatic environments of a temperate region and relationship with some biotic and abiotic environmental parameters. *Zentralbl Hyg Umweltmed* 190, 344–356.

Chubaka, C. E., Whiley, H., Edwards, J. W., and Ross, K. E. (2018). A review of roof harvested rainwater in Australia. *J. Environ. Public Health* 2018, 6471324. doi: 10.1155/2018/6471324

Czaplewski, L., Bax, R., Clokie, M., Dawson, M., Fairhead, H., Fischetti, V. A., et al. (2016). Alternatives to antibiotics-a pipeline portfolio review. *Lancet Infect Dis.* 16, 239–251. doi: 10.1016/S1473-3099(15)00466-1

Darling, A. C., Mau, B., Blattner, F. R., and Perna, N. T. (2004). Mauve: multiple alignment of conserved genomic sequence with rearrangements. *Genome Res.* 14, 1394–1403. doi: 10.1101/gr.2289704

Dedrick, R. M., Guerrero-Bustamante, C. A., Garlena, R. A., Russell, D. A., Ford, K., Harris, K., et al. (2019). Engineered bacteriophages for treatment of a patient with a disseminated drug-resistant Mycobacterium abscessus. *Nat. Med.* 25, 730–733. doi: 10.1038/s41591-019-0437-z

DeNicola, E., Aburizaiza, O. S., Siddique, A., Khwaja, H., and Carpenter, D. O. (2015). Climate change and water scarcity: the case of saudi Arabia. *Ann. Glob. Health* 81, 342–353. doi: 10.1016/j.aogh.2015.08.005

Donlan, R. M., and Costerton, J. W. (2002). Biofilms: survival mechanisms of clinically relevant microorganisms. *Clin. Microbiol. Rev.* 15, 167–193. doi: 10.1128/cmr.15.2.167-193.2002

Dryden, M., and Munro, R. (1989). Aeromonas septicemia: relationship of species and clinical features. *Pathology* 21, 111–114. doi: 10.3109/00313028909059546

Dziewit, L., and Radlinska, M. (2016). Two novel temperate bacteriophages co-existing in Aeromonas sp. *Arm*81 - characterization of their genomes, proteomes and Dna methyltransferases. *J. Gen. Virol.* 97, 2008–2022. doi: 10.1099/jgv.0.000504

Forn-Cuni, G., Tomas, J. M., and Merino, S. (2016a). Genome sequence of *Aeromonas hydrophila* strain Ah-3 (Serotype O34). *Genome Announc.* 4:e00919-16.

Forn-Cuni, G., Tomas, J. M., and Merino, S. (2016b). Whole-genome sequence of *Aeromonas hydrophila* strain Ah-1 (Serotype O11). *Genome Announc.* 4:e00920-16. doi: 10.1128/genomeA.00920-16

Gibb, E. A., and Edgell, D. R. (2007). Multiple controls regulate the expression of mobE, an Hnh homing endonuclease gene embedded within a ribonucleotide reductase gene of phage Aeh1. *J. Bacteriol.* 189, 4648–4661. doi: 10.1128/jb.00321-07

Golkar, Z., Bagasra, O., and Pace, D. G. (2014). Bacteriophage therapy: a potential solution for the antibiotic resistance crisis. *J. Infect Dev. Ctries* 8, 129–136. doi: 10.3855/jidc.3573

Grissa, I., Vergnaud, G., and Pourcel, C. (2007). Crisprfinder: a web tool to identify clustered regularly interspaced short palindromic repeats. *Nucleic Acids Res.* 35, W52–W57.

Gunathilaka, G. U., Tahlan, V., Mafiz, A., Polur, M., and Zhang, Y. (2017). Phages in urban wastewater have the potential to disseminate antibiotic resistance. *Int. J. Antimicrob. Agents* 50, 678–683. doi: 10.1016/j.ijantimicag.2017.08.013

Hansen, M. F., Svenningsen, S. L., Røder, H. L., Middelboe, M., and Burmølle, M. (2019). Big Impact of the Tiny: bacteriophage–bacteria Interactions in Biofilms. *Trends Microbiol.* 27, 739–752. doi: 10.1016/j.tim.2019.04.006

Igbinosa, I. H., Igumbor, E. U., Aghdasi, F., Tom, M., and Okoh, A. I. (2012). Emerging *Aeromonas* species infections and their significance in public health. *Sci. World J.* 2012:625023.

Janda, J. M., and Abbott, S. L. (2010). The genus *Aeromonas*: taxonomy, pathogenicity, and infection. *Clin. Microbiol. Rev.* 23, 35–73. doi: 10.1128/CMR.00039-09

Jia, B., Raphenya, A. R., Alcock, B., Waglechner, N., Guo, P., Tsang, K. K., et al. (2017). Card 2017: expansion and model-centric curation of the comprehensive antibiotic resistance database. *Nucleic Acids Res.* 45, D566–D573. doi: 10.1093/nar/gkw1004

Julia Manresa, M., Vicente Villa, A., Gene Giralt, A., and Gonzalez-Ensenat, M. A. (2009). Aeromonas hydrophila folliculitis associated with an inflatable swimming pool: mimicking *Pseudomonas aeruginosa* infection. *Pediatr. Dermatol.* 26, 601–603. doi: 10.1111/j.1525-1470.2009.00993.x

Jun, J. W., Kim, J. H., Shin, S. P., Han, J. E., Chai, J. Y., and Park, S. C. (2013). Protective effects of the *Aeromonas* phages pAh1-C and pAh6-C against mass mortality of the cyprinid loach (*Misgurnus anguillicaudatus*) caused by Aeromonas hydrophila. *Aquaculture* 416, 289–295. doi: 10.1016/j.aquaculture.2013.09.045

Kazimierczak, J., Wojcik, E. A., Witaszewska, J., Guzinski, A., Gorecka, E., Stanczyk, M., et al. (2019). Complete genome sequences of *Aeromonas* and *Pseudomonas* phages as a supportive tool for development of antibacterial treatment in aquaculture. *Virol. J.* 16:4. doi: 10.1186/s12985-018-1113-5

Larranaga, O., Brown-Jaque, M., Quiros, P., Gomez-Gomez, C., Blanch, A. R., Rodriguez-Rubio, L., et al. (2018). Phage particles harboring antibiotic resistance genes in fresh-cut vegetables and agricultural soil. *Environ. Int.* 115, 133–141. doi: 10.1016/j.envint.2018.03.019

Laslett, D., and Canback, B. (2004). Aragorn, a program to detect trna genes and tmrna genes in nucleotide sequences. *Nucleic Acids Res.* 32, 11–16. doi: 10.1093/nar/gkh152

Le, T. S., Nguyen, T. H., Vo, H. P., Doan, V. C., Nguyen, H. L., Tran, M. T., et al. (2018). Protective effects of *Bacteriophages against Aeromonas hydrophila* species causing motile *Aeromonas* septicemia (Mas) in striped catfish. *Antibiotics* 7, E16. doi: 10.3390/antibiotics7010016

Lowe, T. M., and Chan, P. P. (2016). trnascan-Se On-line: integrating search and context for analysis of transfer Rna genes. *Nucleic Acids Res.* 44, W54–W57. doi: 10.1093/nar/gkw413

Malik, D. J., Sokolov, I. J., Vinner, G. K., Mancuso, F., Cinquerrui, S., Vladisavljevic, G. T., et al. (2017). Formulation, stabilisation and encapsulation of bacteriophage for phage therapy. *Adv. Colloid. Interface Sci.* 249, 100–133. doi: 10.1016/j.cis.2017.05.014

Mateos, D., Anguita, J., Naharro, G., and Paniagua, C. (1993). Influence of growth temperature on the production of extracellular virulence factors and pathogenicity of environmental and human strains of *Aeromonas hydrophila*. *J. Appl. Bacteriol.* 74, 111–118. doi: 10.1111/j.1365-2672.1993.tb03003.x

Merino, S., Camprubi, S., and Tomas, J. M. (1990a). Isolation and characterization of bacteriophage Pm2 from Aeromonas hydrophila. *Fems Microbiol. Lett.* 56, 239–244. doi: 10.1111/j.1574-6968.1990.tb13944.x

Merino, S., Camprubi, S., and Tomas, J. M. (1990b). Isolation and characterization of bacteriophage Pm3 from Aeromonas hydrophila the bacterial receptor for which is the monopolar flagellum. *Fems Microbiol. Lett.* 57, 277–282. doi: 10.1111/j.1574-6968.1990.tb04244.x

Merritt, J. H., Kadouri, D. E., and O'toole, G. A. (2005). Growing and analyzing static biofilms. *Curr. Protoc. Microbiol.* 1:Unit 1B.1. doi: 10.1002/9780471729259.mc01b01s00

Mount, D. W. (2007). Using the basic local alignment search tool (Blast). *Csh. Protoc.* 2007:dbto17. doi: 10.1101/pdb.top17

Moura, Q., Fernandes, M. R., Cerdeira, L., Santos, A. C. M., De Souza, T. A., Ienne, S., et al. (2017). Draft genome sequence of a multidrug-resistant *Aeromonas hydrophila* St508 strain carrying rmtD and blactx-M-131 isolated from a bloodstream infection. *J. Glob. Antimicrob. Resist.* 10, 289–290. doi: 10.1016/j.jgar.2017.07.007

Neyts, K., Huys, G., Uyttendaele, M., Swings, J., and Debevere, J. (2000). Incidence and identification of mesophilic *Aeromonas* spp. from retail foods. *Lett. Appl. Microbiol.* 31, 359–363. doi: 10.1046/j.1472-765x.2000.00828.x

Nir-Paz, R., Gelman, D., Khouri, A., Sisson, B. M., Fackler, J., Alkalay-Oren, S., et al. (2019). Successful treatment of antibiotic resistant poly-microbial bone infection with bacteriophages and antibiotics combination. *Clin. Infect Dis.* 69, 2015–2018. doi: 10.1093/cid/ciz222

Picard, B., and Goullet, P. (1987). Seasonal prevalence of nosocomial *Aeromonas hydrophila* infection related to aeromonas in hospital water. *J. Hosp. Infect.* 10, 152–155. doi: 10.1016/0195-6701(87)90141-1

Rasmussen-Ivey, C. R., Figueras, M. J., Mcgarey, D., and Liles, M. R. (2016). Virulence Factors of *Aeromonas hydrophila*: in the wake of reclassification. *Front. Microbiol.* 7:1337. doi: 10.3389/fmicb.2016.01337

Saha, D., and Mukherjee, R. (2019). Ameliorating the antimicrobial resistance crisis: phage therapy. *Iubmb. Life* 71, 781–790. doi: 10.1002/iub.2010

Schmidt, C. (2019). Phage therapy's latest makeover. *Nat. Biotechnol.* 37, 581–586. doi: 10.1038/s41587-019-0133-z

Shen, C. J., Liu, Y. J., and Lu, C. P. (2012). Complete genome sequence of *Aeromonas hydrophila* Phage Cc2. *J. Virol.* 86:10900. doi: 10.1128/JVI.01882-12

Sinclair, H. A., Heney, C., Sidjabat, H. E., George, N. M., Bergh, H., Anuj, S. N., et al. (2016). Genotypic and phenotypic identification of Aeromonas species and CphA-mediated carbapenem resistance in Queensland, Australia. *Diagn. Microbiol. Infect Dis.* 85, 98–101. doi: 10.1016/j.diagmicrobio.2016.02.005

Talagrand-Reboul, E., Jumas-Bilak, E., and Lamy, B. (2017). The social life of aeromonas through biofilm and quorum sensing systems. *Front. Microbiol.* 8:37. doi: 10.3389/fmicb.2017.00037

Tan, W. S., Yin, W. F., and Chan, K. G. (2015a). Insights into the quorum-sensing activity in *Aeromonas hydrophila* strain M013 as revealed by whole-genome sequencing. *Genome Announc.* 3:e01372-14. doi: 10.1128/genomeA.01372-14

Tan, W. S., Yin, W. F., Chang, C. Y., and Chan, K. G. (2015b). Whole-genome sequencing analysis of quorum-sensing *Aeromonas hydrophila* Strain M023 from freshwater. *Genome Announc.* 3:e01548-14. doi: 10.1128/genomeA.01548-14

Vally, H., Whittle, A., Cameron, S., Dowse, G. K., and Watson, T. (2004). Outbreak of *Aeromonas hydrophila* wound infections associated with mud football. *Clin. Infect. Dis.* 38, 1084–1089. doi: 10.1086/382876

Varela, A. R., Nunes, O. C., and Manaia, C. M. (2016). Quinolone resistant *Aeromonas* spp. as carriers and potential tracers of acquired antibiotic resistance

in hospital and municipal wastewater. *Sci. Total Environ.* 542, 665–671. doi: 10.1016/j.scitotenv.2015.10.124

Vincent, A. T., Paquet, V. E., Bernatchez, A., Tremblay, D. M., Moineau, S., and Charette, S. J. (2017). Characterization and diversity of phages infecting *Aeromonas salmonicida* subsp. *salmonicida*. *Sci. Rep.* 7:7054. doi: 10.1038/s41598-017-07401-7

Wang, J. B., Lin, N. T., Tseng, Y. H., and Weng, S. F. (2016). Genomic characterization of the novel *Aeromonas hydrophila* phage ahp1 suggests the derivation of a new subgroup from phikmv-like family. *PloS One* 11:e0162060. doi: 10.1371/journal.pone.0162060

Wang, Q., Zeng, X., Yang, Q., and Yang, C. (2018). Identification of a bacteriophage from an environmental multidrug-resistant *E. coli* isolate and its function in horizontal transfer of Args. *Sci. Total Environ.* 639, 617–623. doi: 10.1016/j.scitotenv.2018.05.213

World Health Organisation [WHO] (2014). *Antimicrobial Resistance: Global Report on Surveillance 2014*. Geneva: WHO.

Xia, X., and Yuen, K. Y. (2005). Differential selection and mutation between dsdna and ssdna phages shape the evolution of their genomic At percentage. *Bmc Genet.* 6:20.

Yu, H. B., Kaur, R., Lim, S., Wang, X. H., and Leung, K. Y. (2007). Characterization of extracellular proteins produced by Aeromonas hydrophila Ah-1. *Proteomics* 7, 436–449. doi: 10.1002/pmic.200600396

Yuan, S., Chen, L., Liu, Q., Zhou, Y., Yang, J., Deng, D., et al. (2018). Characterization and genomic analyses of Aeromonas hydrophila phages AhSzq-1 and AhSzw-1, isolates representing new species within the T5virus genus. *Arch. Virol.* 163, 1985–1988. doi: 10.1007/s00705-018-3805-y

Conflict of Interest: The authors declare that the research was conducted in the absence of any commercial or financial relationships that could be construed as a potential conflict of interest.

Copyright © 2020 Kabwe, Brown, Speirs, Ku, Leach, Chan, Petrovski, Lock and Tucci. This is an open-access article distributed under the terms of the Creative Commons Attribution License (CC BY). The use, distribution or reproduction in other forums is permitted, provided the original author(s) and the copyright owner(s) are credited and that the original publication in this journal is cited, in accordance with accepted academic practice. No use, distribution or reproduction is permitted which does not comply with these terms.

frontiers in Microbiology

ORIGINAL RESEARCH
published: 21 February 2020
doi: 10.3389/fmicb.2020.00259

Isolation and Characterization of the Novel Phages vB_VpS_BA3 and vB_VpS_CA8 for Lysing *Vibrio parahaemolyticus*

Meiyan Yang[1,2†], Yongjian Liang[1,2†], Shixuan Huang[2], Jumei Zhang[1,2], Jing Wang[2], Hanfang Chen[1,2], Yuanming Ye[1,2], Xiangyang Gao[3], Qingping Wu[1,2] and Zhiyuan Tan[1]**

[1] College of Agriculture, South China Agricultural University, Guangzhou, China, [2] State Key Laboratory of Applied Microbiology Southern China, Guangdong Provincial Key Laboratory of Microbiology Culture Collection and Application, Guangdong Open Laboratory of Applied Microbiology, Guangdong Institute of Microbiology, Guangzhou, China, [3] Guangdong Provincial Key Laboratory of Nutraceuticals and Functional Foods, College of Food Science, South China Agricultural University, Guangzhou, China

OPEN ACCESS

Edited by:
Sutthirat Sitthisak,
Naresuan University, Thailand

Reviewed by:
Yong Jiang,
Ocean University of China, China
Aunchalee Thanwisai,
Naresuan University, Thailand
Rapee Thummeepak,
Naresuan University, Thailand, in collaboration with reviewer AT

***Correspondence:**
Qingping Wu
wuqp203@163.com
Zhiyuan Tan
zytan@scau.edu.cn

[†]These authors have contributed equally to this work

Specialty section:
This article was submitted to Virology, a section of the journal Frontiers in Microbiology

Received: 17 September 2019
Accepted: 04 February 2020
Published: 21 February 2020

Citation:
Yang M, Liang Y, Huang S, Zhang J, Wang J, Chen H, Ye Y, Gao X, Wu Q and Tan Z (2020) Isolation and Characterization of the Novel Phages vB_VpS_BA3 and vB_VpS_CA8 for Lysing Vibrio parahaemolyticus. Front. Microbiol. 11:259. doi: 10.3389/fmicb.2020.00259

Accumulating evidence has indicated that the multiple drug resistant *Vibrio parahaemolyticus* may pose a serious threat to public health and economic concerns for humans globally. Here, two lytic bacteriophages, namely vB_VpS_BA3 and vB_VpS_CA8, were isolated from sewage collected in Guangzhou, China. Electron microscopy studies revealed both virions taxonomically belonged to the *Siphoviridae* family with icosahedral head and a long non-contractile tail. The double-stranded DNA genome of phage BA3 was composed of 58648 bp with a GC content of 46.30% while phage CA8 was 58480 bp with an average GC content of 46.42%. In total, 85 putative open reading frames (ORFs) were predicted in the phage BA3 genome while 84 were predicted in that of CA8. The ORFs were associated with phage structure, packing, host lysis, DNA metabolism, and additional functions. Furthermore, average nucleotide identity analysis, comparative genomic features and phylogenetic analysis revealed that BA3 and CA8 represented different isolates but novel members of the family, *Siphoviridae*. Regarding the host range of the 61 *V. parahaemolyticus* isolates, BA3 and CA8 had an infectivity of 8.2 and 36.1%, respectively. Furthermore, ∼100 plaque-forming units (pfu)/cell for phage BA3 and ∼180 pfu/cell for phage CA8 were determined to be the viral load under laboratory growth conditions. Accordingly, the phage-killing assay *in vitro* revealed that phage CA8 achieved approximately 3.65 log unit reductions. The present results indicate that CA8 is potentially applicable for biological control of multidrug resistant *V. parahaemolyticus*.

Keywords: *Vibrio parahaemolyticus*, *Vibrio* phage, *Siphoviridae*, lytic bacteriophages, biocontrol, aquaculture

INTRODUCTION

The Food and Agriculture Organization of the United Nations (FAO) reported that gains sufficient and nutritious food is jeopardized by the rapid increase in the human population (FAO, 2019a). As a result, aquaculture, the farming of aquatic organisms, has been a crucial activity that has contributed to aquatic-sourced foods for national food security and economic development.

Currently, valuable aquatic species, such as farmed shrimp, marine fish, and freshwater fish, are considered as commodities for the export market and monetary gain. Total production of global farmed shrimp reached almost 4 million ton in 2018, increasing by 3 to 5% over 2017 (FAO, 2019a). Global fish production was also estimated to increase by 2.1% to 178.8 million ton in 2018, with 87 million tons (48.7%) being derived from aquaculture and 91.8 million tons (51.3%) from capture fisheries (FAO, 2019a). Such substantial change in the aquaculture sector resulted in the amount of wild capture fisheries for human consumption being surpassed. Moreover, consumer behaviors have become increasingly universal, especially in developed countries and China. For example, the US per capita shrimp consumption is bound to be historically high, crossing the 4.5-lb maximum in 2018 (FAO, 2019a). Mainland China produced 66.8 million ton of fish for human consumption in 2016, with 49.2 million ton (74%) from aquaculture and 17.6 million ton (26%) from wild capture (FAO, 2019b).

Unfortunately, aquaculture-associated bacterial diseases, which are typically caused by *Vibrio parahaemolyticus*, are considered to be a challenge to food safety, economic development, and human health. *V. parahaemolyticus* is a gram-negative bacterium that has been commonly associated with infections in aquatic organisms in aquaculture farm and the wild. The cost of such disease is significantly greater than previous official estimates and demonstrates the serious problems exerted by foodborne illnesses (commonly known as food poisoning) on social and economic systems. Anyone who consumes raw or undercooked fish, shrimp, shellfish, and other seafood is at risk of contracting *V. parahaemolyticus* (Thompson et al., 2004). Foodborne illness, which is closely related to *V. parahaemolyticus*, is often caused by consuming food contaminated by bacteria and their toxins, such as thermostable direct hemolysin (TDH), TDH-related hemolysin (TRH), and type III secretion system 1 (T3SS1) and system 2 (T3SS2) (Raimondi et al., 2000; Naim et al., 2001; Park et al., 2004; Hiyoshi et al., 2010; Letchumanan et al., 2014; Paria et al., 2019). Most people infected with *V. parahaemolyticus* develop symptoms such as diarrhea, vomiting, abdominal cramps, nausea, fever, and stomach pain after approximately 24 h. Moreover, diarrhea tends to be watery and is occasionally bloody. In total, 26 laboratory-confirmed cases of *V. parahaemolyticus* infections were reported in people who ate fresh crab meat from Venezuela on September 27, 2018 (FDA, 2018). When penicillin was discovered in the 1920s, antimicrobial agents were a crucial practice in animal therapy (Aarestrup and Wegener, 1999). Currently, to rapidly and effectively control and terminate the proliferation of pathogenic *Vibrio* sp., the prophylactic and therapeutic use of antibiotics has been widely employed in hatcheries, the transportation and sales chain; this is despite urgent concerns regarding the development and dispersal of multiple antibiotic-resistance in the pathogen community. Indeed, microbiological risk assessments revealed that both aquatic products and ready-to-eat foods in China can be contaminated by antimicrobial-resistant *V. parahaemolyticus*, with the highest resistance rates observed against streptomycin (Xie et al., 2015, 2016, 2017; Xu et al., 2016). Evidently, as antibiotic-resistant strains cause treatment failure, inducing the violent death of these bacteria is a challenge. Increasing researches have indicated that the multiple drug resistant *V. parahaemolyticus* may pose an especially serious threat to public health and economic concerns for humans globally (Lesmana et al., 2001; Ottaviani et al., 2013; Kang et al., 2017). To prevent and control contaminated *V. parahaemolyticus* in aquatic products, an effective practice instead of the abuse of antibiotics is an evident resolution for the economy and food safety.

Bacteriophages (phages) are the most abundant type of biological particles on Earth. They are composed of either DNA or RNA enclosed in a protein coat (Hendrix, 2003). Phage genomes contain a very high proportion of novel genetic sequences of unknown function, and may represent the largest reservoir of unexplored genes (Hatfull, 2008). Unlike antibiotics, lytic phage multiplication in the host (attachment, penetration, biosynthesis, maturation, assembly, and release) can control and kill the bacterium (Yang Z. et al., 2019). With the inevitable and frequent occurrence of drug-resistant pathogenic bacteria and the sharp decline in novel antibiotic discovery, research, and application, phage therapy is regaining attention after years of continuous worsening of antibiotic resistance owing to the great potential of cell disruption by bacteria (Carlton, 1999; Lu and Collins, 2007, 2009). Nowadays, several studies for identification and characterization as well as animal application of *Vibrio* phages have been carried out, including phages pVp 1, A3S, Vpms1, VP-1, VP-2, VP-3, VPp1, Vpp1, Vpp2, Vpp3, Vpp4, Vpp5, Vpp6, VP1, VP7, VP9, OWB, vB_VpaP_VP-ABTNL-1, and vB_VpaS_VP-ABTNL-2 (Jun et al., 2014; Lomelí-Ortega and Martínez-Díaz, 2014; Mateus et al., 2014; Rong et al., 2014; Alagappan et al., 2016; Chang et al., 2016; Zhang et al., 2016; Ren et al., 2019). Therefore, phage therapy is considered to be an environmentally friendly practice with huge potential to reduce and control drug-resistant *V. parahaemolyticus* in aquaculture.

MATERIALS AND METHODS

Bacterial Strains and Phage Isolation

All *V. parahaemolyticus* strains in our work were provided by the Guangdong Institute of Microbiology and stored at −80°C in 15% (v/v) glycerol and cultivated at 37°C, with shaking at 200 rpm in Trypto soya broth (TSB). The *Vibrio* phages were isolated from sewage samples collected in the Huangsha aquatic product market, from the host, *V. parahaemolyticus* O1-1 and O3-11. Phage concentration from the fluid sample was used for membrane filter adsorption and elution as described before (Van Twest and Kropinski, 2009). The water sample was centrifuged at 8000 × *g* for 10 min at room temperature and filtered (0.45-μm syringe filter) to remove large particulates and bacteria. Solid $MgSO_4$ was added to a final concentration of 50 mM and the mixture was filtered slowly through the 0.45-μm (47 mm diameter) mixed cellulose ester GSWP filter. Before placement in the ultrasonic cleaning bath for 10 min, the filter was cut into many pieces, which were then placed in a flask with 50 mL of eluting solution [1% (w/v) Bacto beef extract and 3% (v/v) Tween 80]. To culture the lytic phage of the target

host, the filtered phage concentrate (2.5 mL) was mixed with 2.5 mL of sterile double-strength TSB (4 mM $CaCl_2$) and 100 μL culture (OD_{600} ∼0.2) of *V. parahaemolyticus* isolate (O1-1/O3-11), and then incubated at 37°C for 24 h with shaking. The mixed culture was then centrifuged at 8000 × *g* for 5 min at room temperature and the supernatant was filtered (0.45-μm syringe filter) to remove residual bacterial cells. The process of phage enrichment was repeated at least three times. A 100-μL diluted sample of the phage culture was mixed with 100 μL of *V. parahaemolyticus* cells (mid-log phase) and incubated at 37°C for 15 min. Approximately 5 mL of the top agar (TSB with 0.4% agar) at 45°C was then added, and the mixture was poured onto a TSA plate. The plates of phage BA3/CA8 were then incubated at 37°C for 5 h/8 h to obtain phage plaques. Purification of the two phages was performed at least 10 times. Lastly, purified and targeted phages were stored at 4°C in TSB for 1 month and −80°C in 30% (v/v) glycerol.

CsCl Gradient Purification and Electron Microscopic Analysis

Isopycnic centrifugation through CsCl gradients was performed as previously described, with modifications (Ajuebor et al., 2018). A high titer phage lysate was precipitated using polyethylene glycol (15% w/v PEG8000, 0.5M NaCl) at 4°C overnight and centrifuged at 12000 × *g* for 20 min at 4°C. Thereafter, the pellet was resuspended in SM buffer. The resulting phage preparation was placed on a CsCl step gradient composed of 1.3, 1.5, and 1.7 g/mL layers and spun in a SW 41 Ti rotor (Optima XPN-100 ultracentrifuge, Beckman Coulter, Brea, CA, United States) at 200600 × *g* (34200 rpm) for 3 h at 4°C. The collected phage could be used for electron microscopic analysis. The prepared phages were placed on freshly-prepared carbon films with 2% (w/v) uranyl acetate. Morphological characteristics were observed under a transmission electron microscope (TEM, Hitachi H-7650) at an acceleration voltage of 80 kV with a CDD camera.

DNA Extraction and Genome Sequencing

Genomic DNA was extracted from BA3/CA8 based on a method described in a previous work, with some modifications (Xing et al., 2017). In brief, DNase I and RNase A were added to the phage preparation to a final concentration of 0.1 Units/μL and 3 μg/mL. The mixture was incubated for 1 h at 37°C. After subsequent treatment with SDS, EDTA, and proteinase K, the mixture was further incubated for 30 min at 65°C. An equal volume of phenol was added for DNA extraction. After centrifugation at 12000 × *g* for 5 min at room temperature, the aqueous layer was transferred to a fresh tube containing an equal volume of phenol-chloroform-isoamyl alcohol (25:24:1) and then centrifuged at 12000 × *g* for 5 min at room temperature. The aqueous layer was collected, mixed with an equal volume of isopropanol, and stored for 30 min at −20°C. The mixture was then centrifuged at 4°C for 20 min at 12,000 × *g*, and the DNA pellet was washed twice with 75% ethanol. Lastly, the DNA was air dried at room temperature, resuspended in deionized water, and stored at −20°C.

To obtain the viral DNA required for high-throughput sequencing (HTS), the absence of free and contaminating bacterial DNA was validated via PCR amplification of the bacterial 16S rRNA gene with universal primers, 27F/1492R (Jin et al., 2019). Thereafter, the extracted BA3/CA8 genomic DNA was sequenced using the semiconductor sequencer in an Ion Torrent™ Personal Genome Machine. This technology used emulsion PCR and a sequencing-by-synthesis approach. The integrity and size of DNA preparation were validated by gel electrophoresis. Sonication of genomic DNA was performed on the Covaris® S2 or S220 Systems to generate DNA fragments suitable for 500-base-read libraries for end-repair. These DNA fragments were then ligated to Ion Xpress™ Barcode Adaptors Kits for subsequent nick repair and purification with Agencourt® AMPure® XP Reagent. Purified DNA fragments of ∼500 bp were selected by using E-Gel® SizeSelect™ agarose gel. After amplification and purification of the selected library, emulsion PCR was used for processing. PCR was performed in a water-in-oil microreactor containing a single DNA molecule on a bead. The H^+ Ion Torrent™ signal was detected during the sequencing-by-synthesis process. High quality reads were assembled using the SPAdes v. 3.6.2 program (Bankevich et al., 2012).

Bioinformatic Analysis

Before complete genome analysis, DNA terminus was identified by CLC Genomics Workbench to initially derive high-frequency sequences (HFSs) in next generation sequencing reads. Briefly, HTS data were aligned to the reference assembly using a CLC Genomics Workbench. The CLC module was used with default parameters (mismatch cost 2, insertion cost 3, deletion cost 3, length fraction 0.5, and similarity 0.8) using FASTQ files as the read input and FASTA files as the reference input. Furthermore, High Occurrence Read Termini theory was performed to study the phage genome termini and support the result (Zhang et al., 2018). Firstly, nucleotide sequence data of the phage was analyzed with the nucleotide BLAST search program[1] at the National Centre for Biotechnology Information (NCBI). Furthermore, the average nucleotide identity (ANI) was determined among all pairwise combinations of phage genomes, using the BLASTN alignment tool in the pyani package and plotted in an interactive heatmap using heatmaply to identify phages (Pritchard et al., 2016). Secondly, a putative open reading frame (ORF) was automatically predicted by Prokka 1.1.3 and functional annotation was re-screened by BLASTp against the Non-Redundant Protein Database of NCBI, where the score was set > 50 and e-value $< 1.0 \times 10^{-3}$ (Seemann, 2014). The functional protein characteristics were predicted with the proteomic tools, InterPro (Mitchell et al., 2019). The virulence signature was determined using the Virulence Factor Database (Liu et al., 2019). A coverage of 95% and identity of 90% for any sequence were required. Artemis Comparison Tool (ACT) was used for comparison to other phages in GenBank and identification of feature variations between the genomes of phages, with homology assessed

[1] https://blast.ncbi.nlm.nih.gov/Blast.cgi

using BLASTN (Carver et al., 2005). Global genome comparison map among available phage data in NCBI were visualized by the Easyfig 2.2.3 visualization tool (Sullivan et al., 2011). Lastly, based on the major capsid protein and terminase large subunit, phylogenetic analysis was performed with MEGA X by the neighbor-joining method with 1000 bootstrap replicates (Kumar et al., 2018).

Identification of Proteins Associated With Phage Virions

Samples of the phage were added to the RIPA lysis buffer for protein extraction. Fifty micrograms of protein was transferred into Microcon devices YM-10 (Millipore) and centrifuged at 12000 × *g* at 4°C for 10 min. Subsequently, 200 μL of 50 mM ammonium bicarbonate was added to the concentrate, followed by centrifugation; this step was repeated once. After being reduced by 10 mM DTT at 56°C for 1 h and alkylated by 20 mM IAA at room temperature in dark for 1 h, the mixture was centrifuged at 12000 × *g* at 4°C for 10 min and wash once with 50 mM ammonium bicarbonate. Hundred microliters of 50 mM ammonium bicarbonate and free trypsin were added into the protein solution at a ratio of 1:50, and the solution was incubated overnight at 37°C. The mixture was centrifuged at 12000 × *g* at 4°C for 10 min. Hundred microliters of 50 mM ammonium bicarbonate was added into the device and centrifuged; this step was repeated once. The extracted peptides were lyophilized to near dryness and subsequently resuspend in 50 μL of 0.1% formic acid before LC-MS/MS analysis. The raw MS data were analyzed and searched against the target protein database, based on the species of the samples using MaxQuant 1.6.2.10. The experiment was repeated three times for each phage.

Phage Titer Assay

Determining the concentration of infectious phage particles is a fundamental protocol for researchers working with bacterial viruses. Phage titer for each experiment was determined by the double agar overlay plaque assay as previously-described with some modifications (Kropinski et al., 2009). Briefly, a 100-μL dilution of the phage culture and 100 μL of *V. parahaemolyticus* cells (mid-log phase) were added to 5 mL of top agar (2 mM $CaCl_2$) at 45°C. To form more obvious phage plaques, 0.2% of agar was used in this top plate. Thereafter, the mixture was poured onto a TSA plate and incubated at 37°C for 5 h/8 h to obtain phage plaques for phage BA3/CA8. This assay of suitable dilution was performed with three replicate plates for each dilution. Lastly, we determined the titer of the original phage culture by using the following calculation formula: number of plaques × 10 × reciprocal of counted dilution = pfu/mL.

Phage Host Range Determination

A host range assay was performed for phages BA3 and CA8 using a previously-described protocol for the spot assay with some modifications (Kutter, 2009). Briefly, 100 μL of bacteria in the mid-log phase and 5 mL of TSB containing 0.4% agar (2 mM $CaCl_2$) were mixed and poured onto the TSA plate. After a 5-min standing at room temperature, 2 μL of the 10-fold serially diluted phages in TSB were spotted onto TSB soft agar. The plates were then incubated at 37°C and examined for plaques after 3–24 h. Bacterial sensitivity to a phage was established by a lysis cleared zone at the spot. Based on the clarity of the spot, bacteria were divided into two categories: clear lysis zone (+) and no lysis zone (−).

Optimal Multiplicity of Infection (MOI) Determination and One-Step Growth Assays

To determine the optimal MOI, serial dilutions of *V. parahaemolyticus* O1-1/O3-11 grown to its exponential phase were added to Li et al. (2019) aliquots of a stock solution of BA3/CA8. Based on the proportion of infection, ratios of 0.0001, 0.001, 0.01, 0.1, 1, 10, and 100, plus 100 μL of phage and 100 μL of *V. parahaemolyticus* (1×10^8 cfu/mL) were added to 5 mL of TSB (2 mM $CaCl_2$). Thereafter, the mixtures were shaken at 37°C for 10 h, centrifuged at 8000 × *g* for 5 min at room temperature for cell removal. The precipitate was then removed and the supernatant was filtered through a 0.45-μm membrane. The titer of the phage was determined by a soft agar overlay method. The one which obtained the highest phage titer was the optimal MOI. Three parallel experiments were performed for this MOI test.

The one-step growth curve was generated according to a previous report with minor modifications (Yin et al., 2019). *V. parahaemolyticus* culture (5 mL) was incubated to $OD_{600} = 0.2$ and the bacterial cell suspension was diluted to 1.0×10^8 cfu/mL. Thereafter, the bacterial cells (1 mL) were pelleted via centrifugation (8000 × *g*, 5 min, room temperature), re-suspended in SM buffer (0.9 ml), and mixed with 0.1 mL of a 1.0×10^8 pfu/mL phage suspension (MOI = 0.1, 2 mM $CaCl_2$). The mixture was incubated for 15 min at 37°C. After centrifugation (12,000 × *g*, 2 min, room temperature), the supernatant with free phage was removed and the pellet was suspended in 10 mL TSB (2 mM $CaCl_2$). The mixture was then incubated at 37°C with shaking (200 rpm). Every 10 min, the phage titer was determined via the double-layer agar technique. Burst size was calculated as the ratio of the final count of liberated phage particles to the initial count of infected bacterial cells during the latent period.

Resistance to Environmental Stresses

Heat and pH stability tests were conducted for the phages following a previously-described protocol with some modifications (Laemmli, 1970). Phage suspension (1×10^8 pfu/mL) for each temperature was carried out in a 1.5-mL tube and kept at different water bath temperatures (20, 37, 40, 50, 60, 70, and 80°C) for 1 h. Phage suspensions were incubated at the corresponding selected temperatures. To determine phage pH stability, a gradient of pH was derived to range from 3 to 11. For this experiment, phage suspension (1 mL) was added to the tryptic soy broth (9 mL) with a specific pH followed by incubation at 37°C for 1 h. Three parallel experiments were performed for the stability of the two phages and phage titer was determined via the double-layer agar technique.

In vitro Phage-Killing Assay

Bacterial killing assays were conducted for the phages following a previously-described method with some modifications (Yen et al., 2017). Briefly, 1 mL overnight cultures of *V. parahaemolyticus* isolate (O1-1/O3-11) were added into 50 mL TSB (2 mM $CaCl_2$) and grown to 10^8 cfu/mL at 37°C with shaking (200 rpm), respectively. Bacterial cultures were mixed with phage lysates (MOI 0.1) and incubated for 15 min at 37°C. After that, The mixture was then incubated at 37°C with shaking (200 rpm). At each time point, bacteria were collected, serially diluted, plated onto TSA, and incubated at 37°C for 24 h. Colonies were enumerated to calculate *V. parahaemolyticus* cfu/mL. Each condition was assessed in triplicate.

Statistical Analysis

Data are expressed as means and standard deviation values. GraphPad Prism 8.0.1 was used for statistical analysis.

Nucleotide Sequence Accession Number

The sequence data for the *Vibrio* phages, vB_VpS_BA3 and vB_VpS_CA8, were deposited at GenBank under accession numbers, MN175679 and MN102376.

RESULTS AND DISCUSSION

Origin and Morphology of Phages BA3 and CA8

Several water samples from aquatic product markets were collected and tested for the presence of bacteriophages against *V. parahaemolyticus* isolates. Based on the clear phage plaque on the plate, the targeted phages were purified using the double-layer agar technique. In this study, phages with lytic activity, designated as vB_VpS_BA3 (phage BA3) and vB_VpS_CA8 (phage CA8), were isolated using the double-layer agar assay technique. Our results suggested that phages can be found in virtually all places where their related hosts exist. Several other investigations reported the presence of *Vibrio*-specific lytic phages in environmental water (shrimp ponds, aquaculture system, sea water and aquatic product market) from different regions of the world (Alagappan et al., 2010; Luo et al., 2016; Stalin and Srinivasan, 2016; Katharios et al., 2017; Srinivasan and Ramasamy, 2017; Yang M. et al., 2019).

To date, bacteriophages are classified based on differences in the morphology of their virion. Results from TEM revealed that BA3 (**Figure 1A**) and CA8 (**Figure 1B**) consist of an icosahedral head and a long non-contractile tail. The measurements of head length, head diameter, and tail length of BA3 were 70, 55, and 130 nm while those of CA8 were 70, 55, and 125 nm. By combining their morphological characteristics with the formal guidelines of the International Committee on Taxonomy of Viruses, phages BA3 and CA8 exhibited typical characteristics of phages belonging to the family, *Siphoviridae*, in the order, *Caudovirales* (Lefkowitz et al., 2018). A similar morphological observation was reported for the *Vibrio* phage, VpKK5 (Lal et al., 2016). In previously-reported scientific literature, over 95% of the identified phages were classified as *Caudovirales* (tailed phages).

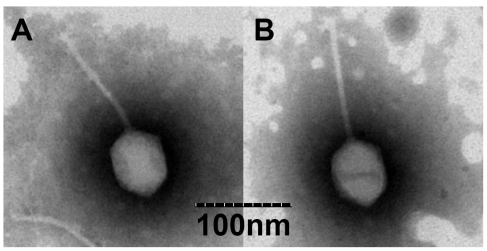

FIGURE 1 | Transmission electron microscopy (TEM) of vB_VpS_BA3 **(A)** and vB_VpS_CA8 **(B)**.

Meanwhile, almost (60%) of all described that phages with long and flexible tails should be assigned to the family, *Siphoviridae*. Researches have focused on phages infecting various foodborne pathogens majorly including *Listeria monocytogenes*, *Escherichia coli,* and *Salmonella* phages. A study focusing on *Vibrio* phages in *Siphoviridae* showed that it was far from enough compared to *Podoviridae* and *Myoviridae* (Chibani et al., 2019). However, related reports of phage therapy mainly and currently focus on *Caudovirales*. Some reports even highlighted that *Siphoviridae* may adapt a broader host range than *Podoviridae*. Therefore, the isolation and characterization of novel phages, especially *Siphoviridae*, are necessary before biocontrol can be achieved for the multidrug resistant *V. parahaemolyticus*.

Host Range Test Analysis

To determine the role of *V. parahaemolyticus* in phage infectivity, we performed a spot assay using 61 *V. parahaemolyticus* strains (11 groups of O antigen). Results showed that phage BA3 infected 5 of the 61 isolates (O1, O2, O3, and O5). Thus, we could conclude that the phage-host range was quite narrow. However, 22 strains of *V. parahaemolyticus* (O1, O2, O3, O4, O5, O8, O9, O10, O11, and O12) were sensitive to lysis by phage CA8 (**Supplementary Table S1**). The lysis effect (22/61) revealed that phage CA8 had the potential to be a candidate for phage therapy. Furthermore, we could predict that phage BA3 and phage CA8 were not cohesive or identical based on the great difference in their host range (Chibani et al., 2019).

Optimal MOI and One-Step Growth Curve

As shown in **Figure 2A**, the *V. parahaemolyticus* strain, O1-1/O3-11, when infected at an MOI of 0.1, generated the maximum bacteriophage titer, indicating that 0.1 was the optimal MOI for the phage BA3/CA8 titer. Owing to the largest titer for the MOI of the two phages, we investigated the latency period and burst size of phages and the results showed in **Figure 2B**. The assays revealed latent periods, defined as the time interval between the adsorption and the beginning of the first burst, of ∼20 min (phage BA3) and ∼30 min (phage CA8). It was determined to be ∼100 plaque-forming units (pfu)/cell for phage BA3 and ∼180 pfu/cell for phage CA8 under the laboratory growth conditions. Previously, the burst size of the phage VP06 infecting strain, YAF1206-1, was reported to be approximately

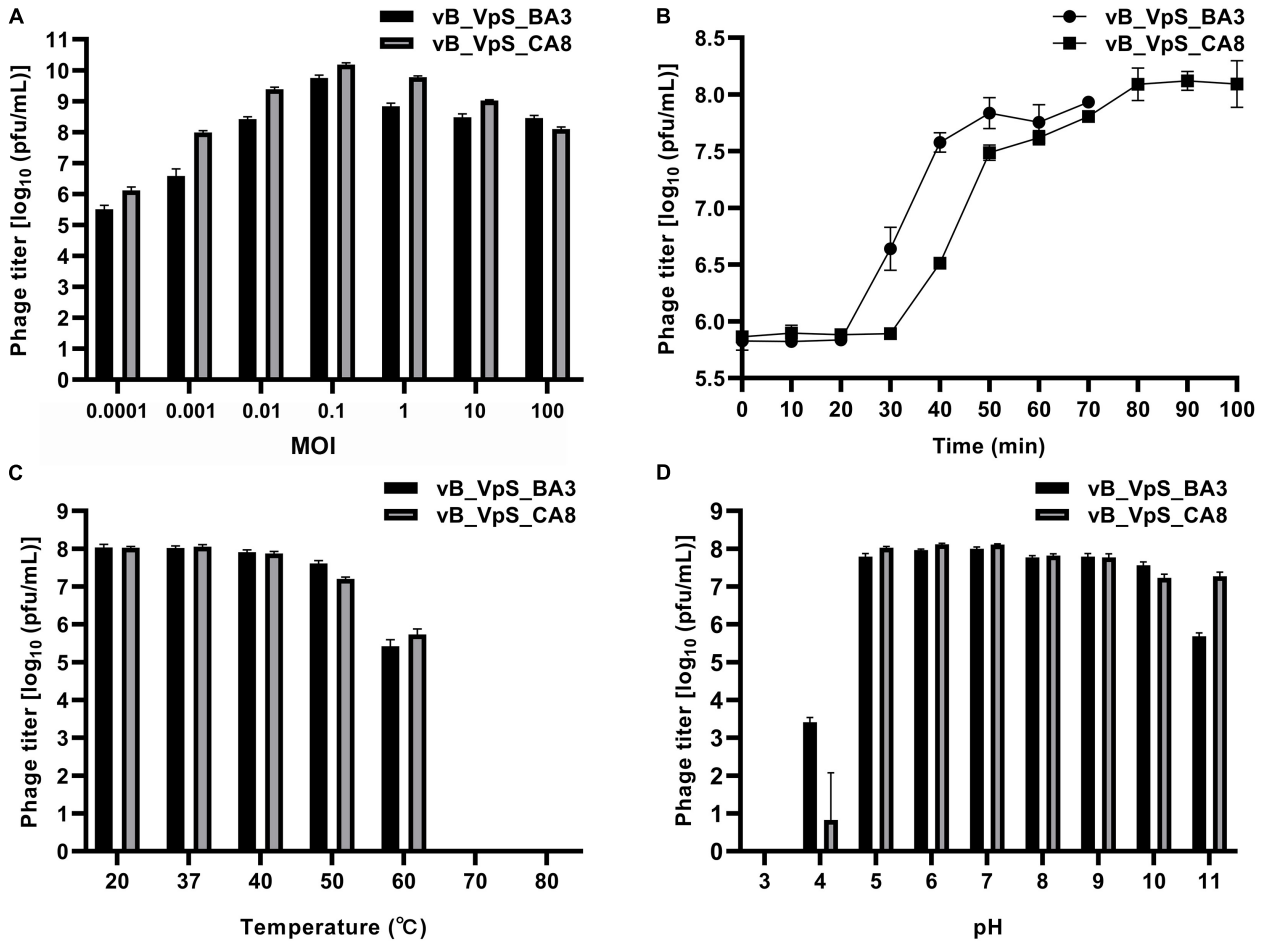

FIGURE 2 | Biological characterization of vB_VpS_BA3 and vB_VpS_CA8. **(A)** Multiplicity of infection; **(B)** Kinetics of progeny production in the single life cycle; **(C)** Thermal stability of two phages treated with different temperature for 1 h; **(D)** pH stability of two phages treated with different pH for 1 h. Results are presented as mean values ± SD and shown as $\log_{10}$ (pfu/mL).

60 pfu/cell, with a latent period of ∼30 min (Wong et al., 2019). Another phage, SIO-2, could readily propagate on SWAT3 with a latent period of approximately 45–60 min and average burst size of 60 viral particles per infected cell (Baudoux et al., 2012). The latent period of the *Vibrio* phage, VpKK5, was short at 24 min but exhibited a large burst size of 180 pfu per infected cell (Lal et al., 2016). Compared to the three phages reported, phage BA3 and CA8 exhibited a short latent period and a large burst size (∼100 pfu per infected cell). Latent period and burst size are critical and necessary in the assessment of phage fitness and identification of a candidate for phage therapy. Thus, our result reflects the lytic effectiveness of both phages toward the *V. parahaemolyticus* isolates.

Resistance to Environmental Stresses

The resistance to environmental stresses assay was performed to investigate the phage application of primary conditions and future prospects (Krasowska et al., 2015). First, phage stability following exposure to varying temperatures and pH was determined. As shown in **Figure 2C**, both phages BA3 and CA8 were stable at 20 and 37°C. Although, the titer of the phages was slightly reduced after 1 h of exposure at 40°C, these phages were stable at temperatures ranging from 20 to 40°C. Incubation at more than 60°C for 1 h was lethal to the phages, thus completely inactivating them. Such characteristics aligned with the results reported in a previous study with the phage VpKK5. Every phage has an optimal pH for survival and biological activity. As shown in **Figure 2D**, phage CA8 had optimal stability from pH 5.0 to pH 7.0 while BA3 was stable between pH 6.0 and pH 7.0. When the pH level was decreased, the titer of the two phages was sharply reduced, and at pH 4.0, the phages were essentially inactive. When the pH level increased to 10 and 11, only a low titer of these phages existed and survived. Therefore, we can infer that both phages caused the primary condition and factor to withstand various environmental stresses for phage therapy in the aquaculture water environment (Tovar et al., 2000).

Bacterial Killing Assays

To further assess potential applications, two phages were used for bacterial killing assays against hosts of *V. parahaemolyticus*. As

shown in **Figure 3**, bacterial density in the bacterial control (BC, VP O1-1 and O3-11) increased by ∼1.00 log cfu/mL after 2 h of incubation. Compared to BC (VP O1-1), the treatment group (VP O1-1 + phage BA3) did not present significant differences before 16 h of incubation. However, the maximum inactivation with phage BA3 was 1.00 log cfu/mL, respectively, achieved at 16 h of incubation. During treatment, the rate of inactivation of phage CA8 was significantly higher than that obtained with phage BA3. Bacterial inactivation of phage CA8 was initiated after 2 h and the bacterial density was 1.21 log cfu/mL less than BC (VP O3-11). Moreover, maximum inactivation with phage CA8 was 3.65 and 3.63 log cfu/mL at 16 and 24 h of incubation. These data revealed that CA8 may have more potential than BA3 for biocontrol of multidrug-resistant *V. parahaemolyticus*.

General Features of the Phage Genome

To further understand the general features of phages, the genome of phage BA3/CA8 was sequenced and analyzed. Mapping revealed that phage BA3 harbored a ∼1.0-kb fragment while phage CA8 harbored a ∼3.2-kb fragment with a ∼2-fold coverage; this revealed the termini considered terminal redundancy. Average frequency, the highest frequency, and ratio (R = highest frequency/average frequency) were calculated to verify the genome termini of both phages. **Table 1** showed that BA3 (R = 54.88) and CA8 (R = 70.44) indicated the preferred termini. Our findings were similar to those of T4 like phages. Unlike the other phages with unique termini, however, functional proteins of both phages were directly predicted using the contig assembly.

The properties of the functional genome, including positions, directions, length, product, and putative functions of each gene are showed in **Supplementary Tables S2, S3**. Both phages had a linear, double-stranded DNA genome. The BA3 genome was 58,648 bp with a GC content of 46.30%, while that of CA8 was 58,480 bp with an average GC content of 46.42%. In total, 85 putative ORFs were predicted in the genome of phage BA3 (**Supplementary Table S2**), with average gene length of 628 bp, and sizes ranging from 126 to 2,529 nucleotides. In contrast, there were 84 putative ORFs in CA8 (**Supplementary Table S3**), with average gene length of 629 bp, and the same size range of nucleotides as BA3. Only 34 ORFs in both phage genomes were predicted and determined to be functional, and 51 in BA3 (50 in CA8) were assigned to hypothetical proteins based on the assumption that sequence homology reflects a functional relationship. Finally, no rRNA was detected, but only one tRNA gene (encoding Pro) was present in both phages. Therefore, the gene inventory of the two phages is largely uncharacterized. All data revealed that both phages had a similar genome size.

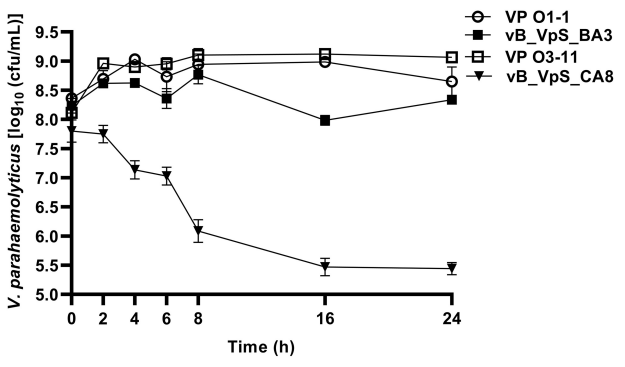

FIGURE 3 | Bacterial growth reduction. Reduction in the exponential growth phase of VP O1-1 and VP O3-11 by phage BA3 and CA8 at an approximate MOI of 0.1. The given values are the means of three determinations.

The Bacterial and Archaeal Viruses Subcommittee (BAVS) described genus as a cohesive group of viruses sharing a high degree of nucleotide sequence similarity (>50%), with two viruses belonging to the same species differing by less than 5% from each other at the nucleotide level using BLASTn. In this study, phage BA3 had high identity (72.59 and 65.52%) to *Prokaryotic dsDNA virus* sp. (GenBank: MK892600.1) and *Vibrio* phage VpKK5 (GenBank: KM378617), with 14% coverage and 9% coverage, respectively. Phage CA8 had the same result in BLASTN with *Prokaryotic dsDNA virus* sp. Besides, it shared 65.25% identity with the *Vibrio* phage, VpKK5, and had 8% coverage. Phage CA8 however shared 69.45, 68.84, 68.84, 68.68, and 68.57% identity with the *Vibrio* phage VP06 (MG893203.1), *Vibrio* phage vB_VpaS_KF4 (MF754114.1), *Vibrio* phage vB_VpaS_KF3 (MF754113.1), *Vibrio* phage R01 (MH599087.1), and *Vibrio* phage VVP001 (MG602476.1), respectively, with 3% coverage. On analyzing the results of the heatmap (**Figure 4**) and regarding the ANIm percentage identity data (**Supplementary Table S4**), phage BA3 and phage CA8 displayed no similarity to any other bacteriophages used in the present ANI analysis. According to these data, we can conclude that both phages BA3 and CA8 had great difference relative to other phages in the NCBI database. Furthermore, we could predict that they are novel phages in the family, *Siphoviridae*. Lastly, nucleotide pairwise sequence alignment based on BLASTN revealed that phages BA3 and CA8 were 97.32% identical to each other while ANI was 96.48%; thus, they can be considered different isolates of the same phage species.

The global genome comparison map among different phages is presented in **Figure 5**. All functional ORFs, displaying homology but low identity to amino acid sequences in the databases, were divided into four modules. Our findings proved that BA3 and CA8 were novel phages of *Siphoviridae*. Among the 34 genes with detected homologs, 94.1% appeared to be related to

TABLE 1 | The criteria for distinguish termini.

Phage	Number of reads	Gemone length (bp)	Highest frequency	Average frequency	Ratio	T1-F/T2-F	T1-R/T2-R	Characteristic
vB_VpS_BA3	66260	58648	0.56	31	54.88	2.07	1.11	Preferred termini
vB_VpS_CA8	74722	58480	0.64	45	70.44	2.81	1.23	Preferred termini

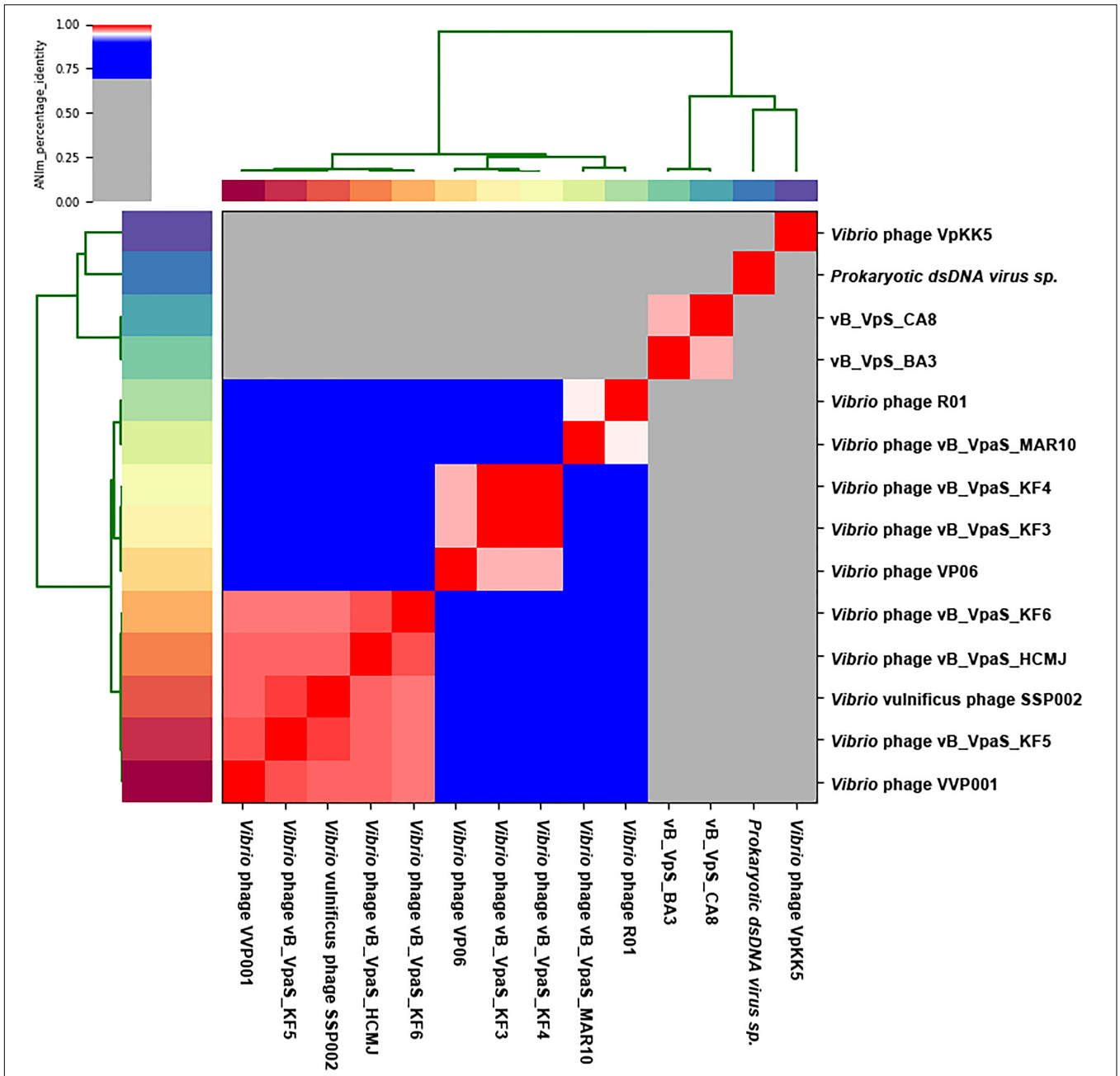

FIGURE 4 | Heatmap of the average nucleotide identity (ANI) values for 14 whole genomes, sequenced from related phages of the family *Siphoviridae* in the NCBI database, including two phages from this study. Values range from 0 (0%) ANI to 1 (100% ANI): gray represents 0% ANI; clusters of highly similar phages are highlighted in pink and red.

viruses while 5.9% had homologs in several groups of bacteria. These modules included DNA metabolism module, lysis module, packaging module, structure module, and additional module (Lal et al., 2016; Wong et al., 2019). In terms of phage therapy, lysis module and structure module (phage tail, receptor binding protein, RBP) played a direct role in bacterial lysis (Nobrega et al., 2018; Cahill and Young, 2019). However, *in silico* analysis of holin and *N*-acetylmuramoyl-L-alanine amidase revealed that phage BA3 and phage CA8 displayed no difference in the lytic mechanism and the ability at the end of the lytic cycle. Although both phages had a high degree of similarity in morphological characteristics and genomic features, the host range between them was not identical. Increasing research confirmed aspects of a process called adsorption between RBP and compatible cell surface structures (receptor) (Nobrega et al., 2018). For siphophages that infect gram-negative bacteria, this process was closely related to a central, straight fiber, as well as side fibers, but not a baseplate-like structure (Nobrega et al., 2018). In this

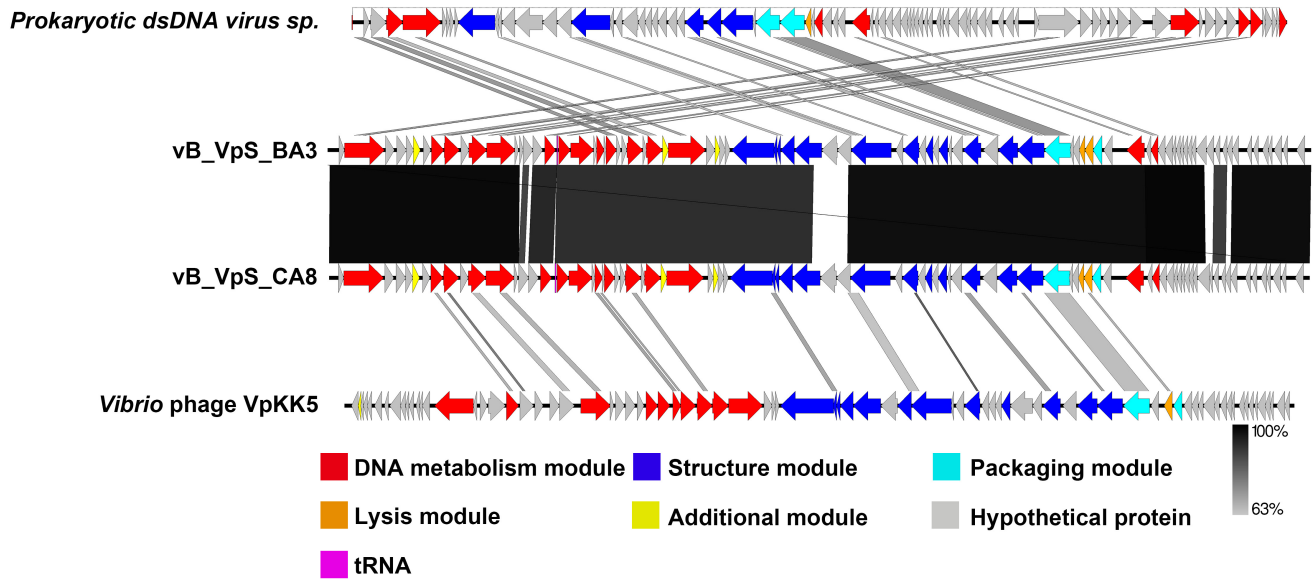

FIGURE 5 | Schematic representation of the genomic organization of vB_VpS_BA3 and vB_VpS_CA8, compared to other related *Vibrio* phages in NCBI. The genome is divided into a DNA metabolism module (red), a lysis module (orange), a packaging module (cyan), a structure module (royal blue), additional functions (yellow), hypothetical proteins (gray), and tRNA (purple). Arrows indicate ORFs with either rightward or leftward direction.

study, any main fiber was either predicted or annotated, but there were five tailed assembly proteins (TAPs) in the genome of two phages. Notably, vB_VpS_BA3 gp35 shared 90.50% identity to vB_VpS_CA8 gp34 and vB_VpS_BA3 gp38 displayed 86.14% identity to vB_VpS_CA8 gp37. Meanwhile, vB_VpS_BA3 gp39 had the lowest identity (63.39%) to vB_VpS_CA8 gp38 among the comparative features of phage tail proteins. The other TAPs, tail length tape-measure protein and tail subunit in phage BA3 shared > 95.00% identity with these proteins in phage CA8. Such features indicated that the great differences in host range between the two phages were primarily caused by the low similarity of TAPs. Although the type II secretion system protein (BA3 gp6 and CA8 gp6) was detected and annotated, there were no core domains or related functions by InterPro. Moreover, no other virulent gene or factor was present, thus, we can conclude that both phages are safe for use in phage therapy for the prevention and control of *V. parahaemolyticus*.

As a common practice, the phylogenetic tree was edited and visualized to analyze the evolution and identification of phage. The major capsid protein and terminase large subunit are conserved proteins in the bacteriophage genomes and regularly used to group phages in families by single gene analysis (Tetart et al., 2001; Fouts et al., 2013). In this study, proteomic comparison of available amino acid sequences of major capsid protein and terminase large subunit were considered to identify distant bacteriophage relatives via phylogenetic analysis. As shown in **Figure 6**, both the major capsid protein tree (**Figure 6A**) and terminase large subunit tree (**Figure 6B**) revealed that the phages BA3, CA8, and VpKK5, which are distinct from other siphophages in the NCBI database, could be divided into the same large cluster. Thus, it is suggested that they could originate from a common distant ancestor. However, phages BA3 and CA8 were still distinct from *Vibrio* phage VpKK5, which indicated that both isolates represented a novel *Vibrio* phage.

Analysis of Phage Virion Proteomes

Siphoviridae phage particle was mainly composed of structural proteins (structure module and packaging module) and a genomic DNA molecule inside its head. Genomic analysis predicted 12 genes in phage BA3 and CA8 genome coding proteins of structure module, including five TAPs, tail length tape-measure protein, tail subunit, virion structural protein, major head protein, minor head protein and structural phage protein. BlastP analysis showed there were terminase large subunit and terminase small subunit of packing module in both phages. All of these proteins were made up of whole phage scaffold. To identify the structural proteins in the mature phage BA3 and CA8, purified phage virions were analyzed by Nano LC-MS/MS.

Results showed that nine structural proteins were identified in phage BA3 virions (**Supplementary Table S5**), including two TAPs (gp38, gp39), tail length tape-measure protein, tail subunit, virion structural protein, major head protein, structural phage protein and terminase large subunit; 11 were identified in phage CA8 (**Supplementary Table S6**), including four TAPs (gp34, gp36, gp37, gp38), tail length tape-measure protein, tail subunit, virion structural protein, major head protein, minor head proteins and structural phage protein and terminase large subunit. Besides, annotated structural proteins in phage BA3 (gp35, gp36, gp37, gp46, gp53, and gp60) and phage CA8 (gp35, gp45, and gp59) were absent in our triplicate repeated proteomic analysis which may due to low copy number (Yuan and Gao, 2016). According to the differences of both host range and TAPs identified by LC-MS/MS between BA3 and CA8, it was considerate that research on transcriptomics and proteomics

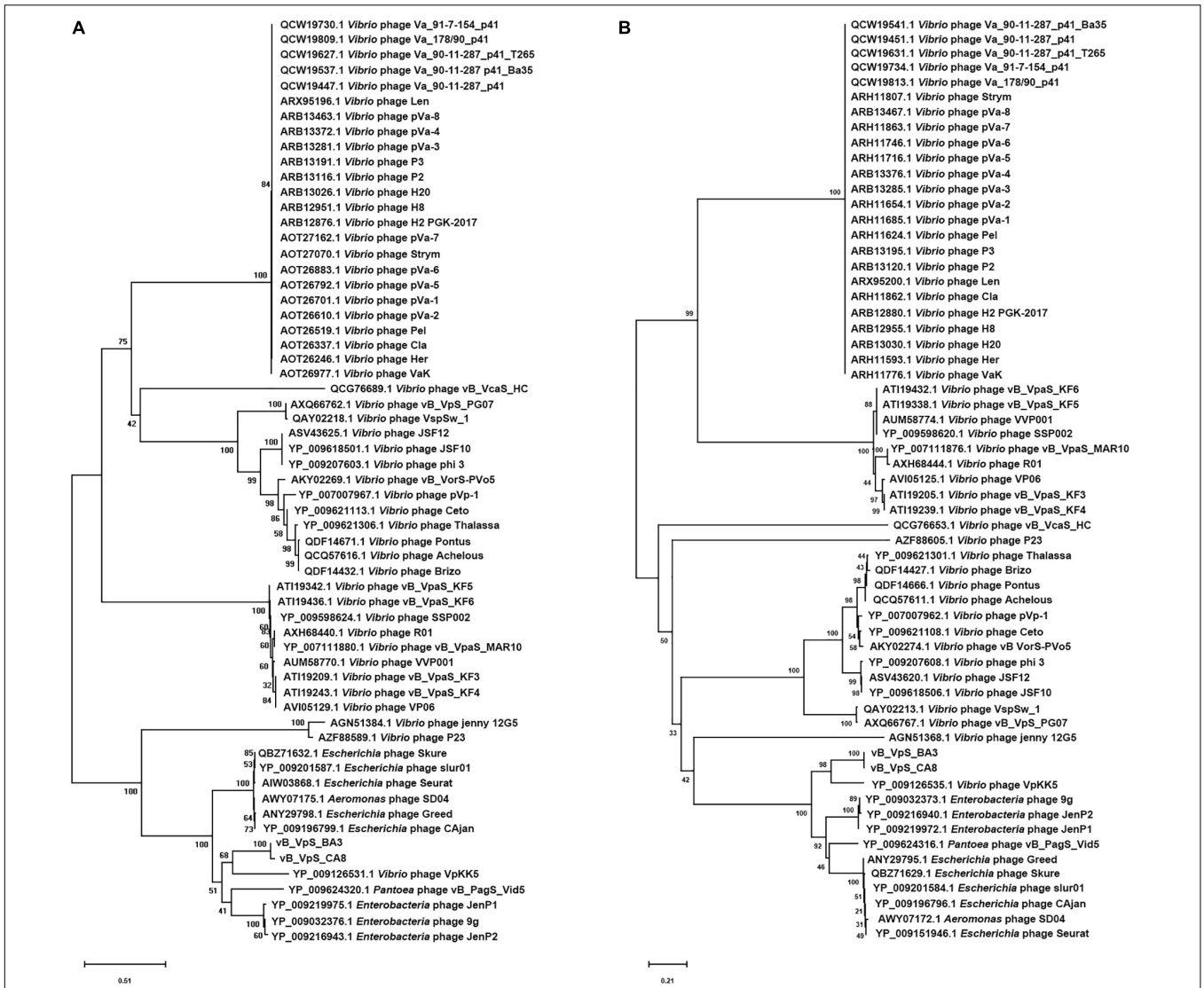

FIGURE 6 | Phylogenetic tree showing vB_VpS_BA3, vB_VpS_CA8, and other related phages of the family *Siphoviridae* and the order *Caudovirales*. The amino acid sequences of **(A)** the major capsid protein and **(B)** the terminase large subunit of the related phages were downloaded from NCBI.

should be performed to further investigate the interaction of host-phage. Interestingly, DNA metabolism module related genes were also determined in our phage particles (BA3 gp2, gp8, gp9, gp12, gp17, gp18, gp19, gp23, gp16, gp28 and gp62; CA8 gp2, gp12 and gp22). It's believed that the real function of these proteins might be involved in DNA translocation, transcription, repair, chromatin rearrangement repair, recombination and replication, which may play important roles in the phage early infection processes and will be our interests in the further studies as well (Lal et al., 2016; Yang M. et al., 2019).

CONCLUSION

Numerous reports have recently warned that *V. parahaemolyticus* is a crucial cause of food poisoning that is associated with the consumption of seafood and ready-to-eat food. Not only is phage therapy a safe and pollution-free treatment, but it is regarded as a promising strategy and activity of biocontrol owing to its specific infectivity toward target *V. parahaemolyticus* and no direct negative effects on aquatic organisms and humans. In this work, we characterized and compared the interaction of vB_VpS_BA3 and vB_VpS_CA8 as novel members of *Siphoviridae* with their own host. Firstly, phage CA8 could infect over 40% *V. parahaemolyticus* isolates than phage BA3 when host range was determined. Secondly, although phage CA8 had a greater burst size than phage BA3, both phages were revealed to be promising candidates of biocontrol. Moreover, both phages with their short latent period could recognize and adsorb the target *V. parahaemolyticus* strains, indicating their ability to control and kill bacterial cells rapidly and effectively. In our further studies, phage therapy *in vitro* could be conducted to support the results.

However, studies regarding potential applications of phages in animal and aquatic products are required to test and verify their safety. As such great number of ORFs could not be identified or characterized, this promoted us to determine the relevant genes and proteins for phage therapy. Because of the absence of virulent genes, both phages in our study were safe for use as phage therapy for the prevention and control of *V. parahaemolyticus*, ultimately stabilizing the progress of aquatic economy, enhancing food safety, and safeguarding human health.

DATA AVAILABILITY STATEMENT

All datasets generated for this study are included in the article/**Supplementary Material**.

AUTHOR CONTRIBUTIONS

JZ, QW, and MY conceived the study. MY and YL designed and conducted the experiments and wrote the manuscript. SH, JW, HC, XG, and YY contributed to the data analyze. QW and ZT guided the experiment. All authors agreed to be accountable for the content of the work.

FUNDING

The authors are grateful to the Science and Technology Planning Project of Guangdong Province (2018A050506074 and 2018A050506075), Key-Area Research and Development Program of Guangdong Province (2018b020205002 and 2018B020205003), and GDAS' Project of Science and Technology Development (2019GDASYL-0103011) for financial supports.

SUPPLEMENTARY MATERIAL

The Supplementary Material for this article can be found online at: https://www.frontiersin.org/articles/10.3389/fmicb.2020.00259/full#supplementary-material

REFERENCES

Aarestrup, F. M., and Wegener, H. C. (1999). The effects of antibiotic usage in food animals on the development of antimicrobial resistance of importance for humans in *Campylobacter* and *Escherichia coli*. *Microb. Infect.* 1, 639–644. doi: 10.1016/s1286-4579(99)80064-1

Ajuebor, J., Buttimer, C., Arroyo-Moreno, S., Chanishvili, N., Gabriel, E. M., O'mahony, J., et al. (2018). Comparison of *Staphylococcus* phage K with close phage relatives commonly employed in phage therapeutics. *Antibiotics* 7:37. doi: 10.3390/antibiotics7020037

Alagappan, K., Karuppiah, V., and Deivasigamani, B. (2016). Protective effect of phages on experimental *V. parahaemolyticus* infection and immune response in shrimp (Fabricius, 1798). *Aquaculture* 453, 86–92. doi: 10.1016/j.aquaculture.2015.11.037

Alagappan, K. M., Deivasigamani, B., Somasundaram, S. T., and Kumaran, S. (2010). Occurrence of *Vibrio parahaemolyticus* and its specific phages from shrimp ponds in east coast of India. *Curr. Microbiol.* 61, 235–240. doi: 10.1007/s00284-010-9599-0

Bankevich, A., Nurk, S., Antipov, D., Gurevich, A. A., Dvorkin, M., Kulikov, A. S., et al. (2012). Spades: a new genome assembly algorithm and its applications to single-cell sequencing. *J. Comput. Biol.* 19, 455–477. doi: 10.1089/cmb.2012.0021

Baudoux, A. C., Hendrix, R. W., Lander, G. C., Bailly, X., Podell, S., Paillard, C., et al. (2012). Genomic and functional analysis of *Vibrio* phage Sio-2 reveals novel insights into ecology and evolution of marine *siphoviruses*. *Environ. Microbiol.* 14, 2071–2086. doi: 10.1111/j.1462-2920.2011.02685.x

Cahill, J., and Young, R. (2019). Phage lysis: multiple genes for multiple barriers. *Adv. Virus Res.* 103, 33–70. doi: 10.1016/bs.aivir.2018.09.003

Carlton, R. M. (1999). Phage therapy: past history and future prospects. *Arch. Immunol. Ther. Exp.* 47, 267–274.

Carver, T. J., Rutherford, K. M., Berriman, M., Rajandream, M. A., Barrell, B. G., and Parkhill, J. (2005). Act: the artemis comparison tool. *Bioinformatics* 21, 3422–3423. doi: 10.1093/bioinformatics/bti553

Chang, H., Hong, J., Lee, N., Chun, H. S., Kim, H. Y., Choi, S., et al. (2016). Growth inhibitory effect of bacteriophages isolated from western and southern coastal areas of Korea against *Vibrio parahaemolyticus* in Manila clams. *Appl. Biol. Chem.* 59, 359–365. doi: 10.1007/s13765-016-0162-y

Chibani, C. M., Farr, A., Klama, S., Dietrich, S., and Liesegang, H. (2019). Classifying the unclassified: a phage classification method. *Viruses* 11:195. doi: 10.3390/v11020195

FAO (2019a). *A Quarterly Update on World Seafood Markets April 2019 Issue, with January–December 2018 Statistics*. Available online at: http://www.fao.org/3/ca5307en/ca5307en.pdf

FAO (2019b). *The State of World Fisheries and Aquaculture 2018 (SOFIA)*. Available online at: http://www.fao.org/3/i9540en/I9540EN.pdf

FDA (2018). *FDA Investigated Multistate Outbreak of Vibrio parahaemolyticus Linked to Fresh Crab Meat Imported from Venezuela*. Available online at: https://www.fda.gov/food/outbreaks-foodborne-illness/fda-investigated-multistate-outbreak-vibrio-parahaemolyticus-linked-fresh-crab-meat-imported

Fouts, D. E., Klumpp, J., Bishop-Lilly, K. A., Rajavel, M., Willner, K. M., Butani, A., et al. (2013). Whole genome sequencing and comparative genomic analyses of two *Vibrio cholerae* O139 Bengal-specific *Podoviruses* to other *N4*-like phages reveal extensive genetic diversity. *Virol. J.* 10:165. doi: 10.1186/1743-422X-10-165

Hatfull, G. F. (2008). Bacteriophage genomics. *Curr. Opin. Microbiol.* 11, 447–453. doi: 10.1016/j.mib.2008.09.004

Hendrix, R. W. (2003). Bacteriophage genomics. *Curr. Opin. Microbiol.* 6, 506–511.

Hiyoshi, H., Kodama, T., Iida, T., and Honda, T. (2010). Contribution of *Vibrio parahaemolyticus* virulence factors to cytotoxicity, enterotoxicity, and lethality in mice. *Infect. Immun.* 78, 1772–1780. doi: 10.1128/IAI.01051-09

Jin, M., Guo, X., Zhang, R., Qu, W., Gao, B., and Zeng, R. (2019). Diversities and potential biogeochemical impacts of mangrove soil viruses. *Microbiome* 7:58. doi: 10.1186/s40168-019-0675-9

Jun, J. W., Shin, T. H., Kim, J. H., Shin, S. P., Han, J. E., Heo, G. J., et al. (2014). Bacteriophage therapy of a *Vibrio parahaemolyticus* infection caused by a multiple-antibiotic-resistant O3:K6 pandemic clinical strain. *J. Infect. Dis.* 210, 72–78. doi: 10.1093/infdis/jiu059

Kang, C. H., Shin, Y., Jang, S., Yu, H., Kim, S., An, S., et al. (2017). Characterization of *Vibrio parahaemolyticus* isolated from oysters in Korea: resistance to various antibiotics and prevalence of virulence genes. *Mar. Pollut. Bull.* 118, 261–266. doi: 10.1016/j.marpolbul.2017.02.070

Katharios, P., Kalatzis, P. G., Kokkari, C., Sarropoulou, E., and Middelboe, M. (2017). Isolation and characterization of a *N4*-like lytic bacteriophage infecting *Vibrio splendidus*, a pathogen of fish and bivalves. *PLoS One* 12:e0190083. doi: 10.1371/journal.pone.0190083

Krasowska, A., Biegalska, A., Augustyniak, D., Los, M., Richert, M., and Lukaszewicz, M. (2015). Isolation and characterization of phages infecting *Bacillus subtilis*. *Biomed. Res. Int.* 2015:179597. doi: 10.1155/2015/179597

Kropinski, A. M., Mazzocco, A., Waddell, T. E., Lingohr, E., and Johnson, R. P. (2009). Enumeration of bacteriophages by double agar overlay plaque assay. *Methods Mol. Biol.* 501, 69–76. doi: 10.1007/978-1-60327-164-6_7

Kumar, S., Stecher, G., Li, M., Knyaz, C., and Tamura, K. (2018). Mega X: molecular evolutionary genetics analysis across computing platforms. *Mol. Biol. Evol.* 35, 1547–1549. doi: 10.1093/molbev/msy096

Kutter, E. (2009). Phage host range and efficiency of plating. *Methods Mol. Biol.* 501, 141–149. doi: 10.1007/978-1-60327-164-6_14

Laemmli, U. K. (1970). Cleavage of structural proteins during the assembly of the head of bacteriophage *T4*. *Nature* 227, 680–685. doi: 10.1038/227680a0

Lal, T. M., Sano, M., and Ransangan, J. (2016). Genome characterization of a novel vibriophage Vpkk5 (Siphoviridae) specific to fish pathogenic strain of *Vibrio parahaemolyticus*. *J. Basic Microbiol.* 56, 872–888. doi: 10.1002/jobm.201500611

Lefkowitz, E. J., Dempsey, D. M., Hendrickson, R. C., Orton, R. J., Siddell, S. G., and Smith, D. B. (2018). Virus taxonomy: the database of the international committee on taxonomy of viruses (Ictv). *Nucleic Acids Res.* 46, D708–D717.

Lesmana, M., Subekti, D., Simanjuntak, C. H., Tjaniadi, P., Campbell, J. R., and Oyofo, B. A. (2001). *Vibrio parahaemolyticus* associated with cholera-like diarrhea among patients in North Jakarta, Indonesia. *Diagn. Microbiol. Infect. Dis.* 39, 71–75. doi: 10.1016/s0732-8893(00)00232-7

Letchumanan, V., Chan, K. G., and Lee, L. H. (2014). *Vibrio parahaemolyticus*: a review on the pathogenesis, prevalence, and advance molecular identification techniques. *Front. Microbiol.* 5:705. doi: 10.3389/fmicb.2014.00705

Li, F., Xing, S., Fu, K., Zhao, S., Liu, J., Tong, Y., et al. (2019). Genomic and biological characterization of the *Vibrio alginolyticus*-infecting *Podoviridae* bacteriophage, vB_ValP_Ime271. *Virus Genes* 55, 218–226. doi: 10.1007/s11262-018-1622-8

Liu, B., Zheng, D., Jin, Q., Chen, L., and Yang, J. (2019). Vfdb 2019: a comparative pathogenomic platform with an interactive web interface. *Nucleic Acids Res.* 47, D687–D692. doi: 10.1093/nar/gky1080

Lomelí-Ortega, C. O., and Martínez-Díaz, S. F. (2014). Phage therapy against *Vibrio parahaemolyticus* infection in the whiteleg shrimp (*Litopenaeus vannamei*) larvae. *Aquaculture* 434, 208–211. doi: 10.1016/j.aquaculture.2014.08.018

Lu, T. K., and Collins, J. J. (2007). Dispersing biofilms with engineered enzymatic bacteriophage. *Proc. Natl. Acad. Sci. U.S.A.* 104, 11197–11202. doi: 10.1073/pnas.0704624104

Lu, T. K., and Collins, J. J. (2009). Engineered bacteriophage targeting gene networks as adjuvants for antibiotic therapy. *Proc. Natl. Acad. Sci. U.S.A.* 106, 4629–4634. doi: 10.1073/pnas.0800442106

Luo, Z., Yu, Y., Jost, G., Liu, W., Huang, X., and Gu, L. (2016). Characterization of two bacteriophages for specific treatment of biofilm formed by a *Vibrio sp* isolated from an abalone farm. *Aquacul. Res.* 47, 3964–3972. doi: 10.1111/are.12846

Mateus, L., Costa, L., Silva, Y. J., Pereira, C., Cunha, A., and Almeida, A. (2014). Efficiency of phage cocktails in the inactivation of *Vibrio* in aquaculture. *Aquaculture* 424-425, 167–173. doi: 10.1016/j.aquaculture.2014.01.001

Mitchell, A. L., Attwood, T. K., Babbitt, P. C., Blum, M., Bork, P., Bridge, A., et al. (2019). InterPro in 2019: improving coverage, classification and access to protein sequence annotations. *Nucleic Acids Res.* 47, D351–D360. doi: 10.1093/nar/gky1100

Naim, R., Yanagihara, I., Iida, T., and Honda, T. (2001). *Vibrio parahaemolyticus* thermostable direct hemolysin can induce an apoptotic cell death in Rat-1 cells from inside and outside of the cells. *FEMS Microbiol. Lett.* 195, 237–244. doi: 10.1111/j.1574-6968.2001.tb10527.x

Nobrega, F. L., Vlot, M., de Jonge, P. A., Dreesens, L. L., Beaumont, H., Lavigne, R., et al. (2018). Targeting mechanisms of tailed bacteriophages. *Nat. Rev. Microbiol.* 16, 760–773. doi: 10.1038/s41579-018-0070-8

Ottaviani, D., Leoni, F., Talevi, G., Masini, L., Santarelli, S., Rocchegiani, E., et al. (2013). Extensive investigation of antimicrobial resistance in *Vibrio parahaemolyticus* from shellfish and clinical sources, Italy. *Int. J. Antimicrob. Agents* 42, 191–193. doi: 10.1016/j.ijantimicag.2013.05.003

Paria, P., Chakraborty, H. J., Behera, B. K., Das, M. P., and Das, B. K. (2019). Computational characterization and molecular dynamics simulation of the thermostable direct hemolysin-related hemolysin (Trh) amplified from *Vibrio parahaemolyticus*. *Microb. Pathog.* 127, 172–182. doi: 10.1016/j.micpath.2018.11.037

Park, K. S., Ono, T., Rokuda, M., Jang, M. H., Okada, K., Iida, T., et al. (2004). Functional characterization of two type Iii secretion systems of *Vibrio parahaemolyticus*. *Infect. Immun.* 72, 6659–6665. doi: 10.1128/iai.72.11.6659-6665.2004

Pritchard, L., Glover, R. H., Humphris, S., Elphinstone, J. G., and Toth, I. K. (2016). Genomics and taxonomy in diagnostics for food security: soft-rotting enterobacterial plant pathogens. *Anal. Methods* 8, 12–24. doi: 10.1039/c5ay02550h

Raimondi, F., Kao, J. P., Fiorentini, C., Fabbri, A., Donelli, G., Gasparini, N., et al. (2000). Enterotoxicity and cytotoxicity of *Vibrio parahaemolyticus* thermostable direct hemolysin in in vitro systems. *Infect. Immun.* 68, 3180–3185. doi: 10.1128/iai.68.6.3180-3185.2000

Ren, H., Li, Z., Xu, Y., Wang, L., and Li, X. (2019). Protective effectiveness of feeding phage cocktails in controlling *Vibrio parahaemolyticus* infection of sea cucumber *Apostichopus japonicus*. *Aquaculture* 503, 322–329. doi: 10.1016/j.aquaculture.2019.01.006

Rong, R., Lin, H., Wang, J., Khan, M. N., and Li, M. (2014). Reductions of *Vibrio parahaemolyticus* in oysters after bacteriophage application during depuration. *Aquaculture* 418-419, 171–176. doi: 10.1016/j.aquaculture.2013.09.028

Seemann, T. (2014). Prokka: rapid prokaryotic genome annotation. *Bioinformatics* 30, 2068–2069. doi: 10.1093/bioinformatics/btu153

Srinivasan, P., and Ramasamy, P. (2017). Morphological characterization and biocontrol effects of *Vibrio vulnificus* phages against *Vibriosis* in the shrimp aquaculture environment. *Microb. Pathog.* 111, 472–480. doi: 10.1016/j.micpath.2017.09.024

Stalin, N., and Srinivasan, P. (2016). Characterization of *Vibrio parahaemolyticus* and its specific phage from shrimp pond in Palk Strait. South East coast of India. *Biologicals* 44, 526–533. doi: 10.1016/j.biologicals.2016.08.003

Sullivan, M. J., Petty, N. K., and Beatson, S. A. (2011). Easyfig: a genome comparison visualizer. *Bioinformatics* 27, 1009–1010. doi: 10.1093/bioinformatics/btr039

Tetart, F., Desplats, C., Kutateladze, M., Monod, C., Ackermann, H. W., and Krisch, H. M. (2001). Phylogeny of the major head and tail genes of the wide-ranging *T4*-type bacteriophages. *J. Bacteriol.* 183, 358–366. doi: 10.1128/jb.183.1.358-366.2001

Thompson, F. L., Iida, T., and Swings, J. (2004). Biodiversity of vibrios. *Microbiol. Mol. Biol. Rev.* 68, 403–431. doi: 10.1128/mmbr.68.3.403-431.2004

Tovar, A., Moreno, C., Mánuel-Vez, M. P., and Garcıìa-Vargas, M. (2000). Environmental impacts of intensive aquaculture in marine waters. *Water Res.* 34, 334–342. doi: 10.1016/s0043-1354(99)00102-5

Van Twest, R., and Kropinski, A. M. (2009). Bacteriophage enrichment from water and soil. *Methods Mol. Biol.* 50, 115–121.

Wong, H. C., Wang, T. Y., Yang, C. W., Tang, C. T., Ying, C., Wang, C. H., et al. (2019). Characterization of a lytic vibriophage Vp06 of *Vibrio parahaemolyticus*. *Res. Microbiol.* 170, 13–23. doi: 10.1016/j.resmic.2018.07.003

Xie, T., Wu, Q., Xu, X., Zhang, J., and Guo, W. (2015). Prevalence and population analysis of *Vibrio parahaemolyticus* in aquatic products from South China markets. *FEMS Microbiol. Lett.* 362:fnv178. doi: 10.1093/femsle/fnv178

Xie, T., Wu, Q., Zhang, J., Xu, X., and Cheng, J. (2017). Comparison of *Vibrio parahaemolyticus* isolates from aquatic products and clinical by antibiotic susceptibility, virulence, and molecular characterisation. *Food Control* 71, 315–321. doi: 10.1016/j.foodcont.2016.06.046

Xie, T., Xu, X., Wu, Q., Zhang, J., and Cheng, J. (2016). Prevalence, molecular characterization, and antibiotic susceptibility of *Vibrio parahaemolyticus* from ready-to-eat foods in China. *Front. Microbiol.* 7:549. doi: 10.3389/fmicb.2016.00549

Xing, S., Zhang, X., Sun, Q., Wang, J., Mi, Z., Pei, G., et al. (2017). Complete genome sequence of a novel, virulent *Ahjdlikevirus* bacteriophage that infects *Enterococcus faecium*. *Arch. Virol.* 162, 3843–3847. doi: 10.1007/s00705-017-3503-1

Xu, X., Cheng, J., Wu, Q., Zhang, J., and Xie, T. (2016). Prevalence, characterization, and antibiotic susceptibility of *Vibrio parahaemolyticus* isolated from retail aquatic products in North China. *BMC Microbiol.* 16:32. doi: 10.1186/s12866-016-0650-6

Yang, M., Liang, Y., Su, R., Chen, H., Wang, J., Zhang, J., et al. (2019). Genome characterization of the novel lytic *Vibrio parahaemolyticus* phage vB_VpP_Ba6. *Arch. Virol.* 164, 2627–2630. doi: 10.1007/s00705-019-04351-5

Yang, Z., Yin, S., Li, G., Wang, J., Huang, G., Jiang, B., et al. (2019). Global Transcriptomic analysis of the interactions between phage Phiabp1 and extensively drug-resistant *Acinetobacter baumannii*. *mSystems* 4:e00068-19. doi: 10.1128/mSystems.00068-19

Yen, M., Cairns, L. S., and Camilli, A. (2017). A cocktail of three virulent bacteriophages prevents *Vibrio cholerae* infection in animal models. *Nat. Commun.* 8:14187. doi: 10.1038/ncomms14187

Yin, Y., Ni, P., Liu, D., Yang, S., Almeida, A., Guo, Q., et al. (2019). Bacteriophage potential against *Vibrio parahaemolyticus*

biofilms. *Food Control* 98, 156–163. doi: 10.3390/microorganisms7030084

Yuan, Y., and Gao, M. (2016). Proteomic analysis of a novel *Bacillus* jumbo phage revealing glycoside hydrolase as structural component. *Front. Microbiol.* 7:745. doi: 10.3389/fmicb.2016.00745

Zhang, H., Li, L., Zhao, Z., Peng, D., and Zhou, X. (2016). Polar flagella rotation in *Vibrio parahaemolyticus* confers resistance to bacteriophage infection. *Sci. Rep.* 6:26147. doi: 10.1038/srep26147

Zhang, X., Wang, Y., and Tong, Y. (2018). Analyzing genome termini of bacteriophage through high-throughput sequencing. *Methods Mol. Biol.* 1681, 139–163. doi: 10.1007/978-1-4939-7343-9_11

Conflict of Interest: The authors declare that the research was conducted in the absence of any commercial or financial relationships that could be construed as a potential conflict of interest.

Copyright © 2020 Yang, Liang, Huang, Zhang, Wang, Chen, Ye, Gao, Wu and Tan. This is an open-access article distributed under the terms of the Creative Commons Attribution License (CC BY). The use, distribution or reproduction in other forums is permitted, provided the original author(s) and the copyright owner(s) are credited and that the original publication in this journal is cited, in accordance with accepted academic practice. No use, distribution or reproduction is permitted which does not comply with these terms.

frontiers in Microbiology

ORIGINAL RESEARCH
published: 06 March 2020
doi: 10.3389/fmicb.2020.00351

The Yersinia Phage X1 Administered Orally Efficiently Protects a Murine Chronic Enteritis Model Against *Yersinia enterocolitica* Infection

Yibing Xue[1†], Shengjie Zhai[1†], Zijing Wang[1†], Yalu Ji[1], Gang Wang[1], Tianqi Wang[2], Xinwu Wang[1], Hengyu Xi[1], Ruopeng Cai[1], Rihong Zhao[1], Hao Zhang[1], Lanting Bi[1], Yuan Guan[1], Zhimin Guo[3], Wenyu Han[1,4]* and Jingmin Gu[1]**

[1] Key Laboratory of Zoonosis Research, Ministry of Education, College of Veterinary Medicine, Jilin University, Changchun, China, [2] College of Clinical Medicine, Jilin University, Changchun, China, [3] Department of Clinical Laboratory, The First Hospital of Jilin University, Changchun, China, [4] Jiangsu Co-Innovation Center for the Prevention and Control of Important Animal Infectious Disease and Zoonose, Yangzhou University, Yangzhou, China

OPEN ACCESS

Edited by:
Krishna Khairnar,
National Environmental Engineering Research Institute (CSIR), India

Reviewed by:
Jack Christopher Leo,
Nottingham Trent University, United Kingdom
Petar Knezevic,
University of Novi Sad, Serbia

***Correspondence:**
Zhimin Guo
amily2222@163.com
Wenyu Han
hanwy@jlu.edu.cn
Jingmin Gu
jingmin0629@163.com

[†] These authors have contributed equally to this work

Specialty section:
This article was submitted to Antimicrobials, Resistance and Chemotherapy, a section of the journal Frontiers in Microbiology

Received: 29 October 2019
Accepted: 18 February 2020
Published: 06 March 2020

Citation:
Xue Y, Zhai S, Wang Z, Ji Y, Wang G, Wang T, Wang X, Xi H, Cai R, Zhao R, Zhang H, Bi L, Guan Y, Guo Z, Han W and Gu J (2020) The Yersinia Phage X1 Administered Orally Efficiently Protects a Murine Chronic Enteritis Model Against Yersinia enterocolitica Infection. Front. Microbiol. 11:351. doi: 10.3389/fmicb.2020.00351

Yersinia enterocolitica is generally considered an important food-borne pathogen worldwide, especially in the European Union. A lytic Yersinia phage X1 (Viruses; dsDNA viruses, no RNA stage; Caudovirales; and Myoviridae) was isolated. Phage X1 showed a broad host range and could effectively lyse 27/51 *Y. enterocolitica* strains covering various serotypes that cause yersiniosis in humans and animals (such as serotype O3 and serotype O8). The genome of this phage was sequenced and analyzed. No toxin, antibiotic-resistance or lysogeny related modules were found in the genome of phage X1. Studies of phage stability confirmed that X1 had a high tolerance toward a broad range of temperatures (4–60°C) and pH values (4–11) for 1 h. The ability to resist harsh acidic conditions and enzymatic degradation *in vitro* demonstrated that phage X1 is suitable for oral administration, and in particular, that this phage can pass the stomach barrier and efficiently reach the intestine *in vivo* without losing infectious ability. The potential of this phage against *Y. enterocolitica* infection *in vitro* was studied. In animal experiments, a single oral administration of phage X1 at 6 h post infection was sufficient to eliminate *Y. enterocolitica* in 33.3% of mice (15/45). In addition, the number of *Y. enterocolitica* strains in the mice was also dramatically reduced to approximately 10^3 CFU/g after 18 h compared with 10^7 CFU/g in the mice without phage treatment. Treatment with phage X1 showed significant improvement by intestinal histopathologic observations. Moreover, proinflammatory cytokine levels (IL-6, TNF-α, and IL-1β) were significantly reduced ($P < 0.05$). These results indicate that phage X1 is a promising candidate to control infection by *Y. enterocolitica in vivo*.

Keywords: *Yersinia enterocolitica*, bacteriophage, chronic enteritis, oral administration, phage therapy

INTRODUCTION

Yersiniosis is mainly caused by *Yersinia enterocolitica*, which is a facultative anaerobic Gram-negative bacterium that belongs to the Yersiniaceae family (Adeolu et al., 2016; Saraka et al., 2017). Yersiniosis is the third most common zoonotic disease in New Zealand and the most country of European Union (e.g., Germany and Finland) following campylobacteriosis and

salmonellosis (Rosner et al., 2010; Strydom et al., 2019). Pigs are asymptomatic carriers and the main reservoir of the *Y. enterocolitica* strain serotype O3, which is the most frequently reported serotype (89%) in the EU (Drummond et al., 2012). *Y. enterocolitica* cause a range of infections including severe diarrhea, enteritis and mesenteric lymphadenitis, reactive arthritis (ReA), nodular erythema (EN) and septicemia (Rosner et al., 2013). It is worth noting that a lot of studies have found that *Y. enterocolitica* has developed resistance to an increasing number of antibiotics, such as the second-generation quinolones, the third-generation cephalosporins, sulfonamides, and streptomycin, which are recognized as first-line treatments for *Y. enterocolitica* infection. Therefore, there is an urgent need for novel therapeutic agents directed against *Y. enterocolitica*.

Many studies have shown the effectiveness of phages in eradicating various food-borne pathogens in humans and animals (Wall et al., 2010; Abedon et al., 2011). Phage is harmless because it is strict bacterial virus that only specifically recognize, infect, and replicate inside host bacteria (Loc-Carrillo and Abedon, 2011). Additionally, phage usually do not destroy intestinal microbiota by specifically targeting host bacteria. Thus, phage therapy possesses great potential as a substitute or supplement for antibiotic treatment (Casey et al., 2018).

From 2000 to 2019, only several *Y. enterocolitica* bacteriophages have been reported (Leon-Velarde et al., 2016; Leskinen et al., 2016). Phage PY100 was administered orally in a murine model of *Y. enterocolitica*, unfortunately, the treatment using this phage with multiple applications and a high dose did not yield satisfying results (Skurnik and Strauch, 2006; Schwudke et al., 2008). Successful phage therapy for *Y. enterocolitica*, especially via oral administration, has rarely been reported.

In this study, the Yersinia phage X1 (Viruses; dsDNA viruses, no RNA stage; Caudovirales; and Myoviridae) was isolated from sewage by using *Y. enterocolitica* strain and the characteristics of this phage was studied. For determining the therapeutic effect of phage X1 on protecting a murine chronic enteritis model against *Y. enterocolitica* infection, the stable of phage X1 within the gastrointestinal tract with oral application and the bactericidal activity of phage X1 was detected *in vivo*.

MATERIALS AND METHODS

Bacterial Strains

The *Y. enterocolitica* strains used in this study are listed in **Supplementary Table S1**. The reference strains ATCC 23715 (serotype O8) and CICC 21565 (serotype O3) were purchased from American Type Culture Collection (Manassas, VA, United States) and China Center of Industrial Culture Collection (Beijing, China), respectively. The 49 clinical isolates of *Y. enterocolitica* were kindly provided by the Yunnan Institute of Endemic Disease Control. After sequencing the 16S rRNA gene with the universal primers 27F (5′-AGAGTTTGATCCTGGCTCAG-3′) and 1492R (5′-GGTTACCTTGTTACGACTT-3′) (Hao et al., 2016), identification of O3, O5, O8, and O9 serotypes was carried out with slide agglutination test by using diagnosis monoclonal antibodies against *Y. enterocolitica* (Wantai Biotech Co., Ltd.; Zhengzhou, China). Strains were cultured in LB (lysogeny broth, containing 5.0 g yeast extract, 10.0 g peptone, and 10.0 g NaCl per 1000 mL) medium (Bertani, 2004) or on plates with selective diagnostic CIN agar (Cefsulodin-Irgasan-Novobiocin; Oxoid, United Kingdom) at 37°C for 18–24 h (Orquera et al., 2012). For long-term storage, bacterial cultures were stored in glycerol [3:1 (v/v)] at −80°C.

Phage Isolation and Characteristics

The bacteriophage was isolated, purified and concentrated according to a previously described method (Gu et al., 2011). ATCC 23715 was used as a host to isolate the phage. Sewage samples were collected from a sewage treatment plant of Changchun City, Jilin Province, China. The phage was purified by the double-layer agar plate method for more than three times. To determine the host range of the phage, spot test and double-layer agar plate methods were used as described previously (Leon-Velarde et al., 2016).

The phage was concentrated as previously described (Synnott et al., 2009) and was spotted on a hydrophilic. Formvar-carbon-coated copper mesh for 2 min and negatively stained with 2% phosphotungstic acid for 30 s, after which the liquid was blotted with filter paper. Phage morphologies were observed under a TEM (H-7650; Hitachi, Japan) at 80 kV.

The multiplicity of infection (MOI) is defined as the ratio of the number of phages to the number of host bacteria (Czajkowski et al., 2015). The host strain was cultured in LB to a logarithmic growth phase (OD_{600} nm = 0.6). The phage and host bacteria (10^9 CFU/mL) were added to LB medium at different MOIs (10^{-7}, 10^{-6}, 10^{-5}, 10^{-4}, 10^{-3}, 10^{-2}, 10^{-1}, or 1) and cultured for 6 h at 37°C with shaking at 180 rpm. Phage titration was measured by the double-layer plate method after the incubation.

The one-step growth curve experiment was conducted with some modifications as explained elsewhere (Xi et al., 2019). The phage was mixed with an ATCC 23715 suspension at an optimal MOI of 1. After centrifugation at 4°C for 5 min (10,000 × *g*), the mixture was suspended in 10 mL of fresh LB medium and incubated at 37°C with shaking (180 rpm). The samples at different time were subjected to phage titer determination.

Genome Sequencing and Bioinformatics Analysis

The phage genome was extracted from the concentrated phage preparation using a viral genome extraction kit (Omega Bio-tek Inc., Norcross, GA, United States). The genome was submitted to BGI Biotechnology Co. Ltd., for genome-wide sequencing via the Illumina HiSeq platform. Potential open reading frames (ORFs) were predicted and analyzed by BLAST (NCBI) and GeneMark (Jeon et al., 2019), and gene function block diagrams were mapped using CLC Main Workbench version 7.7.3 software (CLC Bio-Qiagen, Aarhus, Denmark) (Ji et al., 2019).

Phage Stability Assay

Phage stability experiments *in vitro* were performed for thermal stability and pH according to the method described previously

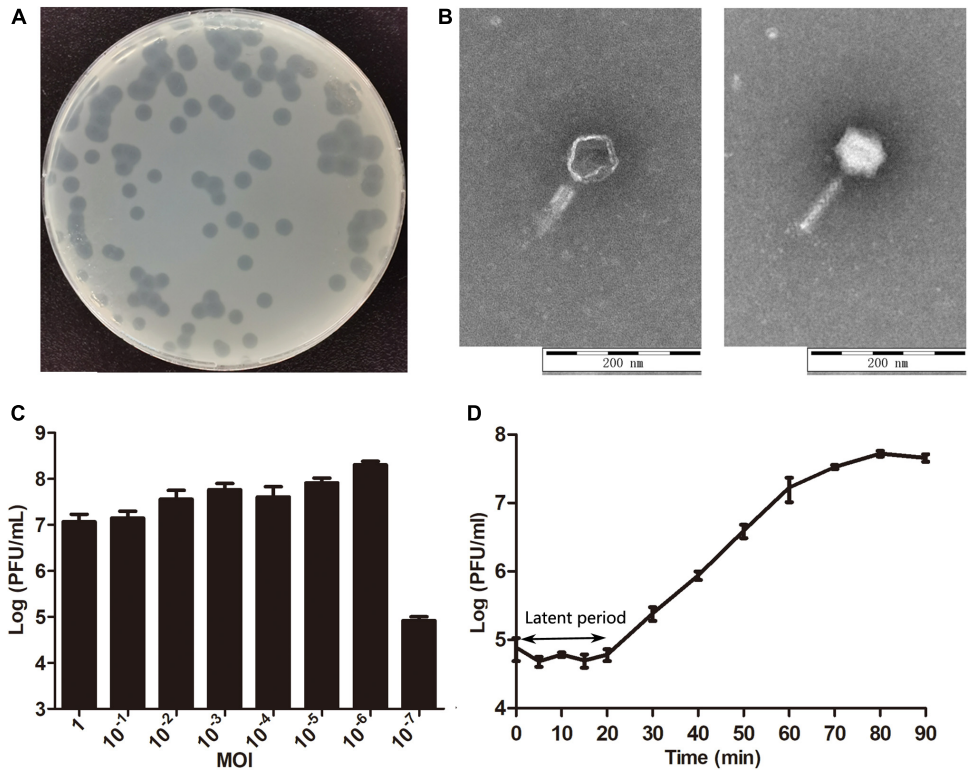

FIGURE 1 | Characteristics of phage X1. **(A)** Plaques induced by phage X1. **(B)** The morphology of phage X1. Transmission electron microscopy (TEM) of phage X1 negatively stained with 2% phosphotungstic acid. The scale bars represent 100 nm. **(C)** Titers of phage X1 under different MOIs in 6 h. When the MOI was 10^{-6}, the titer reached the highest value (2.75×10^8 PFU/mL). **(D)** One-step growth curve of phage X1 with a latent period of 20 min. The phage titer increased rapidly within 70 min and stabilized at 80 min. The titers of samples were measured at different time points. The values represent the mean and standard deviation (SD) ($n = 3$).

(Zhang et al., 2013). Phage suspensions were inoculated in SM buffer (pH range 1.0–13.0) for 1 h at 37°C. In addition, the thermal stability was tested by using a phage suspension (3.75×10^6 PFU/mL) that was incubated at 4, 25, 37, 50, 60, 70, and 80°C for 1 h. Phage titer was determined by double-layer plate assay. After 12 h of fasting, BALB/c mice were euthanized by intravenous injection of Fatal Plus (pentobarbital sodium) (100 mg/kg). The intestinal contents from the stomach, duodenum, jejunum, ileum, cecum, and colon of the mice were harvested. The contents were homogenized in 1 mL of phosphate buffered saline (PBS, pH 7.4) and centrifuged at 4°C for 1 min ($14{,}000 \times g$) to obtain the supernatants (Bosak et al., 2018). The stability of the phage was detected with supernatant of PBS aspirate of corresponding parts of intestinal tract, and the phage titer was measured after incubation at 37°C for 10, 30, 60, and 90 min.

Antibacterial Effect of Phage *in vitro*

Referring to the previous study (Cheng et al., 2017), early exponential cultures of ZTYSG 21 were infected with the phage at five different MOIs (PFU/CFU ratios of 10^{-6}, 10^{-4}, 10^{-2}, and 1), and the mixture was incubated in tubes with shaking at 180 rpm at 37°C. In addition, the uninfected phage group was set as a negative control group. The colony count of the cultures was measured every hour.

Ethics Statement

Female BALB/C mice aged 6–8 weeks (18–20 g) were provided by the Experimental Animal Center of Jilin University, Changchun, China. Experimental animals were placed under specific pathogen-free conditions and provided sterile materials (cages, bedding, water, and food). All animal experiments strictly abided by the National Guidelines for Experimental Animal Welfare (Ministry of Science and Technology of China, 2006) and conducted according to the experimental practices and standards approved by the Animal Welfare and Research Ethics Committee at Jilin University (permit number: 20181227087). All efforts were made to minimize suffering.

Phage Therapy in a Murine Model

To test whether phages could eliminate pathogenic bacteria from the intestinal tract of infected asymptomatic animals, a murine chronic enteritis model was established by previously described methods (Damasko et al., 2005). After being starved for 12 h, the mice were orally administered 0.1 mL ZTYSG 21 by using a feeding syringe. Prior to use, exponential-phase bacteria ZTYSG 21 were washed with PBS and resuspended in PBS to 2.05×10^9 CFU/mL. Phage treatment was orally administered at 6 h post infection. BALB/c mice were randomized into three

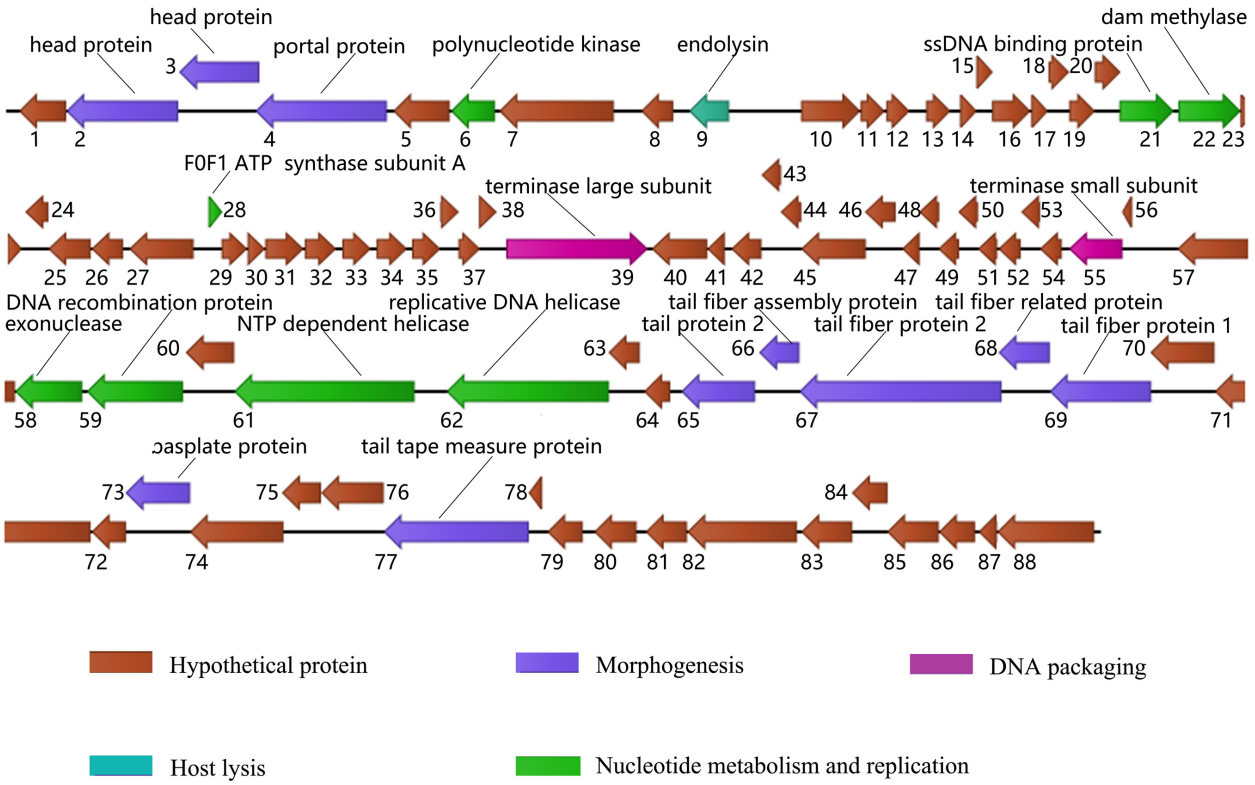

FIGURE 2 | Genome map of phage X1. ORFs are depicted by arrows according to the direction of transcription, and the direction of the arrows represents the direction of gene transcription. Proposed modules are color-coded according to the predicted function of their products. The putative functions and names of the genes are listed above.

experimental groups: (i) Bacteria-PBS group of 15 infected mice treated with 0.1 mL of PBS at 6 h post infection; (ii) Bacteria-Phage group of 15 infected mice treated with phage (0.1 mL, 1.95×10^9 PFU/mL) in a single dose at 6 h post infection; and (iii) PBS-Control group of 15 healthy mice treated with 0.1 mL of PBS as the controls. The experimental animals were monitored for clinical manifestation for 6 days. The experiments were repeated three times.

Colon and cecum tissues were collected under sterile conditions for microbiological analysis at the indicated times. Briefly, after 6 h of challenge, three mice were randomly selected from each group every 3 h for euthanasia by intravenous injection of Fatal Plus (pentobarbital sodium) (100 mg/kg) until 24 h post challenge. After 24 h, three mice were randomly selected from each group every 24 h for euthanasia, and the bacterial load was measured until 6 days after the challenge. The removed organs were homogenized in 1 mL of PBS buffer, then serially diluted with PBS, and plated on *Y. enterocolitica* selective medium (CIN) for counting the number of colonies forming units (CFU).

To determine the phage titer in the Bacteria-Phage group, the supernatants from each time point were centrifuged at 4°C for 15 min (12,000 × *g*) and filtered. The phage titer was determined by agar double-layer plate experiment (Bosak et al., 2018; Jeon et al., 2019).

To assess histological changes, the intestinal tissue samples harvested from euthanized mice were fixed in 10% zinc formalin and stained with hematoxylin and eosin (H&E). Representative tissue sections from each group were imaged. Tissues in cecum were scored blindly for inflammation and pathology using a 13-point system as described before (Barthel et al., 2003). The scoring included submucosal edema (0–3), polymorphonuclear granulocytes (PMN) infiltration into the lamina propria (0–4), goblet cells (0–3), and epithelial integrity (0–3).

Proinflammatory cytokines (TNF-α, IL-6, and IL-1β) in cecum, colon, and spleen tissues were measured. Briefly, three mice were randomly selected from each group at 12, 24, 48, and 72 h after infection. The removed organs were homogenized in 1 mL of PBS buffer, serially diluted with PBS and detected by an enzyme-linked immunosorbent assay kit (BioLegend, San Diego, CA, United States) (Cai et al., 2013).

Statistical Analyses

SPSS version 13.0 software (SPSS, Inc., Chicago, IL, United States) was utilized for the statistical analysis. All experimental data were analyzed by one-way analysis of variance (ANOVA). Error bars represent standard deviation of the mean. $P < 0.05$ was considered statistically significant. $^{*}P < 0.05$; $^{**}P < 0.01$; and $^{***}P < 0.001$.

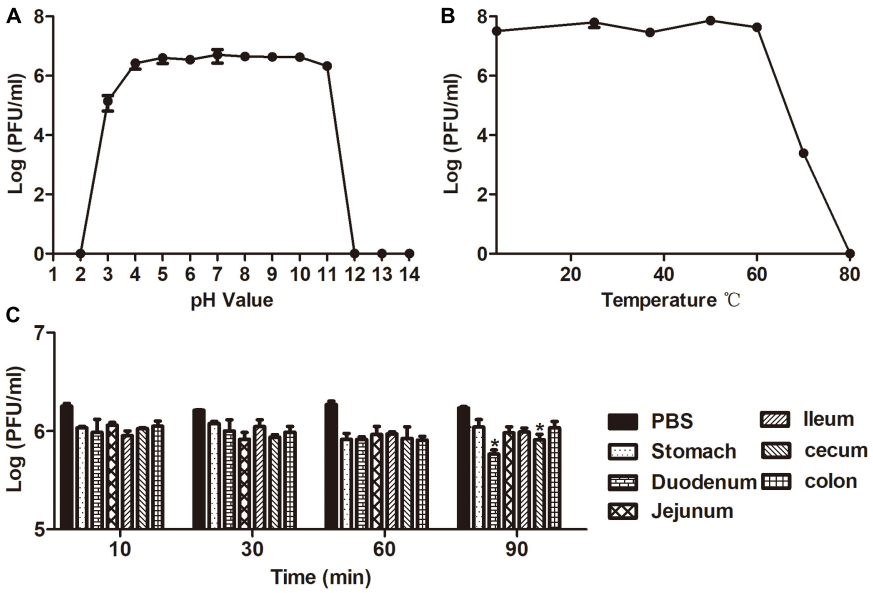

FIGURE 3 | Analysis of the stability of phage X1. **(A)** Stability of phage X1 in different pH values of PBS during 1 h. **(B)** Stability of phage X1 performed at 4, 25, 37, 50, 60, 70, and 80°C during 1 h. **(C)** Stability of phage X1 in gastrointestinal tract content. These values represent the mean and standard deviation (SD) (n = 3). *$P < 0.05$.

RESULTS

Characterization of *Y. enterocolitica* Strains

A total of 49 clinically isolated strains were identified as *Y. enterocolitica* by 16S rRNA sequencing. BLAST analysis showed that the 49 isolates were more than 99% identity to *Y. enterocolitica* strains identified and confirmed in the GenBank database (such as KC776767.1 and LR134492.1). The dominant bacterial serotype was O3 (40%, 18/49), followed by O8 (29%, 13/49), O5 (18%, 8/49), O9 (11%, 5/45), and NT (11%, 5/49) (**Supplementary Table S1**).

Isolation and Characterization of Phage X1

The phage isolated from the sewage was purified by a double-layer agar plate method and designated Yersinia phage X1 (Viruses; dsDNA viruses, no RNA stage; Caudovirales; and Myoviridae). Plaques of phage X1 were 5–7 mm in diameter surrounded by transparent haloes in the periphery that expanded with time (**Figure 1A**). As determined by TEM (**Figure 1B**), phage X1 had an icosahedral head of 70 ± 3 nm and a contracted tail of 90 ± 3 nm in length and belonged to Myoviridae. The host range analysis demonstrated that phage X1 possessed a broad host range and infected 27 (27/51) strains of *Y. enterocolitica* (2 standard strains and 25 clinical isolates), which included pathogens of the following various serotypes: O3 (14/18), O5 (3/8), O8 (6/13), and NT (4/5) (**Supplementary Table S1**). When the MOI was 10^{-6}, the phage titer reached the highest level, approximately 2.75 × 10^{8} PFU/mL (**Figure 1C**). The one-step growth curve results (MOI = 1) indicated that the latent period of phage X1 infection was 20 min. The burst size was approximately 290 particles/infected cell (**Figure 1D**).

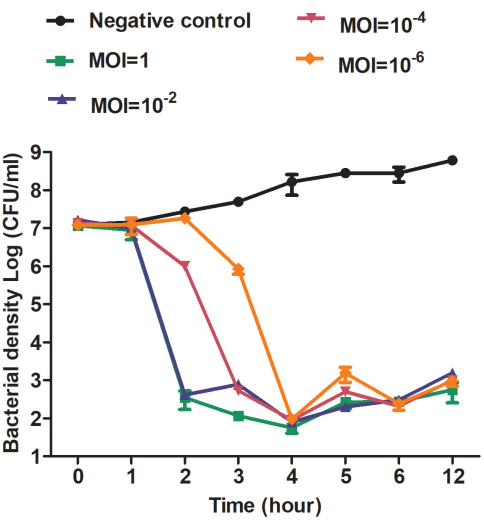

FIGURE 4 | Antibacterial curve of phage X1 *in vitro*. Bacteriolytic activity of phage X1 at different MOIs. ZTYSG21 was infected with phage at the indicated MOI. The colony counts of the negative control group (phage uninfected) and the phage-infected group were determined. The values represent the mean and SD (n = 3).

General Features of the Genome of Phage X1

Whole genome sequencing of phage X1 is available in GenBank (MN617773). The genome of phage X1 was 48,948 bp in length,

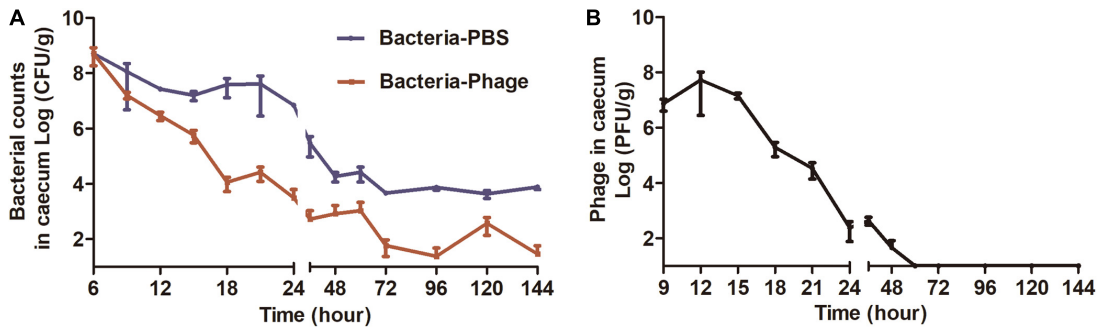

FIGURE 5 | Bacterial and phage loads in the cecum from each group. **(A)** Bacterial load in cecum (CFU/g tissue). Mice infected with ZTYSG21 were sacrificed at the pre-determined times, and 10-fold serial dilutions of cecum homogenates were plated on CIN media to determine bacterial load. **(B)** The titer of the Bacteria-Phage group was observed in the cecum (PFU/g tissue). The experiments were repeated three times. The values represent the means and standard deviations (SDs) (n = 3).

with a G + C content of 47.9%. It was found to have 88 putative ORFs, which included 21 proteins of known putative function and 67 hypothetical proteins (**Figure 2**). ORFs 10–23 and 28–39 were observed to be transcribed on the positive strand and the remaining ORFs were transcribed on the negative stranded. The predicted functional proteins were divided into five modules according to their functions: hypothetical function, structural composition, DNA packaging, host lysis, and nucleic acid metabolism and replication. The host lysis module was the smallest, with only ORF 9 encoding endolysin. No genes related to drug resistance, lysogeny or bacterial virulence were found in the predicted functional genes of phage, at least based on the limited studies.

BLAST analysis showed that the whole genome sequence of phage X1 shows 99.50% sequence identity and 99% genomic coverage with PY100. However, there are differences between X1 and PY100. The size of PY100 genome is 50,291 bp which contains 93 putative ORFs. While, the genome of phage X1 is 48,948 bp and it contains 88 putative ORFs. Though a large part of the ORFs in phage X1 and PY100 show high identity with each other, 10 ORFs in phage X1 shows low query cover and identity with the corresponding putative ORFs that derived from PY100 (as seen from the **Supplementary Table S2**). It is worth noting that, comparing with PY 100, phage X1 lacks a head protein and an HNH endonuclease which was encoded by ORF58 and ORF91 of PY100, respectively. And four other hypothesis ORFs of PY100 were not found in X1. Additionally, the F0F1 ATP synthase subunit A which encoded by ORF28 of X1 was not found in PY100.

Stability of Phage X1

The lytic capability of the phage was stable at pH 4–11 for 1h, and almost no loss of activity was observed (**Figure 3A**). In addition, the sensitivity of phage X1 to various temperatures (4–80°C) is represented in **Figure 3B**. The activity of phage X1 was stable between 4 and 60°C, although phage activity could be maintained after incubation at 70°C for 1 h. Briefly, we found that phage X1 was highly stable over a wide pH and temperature ranges. Similarly, no significant loss of phage activity was observed when phage X1 was incubated with the intestinal contents at 37°C for 60 min, indicating that these phage particles remained stable under gastrointestinal conditions (**Figure 3C**).

Antibacterial Effects of Phage X1 *in vitro*

The activity of phage X1 inhibiting ZTYSG 21 growth *in vitro* is shown in **Figure 4**. As we expected, colony forming unit number increased continuously in the negative control. In contrast, all phage-infected groups dramatically inhibited bacterial growth, although the antibacterial effect was slightly different under different MOIs. With higher MOI values, the bacterium was more sensitive to phage infection. After 4 h, the bacterial counts declined to approximately 10^3–10^4 CFU/mL and remained stable compared to 10^8 PFU/mL in the negative control group.

Therapeutic Effect of Phage X1 *in vivo*

The mice challenged with ZTYSG 21 did not die of infection. Therefore, the bacterial loads in the murine intestinal tract were measured. A single oral administration of phage X1 at 6 h post infection was sufficient to eliminate *Y. enterocolitica* in 33.3% of mice (15/45). The Bacterial-PBS group had a median bacterial load in the cecum and colon of 3.84×10^7 CFU/g and 3.79×10^7 CFU/g, respectively, at 18 h (**Figure 5A** and **Supplementary Figure S1A**). The treatment with phage X1 significantly decreased the bacterial load to 3.13×10^3 CFU/g and 2.15×10^3 CFU/g, respectively. After 24 h of infection, bacterial counts in the tissues decreased to approximately 10^2 CFU/g (the untreated mice were approximately 10^4 CFU/g). No colonies were found in the intestine of PBS group mice. Phage X1 had transient increase after oral administration with a slight uptick of the PFU value in the cecum (**Figure 5B**) and colon (**Supplementary Figure S1B**). The phage was completely cleared after 48 h of infection. It is worth noting that *Y. enterocolitica* also remained in mice, while phage X1 was cleared by the host immune system. Ten colony-forming units isolated from the germ-carrying mice in the Bacteria-Phage group were randomly selected and propagated. Interestingly, the isolated *Y. enterocolitica* strains were lysed by phage X1 suspension *in vitro*.

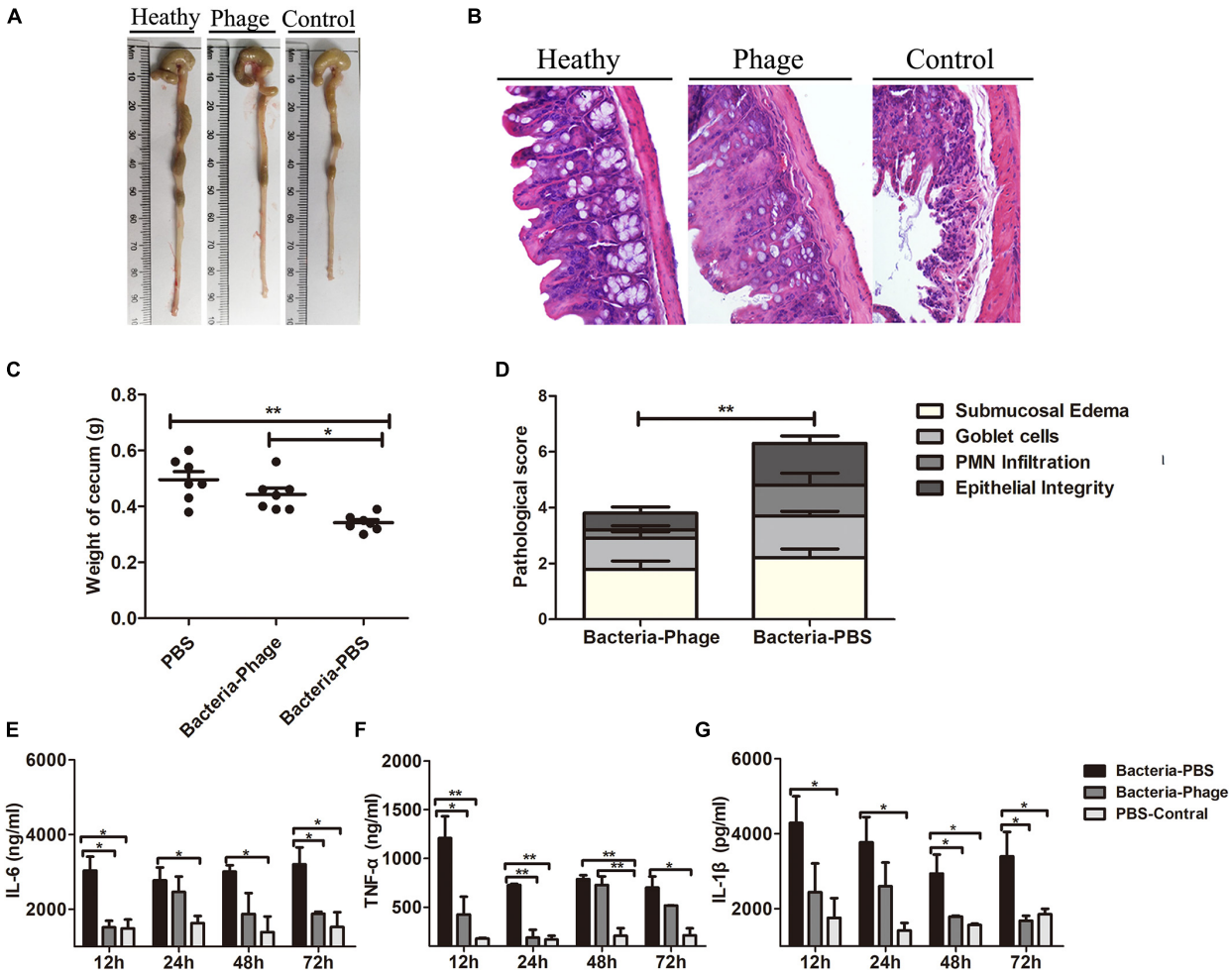

FIGURE 6 | Phage X1 mitigates intestinal inflammation. Representative macroscopic **(A)** and corresponding microscopic images of cecum tissues stained with H&E **(B)**. Images are shown at magnifications of 400. Healthy, phage and control represent the PBS-Control group, Bacteria-Phage group, and Bacteria-PBS group, respectively. **(C)** The weight of the cecum (n = 7) and **(D)** histopathology score were measured (n = 9). **(E–G)** Production of proinflammatory cytokines in cecum lymphocytes. At 12, 24, 48, and 72 h post infection, the levels of TNF-α, IL-6, and IL-1β in the cecum were determined. The tissues of the healthy mice served as controls. The values represent the means and standard deviations (SDs) (n = 3). *P < 0.05; **P < 0.01.

At necropsy, gross and histopathologic lesions in cecum from the different groups were examined. At 48 h post-infection, *Y. enterocolitica* infection induced cecum shortening and increased loss of cecal weight, accompanied by reduced colon size (**Figures 6A,C**). Microscopically, mice in the Bacteria-PBS group displayed greater cecal histopathology scores than mice in the Bacteria-Phage group (**Figure 6D**), represented by a loss of goblet cells, mucosal ulcerations, and odema in the submucosa (**Figure 6B**) and PMN were also observed in the lamina propria of the Bacteria-PBS group mice. In contrast, no significant lesions were observed in the phage-treated mice. The pathological changes were remarkably alleviated in response to X1 treatment.

We also measured the inflammation status in the animals. The levels of the proinflammatory cytokines TNF-α, IL-6, and IL-1β in the cecum (**Figures 6E–G**), spleen (**Supplementary Figure S2A**) and colon (**Supplementary Figure S2B**) of the Bacteria-Phage group were close to the level of healthy mice, whereas they were significantly lower than those of the Bacteria-PBS group (P < 0.05). Taken together, these results indicated that phage X1 could mitigate injury in the cecum against *Y. enterocolitica* infection in mice.

DISCUSSION

Phage treatment for gastrointestinal diseases by oral administration has been studied for a long time. Due to sensitivity to acidic compounds, digestive enzymes, and mucus layer containing IgA antibodies in the gastrointestinal tract, most phages showed limited effect during oral application (Zelasko et al., 2017). The stability of phages under various conditions is an important factor in evaluating their bactericidal potential.

Currently, encapsulation of phages by liposomes (Colom et al., 2015) or alginate nanoparticles (Ma et al., 2016) may also be used to enhance bacteriophage stability and bactericidal activity. The pH in the stomach of mice is 3.0 (fed) and 4.0 (starved) (McConnell et al., 2008). In fact, it was found that phage X1 was stable at pH 4–11 and upon incubation with intestinal contents for 1 h, indicating that phage X1 may be suitable for oral administration treatment without packaging technology, making it a cost-effective, convenient, and quick treatment.

The MOI, short latency period and big burst size indicated that phage X1 has high replication efficiency. Phage X1 exhibited a broad host range with at least four pathogenic serotypes (O3, O5, O8, and O9), which especially included O3 serotypes with epidemiological significance (Fredriksson-Ahomaa et al., 2012). Bacteriophage phiYeO3-12 isolated by Pajunen et al. (2001) was only able to infect the O3 serotype of *Y. enterocolitica*. Phage PY54 displays specificity for the O5 serotype of *Y. enterocolitica* (Hertwig et al., 2003). Bacteriophage vB_YenP_AP5 is able to infect serotypes O3, O2, and O1 (Leon-Velarde et al., 2014). Phage PY100 had a broad host range as X1 in the genus *Yersinia* (Schwudke et al., 2008). Though the genome of phage X1 shows high identity with PY100, there are obvious differences between two phages, which may lead to different biological properties and therapeutic effects. ORF67 in phage X1 genome encodes tail fiber protein (TFP), which showed 91% identity with that of PY100. TFP is responsible for the specific initial recognition of host bacteria (He et al., 2018). Therefore, this discrepancy may lead to different lytic activities. There is a *pac* site in terminase small subunit (terS) of phage X1, just like PY100. The risk of transduction is existing due to this site (Djacem et al., 2017).

In a preliminary animal experiment, 10 strains, including the host bacterial strain ATCC 23715, were chosen to infect mice. Only ZTYSG 21 has the longest colonization time in the mouse intestine and does not result in mouse death (**Supplementary Table S3**). An asymptomatic chronic intestinal infection model in BALB/c mice was established by ZTYSG 21. The murine chronic enteritis model was used to determine the therapeutic effect of phage X1 at a single dose by oral on protecting a murine chronic enteritis model against Y. enterocolitica infection. Phage X1 could lower the number of infected animals and significantly inhibit bacterial growth. Though the phage particles of PY100 were also active for at least 24 h within the gastrointestinal tract (titers between 10^4 and 10^6 PFU/g of organ and feces, respectively), PY100, even multiple doses of treatment, did not remove or prevent *Y. enterocolitica* from colonizing the intestines of mice (Skurnik and Strauch, 2006). The newly identified antibacterial agents enterocoliticin (2005) and colicin FY (2018), which remained stable in a gastrointestinal environment, also failed to prevent colonization of *Y. enterocolitica* in the gastrointestinal tract (Damasko et al., 2005; Bosak et al., 2018). Phage X1 also showed higher bactericidal efficiency *in vivo* than *Y. enterocolitica* antimicrobial agents discovered in recent years.

The level of proinflammatory cytokines in the Bacteria-Phage group was significantly decreased compared with the PBS-treated group ($P < 0.05$). Nevertheless, the level of TNF-α in the spleen of the treatment group was still high at 72 h. A number of studies have shown that TNF-α also has an anti-inflammatory effect in limiting inflammation *in vivo* and autoimmune diseases (Mayordomo et al., 2018).

It is conceivable that phage X1 may also be effective in combating bacterial contamination of food products and in veterinary feed. The U.S. Food and Drug Administration (FDA) approved the administration of phages to replace traditional antibiotics in veterinary medicine and as a safe food additive in food products (Bren, 2007). A large number of studies have shown that phages are effective as biocontrol agents against food pathogens and food spoilage organisms (Guenther et al., 2012). Therefore, in our follow-up studies, we will continue to explore the application of phage X1 for the control of *Y. enterocolitica* on food products, as this study demonstrated the high stability and bactericidal efficacy of this phage.

DATA AVAILABILITY STATEMENT

The datasets generated for this study can be found in the MN617773.

ETHICS STATEMENT

The animal study was reviewed and approved by the Animal Welfare and Research Ethics Committee at Jilin University (permit number: 20181227087).

AUTHOR CONTRIBUTIONS

JG, WH, and ZG conceived and designed the study. YX, SZ, ZW, YJ, GW, TW, XW, HX, RC, RZ, HZ, LB, and YG performed the laboratory testing. YX, SZ, and ZW were responsible for the writing and revision of the manuscript. All authors read and approved the final manuscript.

FUNDING

This work was financially supported through grants from the National Natural Science Foundation of China (Nos. U19A2038, 31872505, and 31572553), the Jilin Province Science Foundation for Youths (Changchun, China; grant no. 20190103106JH), the Achievement Transformation Project of the First Hospital of Jilin University (No. JDYYZH-1902025), and the Fundamental Research Funds for the Central Universities.

SUPPLEMENTARY MATERIAL

The Supplementary Material for this article can be found online at: https://www.frontiersin.org/articles/10.3389/fmicb.2020.00351/full#supplementary-material

REFERENCES

Abedon, S. T., Kuhl, S. J., Blasdel, B. G., and Kutter, E. M. (2011). Phage treatment of human infections. *Bacteriophage* 1, 66–85. doi: 10.4161/bact.1.2.15845

Adeolu, M., Alnajar, S., Naushad, S., and Gupta, R. (2016). Genome-based phylogeny and taxonomy of the '*Enterobacteriales*': proposal for *Enterobacterales* ord. nov. divided into the families Enterobacteriaceae, Erwiniaceae fam. nov., Pectobacteriaceae fam. nov., Yersiniaceae fam. nov., Hafniaceae fam. nov., Morganellaceae fam. nov., and Budviciaceae fam. nov. *Int. J Syst. Evol. Microbiol.* 66, 5575–5599. doi: 10.1099/ijsem.0.001485

Barthel, M., Hapfelmeier, S., Kremer, M., Rohde, M.,, M., Pfeffer, K., et al. (2003). Pretreatment of mice with streptomycin provides a *Salmonella enterica* serovar Typhimurium colitis model that allows analysis of both pathogen and host. *Infect. Immun.* 71, 2839–2858. doi: 10.1128/iai.71.5.2839-2858.2003

Bertani, G. (2004). Lysogeny at mid-twentieth century: P1, P2, and other experimental systems. *J. Bacteriol.* 186, 595–600. doi: 10.1128/jb.186.3.595-600.2004

Bosak, J., Micenkova, L., Hrala, M., Pomorska, K., Krejci, P., Gopfert, E., et al. (2018). Colicin FY inhibits pathogenic *Yersinia enterocolitica* in mice. *Scie Rep.* 8:12242. doi: 10.1038/s41598-018-30729-7

Bren, L. (2007). Bacteria-eating virus approved as food additive. *FDA Consum.* 41, 20–22.

Cai, K., Zhang, Y., Yang, B., and Chen, S. (2013). *Yersinia enterocolitica* ghost with msbB mutation provides protection and reduces proinflammatory cytokines in mice. *Vaccine* 31, 334–340. doi: 10.1016/j.vaccine.2012.11.004

Casey, E., van Sinderen, D., and Mahony, J. (2018). *In vitro* characteristics of phages to Guide 'Real Life' phage therapy suitability. *Viruses* 10:E163.

Cheng, M., Liang, J., Zhang, Y., Hu, L., Gong, P., Cai, R., et al. (2017). The bacteriophage EF-P29 efficiently protects against lethal vancomycin-resistant *Enterococcus faecalis* and alleviates gut microbiota imbalance in a murine bacteremia model. *Front. Microbiol.* 8:837. doi: 10.3389/fmicb.2017.00837

Colom, J., Cano-Sarabia, M., Otero, J., Cortes, P., Maspoch, D., and Llagostera, M. (2015). Liposome-encapsulated bacteriophages for enhanced oral phage therapy against *Salmonella* spp. *Appl. Environ. Microbiol.* 81, 4841–4849. doi: 10.1128/AEM.00812-15

Czajkowski, R., Ozymko, Z., de Jager, V., Siwinska, J., Smolarska, A., Ossowicki, A., et al. (2015). Genomic, proteomic and morphological characterization of two novel broad host lytic bacteriophages PhiPD10.3 and PhiPD23.1 infecting pectinolytic *Pectobacterium* spp. and *Dickeya* spp. *PLoS One* 10:e0119812. doi: 10.1371/journal.pone.0119812

Damasko, C., Konietzny, A., Kaspar, H., Appel, B., Dersch, P., and Strauch, E. (2005). Studies of the efficacy of Enterocoliticin, a phage-tail like bacteriocin, as antimicrobial agent against *Yersinia enterocolitica* serotype O3 in a cell culture system and in mice. *J. Vet. Med. B Infect. Dis. Vet. Public Health* 52, 171–179. doi: 10.1111/j.1439-0450.2005.00841.x

Djacem, K., Tavares, P., and Oliveira, L. (2017). Bacteriophage SPP1 pac cleavage: a precise cut without sequence specificity requirement. *J. Mol. Biol.* 429, 1381–1395. doi: 10.1016/j.jmb.2017.01.005

Drummond, N., Murphy, B. P., Ringwood, T., Prentice, M. B., Buckley, J. F., and Fanning, S. (2012). *Yersinia enterocolitica*: a brief review of the issues relating to the zoonotic pathogen, public health challenges, and the pork production chain. *Foodborne Pathog. Dis.* 9, 179–189. doi: 10.1089/fpd.2011.0938

Fredriksson-Ahomaa, M., Cernela, N., Hachler, H., and Stephan, R. (2012). *Yersinia enterocolitica* strains associated with human infections in Switzerland 2001-2010. *Eur. J. Clin. Microbiol. Infect. Dis.* 31, 1543–1550. doi: 10.1007/s10096-011-1476-7

Gu, J., Xu, W., Lei, L., Huang, J., Feng, X., Sun, C., et al. (2011). LysGH15, a novel bacteriophage lysin, protects a murine bacteremia model efficiently against lethal methicillin-resistant *Staphylococcus aureus* infection. *J. Clin. Microbiol.* 49, 111–117. doi: 10.1128/JCM.01144-10

Guenther, S., Herzig, O., Fieseler, L., Klumpp, J., and Loessner, M. J. (2012). Biocontrol of *Salmonella* Typhimurium in RTE foods with the virulent bacteriophage FO1-E2. *Int. J. Food Microbiol.* 154, 66–72. doi: 10.1016/j.ijfoodmicro.2011.12.023

Hao, H., Liang, J., Duan, R., Chen, Y., Liu, C., Xiao, Y., et al. (2016). *Yersinia* spp. identification using copy diversity in the chromosomal 16S rRNA gene sequence. *PLoS One* 11:e0147639. doi: 10.1371/journal.pone.0147639

He, Y., Shi, Y., Liu, M., Wang, Y., Wang, L., Lu, S., et al. (2018). Nonlytic recombinant phage tail fiber protein for specific recognition of *Pseudomonas aeruginosa*. *Anal. Chem.* 90, 14462–14468. doi: 10.1021/acs.analchem.8b04160

Hertwig, S., Klein, I., Schmidt, V., Beck, S., Hammerl, J. A., and Appel, B. (2003). Sequence analysis of the genome of the temperate *Yersinia enterocolitica* phage PY54. *J. Mol. Biol.* 331, 605–622. doi: 10.1016/s0022-2836(03)00763-0

Jeon, J., Park, J. H., and Yong, D. (2019). Efficacy of bacteriophage treatment against carbapenem-resistant *Acinetobacter baumannii* in *Galleria mellonella* larvae and a mouse model of acute pneumonia. *BMC Microbiol.* 19:70. doi: 10.1186/s12866-019-1443-5

Ji, Y., Cheng, M., Zhai, S., Xi, H., Cai, R., Wang, Z., et al. (2019). Preventive effect of the phage VB-SavM-JYL01 on rabbit necrotizing pneumonia caused by *Staphylococcus aureus*. *Vet. Microbiol.* 229, 72–80. doi: 10.1016/j.vetmic.2018.12.021

Leon-Velarde, C. G., Happonen, L., Pajunen, M., Leskinen, K., Kropinski, A. M., Mattinen, L., et al. (2016). *Yersinia enterocolitica*-specific infection by bacteriophages TG1 and varphiR1-RT is dependent on temperature-regulated expression of the phage host receptor OmpF. *Appl. Environ. Microbiol.* 82, 5340–5353. doi: 10.1128/AEM.01594-16

Leon-Velarde, C. G., Kropinski, A. M., Chen, S., Abbasifar, A., Griffiths, M. W., and Odumeru, J. A. (2014). Complete genome sequence of bacteriophage vB_YenP_AP5 which infects *Yersinia enterocolitica* of serotype O:3. *Virol. J.* 11:188. doi: 10.1186/1743-422X-11-188

Leskinen, K., Blasdel, B. G., Lavigne, R., and Skurnik, M. (2016). RNA-sequencing reveals the progression of phage-host interactions between phiR1-37 and *Yersinia enterocolitica*. *Viruses* 8:111. doi: 10.3390/v8040111

Loc-Carrillo, C., and Abedon, S. T. (2011). Pros and cons of phage therapy. *Bacteriophage* 1, 111–114. doi: 10.4161/bact.1.2.14590

Ma, Y. H., Islam, G. S., Wu, Y., Sabour, P. M., Chambers, J. R., Wang, Q., et al. (2016). Temporal distribution of encapsulated bacteriophages during passage through the chick gastrointestinal tract. *Poult. Sci.* 95, 2911–2920. doi: 10.3382/ps/pew260

Mayordomo, A. C., Silva, J. E., Gorlino, C. V., Arias, J. L., Beron, W., and Di Genaro, M. S. (2018). IL-12/23p40 overproduction by dendritic cells leads to an increased Th1 and Th17 polarization in a model of *Yersinia enterocolitica*-induced reactive arthritis in TNFRp55-/- mice. *PLoS One* 13:e0193573. doi: 10.1371/journal.pone.0193573

McConnell, E. L., Basit, A. W., and Murdan, S. (2008). Measurements of rat and mouse gastrointestinal pH, fluid and lymphoid tissue, and implications for in-vivo experiments. *J. Pharm. Pharmacol.* 60, 63–70. doi: 10.1211/jpp.60.1.0008

Orquera, S., Golz, G., Hertwig, S., Hammerl, J., Sparborth, D., Joldic, A., et al. (2012). Control of Campylobacter spp. and *Yersinia enterocolitica* by virulent bacteriophages. *J. Mol. Genet. Med.* 6, 273–278.

Pajunen, M. I., Kiljunen, S. J., Soderholm, M. E., and Skurnik, M. (2001). Complete genomic sequence of the lytic bacteriophage phiYeO3-12 of *Yersinia enterocolitica* serotype O:3. *J. Bacteriol.* 183, 1928–1937. doi: 10.1128/jb.183.6.1928-1937.2001

Rosner, B. M., Stark, K., and Werber, D. (2010). Epidemiology of reported *Yersinia enterocolitica* infections in Germany, 2001-2008. *BMC Public Health* 10:337. doi: 10.1186/1471-2458-10-337

Rosner, B. M., Werber, D., Hohle, M., and Stark, K. (2013). Clinical aspects and self-reported symptoms of sequelae of *Yersinia enterocolitica* infections in a population-based study, Germany 2009-2010. *BMC Infect. Dis.* 13:236. doi: 10.1186/1471-2334-13-236

Saraka, D., Savin, C., Kouassi, S., Cisse, B., Koffi, E., Cabanel, N., et al. (2017). *Yersinia enterocolitica*, a neglected cause of human enteric infections in cote d'Ivoire. *PLoS Negl. Trop. Dis.* 11:e0005216. doi: 10.1371/journal.pntd.0005216

Schwudke, D., Ergin, A., Michael, K., Volkmar, S., Appel, B., Knabner, D., et al. (2008). Broad-host-range *Yersinia* phage PY100: genome sequence, proteome analysis of virions, and DNA packaging strategy. *J. Bacteriol.* 190, 332–342. doi: 10.1128/jb.01402-07

Skurnik, M., and Strauch, E. (2006). Phage therapy: facts and fiction. *Int. J. Med. Microbiol.* 296, 5–14. doi: 10.1016/j.ijmm.2005.09.002

Strydom, H., Wang, J., Paine, S., Dyet, K., Cullen, K., and Wright, J. (2019). Evaluating sub-typing methods for pathogenic *Yersinia enterocolitica* to support outbreak investigations in New Zealand. *Epidemiol. Infect.* 147:e186. doi: 10.1017/S0950268819000773

Synnott, A. J., Kuang, Y., Kurimoto, M., Yamamichi, K., Iwano, H., and Tanji, Y. (2009). Isolation from sewage influent and characterization of novel *Staphylococcus aureus* bacteriophages with wide host ranges and potent lytic capabilities. *Appl. Environ. Microbiol.* 75, 4483–4490. doi: 10.1128/AEM.02641-08

Wall, S. K., Zhang, J., Rostagno, M. H., and Ebner, P. D. (2010). Phage therapy to reduce preprocessing *Salmonella* infections in market-weight swine. *Appl. Environ. Microbiol.* 76, 48–53. doi: 10.1128/AEM.00785-09

Xi, H., Dai, J., Tong, Y., Cheng, M., Zhao, F., Fan, H., et al. (2019). The characteristics and genome analysis of vB_AviM_AVP, the first phage infecting *Aerococcus viridans*. *Viruses* 11:104. doi: 10.3390/v11020104

Zelasko, S., Gorski, A., and Dabrowska, K. (2017). Delivering phage therapy per os: benefits and barriers. *Expert Rev. Anti Infect. Ther.* 15, 167–179. doi: 10.1080/14787210.2017.1265447

Zhang, C., Li, W., Liu, W., Zou, L., Yan, C., Lu, K., et al. (2013). T4-like phage Bp7, a potential antimicrobial agent for controlling drug-resistant *Escherichia coli* in chickens. *Appl. Environ. Microbiol.* 79, 5559–5565. doi: 10.1128/AEM.01505-13

Conflict of Interest: The authors declare that the research was conducted in the absence of any commercial or financial relationships that could be construed as a potential conflict of interest.

Copyright © 2020 Xue, Zhai, Wang, Ji, Wang, Wang, Wang, Xi, Cai, Zhao, Zhang, Bi, Guan, Guo, Han and Gu. This is an open-access article distributed under the terms of the Creative Commons Attribution License (CC BY). The use, distribution or reproduction in other forums is permitted, provided the original author(s) and the copyright owner(s) are credited and that the original publication in this journal is cited, in accordance with accepted academic practice. No use, distribution or reproduction is permitted which does not comply with these terms.

frontiers in Microbiology

ORIGINAL RESEARCH
published: 17 March 2020
doi: 10.3389/fmicb.2020.00414

Impact of Frequent Administration of Bacteriophage on Therapeutic Efficacy in an *A. baumannii* Mouse Wound Infection Model

Michael D. Rouse[1,2], Joshua Stanbro[1,2], Jessica A. Roman[1,2], Michelle A. Lipinski[1,2], Anna Jacobs[3], Biswajit Biswas[4], James Regeimbal[5], Matthew Henry[2,4], Michael G. Stockelman[2] and Mark P. Simons[2]*

[1] Henry M Jackson Foundation for the Advancement of Military Medicine, Bethesda, MD, United States, [2] Naval Medical Research Center, Silver Spring, MD, United States, [3] Walter Reed Army Institute of Research, Silver Spring, MD, United States, [4] Biological Defense Research Directorate, Naval Medical Research Center, Fort Detrick, MD, United States, [5] Naval Medical Research Unit-6, Lima, Peru

OPEN ACCESS

Edited by:
Robert Czajkowski,
University of Gdańsk, Poland

Reviewed by:
Catherine Maylin Loc-Carrillo,
The University of Utah, United States
Rodolfo García-Contreras,
National Autonomous University of Mexico, Mexico

***Correspondence:**
Michael D. Rouse
michael.d.rouse11.ctr@mail.mil

Specialty section:
This article was submitted to Antimicrobials, Resistance and Chemotherapy, a section of the journal Frontiers in Microbiology

Received: 05 December 2019
Accepted: 27 February 2020
Published: 17 March 2020

Citation:
Rouse MD, Stanbro J, Roman JA, Lipinski MA, Jacobs A, Biswas B, Regeimbal J, Henry M, Stockelman MG and Simons MP (2020) Impact of Frequent Administration of Bacteriophage on Therapeutic Efficacy in an A. baumannii Mouse Wound Infection Model. Front. Microbiol. 11:414. doi: 10.3389/fmicb.2020.00414

The spread of multidrug antibiotic resistance (MDR) is a widely recognized crisis in the treatment of bacterial infections, including those occurring in military communities. Recently, the World Health Organization published its first ever list of antibiotic-resistant "priority pathogens" – a catalog of 12 families of bacteria that pose the greatest threat to human health with *A. baumannii* listed in the "Priority 1: Critical" category of pathogens. With the increasing prevalence of antibiotic resistance and limited development of new classes of antibiotics, alternative antimicrobial therapies are needed, with lytic bacteriophage (phage) specifically targeted against each of the high priority bacterial infections as a potential approach currently in development toward regulatory approval for clinical use. Balb/c mice were prophylactically administered PBS or phage selected against *A. baumannii* strain AB5075. After 3 weeks, mice were anesthetized, wounded (dorsal), and challenged topically with AB5075. Following infection, mice were subsequently treated with PBS or phage for three consecutive days, and evaluated for 3 weeks to assess the safety and efficacy of the phage treatment relative to the control. We assessed mortality, bacterial burden, time to wound closure, systemic and local cytokine profiles, alterations in host cellular immunity, and finally presence of neutralizing antibodies to the phage mixture. In our study, we found that prophylactic phage administration led to a significant reduction in monocyte-related cytokines in serum compared to mice given PBS. However, we detected no significant changes to circulating blood populations or immune cell populations of secondary lymphoid organs compared to PBS-treated mice. Following prophylactic phage administration, we detected a marked increase in total immunoglobulins in serum, particularly IgG2a and IgG2b. Furthermore, we determined that these antibodies were able to specifically target phage and effectively neutralize their ability to lyse their respective target. In regards to their therapeutic efficacy, administration of phage treatment effectively decreased wound size of mice infected with AB5075 without adverse effects. In conclusion, our data demonstrate that phage can serve as a safe and

effective novel therapeutic agent against *A. baumannii* without adverse reactions to the host and pre-exposure to phage does not seem to adversely affect therapeutic efficacy. This study is an important proof of concept to support the efforts to develop phage as a novel therapeutic product for treatment of complex bacterial wound infections.

Keywords: bacteriophage, *Acinetobacter baumannii*, wound infection, host immunity, therapeutic efficacy

INTRODUCTION

The Infectious Diseases Society of America (IDSA) has categorized antimicrobial resistance as "one of the greatest threats to human health worldwide" (Hospenthal et al., 2011). The augmented frequency of multi-drug resistant (MDR) bacterial pathogens has been closely associated with the clinical use of broad spectrum antibiotics, thus ensuing an amplified mutation rate in attempts to maintain bacterial survival (Ena et al., 1993). In addition, there is a tremendous financial burden associated with these infections, which has been estimated to be between $21 billion and $34 billion in the United States alone (Spellberg et al., 2013). The primary culprits have been identified as the ESKAPE pathogens (*Enterococcus faecium*, *Staphylococcus aureus*, *Klebsiella pneumoniae*, *Acinetobacter baumannii*, *Pseudomonas aeruginosa*, and *Enterobacter* spp.), and can cause severe local and systemic infections (Murray et al., 2009; Hospenthal et al., 2011). *A. baumannii*, for example, is a Gram-negative, encapsulated opportunistic pathogen that can cause various types of infections, such as pneumonia, bloodstream infections, meningitis, urinary tract infections, wound, and surgical site infections (Safdar and Maki, 2002; Maragakis and Perl, 2008). According to the CDC, it is estimated that 63% of *Acinetobacter* strains are found to be MDR *A. baumannii*[1] (Center for Disease Control and Pravention, 2013).

A majority of combat-related injuries are associated with significant tissue destruction, and therefore are at high risk for infectious complications, which have occurred in up to 35% of service members who suffered from combat-related injuries during Operations Iraqi- and Enduring Freedom (Murray et al., 2009; Hospenthal et al., 2011). A majority of these infections involved skin, soft tissue, and wounds, and the prevalence of infection in severe injuries, such as open tibial fractures, was as high as 77% (Johnson et al., 2007). Because of the severity of their injuries, patients with combat-trauma are also at a high risk for acquiring nosocomial infections from MDR bacteria due to prolonged hospitalization, inter-institutional transfer, exposure to invasive devices (e.g., central venous catheters, etc.), and exposure to antibiotics (Safdar and Maki, 2002). Pathogens of the ESKAPE (*E. faecium*, *S. aureus*, *Klebsiella* spp., *A. baumannii*, *P. aeruginosa*, and *Enterobacter* spp.) classification were identified as the most frequent isolates associated with combat-trauma wound infections (Keen et al., 2010). The limited number of treatment options against MDR infections is exacerbated by the continuing shortage of new antibiotics in the development pipeline (Spellberg et al., 2013), thus alternative therapeutic are urgently needed to treat complex infections in both military and civilian populations.

Lytic bacteriophage (phage) are viruses that specifically infect and lyse bacteria. Phages have long been considered for use in therapy based on advantages including the high specificity of phage for the host bacteria, the exponential accumulation of phage when bacteria are present, and rapid removal of phage after bacterial clearance. Currently phage therapy is used to prevent and treat bacterial infections in the countries of Georgia and Poland, but the clinical studies with phage in these countries lack quantitative information and adequate controls to robustly address the safety and efficacy of phage therapy (Boucher et al., 2009). In the current study, we investigated the efficacy of phage as a prophylactic and therapeutic regimen, and the impact that pre-immunization to phage has on subsequent efficacy.

MATERIALS AND METHODS

Mice

Female 6-week-old BALB/c mice were purchased from Charles River. Mice were quarantined for 2 weeks prior to the start of the study. Mice were single housed at the start of the study for 1 week, before being group housed.

Ethics Statement

Research was performed in compliance with the Animal Welfare Act and adheres to principles stated in the *Guide for the Care and Use of Laboratory Animals* (Council, 2011). The study protocol was reviewed and approved by the Institutional Animal Care and Use Committee at the Walter Reed Army Institute of Research and Naval Medical Research Center in compliance with all applicable Federal regulations governing the protection of animals in research.

Reagents and Monoclonal Antibodies

The reagents were purchased as follows: red blood cell lysis buffer from Sigma-Aldrich (St. Louis, MO, United States); Percoll, phosphate-buffered saline (PBS) and fetal bovine serum (FBS) from Fisher Scientific; fixation solution from Biolegend.

The following anti-mouse monoclonal antibodies were purchased from BioLegend (San Diego, CA, United States): CD3 APC-Cy7 (17A2), CD4 Brilliant Violet 605 (GK1.5), CD8a PE-Cy7 (53-6.7), CD19 FITC (6D5), TCRγδ PE (GL3), and F4/80 Brilliant Violet 510 (BM8). The following anti-mouse monoclonal antibodies were purchased from BD Biosciences (San Diego, CA, United States): CD11c APC-R700 (N418). The following anti-mouse monoclonal antibodies were purchased

[1]https://www.cdc.gov/drugresistance/pdf/ar-threats-2013-508.pdf

from Bio-Rad (Hercules, CA, United States): Ly6B.2 Alexa Fluor 647 (7/4). The following anti-mouse monoclonal antibodies were purchased from Thermo Fisher Scientific: Live/Dead Fix Blue (L23105).

Bacterial Strains and Phage Mixture

In order to visualize wound bacterial burden during animal studies, in the current study, the bioluminescent strain AB5075 *att*Tn*7*:*luxCDABE* (AB5075:lux) (see **Supplementary Material** for antibiotic susceptibility profile), previously described by Regeimbal et al. (2016), was used to inoculate and infect naïve Balb/c. AB5075:lux, which was used to determine wound bacterial burden via luminescent signal, was maintained on tryptic soy broth (TSB; Becton, Dickinson and Company) or Lennox LB broth (Becton, Dickinson and Company) and stored in 20–40% glycerol at −80°C. The five member phage mixture (AbArmy ϕ1, AbNavy ϕ1, AbNavy ϕ2, AbNavy ϕ3, and AbNavy ϕ4) that was designed to be lytic against AB5075:lux was added at equal volumes to generate a stock concentration of 1×10^9 PFU/mL and was described previously by Regeimbal et al. (2016).

Immunophenotyping

Various tissues [spleen, lymph nodes (LN), and liver] were collected at various time points from naïve mice following administration of either PBS (control) or AB5075 phage mixture to determine changes to the frequency of different immune cell populations. Tissues were homogenized into a single cell suspension. Mononuclear cells from liver homogenates were enriched using a 33% Percoll gradient. Tissue homogenates were subjected to red blood cell lysis and total cell count enumerated using a BioRad automated cell counter. For analysis, 2×10^6 cells were stained with Live/Dead Fix Blue according to the manufacturer's protocol, followed by immunostaining with anti-mouse monoclonal antibodies target against extracellular markers to various immune cell populations for 20 min at 4°C in the presence of 1× PBS supplemented with 2% FBS. Cells were then washed twice, fixed with 4% paraformaldehyde 20 min at 4°C, washed again, and finally suspended in PBS. All samples were ran on a BD LSR Fortessa (BD Biosciences, San Diego, CA, United States) by collecting ≥10,000 events and analyzed using FlowJo software. Negative gates were set using fluorescence-minus-one controls. The following gating strategy was used to assess different immune cell populations: SSC/FSC panel was gated on cells to exclude debris → singlets were gated → live cells only (based on the live/dead stain). From the live cell gate, CD3 (alone), CD11c, CD19, and F4/80 were then assessed. Subsets of CD3+ cells were further differentiated based on the positive gated population CD3 to determine CD3+/CD4+, CD3+/CD8+, and CD3+/γδTCR+ populations.

Phage Neutralization Assay

Serum collected from at various time points from naïve mice following administration of either PBS (control) or AB5075 phage mixture were stored in a −80°C freezer until the assay was performed. Serum was serially diluted in 96-well microtiter plates. AB5075 phage mixture was diluted to a titer of 2×10^6 PFU/mL in PBS. Phage (4×10^4 total PFU) was incubated at 37°C with respective serum at a 1:10 ratio. Samples of the incubated phage-serum mixture were taken at various time intervals and further diluted 1:100 in PBS to stop the antibody reaction. The diluted PBS-phage-serum mixture was spot plated on a lawn of *A. baumannii* and assessed for plaque formation. The neutralization rate (K-value) was determined by the following equation to indicate the rate of 90% phage inactivation as described in Lusiak-Szelachowska et al. (2014): $K = (2.3\ D/t) \times \log\ (p_0/p)$.

Cytokine/Chemokine Analysis

Serum cytokines/chemokines levels were assessed at various time points from naïve mice following administration of either PBS (control) or AB5075 phage mixture. A custom Millipore 25-plex Mouse Cytokine/Chemokine Magnetic Bead Panel kit (MCYTOMAG-70K-PMX, Burlington, MA, United States) was purchased and used according to the manufacturer's instructions to analyze the following: G-CSF, IFNγ, IL-1α, IL-1β, IL-2, IL-4, IL-5, IL-6, IL-7, IL-9, IL-10, IL-12p40, IL-12p70, IL-13, IL-15, IL-17, IP-10, KC, MCP-1 MIP-1a, MIP-1b, MIP-2, RANTES, TNFα, and GM-CSF.

Total Immunoglobulin Measurements

Total immunoglobulins for serum were assessed at various time points from naïve mice following administration of either PBS (control) or AB5075 phage mixture. A custom Millipore Mouse Immunoglobulin Isotyping Magnetic Bead Panel kit (MGAMMAG-300K, Burlington, MA, United States) was purchased and used according to the manufacturer's instructions to analyze the following: IgA, IgG1, IgG2a, IgG2b, IgG3, and IgM.

Full Thickness Dorsal Wound Mouse Model

Phage treatment was assessed using a previously described mouse wound model (Thompson et al., 2014) with some modifications. Briefly, 6-week-old female BALB/c mice were randomly separated and administered either 100 μL of PBS or 1×10^9 PFU (1×10^8 total PFU) of phages in PBS intraperitoneally (i.p.) at Days 20 and 10 (**Figure 1**). Mice were immunosuppressed via cyclophosphamide injection on Days 4 and 1. On Day 0, their backs were shaved, and a full-thickness wound was created on the dorsal side of each mouse using a sterile 6 mm biopsy punch (∼0.3 cm^2). Each wound was inoculated with $\sim 5 \times 10^6$ total CFU of AB5075:lux, and a Tegaderm bandage was placed over the wound. Mice were housed singly from day 0 (inoculation) to day 6. Mice were then further separated into four group based on their pre-treatment/post-treatment regimen: (1) PBS–PBS, (2) PBS–Phage, (3) Phage–PBS, and (4) Phage–Phage. For phage treatments, mice received both 100 μL of 1×10^9 PFU (1×10^8 total PFU) of phages in PBS i.p. and 50 mL 1×10^9 PFU (5×10^7 total PFU) of phages in PBS delivered topically under the Tegaderm dressing, on top of the wound. Treatments were administered at 4, 24, and 48 h post-infection. On day 6 post-infection, each Tegaderm dressing was removed and the wounds were left exposed to air for the remainder of the experiment. An IVIS *in vivo* imaging

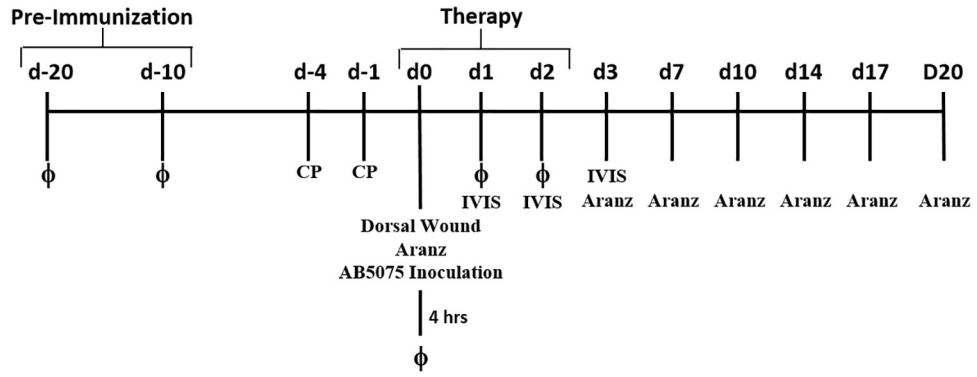

FIGURE 1 | Experimental timeline. Diagram of experimental treatments and model design.

system (IVIS) (PerkinElmer, Waltham, MA, United States) was used to measure the bioluminescent signal of AB5075:lux as a means to visualize and perform relative quantification of bacterial burdens in the wound beds of anesthetized mice over the course of the experiment. Living Image Software version 4.2 (PerkinElmer, Waltham, MA, United States) was used to analyze and quantify *in vivo* bioluminescence as defined with the "Auto ROI" function with a threshold of 10%. The Aranz Silhouette wound measurement device was used to image and measure the physical wound size of mice at various time points throughout the study (Aranz Medical Ltd., Christchurch, New Zealand).

Detection of Phage Titers in Organs

Naïve 6-week-old female BALB/c mice were randomly separated and administered either 100 μL of PBS or 1×10^9 PFU (1×10^8 total PFU) of phages in PBS i.p. at Days 20 and 10 (**Figure 1**). Mice were euthanized at Days 19, 15, and 5, and various organs were excised for the presence of phage. Tissues were homogenized in 5 mL PBS, dilutions of 10^{-1}–10^{-8} were generated, and the various dilutions were spot plated on a lawn of *A. baumannii* AB5075:lux. Samples were allowed to incubate at 37°C overnight and phage plaques were enumerated the next day.

Statistical Analysis

The data shown in this paper is pooled from at least three independent experiments. The mean ± standard error of the mean (SEM) is shown for experiments that are applicable. The statistical differences within experiments were calculated using an analysis of variance (ANOVA). A P-value < 0.05 was considered to be statistically significant.

RESULTS

Distribution of Phage Upon Administration

Phage are viruses that have evolved to interact and target a specific bacterial host. Considering the diverse composition of phage, in addition to their ability lyse select bacterial strains and subsequently release components of lysed bacterial cells into the environment, phage may either directly or indirectly influence the mammalian host immune system. In order to better understand the immunogenicity and limitations of phage therapy, we wanted to first determine where phage migrate upon systemic administration. Therefore, we administered either sterile PBS or 10^8 total PFU of a five member AB5075 phage mixture i.p. to naïve Balb/c mice. After 24 h, we collected peripheral tissues, such as spleen, liver, and lymph nodes (LN) pooled from throughout the body, and examined them for the presence of phage. We found in mice administered phage, the spleen possessed the highest titer of phage ($2.02 \times 10^5 \pm 1.34 \times 10^5$ PFU/mL) followed by liver ($8.71 \times 10^2 \pm 1.29 \times 10^2$ PFU/mL) and LN ($4.43 \times 10^5 \pm 1.97 \times 10^2$ PFU/mL), whereas control animals had undetectable titers in all organs (**Figure 2**).

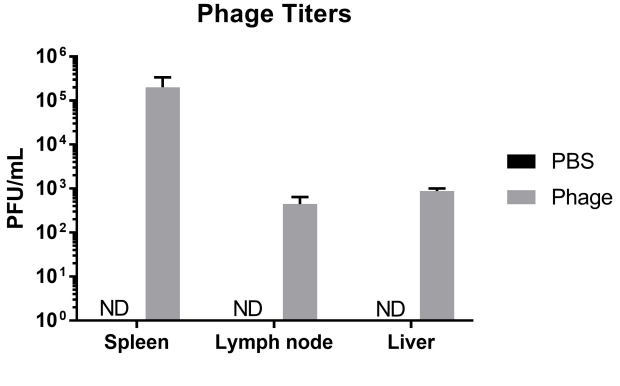

FIGURE 2 | Distribution of phage upon administration. Naïve Balb/c mice were assessed for phage titers 24 h after PBS or phage mixture administration. $N = 7$ per group (ND = not detected).

Phage Mixture Administration Decreases Monocyte-Related Cytokines/Chemokines in Serum.

Next, we sought to determine whether the AB5075 phage mixture impelled cytokine and chemokine production following systemic administration. Thus, we administered either 100 μL of sterile PBS or 1×10^9 PFU of the AB5075 phage mixture i.p. to naïve Balb/c mice at Days 20 and 10, and

collected serum at various time points (Days 19, 15, and 5) (**Figure 3**). Of the 25 cytokines/chemokines in our panel, only 8 illustrated a difference between PBS- and phage-treated mice (**Figure 3**). These circulating factors included G-CSF, IL-12 (p40), IL-13, IP-10/CXCL10, MIP1α, MIP1β, MIP2, and RANTES, which have been shown to be associated with the maturation and function of monocytes. Interestingly, the AB5075 phage mixture was observed to significantly downregulate these eight cytokine/chemokine levels in serum within 5 days of a single administration to naïve mice compared to PBS control. Moreover, some of their levels were further decreased following a second administration. We found no significant differences in IL-1a, IL-5, IL-9, IL-15, and MCP-1 between PBS and phage administered naïve mice (**Figure 3**). The remaining 12 cytokines/chemokines in the panel, which included prominent pro-inflammatory markers IFNγ and TNFα as well as anti-inflammatory markers IL-4 and IL-10, were measured as below detectable levels.

Administration of Phage Mixture Does Not Modulate Immune Cell Populations

Due to the altered cytokine/chemokine profile following systemic administration of the AB5075 phage mixture, we wanted to establish its potential effects on other facets of the immune system. Thus, we collected whole blood at various time points from naïve mice administered PBS or AB5075 phage mixture at Days 20 and 10. Subsequently, we examined their complete blood count (CBC) profile, focusing on the frequency and total cell number of immune cell populations, such as neutrophils, monocytes, lymphocytes, and eosinophils (**Figure 4**). As a result, we observed no statistical differences or trends between groups at any of the time points collected.

After seeing no impact on systemic immune cell populations, we took a closer look at cell populations that reside in secondary lymphoid tissues, such as spleen, LN, and liver (**Figure 5**). We examined these tissues for any gross changes that may occur in the prominent immune bionetwork using flow cytometry. Similar to what we observed in the CBC profiles, AB5075 phage mixture appeared to elicit no significant impact on the frequency of T-cells ($CD3^+$: $CD4^+$, $CD8^+$, $TCR\gamma\delta^+$), B-cells ($CD19^+$), dendritic cells ($CD11c^+$), or macrophages ($F4/80^+$) in any of the tissues.

Phage Mixture Administration Promotes IgG2a and IgG2b Antibody Generation

Unlike cytokines, which can be produced and secreted by any cell type, antibodies, or immunoglobulins can only be derived from plasma B-cells. In the current study, we investigated immunoglobulin levels in circulation following single or multiple administrations of PBS or AB5075 phage mixture (**Figure 6**). We found serum IgM levels to sustain around $\sim 3 \times 10^6$ ng/mL at the various time points for either PBS or AB5075 phage mixture treated mice. Similarly, AB5075 phage mixture administration did not alter the immunoglobulin titers IgA, IgG1, or IgG3 compared to PBS treated mice on a day-to-day basis (**Figure 6**). Surprisingly, mice given AB5075 phage mixture revealed a prompt induction of antibody titer for both Ig2a and Ig2b within 24 h of administration in comparison to PBS mice. Moreover, Ig2a and Ig2b serum levels continued to be enhanced 5 days after the first administration of AB5075 phage mixture given on Day 20 and continued to be augmented following the second administration on Day 10.

Detection of Serum Neutralizing Antibodies Against *A. baumannii* Phage Mixture

Upon detecting significant amounts of immunoglobulin titers in serum following AB5075 phage mixture administration, we set out to determine whether those antibodies specifically targeted our phage mixture as well as potentially impeded the mixture's therapeutic functions and efficacy (**Figure 7**). In testing for the presence of neutralizing antibodies, we diluted a set of previously collected serum samples from PBS or AB5075 phage treated mice. The diluted serum was then incubated with a known titer of AB5075 phage mixture (4×10^4 total PFU) before being added to a lawn of AB5075. After overnight incubation, the agar plates were assessed for plaque formation, which would indicate the ability of the phage mixture to bind and lyse that targeted bacteria. Accordingly, a *K*-value was calculated to signify the rate at which 90% phage were neutralized and unable to lyse their intended target compared to unhindered phage titer control. Interestingly, despite the fact that we were able to detect high titers of immunoglobulins as early as Day 19, we were only able to detect the initial trend of neutralizing antibodies at Day 15 as illustrated by the *K*-value of 1.511 ± 0.869 max *K*/min observed from AB5075 phage treated mice compared to 0.058 ± 0.061 max *K*/min of PBS-treated mice. More importantly, the occurrence of neutralizing antibodies was found to peak markedly at Day 5, where the *K*-value was roughly 18-fold greater in AB5075 phage treated mice compared to those given PBS (AB5075 phage: 26.36 ± 5.063 max *K*/min vs. PBS: 1.408 ± 1.372 max *K*/min). Surprisingly, this notable increase hastily appeared to subside to almost baseline by Day 0 (AB5075 phage: 8.262 ± 4.469 max *K*/min vs. PBS: 0.047 ± 0.046 max *K*/min).

Effects of Phage Mixture on Wound Closure and Bacterial Burden Following *A. baumannii* Infection

The presence of a bacterial infection compounds the stresses and burdens placed on the host's immune system. Moreover, in the case of an open wound, it can prolong the wound healing process and exacerbate inflammation and tissue damage. As an alternative approach to standard of care antibiotics, our institute has previous shown that phage therapy may serve as a selective and effective tool against bacterial pathogens, even those that have become resistant to current treatment regimens (Regeimbal et al., 2016). The potential caveat in phage therapy lies in the host's immune system generating a response against the phage following multiple treatment regimens and clearing them before the treatment has a chance of clearing the infection. This is important to note given the fact that in the current study, we not only observed a significant increase in the presence of immunoglobulins, particularly IgG2a and IgG2b, but we also

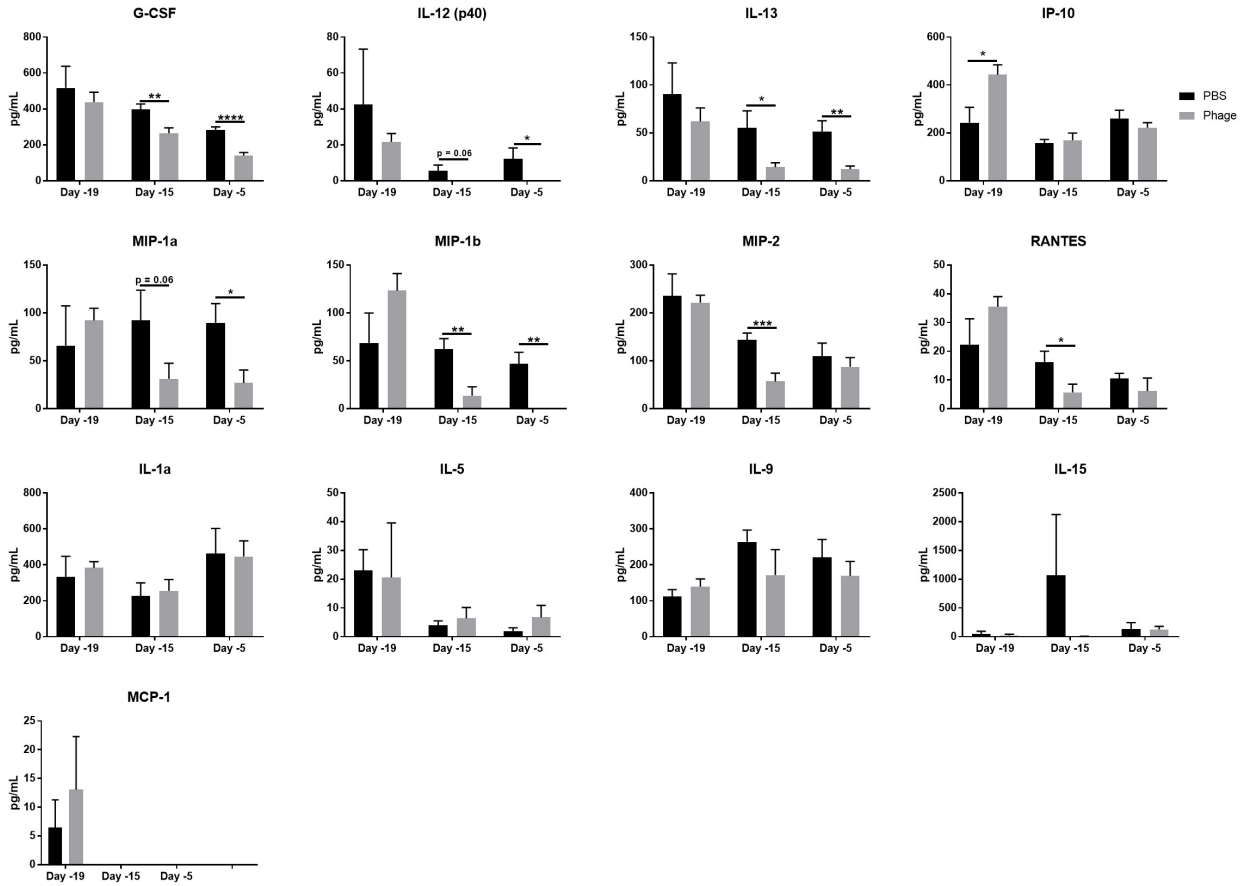

FIGURE 3 | Phage mixture administration decreases monocyte-related cytokines/chemokines in serum. Serum collected from naïve mice given PBS (control) or phage mixture were analyzed for cytokines/chemokines using a 25-plex panel. $N = 10$ per group for each time point; $^{*}p < 0.05$, $^{**}p < 0.01$, $^{***}p < 0.001$, and $^{****}p < 0.0001$.

found that these serum antibodies were able to neutralize the lytic function of phage in our *in vitro* assays. Therefore, we wanted to evaluate the therapeutic effects of our phage mixture during an *A. baumannii* wound infection following single and multi-dose regimens.

In our mouse dorsal wound infection model, we randomly separated mice into four groups where PBS or AB5075 phage mixture were given as prophylactic (in parentheses) or post-infection/treatment regimens in various combinations: PBS–PBS, Phage–PBS, PBS–Phage, and Phage–Phage. Prophylactic regimens were administered i.p. to naïve mice at Days 20 and 10 with either 100 μL of PBS or AB5075 phage mixture (1×10^8 total PFU). Mice were moderately immunosuppressed using cyclophosphamide standardized in our model prior to introducing a 6-mm dorsal wound and subsequent topical infection with *A. baumannii* strain AB5075: *lux*. Post-infection treatment regimens were administered both i.p. and topically at 4 h after infection on Days 0, 1, and 2. We found that PBS–PBS-treated mice subsequently infected with AB5075: *lux* had a high bacterial bioburden 24 h after infection as measured by capturing the bacterial luminescence signal using an IVIS. Bacterial burden did not appear to be altered by prophylactic administration of AB5075 phage mixture, designated as Phage-PBS (**Figure 8B**). The treatment regimen of AB5075 phage mixture [PBS-Phage], on the other hand, was able to promptly reduce bacterial bioburden compared to PBS–PBS mice ($3.32 \times 10^8 \pm 8 \times 10^7$ vs. $6.35 \times 10^8 \pm 2 \times 10^8$ p/s/cm^2/sr) (**Figure 8A**). Meanwhile, the additive measures of including both a pre- and post-infection treatment regimen, Phage–Phage, provided an intermediary effect between PBS–PBS and PBS–Phage mice. In regards to wound size following infection with AB5075: *lux*, we observed that wounds of PBS–PBS mice rapidly increased from 0.3 ± 0.01 cm^2 on Day 0 to 1.27 ± 0.09 cm^2 by Day 8. Furthermore, wounds of PBS–PBS mice only returned to size of the original injury (0.3 ± 0.01 cm^2) around Day 17, but never closed by the end of the study (**Figure 8B**). In comparison, Phage–PBS mice exhibited a similar healing profile and wound sizes as PBS–PBS mice throughout the study, suggesting the prophylactic regimen of AB5075 phage mixture was not effective in mitigating the bioburden and collateral damage of the infectious pathogen. PBS–Phage mice, however, showed reduced wound size throughout the study, especially at the apex on Day 8 in which overall wound sizes were limited to $0.832 \pm 0.0.09$ cm^2. Additionally, wounds of PBS–Phage not only returned to baseline

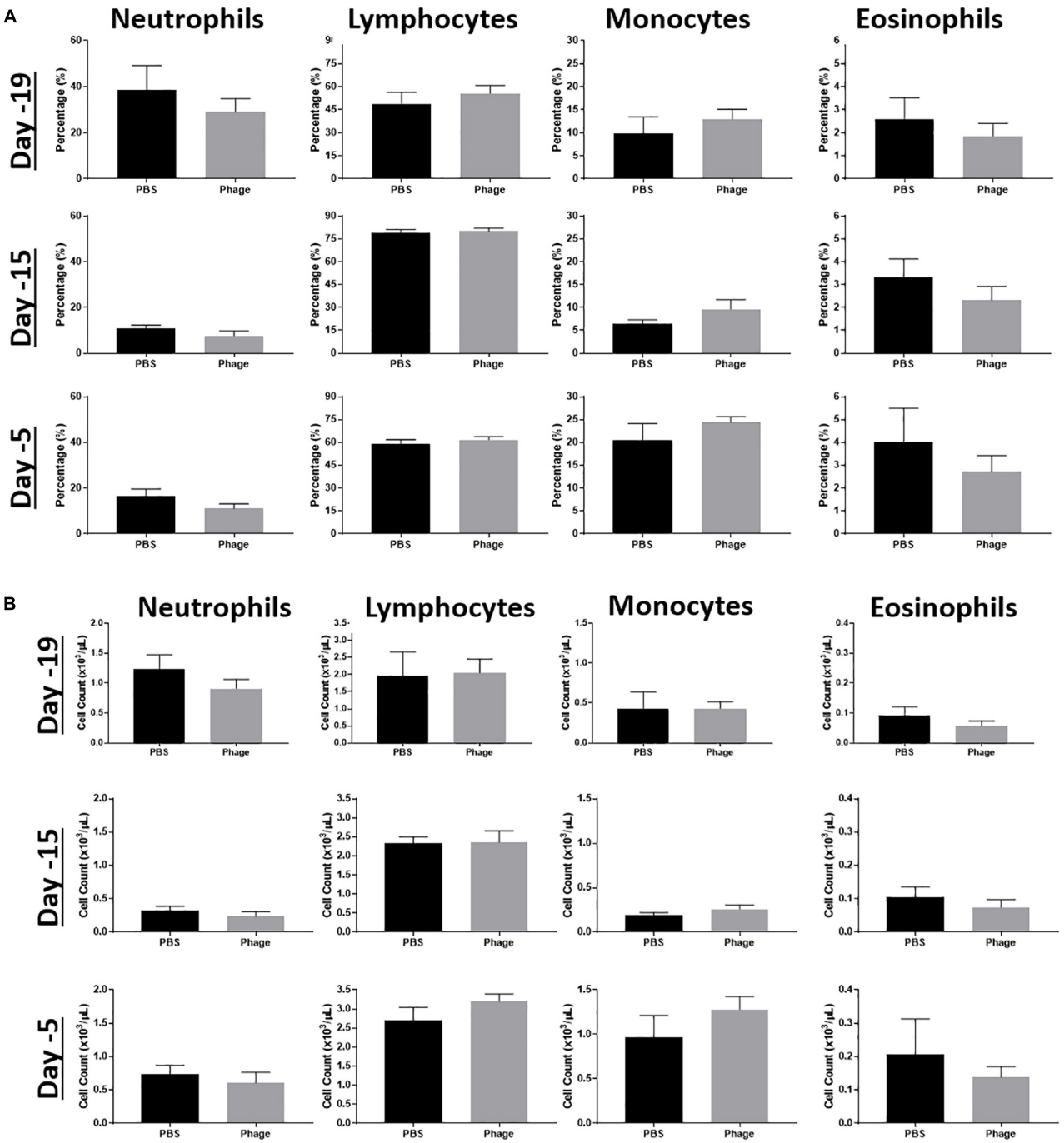

FIGURE 4 | Effects of phage mixture on peripheral immune cell populations. Complete blood counts, **(A)** percentages and **(B)** cell count were measured from whole blood at various time points following PBS (control) or phage mixture administration in naïve mice. *N* = 6 per group per time point.

by Day 14, which was a full 3 days before PBS–PBS mice, but were fully closed by Day 17. When we examined if there was a change in efficacy following multiple administrations of the same phage mixture, we found that Phage–Phage mice had condensed wound sizes, peaking on Day 8 at $0.9 \pm 0.0.09$ cm^2. Similar to PBS–Phage mice, Phage–Phage mice also presented wounds that returned to original size by Day 14 and complete closure by Day 17.

DISCUSSION

The prevalence of MDR bacterial pathogens is a growing threat to public health due to a variety of factors, such as immune competence, educational awareness and intervention, and overuse of antibiotics in food products and patients. Thus, there is an urgent need for new therapeutics against the MDR

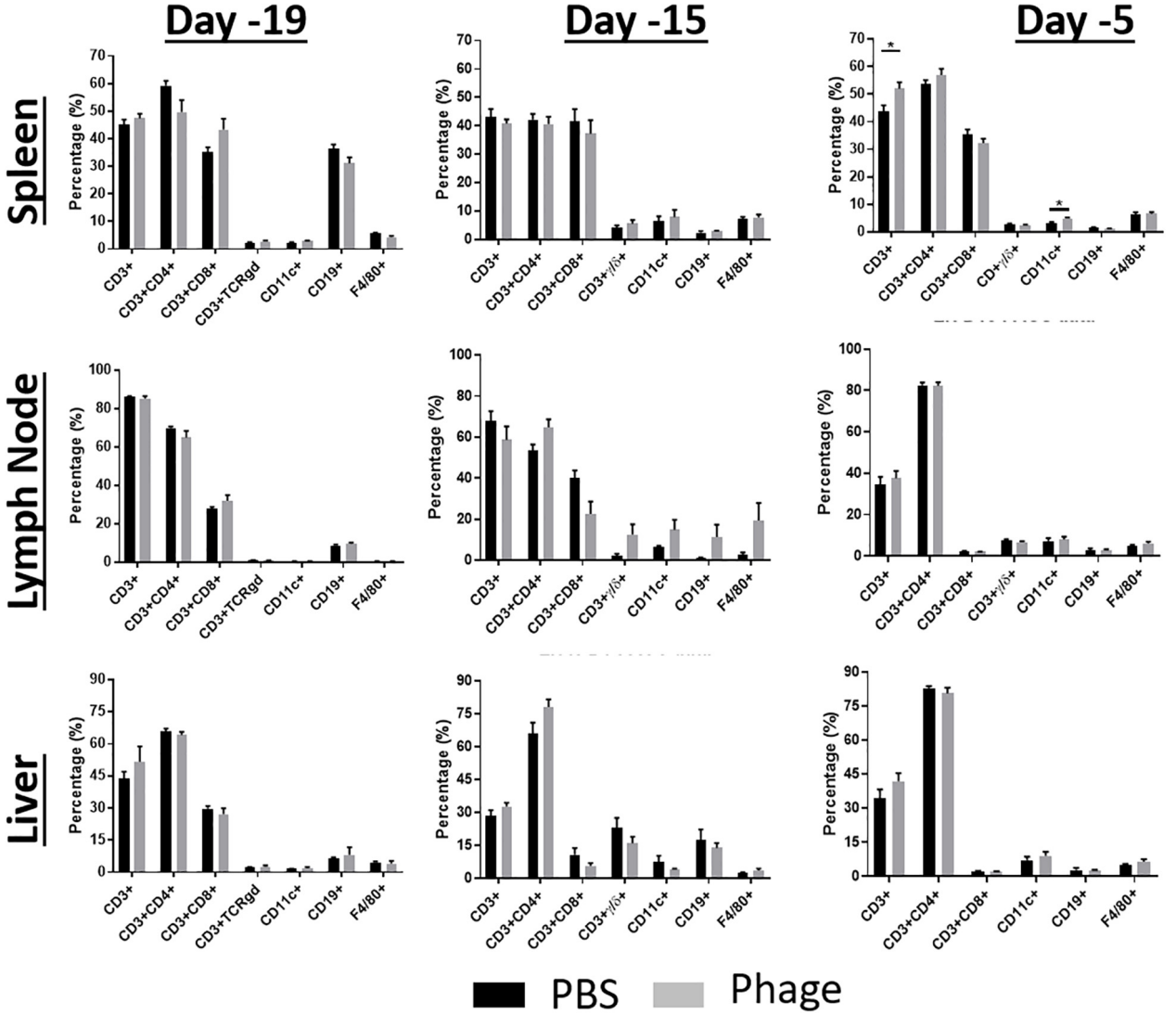

FIGURE 5 | Administration of phage mixture does not modulate immune cell populations. Immune cell populations were assessed at various time points from naïve mice following PBS (control) or phage mixture administration (i.p.). $N = 6$ per group per time point; $^{*}p < 0.05$.

pathogens, including *A. baumannii*, that either replace or work in tandem with current standard of care. Recently, phages have reemerged as potential antibacterial candidates due to their narrow spectrum and targeted actions. In the current study, we demonstrate that phages can serve as a safe and effective novel therapeutic agent against *A. baumannii* when given as a single or sequential regimen without adverse reactions. Moreover, this study helps provide a deeper understanding of the interactions between host immune, bacteria, and phage to better predict bacterial pathogenesis and further develop phages as a novel and effective therapeutic product for treatment of complex infections in military beneficiaries.

The microbiota of healthy humans comprises of a variety of bacterial populations as well as a large number of bacterial viruses, such as phages (Reyes et al., 2012). Ironically, one of the primary benefits of using phage as an antibacterial therapeutic is that they are extremely narrow spectrum, even to the subspecies level, which minimizes the potential damage to the host microbiome. Phages have been found to colonize sites all over the body, including the skin (Foulongne et al., 2012; Oh et al., 2016), oral cavity (Pride et al., 2012), lungs (Dickson and Huffnagle, 2015), gut (Reyes et al., 2010; Minot et al., 2011), urinary tract (Santiago-Rodriguez et al., 2015), and blood (Breitbart and Rohwer, 2005). In the gut, for example, it is estimated that there are 10^9 viruses per gram of feces (Kim et al., 2011; Reyes et al., 2013), which equates to approximately 90% of the gut virome being phages (Scarpellini et al., 2015). Furthermore, studies have shown that phage can enter and cross different types of epithelial cell layers (e.g., gut, lung, liver, kidney, and brain cells) and for diverse phage types and morphologies (e.g., *Myoviridae*, *Siphoviridae*, and *Podoviridae*) by a non-specific transcytosis mechanism (Nguyen et al., 2017). Thus, it is

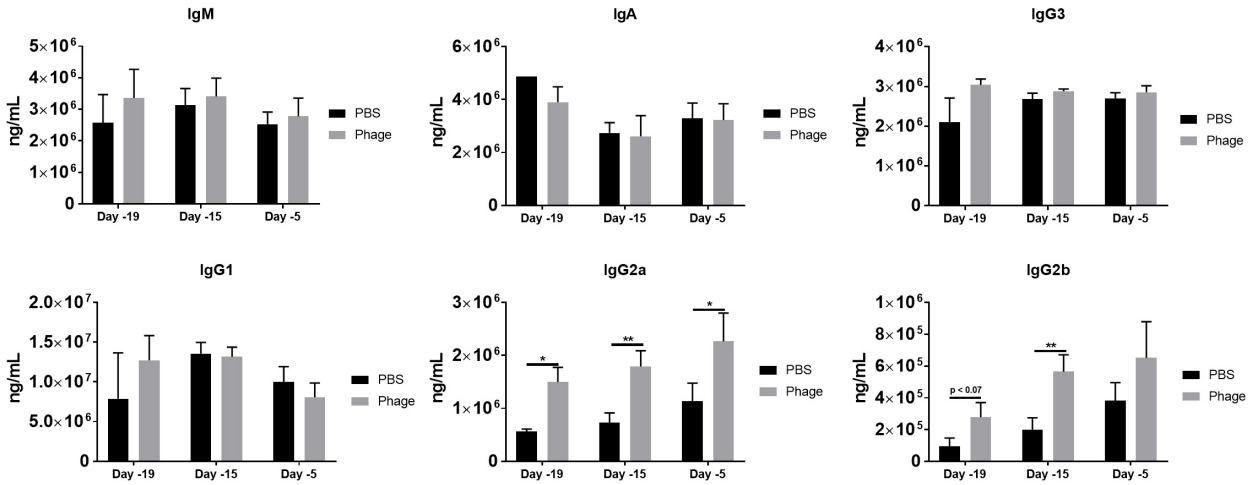

FIGURE 6 | Phage mixture administration promotes IgG2a and IgG2b generation. Serum collected from naïve mice given PBS or phage mixture were analyzed for total immunoglobulins. $N = 10$ per group for each time point; $^{*}p < 0.05$, $^{**}p < 0.01$.

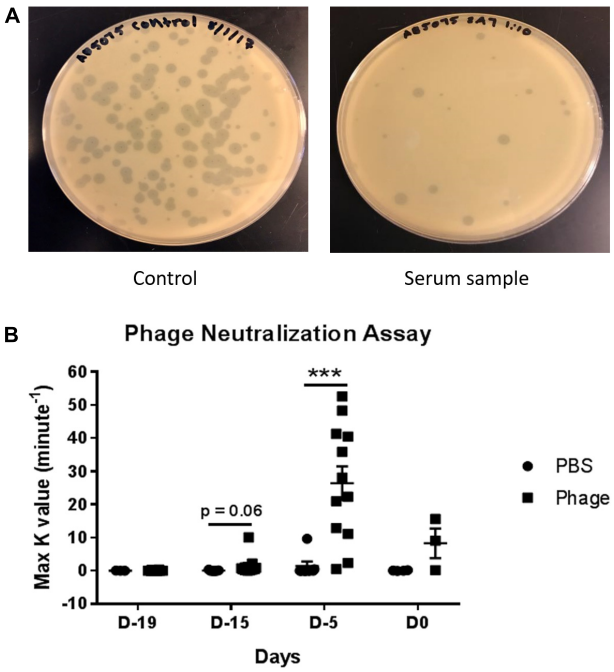

FIGURE 7 | Detection of serum neutralizing antibodies against *A. baumannii* phage mixture. Dilutions were made from serum collected from naïve mice given PBS (control) or phage mixture and incubated with a known titer of phage mixture (4×10^4 total PFU). **(A)** The mixtures were then added to an inoculum of AB5075 and plated in warm agar. **(B)** After 24 h incubation at 37°C, rate of phage neutralization was measured. $N = 7$ for PBS, $N = 13$ for Phage per time point; $^{***}p < 0.001$.

important to recognize and determine the potential interactions between phage and commensal bacteria, and how their co-inhabitance impact the function of the immune system and influence the spread of pathogens (Duerkop and Hooper, 2013).

In the current study, we detected that a significant amount of phage transmigrated to secondary lymphoid organs, such as the spleen, liver, and LN, within 24 h following intraperitoneal administration in naïve mice. Similarly, other studies have also found a high degree of phage titers in the spleen and liver, primarily attributed to the mononuclear phagocyte system (MPS) (Nungester and Watrous, 1934). The MPS, which helps filter and neutralize foreign objects from circulation (Hodyra-Stefaniak et al., 2015), has also been reported to rapidly remove wild-type phage λ from the circulatory system following administration in humans (Geier et al., 1973). As a part of the phagocytosis process, phages demonstrated the ability to enhance phagocytosis either by opsonization of bacterial cells or release of contributing factors during the degradation (Kaur et al., 2014).

In a number of studies, phages have demonstrated the ability to induce cytokine and chemokine production. However, it is sometimes difficult to determine the extent of phage influence due to purified phage vs. lystates, bacterial contaminants (e.g., LPS, cytosolic proteins, or membrane particles), and types of phage being investigated (Weber-Dabrowska et al., 2000; Kaur et al., 2014). In our study, we found that our five-member *A. baumannii* phage mixture did not appear to alter any of the mainstream pro-inflammatory and anti-inflammatory cytokines, such as IFNg, TNFα, IL-6, and IL-10. Interestingly, our phage mixture was able to significantly decrease 10 serum cytokines/chemokines in naïve mice that are associated with monocyte maintenance and function. Current literature supports the notion of phages' ability to modulate cytokine responses upon treatment. Park et al. (2014), for example, demonstrated that mice fed phage T7 daily for 10 days only led to subtle increases in inflammatory cytokine production and no significant histopathological changes. Similarly, mice i.p. administered highly purified preparations of either whole phage T4 particles, or four phage T4 capsid proteins (i.e., gp23*, gp24*, Hoc, and Soc) expressed no inflammatory

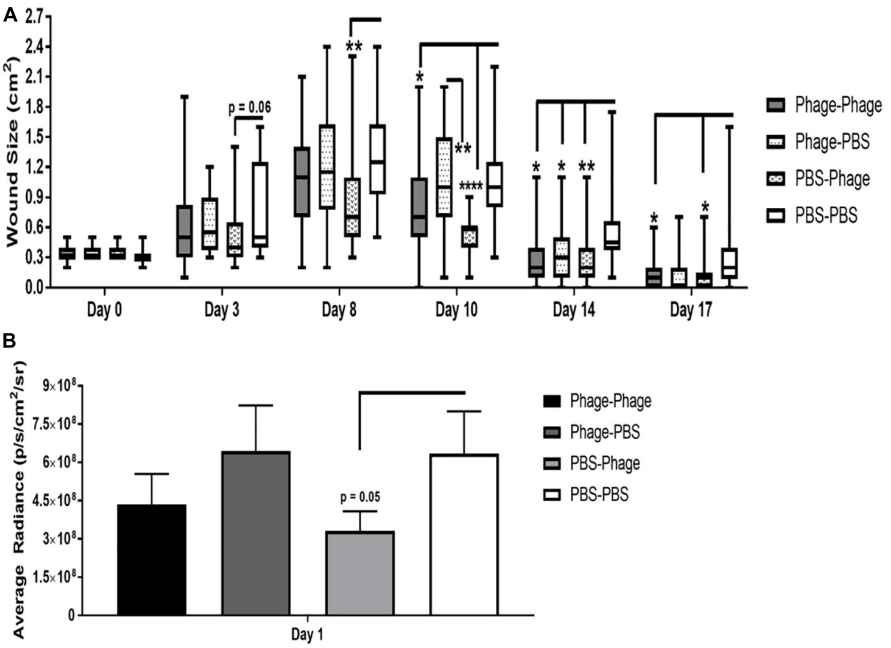

FIGURE 8 | Effects of phage mixture on wound closure and bacterial burden following *A. baumannii* infection. Balb/c mice pre-immunized with PBS or phage mixture were immunosuppressed with cyclophosphamide before wounding (dorsal full thickness injury) and challenged topically with AB5075-lux. **(A)** Wound size measure by Aranz system. **(B)** Bacterial burden measured by IVIS. $N = 27$ per group per time point; $^{*}p < 0.05$, $^{**}p < 0.01$, $^{****}p < 0.0001$.

cytokines (Miernikiewicz et al., 2013). In a 2000 study, 51 patients with long-term suppurative infections of various tissues and organs caused by drug-resistant strains of bacteria were treated with phage (Miernikiewicz et al., 2013). As a result, the patients treated with phage exhibited a significant reduction in TNF-a and IL-6, which may have also been attributed to the decreased number of pathogenic bacteria in the body following therapeutic application of the phage. In another study, five highly purified phages targeting two different pathogens, *P. aeruginosa* and *S. aureus*, were shown to augment suppressor of cytokine signaling 3 (SOSC3), IL-1 receptor antagonist (IL1RN), and IL-6 levels in PBMCs derived from healthy human donors (Van Belleghem et al., 2017). Meanwhile, evidence suggest that *S. aureus* phage, vB_SauM_JS25, is able to suppress LPS-induced inflammation (Zhang et al., 2018).

Recently, it has been suggested that commensal phages may have the potential to stimulate low-level immune responses without causing any overt symptoms as a means to continuously prime innate immune responses (Farrar and Schreiber, 1993; Duerkop and Hooper, 2013). In our study, we observed no significant changes in immune cell populations in circulation or secondary lymphoid organs with our phage mixture. However, Tiwari et al. (2011) have demonstrated the importance of neutrophil-phage cooperation in the resolution of *P. aeruginosa* infections, where the presence of neutrophils was imperative to remove resistant bacteria that emerged during phage treatment. Similar results were achieved by Roach et al. (2017) and Pincus et al. (2015).

Phages have also displayed the ability to induce humoral immunity. Although we were unable to detect any cellular changes upon phage administration in naïve mice, we did find enhanced immunoglobulin levels in serum. There are five major classes of immunoglobulins (IgA, IgD, IgE, IgG, and IgM), which vary in their chemical structure, number of antigen binding sites, and specificity to select antigen. IgA, for example, is dimer that is generally found in high concentrations in the mucous membranes, such as respiratory passages and gastrointestinal tract, as well as in saliva, bile, and tears. IgD, on the other hand, is often detected in only trace amounts in the blood. IgE is primarily found in the lungs, skin, and mucous membranes. Additionally, this immunoglobulin is associated with allergic reactions and results in the release of histamine. IgM, which is found mainly in the blood and lymph fluid, is a pentamer that is responsible for primary antibody responses. As a result, it is the first antibody to emerge upon detection of a foreign antigen and activates the complement system to fight and eliminate new threats. IgG, which includes the subclasses IgG1, IgG2a, and IgG2b, is the most abundant type of antibody. It is generally found in all body fluids and protects against bacterial and viral infections due to its ability to incorporate opsonization and the complement system.

Under "normal" circumstances, naive B cells only express cell-surface IgM and IgD with identical antigen binding regions. Upon introduction to foreign antigen and generation of cytokines, these cells become activated and undergo a process known as class switching. This process induces the expression of IgG, IgA, and IgE, as well as inherent changes in antibody structure, antigen specificity, and overall functionally that allow

it to work more effectively and efficiently at clearing present and future infections (Al-Lazikani et al., 1997). In the current study, we found IgG2a and IgG2b titers were significantly increased over time following phage administration, despite no changes in IgM compared to mice given PBS. Subsequently, we were able to determine that the antibodies generated were capable of neutralizing the lytic activity of our phage mixture. However, data suggest that either the presence of the antibodies or neutralizing activity may be transient, given the fact we observed a substantial decrease in neutralizing activity following Day 5. In alignment with our findings, a number of other studies have also detected the presence of phage-neutralizing antibodies against naturally occurring phages (e.g., not therapeutically administered) in the sera of different species (e.g., mice, horse, or human) (Dabrowska et al., 2014). In 2014, Dabrowska et al. (2014) evaluated 50 healthy volunteers who had never been subjected to phage therapy nor involved in phage work for the presence of naturally occurring phage-antibodies against phage T4. As a result, 81% displayed the presence of anti-phage antibodies, which exhibited specificity to phage proteins gp23, gp24, Hoc, and Soc. Interestingly, in a separate study, evidence suggests that phage T4 Hoc protein and gp12 were potent inducers of IgG and IgA antibody production in the blood and gut, respectively, whereas gp23, gp24, and Soc were found to induce low responses (Majerczyk et al., 2010). In a study involving patients that were administered orally or locally the MS-1 phage mixture, which comprises of three lytic *S. aureus* phages, the majority of the patients possessed no detectable presence of neutralizing antibodies (Zaczek et al., 2016). Moreover, the few patients who presented with elevated IgM or IgG levels still had positive clinical outcomes following phage therapy, suggesting these serum neutralizing antibodies did not impede the efficacy of the delivered phage.

In the current study, we demonstrate that upon systemic administration, phage have the propensity to permeate throughout the host's body, but is quickly sequestered into secondary lymphoid tissues. Based on the abilities of phages to act both as a direct antimicrobials as well as immunomodulatory agents to promote bacterial clearance, they serve as a unique tool capable of complementing and potentially sparing the use of standard of care antibiotics. Although phage are generally characterized as being safe and non-toxic, individual phage and phage mixtures still have the capability of eliciting unique signatures in regards to host responses and the immune system. For example, we observed a rise of select serum cytokines/chemokines and immunoglobulins, as well as induction of neutralizing antibodies upon administration of our AB5075 phage mixture. Recent computational models have been used to depict and elucidate the relationship and interactions between host immunity, phage, and bacteria (Levin and Bull, 2004; Roach et al., 2017). Thus, in a clinical setting, these modulatory effects may influence not just pathogen susceptibility and defenses, but also may dictate the timing and overall efficacy of phage therapy. Collectively, the kinetics of phage propagation vs. bacterial killing can be simplified to five basic parameters: the growth rate and density of the bacteria, the infectivity of the phage, the latency period vs. rate of degradation/removal of phage, the burst size, and the multiplicity of infection of the phage (Levin and Bull, 2004). Understanding these parameters and kinetics will be important to optimize the efficacy of phage therapy in various clinical situations, with patients of different immunocompetency, simultaneous use of different classes of antibiotics of which for some phage may be complementary and others not, and for different types of infections with different pathogens both in monomicrobial and in polymicrobial infections. Our findings, along with others, are highly suggestive of the potential efficacy of phage therapy, even in the presence of a potentially blunting immune response. Further preclinical and clinical studies are needed to elucidate the mechanisms and limitations of phage therapy in order to fulfill the potential promise of phage as a disruptive therapeutic to counter the ever increasing threat of MDR bacterial infections.

DATA AVAILABILITY STATEMENT

All datasets generated for this study are included in the article/**Supplementary Material**.

ETHICS STATEMENT

The animal study was reviewed and approved by the Institutional Animal Care and Use Committee at the Walter Reed Army Institute of Research and Naval Medical Research Center.

AUTHOR CONTRIBUTIONS

MR designed and performed the experiments, collected and analyzed the data, and prepared the manuscript. JS, JAR, and ML performed the experiments and collected the data. AJ, BB, JR, and MH designed the experiments. MGS designed the experiments and performed the data analysis. MPS designed and performed the experiments, analyzed the data, and prepared the manuscript.

FUNDING

The work presented here was funded through the Military Infectious Disease Research Program (W0121_14_NM).

SUPPLEMENTARY MATERIAL

The Supplementary Material for this article can be found online at: https://www.frontiersin.org/articles/10.3389/fmicb.2020.00414/full#supplementary-material

FIGURE S1 | Detection of serum neutralizing antibodies against individual phage comprising the *A. baumannii* phage mixture. Dilutions were made from serum collected at Day 5 from naïve mice given PBS (control) or phage mixture and incubated with a known titer of the individual phage that comprised the phage mixture phage mixture (4×10^4 total PFU), respectively. The mixtures were then added to an inoculum of AB5075 and plated in warm agar. After 24 h incubation at 37°C, rate of phage neutralization was measured.

TABLE S1 | Antibiotic susceptibility profile of *A. baumannii* AB5075.

REFERENCES

Al-Lazikani, B., Lesk, A. M., and Chothia, C. (1997). Standard conformations for the canonical structures of immunoglobulins. *J. Mol. Bio.* 273, 927–948.

Boucher, H. W., Talbot, G. H., Bradley, J. S., Edwards, J. E., Gilbert, D., Rice, L. B., et al. (2009). Bad bugs, no drugs: no ESKAPE! An update from the Infectious Diseases Society of America. *Clin. Infect. Dis.* 48, 1–12. doi: 10.1086/595011

Breitbart, M. R., and Rohwer, F. (2005). Method for discovering novel DNA viruses in blood using viral particle selection and shotgun sequencing. *Biotechniques* 39, 729–736.

Center for Disease Control and Pravention (2013). *Center for Disease Control and Pravention*. Available online at: https://www.cdc.gov/drugresistance/pdf/ar-threats-2013-508.pdf (accessed March 6, 2020).

Council, N. R. (2011). *Guide for the Care and Use of Laboratory Animals*, 8th Edn. Washington, DC: National Academies Press.

Dabrowska, K., Miernikiewicz, P., Piotrowicz, A., Hodyra, K., Owczarek, B., Lecion, D., et al. (2014). Immunogenicity studies of proteins forming the T4 phage head surface. *J. Virol.* 88, 12551–12557. doi: 10.1128/JVI.02043-14

Dickson, R. P. H., and Huffnagle, G. B. (2015). The lung microbiome: new principles for respiratory bacteriology in health and disease. *PLoS Pathog.* 11:e1004923. doi: 10.1371/journal.ppat.1004923

Duerkop, B., and Hooper, A. H. (2013). Resident viruses and their interactions with the immune system. *Nat. Immunol.* 14, 654–659. doi: 10.1038/ni.2614

Ena, J., Dick, R. W., Jones, R. N., and Wenzel, R. P. (1993). The epidemiology of intravenous vancomycin usage in a university hospital. *A* 10-year study. *JAMA* 269, 598–602.

Farrar, M. A., and Schreiber, R. D. (1993). The molecular cell biology of Interferon-gamma and its Receptor. *Annu. Rev. Immunol* 11, 571–611.

Foulongne, V., Sauvage, V., Hebert, C., Dereure, O., Cheval, J., Gouilh, M. A., et al. (2012). Human skin Microbiota: high diversity of DNA viruses identified on the human skin by high throughput sequencing. *PLoS One* 7:e38499. doi: 10.1371/journal.pone.0038499

Geier, M. R., Trigg, M. E., and Merril, C. R. (1973). Fate of bacteriophage lamba in non-immune germ-free mice. *Nature* 246, 221–223.

Hodyra-Stefaniak, K., Miernikiewicz, P., Drapala, J., Drab, M., Jonczyk-Matysiak, E., Lecion, D., et al. (2015). Mammalian Host-Versus-Phage immune response determines phage fate in vivo. *Sci. Rep.* 5:14802. doi: 10.1038/srep14802

Hospenthal, D. R., Murray, C. K., Andersen, R. C., Bell, R. B., Calhoun, J. H., Cancio, L. C., et al. (2011). Guidelines for the prevention of infections associated with combat-related injuries: 2011 update: endorsed by the infectious diseases society of america and the surgical infection society. *J. Trauma* 71(2 Suppl. 2), S210–S234.

Johnson, E. N., Burns, T. C., Hayda, R. A., Hospenthal, D. R., and Murray, C. K. (2007). Infectious complications of open type III tibial fractures among combat casualties. *Clin. Infect. Dis.* 45, 409–415.

Kaur, S., Harjai, K., and Chhibber, S. (2014). Appl. microbiol. biotechnol. bacteriophage-aided intracellular killing of engulfed methicillin-resistant *Staphylococcus aureus* (MRSA) by murine macrophages. *Methods Protocols* 98, 4653–4661. doi: 10.1007/s00253-014-5643-5

Keen, E. F., Murray, C. K., Robinson, B. J., Hospenthal, D. R., Co, E. M., and Aldous, W. K. (2010). Changes in the Incidences of multidrug-resistant and extensively drug-resistant organisms isolated in a military medical center. *Infect. Control Hosp. Epidemiol.* 31, 728–732. doi: 10.1086/653617

Kim, M.-S., Park, E.-J., Roh, S. W., and Bae, J.-W. (2011). Diversity and abundance of single-stranded DNA viruses in human feces. *Appl. Environ. Microbiol.* 77, 8062–8070. doi: 10.1128/AEM.06331-11

Levin, B. R., and Bull, J. J. (2004). Population and evolutionary dynamics of phage therapy. *Nat. Rev. Microbiol.* 2, 166–173.

Lusiak-Szelachowska, M., Zaczek, M., Weber-Dabrowska, B., Miedzybrodzki, R., Klak, M., Fortuna, W., et al. (2014). Phage neutralization by sera of patients receiving phage therapy. *Viral. Immunol.* 27, 295–304. doi: 10.1089/vim.2013.0128

Majerczyk, C. D., Dunman, P. M., Luong, T. T., Lee, C. Y., Sadykov, M. R., Somerville, G. A., et al. (2010). Direct targets of CodY in *Staphylococcus aureus*. *J. Bacteriol.* 192, 2861–2877. doi: 10.1128/JB.00220-10

Maragakis, L. L., and Perl, T. M. (2008). *Acinetobacter baumannii*: epidemiology, antimicrobial resistance, and treatment options. *Clin. Infect. Di.* 46, 1254–1263.

Miernikiewicz, P., Dabrowska, K., Piotrowicz, A., Owczarek, B., Wojas-Turek, J., Kicielinska, J., et al. (2013). T4 phage and its head surface proteins do not stimulate inflammatory mediator production. *PLoS One* 8:e71036. doi: 10.1371/journal.pone.0071036

Minot, S., Sinha, R., Chen, J., Li, H., Keilbaugh, S. A., Wu, G. D., et al. (2011). The human gut virome: Inter-individual variation and dynamic response to diet. *Genome Res.* 21, 1616–1625. doi: 10.1101/gr.122705.111

Murray, C. K., Wilkins, K., Molter, N. C., Li, F., Yu, L., Spott, M. A., et al. (2009). Infections in combat casualties during Operations Iraqi and Enduring Freedom. *J. Trauma* 66, S138–S144.

Nguyen, S., Baker, K., Padman, B. S., Patwa, R., Dunstan, R. A., Weston, T. A., et al. (2017). Bacteriophage transcytosis provides a mechanism to cross epithelial cell layers. *MBio* 8:01874-17. doi: 10.1128/mBio.01874-17

Nungester, W. J., and Watrous, R. M. (1934). Accumulation of bacteriophage in spleen and liver following its intravenous inoculation. *Exp. Biol. Med.* 31, 901–905.

Oh, J., Byrd, A. L., Park, M., Kong, H. H., and Segre, J. A. (2016). Temporal stability of the human skin microbiome. *Cell* 165, 854–866. doi: 10.1016/j.cell.2016.04.008

Park, K., Cha, K. E., and Myung, H. (2014). Observation of inflammatory responses in mice orally fed with bacteriophage T7. *Appl, J. Microbiol.* 117, 627–633. doi: 10.1111/jam.12565

Pincus, N. B., Reckhow, J. D., Saleem, D., Jammeh, M. L., Datta, S. K., and Myles, I. A. (2015). Strain specific phage treatment for *Staphylococcus aureus* Infection is influenced by host immunity and site of infection. *PLoS One* 10:e0124280. doi: 10.1371/journal.pone.0124280

Pride, D. T., Salzmam, J., Haynes, M., Rohwer, F., Davis-Long, C., White, R. A., et al. (2012). Evidence of a robust resident bacteriophage population revealed through analysis of the human salivary virome. *ISME J.* 6, 915–926. doi: 10.1038/ismej.2011.169

Regeimbal, J. M., Jacobs, A. C., Corey, B. W., Henry, M. S., Thompson, M. G., Pavlicek, R. L., et al. (2016). Personalized therapeutic cocktail of wild environmental phages rescues mice from *Acinetobacter baumannii* Wound infections. *Antimicrob. Agents Chemother.* 60, 5806–5816. doi: 10.1128/AAC.02877-15

Reyes, A., Haynes, M., Hanson, N., Angly, F. E., Heath, A. C., Rohwer, F., et al. (2010). Viruses in the faecal microbiota of monozygotic twins and their mothers. *Nature* 466, 334–338. doi: 10.1038/nature09199

Reyes, A., Semenkovich, N. P., Whiteson, K., Rohwer, F., and Gordon, J. I. (2012). Going viral: next-generation sequencing applied to phage populations in the human gut. *Nat. Rev. Microbiol.* 10, 607–617. doi: 10.1038/nrmicro2853

Reyes, A., Wu, M., McNulty, N. P., Rohwer, F. L., and Gordon, J. I. (2013). Gnotobiotic mouse model of phage–bacterial host dynamics in the human gut. *Proc. Natl. Acad. Sci. U.S.A.* 110, 20236–20241. doi: 10.1073/pnas.1319470110

Roach, D. R., Leung, C. Y., Henry, M., Morello, E., Singh, D., Di, Santo JP, et al. (2017). Synergy between the host immune system and bacteriophage is essential for successful phage therapy against an acute respiratory pathogen. *Cell Host Microbe* 22, 38–47. doi: 10.1016/j.chom.2017.06.018

Safdar, N., and Maki, D. G. (2002). The commonality of risk factors for nosocomial colonization and infection with antimicrobial-resistant *Staphylococcus aureus*, enterococcus, gram-negative bacilli. Clostridium difficile, and Candida. *Ann. Intern. Med.* 136, 834–844.

Santiago-Rodriguez, T. M., Ly, M., Bonilla, N., and Pride, D. T. (2015). The human urine virome in association with urinary tract infections. *Front. Microbiol* 6:14. doi: 10.3389/fmicb.2015.00014

Scarpellini, E., Ianiro, G., Attili, F., Bassanelli, C., De Santis, A., and Gasbarrini, A. (2015). The human gut microbiota and virome: potential therapeutic implications. *Dig. Liver Dis.* 47, 1007–1012. doi: 10.1016/j.dld.2015.07.008

Spellberg, B., Bartlett, J. G., and Gilbert, D. N. (2013). The future of antibiotics and resistance. *N. Engl. J. Med.* 368, 299–302.

Thompson, M. G., Black, C. C., Pavlicek, R. L., Honnold, C. L., Wise, M. C., Alamneh, Y. A., et al. (2014). Validation of a novel murine wound model of *Acinetobacter baumannii* Infection. *Antimicrob. Agents Chemother.* 58, 1332–1342. doi: 10.1128/AAC.01944-13

Tiwari, B. R., Kim, S., Rahman, M., and Kim, J. (2011). Antibacterial efficacy of lytic *Pseudomonas* bacteriophage in normal and neutropenic

mice models. *Microbiol, J.* 49, 994–999. doi: 10.1007/s12275-011-1512-4

Van Belleghem, J. D., Clement, F., Merabishvili, M., Lavigne, R., and Vaneechoutte, M. (2017). Pro- and anti-inflammatory responses of peripheral blood mononuclear cells induced by *Staphylococcus aureus* and *Pseudomonas aeruginosa* phages. *Sci. Rep.* 7:8004. doi: 10.1038/s41598-017-08336-9

Weber-Dabrowska, B., Zimecki, M., and Mulczyk, M. (2000). Effective phage therapy is associated with normalization of cytokine production by blood cell cultures. *Arch. Immunol. Ther. Exp.* 48, 31–37.

Zaczek, M., Lusiak-Szelachowska, M., Jonczyk-Matysiak, E., Weber-Dabrowska, B., Miedzybrodzki, R., Owczarek, B., et al. (2016). Antibody production in response to staphylococcal MS-1 phage cocktail in patients undergoing Phage Therapy. *Front. Microbiol.* 7:1681. doi: 10.3389/fmicb.2016.01681

Zhang, L., Hou, X., Sun, L., He, T., Wei, R., Pang, M., et al. (2018). *Staphylococcus aureus* Bacteriophage suppresses LPS-Induced inflammation in MAC-T bovine mammary epithelial cells. *Front. Microbiol.* 9:1614. doi: 10.3389/fmicb.2018.01614

Disclaimer: The views expressed in this article are those of the authors and do not necessarily reflect the official policies or positions of the Department of the Navy, the Department of the Army, the Department of Defense, or the U.S. Government. The material has been reviewed by the Naval Medical Research Center, and there is no objection to its presentation and/or publication.

Conflict of Interest: The authors declare that the research was conducted in the absence of any commercial or financial relationships that could be construed as a potential conflict of interest.

Copyright © 2020 Rouse, Stanbro, Roman, Lipinski, Jacobs, Biswas, Regeimbal, Henry, Stockelman and Simons. This is an open-access article distributed under the terms of the Creative Commons Attribution License (CC BY). The use, distribution or reproduction in other forums is permitted, provided the original author(s) and the copyright owner(s) are credited and that the original publication in this journal is cited, in accordance with accepted academic practice. No use, distribution or reproduction is permitted which does not comply with these terms.

frontiers in Microbiology

ORIGINAL RESEARCH
published: 08 April 2020
doi: 10.3389/fmicb.2020.00484

Genomic Analysis of Mic1 Reveals a Novel Freshwater Long-Tailed Cyanophage

Feng Yang, Hua Jin, Xiao-Qian Wang, Qiong Li, Jun-Tao Zhang, Ning Cui, Yong-Liang Jiang, Yuxing Chen, Qing-Fa Wu, Cong-Zhao Zhou* and Wei-Fang Li**

Hefei National Laboratory for Physical Sciences at the Microscale and School of Life Sciences, University of Science and Technology of China, Hefei, China

OPEN ACCESS

Edited by:
Krishna Khairnar, National Environmental Engineering Research Institute (CSIR), India

Reviewed by:
George S. Bullerjahn, Bowling Green State University, United States
Daichi Morimoto, Kyoto University, Japan

***Correspondence:**
Qing-Fa Wu
wuqf@ustc.edu.cn
Cong-Zhao Zhou
zcz@ustc.edu.cn
Wei-Fang Li
liwf@ustc.edu.cn

Specialty section:
This article was submitted to Virology, a section of the journal Frontiers in Microbiology

Received: *12 October 2019*
Accepted: *05 March 2020*
Published: *08 April 2020*

Citation:
Yang F, Jin H, Wang X-Q, Li Q, Zhang J-T, Cui N, Jiang Y-L, Chen Y, Wu Q-F, Zhou C-Z and Li W-F (2020) Genomic Analysis of Mic1 Reveals a Novel Freshwater Long-Tailed Cyanophage. Front. Microbiol. 11:484. doi: 10.3389/fmicb.2020.00484

Lake Chaohu, one of the five largest freshwater lakes in China, has been suffering from severe cyanobacterial blooms in the summer for many years. Cyanophages, the viruses that specifically infect cyanobacteria, play a key role in modulating cyanobacterial population, and thus regulate the emergence and decline of cyanobacterial blooms. Here we report a long-tailed cyanophage isolated from Lake Chaohu, termed Mic1, which specifically infects the cyanobacterium *Microcystis aeruginosa*. Mic1 has an icosahedral head of 88 nm in diameter and a long flexible tail of 400 nm. It possesses a circular genome of 92,627 bp, which contains 98 putative open reading frames. Genome sequence analysis enabled us to define a novel terminase large subunit that consists of two types of intein, indicating that the genome packaging of Mic1 is under fine control via posttranslational maturation of the terminase. Moreover, phylogenetic analysis suggested Mic1 and mitochondria share a common evolutionary origin of DNA polymerase γ gene. All together, these findings provided a start-point for investigating the co-evolution of cyanophages and its cyanobacterial hosts.

Keywords: freshwater cyanosiphophage, Lake Chaohu, genome sequence, terminase large subunit, DNA polymerase γ, evolution

INTRODUCTION

Cyanobacteria, which have existed on the earth for more than 3.5 billion years, are widely distributed in aquatic environments (Zhang and Gui, 2018). As a group of photosynthetic bacteria, cyanobacteria provide the source of primary production of oxygen, nitrogen, and carbon, and act as a model organism for studying the coordination of carbon and nitrogen metabolisms (Jiang et al., 2018). Beyond contributing to biogeochemical cycle, blooms also yield toxicity and hypoxia of waterbodies, which was first investigated in the Lake Alexandrina of Australia in 1878 (Francis, 1878). From the ecological perspective, blooms are increasing in frequency, magnitude, and duration in recent years, and cause the death of fish and risk to human diet (Paerl et al., 2001; Huisman et al., 2018). Therefore, it becomes imperative to devise an effective strategy to mitigate and control the water blooms.

Cyanophage, the classic companion virus of cyanobacteria, is a key factor that mediates the host communities, food web, carbon cycling, and nutrient recycling. It also has a potential impact on the regulation of cyanobacterial bloom through lysis-induced mortality, metabolic outputs as well as altering diversity and community structures (Zhang and Gui, 2018). Since the first complete genome sequence of cyanophage P60 that infects the marine *Synechococcus* was reported in 2002 (Chen and Lu, 2002), the genomes of 112 cyanophages have been sequenced and deposited in Virus-Host Database.[1] However, only 14 genomes of freshwater cyanophages have been sequenced. The first one came from the myophage Ma-LMM01 of *Microcystis aeruginosa* in 2008 (Yoshida et al., 2008). Afterward, four contractile-tailed phages, MaMV-DC (Ou et al., 2015a), S-CRM01 (Dreher et al., 2011), A-1 and N-1 (Chenard et al., 2016), five short-tailed phages, PP (Zhou et al., 2013), Pf-WMP3 (Liu et al., 2008), Pf-WMP4 (Liu et al., 2007), A-4L (Ou et al., 2015b) and S-EIV1 (Chenard et al., 2015) and one so-called tailless phage PaV-LD (Gao et al., 2012) were sequentially isolated from different sources of freshwater. Nevertheless, only three complete genomes of freshwater siphophages, S-2L (Marliere, 2006), S-LBS1 (Zhong et al., 2018), and CrV-01T (Martin et al., 2019) have been reported to date.

Lake Chaohu (117°16′54″E-117°51′46″E, 30°25′28″N-31°43′28″N), located at the south of the capital city Hefei of Anhui province, is one of the five largest freshwater lakes in China. It annually suffers from massive water blooms due to the fast growth of cyanobacteria, accompanied with the rapid industrialization and urbanization of the surrounding areas in the past decades. We successfully isolated a freshwater cyanosiphophage Mic1 from Lake Chaohu. Genome sequencing showed that Mic1, which depicts *Microcystis*-specific, possesses a genome of 92,627 bp (GenBank accession No. MN013189), consisting of 98 putative open reading frames (ORFs). Genome sequence analysis indicated that Mic1 contains a hypothetical ParABS plasmid partition system and a prophage antirepressor, suggesting that the prophage of Mic1 might also exist in the host. Moreover, Mic1 encodes a novel terminase large subunit that consists of two types of intein, which might be involved in the fine control of DNA packaging and phage maturation. In addition, Mic1 encodes a mitochondrion-like DNA polymerase gene, which might be transferred from a common ancestor of mitochondrion or its companion phage.

MATERIALS AND METHODS

Isolation and Purification of Cyanophage

Water samples were collected semimonthly from the estuaries of 11 rivers toward Lake Chaohu since 2016 (**Figure 1A**). After being concentrated to about 100-fold by ultrafiltration, the water samples were applied to infect 11 cyanobacterial strains isolated from Lake Chaohu (data not shown), then the lytic cyanophages infecting previously named *Microcystis wesenbergii* FACHB 1339 were further isolated by the serial dilution method (Yoshida et al., 2006). Notably, the host *Microcystis wesenbergii* FACHB 1339, which was bought from the Freshwater Algae Culture Collection at the Institute of Hydrobiology, Wuhan, should be classified into *Microcystis aeruginosa* (Harke et al., 2016). Then the crude lysate after phage infection was treated with 1 μg/mL DNase I and RNase at 37°C for 1 h. Afterward, NaCl was added to a final concentration of 0.5 M, followed by incubation at 4°C for 1 h. After centrifugation at 8,000 g for 20 min, the cyanophage particles in the supernatant were pooled and incubated with 10% polyethylene glycol 6,000 at 4°C for 10 h. The pellets after centrifugation were resuspended in SM buffer (50 mM Tris, pH 7.5, 10 mM $MgSO_4$, 100 mM NaCl), and further purified by ultracentrifugation at 100,000 g for 4 h with a CsCl density gradient. The cyanophage band with the highest opalescence was collected by a syringe and dialyzed against SM buffer. The isolated cyanophage was named Mic1, denoting the first strain of cyanosiphophage toward its host *M. aeruginosa*.

Transmission Electron Microscopy

The 4 μL suspension of freshly purified cyanophage Mic1 was layered onto a hydrophilized carbon-coated copper grid, and Mic1 particles were negatively stained with 2% uranyl acetate for 1 min. The particles were examined with a Tecnai G2 Spirit BioTWIN 120 kV transmission electron microscope (FEI Company).

Genomic DNA Extraction

The phage sample in 2 × lysis buffer (20 mM EDTA and 0.5% SDS) was incubated with 50 μg/mL proteinase K at 56°C for 1 h. The phage suspension was sequentially treated with an equal volume of phenol, phenol-chloroform-isoamyl alcohol (25:24:1) and chloroform, respectively. Subsequently, the DNA was precipitated with 0.3 mol/L CH_3COONa, pH 7.5 and 3-fold volume of ethanol at −80°C for 1 h. The precipitate of phage genomic DNA was washed twice with 70% ethanol and resuspended with sterile water.

Genome Sequencing

The sequencing library of phage genomic DNA was constructed using TruePrep DNA library Prep Kit V2, and a total of 10 Gb raw data was generated using Illumina Hiseq 2000 platform. The software Velvet (Version 1.2.07) was applied for genome assembly and 12 contigs showing somewhat similarity with known cyanophages at the protein sequence level were chosen for further analysis. The order and orientation of the 12 contigs were determined by PCR and Sanger sequencing. Finally, the assembled genome was verified using DNAMAN (Lynnon Biosoft).

Genome Annotation and Characterization

The ORFs were predicted using Glimmer (Delcher et al., 1999) and GeneMarkS (Lukashin and Borodovsky, 1998). The translated ORFs were compared with nr protein database in NCBI[2] using BLASTp program with *e*-values $<10^{-3}$ and

[1] https://www.genome.jp/virushostdb/index/virus/all

[2] https://www.ncbi.nlm.nih.gov/

the protein hits with the minimal *e*-value in each species were considered to be orthologs. HHpred analysis against the pfamA database was carried out using the default parameters.[3] Promoters of the genome were predicted by BPROM (LDF > 5).[4] Multiple-sequence alignment was performed using the Multalin program.[5] The circular genome map was drawn using CGView.[6] The cyanophage proteomic tree and genome alignments were conducted with Viptree[7] (Nishimura et al., 2017). The genome-wide similarity score (SG) cutoff for clustering was set to ≥0.15 (viral genus-level cutoff, where the SG value of 1 stands for two identical genomes and 0 for no detectable high-scoring segment pairs by tBLASTx), according to the previous study (Morimoto et al., 2019). The heatmap was generated using Gegenees (tBLASTx method, accurate parameters-fragment length: 200 bp; step size: 100 bp), and the Splits Tree dendrogram was calculated using the Nexus file exported from Gegenees.

Mass-Spectrometric Identification of Phage Proteins

The phage proteins separated by 4–12% gradient polyacrylamide gel were analyzed by liquid chromatography/mass spectrometry (LC-MS/MS) using ion-trap mass spectrometer (Thermo LUMOS) and identified by comparing to the protein/peptide sequences deduced from Mic1 genome as previously described (Jin et al., 2019).

RESULTS AND DISCUSSION

Isolation and Morphology of Mic1

Lake Chaohu has been severely polluted in recent years, owing to a large amount of industrial waste water and domestic sewage flowing from the rivers of Shiwuli, Nanfei, Shuangqiao and Xiapai, which are major rivers to the lake. Accordingly, we chose the estuaries of 11 major rivers entering Lake Chaohu (**Figure 1A**) to investigate the cyanophages and their hosts. Cyanophage Mic1 was isolated from a surficial water sample collected at Shuangqiao estuary on October 21st, 2017, which was enriched with *Microcystis*-dominated blooms. Host-range assays showed that Mic1 is only able to lyse a strain of *Microcystis aeruginosa* (previously named *M. wesenbergii* FACHB 1339) isolated from Lake Chaohu, indicating that the infectivity of Mic1 is limited to specific cyanobacterial strains.

Purification of Mic1 from the lysate was performed by CsCl density gradient centrifugation, and the fourth opalescence band containing cyanophages was collected (**Figure 1B**). The purified cyanophage particles were negatively stained for morphological analysis by electron microscopy, revealing that all particles have a siphoviridal morphotype. As shown in **Figure 1C**, Mic1 has an icosahedral head with a diameter of 88 nm and a flexible and non-contractile tail of 400 nm in length.

Genome Sequence of Mic1

Mic1 has a circular double-stranded DNA genome of 92,627 bp with a G + C content of 35% (**Figure 2A**). BLASTp and HHpred analyses indicated that Mic1 has 98 ORFs, which encode hypothetical proteins/peptides of 36–2,572 residues in length. Sequence comparison indicated that only 50 hypothetical proteins have homologs, 36 of which have known functions (**Supplementary Table 1**). These 36 proteins could be divided into five groups: structural proteins, nucleotide metabolism, DNA replication and packing, auxiliary metabolism and others (**Figure 2A**).

Bioinformatics analyses revealed that the majority of Mic1 structural proteins are similar to those found in other long-tailed phages, for example, the portal protein (ORF2), receptor binding protein (ORF16), phage minor tail (ORF27, ORF32, ORF34), phage tail (ORF28), phage tail L (ORF31), and tail tape measure (ORF35). Moreover, the cryoelectron microscopy (cryo-EM) structure of the icosahedral capsid of Mic1 demonstrated that the major capsid protein and the cement protein are encoded by ORF40 and ORF47, respectively (Jin et al., 2019). To further identify the structural proteins, the purified Mic1 particles were analyzed by mass spectrometry, which identified 23 proteins in total (Jin et al., 2019). As expected, the most abundant proteins are the major capsid protein ORF40 and tail tube protein ORF20. The genes encoding the 23 structural proteins are mainly distributed in three regions (**Figure 2B**): portal protein ORF2 followed by two proteins ORF3 and ORF4 of unknown function, tail-related proteins containing ORF20 to ORF35 in addition to a downstream receptor-binding protein ORF16, and major capsid ORF40 with accessory proteins (such as the head scaffold and cement). Notably, most of the 23 structural genes are transcribed in the opposite direction against the majority of non-structural genes. In addition, Mic1 harbors two auxiliary metabolic genes, *phoH* (ORF97) and *mazG* (ORF98), the products of which are involved in elevating the phage fitness by altering host metabolism during infection. PhoH belongs to the phosphate regulon that regulates phosphate uptake and metabolism under conditions of low-phosphate and phosphate limitation (Goldsmith et al., 2011), whereas MazG is responsible to reactivate the macromolecular synthesis pathways, via modulating the ppGpp pool, for the propagation of phage progenies in the nutrient-limited cyanobacteria (Bryan et al., 2008; Dreher et al., 2011). Besides, Mic1 encodes nine hypothetical proteins, which share no sequence similarity to any previously identified proteins (**Supplementary Table 1** and **Figure 2A**).

Comparison with the genomes of three freshwater cyanosiphophages CrV-01T, S-LBS1 and S-2L, which are of 104,262, 34,236, and 42,000 bp, respectively, Mic1 possesses genome of 92,627 bp. Despite sharing a similar genome architecture, Mic1 encodes 22 unique components, including ParA (ORF5), ParB (ORF82), head scaffold (ORF42), cement (ORF47), and DNA polymerase γ (ORF85 and ORF86) (**Figure 2C**).

[3] https://toolkit.tuebingen.mpg.de/hhpred

[4] http://www.softberry.com/berry.phtml?topic=bprom&group=programs&subgroup=gfi

[5] http://multalin.toulouse.inra.fr/multalin/

[6] http://cgview.ca/

[7] https://www.genome.jp/viptree/

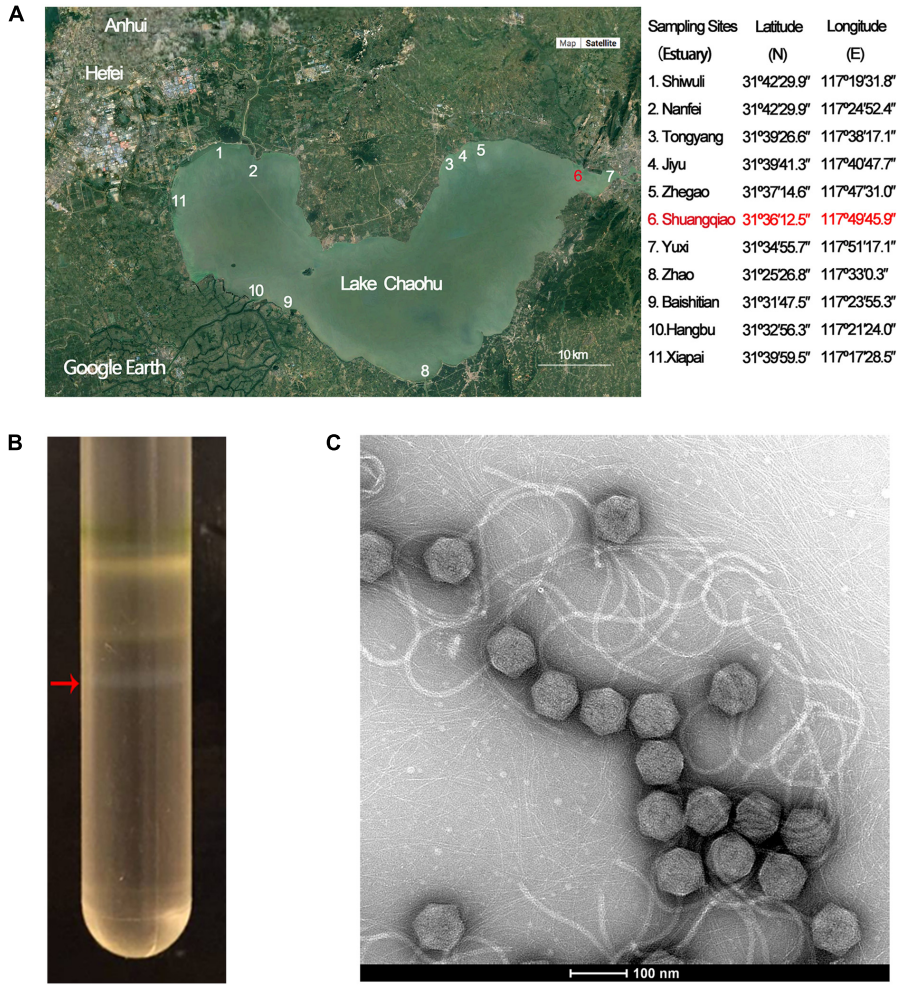

Sampling Sites (Estuary)	Latitude (N)	Longitude (E)
1. Shiwuli	31°42'29.9"	117°19'31.8"
2. Nanfei	31°42'29.9"	117°24'52.4"
3. Tongyang	31°39'26.6"	117°38'17.1"
4. Jiyu	31°39'41.3"	117°40'47.7"
5. Zhegao	31°37'14.6"	117°47'31.0"
6. Shuangqiao	31°36'12.5"	117°49'45.9"
7. Yuxi	31°34'55.7"	117°51'17.1"
8. Zhao	31°25'26.8"	117°33'0.3"
9. Baishitian	31°31'47.5"	117°23'55.3"
10.Hangbu	31°32'56.3"	117°21'24.0"
11.Xiapai	31°39'59.5"	117°17'28.5"

FIGURE 1 | Isolation, purification, and morphological identification of Mic1. **(A)** Location of Lake Chaohu (from the Google Earth) and the coordinates of 11 major river estuaries to Lake Chaohu. The red mark shows the site where Mic1 was isolated. **(B)** CsCl density gradient ultracentrifugation of Mic1. Mic1 concentrated in the fourth layer gradient is indicated by a red arrow. **(C)** Electron micrograph negatively stained Mic1 particles. The cyanophage Mic1 were negatively stained with uranyl acetate and visualized by transmission electron microscopy at 120 kV accelerating voltage. The phages have an isometric head of ∼88 nm in diameter and a long, non-contractile tail of ∼400 nm in length.

Notably, we presented here the first report of a cyanophage encoding ParA and ParB, which are involved in DNA partition. ParA and ParB were reported to exist in the low-copy-number phage-plasmids, such as *Escherichia coli* bacteriophage P1 (Vecchiarelli et al., 2010) and N15 (Ravin, 2011). Moreover, a palindromic sequence ($_{8828}$AAATCACCTAAGTTAGGTGATTT$_{8850}$) was also found at the downstream of *parA* gene in Mic1 genome (**Figure 3**), similar to the previously reported *parS* partition site at the upstream or downstream of *parAB* operon (Brooks and Hwang, 2017). Identification of ParA/B homologs combined with the *parS*-like site indicated that Mic1 might also adopt the ParABS plasmid partition system in the lysogenic cycle, similar to that of phage P1 (Vecchiarelli et al., 2010) and N15 (Ravin, 2011). Moreover, we found that ORF17 of Mic1 most likely encodes a prophage antirepressor (**Figure 3A**), which was proposed to mediate the lytic induction among temperate phages in the order Caudovirale (Kim and Ryu, 2013). In fact, the phenomena of the bull's-eyed plaques were found when amplifying Mic1 (**Figure 3B**). However, the defined condition that switches the lysis–lysogeny transition remains unknown, despite the lysogenic state is most likely favored at the conditions such as low productivity of host cells, poor nutrients, exposure to high temperature or UV (Howard-Varona et al., 2017). Altogether, identification of the ParABS plasmid partition system and the prophage antirepressor strongly indicated that Mic1 might also have a lysogenic cycle at some yet unknown conditions.

Phylogenetic analysis based on the large terminase subunit TerL showed that Mic1 falls into the "P22-like headful" cluster (**Figure 4A**), which has a terminally redundant and circularly permuted genome (Casjens and Gilcrease, 2009). Mic1 is closely related to siphovirus *Lactobacillus thermophilus* prophage Lj964 (Desiere et al., 2000) and *Staphylococcus aureus* phage phiETA

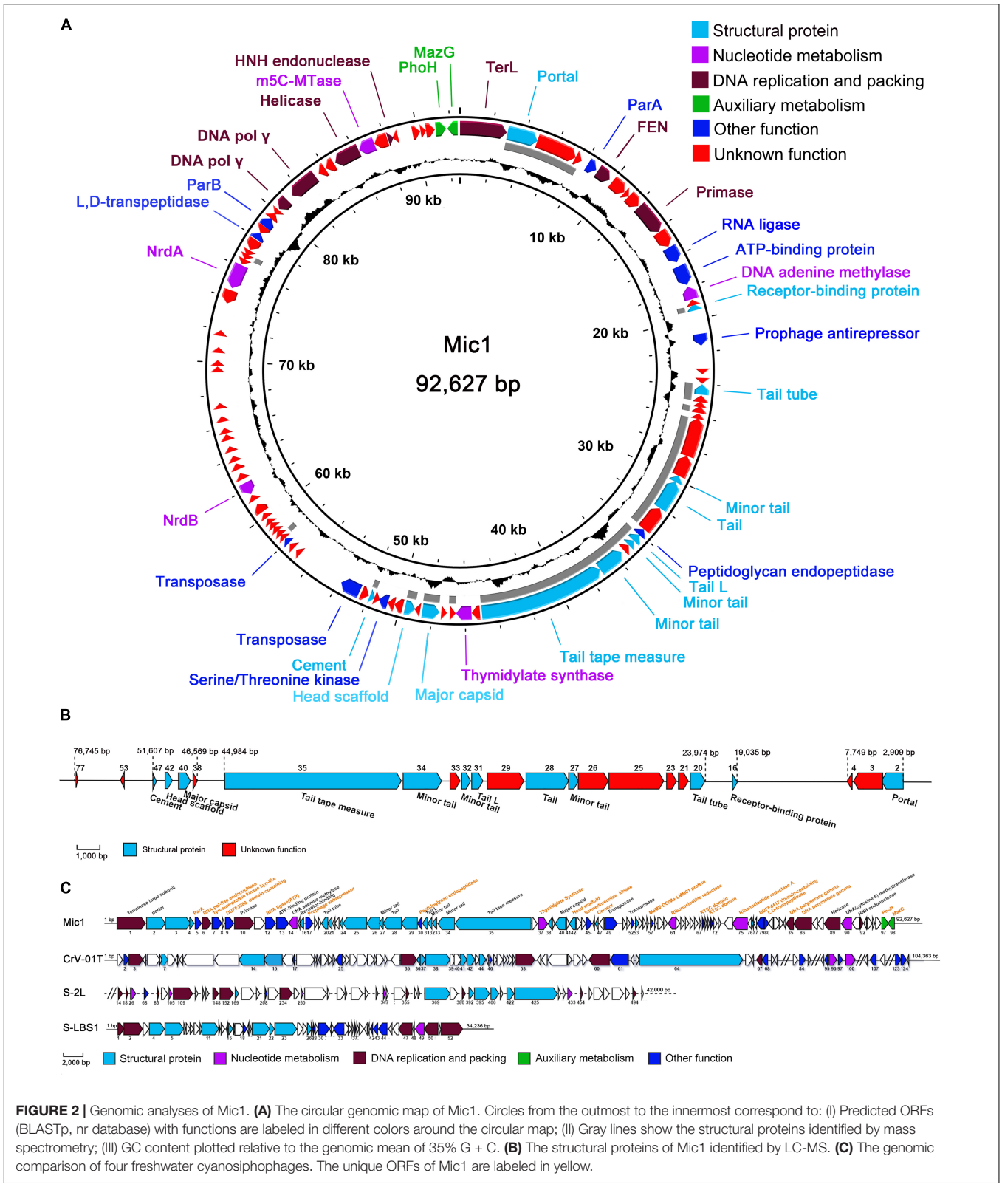

FIGURE 2 | Genomic analyses of Mic1. **(A)** The circular genomic map of Mic1. Circles from the outmost to the innermost correspond to: (I) Predicted ORFs (BLASTp, nr database) with functions are labeled in different colors around the circular map; (II) Gray lines show the structural proteins identified by mass spectrometry; (III) GC content plotted relative to the genomic mean of 35% G + C. **(B)** The structural proteins of Mic1 identified by LC-MS. **(C)** The genomic comparison of four freshwater cyanosiphophages. The unique ORFs of Mic1 are labeled in yellow.

(Yamaguchi et al., 2000) based on the pac-site DNA packaging and long tail morphogenesis modules, but distinct from the λ-like freshwater cyanosiphophage S-LBS1 (Zhong et al., 2018).

Notably, TerL of Mic1 contains two different inteins, which are inserted in the ATPase domain and the nuclease domain, respectively; and moreover, the large intein has a homing

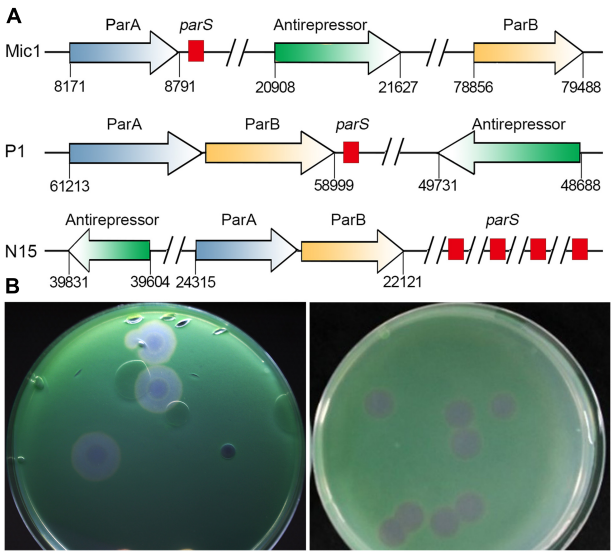

FIGURE 3 | Analyses of Mic1 ParABS system. **(A)** Partitioning loci location in Phages. Genes that encode ParA are depicted by blue arrows, ParB by yellow arrows, the sequences of *parS* are depicted by red box. Genes that encode antirepressor are depicted by green arrows. **(B)** The phage plaques of Mic1. Plaques in the left dish are at lysogenic status, featured with cloudy circular plaques with a bull's eye at the center, whereas the clear plaques in the right dish are at lytic status.

endonuclease domain (HED) (**Figure 4B**). Inteins are often mobile, with the ability to post-translationally excise themselves out of the precursor proteins (Perler et al., 1994), usually triggered by external stimuli, such as reactive oxygen species and reactive nitrogen species (Topilina et al., 2015a), reducing agent (Callahan et al., 2011), high temperature (Topilina et al., 2015b), low pH (Wood et al., 1999), high concentration of salt (Reitter et al., 2016), or DNA damage (Lennon et al., 2016). Thus inteins are thought to be biosensors that allow instantaneous splicing to produce the activated proteins. We proposed that the two inteins in the TerL precursor might act as biosensors to control the DNA packaging and maturation of Mic1.

Sequence analysis showed that Mic1 genome has some highly repetitive sequences in the non-coding region. For example, the motif.

GGRYATAT(A)ACAWWTCTAAAAAAAGATGACATAATG GTAACATAAAGAAAAACACAGG that contains the predicted promoter (−35 box TATACA ∼ −10 box TGACATAAT) repeats 10 times in the region from 66,031 to 71,646. Another motif GTGCCAGTTYATAAAGTGTCACAATTAGAYTTGACAAAA AGCAAAGTTTATGCAGGC(G)ATAAT containing the predicted promoter (−35 box TTGACA ∼ −10 box AGGCAT AAT) repeats 8 times in the region from 67,047 to 69,344. However, more transcriptomic investigations are needed to elucidate the putative multiple promoters that drive the efficient transcription in the lytic cycle of Mic1. In addition, a short repetitive sequence ATCAGTT repeats 20 times in the region from 59,828 to 60,196. In fact, this 7 nt repetitive unit is also widespread in the repetitive regions (ranging from 2 to 40 repetitive units) of *Microcystis aeruginosa* NIES-843 genome. It suggested that this short repetitive unit of Mic1 might come from the host genome through horizontal gene transfer, despite its function in the cyanophage or host remains unknown.

Evolutionary Analyses at the Genome Level

Before Mic1, only 14 cyanosiphophages have been genome-sequenced, including 11 marine and 3 freshwater cyanophages. To determine the degree of genomic variability between the cyanosiphophages, the heatmap was clustered based on Bray-Curtis similarity (Zhong et al., 2018) and compared the gene similarities between two phages (**Figure 5A**). The cyanophages A-HIS1 and A-HIS2 of the unicellular cyanobacterium *Acaryochloris marina* (Chan et al., 2011), CrV-01T of the filamentous *Cylindrospermopsis (Raphidiopsis) raciborskii* (Martin et al., 2019), vB_NpeS-2AV2 of the filamentous nitrogen fixing cyanobacterium *Nodularia* sp. (Coloma et al., 2017), PSS2 of *Prochlorococcus (Sullivan et al., 2009)* were clustered according to their hosts, respectively. In contrast, the two fresh water cyanophage S-LBS1, S-2L were clustered with six marine siphophages S-CBS (1,3,4), KBS-S-2A, S-ESS1, S-SKS1, most likely because they all infect similar hosts of unicellular cyanobacterium *Synechococcus* (**Figure 5A**). Notably, Mic1, which infects the abundant freshwater unicellular cyanobacteria in the genera *Microcystis*, is distinct from the 14 previously sequenced cyanosiphophages and classified in a unique category. These results implied that cyanosiphophages infecting different host cyanobacteria might possess different genetic lineages.

To further define the relationship between Mic1 and other known cyanophages, proteomic tree was constructed using Viptree based on the genomes of 112 completely sequenced cyanophages from Virus-Host Database (**Figure 5B**). The cyanophages were grouped into four clusters based on the genome similarity scores (SG): the cyanosiphophages, cyanopodophages and cyanomyophages from marine belong to the clusters I, III, and IV, respectively, whereas most of the freshwater cyanophages including Mic1 fall into cluster II. Despite there is a clear boundary between cluster I and II, some freshwater cyanophages and marine cyanosiphophages are chimerically distributed in clusters I and II, respectively. For example, four freshwater cyanophages CrV-01T, S-EIV1, S-LBS1, and S-2L were grouped into the cluster I, mainly due to homology in tail components or nucleotide synthesis enzymes with their neighboring marine cyanosiphophages. A fine proteomic comparison of cyanophages in cluster II revealed that Mic1 shares similar DNA replication components with A-HIS1, A-HIS2, and S-CBWM1, such as DNA polymerase γ, flap endonuclease (FEN, also known as 5′ nuclease, ORF6), DNA helicase (ORF89) and primase (ORF10). Moreover, Mic1 encodes a DNA polymerase γ with a relatively high similarity to those of A-HIS1, A-HIS2, and S-CBWM1 up to 29–32% sequence identity.

To have a global view of the evolutionary position of Mic1 among the phages, we constructed the proteomic tree (**Figure 5C**) with the reference genomes of 2,697 phages, in

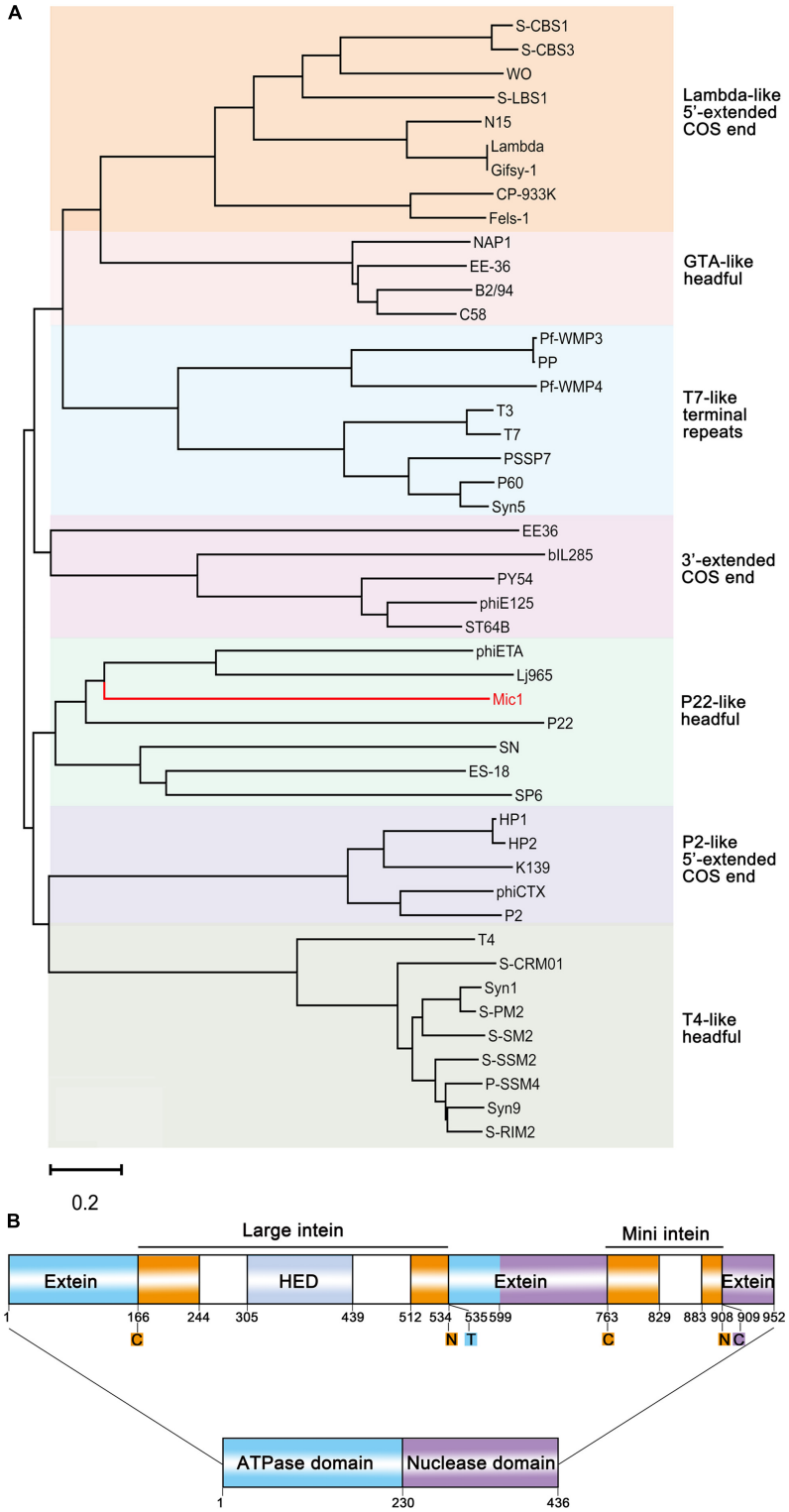

FIGURE 4 | Analyses of Mic1 TerL. **(A)** Phylogenetic tree of TerL proteins from different phages inferred by Neighbor Joining. Colored boxes indicate the characterized clusters which have similar DNA ends. The sequences, except that of Mic1, were classified as described previously (Casjens and Gilcrease, 2009; Huang et al., 2012), and bootstrap analysis was performed with 1,000 repetitions. The scale bar represents 0.2 changes per amino acid. **(B)** Domain organization of TerL. ATPase domain and nuclease domain are indicated by blue and purple box, respectively. The termini of intein are indicated by orange boxes, and the homing endonuclease domain (HED) in the large intein is indicated by the light gray box. Color blocks indicate the conserved amino acid residues at split sites, the oranges (cysteine, asparagine) for the boundary of intein, the blue (threonine) and purple (cysteine) for the boundary of extein.

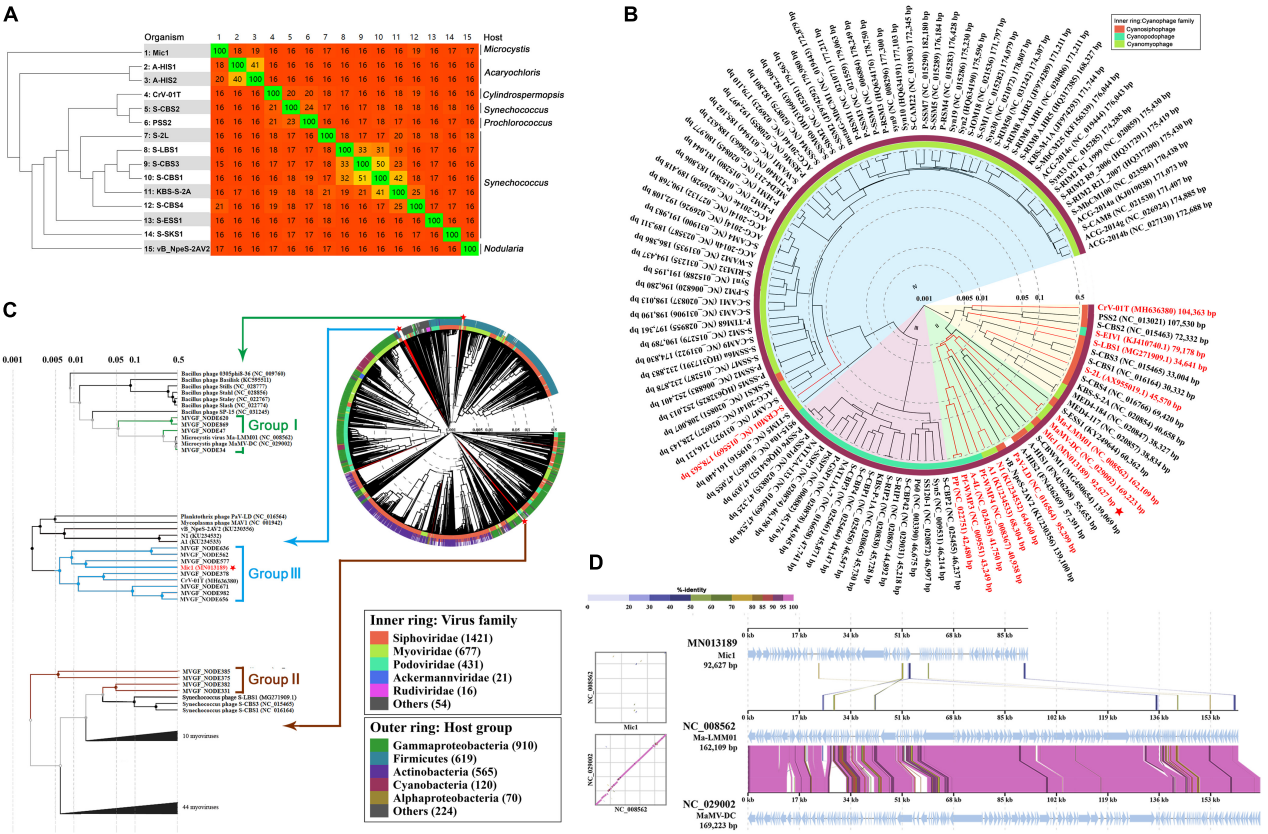

FIGURE 5 | The evolutionary analyses of Mic1. **(A)** Heatmap and phylogenomic tree analyses of cyanosiphophages. The heatmap was generated using Gegenees (tBLASTx method, accurate parameters-fragment length: 200 bp, step size: 100 bp). The numbers show the percentage similarity between the conserved regions of the genomes, whereas the colors reflect the similarity ranging from low (red) to high (green). The Splits Tree dendrogram at the left was calculated using the Nexus file exported from Gegenees. **(B)** The proteomic tree was constructed based on the complete genome sequences of 112 cyanophages. The genome sequences of 12 phages (Mic1, S-2L, S-LBS1, KBS-S-2A, S-EIVI, CrV-01T, A1, N1, S-CBWM1, S-ESSI, A-HIS1, and A-HIS2 were obtained from GenBank and added into ViPTree. The other 100 genome sequences were obtained from Virus-Host Database (https://www.genome.jp/virushostdb/). Cyanophages in the four clusters are shaded in different colors: (I) marine siphophages (yellow), (II) freshwater cyanophages (green), (II) marine podophages (pink), (IV) marine myophages (blue). The previously reported freshwater cyanophages are marked in red, and Mic1 is labeled with a red star. **(C)** Proteomic tree of the complete genome sequences of 2697 dsDNA phages and 15 *Microcystis* viral genomic fragments (MVGFs). Mic1 is labeled with a red star. The whole proteomic tree was generated by ViPTree server ver.1.9. Branch lengths were logarithmically scaled from the root of the entire proteomic tree. **(D)** Genome alignment of Mic1, Ma-LMM01, and MaMV-DC. All tBLASTx alignments are represented by colored lines between two genomes. Color scale represents the tBLASTx percent identity.

addition to 15 *Microcystis* viral genomic fragments (MVGFs) from Hirosawaniike pond in Japan recently sequenced by metagenomic approaches (Morimoto et al., 2019), using Viptree as previously described (Nishimura et al., 2017). It also indicated that Mic1 possesses a genome distinct from other phages. Moreover, the *Microcystis* cyanophage genomes and the 15 MVGFs could be classified into three groups; and Mic1 falls into group III, the cyanophages of which were reported to have a narrow-host-range that infect highly abundant hosts (Morimoto et al., 2019). It is also consistent with the specificity of Mic1 toward *M. aeruginosa* FACHB 1339, which is one of the most dominant bloom-forming cyanobacterial species in Lake Chaohu.

Despite falling into different groups as shown in **Figure 5C**, the three genome-sequenced *M. aeruginosa* cyanophages Mic1, Ma-LMM01, and MaMV-DC showed a relatively high similarity at the genome level (**Figure 5B**). Sequence alignment of the genomes of these three phages also revealed high homology in several coding regions (**Figure 5D**), especially those corresponding to four Mic1 proteins: ORF45 (Serine/Threonine

TABLE 1 | Homologs in cyanophages that infect *M. aeruginosa*.

Mic1	Function	Homologs in Ma-LMM01 (Yoshida et al., 2008)		Homologs in MaMV-DC (Ou et al., 2015a)	
ORF		ORF	Identity (%)	ORF	Identity (%)
45	Serine/Threonine kinase	25	58.24	40	59.34
49	Transposase	31	39.44	127	32.47
97	PhoH	183	37.32	169	37.32
57	Hypothetical protein	158	64.22	145	73.39

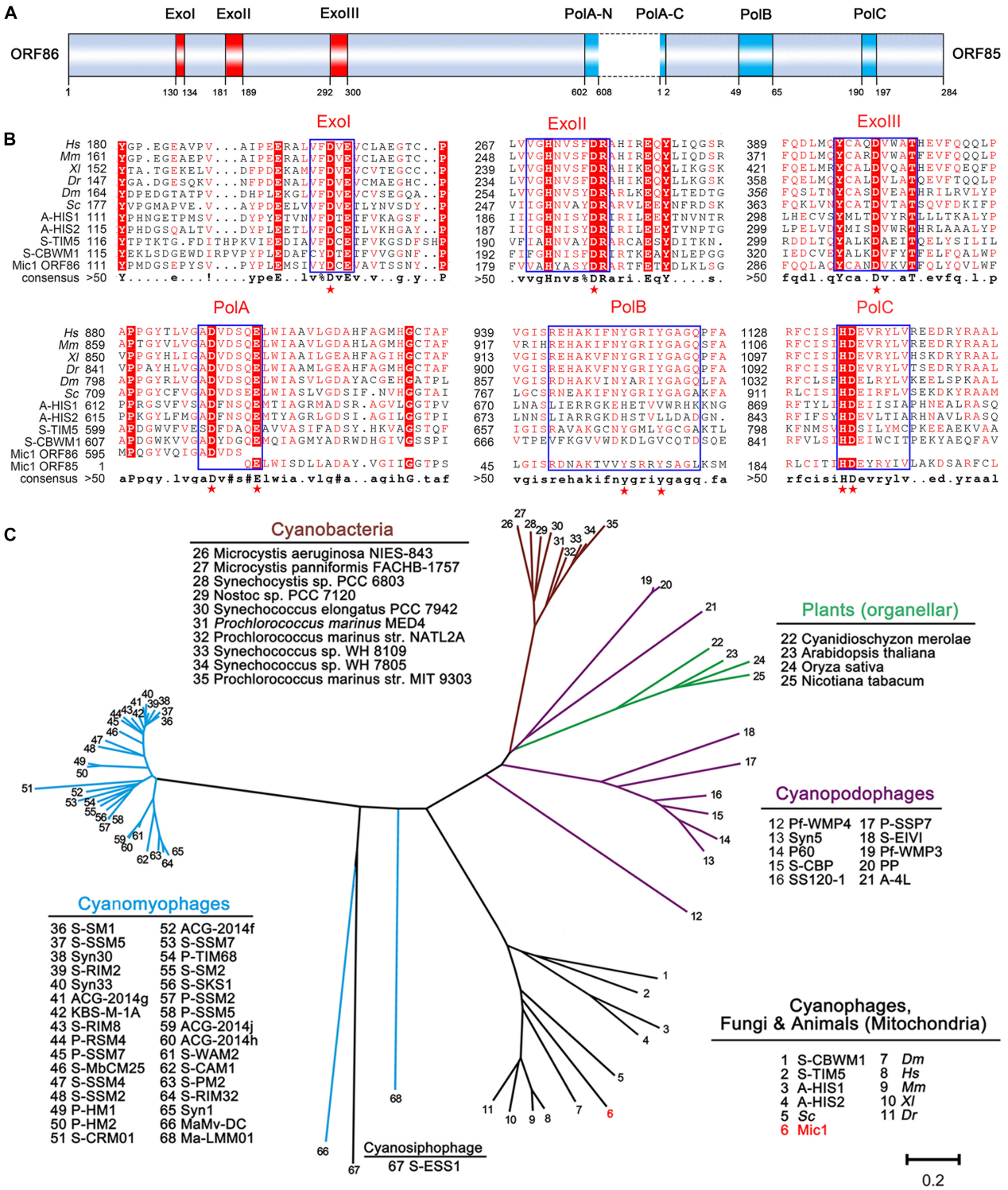

FIGURE 6 | Analyses of DNA polymerase γ. **(A)** Domain organization of Mic1 DNA polymerase γ. The red and blue boxes indicate the conserved exonuclease motifs I–III and polymerase motifs A–C of DNA polymerase γ, respectively. The dotted box indicates the intron between ORF85 and ORF86. **(B)** Multiple-sequence alignment of the conserved DNA polymerase γ from different species. Boxes frame the sequences that are highly conserved, and the key conserved amino acid residues in the exonuclease and polymerase domains are depicted by red stars. The abbreviations are *Hs*, *Homo sapiens*; *Mm*, *Mus musculus*; *Xl*, *Xenopus laevis*; *Dr*, *Danio rerio*; *Dm*, *Drosophila melanogaster*; *Sc*, *Saccharomyces cerevisiae*; A-HIS1 and A-HIS2, *Acaryochloris marina* siphovirus; S-TIM5, *Synechococcus marina* myovirus, S-CBWM1, *Synechococcus marina* myovirus. **(C)** Phylogenetic relationship of DNA polymerases among cyanophages, cyanobacteria and plant organelles. Unrooted phylogenetic tree was constructed based on the neighbor-joining method. The scale bar represents 0.2 changes per amino acid.

kinase), ORF49 (transposase), ORF97 (PhoH), and ORF57 (hypothetical protein) (**Table 1**).

Mic1 Encodes a DNA Polymerase γ

DNA polymerase γ, which is specifically localized in the mitochondria, is responsible for the replication of mitochondrial DNA in eukaryotes (Bolden et al., 1977). Despite mitochondria were proposed to be derived from α-proteobacteria, to date no DNA polymerase γ gene has ever been found in any bacteria (Chan et al., 2011). Since 2011, the DNA polymerase γ gene was found in a couple of marine cyanophages, including cyanosiphophages A-HIS1 and A-HIS2 of *Acaryochloris* (Chan et al., 2011), cyanomyophages S-TIM5 (Sabehi et al., 2012), and S-CBWM1 (Xu et al., 2018) of *Synechococcus*. Here we reported a DNA polymerase γ gene in the freshwater cyanophage. The DNA polymerase γ of Mic1 is encoded by ORF85 and ORF86, with an intron of 298 bp between the two ORFs (**Figure 6A**). Similar to the motif organization of DNA polymerase γ in the model eukaryotes and previously reported cyanophages, ORF86 encodes ExoI∼III motifs and N-terminal moiety of PolA, and ORF85 encodes C-terminal moiety of PolA, PolB, and PolC motifs (**Figure 6B**). Notably, like the mitochondrial DNA polymerase γ, Mic1 and S-TIM5 possess a PolB motif with a conserved tyrosine, which is absent in A-HIS1/A-HIS2 and S-CBWM1.

To date, the evolutionary origin of mitochondrial DNA polymerase remains unclear. Filee et al. (2002) hypothesized that the replication apparatus of mitochondrial DNA polymerase γ gene was originated from phage, and replaced that of bacterial ancestor. However, the homologs of DNA polymerase γ have been only found in cyanophages, but not present in heterotrophic bacteria or their phages by metagenomic recruitment assays (Xu et al., 2018). As shown in the phylogenetic tree (**Figure 6C**), DNA polymerases γ of Mic1, together with A-HIS1/A-HIS2, S-TIM5, and S-CBWM1, share a common origin with mitochondrial DNA polymerases in opisthokonts (fungi and animals), but distinct from those in photosynthetic eukaryotes, which belong to origin-unknown plant organellar DNA polymerases (Moriyama et al., 2011; Cupp and Nielsen, 2014). Thus we can predict that, with more cyanophage genome sequences and metagenomics data available, more homologs of mitochondrial DNA polymerase γ genes will be identified. All together, we propose that the DNA polymerase γ genes in mitochondria and cyanophages share a common ancestor.

DATA AVAILABILITY STATEMENT

The raw datasets for this study can be found in GeneBank, accession No. MN013189.

AUTHOR CONTRIBUTIONS

W-FL, C-ZZ, and Q-FW conceived, designed, and supervised the project. FY, HJ, X-QW, QL, and J-TZ performed the cyanophage isolation and characterization experiments. FY and Q-FW analyzed the genome data. NC, Y-LJ, and YC provided some good suggestions for the subject. W-FL, C-ZZ, and FY analyzed data and wrote the manuscript. W-FL and C-ZZ revised the manuscript. All authors discussed the data and read the manuscript.

FUNDING

This work was supported by the Ministry of Science and Technology of China (http://www.most.gov.cn, Grant No. 2018YFA0903100) and the National Natural Science Foundation of China (http://www.nsfc.gov.cn, Grant No. 31630001).

SUPPLEMENTARY MATERIAL

The Supplementary Material for this article can be found online at: https://www.frontiersin.org/articles/10.3389/fmicb.2020.00484/full#supplementary-material

REFERENCES

Bolden, A., Noy, G. P., and Weissbach, A. (1977). DNA-polymerase of Mitochondria is a gamma-polymerase. *J. Biol. Chem.* 252, 3351–3356.

Brooks, A. C., and Hwang, L. C. (2017). Reconstitutions of plasmid partition systems and their mechanisms. *Plasmid* 91, 37–41. doi: 10.1016/j.plasmid.2017.03.004

Bryan, M. J., Burroughs, N. J., Spence, E. M., Clokie, M. R., Mann, N. H., and Bryan, S. J. (2008). Evidence for the intense exchange of MazG in marine cyanophages by horizontal gene transfer. *PLoS One* 3:e2048. doi: 10.1371/journal.pone.0002048

Callahan, B. P., Topilina, N. I., Stanger, M. J., Van Roey, P., and Belfort, M. (2011). Structure of catalytically competent intein caught in a redox trap with functional and evolutionary implications. *Nat. Struct. Mol. Biol.* 18, 630–633. doi: 10.1038/nsmb.2041

Casjens, S. R., and Gilcrease, E. B. (2009). Determining DNA packaging strategy by analysis of the termini of the chromosomes in tailed-bacteriophage virions. *Methods Mol. Biol.* 502, 91–111. doi: 10.1007/978-1-60327-565-1_7

Chan, Y. W., Mohr, R., Millard, A. D., Holmes, A. B., Larkum, A. W., Whitworth, A. L., et al. (2011). Discovery of cyanophage genomes which contain mitochondrial DNA polymerase. *Mol. Biol. Evol.* 28, 2269–2274. doi: 10.1093/molbev/msr041

Chen, F., and Lu, J. (2002). Genomic sequence and evolution of marine cyanophage P60: a new insight on lytic and lysogenic phages. *Appl. Environ. Microbiol.* 68, 2589–2594. doi: 10.1128/AEM.68.5.2589-2594.2002

Chenard, C., Chan, A. M., Vincent, W. F., and Suttle, C. A. (2015). Polar freshwater cyanophage S-EIV1 represents a new widespread evolutionary lineage of phages. *ISME J.* 9, 2046–2058. doi: 10.1038/ismej.2015.24

Chenard, C., Wirth, J. F., and Suttle, C. A. (2016). Viruses infecting a freshwater filamentous cyanobacterium (*Nostoc* sp.) encode a functional CRISPR array and a proteobacterial DNA polymerase B. *mBio* 7:e667-16. doi: 10.1128/mBio.00667-16

Coloma, S. E., Dienstbier, A., Bamford, D. H., Sivonen, K., Roine, E., and Hiltunen, T. (2017). Newly isolated *Nodularia* phage influences cyanobacterial community dynamics. *Environ. Microbiol.* 19, 273–286. doi: 10.1111/1462-2920.13601

Cupp, J. D., and Nielsen, B. L. (2014). Minireview: DNA replication in plant mitochondria. *Mitochondrion* 19(Pt B), 231–237. doi: 10.1016/j.mito.2014.03.008

Delcher, A. L., Harmon, D., Kasif, S., White, O., and Salzberg, S. L. (1999). Improved microbial gene identification with GLIMMER. *Nucleic Acids Res.* 27, 4636–4641. doi: 10.1093/nar/27.23.4636

Desiere, F., Pridmore, R. D., and Brossow, H. (2000). Comparative genomics of the late gene cluster from *Lactobacillus* phages. *Virology* 275, 294–305. doi: 10.1006/viro.2000.0498

Dreher, T. W., Brown, N., Bozarth, C. S., Schwartz, A. D., Riscoe, E., Thrash, C., et al. (2011). A freshwater cyanophage whose genome indicates close relationships to photosynthetic marine cyanomyophages. *Environ. Microbiol.* 13, 1858–1874. doi: 10.1111/j.1462-2920.2011.02502.x

Filee, J., Forterre, P., Sen-Lin, T., and Laurent, J. (2002). Evolution of DNA polymerase families: evidences for multiple gene exchange between cellular and viral proteins. *J. Mol. Evol.* 54, 763–773. doi: 10.1007/s00239-001-0078-x

Francis, G. (1878). Poisonous Australian lake. *Nature* 18, 11–12. doi: 10.1038/018011d0

Gao, E. B., Gui, J. F., and Zhang, Q. Y. (2012). A novel cyanophage with a cyanobacterial nonbleaching protein A gene in the genome. *J. Virol.* 86, 236–245. doi: 10.1128/JVI.06282-11

Goldsmith, D. B., Crosti, G., Dwivedi, B., McDaniel, L. D., Varsani, A., Suttle, C. A., et al. (2011). Development of phoH as a novel signature gene for assessing marine phage diversity. *Appl. Environ. Microbiol.* 77, 7730–7739. doi: 10.1128/AEM.05531-11

Harke, M. J., Steffen, M. M., Gobler, C. J., Otten, T. G., Wilhelm, S. W., Wood, S. A., et al. (2016). A review of the global ecology, genomics, and biogeography of the toxic cyanobacterium, *Microcystis* spp. *Harmful Algae* 54, 4–20. doi: 10.1016/j.hal.2015.12.007

Howard-Varona, C., Hargreaves, K. R., Abedon, S. T., and Sullivan, M. B. (2017). Lysogeny in nature: mechanisms, impact and ecology of temperate phages. *ISME J.* 11, 1511–1520. doi: 10.1038/ismej.2017.16

Huang, S. J., Wang, K., Jiao, N. Z., and Chen, F. (2012). Genome sequences of siphoviruses infecting marine *Synechococcus* unveil a diverse cyanophage group and extensive phage-host genetic exchanges. *Environ. Microbiol.* 14, 540–558. doi: 10.1111/j.1462-2920.2011.02667.x

Huisman, J., Codd, G. A., Paerl, H. W., Ibelings, B. W., Verspagen, J. M. H., and Visser, P. M. (2018). Cyanobacterial blooms. *Nat. Rev. Microbiol.* 16, 471–483. doi: 10.1038/s41579-018-0040-41

Jiang, Y. L., Wang, X. P., Sun, H., Han, S. J., Li, W. F., Cui, N., et al. (2018). Coordinating carbon and nitrogen metabolic signaling through the cyanobacterial global repressor NdhR. *Proc. Natl. Acad. Sci. U.S.A.* 115, 403–408. doi: 10.1073/pnas.1716062115

Jin, H., Jiang, Y. L., Yang, F., Zhang, J. T., Li, W. F., Zhou, K., et al. (2019). Capsid structure of a freshwater cyanophage siphoviridae Mic1. *Structure* 27, 1–9. doi: 10.1016/j.str.2019.07.003

Kim, M., and Ryu, S. (2013). Antirepression system associated with the life cycle switch in the temperate Podoviridae phage SPC32H. *J. Virol.* 87, 11775–11786. doi: 10.1128/JVI.02173-2113

Lennon, C. W., Stanger, M., and Belfort, M. (2016). Protein splicing of a recombinase intein induced by ssDNA and DNA damage. *Genes Dev.* 30, 2663–2668. doi: 10.1101/gad.289280.116

Liu, X., Kong, S., Shi, M., Fu, L., Gao, Y., and An, C. (2008). Genomic analysis of freshwater cyanophage Pf-WMP3 Infecting cyanobacterium *Phormidium foveolarum*: the conserved elements for a phage. *Microb. Ecol.* 56, 671–680. doi: 10.1007/s00248-008-9386-9387

Liu, X., Shi, M., Kong, S., Gao, Y., and An, C. (2007). Cyanophage Pf-WMP4, a T7-like phage infecting the freshwater cyanobacterium *Phormidium foveolarum*: complete genome sequence and DNA translocation. *Virology* 366, 28–39. doi: 10.1016/j.virol.2007.04.019

Lukashin, A. V., and Borodovsky, M. (1998). GeneMark.hmm: new solutions for gene finding. *Nucleic Acids Res.* 26, 1107–1115. doi: 10.1093/nar/26.4.1107

Marliere, P. (2006). *Genomic Library of Cyanophage s-2l and Functional Analysis*. U.S. Patent No 2006027.0005A1. Washington, DC: U.S. Patent and Trademark Office.

Martin, R. M., Moniruzzaman, M., Mucci, N. C., Willis, A., Woodhouse, J. N., Xian, Y., et al. (2019). *Cylindrospermopsis raciborskii* virus and host: genomic characterization and ecological relevance. *Environ. Microbiol.* 21, 1942–1956. doi: 10.1111/1462-2920.14425

Morimoto, D., Tominaga, K., Nishimura, Y., Yoshida, N., Kimura, S., Sako, Y., et al. (2019). Cooccurrence of broad- and narrow-host-range viruses infecting the bloom-forming toxic cyanobacterium *Microcystis aeruginosa*. *Appl. Environ. Microbiol.* 85:e1170-19. doi: 10.1128/aem.01170-1119

Moriyama, T., Terasawa, K., and Sato, N. (2011). Conservation of POPs, the plant organellar DNA polymerases, in eukaryotes. *Protist* 162, 177–187. doi: 10.1016/j.protis.2010.06.001

Nishimura, Y., Yoshida, T., Kuronishi, M., Uehara, H., Ogata, H., and Goto, S. (2017). ViPTree: the viral proteomic tree server. *Bioinformatics* 33, 2379–2380. doi: 10.1093/bioinformatics/btx157

Ou, T., Gao, X. C., Li, S. H., and Zhang, Q. Y. (2015a). Genome analysis and gene nblA identification of *Microcystis aeruginosa* myovirus (MaMV-DC) reveal the evidence for horizontal gene transfer events between cyanomyovirus and host. *J. Gen. Virol.* 96, 3681–3697. doi: 10.1099/jgv.0.000290

Ou, T., Liao, X. Y., Gao, X. C., Xu, X. D., and Zhang, Q. Y. (2015b). Unraveling the genome structure of cyanobacterial podovirus A-4L with long direct terminal repeats. *Virus Res.* 203, 4–9. doi: 10.1016/j.virusres.2015.03.012

Paerl, H. W., Fulton, R. S. III, Moisander, P. H., and Dyble, J. (2001). Harmful freshwater algal blooms, with an emphasis on cyanobacteria. *Sci. World J.* 1, 76–113. doi: 10.1100/tsw.2001.16

Perler, F. B., Davis, E. O., Dean, G. E., Gimble, F. S., Jack, W. E., Neff, N., et al. (1994). Protein splicing elements - inteins and exteins - a definition of terms and recommended nomenclature. *Nucleic Acids Res.* 22, 1125–1127. doi: 10.1093/nar/22.7.1125

Ravin, N. V. (2011). N15: the linear phage-plasmid. *Plasmid* 65, 102–109. doi: 10.1016/j.plasmid.2010.12.004

Reitter, J. N., Cousin, C. E., Nicastri, M. C., Jaramillo, M. V., and Mills, K. V. (2016). Salt-dependent conditional protein splicing of an intein from *Halobacterium salinarum*. *Biochemistry* 55, 1279–1282. doi: 10.1021/acs.biochem.6b00128

Sabehi, G., Shaulov, L., Silver, D. H., Yanai, I., Harel, A., and Lindell, D. (2012). A novel lineage of myoviruses infecting cyanobacteria is widespread in the oceans. *Proc. Natl. Acad. Sci. U.S.A.* 109, 2037–2042. doi: 10.1073/pnas.1115467109

Sullivan, M. B., Krastins, B., Hughes, J. L., Kelly, L., Chase, M., Sarracino, D., et al. (2009). The genome and structural proteome of an ocean siphovirus: a new window into the cyanobacterial 'mobilome'. *Environ. Microbiol.* 11, 2935–2951. doi: 10.1111/j.1462-2920.2009.02081.x

Topilina, N. I., Green, C. M., Jayachandran, P., Kelley, D. S., Stanger, M. J., Piazza, C. L., et al. (2015a). SufB intein of *Mycobacterium tuberculosis* as a sensor for oxidative and nitrosative stresses. *Proc. Natl. Acad. Sci. U.S.A.* 112, 10348–10353. doi: 10.1073/pnas.1512777112

Topilina, N. I., Novikova, O., Stanger, M., Banavali, N. K., and Belfort, M. (2015b). Post-translational environmental switch of RadA activity by extein-intein interactions in protein splicing. *Nucleic Acids Res.* 43, 6631–6648. doi: 10.1093/nar/gkv612

Vecchiarelli, A. G., Han, Y. W., Tan, X., Mizuuchi, M., Ghirlando, R., Biertumpfel, C., et al. (2010). ATP control of dynamic P1 ParA-DNA interactions: a key role for the nucleoid in plasmid partition. *Mol. Microbiol.* 78, 78–91. doi: 10.1111/j.1365-2958.2010.07314.x

Wood, D. W., Wu, W., Belfort, G., Derbyshire, V., and Belfort, M. (1999). A genetic system yields self-cleaving inteins for bioseparations. *Nat. Biotechnol.* 17, 889–892. doi: 10.1038/12879

Xu, Y., Zhang, R., Wang, N., Cai, L., Tong, Y., Sun, Q., et al. (2018). Novel phage-host interactions and evolution as revealed by a cyanomyovirus isolated from an estuarine environment. *Environ. Microbiol.* 20, 2974–2989. doi: 10.1111/1462-2920.14326

Yamaguchi, T., Hayashi, T., Takami, H., Nakasone, K., Ohnishi, M., Nakayama, K., et al. (2000). Phage conversion of exfoliative toxin A production in *Staphylococcus aureus*. *Mol. Microbiol.* 38, 694–705. doi: 10.1046/j.1365-2958.2000.02169.x

Yoshida, T., Nagasaki, K., Takashima, Y., Shirai, Y., Tomaru, Y., Takao, Y., et al. (2008). Ma-LMM01 infecting toxic *Microcystis aeruginosa* illuminates diverse cyanophage genome strategies. *J. Bacteriol.* 190, 1762–1772. doi: 10.1128/JB.01534-1537

Yoshida, T., Takashima, Y., Tomaru, Y., Shirai, Y., Takao, Y., Hiroishi, S., et al. (2006). Isolation and characterization of a cyanophage infecting the toxic

cyanobacterium *Microcystis aeruginosa*. *Appl. Environ. Microbiol.* 72, 1239–1247. doi: 10.1128/AEM.72.2.1239-1247.2006

Zhang, Q. Y., and Gui, J. F. (2018). Diversity, evolutionary contribution and ecological roles of aquatic viruses. *Sci. China Life Sci.* 61, 1486–1502. doi: 10.1007/s11427-018-9414-7

Zhong, K. X., Suttle, C. A., Baudoux, A. C., Derelle, E., Colombet, J., Cho, A., et al. (2018). A new freshwater cyanosiphovirus harboring integrase. *Front. Microbiol.* 9:2204. doi: 10.3389/fmicb.2018.02204

Zhou, Q., Wei, N., Zheng, L., and Song, L. (2013). Host re-identification of cyanophage PP and its implications for host range and specificity. *Virol. Sin.* 28, 306–308. doi: 10.1007/s12250-013-3356-z

Conflict of Interest: The authors declare that the research was conducted in the absence of any commercial or financial relationships that could be construed as a potential conflict of interest.

Copyright © 2020 Yang, Jin, Wang, Li, Zhang, Cui, Jiang, Chen, Wu, Zhou and Li. This is an open-access article distributed under the terms of the Creative Commons Attribution License (CC BY). The use, distribution or reproduction in other forums is permitted, provided the original author(s) and the copyright owner(s) are credited and that the original publication in this journal is cited, in accordance with accepted academic practice. No use, distribution or reproduction is permitted which does not comply with these terms.

frontiers in Microbiology

ORIGINAL RESEARCH
published: 08 May 2020
doi: 10.3389/fmicb.2020.00883

Deciphering the Role of Holin in Mycobacteriophage D29 Physiology

*Varun Rakeshbhai Bavda and Vikas Jain**

Microbiology and Molecular Biology Laboratory, Department of Biological Sciences, Indian Institute of Science Education and Research (IISER), Bhopal, India

In the era of antibiotic resistance, phage therapy is gaining attention for the treatment of pathogenic organisms such as *Mycobacterium tuberculosis*. The selection of phages for therapeutic purposes depends upon several factors such as the host range that a phage can infect, which can be narrow or broad, time required for the host cell lysis, and the burst size. Mycobacteriophage D29 is a virulent phage that has the ability to infect and kill several slow- and fast-growing mycobacterial species including the pathogenic *M. tuberculosis*. It, therefore, has the potential to be used in phage therapy against *M. tuberculosis*. D29 lytic cassette encodes three proteins *viz*. peptidoglycan hydrolase (LysA), mycolylarabinogalactan esterase (LysB), and holin, which together ensure host cell lysis in a timely manner. In this work, we have scrutinized the importance of holin in mycobacteriophage D29 physiology. Bacteriophage Recombineering of Electroporated DNA (BRED) approach was used to generate D29 holin knockout (D29Δ*gp11*), which was further confirmed by the Deletion amplification detection assay (DADA)-PCR. Our results show that D29Δ*gp11* is viable and retains plaque-forming ability, although with reduced plaque size. Additionally, the host cell lysis governed by the mutant phage is significantly delayed as compared to the wild-type D29. In the absence of holin, D29 shows increased latent period and reduced burst size. Thus, our experiments show that while holin is dispensable for phage viability, it is essential for the optimal phage-mediated host cell lysis and phage propagation, which further points to the significance of the "clock" function of holin. Taken together, we show the importance of holin in governing timely and efficient host cell lysis for efficient progeny phage release, which further dictates its critical role in phage biology.

Keywords: phage infection, phage therapy, mycobacteria, transmission electron microscopy, recombineering

OPEN ACCESS

Edited by:
Krishna Mohan Poluri,
Indian Institute of Technology Roorkee, India

Reviewed by:
Madalena Pimentel,
Research Institute for Medicines (iMed.ULisboa), Portugal
Sebastian Leptihn,
Zhejiang University-University of Edinburgh Institute, China

***Correspondence:**
Vikas Jain
vikas@iiserb.ac.in

Specialty section:
This article was submitted to Virology, a section of the journal Frontiers in Microbiology

Received: *15 February 2020*
Accepted: *16 April 2020*
Published: *08 May 2020*

Citation:
Bavda VR and Jain V (2020) Deciphering the Role of Holin in Mycobacteriophage D29 Physiology. Front. Microbiol. 11:883. doi: 10.3389/fmicb.2020.00883

INTRODUCTION

Tuberculosis (TB) is an infectious disease caused by the pathogenic *Mycobacterium tuberculosis*. With an estimated death of 1.5 million people in year 2018, TB is among top 10 cause of death (Harding, 2020). Further in recent years, TB epidemic has been enhanced by the rapid emergence of multi drug resistant and extensively drug resistant *M. tuberculosis* strains (Koul et al., 2011; Coll et al., 2018). Thus being a global health threat, TB requires an urgent need of alternative approach to combat the failure of treatment with antibiotics.

Mycobacteriophages are viruses that require mycobacterial host for their propagation (Sarkis and Hatfull, 1998; Hatfull, 2014a,b, 2018). Being the natural killer of their hosts, mycobacteriophages have the potential to be developed as the next-generation phage-based

therapeutics against TB and other pathogenic mycobacterial infections, especially when the antibiotics against the pathogens become ineffective. Indeed, mycobacteriophages have not only shown their potential to treat *Mycobacterium abscessus* infection (Dedrick et al., 2019), but they have also been used for the development of phage-based diagnostics (Jacobs et al., 1993; Pearson et al., 1996; Park et al., 2003). Among the many mycobacteriophages, D29, which is a virulent phage and is capable of infecting and killing both slow and fast growing mycobacterial species (Ford et al., 1998; Rybniker et al., 2006), and its lysis enzymes have been used to kill *M. tuberculosis* and other mycobacteria in various animal-based experiments (Carrigy et al., 2019; Fraga et al., 2019). The host cell lysis is governed by the protein products of the "Lytic cassette" genes. In D29, the lytic cassette comprises *gp10* coding for an endolysin LysA that targets the peptidoglycan cell wall and *gp12* producing LysB that targets the outer mycolic acid layer of mycobacteria (Payne et al., 2009; Fraga et al., 2019). Additionally, *gp11*, which is sandwiched between *gp10* and *gp12*, produces holin that perforates the cell membrane of mycobacteria thus allowing for the diffusion of the hydrolytic enzymes to the periplasm and ensuing cell lysis (Catalao et al., 2013; Kamilla and Jain, 2016).

Data available from other phages suggest that holin not only allows for the lysins release to the periplasm, but it also functions as a "clock", and times the lysis event during phage infection (Wang et al., 2000; Grundling et al., 2001). Holins that form large holes to allow the diffusion of folded lysins to the periplasm are called canonical holin (Wang et al., 2003; Savva et al., 2014; To and Young, 2014). On the other hand, several phages code for pinholins that form small holes that disrupt proton gradient across the membrane, but are not involved in the periplasmic delivery of endolysins (Park et al., 2007; Catalao et al., 2010; Young, 2013; Cahill and Young, 2019). Holin, therefore, times the lysis of the host cell and hence functions as "clock" (Wang et al., 2000). In the case of D29, although the holin protein has been shown to form large holes (Catalao et al., 2011; Kamilla and Jain, 2016), its endolysin LysA, however, can translocate to periplasm even in the absence of holin when it is expressed in *Mycobacterium smegmatis* (Pohane et al., 2014).

The functioning of λ phage holin has been dissected in great detail. It has been suggested that holin, upon its expression, initially accumulates in the plasma membrane without disrupting the membrane integrity. This gives sufficient time for the progeny phages to assemble inside the host cell. After reaching a threshold concentration in the membrane, holin spontaneously changes its structure and forms mature holes (Ryan and Rutenberg, 2007; White et al., 2011). These holes dissipate the proton motive force across the plasma membrane and allow the free diffusion of endolysins already accumulated within cytoplasm (Wang et al., 2000; Grundling et al., 2001; Saier and Reddy, 2015). It is conceivable, therefore, that by controlling the timing of lysis, holin determines the duration of the infective cycle of phage, and that an alteration in this function may lead to premature or delayed host lysis, resulting in a loss of phage fitness either in terms of progeny phage number or loss of progeny phages, respectively (Wang, 2006).

While holins from other phages have been studied in great detail (Wang et al., 2000), the structure-function relationship of mycobacteriophage holin and how it regulates mycobacterial cell lysis are not well characterized. We have previously shown that D29 holin possesses two transmembrane domains (TMD) at its N-terminus and a highly charged C-terminal region (Kamilla and Jain, 2016; Lella et al., 2016), and that its expression is extremely toxic to both *Escherichia coli* and mycobacteria. However, an observation that the expression of D29 LysA in *M. smegmatis* is sufficient to kill the bacterium even in the absence of holin (Pohane et al., 2014) tempted us to speculate if holin is an essential protein for the D29 phage survival. Therefore, in order to understand the role of holin in phage biology, we deleted holin gene from D29 phage genome and examined its physiology. Here we show that D29 phage devoid of holin, although viable with poor plaque forming ability, shows delayed host cell lysis, which may hint towards the importance of "clock" function of this protein in mycobacteriophage biology.

MATERIALS AND METHODS

Bacterial Strains, Plasmid, Media, and Growth Conditions

Wild-type *M. smegmatis* strain mc^2155 was grown at 37°C with constant shaking unless specified otherwise in Middlebrook 7H9 (MB7H9) (Difco) medium supplemented with 2% glucose and 0.05% tween 80. For recombineering experiments, electrocompetent *M. smegmatis* cells carrying pJV53 plasmid were prepared as described previously (van Kessel and Hatfull, 2007; Marinelli et al., 2008). For all phage infection experiments, *M. smegmatis* was grown in MB7H9 supplemented with 10% OADC (Difco) along with 1 mM $CaCl_2$. For preparation of solid culture medium, 1.5% agar and 2% glucose were additionally added to the growth medium. For soft agar preparation, 0.75% agar was added to the growth medium in order to perform agar overlay for phage infection experiments. In all experiments, cultures were incubated at 37°C.

Deletion of Holin Gene in D29 Phage and Its Confirmation

Bacteriophage Recombineering of Electroporated DNA (BRED) assay was performed to generate holin knockout of D29 phage essentially as described previously (van Kessel and Hatfull, 2007; Marinelli et al., 2008). Briefly, the allelic exchange substrate (AES) was generated by PCR using the primers listed in **Table 1**, confirmed by DNA sequencing, and co-electroporated with D29 genomic DNA in *M. smegmatis* carrying pJV53 plasmid. Screening of plaques was carried out by Deletion Amplification Detection Assay (DADA) PCR (Swaminathan et al., 2001; Marinelli et al., 2008) using the primers P5 and P6 as listed in **Table 1**. The plaques were further purified to obtain pure mutant phage essentially as described previously (Joshi et al., 2019). Briefly, primary plaques which showed DADA PCR amplification corresponding to both wildtype and knockout phages were selected and diluted further for carrying out phage infection with

TABLE 1 | List of primers used in the present study.

S. No.	Primer name	Primer sequence (5′–3′)
1	P1	GCTCCCCCGAGTTCATCGCAC
2	P2	CCAGGGCTTGCTCATAGGGCTCCATTCCTGG
3	P3	GAGCCCTATGAGCAAGCCCTGGCTGTTCACC
4	P4	GATGTCAAGTACGTCGCGTGCCGTATCG
5	P5	CCAGAGGATCCGGCGACCAACTACTGACTC
6	P6	GAACGGTGAACAGCCAGGGCTTGCTC

M. smegmatis cells to isolate pure holin knockout phage. The pure holin knockout phage (D29Δ*gp11*) was further confirmed by DNA sequencing. Pairwise alignment of the sequencing data with the predicted genomic DNA sequence was carried out using CLUSTAL Omega (Madeira et al., 2019).

Western Blotting Analysis

M. smegmatis cells were grown at 37°C till OD_{600} of the culture reached 0.6. Bacteria were infected with either D29WT or D29Δ*gp11* at multiplicity of infection (MOI) of 1 for 1 h at 37°C. Cells were then harvested and resuspended in a lysis buffer containing 40 mM Tris-Cl pH 8.0, 200 mM NaCl, 5 mM imidazole, 5 mM 2-mercaptoethanol and 8 M urea, and lysed by sonication. Cell lysate thus obtained was centrifuged at high speed and the supernatant was mixed with SDS-loading dye to separate the proteins on polyacrylamide gel. The production of LysA and LysB proteins was examined by western blotting essentially as described previously (Pohane et al., 2014) using anti-LysA (Pohane et al., 2014) and anti-LysB antibodies. Polyclonal anti-LysB antibodies were raised in rabbit using purified LysB protein (Bioneeds India Private Limited, India).

Host Cell Viability and Cell Lysis Attributed by Phage

M. smegmatis log phase culture was infected with either D29WT or D29Δ*gp11* phage at MOI of 1, and the viability of cells after phage infection was measured using AlamarBlue (BIO-RAD) cell viability reagent essentially as described previously (Warrier et al., 2012; Joshi et al., 2019; Patil and Jain, 2019) at different time points post-infection. Phage-induced bacterial cell lysis was also monitored by measuring the optical density of the culture at 600 nm (OD_{600}) at specified time points on a spectrophotometer (Jenway, Bibby scientific). The amount of ATP released into the culture supernatant upon cell lysis was determined by BacTiter-Glo Microbial Cell Viability Assay kit (Promega) as described previously (Joshi et al., 2019; Patil and Jain, 2019).

Transmission Electron Microscopy (TEM) Imaging of Phages

Imaging of phages on a transmission electron microscope was carried out as described previously (Ackermann, 2009). Briefly, both D29WT and D29Δ*gp11* were purified in high titre with at least 1×10^{11} PFU/ml. Formvar/Carbon coated Cu grid (400 mesh) was procured from TED-PELLA, INC. Approximately 5–10 μl of filtered phage was put onto the Cu grid and after a brief incubation (5–10 min) at room temperature, the extra liquid was removed by blotting paper. A drop of 2% uranyl acetate stain was applied on the grid and was incubated for not more than 1 min. Extra stain was then removed by blotting paper, and the grid was washed thrice with Milli-Q water. The grid was then allowed to dry in a desiccator overnight at RT. Grid was then used for TEM imaging on FEI Talos 200S system equipped with a 200-kV field emission gun.

Phage Adsorption Kinetics and One Step Growth

Mycobacteriophage adsorption kinetics was measured as described previously (Delbruck, 1940; Hendrix and Duda, 1992; Kropinski, 2009), with some modifications. Briefly, 1 ml of log phase culture (OD_{600} ∼0.6) of *M. smegmatis* was mixed with either D29WT or D29Δ*gp11* keeping MOI of 1. At regular intervals, equal amount of phage-infected culture was collected in each case and immediately centrifuged at 14000 rpm at 4°C to separate uninfected and infected host from free phages. The number of free phages present in the supernatant thus obtained was estimated by performing phage infection and plotted as percentage of free phages with respect to time 0 being 100% (no infection). One step growth was performed for both D29WT and D29Δ*gp11* essentially as described previously (Hyman and Abedon, 2009; Catalao et al., 2011). Briefly, at regular time intervals, 1 ml of diluted phage-infected sample was used to estimate number of phage particles present in it by carrying out secondary infection. Relative phage titre was determined and was plotted (Hyman and Abedon, 2009).

RESULTS

Construction of Mycobacteriophage D29 Holin Knockout

D29 lytic cassette possesses three overlapping genes *viz. gp10*, *gp11*, and *gp12*. In order to generate a holin knock-out (D29Δ*gp11*), we followed the BRED strategy (Marinelli et al., 2008), which we used earlier to also mutate the gp10 gene in D29 (Joshi et al., 2019). The schematic of the holin deletion is presented in **Supplementary Figure S1A**. The 100 bp upstream and 99 bp downstream regions of *gp11* were PCR amplified and fused by overlapping PCR to generate AES of 199 bp (**Supplementary Figures S1B,C**). It is important to note here that the start codon of *gp11* is overlapped with the stop codon of *gp10*; similarly, the stop codon of *gp11* overlaps with the start codon of *gp12* (**Supplementary Figure S2**). Therefore, the overlapping regions were retained in this fashion in the AES so that *gp10* and *gp12* share the same overlapping region and the open reading frame is not changed. Next, to generate D29Δ*gp11*, purified genomic DNA of D29 and AES were co-electroporated into electrocompetent *M. smegmatis* cells containing pJV53 plasmid as shown in schematic (**Supplementary Figure S1D**). The pJV53 encodes for recombinase that allows for the recombination to occur between the AES and its homologous region of the

phage genomic DNA (Marinelli et al., 2008). The recovered cells were plated using soft agar method and the plaques thus obtained (**Supplementary Figure S3A**) were screened for the mutated phage by DADA PCR (Marinelli et al., 2008). Initially-obtained plaques were found to be having both the knock-out and the wild-type (WT) phages (**Supplementary Figure S3B**). Secondary and further phage infections as shown in the schematic (**Supplementary Figure S3C**) were then carried out to obtain pure D29Δ*gp11* phage, which gave correct size amplicon of ∼400 bp in PCR (**Supplementary Figure S3D**); the amplicon was further sequenced to confirm the deletion of *gp11* (**Supplementary Figure S4**). We next performed western blotting of the D29WT- and D29Δ*gp11*-infected *M. smegmatis* culture to assess the expression of *gp10* and *gp12* genes during phage infection. We found both of these proteins being produced during infection (**Figure 1**), which indicates that the deletion of holin does not hamper expression of the neighboring genes.

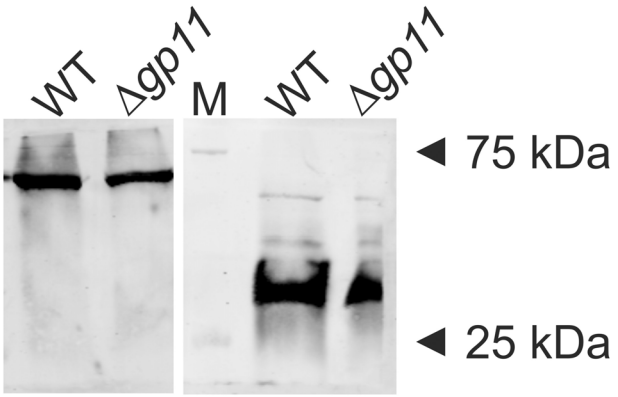

FIGURE 1 | LysA and LysB protein expression analysis by western blotting. The blots show the production of LysA and LysB by both D29WT (WT) and holin knockout (Δ*gp11*) phages. Only one representative blot in each case is shown here. "M" depicts molecular weight marker with two bands marked.

Deletion of Holin Results in Smaller Plaques by D29 Phage

We next assessed morphology of the plaques obtained for D29Δ*gp11* phage and compared the same with the D29WT. *M. smegmatis* was infected with either D29Δ*gp11* or WT and the plaques were observed post 24 h incubation at 37°C. Interestingly, the plaques obtained for the D29Δ*gp11* are found to be significantly smaller than that obtained for the WT D29 phage (**Figure 2A**). We also measured the plaque size using ImageJ software (Schneider et al., 2012). The diameter of plaques for D29 WT and D29Δ*gp11* was found to be ∼5.5 and ∼4 mm, respectively (**Figure 2B**).

D29Δ*gp11* Phage Shows Significantly Delayed Cell Lysis

In order to determine the effect of holin on phage-mediated cell lysis, we monitored the optical density of phage infected cultures. *M. smegmatis* log phase culture was infected with D29WT and D29Δ*gp11* at MOI = 1, and the OD_{600} was measured at regular intervals. Interestingly, whereas the culture infected with D29WT showed a decrease in OD_{600} at 90 min, the culture infected with D29Δ*gp11* phage demonstrated a significant delay in host cell lysis with an OD_{600} decreasing at 120 min (**Figure 3A**). The uninfected culture here was taken as negative control that showed normal growth. In order to further confirm the host cell lysis due to phage infection, we measured the ATP release upon cell lysis. The released ATP in the culture supernatant obtained for each time point samples was measured using the ATP estimation kit. Luminescence data thus obtained showed surge in ATP amounts in the culture supernatant at 90 min post-infection of *M. smegmatis* with D29WT phage, whereas no significant increase in the ATP level was detected in case of culture infected with D29Δ*gp11* at the same time point; in the latter, the ATP amount increased in the culture supernatant only after 120 min of infection (**Figure 3B**), clearly indicating a delay in the host cell lysis by the mutant phage. We also assessed the host cell viability during phage infection by following the alamarBlue assay (Warrier et al., 2012; Joshi et al., 2019; Patil and Jain, 2019). The assay was performed at different time points after infecting *M. smegmatis* with either D29WT or D29Δ*gp11* phage. Here, in presence of viable cells, the blue color dye is reduced to give fluorescent pink color (**Figure 3C**), which is then measured on a fluorescence spectrophotometer with an excitation/emission wavelengths as 540/590 nm, respectively. Expectedly, we observed that the cells infected with the D29Δ*gp11* phage were able to reduce the dye only at a significantly later time point as compared with the D29WT (**Figure 3D**). This data suggests that when *M. smegmatis* is infected with holin knockout phage, hosts cells are viable for longer time than when infected with WT phage.

Mycobacteriophage D29 WT and Δ*gp11* Show Indifferent Morphology and Adsorption Kinetics

The delay in the host cell lysis observed in the case of D29Δ*gp11* phage tempted us to ask if it was because of differences in the morphology of the two phages or the attachment of phage to the host cells. We therefore first assessed the morphology of both the phages by transmission electron microscopy. Our data show that the two phages are identical in terms of general morphology (**Figures 4A–D**). We next performed adsorption kinetics with both the phages. Here, we allowed both WT and D29Δ*gp11* phages to attach to the log phase *M. smegmatis* culture at 37°C. This was followed by the determination of the fraction of free phages present in the supernatant at regular time interval by agar overlay method. The free phages obtained at different time point were plotted as free PFU/ml (**Figure 4E**) and also normalized with the free phages at initial time point (**Figure 4F**). Our data clearly show that nearly 90% of the phages (both WT and the mutant) are adsorbed within first 10 min of infection, thus suggesting that both WT and D29Δ*gp11* phages adsorb to host cell equally efficiently. We conclude from

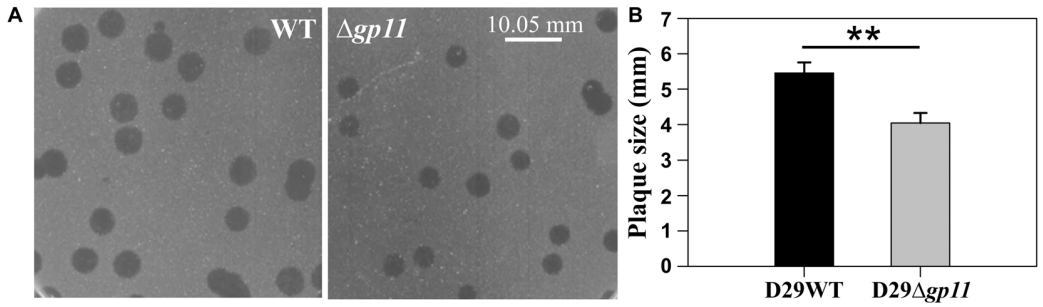

FIGURE 2 | Plaque morphology analysis. **(A)** represents the agar plate images showing the plaques obtained after infecting *M. smegmatis* with either D29WT (WT; Left) or Δ*gp11* (right) phage. The diameter of the obtained plaques was measured using ImageJ software and plotted **(B)**. The experiments were performed at least three times and the total mean value of diameter (in mm) was plotted with standard deviation. *P* value; **< 0.05.

these data that the differences in the host cell lysis by the two phages are not contributed by either phage morphology or host attachment efficiency.

D29Δ*gp11* Shows Increased Latent Period and Decreased Relative Phage Titre

Holin is known to be primarily involved in carrying out a timely lysis of the host bacterium. Conceivably, therefore, a deletion of holin would result in loss of this property of the phage and may affect phage physiology. We, therefore, carried out the one step growth curve analysis to examine the effect of holin deletion on the latent period of phage infection. Our data show that in the absence of holin, the latent period is drastically changed. We observe that when *M. smegmatis* log phase culture is infected with D29WT phage, there is a significant increase in the phage titre at 90 min. In contrast, such increase at 90 min is not observed when the culture is infected with D29Δ*gp11*; in this case, an increase in phage titre is seen only at 120 min. Our data suggest that the latent period of WT phage is ∼60 min, whereas it is 90 min for the D29Δ*gp11* phage (**Figure 5**). Thus an increase of 30 min in the latent period clearly indicates the importance of holin in the timing of lysis of the host bacterium at the end of lytic cycle after D29 phage infection. It also did not escape our notice that a rise in the relative phage titre of D29Δ*gp11* at later time point is ∼2 fold lower than that of the WT phage, which immediately suggests a decrease in the burst size of the D29Δ*gp11* phage. At this juncture, we believe that the less titre observed in D29Δ*gp11* phage is a result of an inefficient host cell lysis in the absence of holin, since the other two proteins, LysA and LysB, expressed efficiently in the cells infected with holin knockout phage. Taken together, our data suggest that holin is crucial for timely and efficient host cell lysis by D29 phage.

DISCUSSION

The underlying mechanism behind holin function is well understood in phages infecting *E. coli*. In addition to holin, several phages express antiholin, which prevents the premature hole formation. Mutations in these alleles have been shown to cause defective cell lysis, with holin null mutants giving rise to an absolute lysis defective phenomenon and phages losing their ability of plaque formation (Wang et al., 2000). In a separate study, point mutation in S^{λ} holin gene A52G has been shown to cause early lysis, thus reducing burst size as compared to WT allele (Johnson-Boaz et al., 1994).

Mycobacteriophage D29 is one of the few virulent phages that can infect and kill both slow-growing *M. tuberculosis* and fast-growing *M. smegmatis*. Host cell lysis by the D29 is solely timed by holin, and thus far, no antiholin has been discovered. In this manuscript, we show how holin protein is important for governing host cell lysis in a time-dependent fashion, and how a deletion of holin influences D29 physiology.

By generating holin knockout, we show that unlike *E. coli* phages, mycobacteriophage D29 is viable. However, we observed notably smaller plaques with the holin knockout phage. Further to check the "clock" function of holin, we measured the rate of host *M. smegmatis* cell lysis upon infection with knockout phage and compared that with D29WT. We find a remarkable difference in the timing of cell lysis exhibited by both the phages. Our experiments show that D29Δ*gp11* displays a 30 min delay in cell lysis as compared to the D29WT. This was further corroborated by the ATP release into the culture supernatant as a consequence of the cell lysis, and the cell viability assays carried out by measuring OD_{600} as well as AlamarBlue dye reduction. Moreover, this notable delay in the host cell lysis cannot be attributed to either a change in phage morphology or its adsorption property as confirmed by our TEM and phage adsorption kinetics data, respectively. Our electron microscopy data show that both WT and holin knockout phages have the same morphology. Additionally, the adsorption kinetics data suggest that nearly 90% of both WT and D29Δ*gp11* phages are adsorbed to the host cell within initial 10 min of phage addition, and no distinguishable differences could be observed. Finally, our one step growth curve experiment with the knockout phage shows an increase in the burst time and a decrease in the burst size. Here, the latent period was found to be increased by 30 min, which concurs well with all other data as discussed above. These observations are in agreement with a previous study with Ms6 phage, wherein a deletion of holin-like proteins such as *gp4* or *gp5* has been shown to cause early or delayed host cell lysis coupled with very small

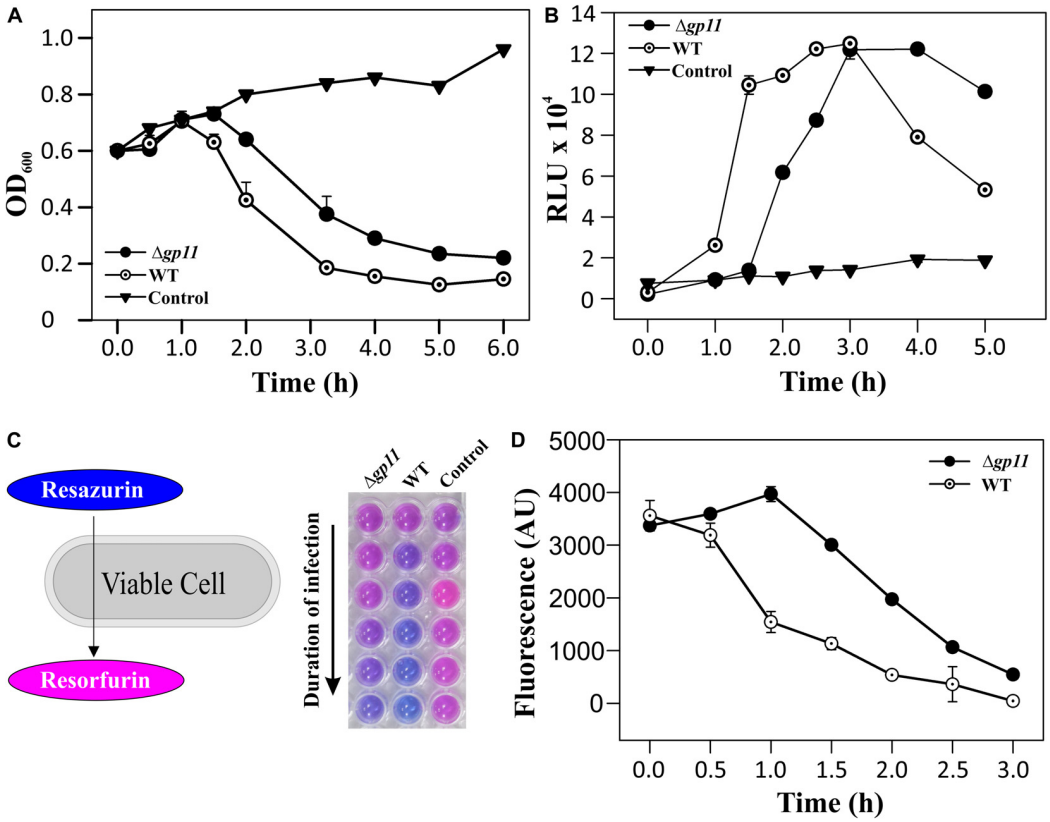

FIGURE 3 | Phage infection with D29Δ*gp11* shows delayed host cell lysis. **(A)** depicts the lysis curve obtained after infecting *M. smegmatis* with either D29WT (WT) or D29Δ*gp11* (Δ*gp11*). The optical density of the culture at 600 nm (OD_{600}) was measured at specified time points and plotted. **(B)** shows the ATP released into the culture supernatant at specified time points, in the form of relative luminescence unit (RLU). **(C)** shows the schematic for the alamarBlue assay; the blue color Resazurin dye is converted into pink colored Resorfurin by live cells. Here, a representative multiwell plate image is shown with *M. smegmatis* culture infected with phage with the duration of infection marked with an arrow; the change in color is observed due to presence of viable cells remaining after phage infection. In all the three panels, "Control" represents the *M. smegmatis* culture without D29 phage infection. In panel **(D)** fluorescence obtained from Resorfurin dye in the alamarBlue cell viability assay at specified time points is plotted for both D29WT (WT) and holin knockout (Δ*gp11*) phage-infected *M. smegmatis*. In panels **(A,B,D)**, only one representative plot is shown with error bars representing standard error.

or large size plaques, respectively (Catalao et al., 2011). Taken together, our data show that while holin is important for the general maintenance of phage physiology, it is dispensable for phage viability. Thus the ability of D29Δ*gp11* to lyse host cell in the absence of holin with a simultaneous decrease in the burst size strongly indicates an inefficient host cell lysis.

Since canonical holins are involved in pore formation in the membrane to let the endolysin diffuse to the peptidoglycan (PG) layer (the substrate of endolysin), what allows D29 endolysin to function in a holin knockout phage? Previous works from our group and Payne & Hatfull have shown that the expression of D29 LysA in *M. smegmatis* results in cell lysis in a holin-independent manner (Payne and Hatfull, 2012; Pohane et al., 2014). These data strongly suggest that holin of D29 is not required for the LysA translocation to the periplasm. It is thus likely that LysA protein translocates to periplasm by secretion via a yet unidentified mechanism post-expression. However, the delay in cell lysis by D29Δ*gp11* phage can be explained by the "clock" function of holin. In other words, it is likely that while holin may not be required for LysA translocation, it is needed for the LysA to become fully active in the periplasm in a timely fashion, as has been suggested in the case of holin-independent (Young, 2002; Park et al., 2007; Briers et al., 2011) as well as canonical endolysins where membrane depolarization is necessary for their activation (Garcia et al., 2010; Proenca et al., 2015; Fernandes and Sao-Jose, 2016). For example, a previous work involving a canonical endolysin of *Bacillus subtilis* phage SPP1 suggested that holin is required for the activation of endolysin after its translocation to the periplasm (Fernandes and Sao-Jose, 2016). Nonetheless, whether D29 holin is involved in LysA activation (and probably its translocation also) is presently not known.

While these data may point to why holin deletion leads to a delay in the host cell lysis upon phage infection, they do not completely explain the observed lower burst size in the case of D29Δ*gp11*. For example, in an earlier study, we reported a D29 phage having a mutation in its LysA protein displayed a late lysis phenotype but with an increase in burst size (Joshi et al., 2019). However, a previous report on an esterase mutant (Δ*lysB*) of mycobacteriophage Giles suggested that LysB is required for efficient phage release (Payne et al., 2009). Similarly, deletion of

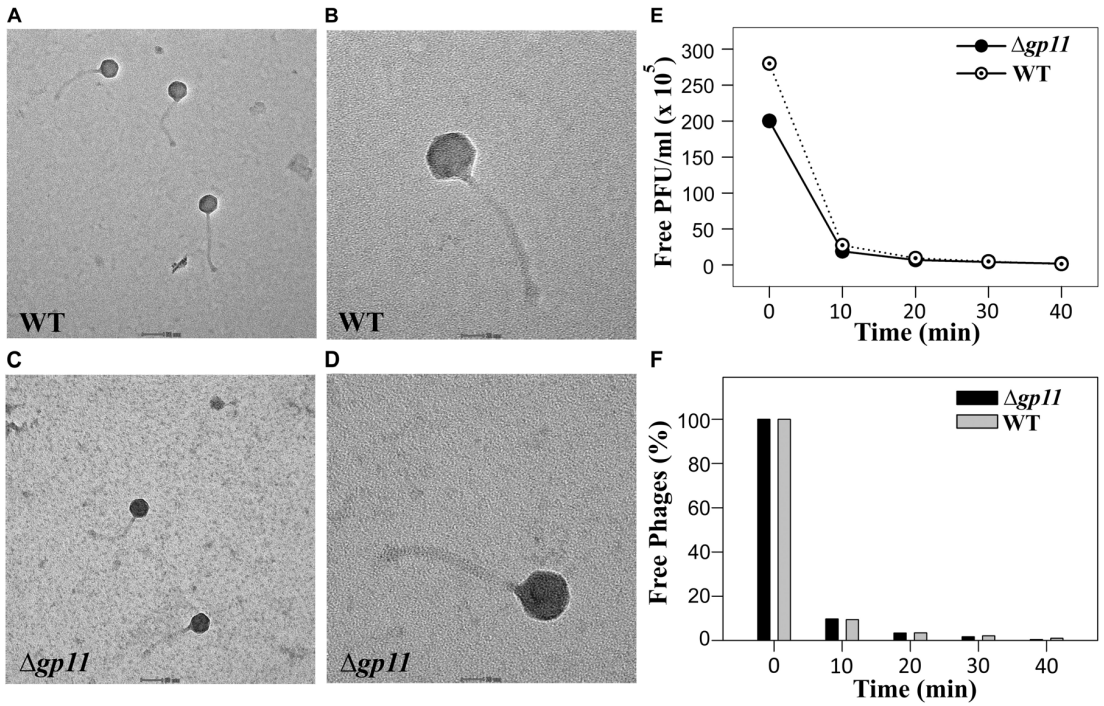

FIGURE 4 | Transmission electron microscopy (TEM) and Phage adsorption kinetics. **(A–D)** show the TEM imaging of D29WT (Panels A & B) and D29Δ*gp11* **(C,D)**. The scale bar in **(A)** and **(C)** correspond to 50 nm; in **(B)** and **(D)**, it is 20 nm. **(E)** and **(F)** show the phage adsorption kinetics for both D29WT and D29Δ*gp11*, wherein a decrease in the free phage titre is plotted as free PFU/ml **(E)** and as percentage of free phages present in culture supernatant after infection **(F)**, with respect to time.

LysB in Ms6 phage has also been shown to result in low number of phage progeny release after infection (Gigante et al., 2017). These studies allow us to suggest that in D29 phage, holin is required for the translocation of LysB. Taken together, we speculate that the lower burst size in D29Δ*gp11* is observed not only because LysB is unable to reach its site of action, i.e., mycolylarabinogalactan layer, but also because while LysA translocates to the periplasm in a holin-independent manner, it is not fully activated to perform its function in the absence of holin.

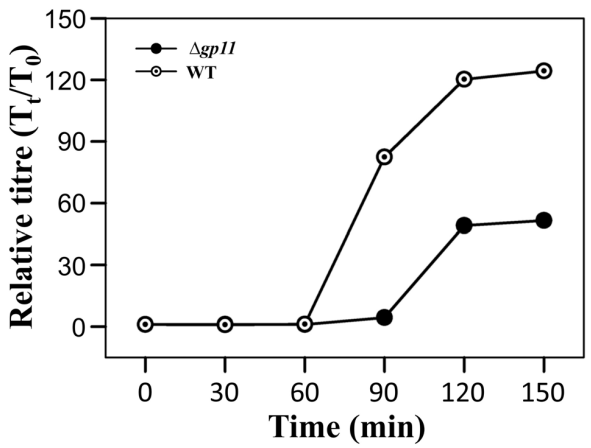

FIGURE 5 | One step growth curve and latent period determination. The plots depict one step growth curve to determine the latent period of infection for both D29WT (WT) and D29Δ*gp11* (Δ*gp11*). The relative phage titre T_t/T_0, where T_0 is the initial PFU and T_t is the PFU at time *t*, obtained at specified time points is plotted. Here, the latent period is the time after which the relative phage titre increases (for D29WT, it is 60 min, whereas for D29Δ*gp11*, it is 90 min).

Phages have the capability to proliferate inside the host and lyse it. Hence, they are also known as "Self-replicating pharmaceuticals" (Payne et al., 2000). Mycobacteriophages are actively being considered for phage therapy against mycobacterial diseases including that caused by the pathogenic *M. tuberculosis* (Hatfull, 2014a) and other mycobacteria (Dedrick et al., 2019), due to the rapid emergence of drug resistant strains. We have earlier reported a mutant D29 phage with a late lysis phenotype but with an increase burst size. Since holin decides the "clock" function of the phage-mediated cell lysis, we believe that by incorporating altered holin gene in our holin knockout phage, novel mycobacteriophage with shorter latent period can be engineered, which may lead to a rapid clearance of bacteria from infection. Such designed phages can be readily used as novel next-generation phage-based therapeutics.

DATA AVAILABILITY STATEMENT

All datasets generated for this study are included in the article/**Supplementary Material**.

AUTHOR CONTRIBUTIONS

VJ conceived the idea. VB and VJ designed the research. VB performed the research. VB and VJ analyzed the data and wrote the manuscript.

FUNDING

This work was supported by the intramural funds from IISER Bhopal to VJ. Funders had no role in designing or execution of the study or preparation of the manuscript and its submission.

ACKNOWLEDGMENTS

VB acknowledges IISER Bhopal for the fellowship. We thank Minakshi Nandanwar for preparing anti-LysB antibodies. We thank DST-FIST facility at IISER Bhopal for the TEM imaging.

SUPPLEMENTARY MATERIAL

The Supplementary Material for this article can be found online at: https://www.frontiersin.org/articles/10.3389/fmicb.2020.00883/full#supplementary-material

FIGURE S1 | Recombineering of mycobacteriophage D29 using BRED (Bacteriophage Recombineering of Electroporated DNA) method for generating holin knockout. Panel A shows the schematic representation of the construction of AES (allelic exchange substrate). Mycobacteriophage D29 genomic DNA (gDNA) consists of lytic cassette encoding three overlapping genes *gp10*, *gp11*, and *gp12* shown as colored boxes. AES was constructed by performing overlapping PCR with the products generated from primers P1/P2 and P3/P4. Panel B shows agarose gel for the PCR amplified AES Up (Primer P1 and P2) and AES Down (Primer P3 and P4) fragments of ∼100 bp each. Panel C shows the AES of ∼200 bp generated by overlapping PCR using primers P1 and P4. In both panels, L represents the DNA ladder with two bands marked for their sizes. Panel D shows the schematic representation of recombineering between D29 gDNA and AES co-electroporated in *M. smegmatis* carrying pJV53 plasmid. pJV53 plasmid produces recombinase that allows for the homologous recombination between the D29 gDNA and AES.

FIGURE S2 | Start and stop codons overlap for the lytic cassette genes. The DNA sequence on the top corresponds to the *gp10* and *gp11* gene sequences. The start codon (ATG) for *gp11* and the stop codon (TGA) for *gp10* are marked with arrows. Similarly, the DNA sequence at the bottom corresponds to the *gp11* and *gp12* gene sequences. The start codon (ATG) for *gp12* and the stop codon (TGA) for *gp11* are marked with arrows.

FIGURE S3 | Screening of knockout phage by DADA PCR. Panel A shows the agar plate image containing plaques recovered after co-electroporation of phage gDNA and AES. A few of the plaques are marked with arrows. Panel B shows screening of individual recovered plaques (1–8) by DADA PCR (using primers P5 & P6). Panel C shows the schematic of the screening of plaques obtained after each phage infection of the positive samples obtained after performing DADA PCR in panel B. Panel D shows the desired amplification of ∼ 400 bp PCR product in all the pure knockout plaques (1–8) obtained after subsequent phage infections. In both B and D, L represents DNA ladder with few bands marked.

FIGURE S4 | Sequence alignment of overlapping *gp10* and *gp12* after holin deletion in D29Δ*gp11*. Shown is the pairwise sequence alignment of the expected and the observed D29Δ*gp11* DNA. "Theoretical" sequence here corresponds to the DNA sequence that is expected after *gp11* deletion, whereas the "Sequencing" DNA depicts the DNA that was obtained after DNA sequencing. Blue and orange colored sequences represent *gp10* and *gp12*, respectively. Only a small region of the two genes is shown to depict the deletion of *gp11* from D29 genome, along with intact overlapping region as desired (underlined). ATG present in the underlined region is the start codon in *gp12*. "*" represents consensus sequence.

REFERENCES

Ackermann, H. W. (2009). Basic phage electron microscopy. *Methods Mol. Biol.* 501, 113–126. doi: 10.1007/978-1-60327-164-6_12

Briers, Y., Peeters, L. M., Volckaert, G., and Lavigne, R. (2011). The lysis cassette of bacteriophage varphiKMV encodes a signal-arrest-release endolysin and a pinholin. *Bacteriophage* 1, 25–30. doi: 10.4161/bact.1.1.14868

Cahill, J., and Young, R. (2019). Phage lysis: multiple genes for multiple barriers. *Adv. Virus Res.* 103, 33–70. doi: 10.1016/bs.aivir.2018.09.003

Carrigy, N. B., Larsen, S. E., Reese, V., Pecor, T., Harrison, M., Kuehl, P. J., et al. (2019). Prophylaxis of *Mycobacterium tuberculosis* H37Rv infection in a preclinical mouse model via inhalation of nebulized bacteriophage D29. *Antimicrob. Agents Chemother.* 63:e00871-19. doi: 10.1128/AAC.00871-19

Catalao, M. J., Gil, F., Moniz-Pereira, J., and Pimentel, M. (2010). The mycobacteriophage Ms6 encodes a chaperone-like protein involved in the endolysin delivery to the peptidoglycan. *Mol. Microbiol.* 77, 672–686. doi: 10.1111/j.1365-2958.2010.07239.x

Catalao, M. J., Gil, F., Moniz-Pereira, J., and Pimentel, M. (2011). Functional analysis of the holin-like proteins of mycobacteriophage Ms6. *J. Bacteriol.* 193, 2793–2803. doi: 10.1128/JB.01519-10

Catalao, M. J., Gil, F., Moniz-Pereira, J., Sao-Jose, C., and Pimentel, M. (2013). Diversity in bacterial lysis systems: bacteriophages show the way. *FEMS Microbiol. Rev.* 37, 554–571. doi: 10.1111/1574-6976.12006

Coll, F., Phelan, J., Hill-Cawthorne, G. A., Nair, M. B., Mallard, K., Ali, S., et al. (2018). Genome-wide analysis of multi- and extensively drug-resistant *Mycobacterium tuberculosis*. *Nat. Genet.* 50, 307–316. doi: 10.1038/s41588-017-0029-0

Dedrick, R. M., Guerrero-Bustamante, C. A., Garlena, R. A., Russell, D. A., Ford, K., Harris, K., et al. (2019). Engineered bacteriophages for treatment of a patient with a disseminated drug-resistant *Mycobacterium abscessus*. *Nat. Med.* 25, 730–733. doi: 10.1038/s41591-019-0437-z

Delbruck, M. (1940). Adsorption of bacteriophage under various physiological conditions of the host. *J. Gen. Physiol.* 23, 631–642. doi: 10.1085/jgp.23.5.631

Fernandes, S., and Sao-Jose, C. (2016). More than a hole: the holin lethal function may be required to fully sensitize bacteria to the lytic action of canonical endolysins. *Mol. Microbiol.* 102, 92–106. doi: 10.1111/mmi.13448

Ford, M. E., Sarkis, G. J., Belanger, A. E., Hendrix, R. W., and Hatfull, G. F. (1998). Genome structure of mycobacteriophage D29: implications for phage evolution. *J. Mol. Biol.* 279, 143–164. doi: 10.1006/jmbi.1997.1610

Fraga, A. G., Trigo, G., Murthy, R. K., Akhtar, S., Hebbur, M., Pacheco, A. R., et al. (2019). Antimicrobial activity of Mycobacteriophage D29 Lysin B during *Mycobacterium ulcerans* infection. *PLoS Negl. Trop. Dis.* 13:e0007113. doi: 10.1371/journal.pntd.0007113

Garcia, P., Martinez, B., Rodriguez, L., and Rodriguez, A. (2010). Synergy between the phage endolysin LysH5 and nisin to kill *Staphylococcus aureus* in pasteurized milk. *Int. J. Food Microbiol.* 141, 151–155. doi: 10.1016/j.ijfoodmicro.2010.04.029

Gigante, A. M., Hampton, C. M., Dillard, R. S., Gil, F., Catalao, M. J., Moniz-Pereira, J., et al. (2017). The Ms6 Mycolyl-arabinogalactan esterase LysB is essential for an efficient mycobacteriophage-induced lysis. *Viruses* 9:343. doi: 10.3390/v9110343

Grundling, A., Manson, M. D., and Young, R. (2001). Holins kill without warning. *Proc. Natl. Acad. Sci. U.S.A.* 98, 9348–9352. doi: 10.1073/pnas.151247598

Harding, E. (2020). WHO global progress report on tuberculosis elimination. *Lancet Respir. Med.* 8:19. doi: 10.1016/S2213-2600(19)30418-7

Hatfull, G. F. (2014b). Molecular genetics of mycobacteriophages. *Microbiol. Spectr.* 2, 1–36.

Hatfull, G. F. (2014a). Mycobacteriophages: windows into tuberculosis. *PLoS Pathog.* 10:e1003953. doi: 10.1371/journal.ppat.1003953

Hatfull, G. F. (2018). Mycobacteriophages. *Microbiol. Spectr.* 6:GPP3-0026-2018. doi: 10.1128/microbiolspec.GPP3-0026-2018

Hendrix, R. W., and Duda, R. L. (1992). Bacteriophage lambda PaPa: not the mother of all lambda phages. *Science* 258, 1145–1148. doi: 10.1126/science.1439823

Hyman, P., and Abedon, S. T. (2009). Practical methods for determining phage growth parameters. *Methods Mol. Biol.* 501, 175–202. doi: 10.1007/978-1-60327-164-6_18

Jacobs, W. R. Jr., Barletta, R. G., Udani, R., Chan, J., Kalkut, G., Sosne, G., et al. (1993). Rapid assessment of drug susceptibilities of *Mycobacterium tuberculosis* by means of luciferase reporter phages. *Science* 260, 819–822. doi: 10.1126/science.8484123

Johnson-Boaz, R., Chang, C. Y., and Young, R. (1994). A dominant mutation in the bacteriophage lambda S gene causes premature lysis and an absolute defective plating phenotype. *Mol. Microbiol.* 13, 495–504. doi: 10.1111/j.1365-2958.1994.tb00444.x

Joshi, H., Nair, G., Gangakhedkar, R., and Jain, V. (2019). Understanding the role of the lysozyme-like domain of D29 mycobacteriophage-encoded endolysin in host cell lysis and phage propagation. *Microbiology* 165, 1013–1023. doi: 10.1099/mic.0.000831

Kamilla, S., and Jain, V. (2016). Mycobacteriophage D29 holin C-terminal region functionally assists in holin aggregation and bacterial cell death. *FEBS J.* 283, 173–190. doi: 10.1111/febs.13565

Koul, A., Arnoult, E., Lounis, N., Guillemont, J., and Andries, K. (2011). The challenge of new drug discovery for tuberculosis. *Nature* 469, 483–490. doi: 10.1038/nature09657

Kropinski, A. M. (2009). Measurement of the rate of attachment of bacteriophage to cells. *Methods Mol. Biol.* 501, 151–155. doi: 10.1007/978-1-60327-164-6_15

Lella, M., Kamilla, S., Jain, V., and Mahalakshmi, R. (2016). Molecular mechanism of holin transmembrane domain I in pore formation and bacterial cell death. *ACS Chem. Biol.* 11, 910–920. doi: 10.1021/acschembio.5b00875

Madeira, F., Park, Y. M., Lee, J., Buso, N., Gur, T., Madhusoodanan, N., et al. (2019). The EMBL-EBI search and sequence analysis tools APIs in 2019. *Nucleic Acids Res.* 47, W636–W641. doi: 10.1093/nar/gkz268

Marinelli, L. J., Piuri, M., Swigonova, Z., Balachandran, A., Oldfield, L. M., van Kessel, J. C., et al. (2008). BRED: a simple and powerful tool for constructing mutant and recombinant bacteriophage genomes. *PLoS One* 3:e3957. doi: 10.1371/journal.pone.0003957

Park, D. J., Drobniewski, F. A., Meyer, A., and Wilson, S. M. (2003). Use of a phage-based assay for phenotypic detection of mycobacteria directly from sputum. *J. Clin. Microbiol.* 41, 680–688. doi: 10.1128/jcm.41.2.680-688.2003

Park, T., Struck, D. K., Dankenbring, C. A., and Young, R. (2007). The pinholin of lambdoid phage 21: control of lysis by membrane depolarization. *J. Bacteriol.* 189, 9135–9139. doi: 10.1128/JB.00847-07

Patil, V., and Jain, V. (2019). Insights into the physiology and metabolism of a mycobacterial cell in an energy-compromised state. *J. Bacteriol.* 201:19. doi: 10.1128/JB.00210-19

Payne, K., Sun, Q., Sacchettini, J., and Hatfull, G. F. (2009). Mycobacteriophage Lysin B is a novel mycolylarabinogalactan esterase. *Mol. Microbiol.* 73, 367–381. doi: 10.1111/j.1365-2958.2009.06775.x

Payne, K. M., and Hatfull, G. F. (2012). Mycobacteriophage endolysins: diverse and modular enzymes with multiple catalytic activities. *PLoS One* 7:e34052. doi: 10.1371/journal.pone.0034052

Payne, R. J., Phil, D., and Jansen, V. A. (2000). Phage therapy: the peculiar kinetics of self-replicating pharmaceuticals. *Clin. Pharmacol. Ther.* 68, 225–230. doi: 10.1067/mcp.2000.109520

Pearson, R. E., Jurgensen, S., Sarkis, G. J., Hatfull, G. F., and Jacobs, W. R. Jr. (1996). Construction of D29 shuttle phasmids and luciferase reporter phages for detection of mycobacteria. *Gene* 183, 129–136. doi: 10.1016/s0378-1119(96)00530-6

Pohane, A. A., Joshi, H., and Jain, V. (2014). Molecular dissection of phage endolysin: an interdomain interaction confers host specificity in Lysin A of *Mycobacterium* phage D29. *J. Biol. Chem.* 289, 12085–12095. doi: 10.1074/jbc.M113.529594

Proenca, D., Leandro, C., Garcia, M., Pimentel, M., and Sao-Jose, C. (2015). EC300: a phage-based, bacteriolysin-like protein with enhanced antibacterial activity against Enterococcus faecalis. *Appl. Microbiol. Biotechnol.* 99, 5137–5149. doi: 10.1007/s00253-015-6483-7

Ryan, G. L., and Rutenberg, A. D. (2007). Clocking out: modeling phage-induced lysis of *Escherichia coli*. *J. Bacteriol.* 189, 4749–4755. doi: 10.1128/JB.00392-07

Rybniker, J., Kramme, S., and Small, P. L. (2006). Host range of 14 mycobacteriophages in *Mycobacterium ulcerans* and seven other mycobacteria including *Mycobacterium tuberculosis*–application for identification and susceptibility testing. *J. Med. Microbiol.* 55(Pt 1), 37–42. doi: 10.1099/jmm.0.46238-0

Saier, M. H. Jr., and Reddy, B. L. (2015). Holins in bacteria, eukaryotes, and archaea: multifunctional xenologues with potential biotechnological and biomedical applications. *J. Bacteriol.* 197, 7–17. doi: 10.1128/JB.02046-14

Sarkis, G. J., and Hatfull, G. F. (1998). Mycobacteriophages. *Methods Mol. Biol.* 101, 145–173. doi: 10.1385/0-89603-471-2:145

Savva, C. G., Dewey, J. S., Moussa, S. H., To, K. H., Holzenburg, A., and Young, R. (2014). Stable micron-scale holes are a general feature of canonical holins. *Mol. Microbiol.* 91, 57–65. doi: 10.1111/mmi.12439

Schneider, C. A., Rasband, W. S., and Eliceiri, K. W. (2012). NIH Image to ImageJ: 25 years of image analysis. *Nat. Methods* 9, 671–675. doi: 10.1038/nmeth.2089

Swaminathan, S., Ellis, H. M., Waters, L. S., Yu, D., Lee, E. C., Court, D. L., et al. (2001). Rapid engineering of bacterial artificial chromosomes using oligonucleotides. *Genesis* 29, 14–21. doi: 10.1002/1526-968x(200101)29:1<14::aid-gene1001>3.0.co;2-x

To, K. H., and Young, R. (2014). Probing the structure of the S105 hole. *J. Bacteriol.* 196, 3683–3689. doi: 10.1128/JB.01673-14

van Kessel, J. C., and Hatfull, G. F. (2007). Recombineering in *Mycobacterium tuberculosis*. *Nat. Methods* 4, 147–152. doi: 10.1038/nmeth996

Wang, I. N. (2006). Lysis timing and bacteriophage fitness. *Genetics* 172, 17–26. doi: 10.1534/genetics.105.045922

Wang, I. N., Deaton, J., and Young, R. (2003). Sizing the holin lesion with an endolysin-beta-galactosidase fusion. *J. Bacteriol.* 185, 779–787. doi: 10.1128/jb.185.3.779-787.2003

Wang, I. N., Smith, D. L., and Young, R. (2000). Holins: the protein clocks of bacteriophage infections. *Annu. Rev. Microbiol.* 54, 799–825. doi: 10.1146/annurev.micro.54.1.799

Warrier, T., Tropis, M., Werngren, J., Diehl, A., Gengenbacher, M., Schlegel, B., et al. (2012). Antigen 85C inhibition restricts *Mycobacterium tuberculosis* growth through disruption of cord factor biosynthesis. *Antimicrob. Agents Chemother.* 56, 1735–1743. doi: 10.1128/AAC.05742-11

White, R., Chiba, S., Pang, T., Dewey, J. S., Savva, C. G., Holzenburg, A., et al. (2011). Holin triggering in real time. *Proc. Natl. Acad. Sci. U.S.A.* 108, 798–803. doi: 10.1073/pnas.1011921108

Young, R. (2002). Bacteriophage holins: deadly diversity. *J. Mol. Microbiol. Biotechnol.* 4, 21–36.

Young, R. (2013). Phage lysis: do we have the hole story yet? *Curr. Opin. Microbiol.* 16, 790–797. doi: 10.1016/j.mib.2013.08.008

Conflict of Interest: The authors declare that the research was conducted in the absence of any commercial or financial relationships that could be construed as a potential conflict of interest.

Copyright © 2020 Bavda and Jain. This is an open-access article distributed under the terms of the Creative Commons Attribution License (CC BY). The use, distribution or reproduction in other forums is permitted, provided the original author(s) and the copyright owner(s) are credited and that the original publication in this journal is cited, in accordance with accepted academic practice. No use, distribution or reproduction is permitted which does not comply with these terms.

frontiers in Microbiology

ORIGINAL RESEARCH
published: 13 May 2020
doi: 10.3389/fmicb.2020.00728

Isolation and Characterization of a New Phage Infecting *Elizabethkingia anophelis* and Evaluation of Its Therapeutic Efficacy *in vitro* and *in vivo*

Shih-Yi Peng[1,2†], Li-Kuang Chen[3†], Wen-Jui Wu[1], Prajna Paramita[1], Po-Wei Yang[1], Yun-Zhong Li[3], Meng-Jiun Lai[1] and Kai-Chih Chang[1,4]**

[1] Department of Laboratory Medicine and Biotechnology, Tzu Chi University, Hualien, Taiwan, [2] Department of Biochemistry, Tzu Chi University, Hualien, Taiwan, [3] Department of Clinic Pathology, Buddhist Tzu Chi General Hospital, Hualien, Taiwan, [4] Department of Laboratory Medicine, Buddhist Tzu Chi General Hospital, Hualien, Taiwan

OPEN ACCESS

Edited by:
Sutthirat Sitthisak,
Naresuan University, Thailand

Reviewed by:
Shuguang Lu,
Third Military Medical University, China
Elina Roine,
University of Helsinki, Finland

***Correspondence:**
Meng-Jiun Lai
monjou@mail.tcu.edu.tw
Kai-Chih Chang
kaichih@mail.tcu.edu.tw

† These authors have contributed equally to this work

Specialty section:
This article was submitted to Antimicrobials, Resistance and Chemotherapy, a section of the journal Frontiers in Microbiology

Received: 29 November 2019
Accepted: 27 March 2020
Published: 13 May 2020

Citation:
Peng S-Y, Chen L-K, Wu W-J, Paramita P, Yang P-W, Li Y-Z, Lai M-J and Chang K-C (2020) Isolation and Characterization of a New Phage Infecting Elizabethkingia anophelis and Evaluation of Its Therapeutic Efficacy in vitro and in vivo. Front. Microbiol. 11:728. doi: 10.3389/fmicb.2020.00728

Elizabethkingia spp. are a group of non-fermentative, Gram-negative, catalase-positive, and non-motile bacilli. They can cause meningitis in neonates and immunosuppressed patients, and lead to high mortality. Considering the rising trend of drug resistance among bacteria pathogens, bacteriophage (phage) therapy is a potential alternative to antibiotics for treating multidrug-resistant bacterial infections. However, so far, no phages specific for *Elizabethkingia* spp. have been reported. Using a clinically isolated *Elizabethkingia anophelis* as the host, the phage TCUEAP1 was isolated from wastewater of Hualien Tzu Chi hospital. The phage particle of TCUEAP1 under electron microscopy was revealed to belong to the siphoviridae family, with a head size of 47 nm, and a tail dimension 12 nm in diameter and 172 nm in length. The one-step growth analysis showed that the latent period of TCUEAP1 was about 40 min with a rise period lasting about 20 min, yielding a burst size of approximately 10 PFU/cell. The adsorption rate of TCUEAP1 reached about 70% in 20 min. Using 20 isolates of *Elizabethkingia* spp. to test the host range of TCUEAP1, it displayed narrow spectrum infecting three strains of *E. anophelis*, but forming spot lysis on 16 strains. The sequence result showed that the genome of TCUEAP1 is a double-stranded DNA of 49,816 bp, containing 73 predicted open reading frames. Further genomic analysis showed TCUEAP1 to be a new phage with no resemblance to publicly available phage genomes. Finally, in a mouse intraperitoneal infection model, at 6 h after the bacterial injection, TCUEAP1 decreased the bacterial load by fivefold in blood. Also, TCUEAP1 rescued 80% of mice heavily infected with *E. anophelis* from lethal bacteremia. We hope that the isolation and characterization of TCUEAP1, the first phage infecting *Elizabethkingia* spp., can promote more studies of the phages targeting this newly emerging bacterial pathogen.

Keywords: *Elizabethkingia anophelis*, bacteriophage, phage therapy, genome analysis, mouse model

INTRODUCTION

The genus *Elizabethkingia* comprises Gram-negative, non-fermenting, non-motile, obligate aerobic bacteria in the family *Flavobacteriaceae*. This genus was originally designated *Flavobacterium meningoseptica* by King (1959). It was subsequently reclassified into the genus *Chryseobacterium* in 1994 (Vandamme et al., 1994). In 2005, based mainly on 16S rRNA gene sequencing, it was moved to the new genus *Elizabethkingia* (Kim et al., 2005). Genome mapping has enabled further identification of species belonging to this genus, including the *E. meningoseptica*, *Elizabethkingia anophelis*, and *E. miricola* cluster. Notably, accumulating evidence indicates that what previously have been identified as *E. meningoseptica* strains causing sporadic cases of meningitis and bacteremia are actually *E. anophelis* (Coyle, 2017; Han et al., 2017).

Elizabethkingia anophelis has been reported to cause neonatal meningitis (Frank et al., 2013), bacteremia (Lau et al., 2016), and nosocomial outbreaks (Teo et al., 2013). Most studies investigating the antimicrobial resistance of *E. meningoseptica* were performed before the proposal of *E. anophelis*; therefore, these studies may actually represent the antimicrobial susceptibility patterns of all *Elizabethkingia* species, particularly *E. anophelis*. Several studies applied reliable species identification methods, and have demonstrated that *E. anophelis* isolates were resistant to most β-lactams, β-lactam/β-lactam inhibitor combinations, carbapenems, and aminoglycosides (Perrin et al., 2017; Lin et al., 2018, 2019; Cheng et al., 2019). A wide variation exists in the susceptibility of *E. anophelis* to piperacillin, piperacillin-tazobactam, ciprofloxacin, levofloxacin, trimethoprim-sulfamethoxazole, and vancomycin (Lin et al., 2019). The treatment options for *E. anophelis* infections are becoming increasingly limited (Janda and Lopez, 2017). For these reasons, there is an urgent need to develop new antibacterial agents to combat the infections caused by *Elizabethkingia* species.

Bacteriophages (phages) are attractive alternatives to antibiotics for treating bacterial infections (Caflisch and Patel, 2019). They have a low environmental impact compared to chemical antibiotics due to their natural origin (Wittebole et al., 2014). They target both Gram-positive and Gram-negative bacteria, and many *in vitro* and *in vivo* models have shown that phages are effective against multidrug-resistant bacteria (Schooley et al., 2017; Dedrick et al., 2019). As antibiotic resistance grows, phages retain the ability to kill antibiotic-resistant bacteria due to their differing mechanisms of action (Abedon et al., 2017). They are highly specific, lysing only their bacterial hosts, and are auto "dosing" in that phage replication at the site of infection, leading to marked increases in their titer (Merril et al., 2003; Abedon et al., 2017). So far, there are no reports of isolation of the phages infecting *Elizabethkingia* species. In this study, we present the isolation and characterization of the world's first strain of the virulent phage against *E. anophelis*, termed TCUEAP1, from the wastewater of Hualien Tzu Chi hospital. The *in vitro* and *in vivo* therapeutic efficacy of phage TCUEAP1 was also evaluated.

MATERIALS AND METHODS

Bacterial Strains and Growth Conditions

The bacteria used in this study are summarized in **Table 1**. Among the 20 strains of the *Elizabethkingia* species, the reference strain of *E. meningoseptica* was obtained from the Bioresource Collection and Research Center (BCRC), and the other 19 non-repetitive isolates were collected from two branches (Hualien and Taipei) of the Buddhist Tzu Chi General Hospital in Taiwan. The species were initially identified using the Vitek 2 compact system (Biomerieux, France). Further differentiation of these isolates as *E. meningoseptica* or *E. anophelis* was performed using PCR, based on the method described by Chew et al. (2018). When isolates could not be identified as *E. meningoseptica* or *E. anophelis* by PCR, sequencing of the 16S rRNA gene was used as the reference standard for species identification (Chang et al., 2014). To analyze the homology of the collected strains, pulsed-field gel electrophoresis (PFGE) was performed (Chang et al., 2014). Bacteria were cultivated in Luria Bertani (LB) broth or LB agar (BioShop Canada Inc., Burlington) at 25 or 37°C. The growth of bacteria was monitored by measuring the optical density at 600 nm (OD_{600}), where an OD unit of 1.0 corresponded to 1×10^9 cells/ml.

Isolation and Purification of Bacteriophage

All the wastewater samples were collected in Hualien Tzu Chi hospital and were used for screening phages specific to the isolated *Elizabethkingia* strains. Thirty milliliters of wastewater samples were centrifuged at 10,000 × *g* for 10 min to clear bacteria and debris, and filtered through a 0.22-μm Millipore filter. To enrich the phages in the wastewater samples, each time 25 ml of filtrate was mixed with 500 μl of bacterial solution consisting of five *Elizabethkingia* strains (10^8 CFU each) all in log-phase and incubated at 37°C for 4 h. In total, 20 strains were used for the enrichment procedure. After the enrichment period, the mixtures were centrifuged at 10,000 × *g* for 10 min and filtered through 0.22-μm Millipore filters. For each tested bacterial strain, 1 ml of the filtrate was mixed with 100 μl of bacteria culture (10^8 CFU) in log phase. The mixture was added to 5 ml of soft LB agar (0.7%) and then poured over solidified LB agar plates. The plates were incubated overnight at 25°C. For the enriched samples showing inhibited bacterial growth, the clear zone of the single plaque was picked using a sterile Pasteur pipette tip, and propagated in a new culture. The new mixture was serially diluted and plated on soft agar medium (0.7%) again for plaque formation. This procedure was repeated three times for phage purification.

Phage Purification

Lysates for TCUEAP1 phage purification were prepared by infecting 200 ml of *E. anophelis* ANO15 in early log-phase with TCUEAP1 at a multiplicity of infection (MOI) of about 1.0, and incubating with aeration for 4 h. Crude lysates were centrifuged and the supernatants were passed through a membrane filter with a pore size of 0.45 μm. The phage particles were concentrated by

TABLE 1 | Bacterial strains used to screen the phages from wastewater and to perform the host range analysis of TCUEAP1.

No.	Bacterial strain	Plaque formation[a]	TCUEAP1 spot test[b]	Source
E. meningoseptica				
1	*E. meningoseptica* BCRC 10677	-	N	BCRC
2	*E. meningoseptica* MEN1	-	P	Clinical isolate from Buddhist Tzu Chi General Hospital (BTCGH), Hualien
E. anophelis				
3	*E. anophelis* ANO1	–	P	Clinical isolates from BTCGH, Hualien
4	*E. anophelis* ANO2	–	P	
5	*E. anophelis* ANO3	–	P	
6	*E. anophelis* ANO5	–	P	
7	*E. anophelis* ANO9	–	P	
8	*E. anophelis* ANO10	+	P	
9	*E. anophelis* ANO12	+	P	
10	*E. anophelis* ANO13	–	P	
11	*E. anophelis* ANO14	–	P	
12	*E. anophelis* ANO15	+	P	
13	*E. anophelis* ANO16	–	N	
14	*E. anophelis* ANO17	–	P	
15	*E. anophelis* ANO18	–	P	
16	*E. anophelis* ANO19	–	P	Clinical isolate from BTCGH, Taipei
17	*E. anophelis* ANO20	–	P	
18	*E. anophelis*eANO21	–	P	
E. miricola				
19	*E. miricola* MIR1	–	N	Clinical isolates from BTCGH, Taipei
20	*E. miricola* MIR2	–	N	

[a]**+**, *susceptibility to TCUEAP1; –, no susceptibility to TCUEAP1.*
[b]***P***, *clear spot could be seen;* ***N***, *no clear spot could be seen.*

centrifugation for 2 h at 39,000 × *g* in a Beckman Avanti J-25I. The pellets were re-suspended in 1.0 ml of TE buffer and purified by banding on the block gradient of CsCl representing 1.2, 1.3, and 1.4 g/cm^3 (2 ml for each block) in ultracentrifugation. The ultracentrifugation conditions were 107,200 × *g* for 3 h at 4°C with the SW41Ti rotor in a Beckman LE-80K. The phage band collected was dialyzed against the TE buffer and then stored at 4°C until further use.

Transmission Electron Microscopy (TEM) of Phage Particles

Phage morphology was examined by TEM with negatively stained preparations. A drop of purified phages with a titer of approximately 10^{10} PFU/ml was applied to the surface of a formvar-coated grid (200-mesh copper grids), followed by negative staining with 2% uranyl-acetate (pH 3). The phage morphology was examined by using a Hitachi H-7500 transmission electron microscope operated at 80 kV (Hitachi Company, Japan).

Phage DNA Preparation, Genome Sequencing, and Annotation

DNA of the purified phage TCUEAP1 was prepared by extraction with phenol/chloroform and ethanol precipitation. The genome was sequenced by MiSeq (Illumina, Inc., San Diego, CA, United States). Raw reads were assembled using Bowtie (v1.1.1) (Langmead et al., 2009). The termini and package mode of the genome were analyzed by PhageTerm (Garneau et al., 2017). Putative protein-encoding open reading frames (ORFs) on the resulting whole genome were predicted using the program Prodigal (Hyatt et al., 2010). The functions of the proteins were annotated by running NCBI protein BLAST[1] against *nr* database. Further annotations were helped by restricting the BLAST search to the organism *virus* (taxid 10239). The genomic sequence of phage TCUEAP1 has been submitted to NCBI (GenBank accession number MN732896).

Determination of Optimal MOI

Host strain *E. anophelis* ANO15 was grown in LB medium at 37°C to the early log phase (10^8 CFU/ml). Six different ratios of TCUEAP1 to the host strain were added to LB medium, for MOI 0.001, 0.01, 0.1, 1, 10, and 100 PFU/CFU. After 3.5 h of incubation at 25 or 37°C, the samples were collected, and the titers of the phages were determined by serial dilution and the double-layer method (Adams, 1959). All experiments were performed in triplicate.

In vitro Adsorption Assay

The adsorption experiment was performed according to Adams (1959). When the growth of the host strain *E. anophelis* ANO15 and the control strain *E. meningoseptica* BCRC 10677 reached an OD_{600} of 1.0, 2 ml of each culture was harvested and fresh LB broth was added to a final volume of 20 ml. Phage stock of TCUEAP1 was added to each diluted culture at an MOI of 1 and

[1]http://www.ncbi.nlm.nih.gov/

incubated at 25°C for 30 min. Aliquots of 100-μl samples were collected from 0 to 30 min at 5-min intervals, and centrifuged at 10,000 *g* for 10 min. The supernatants containing the non-adsorbed phages were titrated by serial dilution and the double-layer method. The percentage of free phages was calculated by dividing the phage titer in the supernatant to that in the initial phage stock. All experiments were performed in triplicate.

One-Step Growth Curve

The culture of the host strain was incubated to an OD_{600} of 1.0. Three-milliliter aliquots of the bacterial culture were mixed with the phage TCUEAP1 at an MOI of 1, and the phages were allowed to adsorb to the host for 10 min at 25°C. The mixture was centrifuged, and the supernatant was discarded to remove free phage particles. The pellets were re-suspended in 30 ml of fresh LB broth and incubated at 25°C. Two sets of the samples were collected every 10 min, for 80 min. One of the two samples was treated with 1% chloroform (final concentration) to release intracellular phages. Then, the sets of the samples were immediately titrated by serial dilution and the double-layer method. All experiments were performed in triplicate. The latent period, eclipse period, and burst size of TCUEAP1 were derived from the growth curve.

Phage Infection Assay

The culture of the host strain *E. anophelis* ANO15 was incubated to an OD_{600} of 0.5 and then was mixed with the phage TCUEAP1 at different MOIs (from 0.0001 to 10) at 25 or 37°C. The control experiments were performed using equal volume of phage buffer [10 mM Tris-HCl (pH 7.5), 10 mM $MgSO_4$, 68.5 mM NaCl, and 1 mM $CaCl_2$] to replace the phage stock. The post-infection OD_{600} values were measured for 14 h, at 30-min intervals for the first 7 or 8 h.

Host Range Analysis

The host range of TCUEAP1 was examined by both the double-layer method (Adams, 1959) and the spot test (Romig and Brodetsky, 1961) on the 20 *Elizabethkingia* spp. used to screen phages from the water samples (**Table 1**). The bacterial strains were separately cultured to reach an OD_{600} of 1. For the double-layer method, 100 μl of 10-fold serially diluted (10^1 to 10^9) phage stock was mixed with 100 μl of the bacterial culture and 5 ml of soft LB agar (0.7%) and then poured over the solid LB agar plates. Plates were incubated overnight at 25°C. For the spot test, 100 μl of the bacterial culture was included in the top agar of the double-layered agar plates, and 10 μl of phage-containing solution (10^5 PFU) was spotted onto the bacterial lawns. Plates were dried in a laminar flow hood for 10 min and incubated at 25°C for 18 to 20 h. The observation of plaques on the bacterial lawn was recorded. Each test was repeated three times.

Effect of Temperature and pH on TCUEAP1 Stability

Thermal and pH stability tests were carried out using the double-layer method (Adams, 1959). In the thermal stability tests, aliquots of phage TCUEAP1 preparations (10^9 CFU/ml) were treated at pH 7 and different temperatures (4, 25, 37, 50, 60, and 70°C) in distilled water for 1 h. For the pH stability experiments, phage preparations were treated with various pH buffers (pH 2, 4, 7, and 11) at 25°C in distilled water for 1 h. The number of the remaining infective phages was determined by the double-layer method at 25°C.

Phage Therapy in the Mouse Sepsis Model

To evaluate the ability of phage TCUEAP1 to control the bacterial load and prevent lethal bacteremia, three experimental conditions were tested. Thirty eight-week-old male BALB/c mice (provided by NLAC Company, Taiwan) were randomly assigned to three groups (n = 10 per group). *E. anophelis* ANO15 was grown in LB broth at 37°C for 18 h and adjusted to the appropriate concentration (1×10^{10} CFU/ml) in normal saline (0.9% NaCl). The first group was only inoculated intraperitoneally with 100 μl of normal saline and phage TCUEAP1 (1×10^9 PFU/mouse, 100 μl/mouse) to assess the phage toxicity to mice. The remaining two groups were inoculated intraperitoneally with 1×10^9 CFU of *E. anophelis* ANO15 (1×10^9 CFU/mouse, 100 μl/mouse), and 2 h later, intraperitoneal administration with either phage TCUEAP1 (1×10^9 PFU/mouse, 100 μl/mouse) or 100 μl of normal saline. After 6 h post-infection, seven mice were randomly selected from each of the two groups and 50 μl of blood was taken by tail vein sampling to evaluate the bacterial load. The animals were monitored for 7 days and the survival rate of each group was calculated.

Statistical Analysis

Data are expressed as the mean ± standard deviation. The statistical significance of all the data was analyzed with the Student's t-test. Statistical significance was defined as $p < 0.05$. Statistical analysis of the mouse survival rate evaluations was performed using GraphPad Prism software 6.0 with $p < 0.05$.

Ethics Statement

All experiments involving the mice and all the care and handling of the mice were performed using protocols approved by the Institutional Animal Care and Use Committee of Tzu Chi University (No. 107083). All methods were performed under the relevant guidelines.

RESULTS

Isolation of a New Phage for *E. anophelis*

Dozens of wastewater samples around Hualien Tzu Chi hospital were collected and screened by the double-layer method using 20 strains of *Elizabethkingia* spp. One obtained phage that formed clear and haloed round plaques of about 1–2 mm in diameter (**Figure 1A**) on *E. anophelis* ANO15 was designated as TCUEAP1. TEM showed that TCUEAP1 possessed an icosahedral head with a diameter of approximately 47 ± 3 nm, and a tail that was 172 ± 3 nm long and 12 ± 1 nm in diameter

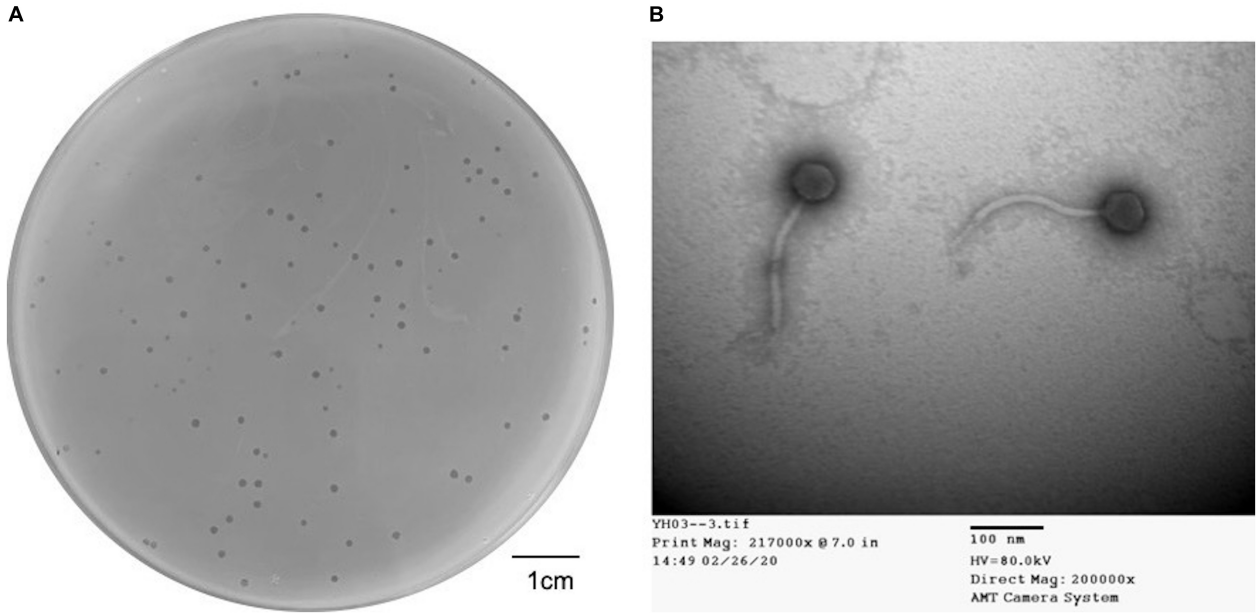

FIGURE 1 | Plaque and transmission electron microscopic (TEM) image of phage TCUEAP1. **(A)** Plaques formed by phage TCUEAP1. Scale bar: 1 cm. **(B)** Morphology of phage TCUEAP1 revealed under TEM. Scale bar: 100 nm.

(**Figure 1B**). The morphology suggested that TCUEAP1 could be assigned to the order *Caudovirales* and family *Siphoviridae*.

Optimal MOI of Phage TCUEAP1

We tested the MOI ranging from 0.001 to 100 to determine the optimal values for producing maximal phage titers at 25 and 37°C (**Figure 2**). The results showed that at both temperatures, the optimal MOI was 1, at which the phage titer at 25°C (about 10^{11} PFU/ml) was even higher than at 37°C (about 10^{10} PFU/ml). This MOI was used for the following experiments.

Biological Characterization of TCUEAP1

The adsorption experiment performed at an MOI of 1 at 25°C showed that approximately 70% of the phage particles of TCUEAP1 were adsorbed to the host *E. anophelis* ANO15 within 20 min of incubation, and no significant rise was observed as the incubation time increased further (**Figure 3A**). To characterize the infection process of the phage, the one-step growth curve of TCUEAP1 on *E. anophelis* ANO15 at an MOI of 1 at 25°C was determined.

The growth curves revealed that the eclipse and latent period of TCUEAP1 were around 30 and 40 min, respectively. The rise period lasted for about 20 min, and released a small burst size of about 10 PFU per infected cell (**Figure 3B**). The stability of phage TCUEAP1 at varying temperatures and pH conditions was also investigated. TCUEAP1 phages showed their viability at the tested temperature from 4 to 50°C, maximally at 25 and 37°C, and were quickly inactivated when heated to 60°C (**Figure 3C**). At pH 7 and 11, phage TCUEAP1 survived generally well, while no titer was recorded at a pH of 2 and 4 (**Figure 3D**).

Host Specificity and Host Growth Inhibition of TCUEAP1

To evaluate the host specificity of TCUEAP1, phage lysates were tested using the double-layer method and the spot test against 20 strains of *Elizabethkingia* species listed in **Table 1**. None of them share the same pulsotypes. The results of the double-layer method indicated that TCUEAP1 could only form plaques against three strains of *E. anophelis*, including the host strain *E. anophelis* ANO15. In contrast, the results of the spot test showed that TCUEAP1 solution was able to form clear spots on 16 isolates of *Elizabethkingia* spp., including one *E. meningoseptica* strain (**Table 1**). The infection assays of phage TCUEAP1 against *E. anophelis* ANO15 at 25 and 37°C were performed *in vitro*. The results (**Figure 4**) showed that at 25°C, even at MOI 0.001, phage TCUEAP1 could effectively reduce the growth of *E. anophelis* ANO15. In contrast, the results at 37°C showed that when the MOI was under 0.01, TCUEAP1 had no observable effect on the growth of the host.

Sequencing and Bioinformatics Analysis of TCUEAP1 Genomic DNA

Raw reads of the genome of TCUEAP1 were assembled into a circularly permutated form. By detecting the biases in the number of sequence reads, PhageTerm (Garneau et al., 2017) software predicted the genome to be a concatemeric DNA packaged through a headful packaging mechanism. The resulting genome of TCUEAP1 is a double-stranded linear DNA with a length of 49,816 bp and GC content of 39.34%. It was predicted by Prodigal (Hyatt et al., 2010) to contain 73 ORFs, all located on the positive strand. No tRNA genes were detected by the tRNAscan-SE 2.0 web server. Through the protein BLAST analysis, only

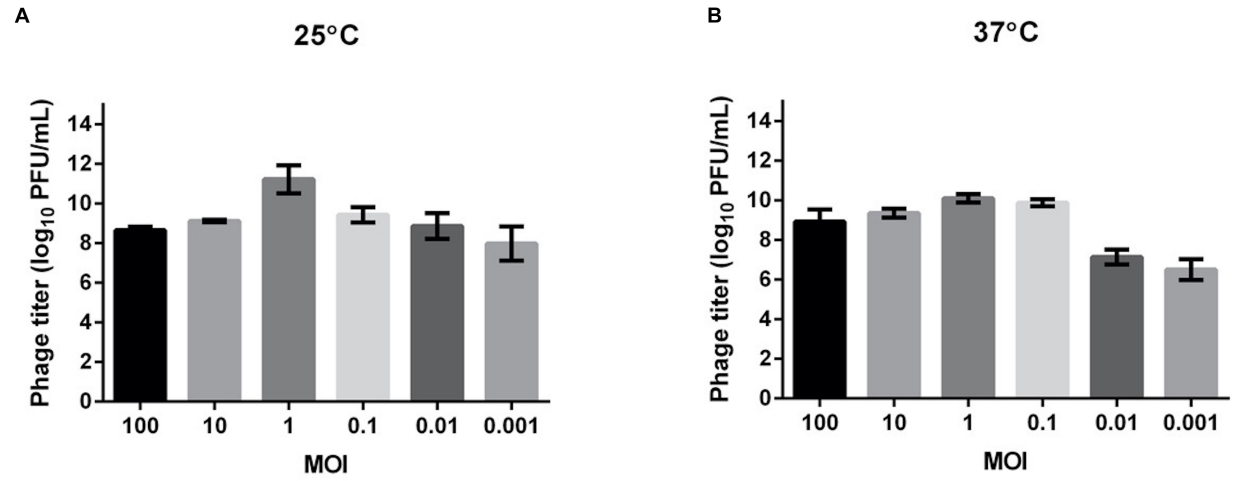

FIGURE 2 | Determination of the optimal multiplicity of infection (MOI) for TCUEAP1. Comparison of the phage titers after 3.5 h of incubation at six MOI values (0.001, 0.01, 0.1, 1, 10, and 100 PFU/CFU) at 25°C **(A)** and 37°C **(B)**. The experiments were repeated three times.

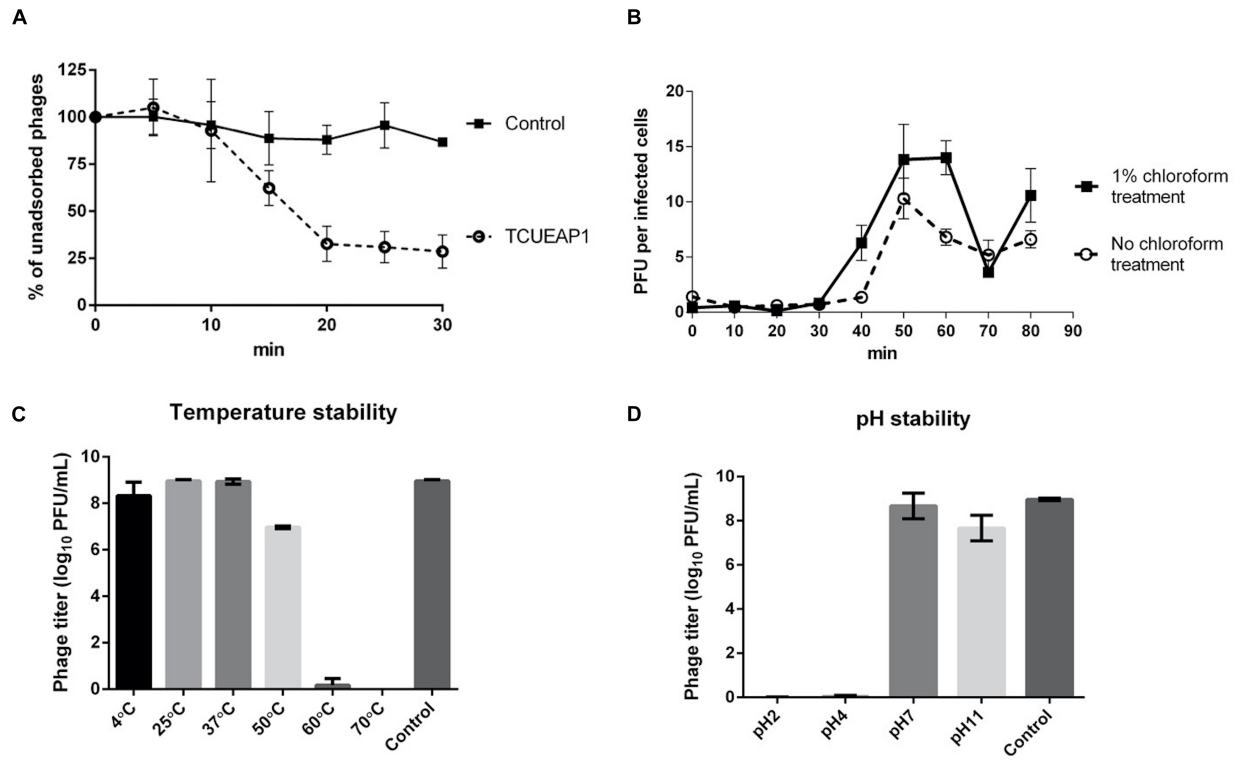

FIGURE 3 | Characterization of TCUEAP1. **(A)** Adsorption curve of the phage TCUEAP1 to the host *E. anophelis* ANO15 and the control *E. meningoseptica* BCRC 10677 at an MOI of 1 at 25°C. Aliquots were taken at intervals of 5 min (up to 30 min), and the supernatant containing the non-adsorbed phages were titrated. Percentage unadsorbed phages is the ratio of the phage titer in the supernatant to that in the initial phage stock. **(B)** One-step growth curve of the phage TCUEAP1 on *E. anophelis* ANO15 at 25°C. PFU per infected cells in chloroform-treated and chloroform-untreated cultures are shown at different time points. **(C)** The effect of temperature. TCUEAP1 was incubated at different temperature values for 1 h before determining the phage titer. **(D)** The effect of pH on TCUEAP1. TCUEAP1 was incubated at different pH values for 1 h before determining the phage titer. All experiments were repeated three times.

putative products from 21 ORFs could find statistically significant ($E < 0.001$) matches, of which six only matched to hypothetical proteins in the databases. The annotations adopted in this paper were based on the BLAST search against the proteins of virus (taxid) origins (**Supplementary Table S1**). Overall, annotations (**Figure 5**) showed that the ORFs predicted to

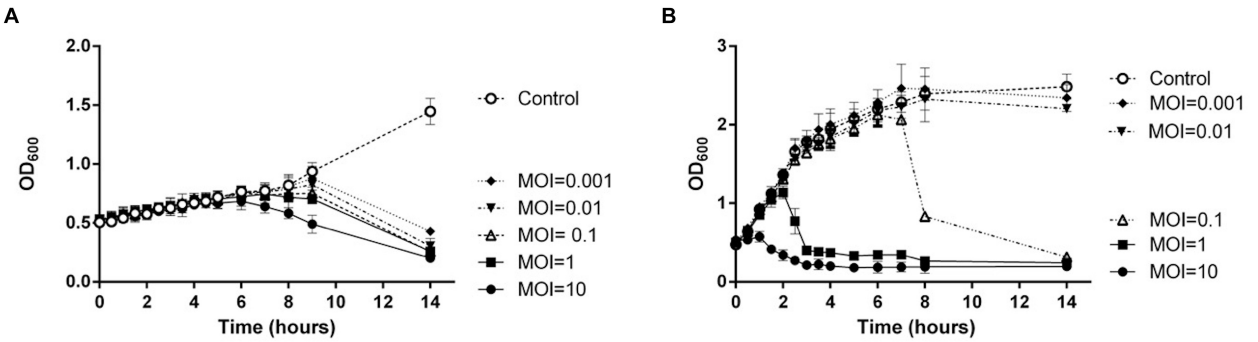

FIGURE 4 | The infection assay of the phage TCUEAP1 against *E. anophelis* ANO15 *in vitro* at 25°C **(A)** and 37°C **(B)**. *E. anophelis* ANO15 was infected by the phage TCUEAP1 at MOI values of 10, 1, 0.1, 0.01, or 0.001, and cultured for 14 h. The control experiments were performed using equal volumes of phage buffer. This experiment was repeated three times.

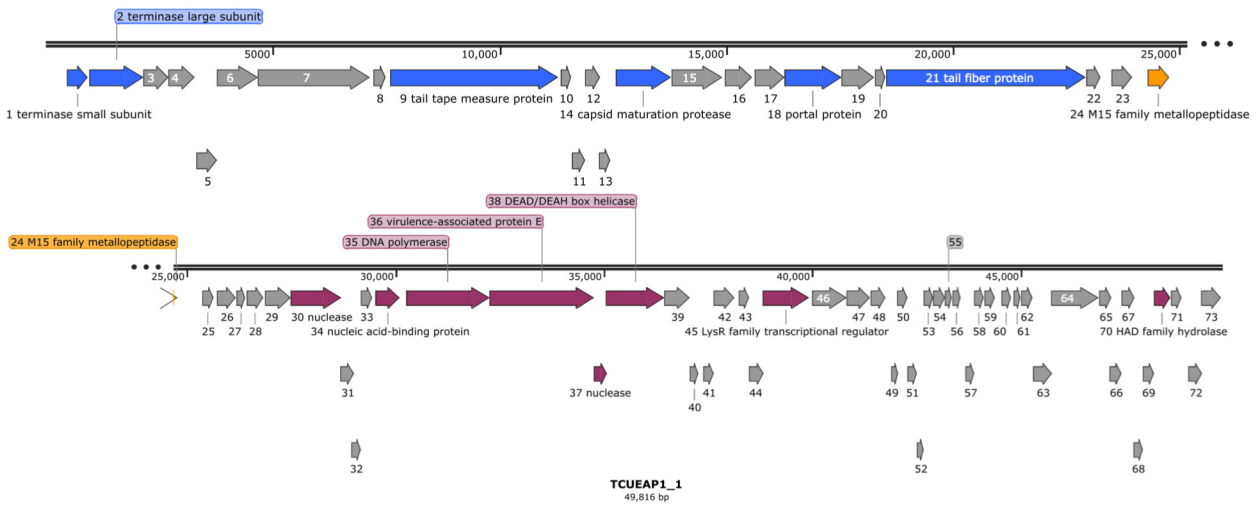

FIGURE 5 | The genomic organization of phage TCUEAP1. Predicted open reading frames (ORFs) are represented as arrows with colors referring to the predicted functions for the derived proteins. Gray color shows hypothetical proteins with unknown functions; blue color, structural proteins; orange color, a possible lysis module; magenta color, replication and regulation-related proteins. The figure was generated using the program SnapGene Viewer (v. 4.3.11) http://www.snapgene.com/.

encode structural products were located in the upstream genomic cluster, and the ORFs related to replication and regulation were in the downstream genomic cluster. ORF 24 between the two clusters encodes a putative product containing the M15 metallopeptidase domain, a functional module related to phage endolysin (Mikoulinskaia et al., 2009). No lysogenic characteristics, such as integration-related or CI repressor genes were identified.

Phage Therapy in the Mouse Sepsis Model

Since lethal bacteremia is a common outcome of *E. anophelis* infection, we investigated the ability of phage TCUEAP1 to rescue mice from lethal sepsis induced by intraperitoneal injection of *E. anophelis*. The minimum lethal dose of *E. anopheles* to BALB/c mice was determined to be 1×10^9 CFU/mouse (**Supplementary Figure S1**). To assess the biosafety of phage TCUEAP1, 10 mice were inoculated intraperitoneally with phage TCUEAP1 (1×10^9 PFU/mouse) and monitored for 7 days. The results showed that all mice in the control group had normal vital signs and survived the 7 days of observation period (**Figure 6A**). Each mouse received 10^9 CFU of *E. anophelis* intraperitoneally, and was treated 2 h later with a single dose of 10^9 PFU of phage TCUEAP1 or normal saline by the same route. While 70% of normal saline-treated mice died within 1 day, the phage TCUEAP1-treated mice had a significantly higher rate of survival, with 80% being rescued from the lethal dose of *E. anophelis* (**Figure 6A**). To quantify the ability of phage TCUEAP1 to reduce *E. anophelis* load *in vivo*, after 6 h post-*E. anophelis* infection, seven mice were randomly selected from each of the two groups to measure the bacterial load in the blood. There was approximately 5×10^5 CFU/ml of bacteria in the blood from the normal saline-treated mice (**Figure 6B**). In contrast, the bacterial load in the blood collected from the mice treated with phage TCUEAP1 was reduced at

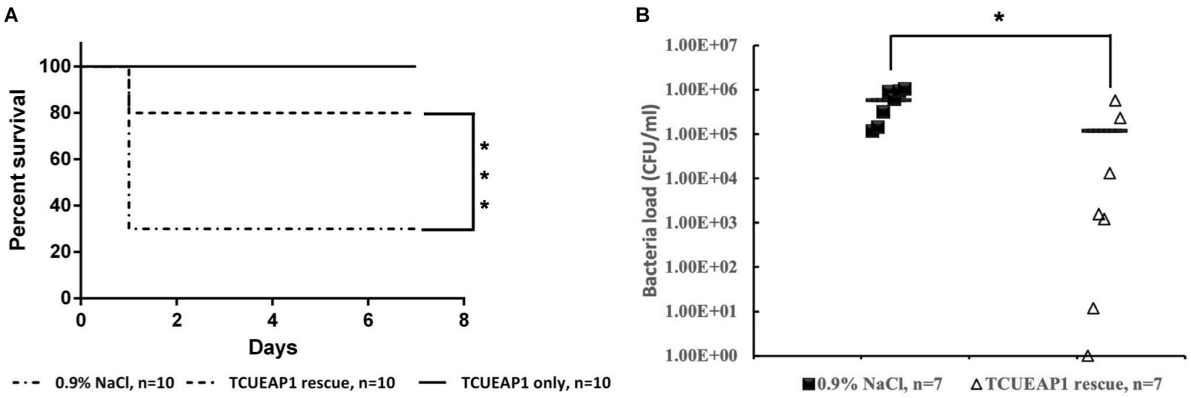

FIGURE 6 | Therapeutic efficacy of phage TCUEAP1 against mice with sepsis induced by *E. anophelis* infection. **(A)** The survival of the mice treated with a single dose of phage TCUEAP1 or normal saline intraperitoneally after *E. anophelis* infection. The survival of the mice was monitored for 7 days. ***$p < 0.001$ for normal saline versus phage TCUEAP1. **(B)** Blood samples of mice treated with normal saline (solid square) versus those of mice treated with phage TCUEAP1 (open triangle) at 6 h after bacterial inoculation. The line indicates mean bacterial load; *$p < 0.05$ for normal saline versus phage TCUEAP1.

least fivefold ($p < 0.05$), to the level about 1×10^5 CFU/ml. These results collectively indicate that phage TCUEAP1 has good antimicrobial activity *in vivo*.

DISCUSSION

As more studies have employed advanced species-identification methods, the clinical importance of *E. anophelis* has begun to emerge, having been identified as a novel human pathogen in just a few years (Janda and Lopez, 2017). The rising trend of drug resistance among bacterial pathogens prompts a consideration of phage therapy (Gorski et al., 2018; Caflisch and Patel, 2019). Among the flourish of various phage studies, there is no discussion of use against the novel pathogen *Elizabethkingia*. In this work, from dozens of wastewater samples, we isolated TCUEAP1, the virulent phage infecting *E. anophelis*. Characterization and genome analysis of TCUEAP1 were performed.

The stability studies showed that the phage could not resist high temperatures (above 60°C) and was very sensitive to an acidic environment (pH 2 and pH 4). The specificity test using 20 bacterial strains showed that while TCUEAP1 could only infect three strains, the phage lysate had a broad lytic spectrum against 16 strains. The difference may imply the possible existence of phage-encoded products, such as endolysin and hydrolase in the phage lysates. The adsorption rate of TCUEAP1 to the host bacteria could reach 70% in 20 min, but then appeared to encounter a limit and did not change much after further 10 min. As stated earlier, in the optimal MOI and infection assays of TCUEAP1 at 25 and 37°C, TCUEAP1 propagated better at 25°C, and could reduce the growth of the host bacteria even when the MOI was as low as 0.001. This matched our experience when we tried to isolate the phages targeting *Elizabethkingia* from the environment. We found it helpful to perform the co-culture of TCUEAP1 with its host at 25°C to slow down the bacterial growth rate and allow the phage to propagate to a suitable amount.

The genome of phage TCUEAP1 was sequenced and analyzed. For more than 70% (52 out of 73) of possible proteins derived from the TCUEAP1 genome, we could not identify any homologs using BLAST searches. Also, as we tried to identify the evolutionary related phages of TCUEAP1, among the 73 putative protein products, maximally only seven of them (mainly products of ORF 34 to 38) could find possible homologs from a single phage origin by BLAST. This patchy sequence similarity means that the traditional linear phylogenetic relationship is not suitable for TCUEAP1. We then tried to use vConTACT2 (v0.9.15) to assign the taxonomic status of TCUEAP1. vConTACT2 is a network-based application using phage genomes and their protein content for phage classification (Bin Jang et al., 2019). This type of program was regarded to be more suitable for the highly mosaic phenomenon seen on phage genomes (Dion et al., 2020). The analysis indicated TCUEAP1 to be a "singleton" virus, meaning no close relatives could be identified in the phage genome database (ProkaryoticViralRefSeq97-Merged). This means that more viral genome space needs to be sampled to build up the connections of TCUEAP1 to other phages.

The putative product of ORF36 was suggested to be a virulence-associated protein E (vapE) in BLAST results. Apart from one report showing that, in the bacterial pathogen of swine, deleting the vapE gene reduced the bacterial pathogenesis in mice (Ji et al., 2016), no details about the nature of the virulence have been identified so far. Among the BLAST results, there were a few protein hits for the predicted product of ORF36 being annotated as DNA primase (**Supplementary Table S1**), revealing another possible function for the predicted ORF36.

Endolysin, also termed phage lysin, is the protein encoded by phages to degrade the peptidoglycan of bacteria. It has been suggested to be a potent antibacterial agent separately from the entire phage (Lai et al., 2011). The potential product of ORF24 in the TCUEAP1 genome was identified to contain the M15 family peptidase domain, implying its possible connection to endolysin function. This presumption is currently under investigation.

When applied to the mice with sepsis induced by *E. anophelis*, TCUEAP1 was able to decrease the bacterial load by over fivefold and enhanced mice survival. Considering the new clinical challenges from *Elizabethkingia*, we believe that the isolation and characterization of the world's first phage against *Elizabethkingia* is valuable. It not only provides a way to understand the *Elizabethkingia* bacteria but can also further the preparation of weapons to combat *Elizabethkingia* infections in the future.

DATA AVAILABILITY STATEMENT

The datasets generated for this study can be found in the GenBank accession number MN732896.

ETHICS STATEMENT

The animal study was reviewed and approved by Institutional Animal Care and Use Committee of Tzu Chi University (No. 107083).

AUTHOR CONTRIBUTIONS

K-CC conceived and guided this project. K-CC and M-JL analyzed the results and wrote the manuscript. S-YP, L-KC, PP, P-WY, and Y-ZL performed the characterization of the phage TCUEAP1. S-YP and W-JW performed the animal studies. All authors reviewed the manuscript.

FUNDING

This work was supported partly by grants (contract number TCRPP107005) from Tzu Chi University and partly by the grants 106-2320-B-320-008-MY2 and 108-2320-B-320-007-MY2 from the Ministry of Science and Technology of Taiwan.

ACKNOWLEDGMENTS

We thank the Electron Microscopy Laboratory of the Department of Anatomy of Tzu Chi University for technical assistance.

SUPPLEMENTARY MATERIAL

The Supplementary Material for this article can be found online at: https://www.frontiersin.org/articles/10.3389/fmicb.2020.00728/full#supplementary-material

REFERENCES

Abedon, S. T., Garcia, P., Mullany, P., and Aminov, R. (2017). Editorial: phage therapy: past. Present and future. *Front. Microbiol.* 8:981. doi: 10.3389/fmicb.2017.00981

Adams, M. H. (1959). *Bacteriophages*. New York, NY: Interscience Publishers.

Bin Jang, H., Bolduc, B., Zablocki, O., Kuhn, J. H., Roux, S., Adriaenssens, E. M., et al. (2019). Taxonomic assignment of uncultivated prokaryotic virus genomes is enabled by gene-sharing networks. *Nat. Biotechnol.* 37, 632–639. doi: 10.1038/s41587-019-0100-8

Caflisch, K. M., and Patel, R. (2019). Implications of bacteriophage- and bacteriophage component-based therapies for the clinical microbiology laboratory. *J. Clin. Microbiol.* 57:00229-19. doi: 10.1128/JCM.00229-19

Chang, Y. C., Lo, H. H., Hsieh, H. Y., and Chang, S. M. (2014). Identification and epidemiological relatedness of clinical *Elizabethkingia meningoseptica* isolates from central Taiwan. *J. Microbiol. Immunol. Infect.* 47, 318–323. doi: 10.1016/j.jmii.2013.03.007

Cheng, Y. H., Perng, C. L., Jian, M. J., Cheng, Y. H., Lee, S. Y., Sun, J. R., et al. (2019). Multicentre study evaluating matrix-assisted laser desorption ionization-time of flight mass spectrometry for identification of clinically isolated *Elizabethkingia* species and analysis of antimicrobial susceptibility. *Clin. Microbiol. Infect.* 25, 340–345. doi: 10.1016/j.cmi.2018.04.015

Chew, K. L., Cheng, B., Lin, R. T. P., and Teo, J. W. P. (2018). *Elizabethkingia anophelis* Is the dominant *Elizabethkingia* species found in blood cultures in Singapore. *J. Clin. Microbiol.* 56:e01445-17. doi: 10.1128/JCM.01445-17

Coyle, A. L. (2017). *Elizabethkingia anophelis*: exploring the outbreak of disease in the Midwest. *Nursing* 47, 61–63. doi: 10.1097/01.NURSE.0000512887.67622.84

Dedrick, R. M., Guerrero-Bustamante, C. A., Garlena, R. A., Russell, D. A., Ford, K., Harris, K., et al. (2019). Engineered bacteriophages for treatment of a patient with a disseminated drug-resistant *Mycobacterium abscessus*. *Nat. Med.* 25, 730–733. doi: 10.1038/s41591-019-0437-z

Dion, M. B., Oechslin, F., and Moineau, S. (2020). Phage diversity, genomics and phylogeny. *Nat. Rev. Microbiol.* 18, 125–138. doi: 10.1038/s41579-019-0311-5

Frank, T., Gody, J. C., Nguyen, L. B., Berthet, N., Le Fleche-Mateos, A., Bata, P., et al. (2013). First case of *Elizabethkingia anophelis* meningitis in the Central African Republic. *Lancet* 381:1876. doi: 10.1016/S0140-6736(13)60318-9

Garneau, J. R., Depardieu, F., Fortier, L. C., Bikard, D., and Monot, M. (2017). PhageTerm: a tool for fast and accurate determination of phage termini and packaging mechanism using next-generation sequencing data. *Sci. Rep.* 7:8292. doi: 10.1038/s41598-017-07910-5

Gorski, A., Miedzybrodzki, R., Lobocka, M., Glowacka-Rutkowska, A., Bednarek, A., Borysowski, J., et al. (2018). Phage therapy: what have we learned? *Viruses* 10:288.

Han, M. S., Kim, H., Lee, Y., Kim, M., Ku, N. S., Choi, J. Y., et al. (2017). Relative prevalence and antimicrobial susceptibility of clinical isolates of *Elizabethkingia* species based on 16S rRNA gene sequencing. *J. Clin. Microbiol.* 55, 274–280. doi: 10.1128/JCM.01637-16

Hyatt, D., Chen, G. L., Locascio, P. F., Land, M. L., Larimer, F. W., and Hauser, L. J. (2010). Prodigal: prokaryotic gene recognition and translation initiation site identification. *BMC Bioinformatics* 11:119. doi: 10.1186/1471-2105-11-119

Janda, J. M., and Lopez, D. L. (2017). Mini review: new pathogen profiles: *Elizabethkingia anophelis*. *Diagn. Microbiol. Infect. Dis.* 88, 201–205. doi: 10.1016/j.diagmicrobio.2017.03.007

Ji, X., Sun, Y., Liu, J., Zhu, L., Guo, X., Lang, X., et al. (2016). A novel virulence-associated protein, vapE, in Streptococcus suis serotype 2. *Mol. Med. Rep.* 13, 2871–2877. doi: 10.3892/mmr.2016.4818

Kim, K. K., Kim, M. K., Lim, J. H., Park, H. Y., and Lee, S. T. (2005). Transfer of Chryseobacterium meningosepticum and *Chryseobacterium miricola* to *Elizabethkingia* gen. nov. as *Elizabethkingia meningoseptica* comb. nov. and *Elizabethkingia miricola* comb. nov. *Int. J. Syst. Evol. Microbiol.* 55, 1287–1293. doi: 10.1099/ijs.0.63541-0

King, E. O. (1959). Studies on a group of previously unclassified bacteria associated with meningitis in infants. *Am. J. Clin. Pathol.* 31, 241–247. doi: 10.1093/ajcp/31.3.241

Lai, M. J., Lin, N. T., Hu, A., Soo, P. C., Chen, L. K., Chen, L. H., et al. (2011). Antibacterial activity of *Acinetobacter baumannii* phage varphiAB2 endolysin (LysAB2) against both gram-positive and gram-negative bacteria. *Appl. Microbiol. Biotechnol.* 90, 529–539. doi: 10.1007/s00253-011-3104-y

Langmead, B., Trapnell, C., Pop, M., and Salzberg, S. L. (2009). Ultrafast and memory-efficient alignment of short DNA sequences to the human genome. *Genome Biol.* 10, R25. doi: 10.1186/gb-2009-10-3-r25

Lau, S. K., Chow, W. N., Foo, C. H., Curreem, S. O., Lo, G. C., Teng, J. L., et al. (2016). *Elizabethkingia anophelis* bacteremia is associated with clinically significant infections and high mortality. *Sci. Rep.* 6:26045. doi: 10.1038/srep26045

Lin, J. N., Lai, C. H., Yang, C. H., and Huang, Y. H. (2018). Comparison of clinical manifestations, antimicrobial susceptibility patterns, and mutations of fluoroquinolone target genes between *Elizabethkingia meningoseptica* and *Elizabethkingia anophelis* Isolated in Taiwan. *J. Clin. Med.* 7:538.

Lin, J. N., Lai, C. H., Yang, C. H., and Huang, Y. H. (2019). *Elizabethkingia* infections in humans: from genomics to clinics. *Microorganisms* 7:295. doi: 10.3390/microorganisms7090295

Merril, C. R., Scholl, D., and Adhya, S. L. (2003). The prospect for bacteriophage therapy in western medicine. *Nat. Rev. Drug. Discov.* 2, 489–497. doi: 10.1038/nrd1111

Mikoulinskaia, G. V., Odinokova, I. V., Zimin, A. A., Lysanskaya, V. Y., Feofanov, S. A., and Stepnaya, O. A. (2009). Identification and characterization of the metal ion-dependent L-alanoyl-D-glutamate peptidase encoded by bacteriophage T5. *FEBS J.* 276, 7329–7342. doi: 10.1111/j.1742-4658.2009.07443.x

Perrin, A., Larsonneur, E., Nicholson, A. C., Edwards, D. J., Gundlach, K. M., Whitney, A. M., et al. (2017). Evolutionary dynamics and genomic features of the *Elizabethkingia anophelis* 2015 to 2016 Wisconsin outbreak strain. *Nat. Commun.* 8:15483. doi: 10.1038/ncomms15483

Romig, W. R., and Brodetsky, A. M. (1961). Isolation and preliminary characterization of bacteriophages for *Bacillus subtilis*. *J. Bacteriol.* 82, 135–141.

Schooley, R. T., Biswas, B., Gill, J. J., Hernandez-Morales, A., Lancaster, J., Lessor, L., et al. (2017). Development and use of personalized bacteriophage-based therapeutic cocktails to treat a patient with a disseminated resistant *Acinetobacter baumannii* infection. *Antimicrob. Agents. Chemother.* 61:e00954-17. doi: 10.1128/AAC.02221-18

Teo, J., Tan, S. Y., Tay, M., Ding, Y., Kjelleberg, S., Givskov, M., et al. (2013). First case of *E. anophelis* outbreak in an intensive-care unit. *Lancet* 382, 855–856. doi: 10.1016/S0140-6736(13)61858-9

Vandamme, P., Bernardet, J. F., Segers, P., Kersters, K., and Holmes, B. (1994). NOTES: new perspectives in the classification of the flavobacteria: description of *Chryseobacterium* gen. nov., *Bergeyella gen*. nov., and *Empedobacter nom*. rev. *Int. J. Syst. Bacteriol.* 44, 827–831.

Wittebole, X., De Roock, S., and Opal, S. M. (2014). A historical overview of bacteriophage therapy as an alternative to antibiotics for the treatment of bacterial pathogens. *Virulence* 5, 226–235. doi: 10.4161/viru.25991

Conflict of Interest: The authors declare that the research was conducted in the absence of any commercial or financial relationships that could be construed as a potential conflict of interest.

Copyright © 2020 Peng, Chen, Wu, Paramita, Yang, Li, Lai and Chang. This is an open-access article distributed under the terms of the Creative Commons Attribution License (CC BY). The use, distribution or reproduction in other forums is permitted, provided the original author(s) and the copyright owner(s) are credited and that the original publication in this journal is cited, in accordance with accepted academic practice. No use, distribution or reproduction is permitted which does not comply with these terms.

frontiers in Microbiology

ORIGINAL RESEARCH
published: 03 June 2020
doi: 10.3389/fmicb.2020.00885

Characterization and Genome Structure of Virulent Phage EspM4VN to Control *Enterobacter* sp. M4 Isolated From Plant Soft Rot

*Nguyen Cong Thanh[1,2], Yuko Nagayoshi[1], Yasuhiro Fujino[1], Kazuhiro Iiyama[3], Naruto Furuya[3], Yasuaki Hiromasa[4], Takeo Iwamoto[5] and Katsumi Doi[1]**

[1] Microbial Genetics Division, Institute of Genetic Resources, Faculty of Agriculture, Kyushu University, Fukuoka, Japan, [2] Plant Protection Research Institute, Hanoi, Vietnam, [3] Laboratory of Plant Pathology, Faculty of Agriculture, Kyushu University, Fukuoka, Japan, [4] Attached Promotive Center for International Education and Research of Agriculture, Faculty of Agriculture, Kyushu University, Fukuoka, Japan, [5] Core Research Facilities for Basic Science, Research Center for Medical Sciences, The Jikei University School of Medicine, Tokyo, Japan

OPEN ACCESS

Edited by:
Robert Czajkowski,
University of Gdańsk, Poland

Reviewed by:
Konstantin Anatolievich Miroshnikov,
Institute of Bioorganic Chemistry (RAS), Russia
Abdelmonim Ali Ahmad,
Pennsylvania State University, United States

***Correspondence:**
Katsumi Doi
doi@agr.kyushu-u.ac.jp

Specialty section:
This article was submitted to Virology, a section of the journal Frontiers in Microbiology

Received: 12 February 2020
Accepted: 16 April 2020
Published: 03 June 2020

Citation:
Thanh NC, Nagayoshi Y, Fujino Y, Iiyama K, Furuya N, Hiromasa Y, Iwamoto T and Doi K (2020) Characterization and Genome Structure of Virulent Phage EspM4VN to Control Enterobacter sp. M4 Isolated From Plant Soft Rot. Front. Microbiol. 11:885. doi: 10.3389/fmicb.2020.00885

Enterobacter sp. M4 and other bacterial strains were isolated from plant soft rot disease. Virulent phages such as EspM4VN isolated from soil are trending biological controls for plant disease. This phage has an icosahedral head (100 nm in diameter), a neck, and a contractile sheath (100 nm long and 18 nm wide). It belongs to the Ackermannviridae family and resembles *Shigella* phage Ag3 and *Dickeya* phages JA15 and XF4. We report herein that EspM4VN was stable from 10°C to 50°C and pH 4 to 10 but deactivated at 70°C and pH 3 and 12. This phage formed clear plaques only on *Enterobacter* sp. M4 among tested bacterial strains. A one-step growth curve showed that the latent phase was 20 min, rise period was 10 min, and an average of 122 phage particles were released from each absorbed cell. We found the phage's genome size was 160,766 bp and that it annotated 219 open reading frames. The genome organization of EspM4VN has high similarity with the *Salmonella* phage SKML-39; *Dickeya* phages Coodle, PP35, JA15, and Limestone; and *Shigella* phage Ag3. The phage EspM4VN has five tRNA species, four tail-spike proteins, and a thymidylate synthase. Phylogenetic analysis based on structural proteins and enzymes indicated that EspM4VN was identified as a member of the genus *Agtrevirus*, subfamily Aglimvirinae, family Ackermannviridae.

Keywords: virulent phage, *Enterobacter*, *Agtrevirus*, soft rot disease, genome

INTRODUCTION

Soft rot is a serious disease of worldwide economic significance that occurs on fleshy vegetables such as potato, carrot, eggplant, squash, and tomato and is caused by *Pectobacterium* and *Dickeya* species (formerly known as the soft rot *Erwinia*) (Ma et al., 2007; Masyahit et al., 2009; Thanh et al., 2009; Lim et al., 2013; George et al., 2018; Rossmann et al., 2018). Both bacterial species are in the soft rot Pectobacteriaceae (SRP) family. Recently, *Enterobacter asburiae* was found to cause mulberry wilt disease and soft rot on *Amorphophallus konjac* in China (Wang et al., 2010; Wu et al., 2011). *E. asburiae* is a gram-negative, facultative anaerobic, oxidase negative, non-motile, and non-pigmented rod-shaped species isolated from soil, water, and food products and previously

known as an epiphytic bacteria (Lau et al., 2014). In addition, *Enterobacter cloacae* was identified as the cause of an unreported bacterial disease in chili pepper (*Capsicum annuum* L.) (García-González et al., 2018) and bacterial soft rot disease in dragon fruit (*Hylocereus* spp.) (Masyahit et al., 2009). The genus *Enterobacter* is classified in the *Enterobacter–Escherichia* clade, which is different from the *Pectobacterium–Dickeya* clade of the order Enterobacteriales (Adeolu et al., 2016). The harmful effects of *Enterobacter* species to soft rot have been argued. Kõiv et al. (2015) reported that *Enterobacter* and *Pseudomonas* were the most dominant genera in infected potato tissues.

In Southeast Asian countries such as Vietnam, chemical agents have been a dominant strategy for controlling plant disease. The use of pesticides in the region has been increasing annually and has caused severe issues for human health and the natural environment due to residual concentration in products, land, air, and water. Roughly 10,000 tons of pesticides was used annually in the 1980s, and this number reached 40,000 tons in the early 2000s (Engineering and Consulting Firms Association, 2006). In addition to pesticides, integrated pest management involving cultivation and pest-resistant plants has been applied widely. However, various bacterial organisms have developed pesticide resistance such as kasugamycin resistance tested in *Erwinia* sp. or carbapenem and cephalosporin resistance reported in *Enterobacteriaceae* (McGhee and Sundin, 2011). Despite a growing need for innovative solutions to this problem, the use of biological control agents such as bacteriophages has not been significantly considered.

Bacteriophages (phage, φ) are viruses specific to bacteria. These viruses have been playing an important role in plant disease control, known as phage therapy (Jones et al., 2007; Balogh et al., 2010). More interestingly, no serious side effects have yet been found on human and animal cells (Sulakvelidze and Kutter, 2005; Kusradze et al., 2016). Therefore, phage control may provide a promising solution for environment- and human-friendly treatment of bacteria-related plant disease. However, the utility of phage therapy often presents a challenge because of specificity to their host bacteria. Two broad-host lysates, φPD10.3 and φPD23.1, have been used for effectively controlling the strains of *Pectobacterium* and *Dickeya* spp. (Czajkowski et al., 2015a). Gašić et al. (2018) reported that *Xanthomonas euvesicatoria* phage Kφ1 had potential for biological control against pepper bacterial spot. Additionally, phage typing was also widely used in bacterial characterization and differentiation. For example, it was reported that nine of 22 *Enterobacter* phages investigated were isolated and used for distinguishing *Enterobacter* species (Loessner et al., 1993). Biological control using phages for soft rot has been applied to soft rot *Enterobacteriaceae* (SRE) such as *Pectobacterium carotovorum* (Muturi et al., 2019), *Dickeya solani* (Carstens et al., 2018), and *Pectobacterium atrosepticum* (Buttimer et al., 2018) causing potato soft rot. However, there is no report studying phages infecting *Enterobacter* species such as *E. asburiae, E. cloacae*, and *Enterobacter intermedium* and related species. Understanding the biological and genetic characteristics of these phages is beneficial for applying phage therapy against emerging SRE infectious diseases.

Therefore, the aim of this study is to isolate and characterize a phage-infecting *Enterobacter* species to be used against soft rot disease in infected crops.

MATERIALS AND METHODS

Bacterial Strains and Growth Conditions

Acinetobacter baumannii, *Escherichia coli*, *Dickeya chrysanthemi* pv. *zeae* 511-3 S2, two *Pantoea* strains, six *Enterobacter* strains, and seven *Pectobacterium* strains were used in this study (**Table 1**). Bacteria samples were collected from vegetables and fruits in Hanoi and Binh Thuân, Vietnam, and each sample was spread on an LB agar. After incubation for 3 days at 37°C, colonies were selected and purified by streaking on fresh plates three times. Type strains were purchased from the Biological Resource Center, NITE (NBRC, Chiba, Japan), and the *Pectobacterium* species were donated by the Laboratory of Plant Pathology, Kyushu University, for references. All bacteria were cultured in LB broth with shaking. Bacterial strains were cultivated at their optimum temperatures. Grown cells were suspended in 30% glycerol and stored at −80°C until use.

Bacterial Identification

Chromosomal DNA of isolates was isolated using MightyPrep reagent for DNA (TaKaRa Bio Inc., Shiga, Japan). 16S rRNA genes of isolated DNAs were amplified by PCR using Tks Gflex DNA polymerase (TaKaRa Bio Inc) and primer sets 27f (5′-AGAGTTTGATCCTGGCTCAG-3′) and 1492r (5′-ACGGCTACCTTGTTACGACCT-3′). PCR products were cloned into the pTA2 vector (Toyobo Co., Ltd., Osaka, Japan) and sequenced using a BigDye Terminator v3.1 cycle sequencing kit (Life Technologies, Carlsbad, CA, United States). Sequences were determined using an Applied Biosystems Gene Analyzer 3130*xl* (Life Technologies). A phylogenetic tree was constructed using the neighbor-joining method with the program of the GENETYX software (GENETYX, Tokyo, Japan).

Isolation of the Phage

Soil samples were collected from cabbage or potato fields in Bac Ninh province, Vietnam. These samples were suspended with SM buffer (Van Twest and Kropinski, 2009). Soil suspensions were added to a log-phase culture of *Enterobacter* sp. M4 for an enrichment culture. After shaking (37°C, 180 rpm, 24 h), the culture solution was centrifuged (10,000 × *g*, 10 min, 4°C). The supernatant was filtered through a pore size of 0.45 μm (Advantec, Tokyo, Japan). The phage was assayed using the soft agar overlap technique (Adams, 1959). After overnight incubation, typical plaques were suspended in an SM buffer and purified through five rounds of single-plaque isolation.

Purification of Phage

Phage particles were purified using cesium chloride (CsCl) gradient ultracentrifugation according to a previously reported protocol (Sambrook and Russell, 2001). Briefly, enriched phage lysate (5×10^{10} plaque-forming units, pfu) was treated with DNase I (1 μg/ml) and RNase A (1 μg/ml) at 37°C for 1 h.

TABLE 1 | Bacterial strains used in this work and their sensitivities against EspM4VN.

Strain	Source	Accession number	Plaque formation	References
Pantoea dispersa TL3	Dragon fruit	LC498100	–	This work
Enterobacter sp. B3	Cabbage	LC498101	–	This work
Enterobacter sp. B5	Cabbage	LC498102	–	This work
Enterobacter sp. BC7	Cabbage	LC415135	–	This work
Enterobacter sp. M4	Potato	LC415612	+	This work
Enterobacter sp. KT	Potato	LC416590	–	This work
Acinetobacter baumannii TL5	Dragon fruit	LC423530	–	This work
Acinetobacter baumannii NBRC 109757	Urine	Z93435	–	Bouvet and Grimont (1986)
Acinetobacter junii NBRC 109759	Urine	Z93438	–	Bouvet and Grimont (1986)
Enterobacter asburiae NBRC 109912	Human, lochia exudate	CP011863	–	Hoffmann et al. (2005)
Escherichia coli DHα5			–	RBC Bioscience
Pectobacterium carotovorum subsp. *carotovora* 489-4	Cabbage		–	Plant Pathology Laboratory, Kyushu University
Pectobacterium carotovora subsp. *carotovora* 489-5	Cabbage		–	Plant Pathology Laboratory, Kyushu University
Pectobacterium carotovora subsp. *carotovora* 493-1	Potato		–	Plant Pathology Laboratory, Kyushu University
Pectobacterium carotovora subsp. *betavasculorum* ATCC 43762^T	Sugar beet	U80198	–	Gardan et al. (2003)
Pectobacterium carotovora subsp. *wasabiae* ATCC 43316^T	Japanese horseradish	U80199	–	Gardan et al. (2003)
Pectobacterium carotovora subsp. *atroseptica* ATCC 33260^T	Solanum tuberosum	Z96090	–	Gardan et al. (2003)
Pectobacterium carotovora subsp. *carotovora* ATCC 15713^T	Potato	U80197	–	Hauben et al. (1998)
Pectobacterium chrysanthemi pv. *Zeae* 511-3 S2	Corn		–	Plant Pathology Laboratory, Kyushu University
Pectobacterium milletiae 1			–	National Institute of Agrobiological Sciences, Japan

Phage lysates were centrifuged (10,000 × *g*, 10 min, 4°C). The supernatant was mixed with 1 M NaCl and 10% (w/v) polyethylene glycol 8000, and the mixture was stored at 4°C for 2 h. After centrifugation (12,000 × *g*, 30 min, 4°C), the pellets were suspended in 4 ml of TBT buffer (100 mM Tris–HCl at pH 7.5, 100 mM NaCl, and 10 mM $MgCl_2$). The resulting suspension was gently mixed with 4.5 g of CsCl and loaded onto a step-layered CsCl gradient (1 ml of 0.5 g/ml CsCl, 2.5 ml of 0.775 g/ml CsCl, and 2.5 ml of 1 g/ml CsCl) prepared in a 38.5-ml Ultra-Clear tube (Beckman Coulter, Indianapolis, IN, United States). The gradient was centrifuged at 22,000 rpm in the swinging-bucket SW28 rotor for 2 h at 4°C in Optima XE-90 ultracentrifuge (Beckmann Coulter). The phage band was dialyzed against dialysis buffer (10 mM NaCl, 50 mM Tris–HCl at pH 8.0, and 10 mM $MgCl_2$) for 4 h. Purified phage particles were resuspended in SM buffer with 25% glycerol and then stored at −80°C.

Transmission Electron Microscopy

Phage morphology was determined using transmission electron microscopy (TEM) to observe negatively stained preparations (Luo et al., 2012). Phage particles picked up from a purified single plaque were suspended to 2% (wt/vol) phosphotungstic acid (pH 7.2) and then applied to the surface of a glow-discharged carbon/formvar-coated grid (200-mesh copper grid). Negatively stained phage particles were examined using a Hitachi H-7500 transmission electron microscope operated at 80 kV (Hitachi High-Technologies Corp., Tokyo, Japan). The phage size was determined from at least 10 measurements.

Host Range Test

The determination of host range was followed by Addy's description with minor modifications (Addy et al., 2019). Briefly, 10 μl of serial dilutions of phage solution (10^8 pfu/ml) was dropped on double-layer agar plates. The top layer was prepared with 100 μl of each strain (OD_{660} of 0.4) mixed with 7 ml of LB. The plates were incubated overnight at bacterial optimum temperature. The phage sensitivity of the bacteria was confirmed by observation of clear zones or plaques. And then further experiment was performed with plaque essay using the dilutions to confirm if they were affected by the phage.

Determination of the Optimal MOI

Optimal multiplicity of infection (MOI) was determined according to the report of Czajkowski et al. (2015a). The indicator strain (4×10^8 colony-forming units, cfu/ml) at the early log phase was infected with phage at different MOIs of 0.1, 1, and 10. After a 15-min incubation at 37°C, the mixtures were centrifuged (12,000 × *g*, 10 min, room temperature). Supernatants were then filtered through a 0.45-μm pore size filter and titrated as described above. The highest titer was considered the optimal MOI. All experiments were averaged from results of triplicate experiments.

Thermal and pH Stability

Phage stability was carried out as described in our previous report (Luo et al., 2012). Briefly, to examine thermal stability, phage stocks (1.0×10^7 pfu/ml in SM buffer) were incubated separately for 60 min at temperature ranges of 10–60°C. For pH stability, 1.0×10^7 pfu/ml of phage suspension was added to an SM buffer at different pHs (pHs 3–11) and then incubated at 25°C for 24 h. After incubation, the surviving phages were enumerated by the double-layer agar method. All tests were performed in triplicate.

One-Step Growth Curve

One-step growth experiments were performed to determine the latent period and burst size as described previously (Nagayoshi et al., 2016; Addy et al., 2019). *Enterobacter* sp. M4 cells were harvested by centrifugation of the early-log-phase culture (4×10^8 cfu/ml) and resuspended in LB broth. Phage was added at an MOI of 1 and allowed to adsorb for 15 min at 37°C. Cell pellet was washed with 1 ml of fresh LB broth three times. The resuspension was added to 100 ml of LB broth and cultured at 37°C. Samples were taken at 10-min intervals (up to 120 min), and phage titers were then determined by the double-layer agar plate method to obtain one-step curves. The average burst size of the phage was calculated according to the report of Bolger-Munro et al. (2013).

Stability With Surfactants

Phage stability was tested with various concentrations of five surfactants: Tween 20, sodium dodecyl sulfate (SDS), ethanol, skim milk (Becton, Dickinson, and Company, Franklin Lakes, NJ, United States), and sucrose. Tween 20 and SDS were chosen as a non-ionic detergent and anionic surfactant, respectively. Ethanol was examined as a standard disinfectant. Phage particles were suspended in each solution at various concentrations for 2 h at room temperature. The resistant capability was investigated by plaque assay. Experiments were performed in triplicate.

Phage DNA Extraction and Genome Analysis

Purified phage particles were used for phage DNA extraction with TE saturated phenol (pH 8.0) (Nippon Gene Co., Ltd., Tokyo, Japan) and phenol–chloroform and were precipitated with sodium acetate and ethanol. The precipitate was washed twice with 70% ethanol, air-dried, and resuspended in the TE buffer.

Phage whole genome was sequenced using the PacBio RSII platform (Pacific Biosciences of California, Inc., Menlo Park, CA, United States). The filtered reads were assembled using HGAP version 2.3.0 (Chin et al., 2013) and resulted in a one-contig scaffold. Potential open reading frames (ORFs) were predicted by the Microbial Genome Annotation Pipeline (MiGAP[1]). The BLAST algorithm at the National Center of Biotechnology Information (NCBI) was used to search for similarities. Analysis of the nucleotide sequences was performed with Geneious Prime (Biomatters Ltd., Auckland, New Zealand). The search for tRNA genes was performed with tRNAscan-SE (Schattner et al., 2005) and ARAGORN ver. 1.2.38 (Laslett and Canback, 2004). Phylogenetic analysis was performed with ClustalW ver. 2.1[2],

[1]http://www.migap.org/

[2]https://clustalw.ddbj.nig.ac.jp

and phylogenetic trees were generated using the neighbor-joining method. Prediction of promoter regions was carried out with Neural Network Promoter Prediction[3].

Structural Protein Identification by Mass Spectroscopy

To analyze virion proteins, phage particles purified by ultracentrifugation were mixed with lysis buffer (62.5 mM Tris–HCl, pH 6.8, containing 5% 2-mercaptoethanol, 2% SDS, 10% glycerol, and 0.01% bromophenol blue) and boiled for 10 min. Prepared proteins were then separated by electrophoresis on precast SDS 15% polyacrylamide gels (e-PAGEL E-T/R15L, ATTO Corporation, Tokyo, Japan).

In-Gel Digestion

Excised gel pieces were destained with 100 μl of 50% acetonitrile containing 25 mM ammonium bicarbonate solution for 1 h at room temperature with gentle agitation. Destained gel pieces were treated for reduction and alkylation using 100 μl of 10 mM DTT in 25 mm ammonium bicarbonate for 45 min at 56°C and 100 μl of freshly prepared 10 mM iodoacetamide in 25 mM ammonium bicarbonate in the dark for 30 min at 37°C. After gel plugs were dried, 400 ng of sequencing-grade trypsin (Trypsin Gold, Promega, Madison, WI, United States) in 20 μl of 25 mM ammonium bicarbonate was added and incubated for 12 h at 37°C. Digested peptides were recovered from the gel plugs using 50 μl of 50% acetonitrile in 5% formic acid (FA) for 30 min at 25°C. The extracted peptides were concentrated in a speed vacuum concentrator and added to 20 μl of 5% acetonitrile in 0.1% FA.

Tandem Mass Spectrometry-Based Proteomics

A Nano-HPLC system (nanoADVANCE, Bruker-Michrom, Billerica, MA, United States) was used to identify proteins automatically using a micro-column switching device coupled to an autosampler and a nanogradient generator. Peptide solution (5 μl) was loaded onto a C18 reversed-phase capillary column (100 μm ID × 30 cm, Zaplous αPep C18; AMR, Tokyo, Japan) in conjunction with a Magic AQ C18 trapping column (300 μm ID × 10 mm; Bruker-Michrom). The peptides were separated using a nanoflow linear acetonitrile gradient of buffer A (0.1% FA) and buffer B (0.1% FA, 99.9% acetonitrile), going from 5 to 45% buffer B over 50 min at a flow rate of 500 nl/min. The column was then washed in 95% buffer B for 5 min. Hystar 3.2 system control software (Bruker Daltonics Inc., Billerica, MA, United States) was used to control the entire process. The eluted peptides were ionized through a CaptiveSpray source (Bruker Daltonics) and introduced into a Maxis 3G Q-TOF mass spectrometer (Bruker Daltonics) set up in a data-dependent MS/MS mode to acquire full scans (m/z acquisition range from 50 to 2,200 Da). The four most intense peaks in any full scan were selected as precursor ions and fragmented using collision energy. MS/MS spectra were interpreted, and peak lists were generated using DataAnalysis 4.1 and BioTools 3.2.

[3]https://www.fruitfly.org/seq_tools/promoter.html

Protein Identification

The filtered data were searched on the Mascot 2.2 server (Matrix Science) using the NCBInr (NCBI 201805) database and custom expected protein databases for EspM4VN. Fixed modification was set on cysteine with carbamidomethylation. Variable modification was based on methionine with oxidation and asparagine/glutamine with deamidation. Maximum missed cleavage was set to two and limited to trypsin cleavage sites. Precursor mass tolerance (MS) and fragment mass tolerance (MS/MS) were set to 100 ppm and ± 0.6 Da, respectively. Positive protein identifications using a threshold of 0.05 were used. Peptides scoring <20 were automatically rejected, ensuring all protein identifications were based on reliable peptide identifications. Protein identification was set to require at least two unique peptides. Homology searches against matched protein sequences were conducted using the BLASTp program[4].

Accession Number

The whole-genome sequence of phage EspM4VN was submitted to DDBJ under accession number LC373201. The 16S rDNA sequences of the isolates have been deposited in the DDBJ under accession numbers LC415135, LC415612, LC416590, LC423530, LC498100, LC498101, and LC498102.

RESULTS

Identification of Isolated Bacteria

The bacteria used in this study were isolated from diseased plants including potato, cabbage, and dragon fruit (**Table 1**). After colony purification, isolated bacteria were applied to 16S rDNA sequence analysis. The phylogenetic analysis from sequence data showed that the isolated strains B3, B5, and M4 belonged to the *Enterobacter* cluster (**Supplementary Figure S1**). Other isolates, TL3 and TL5, were identified as *Pantoea dispersa* and *A. baumannii*, respectively. Strains BC7 and KT were positioned at another *Enterobacteriaceae* cluster.

Isolation and Morphology of EspM4VN

EspM4VN formed large semi-turbid plaques on a lawn of the strain M4. The plaques were approximately 0.5 mm in diameter with a halo effect (2.5 mm) (**Figure 1A**). Purified phage particles from the plaques were applied to TEM analysis. The phage particles were composed of an icosahedral-shaped head approximately 100 nm in diameter, a neck, and a contractile sheath 100 nm in length and 18 nm in width (**Figure 1B**). Intermediate structures with both prongs and stars appeared as have been observed in some Ackermannviridae phages such as *Agtrevirus* Ag3, *Limestonevirus* JA15, and XF4 (Anany et al., 2011; Day et al., 2017). Thus, the phage morphology of EspM4VN is that of the genus *Agtrevirus* belonging to the Ackermannviridae family according to ICTV rule 3.12 (Adriaenssens et al., 2018).

[4]http://www.ncbi.nlm.nih.gov/

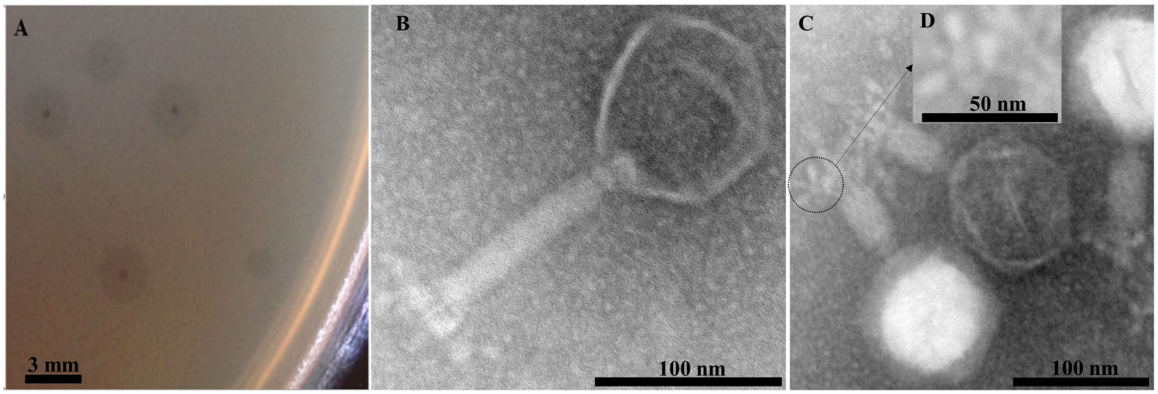

FIGURE 1 | Plaques formed in the top agar layer **(A)**, morphology of the extended tail phage EspM4VN **(B)**, contracted tail phage EspM4VN **(C)**, and displaying an umbrella-like structure **(D)**. Bars indicate 3 mm **(A)**, 100 nm **(B,C)**, and 50 nm **(D)**.

Host Range of EspM4VN4

The host range of EspM4VN was determined with six strains of *Enterobacter*, nine strains of *Pectobacterium*, two *Acinetobacter* species, *A. baumannii* TL5, *P. dispersa* TL3, and *E. coli* DHα5 (**Table 1**). EspM4VN formed clear plaques only on *Enterobacter* strain M4. A phage suspension of 4×10^6 pfu/ml was applied to strain M4 at a low density level for a similar host range experiment used by others (Adriaenssens et al., 2012). It showed a quite narrow host range even in the same *Enterobacter* cluster.

Thermal and pH Stability of EspM4VN

EspM4VN kept stable infectivity at temperatures 10–50°C (**Figure 2A**) and pH 4–10 (**Figure 2B**). The phage was deactivated at 70°C and pHs 3 and 12. Related phages infecting *Dickeya* strains were reported to be stable at temperatures from 4°C to 37°C but not stable at 50°C for 24 h, and they showed stability at pHs 5–12 (Czajkowski et al., 2014).

One-Step Growth of EspM4VN

At an MOI of 1, a one-step growth curve showed that the latent phase of EspM4VN was 20 min, the rise period was 10 min, and an average of 122 phage particles were released from each absorbed cell (**Figure 3**). The latent phase of EspM4VN was much shorter than that of LIMEstone1 and LIMEstone2 (60 and 65 min, respectively) or soilborne lytic phages (40 min) infecting *Dickeya* strains (Adriaenssens et al., 2012; Czajkowski et al., 2014).

Stability of EspM4VN Within Various Chemicals

The stability of EspM4VN was analyzed against detergents and surfactants (**Figure 4**). Phage viability in sterile water was approximately 50% or less compared with that in SM buffer. Up to 1.5% (v/v) Tween 20 and ethanol did not inhibit phage infection. By contrast, the phage showed resistance (>70%) to 0.1 to 1.5% SDS. EspM4VN was stable in skim milk at all concentrations examined.

Genomic Analysis of EspM4VN

Nucleotide sequence analysis of the EspM4VN showed the genome size to be 160,766 bp with a G + C content of 50.7% and that 219 ORFs were annotated (**Figure 5** and **Supplementary Table S1**). BLAST search revealed that the EspM4VN genome showed high similarity to *Agtrevirus* SKML-39 (JX181829; identity 95.3%), *Limestonevirus*, Coodle (MH807820; 95.2%), PP35 (MG266157; 95.2%), JA15 (KY942056; 95.1%), LIMEstone1 (93%), phiDP23.1 (93%), φD3 (93%), and *Agtrevirus* Ag3 (90%) (**Supplementary Table S2**). EspM4VN as a Ackermannviridae infects *Enterobacter*, and its genome has significant homology with other *Enterobacter* phages such as myPSH1140 (MG999954; Manohar et al., 2019), CC31 (GU323318; Petrov et al., 2010), and vB_EaeM_φEap-3 (KT321315; Zhao et al., 2019). Analysis demonstrated that EspM4VN tRNA species and their codons were as follows: $tRNA^{Ser}$ (TCA), $tRNA^{Asn}$ (AAC), $tRNA^{Tyr}$ (TAC), $tRNA^{Ser}$ (AGC), and $tRNA^{Asp}$ (GAT). Two unique regulatory motifs, TTCAAT[N_{14}]TATAAT and CTAAATAcCcc, were found in their entireties in the EspM4VN genome (positions 7219–7244, 143195–143220, 152828–152853, 158832–158857, 61226–61251, and 65377–65387, 70604–70614, 98591–98601, 101772–101782, and 53611–53621). Phylogenetic trees of structural proteins (major capsid protein and baseplate) and enzymes (DNA polymerase and ligase) showed that EspM4VN formed an independent cluster among Ackermannviridae phages (**Figure 6**). Based on the phylogenetic analysis of ligase and major capsid protein, EspM4VN was positioned in the same cluster of *Agtrevirus*, *Shigella* phage Ag3, and *Salmonella* phage SKML-39 and not in the same cluster of *Limestonevirus* and *Kuttervirus* belonging to Ackermannviridae (**Figures 6B,C**). The baseplate protein of EspM4VN was not positioned in *Agtrevirus* but in *Limestonevirus* (**Figure 6D**).

Protein Analysis of EspM4VN

For identification and further characterization of bacteriophage EspM4VN protein, we performed SDS-PAGE and MS analyses of the purified phage. Ten major protein bands were found in the gel, and band patterns including a major band

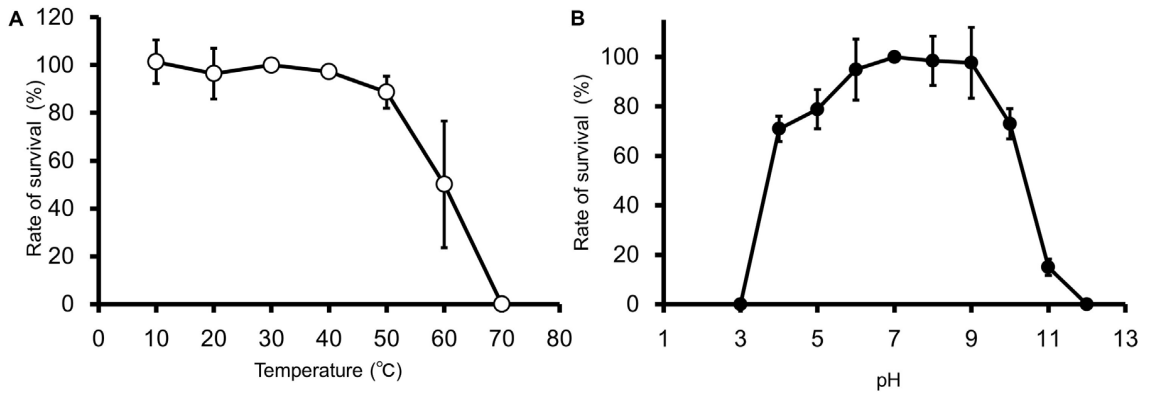

FIGURE 2 | Thermal and pH stability of EspM4VN. Course of survival ratio (%) of EspM4VN particles during heat **(A)** and pH **(B)** treatments is plotted. The mean titer is shown from triplicate assays.

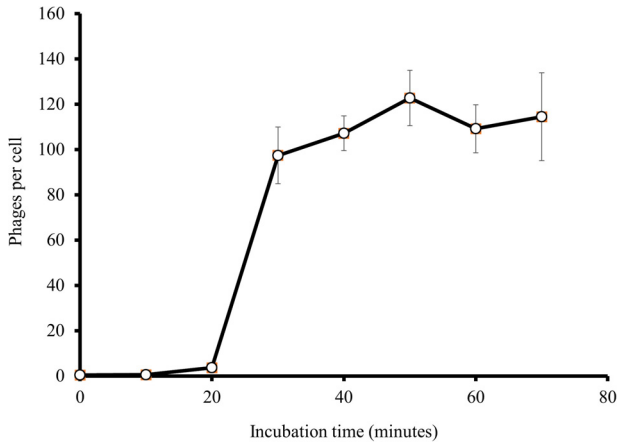

FIGURE 3 | One-step growth curve of the EspM4VN.

around 50 kDa (band 6 in **Figure 7**) were similar to those of *Dickeya* spp. bacteriophage (Czajkowski et al., 2015b), *Shigella boydii* phage Ag3 (Anany et al., 2011), and broad-host-range phages φPD23.1 and φD10.3 (Czajkowski et al., 2015a). Ten protein bands excised from the SDS-PAGE gel were digested by trypsin. Proteomic analysis was performed using a quadrupole time-of-flight tandem mass spectrometer. Peptides were identified by matching the identified peaks to the predicted protein sequence library of the custom EspM4VN gene including 219 ORFs or the NCBInr virus database using the in-house Mascot server. In all 10 gel samples, proteins matched against EspM4VN proteins showed much higher Mascot scores than other bacteriophage proteins including *Dickeya* and *Shigella*, indicating that the purified bacteriophage was from the EspM4VN gene.

A total of 18 EspM4VN proteins were identified and are listed in **Figure 7** along with the gene number, calculated molecular mass, corresponding protein sequence coverage, and predicted annotation by BLASTp protein similarity search. Because 18 identified protein bands were excised from stained bands, these proteins were suggested to be highly expressed proteins. Of these, 16 were identified as structural proteins and two were classified as uncharacterized or unknown proteins. Genes 105 (VriC), 114 (gp18), 116 (gp20), and 121 (gp23) were identified from *Dickeya* phage φD10.3 (Czajkowski et al., 2015a).

Some genes from identified proteins were sequentially located in the genome sequence including genes 25–26, 101–104, and 114–115. BLASTp search indicated that proteins of genes 25–26 were both baseplate subunits and those of 101–104 were all tail-spike-related proteins. Proteins from genes 114–115 were also identified as tail proteins. These proteins were multimeric proteins for function, and all required high expression levels. Analysis of the EspM4VN genome sequence suggested that similar functions or structural proteins were clustered at certain regions as is the case in other phages.

Besides protein identification, Mascot analysis also provides label-free, relative quantitation of proteins, the exponentially modified protein abundance index (emPAI) in a mixture based on protein coverage by the peptide matches in a database search result (Arike and Peil, 2014). The protein of gene 121 yielded the highest emPAI values at gels #6 and #7 (emPAI: 17.9 and 11.2, respectively) and was identified as a major capsid protein, gp23. The gp23 protein nicely migrated at 50 kDa in the gel according to the calculated molecular weight and showed the highest density of the Coomassie Brilliant Blue stain. Other SDS-PAGE analyses showed that the migrations and band densities of EspM4VN were highly similar to those of the *Dickeya* phage φD10.3 sample (Czajkowski et al., 2015a).

Tryptic fragments from the products of genes 92, 100, 114, and 116 included plausible N-terminal sequences (**Supplementary Table S3**). MS/MS analysis showed that all of the peptides started from the amino acid following Met (next to Met) because N-terminal Met could be co-translationally cleaved by methionine aminopeptidase. The gene 116 product included not only N-terminal end Ala^2 but also a C-terminal end Glu^{563}. The calculated molecular weight of this protein (63.23 kDa without Met^1) closely matched with band migration (65 kDa) and was identified as a portal vertex protein, gp20.

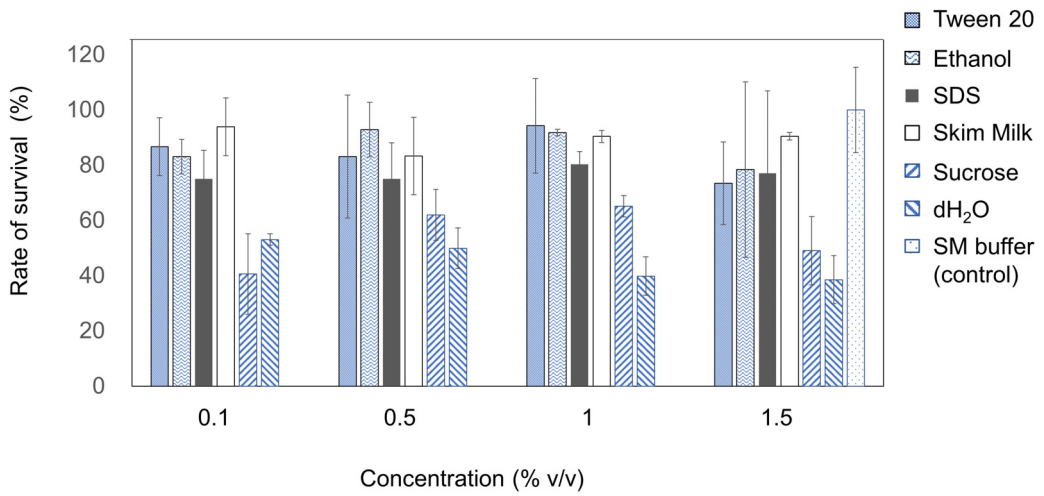

FIGURE 4 | Chemical sensitivity of EspM4VN. Phage particles were inoculated in LB containing different concentrations of Tween 20, ethanol, SDS, skim milk, and sucrose from 0.1 to 1.5?%. SM buffer (outlined bars) was used as a control. Quantification was achieved by plaque assay. The plates were incubated at 37°C for 12 h, and the phage growth was assayed by plaque-forming units (pfu). Experiments were performed in triplicate on three different occasions, and means ± SD are shown.

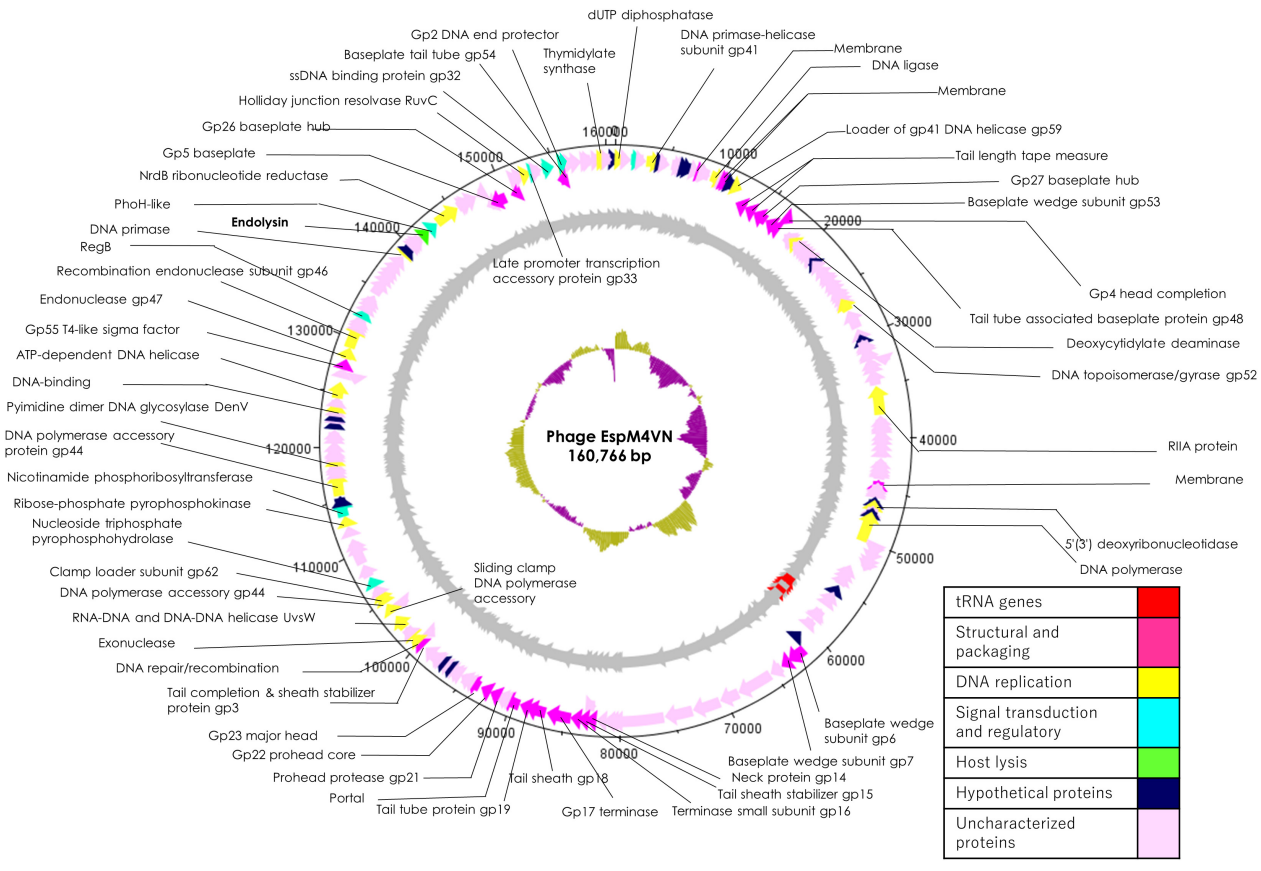

FIGURE 5 | Genome map of EspM4VN. The outer lane represents genes in the plus strand. The next lane illustrates genes on the minus strand. The lane with black peaks and valleys indicate the GC content, while the innermost lane (green and violet) shows a GC skew analysis.

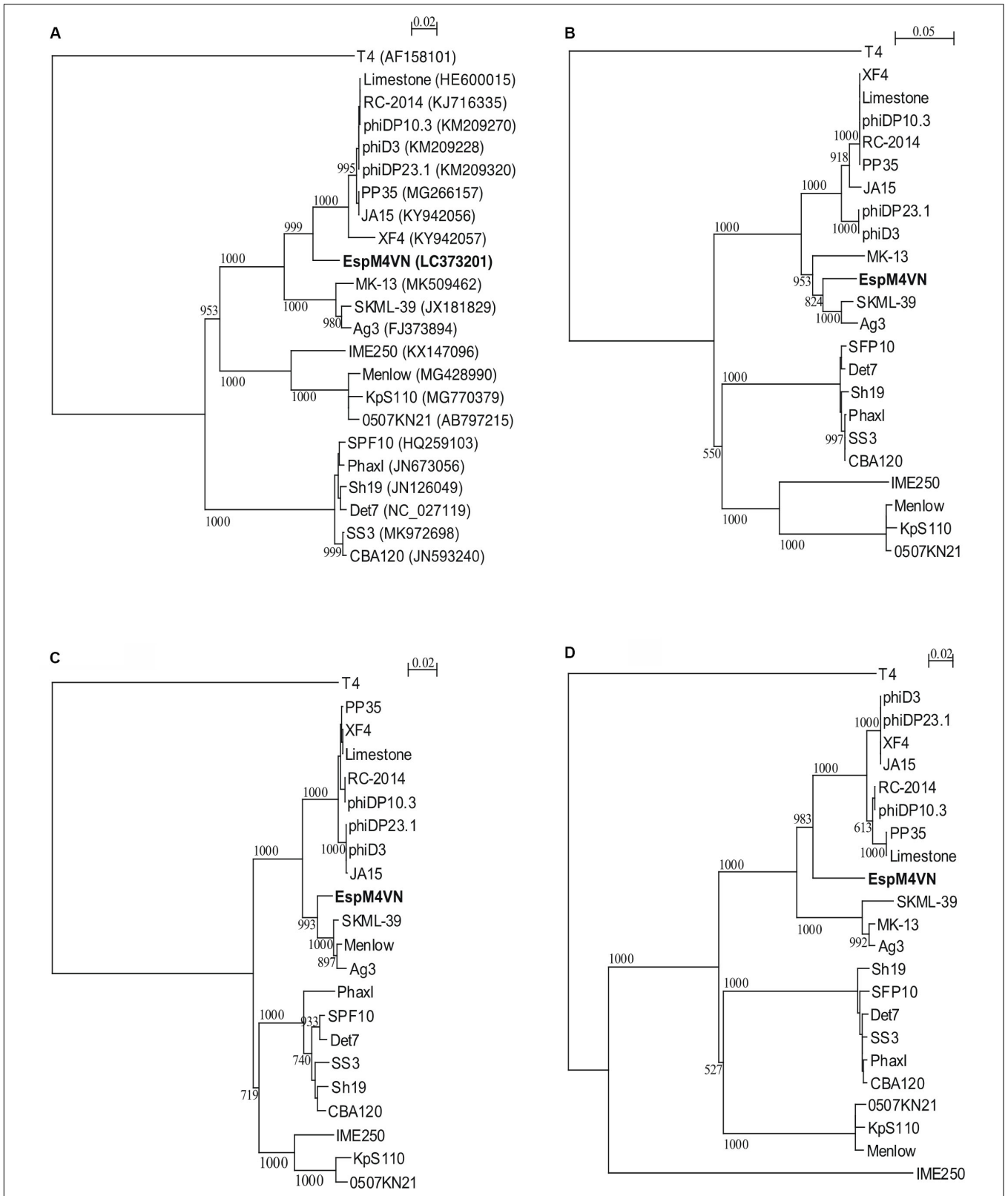

FIGURE 6 | Phylogenetic trees generated based on **(A)** DNA polymerases, **(B)** DNA ligase, **(C)** major capsid protein, and **(D)** baseplate hub subunit of EspM4VN and homologous proteins from other phage members of the Ackermannviridae family. Nucleic acid sequences were compared using ClustalW, and phylogenetic trees were generated using the neighbor-joining method. Numbers in brackets show the gene ID.

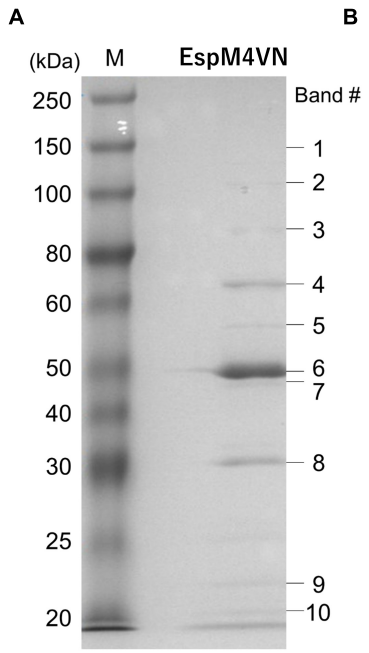

Band #	Gene #	Predicted gene product	ESI-MS analysis		
			MW	Coverage (%)	emPAI
1	105	VriC protein	174760	40	1.35
2	101	Phage tail fiber protein	119592	52	2.21
3	104	Tail fiber protein	92762	50	1.12
	103	Tail fiber protein	93065	35	1.05
4	114	Putative tail sheath protein gp18	68949	61	3.35
	116	Portal vertex protein gp20	63475	53	2.22
	102	Tail fiber protein	63798	61	1.88
	98	Putative baseplate wedge subunit gp6	64822	31	0.98
5	182	Hypothetical protein	60019	59	5.38
6	121	Major head protein gp23	48013	74	17.9
7	100	Unknown structural protein	42806	18	0.32
8	121	Major head protein gp23	48013	55	2.29
9	56	Putative tail tube protein	27677	17	0.71
	26	Putative baseplate wedge subunit gp53	21408	23	0.51
10	92	Phage tail needle protein	18424	86	4.76
	115	Putative tail tube protein gp19	17163	54	4.47
	134	Putative tail completion & sheath stabilizer protein gp3	18502	39	1.21
	160	Uncharacterized protein	17269	13	0.4

FIGURE 7 | Bacteriophage EspM4VN structural proteins separated in SDS-PAGE gel **(A)** and identification of structural proteins with ESI-MS/MS **(B)**. **(A)** For SDS-PAGE, EspM4VN particles (~10^{12} pfu) were mixed with lysis buffer and then boiled for 10 min. Phage proteins were separated in a 15% acrylamide SDS-PAGE gel for approximately 19 h at 50 V at 22°C. The bands were stained with Coomassie Brilliant Blue according to the protocol provided by the manufacturer. For ESI-MS/MS analysis of phage structural proteins, protein bands obtained from SDS-PAGE were excised from the gel with a sterile scalpel.

Among the plausible 219 genes of EspM4VN, gene analysis indicated that 18 proteins did not start from Met at the N-terminal end but Val or Leu. This suggests that EspM4VN uses only the prokaryote expression system as the start codon in the eukaryote expression system is almost exclusively Met (AUG). Gene 115 was found in the gel band #10 sample and included Val as its plausible N-terminal sequence. The expected N-terminal tryptic peptide VTVNFPAFVAGSDTIR was detected seven times via MS/MS with a high Mascot score of 80. In the genome DNA sequence between the stop codon (TGA) of gene 114 and the start codon (GTG) of gene 115, there were no possible Met (AUG) codons found. Based on DNA sequence analysis and MS/MS analysis, we concluded that gene 115 was expressed from Val at the N-terminal amino acid (**Supplementary Figure S2**). BLASTp analysis and quantification analysis showed that gene 115 was identified as a tail tube protein, gp19, at high expression because its emPAI was 4.5.

Gene 101 was found at gel band #2 and had the highest emPAI (2.21) in the gel sample. The molecular weight of gene 101 contained 119,592 Da including 1,109 amino acids. Of the sequence, 52% from the N-terminus to the C-terminus was observed by MS/MS analysis. BLASTp analysis suggested that gene 101 has two unique domains: N-terminal and C-terminal structures. The N-terminal region (1–413) was closely related to other bacteriophage tail proteins (**Figure 8B**). Interestingly, the C-terminal region (436–1109) was similar to a hypothetical protein from bacteria including *Enterobacter* (WP_117582064.1) or *E. coli* (APK16060.1) (**Figure 8C**). BLASTp analysis showed that genes 101, 103, and 104 had a pectin lyase fold motif, a typical motif in tail-spike proteins, including the beta helix structure. Gene 101 has a conserved identical sequence region (L^{371}-D-X-K-T-V-I-Y-D^{379}) with gene 102 (42–50) and gene 103 (42–50). Gene 104 has a part of the identical sequence (V^{46}-I-Y-D^{49}) and has a conserved motif of the tail spike (N-terminal domain at 97–153).

DISCUSSION

Bacterial soft rot is one of the most common diseases of important crops in the world. Therefore, several control strategies including physical methods and chemical treatments using copper sulfate, dimethylammonium chloride, sodium hypochlorite, formaldehyde, and antibiotics have been applied. However, these approaches have the risk of increasing environmental burden and health hazards (Berg, 2001; Dasgupta et al., 2007; Pham et al., 2011; Azaiez et al., 2018). The genus *Enterobacter* contains 14 species and two subspecies (Zhu et al., 2017). Among these, the *E. cloacae* complex (Ecc) including *E. cloacae*, *E. asburiae*, *Enterobacter hormaechei*, *Enterobacter kobei*, *Enterobacter ludwigii*, and *Enterobacter nimipressuralis* has genomic heterogeneity and is therefore difficult to identify (Paauw et al., 2008). In this study, we isolated soft rot disease pathogenic bacteria for usage as phage hosts. Phylogenetic analysis of the isolates with their 16S rDNA sequences showed that they located in the Ecc cluster but had unconfirmed

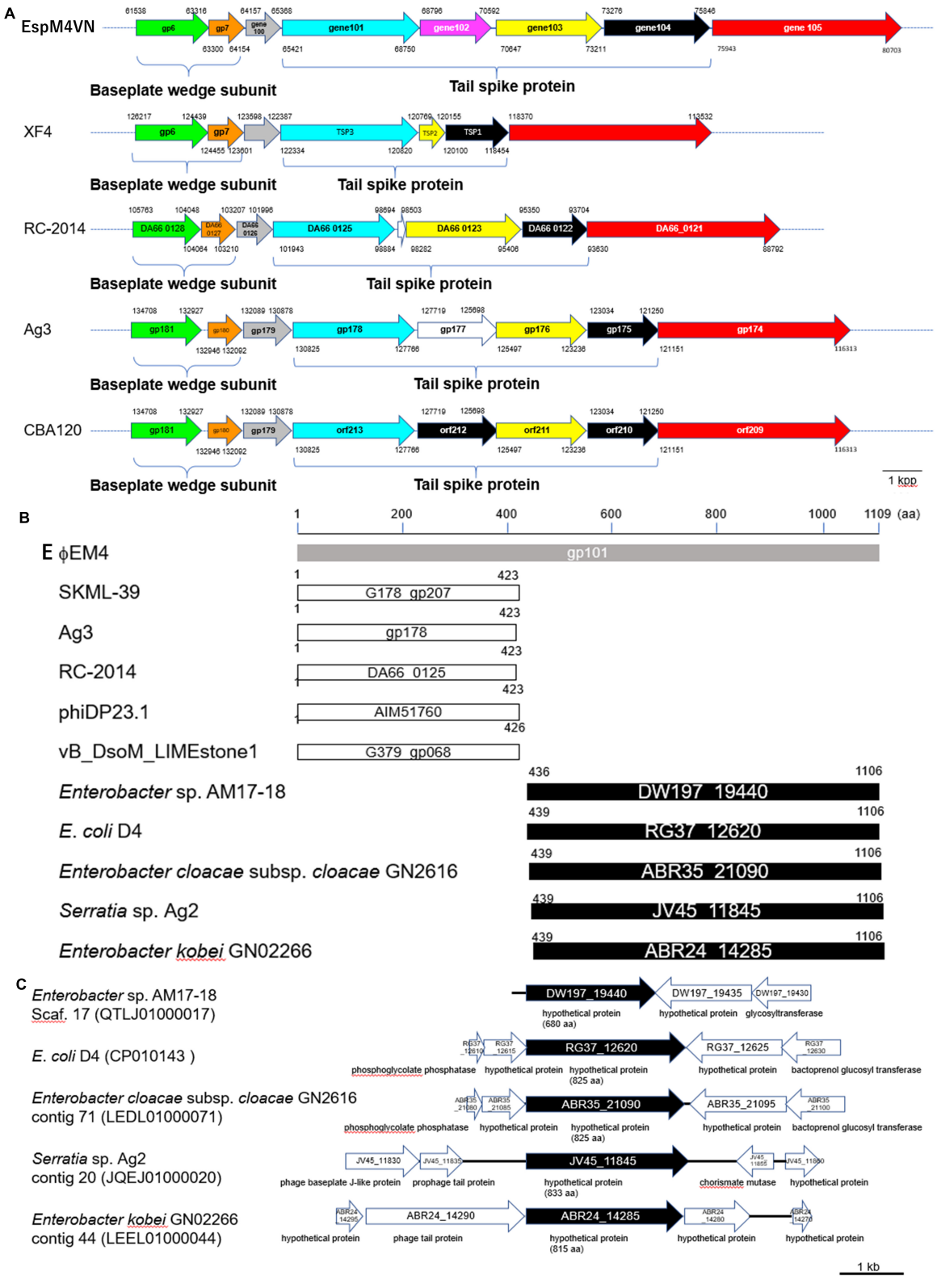

FIGURE 8 | Continued

FIGURE 8 | Comparison of gene organization between tail-protein encoding genes in EspM4VN and its homologous genes. **(A)** Gene clusters of phage tail proteins in EspM4VN and Ackermannviridae family phages. Same-colored arrows indicate homologous genes. Blanked arrows show no homology with gene 102 in EspM4VN. Numbers indicate positions of ORFs in the genome. **(B)** Homologous amino acid sequence distribution of gene 101 product (gray bar). White and black bars show partial regions of phage gene products and bacterial chromosomal gene products, respectively. Numbers indicate amino acid positions in each protein. **(C)** Gene organization adjacent to gene 101 homologs in bacterial chromosomes. Black arrows indicate gene 101 homologous genes. Predicted gene products are shown below each arrow.

identification in the species level. We identified the whole-genome sequence of the strain M4 via *in silico* DNA–DNA hybridization (data not shown). Therefore, the host strain of phage EspM4VN should be *Enterobacter* sp. strain M4, which would be the novel species in the *Enterobacter* genus. It is not enough to prove that isolated strains, including the M4 strain, are the main villain for soft rot disease; therefore, we will examine the function of the strains for maceration with both *in vitro* and in-filed experiments. If so, phage therapy with phage EspM4VN might be a potential solution for soft rot disease.

With morphological observation, EspM4VN belongs to the Ackermannviridae family and resembles *Dickeya* phages φXF4 (Day et al., 2017), but it does not possess short tail spikes as observed in φXF4. Instead, of the gene cluster encoding short-tail-spike proteins of φXF4 (TSP genes), four genes (genes 101–104) consisted of the gene cluster for tail-spike proteins in EspM4VN (**Figure 8A**). The difference in gene organization may cause morphological differentiation of tail structures between EspM4VN and φXF4. In other words, EspM4VN tails with unfolded tail entities, displaying an umbrella-like structure (**Figure 1D**). Based on alignment of thymidylate synthase genes, EspM4VN possess the thymidylate synthase gene, a homolog of the deoxyuridylate hydroxymethyltransferase gene of *Escherichia* phage vB_EcoM Sa157lw (AYC62411) with 71.43% homology.

Phage therapy had been increasingly researched and applied as biological control agents against plant pathogens since the early 1920s (Gill and Abedon, 2003; Jones et al., 2007; Balogh et al., 2010). While the application of phages to an integrated plant disease management strategy is relatively simple, cheap, and effective, phage efficacy is highly dependent on general environmental factors and the susceptibility of the target bacterium. Symptomized soft rot disease is a soilborne infection; hence, we isolated phages from farmland, where the above-mentioned plants have been cultivated. In this study, EspM4VN isolated from soil samples was capable of inhibiting only *Enterobacter* strain M4, indicating that EspM4VN has a narrow host range. This is quite similar to other phages such as WS-EP 19, WS-EP 13, WS-EP 20, WS-EP 26, WS-EP 28, WS-EP 57, WS-EP 32, and WS-EP 94, which infect specific *Enterobacter* strains isolated from milk powder and other foods (Loessner et al., 1993). Therefore, EspM4VN may be used in phage cocktails and classification as phage typing for isolated *Enterobacter* strains. One of the reasons for its restricted host range is the characteristic tail structure of the EspM4VN (**Figures 1B**, **8**). One-step growth curve demonstrated that EspM4VN has a short latent phase and quickly reaches burst size. This phage could be a potential epidemic inhibitor for immediate treatment after an outbreak of plant disease. Furthermore, thermal and pH stability tests indicate that it may be applied in tropical and subtropical zones. In the production industry, pesticides are normally formulated in the presence of surface active agents, which can change pesticide adsorption in the soil–water system. Addition of Tween 20 at low and high concentrations increased the adsorption of diazinon and atrazine into soil (Iglesias-Jiménez et al., 1996). Phage EspM4VN resisted Tween 20, ethanol, SDS, and sucrose at various concentrations as well. Skim milk is one of the best substances for product formulation and long-term storage. In addition to some chemicals used in this study, various materials to extend the life of the phage following exposure to various physical factors may be examined (Jones et al., 2007).

Whole-genome analysis of EspM4VN revealed that five tRNAs (Ser1, Ser2, Tyr, Asn, and Asp) were identified. Those tRNAs may correspond to the short latent phage and large burst size because of their positive influences on reproduction in host cells. However, the homologous phage genome *S. boydii* phage Ag3 had four similar tRNAs and a 52-min latent phase. This contrast may be explained by ampleness of the tRNAs presented in the hosts. In this case, the tRNAs of the phage would have less of an effect on the phage environment during infection (Bailly-Bechet et al., 2007).

Like other phage genome sequences, similar functions or structural proteins were clustered at certain regions in the EspM4VN genome. These results suggested that gene locations were closely related with protein expression. However, genes and gene products of EspM4VN exhibit distinctive features (**Figure 8**). Genes 101 to 104 comprised a gene cluster for tail-spike proteins. Similar cluster structures comprising four genes were observed in *Agtrevirus* (Ag3) and *Limestonevirus* (RC-2014) genomes (**Figure 8A**). In the genome of *Dickeya* phage φXF4 (taxid: 1983656), whose tail-spike structure is similar to that of EspM4VN, there are three genes in the tail-spike protein cluster. Phage XF4 has a gene structure in which three tail-spike genes (TSP1–TSP3) have been sequentially located at the region (118454–122334) (Day et al., 2017). TSP1, TSP2, and TSP3 have sequence similarities with those of genes 104, 103, and 101. In the gene cluster of the tail-spike protein of *Escherichia* virus CBA120 (taxid: 1987159), the TSP1 gene (*orf213*) and TSP3 gene (*orf211*) show significant homology with genes 101 and 103 (**Figure 8A**). TSP2 and TSP4 of GBA120 have partial homologies with the product of gene 104. CBA120-TSP2 binds its substrate and functions to recognize the host receptor (Plattner et al., 2019). These findings suggest that EspM4VN tail-spike proteins might form a heteromeric structure in the phage. Only the product of gene 102 shows high homology with the hypothetical proteins of *Enterobacter mori* (WP_157929994.1), *E. coli* (OJN39208.1), *E. cloacae* (WP_063860747.1), and *Klebsiella aerogenes* (WP_063963681.1). Therefore, the unique structure of the product of gene 102

might be caused by the narrow host range of EspM4VN and the possibility that some gene origin of EspM4VN could be from bacterial chromosomes.

Also, gene 101 might be fused with phage-derived gene and bacterial genome-derived gene (**Figures 8B,C**). Homology analysis of the gene 101 product indicates that its N-terminal region closely resembles a right-handed beta helix region of phage proteins SKML-39 (identity: 94%, 1–423 aa), Ag3 (identity: 94%, 1–423 aa), RC-2014 (identity: 90%, 1–423 aa), phiDP23.1 (identity: 89%, 1–423 aa), and LIMEstone1 (identity: 84%, 1–426 aa) (**Figure 8B**). The C-terminal region of the gene 101 product has high homology with enterobacterial gene products described as follows: *Enterobacter* sp. AM17-18 (identity: 57%, 436–1106 aa), *E. coli* D4 (identity: 56%, 439–1106 aa), *E. cloacae* ssp. *cloacae* GN2616 (identity: 56%, 439–1106 aa), *Serratia* sp. Ag2 (identity: 38%, 439–1106 aa), and *E. kobei* GN02266 (identity: 36%, 439–1106 aa) (**Figure 8B**). From gene locations in their chromosome, some of the homologous genes might be inserted in the glycan metabolic, cell wall, and amino acid biosynthesis pathways in *Enterobacter* sp. AM17-18, *E. coli* D4, and *E. cloacae* ssp. *cloacae* GN2616 (**Figure 8C**). Matilla et al. (2014) suggested that φXF1, φXF3, and φXF4 are very efficient generalized transducers capable of transducing chromosomal markers at high frequencies. The above-mentioned heterogeneous gene structure is reasonable for phage function, as corresponding genes in *Serratia* sp. Ag2 and *E. kobei* GN02266 genomes locate within phage tail gene clusters. This suggests that genes 101 and 102 of EspM4VN existed partially from lysogenic phage genomes or were fused after phage transduction. However, the question remains as to why a tail-spike protein, which is a necessary accessory protein, would start from a rare start codon and whether transcripts longer than 10 kb could be polycistronically synthesized. These and other genetic regulation characteristics of EspM4VN transcription are topics for future studies. We did not observe any lysogenic-related genes such as *int*, *xis*, and *xerD* in the EspM4VN genome; this is a beneficial property of the phage for biocontrol of the plant pathogenic bacteria (Álvarez et al., 2019).

DATA AVAILABILITY STATEMENT

The whole genome sequence of phage EspM4VN was submitted to DDBJ under accession number LC373201. The 16S rDNA sequences of the isolates have been deposited in the DDBJ under accession numbers to LC415135, LC415612, LC416590, LC423530, LC498100, LC498101, and LC498102.

AUTHOR CONTRIBUTIONS

The work presented here was carried out in collaboration between all authors. KD defined the research theme. NT, YN, YF, and KD designed the methods and experiments, carried out the molecular biological and virological experiments, analyzed the data, interpreted the results, and wrote the manuscript. NT, KI, and NF engaged in the experiments using plant pathogens. YH and TI codesigned the protein analysis and ESI-MS/MS experiments and discussed the analyses, interpretation, and presentation. All authors have contributed to, saw, and approved the manuscript.

FUNDING

This work was partly funded by The Toyo Suisan Foundation.

ACKNOWLEDGMENTS

We thank T. Kanemaru for advice on electron microscopic analysis and Y. Shimasaki and Y. Ohshima for helpful advice on Mascot analysis. We thank the referees for comments on the manuscript. We would also like to thank the Japanese Grant Aid for Human Resource Development Scholarship (JDS) and Japanese Government Scholarship (MEXT) program for supporting financial aid.

SUPPLEMENTARY MATERIAL

The Supplementary Material for this article can be found online at: https://www.frontiersin.org/articles/10.3389/fmicb.2020.00885/full#supplementary-material

FIGURE S1 | Phylogenetic tree of isolated strains. Their nucleotide sequences were compared using ClustalW, and phylogenetic trees were generated using the neighbor-joining method.

FIGURE S2 | The nucleotide sequence of the intergeneric spacer region and partial encoding regions of genes 114 and 115. Dotted arrows represent inverted repeats, and an asterisk denotes the stop codon. The detected amino acid residues from MS analysis are underlined. The nucleotide sequence is from position 88621 to 68627 of GenBank Database, accession no. LC373201.2.

TABLE S1 | Annotation table of phage EspM4VN.

TABLE S2 | General features of EspM4VN and related phages' genomes.

TABLE S3 | MS/MS results for phage proteins identified in **Figure 8**.

REFERENCES

Adams, M. H. (1959). *Bacteriophages*. New York, NY: Interscience Publishers Inc.

Addy, H. S., Ahmad, A. A., and Huang, Q. (2019). Molecular and biological characterization of Ralstonia phage RsoM1USA, a new species of *P2virus*, isolated in the United States. *Front. Microbiol.* 10:267. doi: 10.3389/fmicb.2019.00267

Adeolu, M., Alnajar, S., Naushad, S., and Gupta, R. S. (2016). Genome-based phylogeny and taxonomy of the '*Enterobacteriales*': proposal for *Enterobacterales* ord. *nov. divided into the families Enterobacteriaceae, Erwiniaceae fam. nov., Pectobacteriaceae fam. nov., Yersiniaceae fam. nov., Hafniaceae fam. nov., Morganellaceae fam. nov., and Budviciaceae fam. nov. Int. J. Syst. Evol. Microbiol.* 66, 5575–5599. doi: 10.1099/ijsem.0.001485

Adriaenssens, E. M., Van Vaerenbergh, J., Vandenheuvel, D., Dunon, V., Ceyssens, P. J., De Proft, M., et al. (2012). T4-related bacteriophage LIMEstone isolates for the control of soft rot on potato caused by '*Dickeya solani*'. *PLoS One* 7:e33227. doi: 10.1371/journal.pone.0033227

Adriaenssens, E. M., Wittmann, J., Kuhn, J. H., Turner, D., Sullivan, M. B., Dutilh, B. E., et al. (2018). Taxonomy of prokaryotic viruses: 2017 update from the

ICTV bacterial and archaeal viruses subcommittee. *Arch. Virol.* 163, 1125–1129. doi: 10.1007/s00705-018-3723-z

Álvarez, B., López, M. M., and Biosca, E. G. (2019). Biocontrol of the major plant pathogen *Ralstonia solanacearum* in irrigation water and host plants by novel waterborne lytic bacteriophages. *Front. Microbiol.* 10:2813. doi: 10.3389/fmicb.2019.02813

Anany, H., Lingohr, E. J., Villegas, A., Ackermann, H. W., She, Y. M., Griffiths, M. W., et al. (2011). A *Shigella boydii* bacteriophage which resembles *Salmonella* phage ViI. *Virol. J.* 8:242. doi: 10.1186/1743-422X-8-242

Arike, L., and Peil, L. (2014). Spectral counting label-free proteomics. *Methods Mol. Biol.* 1156, 213–222. doi: 10.1007/978-1-4939-0685-7_14

Azaiez, S., Ben Slimene, I., Karkouch, I., Essid, R., Jallouli, S., Djebali, N., et al. (2018). Biological control of the soft rot bacterium *Pectobacterium carotovorum* by *Bacillus amyloliquefaciens* strain Ar10 producing glycolipid-like compounds. *Microbiol. Res.* 217, 23–33. doi: 10.1016/j.micres.2018.08.013

Bailly-Bechet, M., Vergassola, M., and Rocha, E. (2007). Causes for the intriguing presence of tRNAs in phages. *Genome Res.* 17, 1486–1495. doi: 10.1101/gr.6649807

Balogh, B., Jones, J. B., Iriarte, F. B., and Momol, M. T. (2010). Phage therapy for plant disease control. *Curr. Pharm. Biotechnol.* 11, 48–57. doi: 10.2174/138920110790725302

Berg, H. (2001). Pesticide use in rice and rice–fish farms in the Mekong Delta. *Vietnam. Crop Prot.* 20, 897–905. doi: 10.1016/S0261-2194(01)00039-4

Bolger-Munro, M., Cheung, K., Fang, A., and Wang, L. (2013). T4 bacteriophage average burst size varies with *Escherichia coli* B23 cell culture age. *J. Exp. Microbiol. Immunol.* 17, 115–119.

Bouvet, P. J. M., and Grimont, P. A. D. (1986). Taxonomy of the Genus *Acinetobacter* with the Recognition of *Acinetobacter baumannii* sp. *nov., Acinetobacter haemolyticus sp. nov., Acinetobacter johnsonii sp. nov., and Acinetobacter junii sp. nov. and Emended Descriptions of Acinetobacter calcoaceticus and Acinetobacter lwoffii*. *Int. J. Syst. Evol. Microbiol.* 36, 228–240. doi: 10.1099/00207713-36-2-228

Buttimer, C., Hendrix, H., Lucid, A., Neve, H., Noben, J. P., Franz, C., et al. (2018). Novel N4-Like bacteriophages of *Pectobacterium atrosepticum*. *Pharmaceuticals* 11:E45. doi: 10.3390/ph11020045

Carstens, A. B., Djurhuus, A. M., Kot, W., Jacobs-Sera, D., Hatfull, G. F., and Hansen, L. H. (2018). Unlocking the potential of 46 new bacteriophages for biocontrol of *Dickeya solani*. *Viruses* 10:E621. doi: 10.3390/v10110621

Chin, C. S., Alexander, D. H., Marks, P., Klammer, A. A., Drake, J., Heiner, C., et al. (2013). Nonhybrid, finished microbial genome assemblies from long-read SMRT sequencing data. *Nat. Methods* 10, 563–569. doi: 10.1038/nmeth.2474

Czajkowski, R., Ozymko, Z., de Jager, V., Siwinska, J., Smolarska, A., Ossowicki, A., et al. (2015a). Genomic, proteomic and morphological characterization of two novel broad host lytic bacteriophages ΦPD10.3 and ΦPD23.1 infecting pectinolytic *Pectobacterium* spp. and *Dickeya* spp. *PLoS One* 10:e0119812. doi: 10.1371/journal.pone.0119812

Czajkowski, R., Ozymko, Z., Siwinska, J., Ossowicki, A., de Jager, V., Narajczyk, M., et al. (2015b). The complete genome, structural proteome, comparative genomics and phylogenetic analysis of a broad host lytic bacteriophage ΦD3 infecting pectinolytic *Dickeya* spp. *Stand. Genomic Sci.* 10:68. doi: 10.1186/s40793-015-0068-z

Czajkowski, R., Ozymko, Z., and Lojkowska, E. (2014). Isolation and characterization of novel soilborne lytic bacteriophages infecting *Dickeya* spp. *biovar* 3 ('*D. solani*'). *Plant Pathol.* 63, 758–772. doi: 10.1111/ppa.12157

Dasgupta, S., Meisner, C., Wheeler, D., Xuyen, K., and Thi Lam, N. (2007). Pesticide poisoning of farm workers-implications of blood test results from Vietnam. *Int. J. Hyg. Environ. Health* 210, 121–132. doi: 10.1016/j.ijheh.2006.08.006

Day, A., Ahn, J., Fang, X., and Salmond, G. P. C. (2017). Environmental bacteriophages of the emerging enterobacterial phytopathogen, *Dickeya solani*, show genomic conservation and capacity for horizontal gene transfer between their bacterial hosts. *Front. Microbiol.* 8:1654. doi: 10.3389/fmicb.2017.01654

Engineering and Consulting Firms Association, J. (2006). *Study on Strengthening Food Standards and the Certification System in the Socialist Republic of Vietnam*. Study Report. Engineering and Consulting Firms Association, Japan: Overseas Merchandise Inspection Co., Ltd. Available online at: http://www.ecfa.or.jp/japanese/act-pf_jka/H17/renkei/renkei_Vietnam_Food_Eng.pdf

García-González, T., Sáenz-Hidalgo, H. K., Silva-Rojas, H. V., Morales-Nieto, C., Vancheva, T., Koebnik, R., et al. (2018). *Enterobacter cloacae*, an emerging plant-pathogenic bacterium affecting chili pepper seedlings. *Plant Pathol. J.* 34, 1–10. doi: 10.5423/PPJ.OA.06.2017.0128

Gardan, L., Gouy, C., Christen, R., and Samson, R. (2003). Elevation of three subspecies of *Pectobacterium carotovorum* to species level: *Pectobacterium atrosepticum* sp. *nov., Pectobacterium betavasculorum sp. nov. and Pectobacterium wasabiae sp. nov*. *Int. J. Syst. Evol. Microbiol.* 53, 81–91. doi: 10.1099/ijs.0.02423-0

Gašić, K., Kuzmanović, N., Ivanović, M., Prokić, A., Šević, M., and Obradović, A. (2018). Complete genome of the *Xanthomonas euvesicatoria* specific bacteriophage KΦ1, its survival and potential in control of pepper bacterial spot. *Front. Microbiol.* 9:2021. doi: 10.3389/fmicb.2018.02021

George, A. S., Cox, C. E., Desai, P., Porwollik, S., Chu, W., de Moraes, M. H., et al. (2018). Interactions of *Salmonella enterica* Serovar typhimurium and *Pectobacterium carotovorum* within a tomato soft rot. *Appl. Environ. Microbiol.* 84, e1913–e1917. doi: 10.1128/AEM.01913-1917

Gill, J., and Abedon, S. T. (2003). Bacteriophage ecology and plants. *APSnet Feature Art*. Available online at: https://www.apsnet.org/edcenter/apsnetfeatures/Pages/BacteriophageEcology.aspx

Hauben, L., Moore, E. R. B., Vauterin, L., Steenackers, M., Mergaert, J., Verdonck, L., et al. (1998). Phylogenetic position of phytopathogens within the *Enterobacteriaceae*. *Syst. Appl. Microbiol.* 21, 384–397. doi: 10.1016/S0723-2020(98)80048-9

Hoffmann, H., Stindl, S., Ludwig, W., Stumpf, A., Mehlen, A., Heesemann, J., et al. (2005). Reassignment of *Enterobacter* dissolvens to *Enterobacter cloacae* as *E. cloacae subspecies dissolvens comb. nov. and emended description of Enterobacter asburiae and Enterobacter kobei*. *Syst. Appl. Microbiol.* 28, 196–205. doi: 10.1016/j.syapm.2004.12.010

Iglesias-Jiménez, E., Sánchez-Martín, M. J., and Sánchez-Camazano, M. (1996). Pesticide adsorption in a soil-water system in the presence of surfactants. *Chemosphere* 32, 1771–1782. doi: 10.1016/0045-6535(96)00094-X

Jones, J. B., Jackson, L. E., Balogh, B., Obradovic, A., Iriarte, F. B., and Momol, M. T. (2007). Bacteriophages for plant disease control. *Annu. Rev. Phytopathol.* 45, 245–262. doi: 10.1146/annurev.phyto.45.062806.094411

Kõiv, V., Roosaare, M., Vedler, E., Ann Kivistik, P., Toppi, K., Schryer, D. W., et al. (2015). Microbial population dynamics in response to *Pectobacterium atrosepticum* infection in potato tubers. *Sci. Rep.* 5:11606. doi: 10.1038/srep11606

Kusradze, I., Karumidze, N., Rigvava, S., Dvalidze, T., Katsitadze, M., Amiranashvili, I., et al. (2016). Characterization and testing the efficiency of *Acinetobacter baumannii* phage *vB-GEC_Ab-M-G7* as an antibacterial agent. *Front. Microbiol.* 7:1590. doi: 10.3389/fmicb.2016.01590

Laslett, D., and Canback, B. (2004). ARAGORN, a program to detect tRNA genes and tmRNA genes in nucleotide sequences. *Nucleic Acids Res.* 32, 11–16. doi: 10.1093/nar/gkh152

Lau, Y. Y., Yin, W. F., and Chan, K. G. (2014). *Enterobacter asburiae* strain L1: complete genome and whole genome optical mapping analysis of a quorum sensing bacterium. *Sensors* 14, 13913–13924. doi: 10.3390/s140813913

Lim, J. A., Jee, S., Lee, D. H., Roh, E., Jung, K., Oh, C., et al. (2013). Biocontrol of *Pectobacterium carotovorum* subsp. carotovorum using bacteriophage PP1. *J. Microbiol. Biotechnol.* 23, 1147–1153. doi: 10.4014/jmb.1304.04001

Loessner, M. J., Neugirg, E., Zink, R., and Scherer, S. (1993). Isolation, classification and molecular characterization of bacteriophages for *Enterobacter* species. *J. Gen. Microbiol.* 139, 2627–2633. doi: 10.1099/00221287-139-11-2627

Luo, C. H., Chiou, P. Y., Yang, C. Y., and Lin, N. T. (2012). Genome,integration, and transduction of a novel temperate phage of *Helicobacter pylori*. *J. Virol.* 86, 8781–8792. doi: 10.1128/JVI.00446-12

Ma, B., Hibbing, M. E., Kim, H. S., Reedy, R. M., Yedidia, I., Breuer, J., et al. (2007). Host range and molecular phylogenies of the soft rot enterobacterial genera *Pectobacterium* and *Dickeya*. *Phytopathology* 97, 1150–1163. doi: 10.1094/PHYTO-97-9-1150

Manohar, P., Tamhankar, A. J., Lundborg, C. S., and Nachimuthu, R. (2019). Therapeutic characterization and efficacy of bacteriophage cocktails infecting *Escherichia coli*, *Klebsiella pneumoniae*, and *Enterobacter* species. *Front. Microbiol.* 10:574. doi: 10.3389/fmicb.2019.00574

Masyahit, M., Sijam, K., Awang, Y., and Satar, M. G. M. (2009). First report on bacterial soft rot disease on dragon fruit (*Hylocereus* spp.) caused by *Enterobacter cloacae in Peninsular Malaysia*. *Int. J. Agric. Biol.* 11, 659–666.

Matilla, M. A., Fang, X., and Salmond, G. P. (2014). Viunalikeviruses are environmentally common agents of horizontal gene transfer in pathogens and biocontrol bacteria. *ISME J.* 8, 2143–2147. doi: 10.1038/ismej.2014.150

McGhee, G. C., and Sundin, G. W. (2011). Evaluation of kasugamycin for fire blight management, effect on nontarget bacteria, and assessment of kasugamycin resistance potential in *Erwinia amylovora*. *Phytopathology* 101, 192–204. doi: 10.1094/PHYTO-04-10-0128

Muturi, P., Yu, J., Maina, A. N., Kariuki, S., Mwaura, F. B., and Wei, H. (2019). Bacteriophages isolated in China for the control of *Pectobacterium carotovorum* causing Potato Soft Rot in Kenya. *Virol. Sin.* 34, 287–294. doi: 10.1007/s12250-019-00091-97

Nagayoshi, Y., Kumagae, K., Mori, K., Tashiro, K., Nakamura, A., Fujino, Y., et al. (2016). Physiological properties and genome structure of the hyperthermophilic filamentous phage φOH3 which infects *Thermus thermophilus* HB8. *Front. Microbiol.* 7:50. doi: 10.3389/fmicb.2016.00050

Paauw, A., Caspers, M. P., Schuren, F. H., Leverstein-van Hall, M. A., Delétoile, A., Montijn, R. C., et al. (2008). Genomic diversity within the *Enterobacter cloacae* complex. *PLoS One* 3:e3018. doi: 10.1371/journal.pone.0003018

Petrov, V. M., Ratnayaka, S., Nolan, J. M., Miller, E. S., and Karam, J. D. (2010). Genomes of the T4-related bacteriophages as windows on microbial genome evolution. *Virol. J.* 7:292. doi: 10.1186/1743-422X-7-292

Pham, M. H., Sebesvari, Z., Tu, B. M., Pham, H. V., and Renaud, F. G. (2011). Pesticide pollution in agricultural areas of Northern Vietnam: case study in Hoang Liet and Minh Dai communes. *Environ. Pollut.* 159, 3344–3350. doi: 10.1016/j.envpol.2011.08.044

Plattner, M., Shneider, M. M., Arbatsky, N. P., Shashkov, A. S., Chizhov, A. O., Nazarov, S., et al. (2019). Structure and function of the branched receptor-binding complex of bacteriophage CBA120. *J. Mol. Biol.* 431, 3718–3739. doi: 10.1016/j.jmb.2019.07.022

Rossmann, S., Dees, M. W., Perminow, J., Meadow, R., and Brurberg, M. B. (2018). Soft rot *Enterobacteriaceae* are carried by a large range of insect species in potato fields. *Appl. Environ. Microbiol.* 84:e281-18. doi: 10.1128/AEM.00281-218

Sambrook, J., and Russell, D. (2001). *Molecular Cloning: A Laboratory Manual*, 3rd Edn. Harbor, CA: Cold Spring Harbor Laboratory Press.

Schattner, P., Brooks, A. N., and Lowe, T. M. (2005). The tRNAscan-SE, snoscan and snoGPS web servers for the detection of tRNAs and snoRNAs. *Nucleic Acids Res.* 33, W686–W689. doi: 10.1093/nar/gki366

Sulakvelidze, A., and Kutter, E. (2005). "Bacteriophage therapy in humans," in *Bacteriophages: Biology and Applications*, eds E. Kutter and A. Sulakvelidze (Boca Raton, FL: CRC Press), 381–436.

Thanh, D. T., Tarn, L. T. T., Hanh, N. T., Tuyen, N. H., Bharathkumar, S., Lee, S. Y., et al. (2009). Biological control of soilborne diseases on tomato, potato and black pepper by selected PGPR in the greenhouse and field in Vietnam. *Plant Pathol. J.* 25, 263–269. doi: 10.5423/PPJ.2009.25.3.263

Van Twest, R., and Kropinski, A. M. (2009). Bacteriophage enrichment from water and soil. *Methods Mol. Biol.* 501, 15–21. doi: 10.1007/978-1-60327-164-6_2

Wang, G. F., Xie, G. L., Zhu, B., Huang, J. S., Liu, B., Kawicha, P., et al. (2010). Identification and characterization of the *Enterobacter* complex causing mulberry (*Morus alba*) wilt disease in China. *Eur. J. Plant Pathol.* 126, 465–478. doi: 10.1007/s10658-009-9552-x

Wu, J., Ding, Z., Diao, Y., and Hu, Z. (2011). First report on *Enterobacter* sp. causing soft rot of Amorphophallus konjac in China. *J. Gen. Plant Pathol.* 77, 312–314. doi: 10.1007/s10327-011-0330-1

Zhao, J., Zhang, Z., Tian, C., Chen, X., Hu, L., Wei, X., et al. (2019). Characterizing the biology of lytic bacteriophage vB_EaeM_φEap-3 infecting multidrug-resistant *Enterobacter aerogenes*. *Front. Microbiol.* 10:420. doi: 10.3389/fmicb.2019.00420

Zhu, B., Wang, S., Li, O., Hussain, A., Hussain, A., Shen, J., et al. (2017). High-quality genome sequence of human pathogen *Enterobacter asburiae* type strain 1497-78T. *J. Glob. Antimicrob. Resist.* 8, 104–105. doi: 10.1016/j.jgar.2016.12.003

Conflict of Interest: The authors declare that the research was conducted in the absence of any commercial or financial relationships that could be construed as a potential conflict of interest.

Copyright © 2020 Thanh, Nagayoshi, Fujino, Iiyama, Furuya, Hiromasa, Iwamoto and Doi. This is an open-access article distributed under the terms of the Creative Commons Attribution License (CC BY). The use, distribution or reproduction in other forums is permitted, provided the original author(s) and the copyright owner(s) are credited and that the original publication in this journal is cited, in accordance with accepted academic practice. No use, distribution or reproduction is permitted which does not comply with these terms.

frontiers in Microbiology

METHODS
published: 05 June 2020
doi: 10.3389/fmicb.2020.01119

Separation of *Mycobacterium smegmatis* From a Mixed Culture Using the Cell Wall Binding Domain of D29 Mycobacteriophage Endolysin

*Gokul Nair and Vikas Jain**

Microbiology and Molecular Biology Laboratory, Department of Biological Sciences, Indian Institute of Science Education and Research, Bhopal, India

Pathological infection caused by *Mycobacterium tuberculosis* is still a major global health concern. Traditional diagnostic methods are time-consuming, less sensitive, and lack high specificity. Due to an increase in the pathogenic graph of mycobacterial infections especially in developing countries, there is an urgent requirement for a rapid, low cost, and highly sensitive diagnostic method. D29 mycobacteriophage, which is capable of infecting and killing *M. tuberculosis*, projects itself as a potential candidate for the development of novel diagnostic methods and phage therapy of mycobacterial infections. In our previous study, we showed that the cell wall binding domain [C-terminal domain (CTD)] located at the C-terminal end of the D29 mycobacteriophage LysA endolysin very selectively binds to the peptidoglycan (PG) of *Mycobacterium smegmatis* and *M. tuberculosis*. Here, by using *M. smegmatis* as model organism and by exploiting the PG binding ability of CTD, we have developed a method to isolate *M. smegmatis* cells from a mixed culture *via* magnetic separation. We show that green fluorescent protein (GFP)-tagged CTD (CTD-GFP) can bind to *M. smegmatis* cells *in vitro* after treatment with non-ionic detergent Triton X-100. Fluorescence-based assays show that CTD-GFP binding to *M. smegmatis* cells is highly specific and stable, and is not disrupted by an excess of either GFP or BSA. We further fused CTD with glutathione-S-transferase (GST) to generate CTD-GST protein and carried out an anti-GST antibody-mediated coating of CTD-GST on Dynabeads. This allowed us to perform successful magnetic separation of *M. smegmatis* from a mixed culture of bacteria having both Gram-negative and Gram-positive bacteria. Furthermore, the separated cells could be confirmed by a simple PCR. Thus our assay allows us to separate and identify *M. smegmatis* from a mixed culture.

Keywords: mycobacteria, endolysin, mycobacteriophage, phage therapy, TB diagnostic

OPEN ACCESS

Edited by:
Krishna Mohan Poluri,
Indian Institute of Technology Roorkee, India

Reviewed by:
Irene Grant,
Queen's University Belfast, United Kingdom
Maria Joao Catalao,
University of Lisbon, Portugal
Amit Mishra,
Indian Institute of Technology Jodhpur, India
Andaleeb Sajid,
Yale University, United States

***Correspondence:**
Vikas Jain
vikas@iiserb.ac.in

Specialty section:
This article was submitted to Antimicrobials, Resistance and Chemotherapy, a section of the journal Frontiers in Microbiology

Received: *16 February 2020*
Accepted: *05 May 2020*
Published: *05 June 2020*

Citation:
Nair G and Jain V (2020) Separation of Mycobacterium smegmatis From a Mixed Culture Using the Cell Wall Binding Domain of D29 Mycobacteriophage Endolysin. Front. Microbiol. 11:1119. doi: 10.3389/fmicb.2020.01119

INTRODUCTION

Despite tremendous advancement in medical and clinical biology, mycobacterial infections remain one of the major global health concerns. *Mycobacterium tuberculosis*, the bacterium that causes tuberculosis (TB), is listed among one of the highest mortality-causing infection agents, and has caused nearly 1.5 million deaths in 2018 (Harding, 2020). Non-availability of efficient, rapid, and reliable detection methods for TB is one of the major contributors to this high death index

(Caviedes et al., 2000). Most patients carrying mycobacterial infections who are diagnosed early can be cured due to recent advancements in the therapeutics (Sloan et al., 2013). Thus, the need of the hour is to have improved diagnostic methods for mycobacterial infections (McNerney et al., 2012). Currently, there are very few approved diagnostic tools available including molecular tests, smear microscopy, and culture-based tests (Liu et al., 2007; Lange and Mori, 2010). Many of these methods for mycobacterial detection fail to satisfy parameters such as accuracy, sensitivity, and reproducibility, and high throughput techniques require special expertise (De Cock et al., 2013).

Bacteriophage-based therapeutics and diagnostics have always been of interest due to their specificity toward target bacterium (Fischetti, 2008; Abedon et al., 2017). Phages are easy to culture, economic, and can be stored for long periods. Further, the host range for a given phage is narrow and is generally limited to either species or strain suggesting its highly specific nature. Due to these properties, bacteriophages are readily considered as potential tool for bacterial detection and identification (McNerney et al., 1998; Simboli et al., 2005; Schofield et al., 2012; Pohane et al., 2014).

Mycobacteriophage D29 is considered as one of the most potent mycobacteriophages with highly diverse mycobacterial host (Rybniker et al., 2006). To release phage progeny at the end of lytic cycle, the phage produces lytic proteins from its lytic cassette, which then mediate mycobacterial cell lysis by targeting cell envelope (Payne and Hatfull, 2012; Catalao and Pimentel, 2018). LysA of D29 phage lytic cassette specifically targets the peptidoglycan (PG) layer of mycobacterial cell envelope, and therefore plays a crucial role in host cell lysis (Payne and Hatfull, 2012; Pohane et al., 2014; Catalao and Pimentel, 2018). We have previously shown that D29 LysA is a multidomain structure having an N-terminal catalytic domain (NTD), lysozyme like domain (LD), and a C-terminal domain (CTD) that specifically binds to the mycobacterial cell wall PG (Pohane et al., 2014). Thus, CTD plays a crucial role in anchoring LysA to the PG layer thereby mediating its successful degradation and ultimately resulting in mycobacterial cell lysis.

Since PG is one of the major components of mycobacterial cell envelope, it acts as a novel target for the development of rapid and sensitive mycobacteria detection assay. We have previously shown that the CTD binds very specifically to both *Mycobacterium smegmatis* and *M. tuberculosis* PG, but does not bind to the PG of other bacteria (Pohane et al., 2014). Here we have developed a method wherein we use an engineered CTD protein to isolate and identify *M. smegmatis* from a mixed bacterial culture.

METHODS

Bacterial Strains, Media, and Growth Conditions

Escherichia coli strain XL1-Blue (Stratagene) was used for all cloning experiments, and strain BL21(DE3) (Novagen) was used for protein expression and purification. *Mycobacterium smegmatis* mc^{2}155 was grown in Middlebrook 7H9 medium (Difco) supplemented with 2% glucose, 0.05% Tween 80 at 37°C with constant shaking at 200 r/min. *E. coli* MG1665, XL1-Blue, BL21(DE3), and *Bacillus subtilis* cells were cultured in LB broth (Difco) at 37°C with constant shaking at 200 r/min. Wherever required, medium was supplemented with 100 μg/ml ampicillin. For solid medium culture, 1.5% agar was added to the growth medium while excluding Tween 80.

Molecular Cloning

The plasmids used in this study are listed in **Table 1**. Oligonucleotides used in various PCR reactions are given in **Table 2**. Glutathione-S-transferase (GST) tag was added at the C-terminus of CTD by PCR amplifying CTD gene from pETGP10CTD using the oligonucleotides listed in **Table 2**, digesting the amplicon with *Eco*RI and *Bam*HI, and ligating it in pGEX-4T-2 vector at the same sites to yield pGEXCTD-GST.

Expression and Purification of Proteins

Plasmids pETGP10CTD and pETGP10CTD-GFP were used to express and purify CTD and CTD tagged with green fluorescent protein (CTD-GFP), respectively, as described previously (Pohane et al., 2014). For the purification of GST tagged-CTD (CTD-GST), *E. coli* BL21(DE3) carrying pGEXCTD-GST was cultured at 37°C with constant shaking at 200 r/min until the optical density of the culture at 600 nm (OD_{600}) reached ∼0.6. The cells were then induced with 0.3 mM IPTG, and further incubated at 22°C with constant shaking at 150 r/min for 8 h. Cells were then harvested and resuspended in lysis buffer (40 mM Tris-Cl, pH 8.0, 400 mM NaCl, 5 mM 2-mercaptoethanol) and lyzed by sonication. The lysate was clarified by centrifugation at 18,000 r/min at 4°C for 1 h, and the supernatant was incubated with pre-equilibrated Glutathione Sepharose 4 Fast Flow matrix for 2 h. The matrix was washed with buffer containing 40 mM Tris-Cl, pH 8.0, 500 mM NaCl, 100 μM reduced L-glutathione, and 5 mM 2-mercaptoethanol. The protein was then eluted using a buffer containing 40 mM Tris-Cl pH 8.0, 200 mM NaCl, 10 mM reduced L-glutathione, and 5 mM 2-mercaptoethanol. The elution having ample amount of protein was subjected to dialysis in a buffer having 40 mM Tris-Cl pH 8.0, 200 mM NaCl, 1 mM dithiothreitol, and 40% glycerol. The protein was collected, centrifuged at 14,000 r/min for 15 min at 4°C, and analyzed on SDS-PAGE. The supernatant was stored at −20°C until further use.

Mixed Bacterial Sample Preparation and Protein Binding Assays

Different test samples for assay were prepared to have different combinations of *M. smegmatis* mc^{2}155, *E. coli* MG1665, and

TABLE 1 | List of plasmids used in the present study.

Plasmid	Protein	Oligonucleotide	Template
[1]pETGP10CTD	CTD		
[1]pETGP10CTD-GFP	CTD-GFP		
pGEXCTD-GST	CTD-GST	CTD_GFP_GST_for CTD_GST_Rev	pETGP10CTD

The oligonucleotides and the template that were used to generate the respective clones are also mentioned. [1]Source: Laboratory stock (Pohane et al., 2014).

TABLE 2 | List of oligonucleotides used in the present study.

Oligonucleotide	Sequence (5′–3′)	Purpose
CTD_GFP_GST_for	CCAGAGGATCCGGCGACCAACTACTGACTC	Cloning of
CTD_GST_rev	GGTGGAATTCTTGCGGCCGCTAGGGCTCCTGG	CTD-GST
mnoRTfor	TCTGCTTGTTGGTGGACTTG	Detection of *M. smegmatis*
mnoRTrev	GTCGAACCCCAAGGACTACA	by PCR
LacZ_gn_for	GCTGGAGTGACGGCAGTTATCTGGAAG	Detection of *E. coli*
LacZ_gn_rev	CAGAAACTGTTACCCGTAGGTAGTCACG	by PCR
rpoB_BS_gn_for	CCAAGGTACGTGCTACAACCAGCGTC	Detection of *B. subtilis*
rpoB_BS_gn_rev	CCTCATAGTTGTAGCCATCCCACGTC	by PCR

Underlined sequences represent the restriction enzyme site.

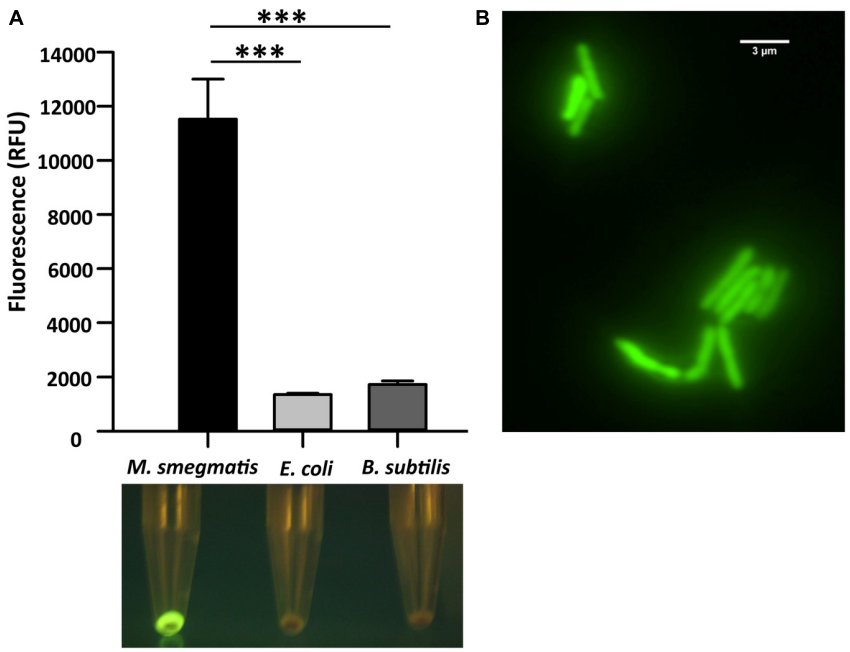

FIGURE 1 | Cell binding assay of CTD-GFP with different bacterial cells. **(A)** The relative fluorescence obtained for CTD-GFP bound to *M. smegmatis*, *E. coli*, and *B. subtilis* cells. Fluorescence was measured by keeping the excitation and emission wavelengths at 488 and 509 nm, respectively. The data represent an average of three experiments with error bars denoting the standard deviation (*p*-value analysis: ***, < 0.0003). The bottom panel shows the image of fluorescing cell pellet obtained after illuminating it with a blue light (~470 nm) source. **(B)** Fluorescence microscopy imaging of CTD-GFP bound *M. smegmatis* cells. The image was taken on a Leica Microsystems fluorescence microscope with a GFP filter.

B. subtilis cells. All the bacteria were individually grown till OD_{600} reached ~0.6, and normalized according to the requirement of the number of cells with respect to experimental setup. The samples were harvested by centrifugation at 8000 r/min at room temperature. The cell pellet was resuspended in 1 ml of binding buffer (25 mM Tris-Cl, pH 8.0, 200 mM NaCl) containing 1% Triton X-100 and incubated at 37°C with constant shaking at 800 r/min using a thermomixer (Eppendorf) for 2 h. Cells were again harvested by centrifugation and resuspended in binding buffer having 0.05% Triton X-100. Resulting cell suspension was then used in the protein binding assays by incubating various bacterial cells with 5 µg of various proteins (CTD, CTD-GFP, GFP, BSA). The proteins were allowed to bind to the cells by constant mixing at 800 r/min at 37°C for 2 h. Cells were harvested post-incubation by centrifugation and washed twice with binding buffer. For fluorescence microscopy, cells were serially diluted, added to an agarose pad (prepared by dissolving 0.5% agarose in TAE buffer and spreading it over a glass slide in the form of pad), and imaged on a fluorescence microscope (Leica DM 2500) under 100X objective with GFP filter. Alternatively, the cell pellet was either resuspended in binding buffer devoid of Triton X-100 for fluorescence measurements or resuspended in binding buffer with 0.05% Triton X-100 to carry out competition assays. 200 µl of the suspension devoid of Triton X-100 was subjected to fluorescence measurement on Spectramax M5 (Molecular Devices). For performing competition experiments, cells were incubated with 20 µg of the competitor protein with constant mixing at 800 r/min at 37°C for 2 h. Cells were again harvested post-incubation by centrifugation and washed twice with binding buffer devoid of Triton X-100, and were used for

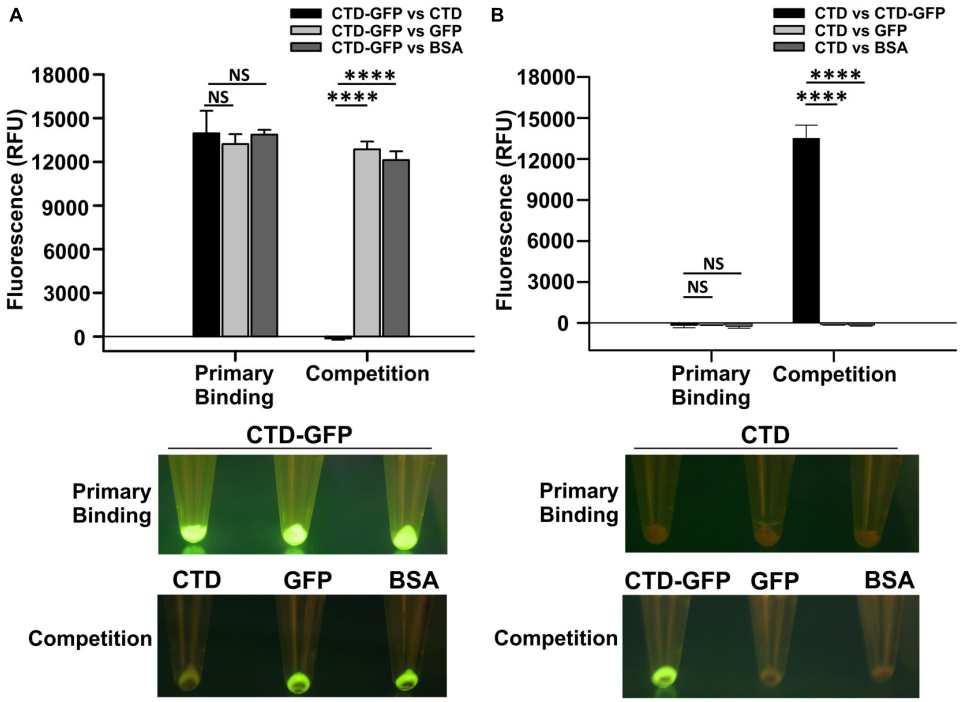

FIGURE 2 | Qualitative and quantitative assessment of CTD binding to *M. smegmatis* cells. **(A)** The relative fluorescence obtained for *M. smegmatis* cells bound to CTD-GFP before (Primary binding) and after competitor addition (Competition). Competitors used are CTD, GFP, and BSA. **(B)** The relative fluorescence obtained for *M. smegmatis* cells bound to CTD before (Primary binding) and after competitor addition (Competition). Competitors used are CTD-GFP, GFP, and BSA. In both **A** and **B**, the data represent an average of three independent experiments with error bars denoting the standard deviation (*p*-value analysis: ****, < 0.0001; NS, not significant). In both **A** and **B**, the bottom panels show the image of fluorescing cell pellet obtained after illuminating it with a blue light (∼470 nm) source before and after the competition.

fluorescence measurements. Additionally, the cell pellet present in the tube was imaged by using a digital camera (Canon) and an amber filter while the tube was illuminated using a blue light transilluminator (∼470 nm).

Magnetic Separation of *M. smegmatis* Cell

Purified CTD-GST protein was used for the *M. smegmatis* cell separation. Dynabeads M-270 Epoxy beads (10 mg) were coupled with the anti-GST monoclonal antibody (Thermo Fisher Scientific) using antibody coupling kit (Thermo Fisher Scientific) following manufacturer's instructions to obtain a final bead concentration of 10 mg/ml. Anti-GST antibody-coupled Dynabeads were next equilibrated in binding buffer before protein coating. Equilibrated beads were incubated with 200 μg CTD-GST protein at 4°C overnight with gentle rotation thus allowing the protein to have efficient interaction with the antibody. The CTD-GST bound Dynabeads were equilibrated in binding buffer and eluted with final volume of 0.5 ml. The bead-protein complex (20 μl) was mixed with bacterial suspension containing *M. smegmatis* in combination with *E. coli and B. subtilis* as prepared above, and the mixture was incubated at 37°C with constant shaking at 800 r/min for 2 h. Next, the mixture was subjected to magnetic separation on a magnet bar (Thermo Fisher Scientific) by following manufacturer's instructions, and the supernatant was collected. The magnetically separated sample was either directly used in PCR or was subjected to competition with CTD-GST protein in order to dissociate the *M. smegmatis* cells bound to Dynabeads, and the eluted cells were then subjected to PCR confirmation. PCR was carried out using Phusion enzyme (Thermo Fisher Scientific) and the oligonucleotides specific for the bacterium (**Table 2**). The amplicons were separated on agarose gel and imaged.

RESULTS

We have previously shown that CTD protein has specific PG binding property for mycobacterial PG (Pohane et al., 2014), which is one of the major components of the mycobacterial cell envelope. Here, we have explored the possibility of CTD to selectively bind to *M. smegmatis* cells directly in order to use this assay as a separation method for *M. smegmatis* cells from a mixed culture.

C-Terminal Domain of LysA Binds to *M. smegmatis* Cells

We first analyzed the *in vitro* binding of CTD of LysA specifically to *M. smegmatis* cells by constructing a GFP-tagged CTD protein. Here, GFP and hexa-histidine tag were added in tandem at the C-terminal of CTD. The recombinant

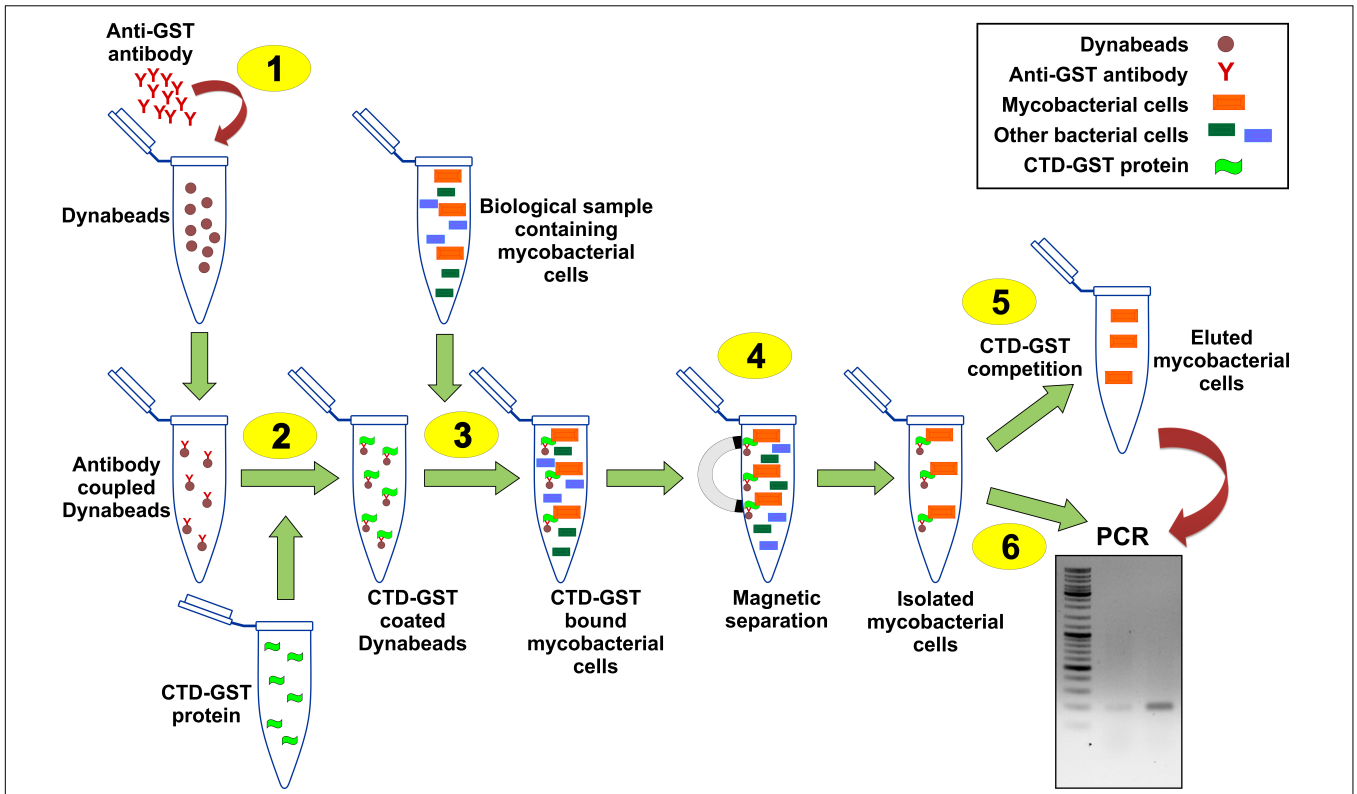

FIGURE 3 | Schematic of CTD-based mycobacterial detection assay. Illustration here shows the general procedure for the isolation of *M. smegmatis* cells present in a given biological sample. 1–6 represent the key steps in the assay as detailed in "Methods" section. Step 1 is the coupling of anti-GST antibodies with Dynabeads. CTD-GST protein is then coated on these beads (Step 2). Step 3 involves the incubation of mixed bacterial sample having *M. smegmatis* cells with the product of step 2. Step 4 involves magnetic separation of the Dynabeads that pulls down *M. smegmatis* cells. The isolated cells can either be eluted by competition with CTD-GST (Step 5) or be used directly in a PCR (Step 6).

protein was purified (**Supplementary Figure S1**), and was used for the *in vitro* binding assays. The purified protein was incubated with *M. smegmatis*, *E. coli*, and *B. subtilis*. The fluorescence of the GFP tag associated with CTD was visualized using a blue light transilluminator and also quantified on Spectramax M5 (Molecular Devices). Our data show that maximum fluorescence of CTD-GFP is obtained in the case of *M. smegmatis* only, whereas negligible fluorescence is observed from the other two bacteria (**Figure 1A**). The bacterial samples and CTD-GFP ratio in each case was kept constant to avoid any bias. We further examined CTD-GFP binding to *M. smegmatis* under the fluorescence microscope. The microscopic images demonstrate clear localization of GFP throughout *M. smegmatis* envelope (**Figure 1B**). Taken together, our data suggest that CTD-GFP is able to interact with intact *M. smegmatis* cells.

CTD–*M. smegmatis* Cell Interaction Is Highly Specific and Stable

Since CTD-GFP readily interacts with *M. smegmatis* cells, we asked if this interaction is both specific and stable. We, therefore, challenged the CTD-GFP–*M. smegmatis* cell interaction with non-specific competitors GFP and BSA as well as specific competitor CTD protein devoid of GFP (**Supplementary Figure S1**). First, cell binding assay was performed with *M. smegmatis* cells as a substrate and CTD-GFP protein as binding partner. Fluorescence of CTD-GFP-bound *M. smegmatis* cells were measured after multiple washes with binding buffer (**Figure 2A**). Next, the CTD-GFP protein bound to *M. smegmatis* cells was challenged with higher amounts of competitors, *viz.*, CTD, GFP, and BSA proteins. Relative fluorescence measurements clearly show a significant decrease in fluorescence when the binding reaction was challenged with CTD, which is in sharp contrast with other two competitor proteins (**Figure 2A**). This competition was also clearly visible when the cells were illuminated on a blue light transilluminator to observe GFP fluorescence (**Figure 2A**). Only the cell pellet where the CTD-GFP was competed out with CTD did not show any fluorescence suggesting the complete displacement of CTD-GFP with CTD.

The above experiment was also attempted in reverse order also to rule out the possibility of GFP binding non-specifically to *M. smegmatis* cells. Here, we first incubated *M. smegmatis* cells with GFP-less CTD, and then challenged the interaction with CTD-GFP, GFP, or BSA. Our data show that only CTD-GFP was able to compete out CTD bound to *M. smegmatis* cells, thus resulting in a significant increase in relative fluorescence;

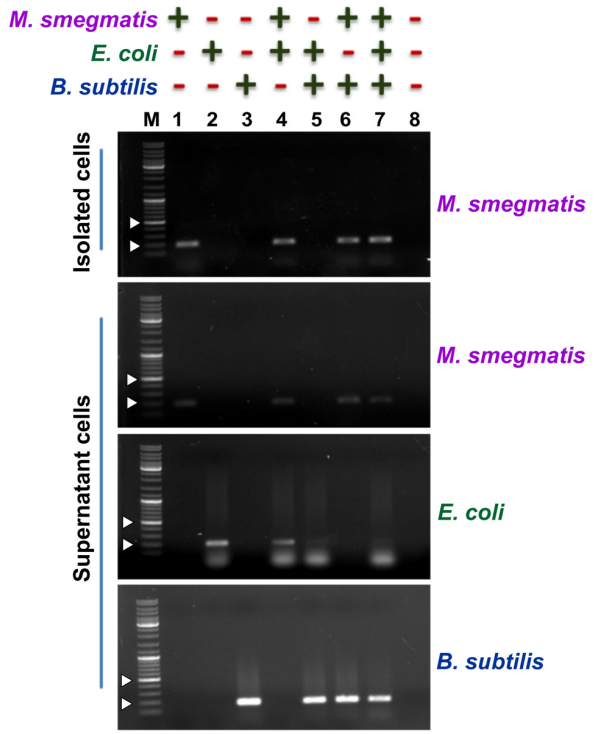

FIGURE 4 | Detection of the presence of bacteria after magnetic separation from mix-samples. The assay was carried out with a bacterial sample having presence (+) or absence (–) of *M. smegmatis*, *E. coli*, and *B. subtilis* as indicated. Agarose gels show the PCR amplicon obtained after carrying out PCR with either the pulled-down cells or the cells present in the supernatant after magnetic separation. Lanes 1–8 represent all the different combinations of samples. PCR was performed using *mno* gene primer for *M. smeg*matis, *lacZ* gene primer for *E. coli*, and *rpoB* gene primer for *B. subtilis*. Obtained amplicon sizes are 188 bp for *mno*, 210 bp for *lacZ*, and 161 bp for *rpoB*. "M" represents the DNA ladder with two bands of 200 and 500 bp marked with white arrowheads.

GFP was unable to show this phenomenon and therefore, no fluorescence was observed in this case when subjected to blue light illumination (**Figure 2B**). This observation was also corroborated by the imaging of cell pellets treated with CTD and competitors; here, only the cell pellet with CTD-GFP as competitor showed fluorescence. These data additionally suggest that GFP does not interact with *M. smegmatis* cells. Taken together, our data show that CTD has a high affinity toward, and shows stable *in vitro* interaction with, *M. smegmatis* cells.

Designing and Validation of CTD-Based *M. smegmatis* Detection Assay

Figure 3 shows the schematic of the *M. smegmatis* cell separation and detection. To develop this assay, we generated CTD-GST protein construct, and used the purified protein (**Supplementary Figure S1**) in our experiments. Because of their magnetic property, Dynabeads were used in this method. These beads were coupled with anti-GST monoclonal antibody by chemical conjugation. The antibody-coupled Dynabeads were first incubated with CTD-GST protein, and, then the protein coated beads were mixed with a bacterial suspension containing *M. smegmatis* cells. The bacterial cells could then be readily separated by using a magnet bar. Here, centrifugation is avoided as that will result in the sedimentation of all the cells, whereas magnetic separation allows the separation of only CTD-GST-bound cells. *M. smegmatis* cells thus isolated were confirmed by PCR. As a proof of concept, by using a bacterial suspension containing other bacteria besides *M. smegmatis*, we demonstrate that the method developed here is applicable to mixed culture as well.

Next, to assess the ability of the designed assay to selectively capture *M. smegmatis* cells, we used *M. smegmatis* cell suspension containing other Gram-positive and Gram-negative bacteria (**Figure 4**). In all, we prepared eight different cell suspensions having one or more of the following three bacteria—*M. smegmatis*, *E. coli*, and *B. subtilis*. Here, $\sim 10^4$ CFU/ml *M. smegmatis* cells were mixed with an equal proportion of *B. subtilis* and/or *E. coli* cells resulting in an equal final ratio of all bacterial cell types in the sample. All the samples were processed through the designed assay (**Figure 3**). Additionally, all the conditions were kept the same for all the samples to avoid any biasness. The eluted fraction after magnetic separation and the supernatant fraction from all the samples were subjected to PCR using bacteria-specific oligonucleotides. Our data show that out of the eight different combinations of bacterial samples, an amplicon with *M. smegmatis* specific oligonucleotides is observed only in the samples containing *M. smegmatis* cells (**Figure 4**). This immediately suggests a successful capture of *M. smegmatis* cells from a mixture having different combination of *M. smegmatis*, *E. coli*, and *B. subtilis*. Moreover, in the separated cells, the other bacteria could not be detected, which immediately suggests that the developed method is very specific. The supernatant obtained after magnetic separation was also harvested and subjected to PCR confirmation with primers specific for *M. smegmatis*, *E. coli*, and *B. subtilis*. In all the cases, the presence of the PCR amplicon on agarose gel clearly indicates and validates the presence of respective bacterium in the sample. Thus, the PCR confirmation of the presence of all bacteria before magnetic separation and the detection of only *M. smegmatis* cells post-magnetic separation clearly demonstrate a successful separation of only *M. smegmatis* cells from the samples having a mixture of bacteria.

Evaluating the Capability of Designed Detection Assay

Since GFP fluorescence can be easily quantified, we used CTD-GFP protein to assess the presence of varied amount of *M. smegmatis* cells in different samples. We incubated different amount of *M. smegmatis* cells with CTD-GFP, and assessed protein binding by measuring the fluorescence after extensive washing of the cell pellet. Our data show a significant fluorescence with samples having 1.1×10^3 CFU/ml *M. smegmatis* cells (**Figure 5A**); with an increase in number of cells, a significant increase in fluorescence is also observed (**Figure 5A**), which indicates that CTD-GFP can be useful as a potential reporter for the varying levels of *M. smegmatis* cells. We next estimated

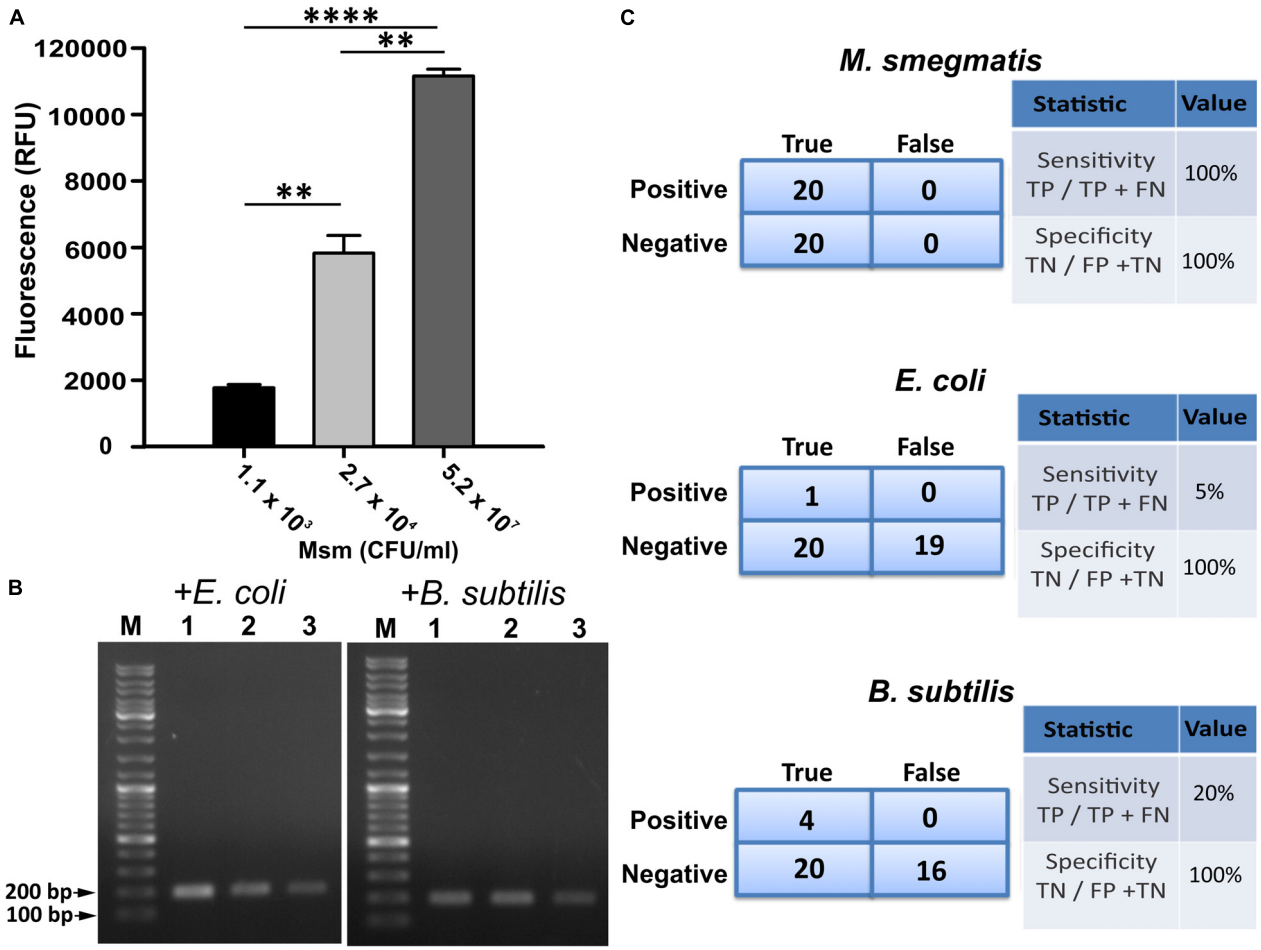

FIGURE 5 | Evaluation of efficiency of designed *M. smegmatis* detection assay. **(A)** CTD-GFP was used for differential quantitative assessment of the presence of *M. smegmatis* in bacterial samples carrying a mixture of varying amount of *M. smegmatis* cells spiked with *E. coli* and *B. subtilis*. *x*-axis represents the CFU/ml of *M. smegmatis* (Msm) present in the sample for assay and *y*-axis represents fluorescence obtained due to CTD-GFP binding to *M. smegmatis* cells (*P*-value analysis: ****, < 0.0001; **, < 0.0002). **(B)** Limit of detection of designed assay analyzed with minimal level of *M. smegmatis* spiked with either *E. coli* or *B. subtilis* as depicted above agarose gel images. Shown are the amplicons obtained by PCR carried out using *mno* gene primer. Lanes 1, 2, and 3 represent 1.1 × 10^3, 2.7 × 10^4, and 5.2 × 10^7 CFU/ml of *M. smegmatis* cells, respectively, present in the samples. "M" represents the DNA ladder with two bands marked. **(C)** Statistical analysis of the specificity and the sensitivity of the detection of *M. smegmatis*, *E. coli*, and *B. subtilis*, as depicted. Experiments were performed multiple times to obtain statistically significant data. "TP," "TN," "FP," and "FN" represent true positive, true negative, false positive, and false negative, respectively.

the efficiency of our assay using the limit of detection as one of the parameters by analyzing the minimum number of cells that can be detected. Samples carrying different amounts of *M. smegmatis* cells mixed with either *E. coli* or *B. subtilis* were subjected to our designed assay, and the presence of *M. smegmatis* cells was confirmed by PCR. Our data show that *M. smegmatis* could be detected in the bacterial samples carrying as low as 1.1 × 10^3 CFU/ml (**Figure 5B**). We thus conclude that our designed assay has a limit of detection in range of 10^3 *M. smegmatis* cells. We wish to add here that previous studies of mycobacterial detection assay suggest a detection limit of *M. tuberculosis* in the range of 10^5 CFU/ml to be considered as significant (Park et al., 2009). Thus, our detection limit of 10^3 CFU/ml in a mixed bacterial culture can be considered as very significant. **Figure 5C** presents the statistical analysis of the sensitivity and specificity of our assay in laboratory conditions. We find that out of the 20 samples analyzed, our assay shows 100% sensitivity and specificity toward *M. smegmatis* in comparison with *E. coli* and *B. subtilis*.

DISCUSSION

Rapid diagnosis of mycobacterial infections such as TB will significantly reduce the disease burden. Several classical and contemporary approaches are being used clinically to detect mycobacterial infections such as smear microscopy, culture identification, histopathology, tuberculin skin test (TST), serological assays, interferon-gamma release assays (IGRAs), and nucleic acid amplification (NAA) tests (Liu et al., 2007; Lange and Mori, 2010). Smear microscopy, although is one of the commonly used methods, has drawbacks owing to low

and variable sensitivity. Similarly, culture identification is time-consuming with a turn-around time of 2–10 weeks (Padmavathy et al., 2003; Haldar et al., 2011; Derese et al., 2012). On the other hand, tissue samples analysis for mycobacterial infection using histopathological approach depends on the presence of granulomatous inflammation and caseous necrosis, and is therefore difficult and suffers from handling error with significant variability (Bravo and Gotuzzo, 2007; Haldar et al., 2011).

PCR-based approaches are considered to be one of the most accurate ways to detect mycobacteria. Not only does it shorten the turn-around time, automation of the procedure also reduces handling error and allows for the differentiation between different types of mycobacterial infections due to availability of novel marker genes for different mycobacterial strains and species (Katoch, 2004). The biggest limitation of the PCR-based approach is the signal to noise ratio in pathological samples, and may lead to a reaction failure if a minimum threshold level of mycobacterial genomic DNA is unavailable in the sample.

Mycobacteriophages, due to their highly specific interaction with mycobacterial host, can be developed as both next-generation therapeutics and diagnostic tools. We and others have previously reported that the cell wall binding domain present in the endolysin protein produced by the phages shows high specificity toward host bacterial cell wall (Kretzer et al., 2007; Schmelcher et al., 2010; Pohane et al., 2014; Yu et al., 2016). Indeed, CBD construct of phage tagged with various reporter proteins such as green, blue, yellow, cyan, and red fluorescent protein have been used to demonstrate its ability to differentiate *Listeria* strains via microscopy (Schmelcher et al., 2010). Similarly unique properties of the CBDs to bind and immobilize *Listeria* cells have been used to recover *Listeria* cells from samples by coating them on paramagnetic beads (Kretzer et al., 2007). In the present study, we have utilized the PG-binding ability of the C-terminal cell wall binding domain of D29 mycobacteriophage LysA to isolate *M. smegmatis cells* from mixed bacterial culture.

We show that the interaction between CTD and *M. smegmatis* cells is highly stable, efficient, and specific. Owing to the presence of outer mycolic acid layer, it was important to carry out Triton X-100 treatment in order to allow CTD to bind directly to *M. smegmatis* cells. We further engineered variants of CTD carrying either GFP or GST that enabled us to exploit its *M. smegmatis* cell wall binding property to develop efficient cell separation and detection assay. For example, our GFP-tagged protein allowed us to visualize *M. smegmatis* directly under a fluorescence microscope. Here, the quantification of GFP fluorescence also suggests that low number of cells can be detected in our assay. We wish to add here that Triton X-100 treatment is essential for the CTD to bind to *M. smegmatis* cells; without Triton X-100 treatment, CTD does not bind *M. smegmatis* (data not shown). To the best of our knowledge, such treatment to directly access the cell wall PG of *M. smegmatis* cell has not been carried out before.

We also generated a GST-tagged CTD protein, which was coated on the Dynabeads by means of anti-GST antibodies. The antibodies against CTD protein were avoided since they will likely interfere in the binding of CTD to the cell wall. Dynabeads can be extracted from the bulk material by magnetic separation. It is this property of Dynabeads that allowed us to capture *M. smegmatis* cells from a suspension containing more than one bacterium. Additionally, CTD-GST-coated Dynabeads can also be stored at 4°C for future use, and are not required to be prepared fresh before every use, thus saving time. *M. smegmatis* after magnetic separation was verified by PCR with primers specific for mycobacterial gene. Very importantly, this method enables us to overcome the major drawback of the PCR-based detection method as discussed above. Thus using CTD, we were able to successfully capture *M. smegmatis* cells from test samples. The designed assay shows 100% sensitivity and specificity toward *M. smegmatis* in comparison with *E. coli* and *B. subtilis*. We have included PCR in this assay as a final confirmation/identification step. Since CTD binds to the *M. tuberculosis* PG also (Pohane et al., 2014), it is worth testing of this designed assay against *M. tuberculosis* and other mycobacterial species to unravel its specificity.

DATA AVAILABILITY STATEMENT

All datasets generated for this study are included in the article/**Supplementary Material**.

AUTHOR CONTRIBUTIONS

VJ conceived the idea. GN and VJ designed the research, analyzed the data, and wrote the manuscript. GN performed the experiments.

FUNDING

This work was supported by the intramural funds from IISER Bhopal to VJ. Funders had no role in the designing of research and the manuscript writing and communication.

ACKNOWLEDGMENTS

GN thanks IISER Bhopal for the senior research fellowship.

SUPPLEMENTARY MATERIAL

The Supplementary Material for this article can be found online at: https://www.frontiersin.org/articles/10.3389/fmicb.2020.01119/full#supplementary-material

FIGURE S1 | SDS-PAGE profiles of the purified recombinant proteins. Panels show the purified CTD, CTD-GFP, and CTD-GST proteins. In each gel, L represents the molecular weight marker with few bands marked.

REFERENCES

Abedon, S. T., Garcia, P., Mullany, P., and Aminov, R. (2017). Editorial: phage therapy: past, present and future. *Front. Microbiol.* 8:981. doi: 10.3389/fmicb.2017.00981

Bravo, F. G., and Gotuzzo, E. (2007). Cutaneous tuberculosis. *Clin. Dermatol.* 25, 173–180.

Catalao, M. J., and Pimentel, M. (2018). Mycobacteriophage lysis enzymes: targeting the mycobacterial cell envelope. *Viruses* 10:428. doi: 10.3390/v10080428

Caviedes, L., Lee, T. S., Gilman, R. H., Sheen, P., Spellman, E., Lee, E. H., et al. (2000). Rapid, efficient detection and drug susceptibility testing of *Mycobacterium tuberculosis* in sputum by microscopic observation of broth cultures. The tuberculosis working group in Peru. *J. Clin. Microbiol.* 38, 1203–1208.

De Cock, K. M., Simone, P. M., Davison, V., and Slutsker, L. (2013). The new global health. *Emerg. Infect. Dis.* 19, 1192–1197. doi: 10.3201/eid1908.130121

Derese, Y., Hailu, E., Assefa, T., Bekele, Y., Mihret, A., Aseffa, A., et al. (2012). Comparison of PCR with standard culture of fine needle aspiration samples in the diagnosis of tuberculosis lymphadenitis. *J. Infect. Dev. Ctries.* 6, 53–57. doi: 10.3855/jidc.2050

Fischetti, V. A. (2008). Bacteriophage lysins as effective antibacterials. *Curr. Opin. Microbiol.* 11, 393–400. doi: 10.1016/j.mib.2008.09.012

Haldar, S., Bose, M., Chakrabarti, P., Daginawala, H. F., Harinath, B. C., Kashyap, R. S., et al. (2011). Improved laboratory diagnosis of tuberculosis–the Indian experience. *Tuberculosis* 91, 414–426. doi: 10.1016/j.tube.2011.06.003

Harding, E. (2020). WHO global progress report on tuberculosis elimination. *Lancet Respir. Med.* 8:19. doi: 10.1016/S2213-2600(19)30418-7

Katoch, V. M. (2004). Newer diagnostic techniques for tuberculosis. *Indian J. Med. Res.* 120, 418–428.

Kretzer, J. W., Lehmann, R., Schmelcher, M., Banz, M., Kim, K. P., Korn, C., et al. (2007). Use of high-affinity cell wall-binding domains of bacteriophage endolysins for immobilization and separation of bacterial cells. *Appl. Environ. Microbiol.* 73, 1992–2000. doi: 10.1128/AEM.02402-06

Lange, C., and Mori, T. (2010). Advances in the diagnosis of tuberculosis. *Respirology* 15, 220–240.

Liu, K. T., Su, W. J., and Perng, R. P. (2007). Clinical utility of polymerase chain reaction for diagnosis of smear-negative pleural tuberculosis. *J. Chin. Med. Assoc.* 70, 148–151; discussion 146–147. doi: 10.1016/S1726-4901(09)70348-X

McNerney, R., Maeurer, M., Abubakar, I., Marais, B., McHugh, T. D., Ford, N., et al. (2012). Tuberculosis diagnostics and biomarkers: needs, challenges, recent advances, and opportunities. *J. Infect. Dis.* 205(Suppl. 2), S147–S158. doi: 10.1093/infdis/jir860

McNerney, R., Wilson, S. M., Sidhu, A. M., Harley, V. S., al Suwaidi, Z., Nye, P. M., et al. (1998). Inactivation of mycobacteriophage D29 using ferrous ammonium sulphate as a tool for the detection of viable *Mycobacterium smegmatis* and *M. tuberculosis*. *Res. Microbiol* 149, 487–495. doi: 10.1016/s0923-2508(98)80003-x

Padmavathy, L., Rao, L., and Veliath, A. (2003). Utility of polymerase chain reaction as a diagnostic tool in cutaneous tuberculosis. *Indian J. Dermatol. Venereol. Leprol.* 69, 214–216.

Park, M. Y., Kim, Y. J., Hwang, S. H., Kim, H. H., Lee, E. Y., Jeong, S. H., et al. (2009). Evaluation of an immunochromatographic assay kit for rapid identification of *Mycobacterium tuberculosis* complex in clinical isolates. *J. Clin. Microbiol.* 47, 481–484. doi: 10.1128/JCM.01253-08

Payne, K. M., and Hatfull, G. F. (2012). Mycobacteriophage endolysins: diverse and modular enzymes with multiple catalytic activities. *PLoS One* 7:e34052. doi: 10.1371/journal.pone.0034052

Pohane, A. A., Joshi, H., and Jain, V. (2014). Molecular dissection of phage endolysin: an interdomain interaction confers host specificity in Lysin A of *Mycobacterium* phage D29. *J. Biol. Chem.* 289, 12085–12095. doi: 10.1074/jbc.M113.529594

Rybniker, J., Kramme, S., and Small, P. L. (2006). Host range of 14 mycobacteriophages in *Mycobacterium ulcerans* and seven other mycobacteria including *Mycobacterium tuberculosis*–application for identification and susceptibility testing. *J. Med. Microbiol.* 55, 37–42. doi: 10.1099/jmm.0.46238-0

Schmelcher, M., Shabarova, T., Eugster, M. R., Eichenseher, F., Tchang, V. S., Banz, M., et al. (2010). Rapid multiplex detection and differentiation of Listeria cells by use of fluorescent phage endolysin cell wall binding domains. *Appl. Environ. Microbiol.* 76, 5745–5756. doi: 10.1128/AEM.00801-10

Schofield, D. A., Sharp, N. J., and Westwater, C. (2012). Phage-based platforms for the clinical detection of human bacterial pathogens. *Bacteriophage* 2, 105–283. doi: 10.4161/bact.19274

Simboli, N., Takiff, H., McNerney, R., Lopez, B., Martin, A., Palomino, J. C., et al. (2005). In-house phage amplification assay is a sound alternative for detecting rifampin-resistant *Mycobacterium tuberculosis* in low-resource settings. *Antimicrob. Agents Chemother.* 49, 425–427. doi: 10.1128/AAC.49.1.425-427.2005

Sloan, D. J., Davies, G. R., and Khoo, S. H. (2013). Recent advances in tuberculosis: new drugs and treatment regimens. *Curr. Respir. Med. Rev.* 9, 200–210. doi: 10.2174/1573398x113099990017

Yu, J., Zhang, Y., Li, H., Yang, H., and Wei, H. (2016). Sensitive and rapid detection of *Staphylococcus aureus* in milk via cell binding domain of lysin. *Biosens. Bioelectron.* 77, 366–371. doi: 10.1016/j.bios.2015.09.058

Conflict of Interest: The authors declare that the research was conducted in the absence of any commercial or financial relationships that could be construed as a potential conflict of interest.

Copyright © 2020 Nair and Jain. This is an open-access article distributed under the terms of the Creative Commons Attribution License (CC BY). The use, distribution or reproduction in other forums is permitted, provided the original author(s) and the copyright owner(s) are credited and that the original publication in this journal is cited, in accordance with accepted academic practice. No use, distribution or reproduction is permitted which does not comply with these terms.

frontiers in Microbiology

ORIGINAL RESEARCH
published: 24 June 2020
doi: 10.3389/fmicb.2020.01358

Characterization of Novel Broad-Host-Range Bacteriophage DLP3 Specific to *Stenotrophomonas maltophilia* as a Potential Therapeutic Agent

*Danielle L. Peters, Jaclyn G. McCutcheon and Jonathan J. Dennis**

Department of Biological Sciences, Faculty of Science, University of Alberta, Edmonton, AB, Canada

A novel *Siphoviridae* phage specific to the bacterial species *Stenotrophomonas maltophilia* was isolated from a pristine soil sample and characterized as a second member of the newly established *Delepquintavirus* genus. Phage DLP3 possesses one of the broadest host ranges of any *S. maltophilia* phage yet characterized, infecting 22 of 29 *S. maltophilia* strains. DLP3 has a genome size of 96,852 bp and a G+C content of 58.4%, which is significantly lower than *S. maltophilia* host strain D1571 (G+C content of 66.9%). The DLP3 genome encodes 153 coding domain sequences covering 95% of the genome, including five tRNA genes with different specificities. The DLP3 lysogen exhibits a growth rate increase during the exponential phase of growth as compared to the wild type strain. DLP3 also encodes a functional erythromycin resistance protein, causing lysogenic conversion of the host D1571 strain. Although a temperate phage, DLP3 demonstrates excellent therapeutic potential because it exhibits a broad host range, infects host cells through the *S. maltophilia* type IV pilus, and exhibits lytic activity *in vivo*. Undesirable traits, such as its temperate lifecycle, can be eliminated using genetic techniques to produce a modified phage useful in the treatment of *S. maltophilia* bacterial infections.

Keywords: *Stenotrophomonas*, bacteriophage, phage, phage therapy, antimicrobial resistance

OPEN ACCESS

Edited by:
Sutthirat Sitthisak, Naresuan University, Thailand

Reviewed by:
Kitiya Vongkamjan, Prince of Songkla University, Thailand
Antonia Sagona, University of Warwick, United Kingdom

***Correspondence:**
Jonathan J. Dennis
jon.dennis@ualberta.ca

Specialty section:
This article was submitted to Antimicrobials, Resistance and Chemotherapy, a section of the journal Frontiers in Microbiology

Received: *25 February 2020*
Accepted: *27 May 2020*
Published: *24 June 2020*

Citation:
Peters DL, McCutcheon JG and Dennis JJ (2020) Characterization of Novel Broad-Host-Range Bacteriophage DLP3 Specific to Stenotrophomonas maltophilia as a Potential Therapeutic Agent. Front. Microbiol. 11:1358. doi: 10.3389/fmicb.2020.01358

INTRODUCTION

Stenotrophomonas maltophilia is a robust, non-sporulating, obligate aerobe Gram-negative bacillus (Brooke, 2012). The genus name *Stenotrophomonas* was originally chosen due to the perceived limited nutritional range of the bacterium (Palleroni and Bradbury, 1993), though many studies have since shown an impressive metabolic versatility (Chatelut et al., 1995; Berg et al., 1999; Hauben et al., 1999; Minkwitz and Berg, 2001; Svensson-Stadler et al., 2012). *S. maltophilia* is often found in close association with plant rhizospheres where they actively promote plant growth through the secretion of growth-promoting compounds (Ryan et al., 2009). This plant growth promotion is now being used commercially; *S. maltophilia* strains are used as biofertilizers due to their ability to fix nitrogen, produce growth-promoting plant hormones, and protect plant roots from phytopathogens (Rathi and Nandabalan, 2017). Additionally, the vast metabolic diversity

observed in *S. maltophilia* enables these bacteria to be used in bioremediation, from heavy metal detoxification of soils and waterways to the degradation of insecticides and volatile organic compounds such as benzene. However, their widespread use in biotechnology and agriculture is problematic due to their ability to cause disease in humans (Berg and Martinez, 2015).

S. maltophilia is an important multidrug resistant, opportunistic pathogen that is most commonly associated with pneumonia and bacteremia in immunocompromised patients. *S. maltophilia* has also been identified as the cause of soft tissue infections, osteomyelitis, meningitis, endocarditis, otitis and scleritis (Brooke, 2012). Several risk factors are associated with *S. maltophilia* infections in the general population, including malignancy, human immunodeficiency virus, cystic fibrosis (CF), intravenous drug use, surgical and accidental trauma, prolonged hospitalization, mechanical ventilation, indwelling catheters, corticosteroids, immunosuppressive therapy, and treatment with broad-spectrum antibiotics (Al-Anazi and Al-Jasser, 2014). One study estimated the nosocomial mortality rates attributed to *S. maltophilia* bacteremia at 16.7%, and the overall mortality rate of patients infected with *S. maltophilia* was 25% (Naidu and Smith, 2012). A recent study on the clinical outcomes of cancer patients with bloodstream infections (BSI) and pneumonia caused by *S. maltophilia* infections in Mexico City indicated that 31.6% died within the first month; 22.1% of the deaths were due to pneumonia and 9.5% were due to BSI (Velazquez-Acosta et al., 2018). A similar study on BSI mortality rates associated with 937 German intensive care units found *S. maltophilia* infections had the highest mortality rates (28.4%), followed next by non-*albicans-Candida spp.* (27.1%) and *Pseudomonas aeruginosa* (25.8%) (Schwab et al., 2018).

Due to a wide array of pathogenicity factors, *S. maltophilia* can be difficult to clear once an infection has been established. *S. maltophilia* pathogenicity mechanisms include swimming and twitching motility (from flagella and type IV pili, respectively), a DNA hypermutator mechanism, iron uptake transporters, biofilm formation, lipopolysaccharide (LPS), many extracellular enzymes encoded such as fibrolysin, lipases, esterase, DNase, RNase, proteases and lecithinase, type II protein secretion systems, host cell invasion, and quorum sensing signaling systems (Brooke, 2012). In addition, clinical *S. maltophilia* isolate culture supernatants applied to Hep-2, HeLa, or Vero cells resulted in cytotoxic effects such as intensive rounding, loss of intercellular junctions, and membrane blebbing followed by cell death within 24 h (Figueiredo et al., 2006). In some cases, endocytosis, hemolytic activity, and cell aggregation were observed, and the addition of protease inhibitors did not prevent cell cytotoxicity. LPS production was shown to be required for attachment to surfaces, and colonization and virulence in a rat lung model (McKay et al., 2003). As well, it was shown that an *O*-polysaccharide synthesis mutant was susceptible to complement-mediated cell killing (Brooke et al., 2008). *S. maltophilia* can form biofilms on many surfaces such as glass, plastics, implanted medical devices, and lung epithelial cells (Huang et al., 2006; Pompilio et al., 2008, 2010; Brooke, 2014). A study focusing on the biofilm formation of CF-derived bronchial epithelial cell monolayers revealed that all *S. maltophilia* isolates were able to form biofilms on bronchial epithelial cells (Pompilio et al., 2010). Type-1 fimbriae genes have only been identified in clinical *S. maltophilia* isolates, which suggests they may play a direct role in the colonization of infected CF individuals (Nicoletti et al., 2011). *In vitro* tissue culture assays have indicated the *S. maltophilia* fimbriae 1 (SMF-1) protein is important for adherence to eukaryotic cells and glass, and anti-SMF-1 antibodies inhibit adherence to eukaryotic cells and glass if the antibodies were applied during early stages of infection (de Oliveira-Garcia et al., 2003). The ability of *S. maltophilia* isolates to form biofilms and invade host cells contributes to the prolonged infections noted in hematology and oncology patients, despite aggressive antibiotic treatments (Lai et al., 2006).

Innate antibiotic resistance in *S. maltophilia* infections is a major contributing factor to treatment failure. Patients who receive the wrong antibiotic at initial infection diagnosis have an increased risk of mortality compared to patients who received appropriate *S. maltophilia* antibiotic treatment initially (Velazquez-Acosta et al., 2018). *S. maltophilia* infections can be further complicated by the emergence of mutants with pleiotropic antibiotic resistance (Denton and Kerr, 1998). Intrinsic resistance is attributed to mechanisms such as reduced membrane permeability (Mett et al., 1988), chromosomally encoded multidrug efflux pumps, and chromosomally encoded Qnr pentapeptide repeat proteins (Sanchez et al., 2008; Sanchez and Martinez, 2010; Chang et al., 2011). Additionally, antibiotic inactivating enzymes such as inducible L1 and L2 β-lactamases (Walsh et al., 1997; Crowder et al., 1998; Okazaki and Avison, 2008), a TEM-2 β-lactamase from a Tn*1*-like transposon (Avison et al., 2000), and aminoglycoside- inactivating enzymes (Okazaki and Avison, 2007; Vetting et al., 2008) have been identified in many *S. maltophilia* isolates. The L1 protein is a molecular class B zinc-dependent metallo-β-lactamase which hydrolyzes virtually all classes of β-lactams, including penicillins, cephalosporins and carbapenems (Avison et al., 2001), whereas the L2 protein is a molecular class A clavulanic acid-sensitive cephalosporinase (Chang et al., 2015). The drug of choice to treat *S. maltophilia* infections continues to be trimethoprim/sulfamethoxazole (TMP/SMX) (Chung et al., 2013; Wang et al., 2016), although resistance to TMP/SMX across clinical isolates is common (30.5%) (Ochoa-Sanchez and Vinuesa, 2017). However, higher rates of TMP/SMX resistance, ranging from 16% to nearly 80%, have been noted in patients with cancer, CF, and in several specific countries (Chang et al., 2015; Rhee et al., 2016). The majority of TMP/SMX resistance is due to the presence of a *sul* gene encoding a sulfonamide resistance protein located on a class 1 integron (sul1) (Barbolla et al., 2004; Chung et al., 2015), and also on insertion sequence common region (ISCR) elements (sul2) (Toleman et al., 2007) rather than through the overexpression of efflux pumps. A *dhfr* gene encoding a dihydrofolate reductase associated with a class 1 integron has also been shown to cause some level of resistance against TMP/SMX (Hu et al., 2011), along with the activity from several RND family efflux pumps, although not to the same degree as the resident *sul* genes (Huang et al., 2013; Lin et al., 2015; Sanchez, 2015). Thus, research into alternative treatment options is critical due to increased

resistance to TMP/SMX noted with specific comorbidities and geographic locations.

Related to this high-level antibiotic resistance, *S. maltophilia* is also capable of tolerating biocides and harsh environments, which makes this bacterium difficult to eradicate from hospital settings. Nosocomial isolation sources for *S. maltophilia* include ultra-pure water, hemodialysis water, nebulizers, hand-washing soap, hospital antiseptic solution, chlorhexidine-cetrimide topical antiseptic solution, hypochlorite cleaners, triclosan, sodium dodecyl sulfate, and antiseptics containing quaternary ammonium compounds (Brooke, 2012; Kampmeier et al., 2017). Non-clinical multidrug resistant isolates of *S. maltophilia* have also been recovered from environments such as soil, water, plants and food sources (Berg et al., 2005; Qureshi et al., 2005; Brooke, 2012; Lin et al., 2017; Furlan and Stehling, 2018; Kim et al., 2018), and have the potential to cause community-acquired infections (Falagas et al., 2009; Chang et al., 2014).

High levels of innate antibiotic resistance in *S. maltophilia* isolates highlights the need for alternative treatment options to combat these infections. The use of bacteriophages, or phages, as viruses specifically lytic toward bacteria, is being investigated as a viable option. Phage therapy requires the isolation and characterization of phages prior to their use as prophylactic or therapeutic agents. Phage therapy holds several advantages over traditional antibiotics (Sulakvelidze et al., 2001; Burrowes et al., 2011; Golkar et al., 2014). First, phages possess a narrow host range, only infecting a few strains within a species, enabling precise targeting of the treatment, and preventing disruption of the patient's normal microbiota. Second, phages are self-replicating, such that phage replication can significantly increase phage abundance at the site of the bacterial infection. Third, phages use a different mechanism of action to kill bacteria than chemical antibiotics, and so are virulent against antibiotic resistant bacteria. Fourth, few side effects have been reported during or after phage application, including immune responses, suggesting that higher organisms are adapted to the presence of phages within tissues or on body surfaces. In addition, the high abundance of phages in the environment make them relatively simple to isolate. As well, phages are relatively easy to manipulate through molecular approaches to create therapeutically enhanced phages which exhibit improved performance *in vivo*, and phage biology is becoming better understood such that the development of new therapeutic phages will progress more rapidly than it has in the past. Ideally, a therapeutic cocktail of multiple phages targeting several bacterial strains with different phage-receptors will be developed to increase the host range of the cocktail and protect against receptor-mutation mediated resistance (Burrowes et al., 2011; Golkar et al., 2014).

Twenty phages specific to *S. maltophilia* have been isolated and characterized to date. Eleven phages (Sm1, IME13, IME15, S3, Sm14, ΦSMA5, DLP1, DLP2, DLP4, DLP5, DLP6) have been isolated and characterized specifically for their therapeutic potential. For example, the *Myoviridae* phage ΦSMA5 has an extensive host range successfully infecting 61 out of 87 strains tested (Chang et al., 2005), while Sm1 is the first *S. maltophilia* phage used in a murine model where it was found to provide 100% protection against *S. maltophilia* infection. The broad host range of ΦSMA5 and significant *in vivo* protection Sm1 provides in a murine model are promising examples of therapeutic phages that can be used for the treatment of antibiotic resistant *S. maltophilia* infections.

MATERIALS AND METHODS

Bacterial Strains and Growth Conditions

Initial phage isolation was accomplished with five clinical *S. maltophilia* strains (D1585, D1571, D1614, D1576, D1568) from the Canadian *Burkholderia cepacia* complex Research and Referral Repository (CBCCRRR; Vancouver, BC, Canada). An additional 22 *S. maltophilia* clinical isolates were obtained from the Provincial Laboratory for Public Health - North (Microbiology), Alberta Health Services for host range analysis. Strains SMDP92 and ATCC 13637 were gifted by Dr. Jorge Giron. Strains were grown aerobically at 30°C on Luria-Bertani solid media until single colonies were visible (16–36 h) or in LB broth with shaking at 225 RPM.

Bacteriophage Isolation, Propagation, and Host Range

The phage DLP3 (vB_SmaS_DLP_3) was isolated from soil collected in Edmonton, Alberta, Canada using host strain *S. maltophilia* D1571. No plants were associated with the soil sample. Approximately 10 ml of soil was mixed with 10 ml of LB broth, 1 ml of modified suspension media (SM) (50 mM Tris-HCl pH 7.5, 100 mM NaCl, 10 mM MgSO4) and 100 μl of a D1571 overnight culture. The slurry was incubated overnight at 30°C with shaking at 225 RPM. The supernatant was filter-sterilized with a Millex-HA 0.45 μm syringe-driven filter (Millipore, Billerica, MA, United States) and stored at 4°C, as performed previously (Peters et al., 2015, 2017, 2019). A single plaque was picked to propagate a working-stock solution for analysis using top-agar overlays. Briefly, 100 μl of overnight D1571 culture and 100 μl DLP3 stock ($\sim 10^9$ PFU/ml) were mixed and incubated for 5 min at room temperature then added to 3 ml of 0.7% LB top agar. The mixture was poured onto an LB plate and incubated for 18 h at 30°C. The top agar of plates showing confluent lysis was scraped into a 50 ml Falcon tube. A 3 ml aliquot of SM was added for each plate scraped and the slurry was shaken for 1 min followed by centrifugation (5 min at 10,000 × *g*) and filter sterilization. Host range analysis was performed on 29 *S. maltophilia* and 19 *Pseudomonas aeruginosa* strains using serially diluted DLP3 lysate into SM. A 10 μl aliquot of each concentration was spotted in triplicate onto a plate containing bacterial culture in a top-agar overlay and incubated overnight at 30°C.

Electron Microscopy

Phage lysate for electron microscopy was prepared using LB plates and top agar made with agarose and filter sterilized using a 0.22 μm filter. A carbon-coated copper

grid was overlaid with 10 μl of phage lysate for 2 min then stained with 4% uranyl acetate for 30 s. A Philips/FEI (Morgagni) transmission electron microscope (TEM) with charge-coupled device camera at 80 kV (University of Alberta Department of Biological Sciences Advanced Microscopy Facility) was used to obtain TEM images. The capsid diameter, tail length and tail width of ten virions were measured using ImageJ and averages calculated using Microsoft Excel.

Phage DNA Isolation, Sequencing, and RFLP Analysis

Genomic DNA was isolated from a high-titer DLP3 stock (10^9 PFU/ml). Lysate was clarified by spinning 10,000 × *g* for 10 min and the supernatant was subsequently treated with 100 μl 100x DNase I buffer (1 M Tris–HCl, 0.25 M MgCl2, 10 mM CaCl2), 10 μl DNase I (Thermo Scientific, Waltham, MA, United States), 6 μl RNase (Thermo Scientific) and incubated 1 h at 37°C. A 400 μl aliquot of 0.5 M EDTA (pH 8.0), SDS (final concentration of 2%) and Proteinase K (final concentration of 400 μg/ml) was added followed by incubation at 55°C overnight. A 1/2 volume of 6 M NaCl was added and the solution was vortexed at high speed for 30 s followed by centrifugation at 17,900 × *g* for 30 min. The supernatant was transferred to a fresh tube with an equal volume of 100% isopropanol and stored at −20°C for at least 1 h to overnight. The DNA was pelleted with centrifugation at 17,900 × *g* for 20 min at 4°C followed by three 70% ethanol washes. The pellet was dried at room temperature and resuspended in nuclease-free water. Purity and concentrations of eluted DNA were checked with a NanoDrop ND-1000 spectrophotometer (Thermo Scientific, Waltham, MA, United States). DLP3 genomic (gDNA) DNA was sequenced using both Illumina and Pacific Biosciences technologies. A Nextera XT library was generated for paired-end sequencing on MiSeq (Illumina) platform using MiSeq v2 reagent kit. Restriction fragment length polymorphism (RFLP) analysis was used with 15 FastDigest (Thermo Scientific) restriction enzymes: *Eco*RI, *Xba*I, *Bam*HI, *Hin*dIII, *Kpn*I, *Sma*I, *Sph*I, *Pst*I, *Sac*I, SaII, *Apa*I, *Cla*I, *Nde*I, *Spe*I, Xhol. Restriction reactions were set up using 1 μl FastDigest enzyme, 2 μl FastDigest restriction buffer, 1 μg of phage DNA and nuclease-free water to bring the final volume to 20 μl. Reactions were separated on a 0.8% (wt/vol) agarose gel in 1x TAE (pH 8.0).

Bioinformatic Analysis of the DLP3 Genome

A 96,852 bp contig assembled from the Illumina reads with SPAdes 3.8.0 was identified for further analysis. No gaps or ambiguous sites were found in the assembly, which has a mean coverage of 114 reads and Q40 of 93.8%. Prediction of open reading frames (ORFs) was accomplished with the GLIMMER plugin (Delcher et al., 2007) for Geneious (Kearse et al., 2012) using the Bacteria and Archaea setting, as well as GeneMarkS for phage (Besemer et al., 2001). Conserved domain searches were performed using CD-Search with the CDD v3.16 – 50369 PSSMs database (Marchler-Bauer et al., 2011). Phyre (Kelley et al., 2015), HHblits (Remmert et al., 2011; Zimmermann et al., 2018) and ITASSER (Yang and Zhang, 2015) were used to gain insights into possible functions of hypothetical proteins or to provide more support for putative functions. BLASTn and BLASTp were used to gain information on relatives based on genomic data and individual proteins, respectively (Altschul et al., 1997). The NCBI non-redundant protein sequence and nucleotide collection databases (update dates for both: 2018/08/26) were used for the BLASTp and BLASTn searches, respectively. BLASTp results above 1.00E-03 were annotated as hypothetical proteins. tRNAs were identified using the general tRNA model with tRNAscan-SE software (Schattner et al., 2005).

D1585 *pilT* Deletion Construction

A *pilT* clean deletion mutant of *S. maltophilia* D1585 was constructed using overlap-extension PCR and allele exchange as previously described (McCutcheon et al., 2018). Briefly, regions upstream and downstream of the *pilT* gene in D1585 were PCR amplified using Phusion High-Fidelity DNA Polymerase (New England Biolabs) with primer pairs UpF-*Hin*dIII (GGGC**AAGCTT**CAGTACCTGCGGCTTCACTG) and UpR-OE (*CTCGAACAGGCGCTTGGACGCTTTGTTCTT*TACGG) for the upstream region, and DnF-OE (*AAGAACAAAGCGTC CAAGCGCCTGTTCGAG*TAAGG) and DnR-*Xba*I (GGGC **TCTAGA**CTTCAGCTTGTGGATCTCGC) for the downstream region. Overlap regions are italicized and restriction enzyme recognition sites are bolded. Following overlap-extension PCR, the deletion cassette was ligated into pEX18Tc and this plasmid, pD1585Δ*pilT*, was transformed into *E. coli* S17-1 for bacterial mating with D1585. Single crossover transconjugants were selected on LB agar containing 100 μg/mL tetracycline and merodiploid status was confirmed by colony PCR with *pilT* specific primers pilTF (GTTCCGTTGAATCAGGAGGC) and pilTR (GAGGGCATGTACCAGGAAAC). Positive merodiploids were grown in LB broth and plated on LB with 10% sucrose to select for double crossover Δ*pilT* mutants that were confirmed by colony PCR as above. For complementation, the D1585 *pilT* gene was cloned into pBBR1MCS using pilTF and pilTR primers with tails for *Hin*dIII and *Xba*I restriction enzymes (Thermo Fisher) to create pD1585*pilT*.

Phage Plaquing Assays

DLP3 plaquing ability on wildtype and mutant strains of D1585 and 280 was determined by spot assay on bacterial lawns as previously described (McCutcheon et al., 2018). Briefly, bacterial strains were grown in 1/2 LB supplemented with 35 μg/mL chloramphenicol at 30°C with aeration at 225 RPM for 18 h. 100 μL of overnight culture was used in a top agar overlay containing 35 μg/mL chloramphenicol and allowed to solidify. DLP3 lysate standardized to 10^{10} PFU/mL on *S. maltophilia* D1571 was ten-fold serially diluted in SM to 10^3 PFU/mL and 5 μL of each dilution was spotted on the prepared plates in triplicate. Plates were incubated upright at 30°C and imaged

after 16 h. Each experiment was repeated in biological and technical triplicate.

Protein Isolation and Mass Spectrometry

Isolation of DLP3 protein for SDS-PAGE analysis was accomplished following a protocol for the formation of ghost particles (Boulanger, 2009). Briefly, sterile DLP3 lysate ($\sim 1 \times 10^9$) was clarified twice with 10,000 × *g* centrifugations and treated with nucleases following the DNA isolation protocol described above. After the incubation, an equal volume of 10 M LiCl was added and the solution was incubated at 46°C for 10 min, followed by 10-fold dilutions into sterile Milli-Q water. The released DLP3 gDNA was digested with an addition of 10 mM $MgCl_2$ and 50 U of RNase-free DNaseI per 1×10^{12} PFU. This solution was incubated overnight at 37°C, followed by ultracentrifugation at 28,700 × *g* for 1.2 h. The supernatant was discarded and pellets were resuspended with 100 μl SM. An aliquot of the sample was diluted in half with 2x Laemmli sample buffer (10% [v/v] beta-mercaptoethanol [BME], 6% [w/v] SDS, 20% [v/v] glycerol, 0.2 mg/ml bromophenol blue) and incubated 10 min at 99°C.

An SDS-PAGE gel with a 4% stack and a 7.5% resolving portion was made with 40% 37.5:1 acrylamide/bis-acrylamide solution (Bio-Rad) and fresh 10% ammonium persulfate. The gel was loaded into a Mini-PROTEAN electrophoresis chamber (Bio-Rad) using 1x running buffer. A 6 μl aliquot of PageRuler Plus Prestained Protein Ladder (Thermo Scientific) was used as a molecular weight standard and 6–12 μl of DLP3 ghost particles in 1x sample buffer was loaded into the remaining wells. The gel was run at 180 kV for 75 min and placed in Coomassie R-250 stain for 1 h with gentle rocking. The gel was destained over 2 h, with the destaining solution replaced every 30 min. The gel was placed in a 50 ml Falcon tube with Milli-Q to transport the gel for mass spectrometry analysis at the Alberta Proteomics and Mass Spectrometry (APM) facility located at the University of Alberta.

In-gel trypsin digestion was performed on the samples. The lane was cut into seven equal gel sections, destained twice in 100 mM ammonium bicarbonate/acetonitrile (ACN) (50:50), reduced (10 mM BME–100 mM bicarbonate) and then alkylated (55 mM iodoacetamide–100 mM bicarbonate). After dehydration, trypsin digestion (6 ng/μl) was allowed to proceed overnight at room temperature. Tryptic peptides were extracted from the gel using 97% water–2% acetonitrile–1% formic acid followed by a second extraction using 50% of the initial extraction buffer and 50% acetonitrile. Fractions containing tryptic peptides were resolved and ionized using nanoflow high-performance liquid chromatography (HPLC) (Easy-nLC 1000; Thermo Scientific) coupled to a Q Exactive Orbitrap mass spectrometer (MS) (Thermo Scientific). Nanoflow chromatography and electrospray ionization were accomplished by using a Pico- Frit fused silica capillary column (ProteoPepII; C18) with a 100-μm inner diameter (New Objective) (300 Å, 5 μm pore size). Peptide mixtures were injected onto the column at a flow rate of 3,000 nl/min and resolved at 500 nl/min using 75-min linear gradients of 4% to 40% (vol/vol) aqueous ACN with 0.2% (vol/vol) formic acid. The mass spectrometer was operated in data-dependent acquisition mode, recording high-accuracy and high-resolution Orbitrap survey spectra using external mass calibration, with a resolution of 35,000 and m/z range of 400 to 2,000. The 15 most intensely multiply charged ions were sequentially fragmented by HCD fragmentation. After two fragmentations, all precursors selected for dissociation were dynamically excluded for 60 s. Data were processed using Proteome Discoverer 1.4 (Thermo Scientific). The UniProt *Stenotrophomonas* database and all DLP3 proteins were searched using SEQUEST (Thermo Scientific). Search parameters included a precursor mass tolerance of 10 ppm and a fragment mass tolerance of 0.8 Da. Peptides were searched with carbamidomethyl cysteine as a static modification and oxidized methionine and deamidated glutamine and asparagine as dynamic modifications.

Determination of DLP3 Lifestyle

Top agar overlay plates showing confluent lysis of D1571 by DLP3 were used to obtain resistant colonies. Briefly, 3 ml of SM was added to the plates and a sterile glass rod was used to gently skim the agar. The SM was collected and placed into microcentrifuge tubes, then centrifuged at 5,000 × *g* for 5 min. The supernatant was discarded and 1 ml of fresh SM was added to resuspend the pellet, followed by centrifugation at 5,000 × *g* for 5 min. This wash step was repeated three times in total. Following the final wash centrifugation, the supernatant was removed and the pellet was resuspended in 500 μl LB broth. Cells were serially diluted with LB and plated on LB plates, then incubated at 30°C for 16 h. Single colony isolates were selected for further study and tested for superinfection resistance using overnight cultures of every isolate in a top agar overlay assay with DLP3. After an 18 h incubation at 30°C, the plates were observed for plaque development. Single colony isolates without plaque development were retained for analysis.

Erm Functionality

Triplicate minimal inhibitory concentration (MIC) experiments on *S. maltophilia* strains D1571 and D1571:DLP3 were conducted using established protocols (Wiegand et al., 2008) to study the functionality of the DLP3-encoded Erm. Overnight cultures were grown at 30°C in 5 mL LB. A 1:100 subculture was grown at 30°C to an OD_{600} of 0.1 in Mueller-Hinton broth (MH) and used in 96 well plates containing an erythromycin dilution series (MP Biomedicals). Following a 16 h incubation, OD_{600} absorbance was obtained using a Wallac 1420 VICTOR2 multilabel counter (PerkinElmer, Waltham, MA, United States) and values were averaged using Excel. Statistical analysis was conducted using GraphPad Prism 7 (GraphPad Software Inc., San Diego, CA, United States) to perform a two-way analysis of variance (ANOVA) with Sidak's multiple comparisons.

Growth Analysis of Wild Type D1571 and the DLP3 Lysogen

Single colony triplicate overnight cultures of wild type D1571 and the lysogen D1571:DLP3 were grown in LB broth at

30°C with shaking. Subcultures (1:100) for each sample were performed using LB broth and each subculture was grown to an OD_{600} of ∼0.32 at 30°C with 225 RPM shaking. Subcultures were distributed in triplicate aliquots of 200 μl in 96 well plates; an LB broth control was included for each plate. The OD_{600} was then obtained for each plate using a Wallac 1420 VICTOR^2 multilabel counter (PerkinElmer, Waltham, MA) at the following time points: 0, 2, 4, 6, 8 h. The OD_{600} data were used to determine the growth rate (μ) with the established formula: $\log_{10} N - \log_{10} N_0 = (\mu/2.303)(t - t_0)$, whereby N_0 is the time zero (t_0) OD_{600} reading and N is the final OD_{600} reading obtained at a specific time (t) in the experiment. Resulting data were analyzed with GraphPad Prism 7 (GraphPad Software Inc., San Diego, CA, United States) to graph the growth curve and growth rate. Statistical analysis of the growth curve and growth rate data were performed in GraphPad Prism 8 using two-way repeated measurement ANOVA with multiple comparisons (Sidak's).

Galleria mellonella Killing and Phage Rescue Assays

G. mellonella infections were performed as previously described, with modifications (Seed and Dennis, 2008; Kamal et al., 2019). Single colony triplicate overnight cultures of wildtype strain D1571 and the DLP3 lysogen, D1571:DLP3, were grown aerobically at 37°C in LB for 19 h corresponding to approximately 2×10^{10} CFU/mL. Cultures were standardized by OD_{600}, washed once in 1× phosphate-buffered saline (PBS, pH 7.4) and serially diluted tenfold in PBS. *G. mellonella* larvae were bred in-house at 30°C using artificial food (wheat germ: 264 g, brewer's yeast: 132 g, beeswax: 210 g, glycerol: 132 g, honey: 132 g, water: 66 g) and larvae weighing approximately 250 mg were selected for experiments. Each experiment consisted of ten larvae per group and 5 μL aliquots of bacterial culture were injected into the rear left proleg of each larva using a 250 μL Hamilton syringe fitted with a repeating dispenser. Sterile PBS injected larvae were used as negative controls and showed 100% survival for the duration of the experiment. Colony counts on LB agar were used to determine the CFUs injected. Following injection, larvae were placed in a static incubator in the dark at 37°C and scored for death every 24 h until 120 h post-infection (hpi). Larvae were considered dead when they did not respond to touch with movement.

For DLP3 phage rescue trials, wildtype D1571 culture was prepared as described above and an inoculum of approximately 8×10^6 CFU/larvae was chosen. DLP3 lysate was used at 8.9×10^{10} PFU/mL. Larvae were injected with 10 μL of DLP3 lysate dilutions to give MOIs of approximately 100 and 50 into the rear right proleg 1.5 hpi with D1571. Aliquots of 5 μL PBS and 10 μL SM were used in place of bacteria and phage, respectively, for negative controls. Each worm was therefore injected with 15 μL total volume. Larvae were incubated and scored for survival as above. Results from three separate trials were combined and survival at each timepoint was plotted using the Kaplan–Meier method with error bars for standard error using GraphPad Prism 8. Statistical analysis of survival differences was completed using the Log-rank (Mantel–Cox) test.

RESULTS AND DISCUSSION

Isolation, Morphology, Host Range, and RFLP Analysis

Bacteriophage DLP3 (vB_SmaS-DLP_3) was isolated from soil using clinical *S. maltophilia* strain D1571. Transmission electron microscopy (TEM) enabled the classification of DLP3 as a *Siphoviridae* of the B1 morphotype (Ackermann and Eisenstark, 1974) due to the long, non-contractile tail averaging 202.2 ± 5.7 nm and isometric capsid with a length and width of 92.8 ± 4.1 and 84.0 ± 2.8 nm, respectively (**Figure 1**). No tail fibers were observed in the TEM images. The host range of DLP3 against all 29 clinical *S. maltophilia* isolates reveals a broad tropism through the successful infection of 22 strains, although DLP3 is not capable of infecting the *P. aeruginosa* strains tested (**Table 1**). The restriction fragment length polymorphism analysis revealed DLP3 genomic DNA is resistant to the 15 restriction enzymes screened. These results suggest DLP3 contains modified DNA, although the exact types of modifications are currently undetermined.

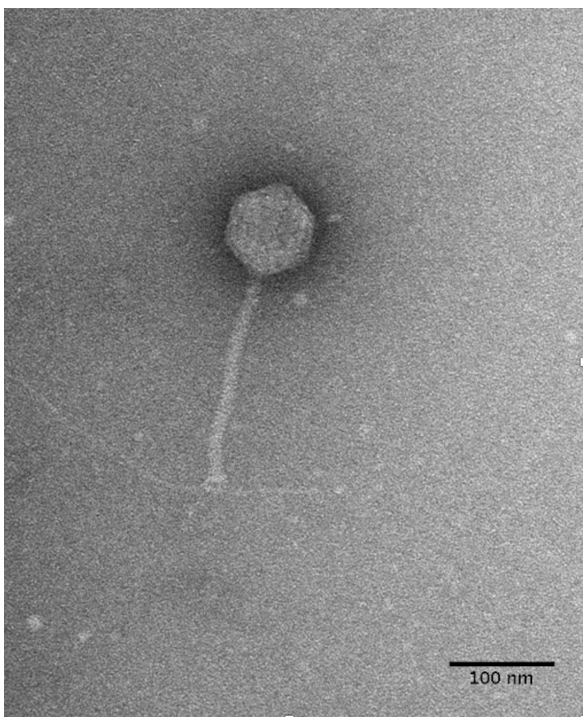

FIGURE 1 | DLP3 *Siphoviridae* morphology. Phage lysate was applied to a carbon-coated copper grid and stained with 4% uranyl acetate. Transmission electron micrographs were obtained at 180,000× magnification. A *S. maltophilia* D1571 pili is shown to be interacting with the baseplate portion of the DLP3 tail. The averaged measurements for tail length, capsid length and width from ten virions is 202, 92, and 84 nm, respectively.

TABLE 1 | Host range analysis for *S. maltophilia* bacteriophage DLP3 on *S. maltophilia* and *P. aeruginosa* strains.

***S. maltophilia* strain**	**Efficiency of plating**
101	++
102[b]	+++
103	++
152	–
155	++++
174	++
176	++++
213	++
214	++
217	–
218	+
219	+++
230	++++
236	+
242	++
249[b]	+
278	–
280	+++
282	+
287	++
446	–
667	+
D1585[a]	+++
D1571[a,b]	++++
D1614[a,b]	–
D1576[a,b]	+++
D1568[a]	–
SMDP92[b]	++++
ATCC13637	–
***P. aeruginosa* strain**	
PA01	–
HER1004	–
HER1012	–
14715	–
Utah3	–
Utah4	–
14655	–
6106	–
pSHU-OTE	–
D1606D[a]	–
D1615C[a]	–
D1619M[a]	–
D1620E[a]	–
D1623C[a]	–
ENV003[a]	–
ENV009[a]	–
FC0507[a]	–
R285	–
14672	–

–, no sensitivity to phage; +, plaques at 10–2; ++, clearing at 10–2; +++, plaques at 10–4; ++++, plaques at 10–6. [a]Isolates from the Canadian Burkholderia cepacia complex Research Referral Repository. [b]Strain susceptible to phage DLP5.

Genomic Characterization

The DLP3 genome is 96,852 bp long with a 58.3% global GC content. No low coverage or ambiguous regions were identified with the assembled contig, which has a mean coverage of 114 and a Q40 of 99.6%. NCBI non-redundant protein sequence database searches indicate that DLP3 shares a high identity to the *Siphoviridae* phage vB_SmaS_DLP_5 (DLP5) (Peters and Dennis, 2018). DLP5 is the type species of the new genus *Delepquintavirus* and based on the genomic similarities between DLP3 and DLP5, DLP3 is also a member of this new genus. Open reading frame calling with Glimmer and GeneMarkS identified a total of 148 protein coding domain sequences (CDS) covering 95% of the genome (**Figure 2** and **Table 2**). DLP3 also encodes five tRNA genes with different specificities: Tyr (GTA), Sup (CTA), Ser (GCT), Ile (GAT), Glu (TTC). A total of 97 proteins could not be assigned functions due to lack of significant results from both BLASTp and CD-Search. The DLP3 genome with putative gene annotations has been deposited in GenBank under accession number MT110073.

The CD-Search did yield 37 DLP3 proteins with conserved domains predicted (**Table 3**). Three of the domains identified are domains of unknown function (DUF) which tended to be distributed throughout Gram-negative bacteria and to a lesser extent in Gram-positive bacteria, according to the species distribution for each DUF in pfam (Finn et al., 2014). There are six conserved domains (CD) identified which are involved in virion morphogenesis: phage portal protein superfamily, gp1; phage capsid family, gp6; phage tail proteins, gp10 and gp24;

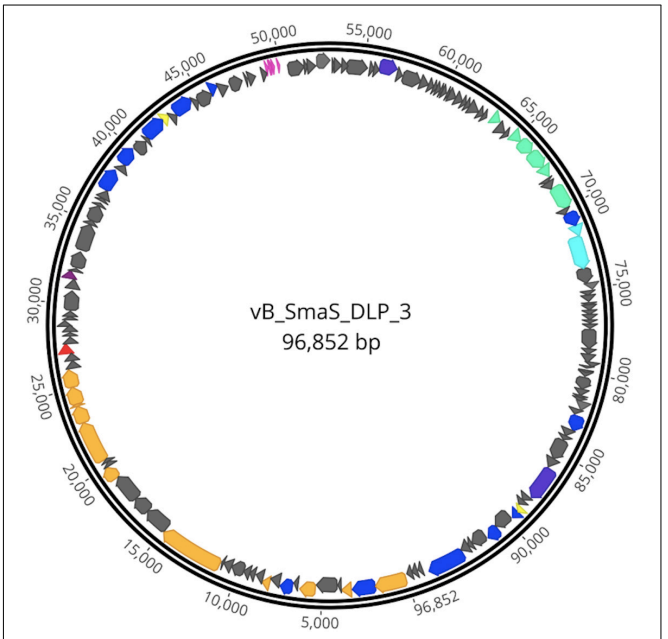

FIGURE 2 | Genome map of DLP3. Scale in bp is shown on the outer periphery. Predicted functions are grouped by color: teal; moron, gray; hypothetical, light blue; DNA packaging, pink; tRNA, red; lysis, green; virion morphogenesis, dark blue; DNA replication and repair, purple; auxiliary metabolism, and yellow; regulatory.

TABLE 2 | Genome annotations for DLP3 obtained from BLASTp and CD-Search data.

CDS	Interval	Length (AA)	Putative function	Species	Coverage (%)	*E*-Value	Identity (%)	Accession
1	48–1856	602	Portal protein	DLP5[a]	98	0	83	ATS92275.1
2	1856–3193	445	ParB-like nuclease domain protein	DLP5	100	0	75	ATS92281.1
3	3249–3854	201	Serine protease	DLP5	98	1.00E-113	80	ATS92325.1
4	3847–4017	56	Hypothetical protein gp_005	DLP5	100	3.00E-24	77	ATS92409.1
5	4090–5307	405	Hypothetical protein gp_006	DLP5	100	0	79	ATS92283.1
6	5340–6272	310	Major capsid protein	DLP5	100	0	93	ATS92299.1
7	6358–6624	88	Hypothetical protein gp_008	DLP5	100	3.00E-33	65	ATS92383.1
8	6693–7436	247	Ribonuclease E	DLP5	100	3.00E-113	73	ATS92315.1
9	7457–8068	203	Hypothetical protein gp_010	DLP5	100	2.00E-121	82	ATS92324.1
10	8068–8493	141	Tail protein	DLP5	99	6.00E-71	77	ATS92347.1
11	8490–8936	148	Hypothetical protein gp_012	DLP5	99	3.00E-82	76	ATS92342.1
12	9012–9305	97	Hypothetical protein gp_013	DLP5	100	5.00E-50	85	ATS92376.1
13	9316–9693	125	Hypothetical protein gp_014	DLP5	100	4.00E-48	67	ATS92360.1
14	9693–10448	251	Hypothetical protein gp_015	DLP5	100	2.00E-152	82	ATS92314.1
15	10465–10959	164	Hypothetical protein gp_016	DLP5	100	9.00E-83	81	ATS92333.1
16	11016–11144	42	Hypothetical protein gp_017	DLP5	95	2.00E-15	83	ATS92415.1
17	11151–14915	1254	Tape measure protein	DLP5	99	0	83	ATS92270.1
18	14917–16500	527	Hypothetical protein gp_019	DLP5	100	0	79	ATS92277.1
19	16500–17474	324	Hypothetical protein gp_020	DLP5	100	0	83	ATS92295.1
20	17474–19153	559	Hypothetical protein gp_021	DLP5	100	0	74	ATS92276.1
21	19150–19968	272	Minor tail protein	DLP5	100	0	90	ATS92307.1
22	19968–20255	95	Hypothetical protein gp_023	DLP5	100	5.00E-62	98	ATS92377.1
23	20252–20455	67	Hypothetical protein gp_024	DLP5	100	1.00E-38	93	ATS92399.1
24	20445–22925	826	Tail protein	DLP5	100	0	86	ATS92271.1
25	22925–23923	332	Tail assembly protein	DLP5	100	0	86	ATS92294.1
26	23926–24102	58	Tail assembly protein	DLP5	100	3.00E-30	88	ATS92406.1
27	24110–25081	323	Tail assembly protein	DLP5	100	2.00E-169	70	ATS92296.1
28	25085–26107	340	Tail protein	Salvo[b]	100	3.00E-76	43	AHB12239.1
29	26183–26611	142	Hypothetical protein gp_030	DLP5	100	1.00E-91	93	ATS92345.1
30	26611–27096	161	Hypothetical protein gp_031	DLP5	100	6.00E-87	91	ATS92334.1
31	27096–27653	185	Lysozyme	DLP5	100	2.00E-120	89	ATS92330.1
32	27655–28059	134	Hypothetical protein gp_033	DLP5	100	3.00E-80	88	ATS92352.1
33	28110–28280	56	Hypothetical protein gp_034	DLP5	78	1.00E-11	70	ATS92408.1
34	28329–28715	128	DUF2500 containing protein	DLP5	100	3.00E-77	89	ATS92350.1
35	28687–28974	95	Hypothetical protein gp_036	DLP5	93	2.00E-57	96	ATS92380.1
36	29077–29271	64	Hypothetical protein					
37	29275–29574	99	Hypothetical protein gp_041	DLP5	95	2.00E-58	95	ATS92374.1

(Continued)

TABLE 2 | Continued

CDS	Interval	Length (AA)	Putative function	Species	Coverage (%)	*E*-Value	Identity (%)	Accession
38	29634–30791	385	Hypothetical protein gp_042	DLP5	100	0	78	ATS92287.1
39	30898–31506	202	Hypothetical protein gp_043	DLP5	87	2.00E-82	70	ATS92323.1
40	31499–31951	150	Phosphoglycerate kinase	DLP5	100	2.00E-103	96	ATS92341.1
41	31951–32136	61	Hypothetical protein gp_046	DLP5	100	2.00E-25	79	ATS92401.1
42	32197–33141	314	Hypothetical protein gp_047	DLP5	100	3.00E-138	85	ATS92300.1
43	33255–34856	533	Hypothetical protein gp_048	DLP5	98	2.00E-156	50	ATS92279.1
44	34856–35137	93	Hypothetical protein gp_049	DLP5	100	5.00E-35	64	ATS92378.1
45	35139–36056	305	Hypothetical protein gp_050	DLP5	100	0	90	ATS92301.1
46	36060–36251	63	Hypothetical protein	BCC[c]	98	5.00E-08	46	WP_046196969.1
47	36389–36571	60	Hypothetical protein gp_052	DLP5	85	1.00E-19	78	ATS92407.1
48	36568–37128	186	Hypothetical protein gp_053	DLP5	100	5.00E-128	93	ATS92329.1
49	37125–38414	429	Helicase	DLP5	100	0	90	ATS92282.1
50	38481–38981	166	Hypothetical protein gp_055	DLP5	100	2.00E-86	80	ATS92331.1
51	38974–39957	327	Primase	DLP5	100	0	77	ATS92297.1
52	40036–40812	258	Hypothetical protein gp_057	DLP5	100	3.00E-157	89	ATS92312.1
53	40860–41075	71	Hypothetical protein gp_058	DLP5	100	4.00E-41	92	ATS92395.1
54	41072–42430	452	Superfamily II DNA or RNA helicase	DLP5	100	0	90	ATS92280.1
55	42427–42828	133	Transcriptional regulator	DLP5	100	6.00E-68	74	ATS92353.1
56	42831–43208	125	Hypothetical protein gp_061	DLP5	100	1.00E-62	81	ATS92362.1
57	43208–44425	405	RecA	DLP5	100	0	90	ATS92285.1
58	44425–44799	124	Hypothetical protein gp_063	DLP5	100	9.00E-83	94	ATS92359.1
59	44799–45680	293	Hypothetical protein gp_064	DLP5	100	0	87	ATS92304.1
60	45677–46174	165	RuvC	DLP5	99	5.00E-111	93	ATS92332.1
61	46152–46766	204	Hypothetical protein gp_066	DLP5	100	5.00E-108	78	ATS92321.1
62	46848–47657	269	Hypothetical protein gp_067	DLP5	96	2.00E-153	83	ATS92308.1
63	47840–47947	35	Hypothetical protein gp_069	DLP5	100	5.00E-13	94	ATS92417.1
64	48028–48504	158	Hypothetical protein gp_070	DLP5	100	3.00E-96	91	ATS92336.1
65	48839–49174	111	Hypothetical protein gp_071	DLP5	100	8.00E-60	82	ATS92357.1
66	50468–51409	313	Hypothetical protein gp_073	DLP5	100	6.00E-127	61	ATS92313.1
67	51397–51585	62	Hypothetical protein					
68	51582–52145	187	Hypothetical protein gp_074	DLP5	100	2.00E-124	91	ATS92328.1
69	52165–52959	264	SPFH domain-containing protein	DLP5	100	0	96	ATS92309.1
70	53058–53210	50	Hypothetical proteins					
71	53207–53653	148	Hypothetical protein gp_077	DLP5	100	3.00E-87	87	ATS92343.1
72	53650–54000	116	Hypothetical protein gp_078	DLP5	100	7.00E-74	90	ATS92365.1
73	53993–55207	404	Hypothetical protein gp_079	DLP5	100	7.00E-96	44	ATS92288.1
74	55279–55548	113	Hypothetical protein gp_081	DLP5	100	1.00E-65	84	ATS92368.1
75	55558–55899	89	Hypothetical protein gp_080	DLP5	98	8.00E-37	66	ATS92369.1

(Continued)

TABLE 2 | Continued

CDS	Interval	Length (AA)	Putative function	Species	Coverage (%)	*E*-Value	Identity (%)	Accession
76	55887–56930	347	UDP-glucose 4-epimerase	DLP5	100	0	83	ATS92289.1
77	56962–57285	107	Hypothetical protein gp_083	DLP5	99	9.00E-56	78	ATS92370.1
78	57355–58425	356	Hypothetical protein gp_084	DLP5	100	0	73	ATS92290.1
79	58418–58939	173	Hypothetical protein gp_087	DLP5	45	6.00E-35	73	ATS92388.1
80	58936–59283	115	Hypothetical protein gp_086	DLP5	86	1.00E-36	64	ATS92361.1
81	59280–59456	58	Hypothetical protein gp_088	DLP5	100	4.00E-17	62	ATS92405.1
82	59465–59737	90	Hypothetical protein BV378_14040	*Nostoc* sp. RF31Y	97	8.00E-19	50	OUL25853.1
83	59737–59862	41	Hypothetical protein					
84	59859–60128	89	Hypothetical protein					
85	60132–60314	60	Hypothetical protein gp_089	DLP5	100	2.00E-05	53	ATS92403.1
86	60318–60737	139	Hypothetical protein gp_090	DLP5	84	3.00E-64	79	ATS92363.1
87	60734–61210	158	Hypothetical protein gp_091	DLP5	98	7.00E-60	62	ATS92339.1
88	61207–61458	83	Hypothetical protein gp_092	DLP5	100	1.00E-22	46	ATS92382.1
89	61455–61709	84	Hypothetical protein					
90	61709–62359	216	Hypothetical protein gp_093	DLP5	100	3.00E-100	65	ATS92319.1
91	62362–62649	95	Hypothetical protein gp_094	DLP5	96	4.00E-35	66	ATS92381.1
92	62646–62885	79	Hypothetical protein gp_095	DLP5	100	4.00E-31	70	ATS92392.1
93	63161–63688	175	Rhomboid membrane protein	DLP5	100	9.00E-96	78	ATS92322.1
94	63746–64342	198	Hypothetical protein gp_097	DLP5	98	8.00E-108	82	ATS92326.1
95	64339–64593	84	Hypothetical protein gp_098	DLP5	96	3.00E-31	68	ATS92385.1
96	64670–65308	212	PIG-L family deacetylase	DLP5	100	6.00E-114	75	ATS92320.1
97	65311–66252	313	WcaG	DLP5	100	0	95	ATS92298.1
98	66252–67298	348	WecE	DLP5	100	0	87	ATS92291.1
99	67295–67975	226	Methyltransferase	DLP5	100	1.00E-139	82	ATS92317.1
100	68043–68228	61	Hypothetical protein gp_103	DLP5	98	5.00E-20	62	ATS92400.1
101	68225–68647	140	Hypothetical protein gp_104	DLP5	97	8.00E-56	68	ATS92346.1
102	68647–70095	482	*N*-acetyl-alpha-D-glucosaminyl l-malate synthase	DLP5	100	0	93	ATS92278.1
103	70092–70403	103	Hypothetical protein gp_106	DLP5	100	1.00E-36	59	ATS92372.1
104	70375–71229	284	ParBc	DLP5	99	0	89	ATS92305.1
105	71229–71879	216	Hypothetical protein gp_108	DLP5	99	5.00E-125	85	ATS92318.1
106	71842–73755	637	Terminase large subunit	DLP5	100	0	91	ATS92274.1
107	73767–74660	297	Hypothetical protein gp_110	DLP5	100	0	95	ATS92303.1
108	74657–75067	136	DUF3310 containing protein	DLP5	100	1.00E-61	71	ATS92351.1
109	75129–75371	80	Hypothetical protein gp_112	DLP5	100	8.00E-37	74	ATS92390.1
110	75373–75765	130	Hypothetical protein gp_113	DLP5	92	7.00E-12	34	ATS92355.1
111	75841–75939	32	Hypothetical protein gp_114	DLP5	100	7.00E-09	81	ATS92418.1

(Continued)

TABLE 2 | Continued

CDS	Interval	Length (AA)	Putative function	Species	Coverage (%)	*E*-Value	Identity (%)	Accession
112	75936–76253	105	Hypothetical protein gp_115	DLP5	96	6.00E-54	81	ATS92371.1
113	76250–76504	84	Hypothetical protein gp_116	DLP5	100	2.00E-42	79	ATS92387.1
114	76494–76859	121	Hypothetical protein gp_117	DLP5	98	6.00E-59	80	ATS92358.1
115	76859–77011	50	Hypothetical protein gp_118	DLP5	100	1.00E-22	88	ATS92412.1
116	77087–77335	82	Hypothetical protein gp_119	DLP5	100	2.00E-43	82	ATS92389.1
117	77389–78528	379	Hypothetical protein gp_120	DLP5	70	2.00E-143	94	ATS92286.1
118	78528–78878	116	Hypothetical protein gp_121	DLP5	99	4.00E-71	90	ATS92364.1
119	78904–79365	153	Hypothetical protein gp_122	DLP5	100	7.00E-78	75	ATS92340.1
120	79331–79561	76	Hypothetical protein gp_123	DLP5	100	3.00E-33	76	ATS92393.1
121	79558–79731	57	Hypothetical protein gp_124	DLP5	96	6.00E-23	78	ATS92404.1
122	79804–79920	38	Hypothetical protein					
123	79920–80228	102	Hypothetical protein gp_125	DLP5	100	3.00E-59	87	ATS92373.1
124	80254–80988	244	Hypothetical protein gp_126	DLP5	100	8.00E-153	83	ATS92316.1
125	80985–81350	121	Hypothetical protein gp_127	DLP5	96	1.00E-64	79	ATS92356.1
126	81347–81523	58	Hypothetical protein					
127	81516–81698	60	Hypothetical protein gp_128	DLP5	96	2.00E-29	86	ATS92402.1
128	81698–82180	160	DUF1643 containing protein	DLP5	100	2.00E-88	80	ATS92337.1
129	82180–82515	111	Hypothetical protein gp_130	DLP5	90	2.00E-44	83	ATS92367.1
130	82589–83485	298	DNA ligase	DLP5	100	0	92	ATS92302.1
131	83482–83895	137	Hypothetical protein gp_133	DLP5	100	4.00E-65	74	ATS92349.1
132	83895–84197	100	Hypothetical protein gp_134	DLP5	97	2.00E-47	77	ATS92375.1
133	84248–85459	403	Hypothetical protein gp_135	DLP5	100	0	81	ATS92284.1
134	85456–86028	190	Hypothetical protein gp_136	DLP5	100	3.00E-119	85	ATS92327.1
135	86122–88065	647	Pyruvate phosphate dikinase	DLP5	100	0	84	ATS92273.1
136	88141–88527	128	Hypothetical protein gp_138	DLP5	98	7.00E-76	90	ATS92348.1
137	88527–88868	113	Hypothetical protein gp_139	DLP5	100	5.00E-63	86	ATS92366.1
138	88879–89238	119	Transcriptional repressor	DLP5	95	3.00E-71	88	ATS92354.1
139	89228–89698	156	Tyrosine phosphatase family protein	DLP5	99	5.00E-93	86	ATS92338.1
140	89740–90759	339	Hypothetical protein gp_142	DLP5	98	0	77	ATS92292.1
141	90756–91532	258	Thymidylate synthase	DLP5	98	6.00E-121	72	ATS92311.1
142	91618–92493	291	Hypothetical protein gp_144	DLP5	97	1.00E-124	65	ATS92306.1
143	92483–92737	84	Hypothetical protein gp_145	DLP5	97	3.00E-35	71	ATS92386.1
144	92734–93231	165	Hypothetical protein gp_146	DLP5	96	1.00E-83	77	ATS92335.1
145	93260–95482	740	DNA polymerase I	DLP5	100	0	85	ATS92272.1
146	95794–96030	78	Hypothetical protein					
147	96134–96415	93	Hypothetical protein gp_149	DLP5	96	6.00E-52	87	ATS92379.1
148	96412–96741	109	Hypothetical protein gp_150	DLP5	100	2.00E-61	85	ATS92310.1

Results below 0.01 were not included and the function was annotated as hypothetical. [a]Stenotrophomonas phage DLP5, [b]Xylella phage Salvo, and [c]Burkholderia cepacia complex.

TABLE 3 | The conserved domains found in the 148 DLP3 gene products.

Gp	Hit type	PSSM-ID	Interval	*E*-Value	Accession	Short name	Superfamily
1	Superfamily	327517	29–471	2.89E-49	cl19194	Phage_portal superfamily	–
2	Specific	214678	359–441	8.46E-06	smart00470	ParB	cl02129
3	Superfamily	317012	5–114	7.39E-23	cl24270	Peptidase_S78_2 superfamily	–
6	Superfamily	331903	20–307	5.06E-12	cl27082	Phage_capsid superfamily	–
10	Superfamily	321796	6–137	7.98E-15	cl02089	Phage_tail_S superfamily	–
17	Superfamily	331332	525–930	5.90E-15	cl26511	Neuromodulin_N superfamily	–
17	Superfamily	333387	163–230	3.22E-03	cl28567	HI1514 superfamily	–
19	Superfamily	316645	14–69	9.95E-03	cl16644	DUF4302 superfamily	–
21	Superfamily	312753	188–264	8.54E-16	cl10710	Phage_BR0599 superfamily	–
21	Superfamily	331404	18–261	5.62E-12	cl26583	DUF2163 superfamily	–
24	Specific	316107	207–368	2.18E-13	pfam13550	Phage-tail_3	cl26145
28	Superfamily	328935	62–184	1.13E-05	cl22861	LamG superfamily	–
31	Superfamily	331815	6–185	4.73E-34	cl26994	Glyco_hydro_108 superfamily	–
38	Superfamily	332389	92–371	4.11E-42	cl27568	TIP49 superfamily	–
41	Superfamily	332243	13–46	5.11E-03	cl27422	SecD superfamily	–
49	Superfamily	333705	167–405	5.02E-22	cl28885	RecA-like_NTPases superfamily	–
51	Superfamily	331610	31–322	7.81E-12	cl26789	Toprim_N superfamily	–
54	Superfamily	331760	51–451	4.03E-38	cl26939	DEXDc superfamily	–
55	Superfamily	322007	53–98	3.22E-04	cl02600	HTH_MerR-SF superfamily	–
57	Superfamily	333705	77–272	2.57E-48	cl28885	RecA-like_NTPases superfamily	–
60	Superfamily	328743	1–140	6.73E-14	cl21482	RuvC_resolvase superfamily	–
69	Specific	307341	23–207	2.15E-17	pfam01145	Band_7	cl19107
76	Specific	224012	1–336	1.19E-76	COG1087	GalE	cl21454
78	Superfamily	330522	59–126	2.19E-04	cl25701	RuvB_N superfamily	–
93	Superfamily	328780	29–159	3.68E-14	cl21536	Rhomboid superfamily	–
96	Specific	308281	5–122	3.46E-11	pfam02585	PIG-L	cl00929
97	Specific	223528	1–297	7.51E-40	COG0451	WcaG	cl25660
98	Superfamily	327488	20–340	5.46E-56	cl18945	AAT_I superfamily	–
99	Superfamily	327401	30–135	1.43E-04	cl17173	AdoMet_MTases superfamily	–
102	Specific	223515	1–323	4.33E-03	COG0438	RfaB	cl28208
104	Specific	214678	18–109	7.28E-17	smart00470	ParB	cl02129
104	Specific	224392	34–187	5.36E-08	COG1475	Spo0J	cl26722
108	Superfamily	314594	17–68	1.07E-11	cl13237	DUF3310 superfamily	–
128	Specific	311648	12–146	4.16E-44	pfam07799	DUF1643	cl01787
130	Superfamily	325160	25–186	2.14E-25	cl12015	Adenylation_DNA_ligase_like superfamily	–
130	Superfamily	330238	112–270	1.28E-08	cl25417	CDC9 superfamily	–
133	Superfamily	332389	206–341	8.78E-33	cl27568	TIP49 superfamily	–
133	Superfamily	332204	43–150	8.52E-03	cl27383	ERCC4 superfamily	–
135	Superfamily	331842	16–471	0.00E+00	cl27021	PtsP superfamily	–
139	Superfamily	330819	39–125	1.50E-10	cl25998	CDC14 superfamily	–
141	Superfamily	330819	85–189	1.80E-05	cl25998	CDC14 superfamily	–
145	Superfamily	322025	107–710	7.76E-64	cl02626	DNA_pol_A superfamily	–

laminin G, gp28; and tape measure protein domain, gp17. Nine proteins with domains involved in DNA replication and repair identified with the CD-Search include two ParB domains, gp2 and 104; two helicases, gp49 and 54; Holliday junction resolvase, gp60; RecA recombinase, gp57; topoisomerase primase, gp51; DNA ligase, gp130; and DNA polymerase A, gp145. The remaining CD results appear to be quite diverse in their functions such as the SpoVK family domain involved in sporulation (gp38) (Fan et al., 1992), protein-tyrosine phosphatases (gp139 and gp141) typically involved in signal transduction (Whitmore and Lamont, 2012), and a membrane-associated serine protease of the rhomboid family (gp93). One CD identified that is of particular interest is the glycosyltransferase domain of gp102. T-even bacteriophages have been shown to use glycosyltransferases for DNA modification by linking a glycosyl group to hydroxymethyl-cytosine, thus protecting the DNA against digestion by bacterial restriction systems (Bair and Black, 2007). Another role for glycosyltransferases within bacteriophages is highlighted by some *Shigella* phages which have been shown to seroconvert their host by modifying the

O-antigen polysaccharides to prevent infection of the bacteria by other O-antigen receptor phages (Allison and Verma, 2000). The specific glycosyltransferase family is RfaB, a protein involved in the assembly of the LPS core of *Escherichia coli* K-12 (Pradel et al., 1992). This result suggests DLP3 may use the glycosyltransferase to modify the host LPS, similar to the seroconverting *Shigella* phages, though this has yet to be confirmed experimentally.

Phage DLP3 Relatedness to Phage DLP5

While characterizing the *Siphoviridae* phage DLP3 genome, it was evident through BLASTn and BLASTp searches that phages DLP3 and DLP5 are closely related. The genome size of DLP3 and DLP5 are similar (96,852 versus 96,542 bp), as is their GC content (58.3 versus 58.4%). BLASTn analysis of DLP3 against DLP5 revealed 81% identity over 90% of the DLP5 genome (0.0 *E*-value). A LASTZ alignment (Harris, 2007) of the phages using DLP5 as the reference sequence shows sequence identity >30% between their genomes, represented as a mustard yellow color in the consensus (**Figure 3**). BLASTn alignment between DLP3 to DLP5 gives a query coverage of 89% and 81% identity. Two small stretches with a breakdown in identity are observed between the DLP5 and DLP3 genomes, which is viewed as a breakdown in the alignment blocks of the dot plot around 30,000 and 60,000 bp (**Figure 3**). These stretches correspond to four genes (DLP05_037 to DLP05_039, plus DLP05_087) encoding hypothetical proteins with no significant matches in the NCBI database, no conserved domains, and no significant results when using structural prediction software such as HHpred and Phyre. Two additional genes, DLP05_045 and DLP05_068, which encode hypothetical proteins, are not present in the DLP3 genome. The DLP05_045 gene product shares 93% coverage with 36% identity (1.0E-08) to a *Polaromonas naphthalenivorans* hypothetical protein which contains no conserved domains, whereas the DLP05_068 gene product did not have similar sequences in the NCBI database or conserved domains predicted. Both phages encode five tRNAs, with four of the five tRNAs sharing the same specificity: Sup-CTA, Glu-TTC, Ser-GCT, Tyr-GTA. Phage DLP3 differs from DLP5 with respect to the fifth tRNA, which is Ile-GAT in DLP3 but Gly-TCC in DLP5. The amino acid usage of each phage does not explain the differences, as they each have the same usage rates for isoleucine (4.7%) and glycine (7.7%), but there are several nucleotide changes observed in this region when comparing DLP3 to DLP5.

Besides the genomic similarities observed between DLP3 and DLP5, they also share morphological similarities. The DLP3 and DLP5 phages have the same measurement averages for their head width (84 nm) and length (92 nm), as well as tail length (202 nm). The host range of DLP3 versus DLP5 is significantly different, with DLP3 exhibiting a broad host range infecting 22 *S. maltophilia* strains, whereas DLP5 only infects six (**Table 1**). Of the six strains DLP5 is capable of infecting (102, 249, D1571, D1614, D1576, SMDP92), DLP3 is only unable to infect the DLP5 host strain D1614. The virion morphogenesis proteins of DLP3 range in sequence identity to the DLP5 equivalents from 43.8% (gp28) to 93.2% (gp6), with all but gp28 having sequence identity greater than 70%. The gp28 proteins of DLP3 and DLP5 are related to the *Xylella* phage Sano tail fiber protein. The annotation of tail fiber for the Sano protein was based solely on synteny to the *Burkholderia* phage BcepNazgul255. There are no shared conserved domains identified between these two proteins, and the Bcep Nazgul protein is 1,270 amino acids long whereas the DLP3 and DLP5 gp28 proteins and the Sano tail fiber protein are only approximately 340 amino acids long; thus, we consider the assignment of tail fiber function to the Sano phage protein to be incorrect.

The gp28 proteins of DLP3 and DLP5 may play a role in host range due to the variability observed between these proteins. The DLP5 gp28 protein shares 62.5% identity with the Sano tail fiber, while DLP3 only has 39.6% identity to the Sano protein and 41.8% identity to the DLP5 protein. The first 242 N-terminal amino acids of the DLP3 and DLP5 gp28 consensus show a high degree of variability at 24.5% pairwise identity. The remaining 104 amino acids from 243 to the C-terminal have high pairwise identity at 88.5%. Variability in the N-terminal region was also observed with a MUSCLE alignment using all three proteins from DLP3, DLP5 and Sano (**Supplementary Figure S1**). The first 258 N-terminal amino acids of the protein consensus share only 35.4% pairwise identity, which increases to 77.8% over the remaining 104 amino acids. The alignment shows at least nine insertion/deletion events have occurred within the DLP3 gene resulting in gaps and insertions in the translated DLP3 protein compared to the Sano and DLP5 proteins. Further investigation into gp28 of DLP3 and DLP5 as a host recognition protein is currently underway to help elucidate whether this protein plays a role in the host range of the *Delepquintavirus* phages.

Receptor Identification

Three *Siphoviridae* phages, DLP1, DLP2 and DLP4, previously isolated on *S. maltophilia* strain D1585, were found to bind the type IV pilus as their cell surface receptor across their host ranges (McCutcheon et al., 2018; Peters et al., 2019). Despite isolating DLP3 on strain D1571, we assessed DLP3 plaquing ability on the previously constructed D1585 and 280 Δ*pilA* mutants lacking the major pilin subunit. Similar to the three previously characterized phages, *S. maltophilia* strains lacking type IV pili are also resistant to infection by DLP3, shown by an absence of cell lysis at high titer (**Figure 4**). Complementation with the endogenous genes restores phage infection to wildtype levels. Unfortunately, the *pilA* gene is undetectable in the incompletely assembled D1571 genome, which prevented construction of pili mutants in this background. In contrast to host range data collected when DLP3 was initially isolated from the environment (**Table 1**), DLP3 efficiency of plating on D1585 and 280 is much lower than initially documented, showing phage activity at 10^9 PFU/mL compared to plaque formation at 10^5 PFU/mL (**Figure 4**). We attribute this reduced plaquing ability on some hosts to the repeated propagation of DLP3 on strain D1571. It is hypothesized that propagating DLP3 on a single host has selected for phages optimized to that host over time, resulting in the differences observed.

An additional mutant was constructed in strain D1585, Δ*pilT*, lacking the retraction ATPase required for depolymerization of the pilus (Burrows, 2005). This mutation results in hyperpiliated, non-motile cells having numerous non-functional pili projecting

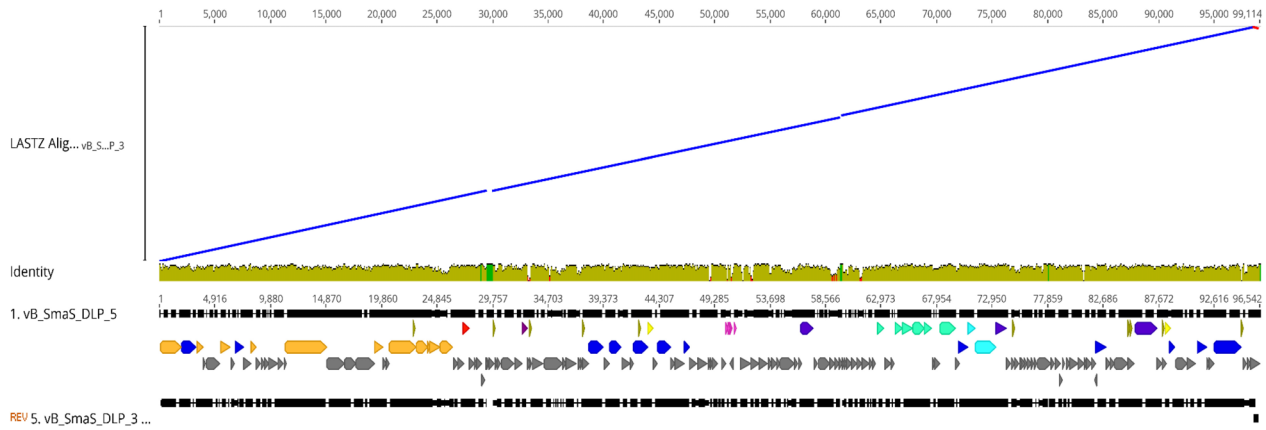

FIGURE 3 | Genomic alignment of DLP3 to DLP5 using the Large-Scale Genome Alignment Tool. Identity is indicated by color: mustard yellow; >30%, green; deletion in DLP3, red; deletion in DLP5.

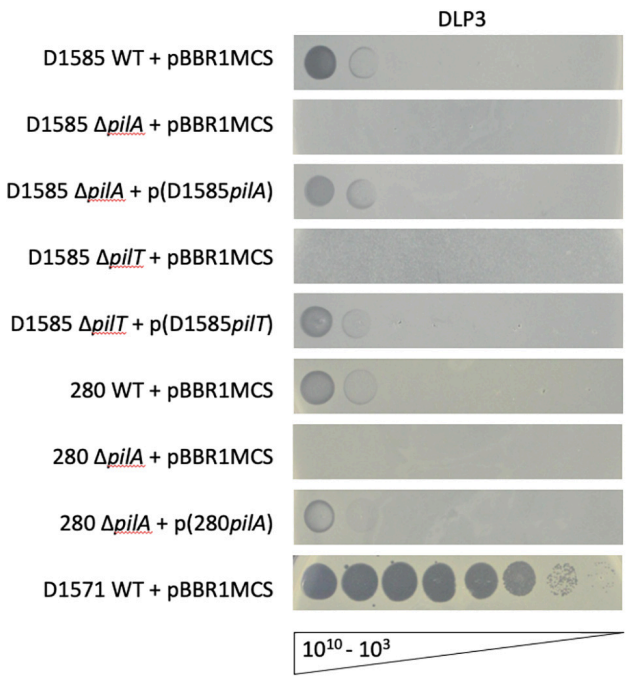

FIGURE 4 | DLP3 requires a functional type IV pilus to infect host strains D1585 and 280. Phage DLP3 is capable of infecting wildtype *S. maltophilia* strains D1585 and 280, infecting both at 10^9 PFU/mL, whereas phage infection is blocked in the Δ*pilA* and Δ*pilT* mutants. Complementation with the endogenous genes restores phage infection to wildtype levels. DLP3 plaquing ability on strain D1571 is shown for titer calculation, however, no mutants were constructed in this background. Images are representative of three biological replicates, each with three technical replicates.

from the cell surface. Similar to the Δ*pilA* mutants, D1585 Δ*pilT* is resistant to DLP3 phage infection. This strain grows poorly in liquid, as observed in the speckled overlay lawn, however, this phenotype, as well as susceptibility to phage, is restored by complementation with the *pilT* gene (**Figure 4**). These results indicate that DLP3 uses the type IV pilus as a cell surface receptor and requires a functional pilus capable of retraction to reach the cell surface for successful host infection. This is the fourth documented *S. maltophilia* phage to use the type IV pilus as its receptor, however, we have yet to identify the receptor for the highly similar phage DLP5. Minor differences in the genomes of these two phages likely explains the significant differences observed in phage host range due to the binding of different receptors.

Analysis of DLP3 Structural Proteins

To further investigate DLP3 morphology, phage structural proteins were analyzed by HPLC-MS and screened against DLP3 proteins and the *Stenotrophomonas* database in UniProt. The SEQUEST results from searching all DLP3 proteins identified 21 (**Table 4**), though only 11 proteins were classified as virion morphogenesis using BLASTp and CD-Search data (**Supplementary Figure S2**). The most abundant protein isolated was the major capsid protein (gp6), which is the main structural component of a bacteriophage capsid (Hendrix and Johnson, 2012). The second most abundant protein found was the portal protein (gp1), which forms the entry site for phage DNA to be packaged into the capsid by the large terminase. The portal protein also functions like a DNA sensor, measuring the amount of DNA packaged into the capsid and signaling the large terminase to end genome-packaging once full (Lokareddy et al., 2017).

Gene products gp14 and gp18 were also identified. Both gene products are hypothetical proteins without conserved domains. Also, they do not have significant results using HHpred; therefore, their structural function is unknown (**Table 4**). Phyre2 analysis of these proteins only suggested a putative function for gp14, which showed structural identity to the major tropism determinant P1 (MTD-P1) of *Bordetella* phage BPP-1 (38.7% confidence, 25% identity). The MTD-P1 protein in BPP-1 is responsible for phage receptor binding (Miller et al., 2008) and uses specific variable residues for target recognition similar to

TABLE 4 | Mass spectrometry protein results with the DLP3 protein database.

Gp	Function	Score	Coverage (%)	Unique Peptides	Peptides	PSMs	AAs	MW [kDa]	calc. pI
6	Major capsid protein	1635.14	91.94	27	27	2709	310	33.7	5.76
14	Hypothetical protein gp_015	189.02	56.57	12	12	282	251	27.4	4.92
1	Portal protein	95.51	51.24	35	36	339	566	62.7	5.41
18	Hypothetical protein gp_019	54.48	19.54	10	10	123	527	58.2	6.27
17	Tape measure protein	45.75	21.85	28	28	78	1254	131.9	6.39
27	Tail assembly protein	33.34	28.48	7	7	46	323	35.4	7.05
19	DUF4302 family protein	30.84	27.47	7	7	69	324	35.8	6.61
24	Tail protein	23.39	26.51	18	18	106	826	90.1	5.08
97	WcaG	22.78	30.99	10	10	52	313	34.8	5.99
21	Minor tail protein	11.39	28.68	9	9	19	272	30.5	7.33
2	ParB-like nuclease domain protein	11.28	20.45	8	8	19	445	49.3	6.96
9	Hypothetical protein gp_010	8.01	31.03	6	6	11	203	22.5	5.94
28	Tail protein	7.74	24.71	10	10	24	340	37.2	8.73
20	Hypothetical protein gp_021	7.56	14.85	9	9	30	559	63.5	5.25
61	Hypothetical protein gp_066	6.45	27.45	7	7	31	204	22.3	9.00
25	Tail assembly protein	4.15	23.80	6	6	15	332	35.5	5.15
12	Hypothetical protein gp_013	2.37	78.35	4	4	7	97	9.6	9.47
3	Serine protease	2.24	9.95	2	2	3	201	22.7	4.67
57	RecA	2.03	15.56	5	5	7	405	43.5	6.46
5	Hypothetical protein gp_006	0.00	6.67	2	2	4	405	43.4	5.39
133	ATPase family protein	0.00	10.67	4	4	9	403	44.6	5.80

Results are ordered by score.

an antibody (Miller, 2006). Another abundant protein identified is gp24, which is predicted to be a structural component of the DLP3 tail with a phage-tail_3 family (PF13550) conserved domain. The tape measure protein (gp17), which is responsible for setting the tail length (Belcaid et al., 2011), is the largest protein identified and the sixth most abundant, though the ∼130 kDa band was faint after fully destaining (**Supplementary Figure S2**). The remaining DLP3 proteins identified and ordered by relative abundance are gene products gp19, gp97, gp27, gp61, gp20, gp28, gp2, gp21, gp25, gp9, gp133, gp12, gp57, gp5, and gp3. Some of the proteins identified are surprising, such as gp2 (Par-B like nuclease domain protein) and gp5 (RecA), but based on the results obtained by screening the *Stenotrophomonas* protein database, it is evident that there were proteins present from the bacterial cell; thus, there may also be DLP3 proteins present that are not structural in function (**Table 4** and **Supplementary Table S2**).

Lysogenic Conversion of D1571 by Temperate Phage DLP3

Stable DLP3 lysogens of *S. maltophilia* strain D1571 have been isolated and due to the presence of ParB domains in two of the DLP3 proteins, DLP3 may lysogenize its host as a phagemid. The closely related phage DLP5 was also found to encode two proteins with ParB domains and was successfully isolated as a phagemid from the lysogenized strain D1614 (Peters and Dennis, 2018). Blastn and PHAST analysis (Altschul et al., 1997; Zhou et al., 2011) of GenBank-deposited *Stenotrophomonas* genomes indicates that phage DLP3 (or phages closely related to DLP3) has also lysogenized *S. maltophilia* strains ABB550, FDAARGOS_325 and ICU331. Phage DLP5 has been previously shown to cause lysogenic conversion of *S. maltophilia* strain D1571 (Peters and Dennis, 2018). Therefore, we sought to further investigate the characteristics of the D1571:DLP3 lysogen relative to wildtype *S. maltophilia* strain D1571.

Identification of Erythromycin Resistance Factor Erm(45)

Annotation of the DLP3 genome revealed the presence of a methyltransferase domain in the gene product encoded by

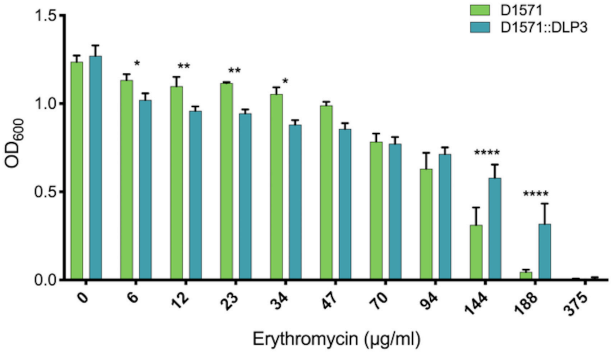

FIGURE 5 | Erythromycin resistance of D1571:DLP3 lysogen increases compared to wild type control D1571. Minimum inhibitory concentration assay was completed in biological and mechanical triplicates. Two-way ANOVA with Sidak's multiple comparisons test was performed on the MIC data. Statistical significance is represented as: ****$P < 0.0001$; **$P < 0.01$; and *$P < 0.05$.

DLP3_099. A specific domain identified is the AdoMet_MTases superfamily comprised of class I S-adenosylmethionine-dependent methyltransferases. The class I family is the largest and most diverse, with members targeting a range of substrate specificities such as small molecules, lipids, nucleic acids, and different target atoms for methylation (Struck et al., 2012). Members of this family are known to maintain structural similarity even when the amino acid sequence diverges to as little as 10% (Schubert et al., 2003). Further investigation into gp69 with HHblits revealed high sequence identity to Erm(45) of *Staphylococcus fleurettii* (HHblits: 100% probability, 2.4e-104 *E*-value). Researchers identified Erm(45) as the enzyme responsible for increased erythromycin resistance in some strains of *S. fleuretti* (Wipf et al., 2015). The erm gene (erythromycin ribosome methylase) encodes a methylase enzyme that provides macrolide resistance by methylating the erythromycin target-site on the ribosome (Prunier et al., 2002). Together, these findings suggested that the DLP3 encoded methyltransferase is an erythromycin resistance protein similar to Erm(45) and could cause an increase in erythromycin resistance of the host cell during lysogeny.

To test the functionality of the DLP3 Erm protein, minimum inhibitory concentration (MIC) assays of the wild type D1571 and lysogen D1571:DLP3 were completed. The results show a statistically significant difference in erythromycin resistance with DLP3 lysogeny over a wide range of concentrations tested (**Figure 5**). There are differences noted between the wild type and lysogenized strains at lower concentrations of erythromycin, with wild type having a statistically significant increase in optical density at lower concentrations (6 and 34 μg/ml; $P < 0.05$, 12 and 23 μg/ml; $P < 0.01$). The cause of the decreased resistance in the lysogen noted at lower concentrations of erythromycin is currently unknown. This trend is reversed at higher concentrations of erythromycin, with the lysogen having significantly higher OD_{600} readings at 144 and 188 μg/ml erythromycin concentrations compared to wild type control ($P < 0.0001$). The increased resistance noted at higher erythromycin concentrations indicates lysogenic conversion of D1571 by lysogenized DLP3 and confirms the functionality of the predicted Erm protein. Fortuitously, *S. maltophilia* strains are already highly resistant toward macrolides, and macrolides such as erythromycin are not considered to be a frontline treatment option.

Differing Growth Characteristics of DLP3 Lysogen *in vitro*

While working with the D1571:DLP3 lysogen and wild type D1571 for the erythromycin resistance assay, it was evident that the lysogen exhibited a faster growth rate as compared to the wild type strain. This difference in growth rate was also observed when growing single colony isolates of the lysogen and wild type on an LB agar plate, with the lysogen having larger single colonies after a 16 h incubation at 30°C as compared to the wild type D1571 (data not shown). To investigate this phenotypic difference further, a growth curve was conducted in mechanical and biological triplicates for the lysogen and wild type over 8 h. The plotted growth curve clearly shows the lysogenized strain exhibiting a faster growth rate than the wild type strain, with significance found following a two-way repeated measures ANOVA with multiple comparisons at 2 h, $P < 0.05$; 4 h, $P < 0.0001$; and 6 h, $P < 0.01$ (**Figure 6A**). This observation was confirmed by converting the OD_{600} data into growth rate (μ) and plotting the resulting data (**Figure 6B**). A two-way repeated measures ANOVA with multiple comparisons revealed significant ($P < 0.0001$) differences between 0- to 2-h and 2- to 4-h time intervals for the lysogen and wild type D1571. The increased growth rate is only observed during the lag and early exponential phase of growth and disappears in the 4- to 6-h and 6- to 8-h growth rate intervals. The cause of the growth

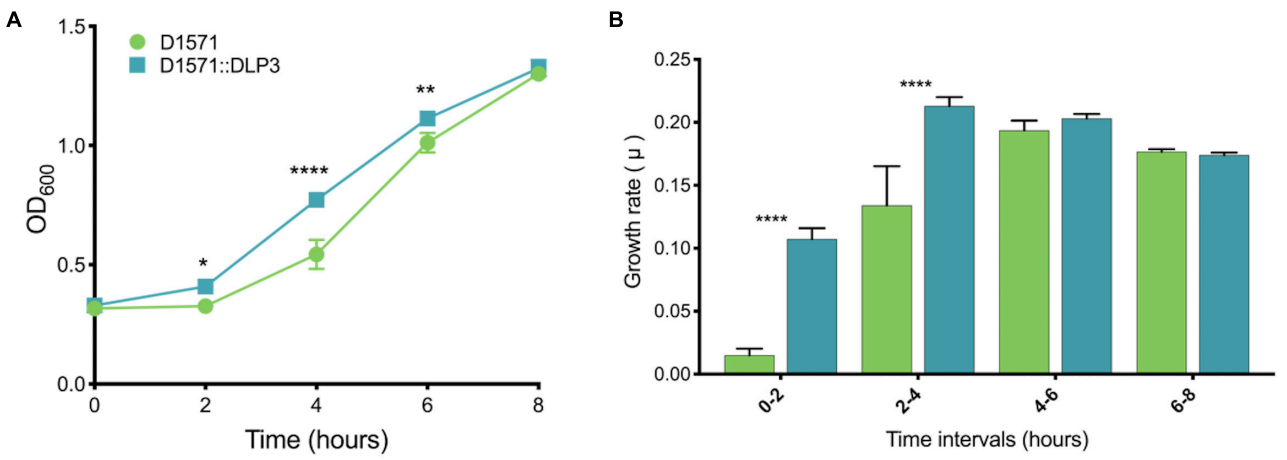

FIGURE 6 | *In vitro* growth analysis of D1571 wild type and D1571:DLP3 lysogen. **(A)** Growth curve of wildtype D1571 compared to D1571:DLP3 strains grown in LB broth over 8 h. Results from biological and mechanical triplicate experiments were averaged and the mean plotted with the standard deviation represented as error bars. **(B)** Growth curve OD_{600} data was converted to the growth rate for wildtype and DLP3 lysogen with the mean plotted and error bars representing standard deviation. Two-way repeated measures ANOVA with multiple comparisons indicates statistical significance (*$P < 0.05$; **$P < 0.01$; ****$P < 0.0001$).

rate differences observed with DLP3 lysogenization is currently unknown, though DLP3 does encode many hypothetical and moron genes which may be expressed to produce this phenotype.

Virulence of D1571:DLP3 and DLP3 Rescue in *G. mellonella*

Based on the differing growth characteristics of D1571:DLP3 lysogen and the wildtype strain, we examined if the increased growth rate of the lysogen observed *in vitro* affected the virulence of strain D1571 *in vivo* using the *G. mellonella* larvae infection model. *G. mellonella* have been used as a non-mammalian eukaryotic model for assessing the virulence of many bacterial pathogens, including *S. maltophilia* (Betts et al., 2014; Tsai et al., 2016; Melloul et al., 2018), as well as a model to study the efficacy of novel antimicrobial compounds and phages (Seed and Dennis, 2009; Kamal and Dennis, 2015; Cutuli et al., 2019). Injection of *G. mellonella* larvae with *S. maltophilia* D1571 results in dose-dependent killing, with the lethal dose for this strain greater than 10^7 CFU per larva (**Figure 7A**). Coinciding with the faster growth rate observed *in vitro*, the D1571:DLP3 lysogen was more virulent than the wildtype D1571 strain, resulting in significantly lower survival for *G. mellonella* larvae injected with 10^7 ($P < 0.01$) or 10^6 ($P < 0.001$) CFU over 120 h (**Figure 7A**). This increased virulence may be due to the faster growth rate of D1571:DLP3, however, CFU were not recovered from the larvae following infection.

Despite the DLP3 lysogen showing increased virulence *in vivo*, we sought to determine if DLP3 could rescue *G. mellonella* from wildtype D1571 infection. An inoculum of approximately 10^6 CFU per larva was chosen to allow for phage rescue at a multiplicity of infection of at least 100, as DLP3 does not propagate higher than 10^{10} PFU/mL. Larvae were injected with DLP3 lysate at 1.5 h post-infection with D1571 and survival

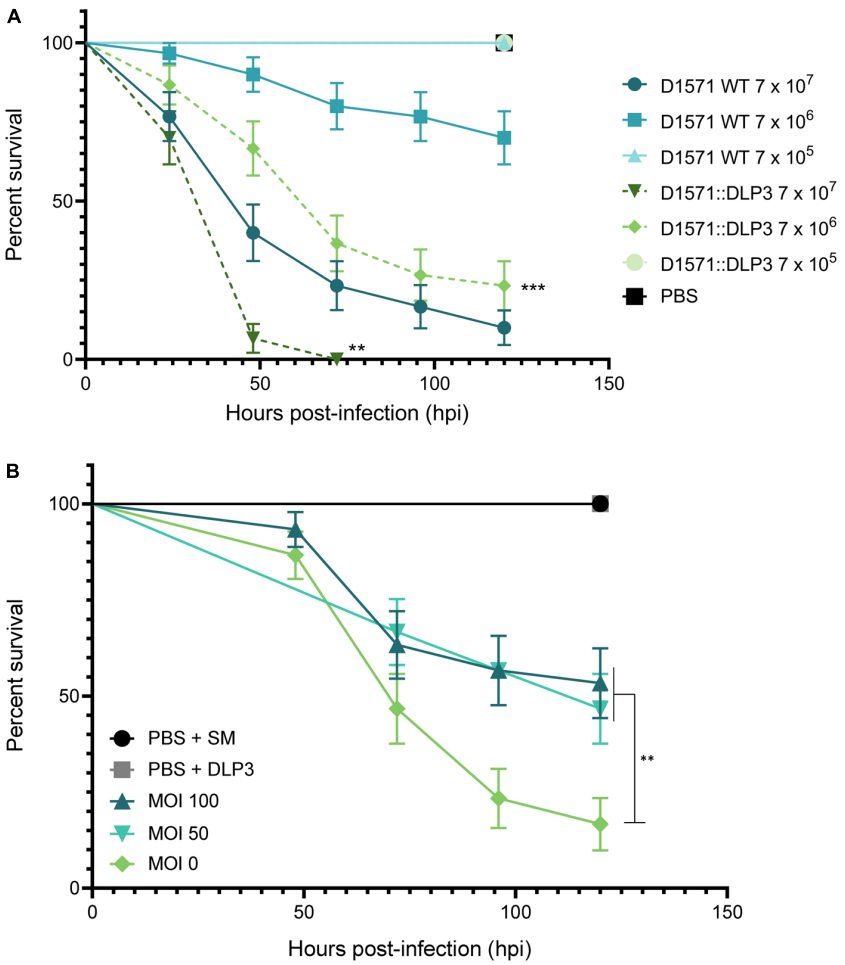

FIGURE 7 | Effect of DLP3 on the virulence of D1571 in *G. mellonella*. **(A)** Survival of *G. mellonella* larvae over 120 h following infection with *S. maltophilia* D1571 wildtype or D1571:DLP3 lysogen at varying CFU. Larvae infected with D1571:DLP3 showed significantly lower survival at 10^7 (**$P < 0.01$) and 10^6 (***$P < 0.001$) CFU than larvae injected with the same inoculum of D1571 (log-rank test). **(B)** Survival of *G. mellonella* larvae injected with 8×10^8 CFU of D1571 over 120 h treated with DLP3 at an MOI of 100 (8.9×10^8 PFU), 50 (4.5×10^8 PFU) or 0 at 1.5 h post-infection. For controls, sterile PBS and SM were used in place of bacteria and phage injections, respectively. A significant difference in survival was observed between untreated larvae (MOI 0) and either phage treatment (**$P < 0.01$; log-rank test). Ten larvae were injected per group and results were obtained from three separate trials and plotted using the Kaplan–Meier method with standard error bars.

monitored over 120 h. Compared to treatment with SM buffer, significantly more larvae survived when given phage at a MOI of 50 or 100 (**Figure 7B**, $P < 0.01$), with an average survival at 120 h of 53% or 47% for worms treated at an MOI of 100 or 50, respectively, compared to 17% survival of untreated larvae. Attempts to concentrate DLP3 to a titer greater than 10^{12} PFU/mL without causing melanization of larvae following phage injection were unsuccessful, however, we expect that treatment at a higher MOI would increase the survival of infected larvae. Increased survival may also occur with repeated phage injections over the course of the experiment, however, this was not tested. Overall, this preliminary investigation using *G. mellonella* indicates the potential of DLP3 as a therapeutic for the treatment of *S. maltophilia* infections.

CONCLUSION

The novel temperate phage DLP3 isolated from a soil sample enabled the identification of a second member of the newly established *Delepquintavirus* genus. DLP3 has a genome size of 96,852 bp and a GC content of 58.4%, which is significantly lower than the host strain D1571 which has a GC content of 66.9%. DLP3 encodes two proteins with ParB conserved domains enabling the stable lysogenization of the host strain D1571. Lysogenization by DLP3 leads to a growth rate increase during the lag and early exponential phase of growth for the host when compared to the wild type strain. DLP3 also encodes a functional Erm protein, allowing for the lysogenic conversion of the host D1571 strain which is observed though increased resistance to erythromycin at 144 and 188 μg/ml concentrations. Despite the temperate lifestyle of this phage, DLP3 is capable of lytic activity *in vivo*.

Like DLP3, many of the *S. maltophilia* temperate phages characterized to date feature moron genes that encode virulence factors or antibiotic resistance proteins that could cause lysogenic conversion of their host (Hagemann et al., 2006; Garcia et al., 2008; Peters and Dennis, 2018; Peters et al., 2019). Genetically modifying these phages by removing adverse genes, such as those encoding virulence factors or lysogeny proteins, will enable the creation of safe and highly targeted therapeutic agents (Lynch et al., 2010; Dedrick et al., 2019). Modified phages have been used in a case study against *Mycobacterium abscessus* (Dedrick et al., 2019) and a clinical trial (NCT04191148) sponsored by Locus Bioscience treating urinary tract infections with their modified crPhage cocktail. The genetically modified phage therapy examples set the precedence for other phages, such as DLP3, to be genetically modified and included in therapeutic phage cocktails. To this end, further study of DLP3 receptor binding proteins will possibly allow for the modification of other *S. maltophilia* phages showing therapeutic potential to target a wider host range.

DATA AVAILABILITY STATEMENT

The datasets generated for this study can be found in GenBank under accession number MT110073.

AUTHOR CONTRIBUTIONS

DP isolated phage DLP3, performed experiments to characterize the genome and viral particle, wrote the original manuscript draft and edited the manuscript. JM performed experiments to characterize the virus, wrote parts of the manuscript, and edited the manuscript. JD conceived of the research, directed the experiments, funded the research, and edited the manuscript. All authors contributed to the article and approved the submitted version.

FUNDING

This research was supported by operating funds to JD from the Natural Sciences and Engineering Research Council of Canada (NSERC-238414-2018). DP gratefully acknowledges Alberta Innovates AITF, and NSERC PGS-D graduate scholarships. JM was kindly supported by a CGS-D award from NSERC and an AIGSS award from Alberta Innovates.

ACKNOWLEDGMENTS

The authors would like to thank Arlene Oatway from the University of Alberta Department of Biological Sciences Advanced Microscopy Facility for assistance with electron microscopy. The authors thank the Canadian *Burkholderia cepacia* complex Research and Referral Repository (CBCCRRR, Vancouver, BC, Canada) and The Provincial Laboratory for Public Health – North (Microbiology), Alberta Health Services, for gifts of the *S. maltophilia* strains used in this study. The authors thank Dr. Andrew Keddie from the University of Alberta for supplying the *G. mellonella* larvae used to establish their lab colony, and thank Dr. Keddie and Dr. Brent Weber for providing information and advice on breeding *G. mellonella*.

SUPPLEMENTARY MATERIAL

The Supplementary Material for this article can be found online at: https://www.frontiersin.org/articles/10.3389/fmicb.2020.01358/full#supplementary-material

FIGURE S1 | MUSCLE multiple sequence alignment of gp28 proteins from phages DLP3 and DLP5, and tail fiber protein of *Xylella* phage Sano. Note the increased amino acid conservation toward the C-termini of the proteins versus the N-termini as observed through protein alignment.

FIGURE S2 | SDS-PAGE gel of DLP3 ghost particles (L) compared to a PageRuler Plus Pre-stained Protein Ladder (Thermo Scientific). Approximate masses are labeled on the right of the gel in kDa. Protein bands labeled using mass spectrometry results from SEQUEST scan of DLP3 and *Stenotrophomonas* protein databases. Stacking and resolving portions of the gel were 4 and 7.5%, respectively. The gel was stained with Coomassie R-250.

TABLE S1 | Bacterial strains and plasmids used in this study.

TABLE S2 | Mass spectrometry protein results using the Stenotrophomonas protein database in UniProt. The results are organized by score.

REFERENCES

Ackermann, H. W., and Eisenstark, A. (1974). The present state of phage taxonomy. *Intervirology* 3, 201–219. doi: 10.1159/000149758

Al-Anazi, K. A., and Al-Jasser, A. M. (2014). Infections caused by *Stenotrophomonas maltophilia* in recipients of hematopoietic stem cell transplantation. *Front. Oncol.* 4:232. doi: 10.3389/fonc.2014.00232

Allison, G. E., and Verma, N. K. (2000). Serotype-converting bacteriophages and O-antigen modification in *Shigella flexneri*. *Trends Microbiol.* 8, 17–23. doi: 10.1016/s0966-842x(99)01646-7

Altschul, S. F., Madden, T. L., Schäffer, A. A., Zhang, J., Zhang, Z., Miller, W., et al. (1997). Gapped BLAST and PSI-BLAST: a new generation of protein database search programs. *Nucleic Acids Res.* 25, 3389–3402. doi: 10.1093/nar/25.17.3389

Avison, M. B., Higgins, C. S., von Heldreich, C. J., Bennett, P. M., and Walsh, T. R. (2001). Plasmid location and molecular heterogeneity of the L1 and L2 beta-lactamase genes of *Stenotrophomonas maltophilia*. *Antimicrob. Agents Chemother.* 45, 413–419. doi: 10.1128/AAC.45.2.413-419.2001

Avison, M. B., von Heldreich, C. J., Higgins, C. S., Bennett, P. M., and Walsh, T. R. (2000). A TEM-2 beta-lactamase encoded on an active Tn1-like transposon in the genome of a clinical isolate of *Stenotrophomonas maltophilia*. *J. Antimicrob. Chemother.* 46, 879–884. doi: 10.1093/jac/46.6.879

Bair, C., and Black, L. W. (2007). Exclusion of glucosyl-hydroxymethylcytosine DNA containing bacteriophages. *J. Mol. Biol.* 366, 779–789. doi: 10.1016/j.jmb.2006.11.049

Barbolla, R., Catalano, M., Orman, B. E., Famiglietti, A., Vay, C., Smayevsky, J., et al. (2004). Class 1 integrons increase trimethoprim-sulfamethoxazole MICs against epidemiologically unrelated *Stenotrophomonas maltophilia* isolates. *Antimicrob. Agents Chemother.* 48, 666–669. doi: 10.1128/AAC.48.2.666-669.2004

Belcaid, M., Bergeron, A., and Poisson, G. (2011). The evolution of the tape measure protein: units, duplications and losses. *BMC Bioinformatics* 12(Suppl. 9):S10. doi: 10.1186/1471-2105-12-S9-S10

Berg, G., Eberl, L., and Hartmann, A. (2005). The rhizosphere as a reservoir for opportunistic human pathogenic bacteria. *Environ. Microbiol.* 7, 1673–1685. doi: 10.1111/j.1462-2920.2005.00891.x

Berg, G., and Martinez, J. L. (2015). Friends or foes: can we make a distinction between beneficial and harmful strains of the *Stenotrophomonas maltophilia* complex? *Front. Microbiol.* 6:241. doi: 10.3389/fmicb.2015.00241

Berg, G., Roskot, N., and Smalla, K. (1999). Genotypic and phenotypic relationships between clinical and environmental isolates of *Stenotrophomonas maltophilia*. *J. Clin. Microbiol.* 37, 3594–3600. doi: 10.1128/jcm.37.11.3594-3600.1999

Besemer, J., Lomsadze, A., and Borodovsky, M. (2001). GeneMarkS: a self-training method for prediction of gene starts in microbial genomes. Implications for finding sequence motifs in regulatory regions. *Nucleic Acids Res.* 29, 2607–2618. doi: 10.1093/nar/29.12.2607

Betts, J. W., Phee, L. M., Woodford, N., and Wareham, D. W. (2014). Activity of colistin in combination with tigecycline or rifampicin against multidrug-resistant *Stenotrophomonas maltophilia*. *Eur. J. Clin. Microbiol. Infect. Dis.* 33, 1565–1572. doi: 10.1007/s10096-014-2101-3

Boulanger, P. (2009). *Bacteriophages: Methods and Protocols, Molecular and Applied Aspects*, Vol. 2, eds M. R. J. Clokie and A. M. Kropinski (Totowa, NJ: Humana Press), 227–238.

Brooke, J. S. (2012). *Stenotrophomonas maltophilia*: an emerging global opportunistic pathogen. *Clin. Microbiol. Rev.* 25, 2–41. doi: 10.1128/cmr.00019-11

Brooke, J. S. (2014). New strategies against *Stenotrophomonas maltophilia*: a serious worldwide intrinsically drug-resistant opportunistic pathogen. *Exp. Rev. Anti Infect. Ther.* 12, 1–4. doi: 10.1586/14787210.2014.864553

Brooke, J. S., Vo, A., Watts, P., and Davis, N. A. (2008). Mutation of a lipopolysaccharide synthesis gene results in increased biofilm of *Stenotrophomonas maltophilia* on plastic and glass surfaces. *Ann. Microbiol.* 58, 35–40. doi: 10.1007/bf03179442

Burrowes, B., Harper, D. R., Anderson, J., McConville, M., and Enright, M. C. (2011). Bacteriophage therapy: potential uses in the control of antibiotic-resistant pathogens. *Expert Rev. Anti Infect. Ther.* 9, 775–785. doi: 10.1586/eri.11.90

Burrows, L. (2005). Weapons of mass retraction. *Mol. Microbiol.* 57, 878–888. doi: 10.1111/j.1365-2958.2005.04703.x

Chang, H. C., Chen, C. R., Lin, J. W., Shen, G. H., Chang, K. M., Tseng, Y. H., et al. (2005). Isolation and characterization of novel giant *Stenotrophomonas maltophilia* phage phi SMA5. *Appl. Environ. Microbiol.* 71, 1387–1393. doi: 10.1128/aem.71.3.1387-1393.2005

Chang, Y. C., Tsai, M. J., Huang, Y. W., Chung, T. C., and Yang, T. C. (2011). SmQnrR, a DeoRtype transcriptional regulator, negatively regulates the expression of Smqnr and SmtcrA in *Stenotrophomonas maltophilia*. *J. Antimicrob. Chemother.* 66, 1024–1028. doi: 10.1093/jac/dkr049

Chang, Y. T., Lin, C. Y., Chen, Y. H., and Hsueh, P. R. (2015). Update on infections caused by *Stenotrophomonas maltophilia* with particular attention to resistance mechanisms and therapeutic options. *Front. Microbiol.* 6:893. doi: 10.3389/fmicb.2015.00893

Chang, Y. T., Lin, C. Y., Lu, P. L., Lai, C. C., Chen, T. C., Chen, C. Y., et al. (2014). *Stenotrophomonas maltophilia* bloodstream infection: comparison between community-onset and hospital-acquired infections. *J. Microbiol. Immunol. Infect.* 47, 28–35. doi: 10.1016/j.jmii.2012.08.014

Chatelut, M., Dournes, J. L., Chabanon, G., and Marty, N. (1995). Epidemiological typing of *Stenotrophomonas* (*Xanthomonas*) maltophilia by PCR. *J. Clin. Microbiol.* 33, 912–914. doi: 10.1128/jcm.33.4.912-914.1995

Chung, H. S., Hong, S. G., Kim, Y. R., Shin, K. S., Whang, D. H., Ahn, J. Y., et al. (2013). Antimicrobial susceptibility of *Stenotrophomonas maltophilia* isolates from Korea, and the activity of antimicrobial combinations against the isolates. *J. Korean Med. Sci.* 28, 62–66. doi: 10.3346/jkms.2013.28.1.62

Chung, H. S., Kim, K., Hong, S. S., Hong, S. G., Lee, K., and Chong, Y. (2015). The *sul1* gene in *Stenotrophomonas maltophilia* with high-level resistance to trimethoprim/sulfamethoxazole. *Ann. Lab. Med.* 35, 246–249. doi: 10.3343/alm.2015.35.2.246

Crowder, M. W., Walsh, T. R., Banovic, L., Pettit, M., and Spencer, J. (1998). Overexpression, purification, and characterization of the cloned metallo-β-lactamase L1 from *Stenotrophomonas maltophilia*. *Antimicrob. Agents Chemother.* 42, 921–926. doi: 10.1128/aac.42.4.921

Cutuli, M. A., Petronio, G. P., Vergalito, F., Magnifico, I., Pietrangelo, L., Venditti, N., et al. (2019). *Galleria mellonella* as a consolidated *in vivo* model hosts: new developments in antibacterial strategies and novel drug testing. *Virulence* 10, 527–541. doi: 10.1080/21505594.2019.1621649

de Oliveira-Garcia, D., Dall'Agnol, M., Rosales, M., Azzuz, A. C., Alcántara, N., Martinez, M. B., et al. (2003). Fimbriae and adherence of *Stenotrophomonas maltophilia* to epithelial cells and to abiotic surfaces. *Cell. Microbiol.* 5, 625–636. doi: 10.1046/j.1462-5822.2003.00306.x

Dedrick, R. M., Guerrero-Bustamante, C. A., Garlena, R. A., Daniel, A., Ford, K., Harris, K., et al. (2019). Engineered bacteriophages for treatment of a patient with a disseminated drug resistant *Mycobacterium abscessus*. *Nat. Med.* 25, 730–733. doi: 10.1038/s41591-019-0437-z

Delcher, A. L., Bratke, K. A., Powers, E. C., and Salzberg, S. L. (2007). Identifying bacterial genes and endosymbiont DNA with Glimmer. *Bioinformatics* 23, 673–679. doi: 10.1093/bioinformatics/btm009

Denton, M., and Kerr, K. G. (1998). Microbiological and clinical aspects of infection associated with *Stenotrophomonas maltophilia*. *Clin. Microbiol. Rev.* 11, 57–80. doi: 10.1128/cmr.11.1.57

Falagas, M. E., Kastoris, A. C., Vouloumanou, E. K., and Dimopoulos, G. (2009). Community-acquired *Stenotrophomonas maltophilia* infections: a systematic review. *Eur. J. Clin. Microbiol. Infect. Dis.* 28, 719–730. doi: 10.1007/s10096-009-0709-5

Fan, N., Cutting, S., and Losick, R. (1992). Characterization of the *Bacillus subtilis* sporulation gene spoVK. *J. Bacteriol.* 174, 1053–1054. doi: 10.1128/jb.174.3.1053-1054.1992

Figueiredo, P. M. S., Furumura, M. T., Santos, A. M., Sousa, A. C., Kota, D. J., Levy, C. E., et al. (2006). Cytotoxic activity of clinical *Stenotrophomonas maltophilia*. *Lett. Appl. Microbiol.* 43, 443–449. doi: 10.1111/j.1472-765X.2006.01965.x

Finn, R. D., Bateman, A., Clements, J., Coggill, P., Eberhardt, R. Y., Eddy, S. R., et al. (2014). Pfam: the protein families database. *Nucleic Acids Res.* 42, D222–D230. doi: 10.1093/nar/gkt1223

Furlan, J. P. R., and Stehling, E. G. (2018). Detection of blaPER on an IncA/C plasmid in *Stenotrophomonas maltophilia* isolated from Brazilian soil. *Water Air Soil Pollut.* 229:142.

Garcia, P., Monjardín, C., Martín, R., Madera, C., Soberón, N., Garcia, E., et al. (2008). Isolation of new *Stenotrophomonas* bacteriophages and genomic

characterization of temperate phage S1. *Appl. Environ. Microbiol.* 74, 7552–7560. doi: 10.1128/aem.01709-08

Golkar, Z., Bagasra, O., and Pace, D. G. (2014). Bacteriophage therapy: a potential solution for the antibiotic resistance crisis. *J. Infect. Dev. Ctries.* 8, 129–136. doi: 10.3855/jidc.3573

Hagemann, M., Hasse, D., and Berg, G. (2006). Detection of a phage genome carrying *a zonula occludens* like toxin gene (*zot*) in clinical isolates of *Stenotrophomonas maltophilia*. *Arch. Microbiol.* 185, 449–458. doi: 10.1007/s00203-006-0115-7

Hanahan, D., Jessee, J., and Bloom, F. R. (1991). Plasmid transformation of *Escherichia coli* and other bacteria. *Methods Enzymol.* 204, 63–113. doi: 10.1016/0076-6879(91)04006-a

Harris, R. S. (2007). *Improved Pairwise Alignment of Genomic DNA*. Ph.D. thesis, The Pennsylvania State University, State College, PA.

Hauben, L., Vauterin, L., Moore, E. R. B., Hoste, B., and Swings, J. (1999). Genomic diversity of the genus *Stenotrophomonas*. *Int. J. Syst. Bacteriol.* 49, 1749–1760. doi: 10.1099/00207713-49-4-1749

Hendrix, R. W., and Johnson, J. E. (2012). Bacteriophage HK97 capsid assembly and maturation. *Adv. Exp. Med. Biol.* 726, 351–363. doi: 10.1007/978-1-4614-0980-9_15

Hoang, T. T., Karkhoff-Schweizer, R. R., Kutchma, A. J., and Schweizer, H. P. (1998). A broad-host-range Flp-FRT recombination system for site-specific excision of chromosomally-located DNA sequences: application for isolation of unmarked *Pseudomonas aeruginosa* mutants. *Gene* 212, 77–86. doi: 10.1016/s0378-1119(98)00130-9

Hu, L. F., Chang, X., Ye, Y., Wang, Z. X., Shao, Y. B., Shi, W., et al. (2011). *Stenotrophomonas maltophilia* resistance to trimethoprim/sulfamethoxazole mediated by acquisition of sul and dfrA genes in a plasmid-mediated class 1 integron. *Int. J. Antimicrob. Agents* 37, 230–234. doi: 10.1016/j.ijantimicag.2010.10.025

Huang, T. P., Somers, E. B., and Wong, A. C. L. (2006). Differential biofilm formation and motility associated with lipopolysaccharide/exopolysaccharide-coupled biosynthetic genes in *Stenotrophomonas maltophilia*. *J. Bacteriol.* 188, 3116–3120. doi: 10.1128/JB.188.8.3116-3120.2006

Huang, Y. W., Hu, R. M., and Yang, T. C. (2013). Role of the pcm-tolCsm operon in the multidrug resistance of *Stenotrophomonas maltophilia*. *J. Antimicrob. Chemother.* 68, 1987–1993. doi: 10.1093/jac/dkt148

Kamal, F., and Dennis, J. J. (2015). *Burkholderia cepacia* complex phage-antibiotic synergy (PAS): antibiotics stimulate lytic phage activity. *Appl. Environ. Microbiol.* 81, 1132–1138. doi: 10.1128/aem.02850-14

Kamal, F., Peters, D. L., McCutcheon, J. G., Dunphy, G. B., and Dennis, J. J. (2019). Use of greater wax moth larvae (*Galleria mellonella*) as an alternative animal infection model for analysis of bacterial pathogenesis. *Methods Mol. Biol.* 1898, 163–171. doi: 10.1007/978-1-4939-8940-9_13

Kampmeier, S., Pillukat, M. H., Pettke, A., Kossow, A., Idelevich, E. A., and Mellmann, A. (2017). Evaluation of a *Stenotrophomonas maltophilia* bacteremia cluster in hematopoietic stem cell transplantation recipients using whole genome sequencing. *Antimicrob. Resist. Infect. Control* 6:115. doi: 10.1186/s13756-017-0276-y

Kearse, M., Moir, R., Wilson, A., Stones-Havas, S., Cheung, M., Sturrock, S., et al. (2012). Geneious Basic: an integrated and extendable desktop software platform for the organization and analysis of sequence data. *Bioinformatics* 28, 1647–1649. doi: 10.1093/bioinformatics/bts199

Kelley, L. A., Mezulis, S., Yates, C. M., Wass, M. N., and Sternberg, M. J. (2015). The Phyre2 web portal for protein modeling, prediction and analysis. *Nat. Protoc.* 10, 845–858. doi: 10.1038/nprot.2015.053

Kim, Y. J., Park, J. H., and Seo, K. H. (2018). Presence of *Stenotrophomonas maltophilia* exhibiting high genetic similarity to clinical isolates in final effluents of pig farm wastewater treatment plants. *Int. J. Hyg. Environ. Health* 221, 300–307. doi: 10.1016/j.ijheh.2017.12.002

Kovach, M. E., Phillips, R. W., Elzer, P. H., Roop, R. M., and Peterson, K. M. (1994). pBBR1MCS: a broad-host-range cloning vector. *Biotechniques* 16, 800–802.

Lai, C. H., Wong, W. W., Chin, C., Huang, C. K., Lin, H. H., Chen, W. F., et al. (2006). Central venous catheter-related *Stenotrophomonas maltophilia* bacteraemia and associated relapsing bacteraemia in haematology and oncology patients. *Clin. Microbiol. Infect.* 12, 986–991. doi: 10.1111/j.1469-0691.2006.01511.x

Lin, L., Wang, S. F., Yang, T. Y., Hung, W. C., Chan, M. Y., and Tseng, S. P. (2017). Antimicrobial resistance and genetic diversity in ceftazidime nonsusceptible bacterial pathogens from ready-to-eat street foods in three Taiwanese cities. *Sci. Rep.* 7:15515.

Lin, Y. T., Huang, Y. W., Chen, S. J., Chang, C. W., and Yang, T. C. (2015). The SmeYZ efflux pump of *Stenotrophomonas maltophilia* contributes to drug resistance, virulence-related characteristics, and virulence in mice. *Antimicrob. Agents Chemother.* 59, 4067–4073. doi: 10.1128/aac.00372-15

Lokareddy, R. K., Sankhala, R. S., Roy, A., Afonine, P. V., Motwani, T., Teschke, C. M., et al. (2017). Portal protein functions akin to a DNA-sensor that couples genome-packaging to icosahedral capsid maturation. *Nat. Commun.* 8:14310. doi: 10.1038/ncomms14310

Lynch, K. H., Seed, K. D., Stothard, P., and Dennis, J. J. (2010). Inactivation of *Burkholderia cepacia* complex phage KS9 gp41 identifies the phage repressor and generates lytic virions. *J. Virol.* 84, 1276–1288. doi: 10.1128/JVI.01843-09

Marchler-Bauer, A., Lu, S., Anderson, J. B., Chitsaz, F., Derbyshire, M. K., DeWeese-Scott, C., et al. (2011). CDD: a Conserved Domain Database for the functional annotation of proteins. *Nucleic Acids Res.* 39, D225–D229. doi: 10.1093/nar/gkq1189

McCutcheon, J. G., Peters, D. L., and Dennis, J. J. (2018). Identification and characterization of type IV pili as the cellular receptor of broad host range *Stenotrophomonas maltophilia* bacteriophages DLP1 and DLP2. *Viruses* 10:E338. doi: 10.3390/v10060338

McKay, G. A., Woods, D. E., MacDonald, K. L., and Poole, K. (2003). Role of phosphoglucomutase of *Stenotrophomonas maltophilia* in lipopolysaccharide biosynthesis, virulence, and antibiotic resistance. *Infect. Immun.* 71, 3068–3075. doi: 10.1128/iai.71.6.3068-3075.2003

Melloul, E., Roisin, L., Durieux, M., Woerther, P., Jenot, D., Risco, V., et al. (2018). Interactions of *Aspergillus fumigatus* and *Stenotrophomonas maltophilia* in an *in vitro* mixed biofilm model: does the strain matter? *Front. Microbiol.* 9:2850. doi: 10.3389/fmicb.2018.02850

Mett, H., Rosta, S., Schacher, B., and Frei, R. (1988). Outer membrane permeability and beta-lactamase content in *Pseudomonas maltophilia* clinical isolates and laboratory mutants. *Rev. Infect. Dis.* 10, 765–769. doi: 10.1093/clinids/10.4.765

Miller, J. L. (2006). *Understanding Receptor Specificity though the Massively Variable Major Tropism Determinant of Bordetella Bacteriophage*. Ph.D. thesis, University of California, Oakland, CA.

Miller, J. L., Le Coq, J., Hodes, A., Barbalat, R., Miller, J. F., and Ghosh, P. (2008). Selective ligand recognition by a diversity-generating retroelement variable protein. *PLoS Biol.* 6:e131. doi: 10.1371/journal.pbio.0060131

Minkwitz, A., and Berg, G. (2001). Comparison of antifungal activities and 16S ribosomal DNA sequences of clinical and environmental isolates of *Stenotrophomonas maltophilia*. *J. Clin. Microbiol.* 39, 139–145. doi: 10.1128/JCM.39.1.139-145.2001

Naidu, P., and Smith, S. (2012). A review of 11 years of *Stenotrophomonas maltophilia* blood isolates at a tertiary care institute in Canada. *Can. J. Infect. Dis. Med. Microbiol.* 23, 165–169. doi: 10.1155/2012/762571

Nicoletti, M., Iacobino, A., Prosseda, G., Fiscarelli, E., Zarrilli, R., De Carolis, E., et al. (2011). *Stenotrophomonas maltophilia* strains from cystic fibrosis patients: genomic variability and molecular characterization of some virulence determinants. *Int. J. Med. Microbiol.* 301, 34–43. doi: 10.1016/j.ijmm.2010.07.003

Ochoa-Sanchez, L. E., and Vinuesa, P. (2017). Evolutionary genetic analysis uncovers multiple species with distinct habitat preferences and antibiotic resistance phenotypes in the *Stenotrophomonas maltophilia* complex. *Front. Microbiol.* 8:1548. doi: 10.3389/fmicb.2017.01548

Okazaki, A., and Avison, M. B. (2007). Aph(3′)-IIc, an aminoglycoside resistance determinant from *Stenotrophomonas maltophilia*. *Antimicrob. Agents Chemother.* 51, 359–360. doi: 10.1128/aac.00795-06

Okazaki, A., and Avison, M. B. (2008). Induction of L1 and L2 β-lactamase production in *Stenotrophomonas maltophilia* is dependent on an AmpR-type regulator. *Antimicrob. Agents Chemother.* 52, 1525–1528. doi: 10.1128/aac.01485-07

Palleroni, N. J., and Bradbury, J. F. (1993). *Stenotrophomonas*, a new bacterial genus for *Xanthomonas maltophilia* (Hugh 1980) Swings et al. 1983. *Int. J. Syst. Bacteriol.* 43, 606–609. doi: 10.1099/00207713-43-3-606

Peters, D. L., and Dennis, J. J. (2018). Complete genome sequence of temperate *Stenotrophomonas maltophilia* bacteriophage DLP5. *Genome Announc.* 6:e00073-18.

Peters, D. L., Lynch, K. H., Stothard, P., and Dennis, J. J. (2015). The isolation and characterization of two *Stenotrophomonas maltophilia* bacteriophages capable

of cross-taxonomic order infectivity. *BMC Genomics* 16:664. doi: 10.1186/s12864-015-1848-y

Peters, D. L., McCutcheon, J. G., Stothard, P., and Dennis, J. J. (2019). Novel *Stenotrophomonas maltophilia* temperate phage DLP4 is capable of lysogenic conversion. *BMC Genomics* 20:300. doi: 10.1186/s12864-019-5674-5

Peters, D. L., Stothard, P., and Dennis, J. J. (2017). The isolation and characterization of *Stenotrophomonas maltophilia* T4-like bacteriophage DLP6. *PLoS One* 12:e0173341. doi: 10.1371/journal.pone.0173341

Pompilio, A., Crocetta, V., Confalone, P., Nicoletti, M., Petrucca, A., Guarnieri, S., et al. (2010). Adhesion to and biofilm formation on IB3-1 bronchial cells by *Stenotrophomonas maltophilia* isolates from cystic fibrosis patients. *BMC Microbiol.* 10:102. doi: 10.1186/1471-2180-10-102

Pompilio, A., Piccolomini, R., Picciani, C., D'Antonio, D., Savini, V., and Di Bonaventura, G. (2008). Factors associated with adherence to and biofilm formation on polystyrene by *Stenotrophomonas maltophilia*: the role of cell surface hydrophobicity and motility. *FEMS Microbiol. Lett.* 287, 41–47. doi: 10.1111/j.1574-6968.2008.01292.x

Pradel, E., Parker, C. T., and Schnaitman, C. A. (1992). Structures of the *rfaB*, *rfaI*, *rfaJ*, and *rfaS* genes of *Escherichia coli* K-12 and their roles in assembly of the lipopolysaccharide core. *J. Bacteriol.* 174, 4736–4745.

Prunier, A. L., Malbruny, B., Tande, D., Picard, B., and Leclercq, R. (2002). Clinical isolates of *Staphylococcus aureus* with ribosomal mutations conferring resistance to macrolides. *Antimicrob. Agents Chemother.* 46, 3054–3056. doi: 10.1128/aac.46.9.3054-3056.2002

Qureshi, A., Mooney, L., Denton, M., and Kerr, K. G. (2005). *Stenotrophomonas maltophilia* in salad. *Emerg. Infect. Dis.* 11, 1157–1158. doi: 10.3201/eid1107.040130

Rathi, M., and Nandabalan, Y. K. (2017). Copper-tolerant rhizosphere bacteria-characterization and assessment of plant growth promoting factors. *Environ. Sci. Pollut. Res.* 24, 9723–9733. doi: 10.1007/s11356-017-8624-2

Remmert, M., Biegert, A., Hauser, A., and Soding, J. (2011). HHblits: lightning-fast iterative protein sequence searching by HMM-HMM alignment. *Nat. Methods* 9, 173–175. doi: 10.1038/nmeth.1818

Rhee, J. Y., Song, J. H., and Ko, K. S. (2016). Current situation of antimicrobial resistance and genetic differences in *Stenotrophomonas maltophilia* complex isolates by multilocus variable number of tandem repeat analysis. *Infect. Chemother.* 48, 285–293. doi: 10.3947/ic.2016.48.4.285

Ryan, R. P., Monchy, S., Cardinale, M., Taghavi, S., Crossman, L., Avison, M. B., et al. (2009). The versatility and adaptation of bacteria from the genus *Stenotrophomonas*. *Nat. Rev. Microbiol.* 7, 514–525. doi: 10.1038/nrmicro2163

Sanchez, M. B. (2015). Antibiotic resistance in the opportunistic pathogen *Stenotrophomonas maltophilia*. *Front. Microbiol.* 6:658. doi: 10.3389/fmicb.2015.00658

Sanchez, M. B., Hernandez, A., Rodriguez-Martinez, J. M., Martinez-Martinez, L., and Martinez, J. L. (2008). Predictive analysis of transmissible quinolone resistance indicates *Stenotrophomonas maltophilia* as a potential source of a novel family of Qnr determinants. *BMC Microbiol.* 8:148. doi: 10.1186/1471-2180-8-148

Sanchez, M. B., and Martinez, J. L. (2010). SmQnr contributes to intrinsic resistance to quinolones in *Stenotrophomonas maltophilia*. *Antimicrob. Agents Chemother.* 54, 580–581. doi: 10.1128/aac.00496-09

Schattner, P., Brooks, A. N., and Lowe, T. M. (2005). The tRNAscan-SE, snoscan and snoGPS web servers for the detection of tRNAs and snoRNAs. *Nucleic Acids Res.* 33, W686–W689. doi: 10.1093/nar/gki366

Schubert, H. L., Blumenthal, R. M., and Cheng, X. (2003). Many paths to methyltransfer: a chronicle of convergence. *Trends Biochem. Sci.* 28, 329–335. doi: 10.1016/s0968-0004(03)00090-2

Schwab, F., Geffers, C., Behnke, M., and Gastmeier, P. (2018). ICU mortality following ICU acquired primary bloodstream infections according to the type of pathogen: a prospective cohort study in 937 Germany ICUs (2006-2015). *PLoS One* 13:e0194210. doi: 10.1371/journal.pone.0194210

Seed, K. D., and Dennis, J. J. (2008). Development of *Galleria mellonella* as an alternative infection model for the *Burkholderia cepacia* complex. *Infect. Immun.* 76, 1267–1275. doi: 10.1128/iai.01249-07

Seed, K. D., and Dennis, J. J. (2009). Experimental bacteriophage therapy increases survival of *Galleria mellonella* larvae infected with clinically relevant strains of the *Burkholderia cepacia* Complex. *Antimicrob. Agents Chemother.* 53, 2205–2208. doi: 10.1128/aac.01166-08

Simon, R., Priefer, U., and Puhler, A. (1983). A broad host range mobilization system for in vivo genetic engineering: transposon mutagenesis in gram negative bacteria. *Nat. Biotechnol.* 1, 784–791. doi: 10.1038/nbt1183-784

Struck, A. W., Thompson, M. L., Wong, L. S., and Micklefield, J. (2012). S-adenosyl-methionine dependent methyltransferases: highly versatile enzymes in biocatalysis, biosynthesis and other biotechnological applications. *Chem. Biochem.* 13, 2642–2655. doi: 10.1002/cbic.201200556

Sulakvelidze, A., Alavidze, Z., and Morris, J. G. Jr. (2001). Bacteriophage therapy. *Antimicrob. Agents Chemother.* 45, 649–659. doi: 10.1128/AAC.45.3.649-659.2001

Svensson-Stadler, L. A., Mihaylova, S. A., and Moore, E. R. (2012). *Stenotrophomonas* interspecies differentiation and identification by *gyrB* sequence analysis. *FEMS Microbiol. Lett.* 327, 15–24. doi: 10.1111/j.1574-6968.2011.02452.x

Toleman, M. A., Bennett, P. M., Bennett, D. M., Jones, R. N., and Walsh, T. R. (2007). Global emergence of trimethoprim/sulfamethoxazole resistance in *Stenotrophomonas maltophilia* mediated by acquisition of sul genes. *Emerg. Infect. Dis.* 13, 559–565. doi: 10.3201/eid1304.061378

Tsai, C. J., Loh, J. M. S., and Proft, T. (2016). *Galleria mellonella* infection models for the study of bacterial diseases and for antimicrobial drug testing. *Virulence* 7, 214–229. doi: 10.1080/21505594.2015.1135289

Velazquez-Acosta, C., Zarco-Marquez, S., Jiminez-Andrade, M. C., Volkow-Fernandez, P., and Cornejo-Juarez, P. (2018). *Stenotrophomonas maltophilia* bacteremia and pneumonia at a tertiary-care oncology center: a review of 16 years. *Support. Care Cancer* 26, 1953–1960. doi: 10.1007/s00520-017-4032-x

Vetting, M. W., Park, C. H., Hegde, S. S., Jacoby, G. A., Hooper, D. C., and Blanchard, J. S. (2008). Mechanistic and structural analysis of aminoglycoside N-acetyltransferase AAC(6′)-Ib and its bifunctional, fluoroquinolone-active AAC(6′)-Ib-cr variant. *Biochemistry* 47, 9825–9835. doi: 10.1021/bi800664x

Walsh, T. R., MacGowan, A. P., and Bennett, P. M. (1997). Sequence analysis and enzyme kinetics of the L2 serine β-lactamase from *Stenotrophomonas maltophilia*. *Antimicrob. Agents Chemother.* 41, 1460–1464. doi: 10.1128/aac.41.7.1460

Wang, C. H., Lin, J. C., Lin, H. A., Chang, F. Y., Wang, N. C., Chiu, S. K., et al. (2016). Comparisons between patients with trimethoprim-sulfamethoxazole-susceptible and trimethoprim-sulfamethoxazole-resistant *Stenotrophomonas maltophilia* monomicrobial bacteremia: a 10-year retrospective study. *J. Microbiol. Immunol. Infect.* 49, 378–386. doi: 10.1016/j.jmii.2014.06.005

Whitmore, S. E., and Lamont, R. J. (2012). Tyrosine phosphorylation and bacterial virulence. *Int. J. Oral Sci.* 4, 1–6. doi: 10.1038/ijos.2012.6

Wiegand, I., Hilpert, K., and Hancock, R. E. W. (2008). Agar and broth dilution methods to determine the minimal inhibitory concentration (MIC) of antimicrobial substances. *Nat. Protoc.* 3, 163–175. doi: 10.1038/nprot.2007.521

Wipf, J. R. K., Schwendener, S., Nielsen, J. B., Westh, H., and Perreten, V. (2015). The new macrolide-lincosamide-streptogramin b resistance gene erm(45) is located within a genomic island in *Staphylococcus fleurettii*. *Antimicrob. Agents Chemother.* 59, 3578–3581. doi: 10.1128/aac.00369-15

Yang, J., and Zhang, Y. (2015). Protein structure and function prediction using I-TASSER. *Curr. Protoc. Bioinformatics* 52, 5.8.1–5.8.15. doi: 10.1002/0471250953.bi0508s52

Zhou, Y., Liang, Y., Lynch, K. H., Dennis, J. J., and Wishart, D. S. (2011). PHAST: a fast phage search tool. *Nucleic Acids Res.* 39, W347–W352. doi: 10.1093/nar/gkr485

Zimmermann, L., Stephens, A., Nam, S. Z., Rau, D., Kübler, J., Lozajic, M., et al. (2018). A completely reimplemented MPI bioinformatics toolkit with a new HHpred server at its core. *J. Mol. Biol.* 17, 30587–30589.

Conflict of Interest: The authors declare that the research was conducted in the absence of any commercial or financial relationships that could be construed as a potential conflict of interest.

Copyright © 2020 Peters, McCutcheon and Dennis. This is an open-access article distributed under the terms of the Creative Commons Attribution License (CC BY). The use, distribution or reproduction in other forums is permitted, provided the original author(s) and the copyright owner(s) are credited and that the original publication in this journal is cited, in accordance with accepted academic practice. No use, distribution or reproduction is permitted which does not comply with these terms.

frontiers in Microbiology

ORIGINAL RESEARCH
published: 21 July 2020
doi: 10.3389/fmicb.2020.01554

Isolation and Characterization of Novel Lytic Bacteriophages Infecting Epidemic Carbapenem-Resistant *Klebsiella pneumoniae* Strains

Min Li[1,2,3†], Min Guo[4†], Long Chen[5], Chaowang Zhu[6], Yuyi Xiao[1,2,3], Pei Li[1,2,3], Hongxiong Guo[7], Liang Chen[8,9], Wei Zhang[1,2,3*] and Hong Du[4*]*

[1] College of Veterinary Medicine, Nanjing Agricultural University, Nanjing, China, [2] Key Lab of Animal Bacteriology, Ministry of Agriculture, Nanjing, China, [3] MOE Joint International Research Laboratory of Animal Health and Food Safety, College of Veterinary Medicine, Nanjing Agricultural University, Nanjing, China, [4] Department of Clinical Laboratory, The Second Affiliated Hospital of Soochow University, Suzhou, China, [5] Department of Clinical Laboratory, Zhangjiagang Hospital Affiliated to Soochow University, Zhangjiagang, China, [6] Department of Clinical Laboratory, The North District of Suzhou Municipal Hospital, Nanjing Medical University, Suzhou, China, [7] Department of Expanded Program on Immunization, Jiangsu Provincial Center for Disease Control and Prevention, Nanjing, China, [8] Center for Discovery and Innovation, Hackensack Meridian Health, Nutley, NJ, United States, [9] Hackensack Meridian School of Medicine, Seton Hall University, Nutley, NJ, United States

Carbapenem-resistant *Klebsiella pneumoniae* (CRKP) poses a significant clinical problem given the lack of therapeutic options available. Alternative antibacterial agents, such as bacteriophages, can be used as a valuable tool to treat the infections caused by these highly resistant bacteria. In this study, we isolated 54 phages from medical and domestic sewage wastewater between July and September 2019 and determined their host ranges against 54 clinical CRKP isolates, collected from a tertiary hospital in eastern China. The 54 CRKP isolates were from 7 sequence types (STs) and belonged to 9 capsular K locus types, harboring bla_{KPC-2} (n = 49), bla_{NDM-1} (n = 5), and bla_{IMP-4} (n = 3). Among them, the epidemic KPC-2-producing ST11 strains were most predominant (88.9%). The 54 phages showed different host ranges from 7 to 52 CRKP isolates. The total host ranges of three phages can potentially cover all 54 CRKP isolates. Among the 54 phages, phage P545, classified as a member of Myoviridae, order Caudovirales, had a relatively wide host range (96.3%), a short latent period of 20 min, and a medium burst size of 82 PFU/cell and was stably maintained at different pH values (4–10) and temperatures (up to 60°C). P545 showed the ability to inhibit biofilm formation and to degrade the mature biofilms. Taken together, the results of our study showed that the newly isolated phage P545 had a relatively wide host range, excellent properties, and antibacterial activity as well as antibiofilm activity against a clinical CRKP ST11 isolate, providing a promising candidate for future phage therapy applications.

Keywords: bacteriophages, carbapenem-resistant, host range, *Klebsiella pneumoniae*, sewage

OPEN ACCESS

Edited by:
Sutthirat Sitthisak, Naresuan University, Thailand

Reviewed by:
Zhongjing Lu, Kennesaw State University, United States
Rattanaruji Pomwised, Prince of Songkla University, Thailand

***Correspondence:**
Hong Du
hong_du@126.com; hongdu@suda.edu.cn
Liang Chen
liang.chen@hmh-cdi.org
Wei Zhang
vszw@njau.edu.cn

† These authors have contributed equally to this work

Specialty section:
This article was submitted to Antimicrobials, Resistance and Chemotherapy, a section of the journal Frontiers in Microbiology

Received: *23 December 2019*
Accepted: *16 June 2020*
Published: *21 July 2020*

Citation:
Li M, Guo M, Chen L, Zhu C, Xiao Y, Li P, Guo H, Chen L, Zhang W and Du H (2020) Isolation and Characterization of Novel Lytic Bacteriophages Infecting Epidemic Carbapenem-Resistant Klebsiella pneumoniae Strains. Front. Microbiol. 11:1554. doi: 10.3389/fmicb.2020.01554

INTRODUCTION

Carbapenem-resistant *Klebsiella pneumoniae* (CRKP) has spread globally and become a significant clinical threat because of the lack of therapeutic options available. The carbapenem-resistant genes were mostly plasmid borne, thereby facilitating the horizontal transfer of resistance between different species and strains. Worrisome is that CRKP strains have recently developed resistance to some last-line antibiotics, such as polymyxin and tigecycline (Zhang et al., 2018). Although some novel β-lactam/β-lactamase inhibitor combinations, e.g., cefatazidime/avibactam, meropenem/vaborbactam, and imipenem/relebactam, were approved for the treatment of CRKP infections, they were not effective against all carbapenemase producers. Consequently, antibiotic therapeutic choices against CRKP remain limited, while other measures, such as phage therapy, have been considered as alternative measures to prevent and control CRKP infections (Ciacci et al., 2018; Anand et al., 2019).

Bacteriophages, also known as phages, are viruses that can invade and replicate in bacterial cells, and for the case of lytic phages, they are able to disrupt bacterial metabolism and cause the bacteria to lyse. Phages were discovered and clinically implemented against bacterial infections approximately 100 years ago, even before the discovery of antibiotics (Kwan et al., 2005). However, phage therapy was gradually ignored along with the wide application of antibiotics (Criscuolo et al., 2017; Lazaro-Perona et al., 2018). The progressive reduction of the effectiveness of antibiotics has recently generated renewed interest in revisiting phage therapy.

During clinical practice, phages can be used systematically through oral or injection administration, or locally on wounds or burns, as well as in the hospital environment and on medical devices. Phage therapy has been used against some Enterobacteriaceae pathogens, and among them, *Escherichia coli* phages (Chen et al., 2017; Cieplak et al., 2018) and *Salmonella* phages (Huang et al., 2018) were the most studied and applied. *K. pneumoniae* phages also had some applications, such as in burns (Chadha et al., 2017) and diabetes-related foot ulcers (Morozova et al., 2018). However, studies on phages against clinical CRKP strains were still limited. In the study reported here, we isolated 54 phages from domestic and hospital sewage wastewater and examined their activities against 54 CRKP strains collected from a tertiary hospital in eastern China, within one of the CRKP endemic regions.

MATERIALS AND METHODS

Bacteria and Growth Conditions

A total of 54 unique (one isolate per patient) CRKP isolates, collected from blood ($n = 7$), abdominal cavity ($n = 5$), respiratory tract ($n = 35$), urinary tract ($n = 4$), and other body sites ($n = 3$), from a tertiary hospital in eastern China between 2016 and 2018 were used as host bacteria to determine the host ranges of phages. Details of the bacterial isolates used in this study are listed in **Table 1**. All isolates were routinely cultured in Luria–Bertani (LB) broth at 37°C on an orbital shaker at 180 rpm. Phosphate-buffered saline (0.1 M Na_2HPO_4, 0.15 M $NaCl_2$, pH 7.2) was used for dilution and wash of *K. pneumoniae* cultures.

Antimicrobial Susceptibility Testing

Antimicrobial susceptibility testing was conducted using the standard broth microdilution method and followed the Clinical & Laboratory Standards Institute (CLSI) guidelines. Meropenem and imipenem were tested from 0.25 to 32 μg/mL. The 2018 CLSI breakpoints were used to interpret the susceptibility results. This experiment was performed in three biological replicates. *Escherichia coli* ATCC®25922 was used as a negative control.

Genetic Background of CRKP Strains

Multilocus sequence typing (MLST) was used to investigate the sequence types (STs) of the total 54 CRKP isolates. In brief, polymerase chain reaction (PCR) detection followed by Sanger sequencing was used to examine seven conserved housekeeping genes including *gapA*, *infB*, *mdh*, *pgi*, *phoE*, *rpoB*, and *tonB* (Diancourt et al., 2005). Allelic profiles and sequence types were determined based on the *Klebsiella* locus/sequence definitions database[1]. Capsular types were determined by *wzi* sequencing (Brisse et al., 2013) and the K locus types (KLs) were inferred using the same *Klebsiella* locus/sequence definitions database as described above. In addition, ST11 KL64 and KL47 capsular types were examined by a multiplex PCR scheme described previously (Yu et al., 2018).

Detection of Carbapenemases, Extended-Spectrum Beta-Lactamases, and AmpC Genes

Polymerase chain reaction was performed to investigate the presence of carbapenemase-encoding genes, including bla_{KPC}, bla_{NDM}, bla_{VIM}, bla_{IMP}, and bla_{OXA-48}-like. In addition, we examined the extended-spectrum beta-lactamases (ESBLs) (CTX-M, SHV, and TEM) and AmpC cephalosporinases (CMY, ACT, and DHA) using PCR followed by Sanger sequencing. Oligonucleotide primers used for screening the aforementioned genes were described in previous reports (Mammeri et al., 2010; Bokaeian et al., 2015; Candan and Aksoz, 2015).

Isolation of Phages

Phages were isolated from the filtered (0.22-μm pore size) sewage, including medical sewage from three sewage treatment stations of local hospitals (site A, B, C) and domestic sewage from a local sewage treatment plant (site D) (**Supplementary Table S1**).

The purification, counting, and propagation of phages were performed using the double-layer agar plate method (Adams, 1959). SM buffer (50 mM Tris−HCl [pH 7.5], 100 mM NaCl, 10 mM $MgSO_4$, and 0.01% gelatin) was used for the dilution of the phages. Phage suspensions were centrifuged at 5000 × *g*, 4°C for 10 min, and then the supernatants were filtered through 0.22-μm filters (Merck Millipore, Germany) and stored at either 4°C

[1]https://bigsdb.pasteur.fr/klebsiella/klebsiella.html

TABLE 1 | Molecular characteristics of the 54 *K. pneumoniae* clinical isolates.

Sequence types (STs)	Number (%)	K locus (KL) types (*n*,%)	Carbapenemases (*n*,%)	ESBLs and AmpC (*n*,%)	Sources (*n*,%)
ST11	48 (88.9)	KL64 (24, 50.0) KL47 (23, 47.9) KL25 (1, 2.1)	KPC-2 (48, 100.0) NDM-1 (2, 4.2)	CTX-M-65 (43, 89.6) CTX-M-14 (1, 2.1) SHV-12 (16, 33.3) DHA-1 (10, 20.8)	Blood (7, 13.0) Abdominal cavity (5, 9.3) Respiratory tract (30, 55.6) Urinary tract (4, 7.4) Others (2, 3.7)
ST147	1 (1.9)	KL107 (1, 100.0)	KPC-2 (1, 100.0)	–	Respiratory tract (1, 1.9)
ST230	1 (1.9)	KL136 (1, 100.0)	IMP-4 (1, 100.0)	CTX-M-3 (1, 100.0)	Respiratory tract (1, 1.9)
ST3155	1 (1.9)	KL139 (1, 100.0)	IMP-4 (1, 100.0)	–	Others (1, 1.9)
ST3369	1 (1.9)	KL116 (1, 100.0)	NDM-1 (1, 100.0)	–	Respiratory tract (1, 1.9)
ST367	1 (1.9)	KL1 (1, 100.0)	IMP-4 (1, 100.0) NDM-1 (1, 100.0)	CTX-M-55 (1, 100.0)	Respiratory tract (1, 1.9)
ST656	1 (1.9)	KL14 (1, 100.0)	NDM-1 (1, 100.0)	CTX-M-3 (1, 100.0)	Respiratory tract (1)

–, negative.

or at -80°C in glycerol (3:1 [v/v]) (Gu et al., 2011). All the sterile operations were carried out in class II biosecurity cabinets with institutional safety approval.

Host Range Determination of Phages

The host ranges of the phages were determined against 54 CRKP strains using spot testing (Chen et al., 2017). Briefly, 10 μL of the purified phage suspensions (∼10^9 PFU/mL) were spotted onto freshly seeded lawns of the isolates and left to dry before incubation for 6 h at 37°C (Kutter, 2009). Host bacteria were determined by the observation of lytic spots. The host-range frequencies were analyzed using the GraphPad Prism 5 software package. Host ranges of 54 phages were illustrated by HemI software (Deng et al., 2014).

Examination of Bacteriophage Morphology by Electron Microscopy

We selected three phages—P545, P539, and P507—for morphological analysis by transmission electron microscopy (TEM), as they had different host ranges and plaque morphology. The filtrates of phages P545, P539, and P507 were applied to a copper grid, respectively, before negative staining with phosphotungstic acid (PTA, 2% w/v). Electron micrographs were observed using an H_7650 transmission electron microscope (Hitachi, Tokyo, Japan). Bacteriophage morphology and taxonomy were confirmed following the guidelines from the International Committee on Taxonomy of Viruses[2].

Optimal Multiplicity of Infection

A relatively wide host-range phage, P545, identified from the current study was further selected to determine its basic characteristics, including optimal multiplicity of infection, one-step growth curve, and thermo and pH stability.

Multiplicity of infection (MOI) refers to the ratio of phages to host bacteria during the processes for infection (Ji et al., 2019). *K. pneumoniae* ST11 strain KP4 was used as the host strain and was grown to logarithmic phase at a final concentration of approximately 2 × 10^8 CFU/mL (OD_{600} ∼0.4). Phage P545 suspensions were then added at different MOIs (phage/bacteria = 10, 1, 0.1, 0.01, 0.001, 0.0001, 0.00001, and 0.000001), and the mixtures were incubated at 37°C for 10 h. The phage titers were then determined immediately by plaque assay after serial dilution (Gong et al., 2016). All assays were conducted in triplicate. The MOI that generated the highest phage titer within 10 h was considered as the optimal MOI.

One-Step Growth Curve of Phage P545

Bacteriophage latent time and burst size were determined by one-step growth curve as previously described (Pajunen et al., 2000). Phage P545 was added to the exponential-phase KP4 culture (∼2 × 10^8 CFU/mL) at an MOI of 0.1, followed by adsorption at 37°C for 10 min. The precipitated KP4 strains were then resuspended in 10 mL of fresh LB medium after discarding unabsorbed phages by centrifugation at 5000 × *g* for 10 min at 4°C, followed by incubation at 37°C with shaking at 180 rpm. Samples were taken out at 5-min intervals for 120 min, and a 1% final concentration of chloroform was added to each subsample to release the intracellular phages for determining phage titers using the double-layer agar plate method. All assays were conducted in triplicate.

Thermo and pH Stability

Thermo and pH stability tests of phage P545 were conducted following a previously described protocol with minor modifications (Laemmli, 1970). In brief, 100 μL of phage was suspended in 900 μL of SM buffer (pH 7.5) and kept at different temperature (i.e., 4, 25, 37, 50, 60, 70, and 80°C) for 1 h. Phage survival rates were determined by the double-layer agar plate method described above. All assays were conducted in triplicate.

To determine pH stability of P545, 100 μL of phage suspension was added to 900 μL of SM buffer with a gradient of pH (range from 1 to 12), followed by incubation at 37°C for 1 h. SM buffer with a gradient of pH (pH 1–12) was adjusted by HCl and NaOH solution, and measured by a pH meter. Similarly, all the samples were diluted and tested immediately by the double-layer agar plate method. All assays were conducted in triplicate.

[2]https://talk.ictvonline.org/taxonomy/

DNA Extraction and Genome Sequencing

The phage P545 suspensions were concentrated and purified for genomic DNA extraction as previously described (Sambrook and Russell, 2006). The phage genome was sequenced using the Illumina HiSeq system (Illumina, San Diego, CA, United States). Sequencing reads were *de novo* assembled using Spades 3.11.1 (Bankevich et al., 2012). The whole-genome sequence of phage P545 was deposited in the GenBank database under accession number MN781108. Annotation of the phage genome was conducted by the RAST server (Aziz et al., 2008), followed by manual curation. Phages closely related to P545 were examined using online BLASTn against the NCBI database[3]. Genome alignment of the phages was illustrated using EasyFig.

Bacteriophage Potency Against Planktonic Cells and Biofilm

To assess the inhibition effectiveness of phage P545 against KP4 planktonic cells, phages were added to the KP4 cultures (OD 0.1, $\sim 5 \times 10^7$ CFU/mL) at MOIs of 0.1, 0.01, and 0.001, followed by incubation at 37°C with shaking at 180 rpm. Bacterial cultures with no phages was used as an untreated group. The OD_{600} values of the cultures were determined at 5-min intervals for 70 min. The inhibition effectiveness of P545 were analyzed by the growth kinetics of host bacteria.

To assess the inhibition effectiveness of phage P545 in biofilm formation, 100 μL of exponential-phase bacteria (OD 0.4, $\sim 2 \times 10^8$ CFU/mL), 20 μL of phages (at MOIs of 0.1, 0.01, and 0.001), and 80 μL of fresh tryptic soy broth (TSB) medium (Merck, Darmstadt, Germany) were added into each well of 96-well flat-bottomed polystyrene microtiter plates (Sigma-Aldrich, St. Louis, MO, United States) as phage-treated groups. The untreated group consisted of 100 μL of bacteria mixed with 100 μL of fresh TSB medium, while 200 μL of fresh TSB medium was used as the negative control group. All plates were incubated for 24 h at 37°C without shaking. The biofilms were stained with 1% crystal violet as described previously (Wu Y. et al., 2019). Optical density values at 595nm (OD_{595}) were measured using an ELISA microplate reader (Biotek, Winooski, VT, United States). Each experiment was performed in triplicate.

The degradation activity of P545 against the established mature biofilms of KP4 was evaluated using previously described protocols with minor modification (Cerca et al., 2005). Following the incubation of logarithmic-phase bacteria (see above) for 24 h at 37°C in 96-well plates, 100 μL of phage P545 at MOIs of 0.1, 0.01, and 0.001 (phage-treated groups), or 100 μL of fresh medium (untreated group) was added to each well. The negative control group was the same as above. Biofilm degradation was evaluated by the crystal violet staining method described above. Each experiment was performed in triplicate.

Statistical Analysis

All statistical analyses in this study were carried out using the GraphPad Prism 5 software package. Mean differences of negative control, untreated, and phage-treated groups of planktonic or biofilm assay were analyzed by Student's *t*-test. Differences at $P \leq 0.05$ were considered significant.

[3]https://blast.ncbi.nlm.nih.gov/Blast.cgi

RESULTS

Molecular Characteristics of the Clinical Isolates

Multilocus sequence typing showed that 54 *K. pneumoniae* belonged to seven different STs, with ST11 being the most common (48/54, 88.9%). Among 48 ST11 isolates, 24 isolates belonged to capsular K locus type KL64, 23 isolates belonged to KL47, and 1 isolate belonged to KL25. The other 6 isolates belonged to ST147, ST230, ST3155, ST3369, ST367, and ST656, and were assigned as capsular K locus type KL10, KL136, KL139, KL116, KL1, and KL30, respectively. All 54 *K. pneumoniae* isolates were carbapenemase producers, harboring bla_{KPC-2} (49/54, 90.7%), bla_{NDM-1} (5/54, 9.3%), and bla_{IMP-4} (3/54, 5.6%). Among them, three isolates coharbored two carbapenemase genes, with two strains harboring both bla_{KPC-2} and bla_{NDM-1}, and the other one harboring both bla_{NDM-1} and bla_{IMP-4}. Meanwhile, 48 isolates (88.9%) were identified to carry ESBLs and/or AmpC-encoding genes. Among them, 47 isolates were found to carry bla_{CTX-M}, including $bla_{CTX-M-65}$ ($n = 43$), $bla_{CTX-M-3}$ ($n = 2$), $bla_{CTX-M-14}$ ($n = 1$), and $bla_{CTX-M-55}$ ($n = 1$), while 16 isolates carried bla_{SHV-12} and 10 isolates contained bla_{DHA-1}. The results are summarized in **Table 1**.

The result of antibiotic susceptibility testing showed 54 (100%) *K. pneumoniae* were all carbapenem resistant (**Table 2**). Fifty (92.6%) isolates (46 KPC-2, 1 IMP-4, and 2 NDM-1 producers and 1 KPC-2 and NDM-1 producer) exhibited minimum inhibitory concentrations (MICs) of 32 or 16 mg/L for meropenem. Fifty (92.6%) isolates (47 KPC-2, 1 NDM-1, and 2 KPC-2 and NDM-1 producers) exhibited MICsof 32 or 16 mg/L for imipenem, while the other 4 (7.4%) isolates (2 IMP-4, 1 NDM-1, and 1 IMP-4 and NDM-1 producer) exhibited MICs of 4 or 8 mg/L for imipenem (**Table 2**).

Phage Isolation

A total of 54 phages were isolated from two types of sewage water samples (medical sewage and domestic sewage) between July and September 2019. Among the 54 phages, 27, 14, and 8 phages were isolated from three medical sewage samples from site C, B, and A respectively, while five phages were isolated from a domestic sewage sample from site D (**Supplementary Table S1**).

Host Ranges of 54 Phages

The 54 phages can lyse on average 25 CRKP strains, and each phage can lyse at least one ST11 strain. The host-range frequency analysis of phages showed that 2 (3.7%), 11 (20.4%), 25 (46.3%), 14 (25.9%), and 2 (3.7%) phages lysed >41, 31–40, 21–30, 11–20, and <10 CRKP strains, respectively (**Figure 1**).

Among these 54 phages, phages P545 and P546, both isolated from a sewage wastewater sample from a local hospital (site C), formed clear lysis spots on the lawns of 52 out of 54 (96.3%)

TABLE 2 | Minimal inhibitory concentration of meropenem and imipenem against *Klebsiella pneumoniae*.

Strain no.	Carbapenemase	MIC (mg/L)		Antimicrobial susceptibility	
		MEM	IPM	MEM	IPM
KP1	KPC-2	32	32	R	R
KP2	KPC-2	16	16	R	R
KP3	NDM-1	16	8	R	I
KP4	KPC-2	16	16	R	R
KP5	KPC-2	16	16	R	R
KP6	KPC-2	16	16	R	R
KP7	KPC-2	32	32	R	R
KP8	KPC-2	16	16	R	R
KP9	KPC-2	16	16	R	R
KP10	KPC-2	16	16	R	R
KP11	KPC-2	16	16	R	R
KP12	KPC-2	16	16	R	R
KP13	KPC-2	16	16	R	R
KP14	KPC-2	16	16	R	R
KP15	KPC-2	16	16	R	R
KP16	KPC-2	16	16	R	R
KP17	KPC-2	16	16	R	R
KP18	KPC-2	16	16	R	R
KP19	KPC-2	16	16	R	R
KP20	KPC-2	16	16	R	R
KP21	KPC-2	16	16	R	R
KP22	KPC-2	16	16	R	R
KP23	KPC-2	32	32	R	R
KP24	KPC-2	16	16	R	R
KP25	KPC-2	16	16	R	R
KP26	KPC-2	16	16	R	R
KP27	KPC-2	16	16	R	R
KP28	KPC-2	16	16	R	R
KP29	IMP-4	16	8	R	I
KP30	KPC-2	16	16	R	R
KP31	KPC-2	16	16	R	R
KP32	KPC-2	16	16	R	R
KP34	KPC-2	16	32	R	R
KP35	KPC-2	16	16	R	R
KP36	NDM-1	16	16	R	R
KP37	KPC-2	16	16	R	R
KP38	KPC-2	16	16	R	R
KP39	KPC-2	32	32	R	R
KP40	KPC-2	16	16	R	R
KP41	KPC-2	16	16	R	R
KP42	KPC-2	16	16	R	R
KP43	KPC-2	16	16	R	R
KP44	KPC-2	NA	16	NA	R
KP45	KPC-2	16	16	R	R
KP46	KPC-2	16	16	R	R
KP47	KPC-2	16	16	R	R
KP48	KPC-2	16	16	R	R
KP49	KPC-2	16	16	R	R
KP50	KPC-2	16	16	R	R
KP51	KPC-2	16	16	R	R
KP55	IMP-4; NDM-1	NA	8	NA	I
KP56	IMP-4	1	4	S	I
KP57	KPC-2; NDM-1	16	16	R	R
KP58	KPC-2; NDM-1	NA	16	NA	R

I, intermediate; IPM, imipenem; MEM, meropenem; R, resistant; S, susceptible. NA, not available. *I, intermediate; IPM, imipenem; MEM, meropenem; S, susceptible. NA, not available.*

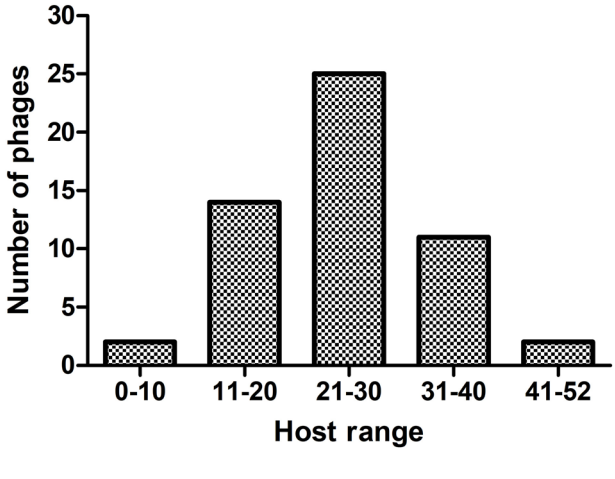

FIGURE 1 | The host-range frequency distribution of phages. The *x*-axis represents five host-range groups based on the number of CRKP host strains. The *y*-axis represents the number of phages.

CRKP strains, including both ST11 (KL47, KL64, and KL25) and non-ST11 strains, indicating that P545/P546 had a relatively wide host range (**Figure 2**). Two CRKP strains—KP24 (ST11, KL47) and KP36 (ST230, KL136) —were insensitive to both phage P545 and P546. By contrast, phage P523 and P508 had narrow host ranges and could form clear lysis spots on the lawns of only eight and seven strains, respectively.

The host ranges of some phages appear to be correlated with the capsular types of host bacteria. Fourteen phages (25.9%) showed an ability to lyse both ST11 KL47-type and KL64-type strains, including phages P506, P507, P509–P512, P547–P551, P557, and P558 isolated from medical sewage, and one phage P565 isolated from domestic sewage. By contrast, eight phages lysed mainly ST11 KL47 strains, including P556, P559–P564 from medical sewage, and P568 from domestic sewage (**Figure 2**). Twenty-three phages lysed mainly KL64-type CRKP strains, for example, P513–P515 and P525–P544, isolated mostly from medical sewage (**Figure 2**).

Morphology Analysis

Two relatively wide host-range phages, P545 and P539, and a high lytic activity phage, P507, were selected for plaque

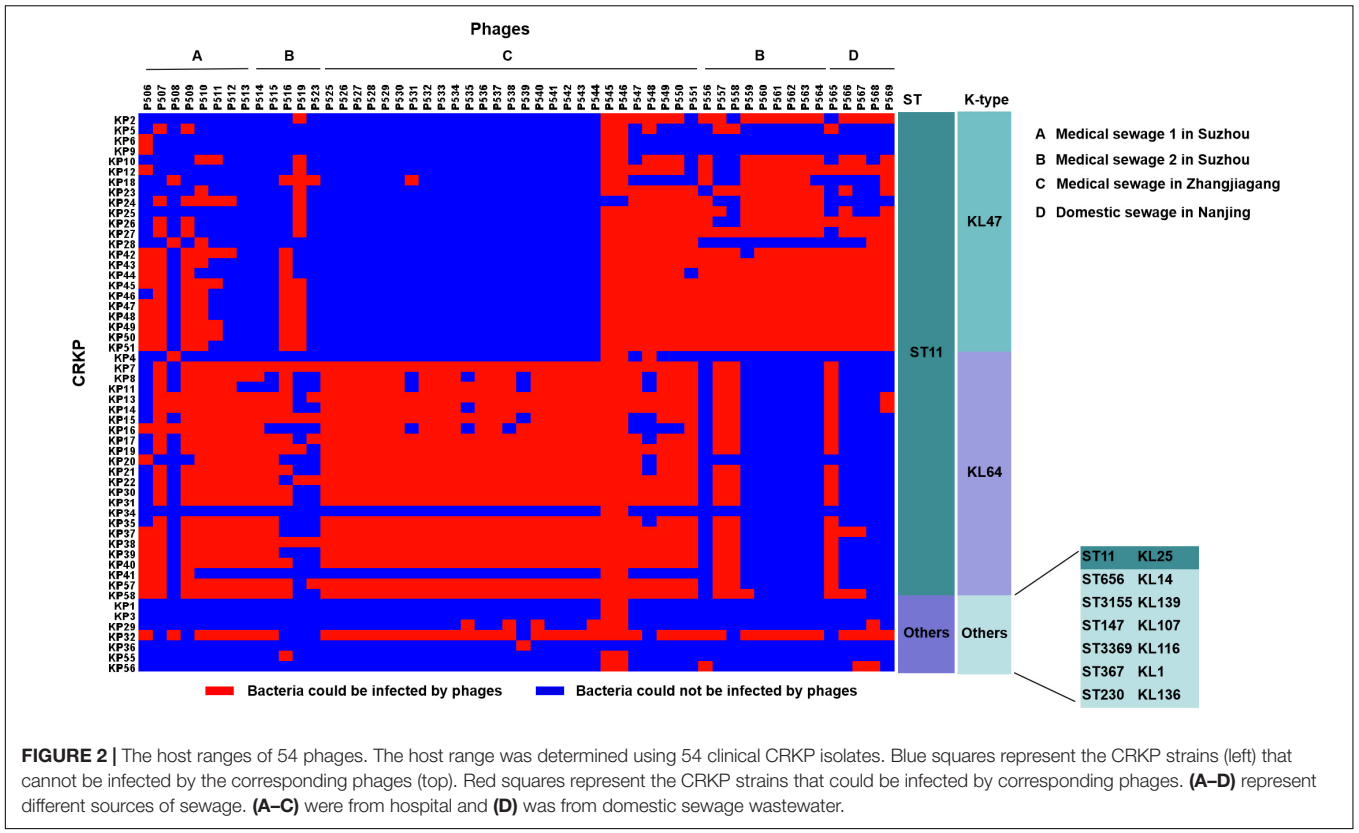

FIGURE 2 | The host ranges of 54 phages. The host range was determined using 54 clinical CRKP isolates. Blue squares represent the CRKP strains (left) that cannot be infected by the corresponding phages (top). Red squares represent the CRKP strains that could be infected by corresponding phages. **(A–D)** represent different sources of sewage. **(A–C)** were from hospital and **(D)** was from domestic sewage wastewater.

morphology analysis. Both P545 and P539 formed small clear and round plaques with a diameter of approximately 0.1 cm. P507 formed large clear and round plaques with a diameter of approximately 0.5 cm surrounded by 0.15-cm enlarged haloes, indicating that P507 most likely encodes depolymerases with polysaccharide-degrading activity (**Figure 3**). In addition, phages P560, P569, and P551 also formed big clear and round plaques surrounded by enlarged haloes (data not shown). TEM confirmed that P545 and P539 belonged to T4-like phages, a member of Myoviridaes, order Caudovirales. P507 belonged to T7-like phage, a member of Podoviridaes, order Caudovirales. The diameter of capsid of P507 was estimated at 50 ± 0.5 nm (**Figure 4**).

Optimal MOI and One-Step Growth Curve

When the MOI was 0.01 or 0.001, the titers of P545 reached maximum values after propagation with a titer of approximately 10^9 PFU/mL (**Figure 5A**). Considering the input–output ratio (or growth multiple) of phages, the low MOI (0.001) was considered as the optimal MOI. The one-step growth curve experiment indicated that the latent time period of phage P545 was approximately 20 min, and the burst size was about 82 phages/cell (**Figure 5B**).

Thermo and pH Stability of the Phages

The stability of phage P545 at various pH values and temperatures was examined. The survival rates of P545 were stable at pH 4 to pH 10 (phage survival rates >80%). However, the survival rates decreased significantly at the acidic (pH < 3) or alkaline (pH > 11) conditions (**Figure 6A**). After incubation for1 h, high survival rates were maintained between 4°C and 37°C (approaching 100.0%). When the temperature reached 50°C to 60°C, the survival rates declined to 95.9% and 86.2%, respectively. When the temperature reached 70°C and 80°C, nearly no phages survived (**Figure 6B**).

Genome Analysis of P545

Next-generation sequencing analysis showed that P545 was a linear dsDNA molecule of 169,725 bp and a GC content of 40.8%. No repeated terminal sequences were detected at the 5′- and 3′-ends. P545 contained a total of 287 putative coding regions (CDSs) and 7 tRNAs. No lysogeny or virulence associated genes were identified in the genome of P545, showing its lytic nature and the potential for therapeutic application. Two putative tail lysozymes (gene loci: 7096–7590 and 157173–158912) were identified based on the RAST predication. Online BLASTn analysis of P545 genome sequence revealed that it is mostly close to *Klebsiella* phage vB_Kpn_F48 (Accession no. MG746602) isolated from a hospital sewage wastewater in Italy (Ciacci et al., 2018), with 99% query coverage and 99% nucleotide identity, and to *Klebsiella* phage AmPh_EK29 (MN434092), isolated from sewage and wastewater in Australia, with 96% query coverage and 98% nucleotide identity (**Figure 7**).

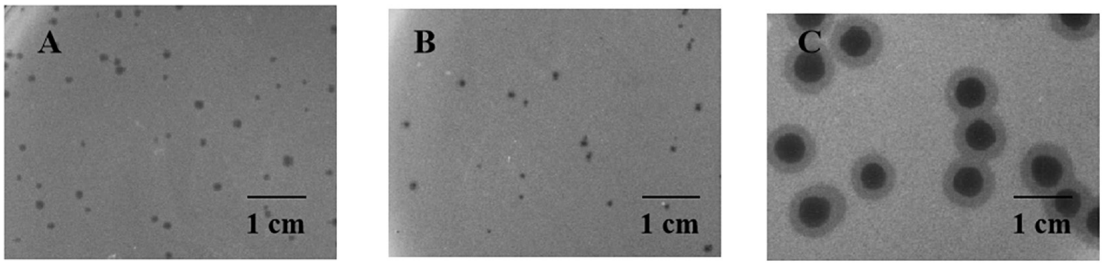

FIGURE 3 | Plaque morphology of P545 **(A)**, P539 **(B)**, and P507 **(C)**. Both P545 **(A)** and P539 **(B)** formed small clear and round plaques with a diameter of approximate 0.1 cm on double layer agar plate. P507 **(C)** formed big clear and round plaques with a diameter of approximately 0.5 cm surrounded by 0.15-cm enlarged haloes.

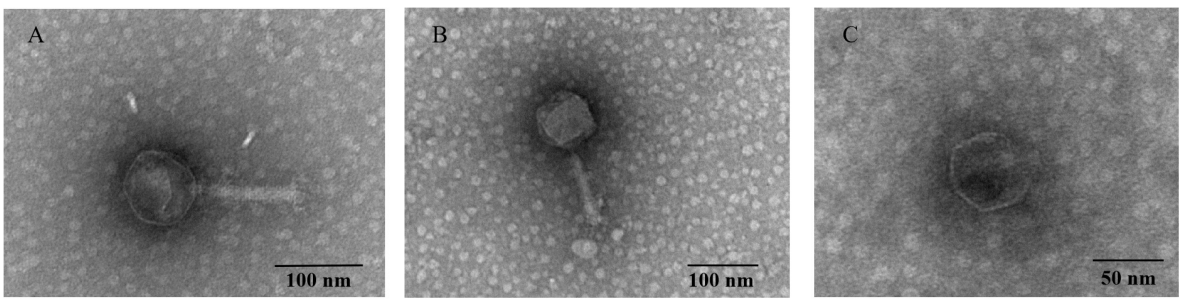

FIGURE 4 | Transmission electron micrograph of phage P545 **(A)**, P539 **(B)**, and P507 **(C)**. The phage filtrate was applied to a copper grid before negative staining with phosphotungstic acid (PTA, 2% w/v). Electron micrographs were observed using an H_7650 (Hitachi, Tokyo, Japan) TEM.

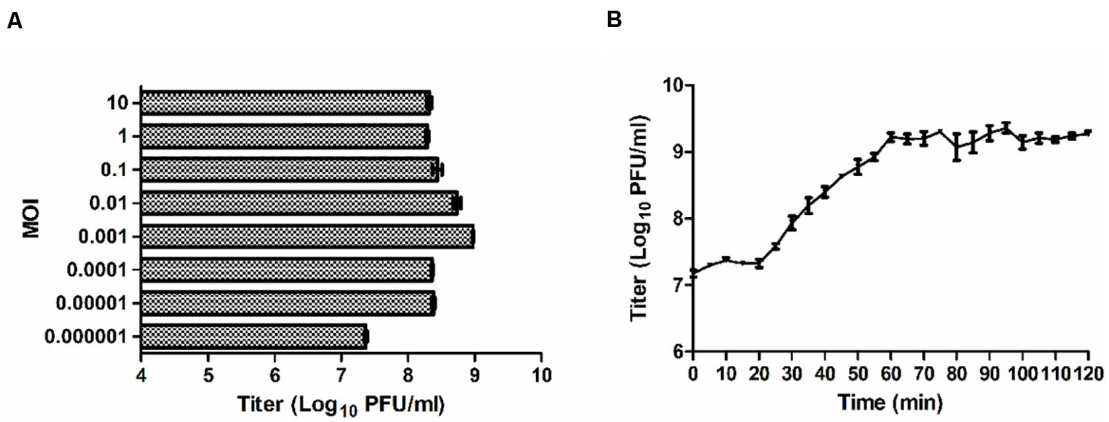

FIGURE 5 | Growth characteristics of P545. **(A)** The phage titers under different MOI (phage/bacteria = 10, 1, 0.1, 0.01, 0.001, 0.0001, 0.00001, 0.000001) are indicated on the *y*-axis. **(B)** One-step growth curve test of P545 was carried out at MOI = 0.1. The results are shown as mean ± SEM from three biological replicates.

Antibacterial and Antibiofilm Activity of Bacteriophage P545

To evaluate the inhibitory activity of phage P545 against planktonic bacteria, P545 suspensions of different concentrations (MOI = 0.1, 0.01, and 0.001) were incubated with CRKP strain KP4 for 70 min. The antibacterial assay showed that the OD_{600} values of three phage-treated groups (MOI = 0.1, 0.01, and 0.001) were significantly lower than those of the untreated group after 50, 60, and 70 min of incubation (**Figure 8**). The results indicated that phage P545 can effectively inhibit bacterial growth.

The inhibitory effect of phage P545 on biofilm formation in the KP4 strain was analyzed using 96-well plates. To evaluate the ability of phage P545 to inhibit biofilm formation, phage P545 suspensions were incubated with CRKP strain KP4 at different MOIs (0.1, 0.01, and 0.001) for 24 h. The results of crystal violet staining assay showed that the OD_{595} values of three different phage-treated groups (MOI 0.1, 0.01, and 0.001)

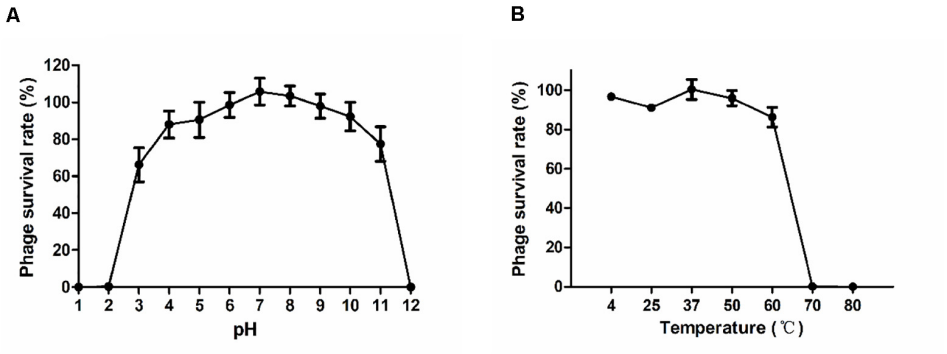

FIGURE 6 | Stability tests of P545. **(A)** pH stability: phage particles were incubated under different pH conditions for 1 h. **(B)** Thermal stability: phage particles were incubated at various temperatures for 1 h. Phage survival rate = (titer after incubation)/(initial titer). SEM are shown as vertical lines.

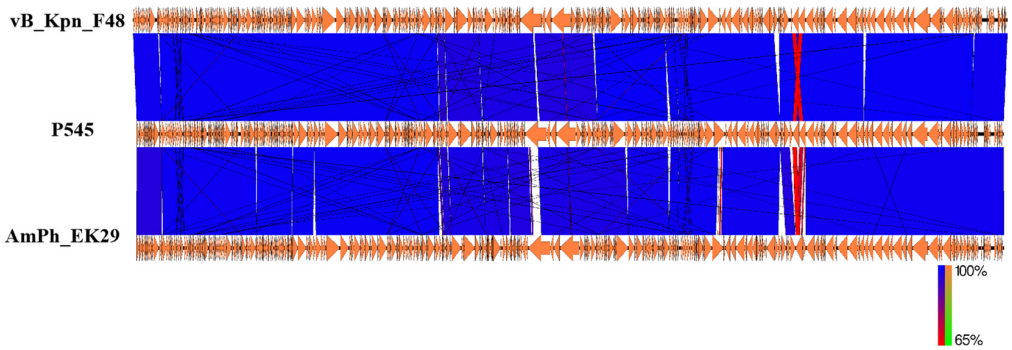

FIGURE 7 | Comparative genome analysis of *K. pneumoniae* P545 bacteriophage. Schematics were produced using EasyFig. The genome sequence of the P545 was compared to those of two most closely related phages, vB_Kpn_F48 (MG746602) and AmPh_EK29 (MN434092) published in NCBI.

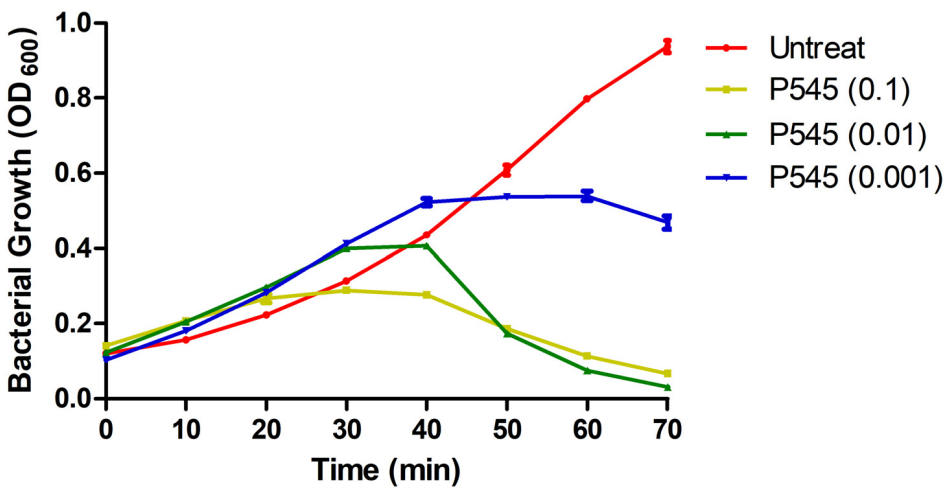

FIGURE 8 | *In vitro* activity of phage P545 at 37°C. Panels show the OD_{600} values of bacterial cultures. The yellow line represents the OD_{600} value of CRKP KP4 treated with phage P545 at MOI 0.1; the green line represents that of KP4 treated with phage P545 at MOI 0.01; the blue line represents that of KP4 treated with phage P545 at MOI 0.001; the red line represents that of untreated KP4.

decreased 0.70, 0.59, and 0.49, respectively, in comparison to that of the untreated group (**Figure 9A**, $P < 0.001$). The ability of P545 to degrade biofilms was also assessed using 24-h-old mature biofilms. The OD_{595} values of the total biomass that remained attached in the phage-treated groups decreased 0.24 (MOI = 0.1), 0.23 (MOI = 0.01), and 0.21 (MOI = 0.001) compared with that

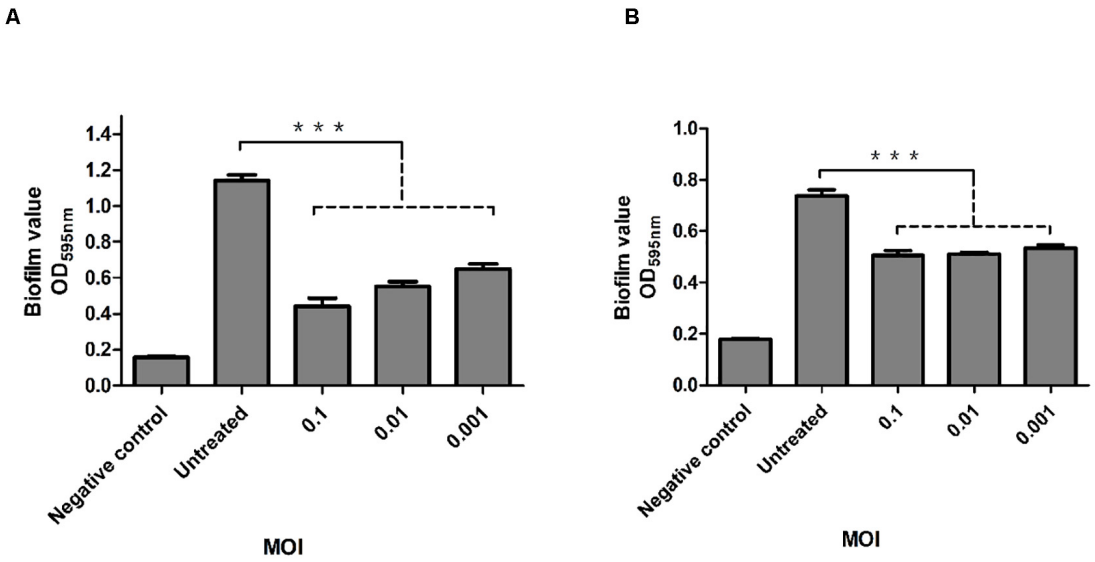

FIGURE 9 | Antibacterial and antibiofilm activity of phage P545. **(A)** P545 inhibited the formation of biofilms. P545 was incubated with CRKP strain KP4 at MOIs of 0.1, 0.01, and 0.001 in 96-well plates for 24 h. **(B)** P545 disrupted the mature biofilm of KP4. Biofilm formation of KP4 was induced in 96-well plates for 24 h, and then the biofilm was treated with P545 at MOIs of 0.1, 0.01, and 0.001 for 24 h. Fresh TSB medium was used as a negative control. The OD_{595} values of the residual biofilms were measured after crystal violet staining. All the data are shown as the mean ± SEM. ***indicates $p < 0.001$.

of the untreated group (**Figure 9B**, $P < 0.001$). These results suggested that P545 can inhibit biofilm formation and degrade the formed mature biofilm.

DISCUSSION

Carbapenem-resistant *Klebsiella pneumoniae* strains have emerged as significant multidrug-resistant bacterial pathogens that pose a serious threat to global public health. The international spreads of CRKP strains were associated with a few high-risk clonal strains, including ST258, ST11, ST14, ST147, and ST307 etc. Among them, ST258 predominates in North America and Europe, whereas ST11 is the primary CRKP clone in East Asia, especially China (Chen et al., 2014; Zhang et al., 2019). In China, ST11 strains accounted for >70% CRKP strains (Liu et al., 2018). CRKP ST11 strains were primarily associated with the bla_{KPC-2} gene in China, but other carbapenemase genes, such as bla_{NDM}, $bla_{OXA-48-like}$, bla_{VIM}, and bla_{IMP}, were frequently identified in ST11 strains elsewhere (Chen et al., 2018; Liu et al., 2018; Wang et al., 2018). For example, in this study, two ST11 strains were also found to carry both bla_{NDM-1} and bla_{KPC-2}. In addition, some CRKP ST11 strains have evolved to be extensively drug resistant (Dorp et al., 2019; Wu X. et al., 2019). ccordingly, combating the infection caused by epidemic CRKP ST11 strains has already become a priority in controlling CRKP strains in China and some other countries.

Bacteriophages are being considered as a potential therapeutic approach against highly drug-resistant pathogens, including CRKP strains (Wu X. et al., 2019). In this study, we isolated 54 phages from domestic and hospital sewage wastewater. Our results suggested that sewage, especially medical sewage, may be a better phage source against clinical CRKP strains, since phages can be efficiently isolated (Peng et al., 2020). Clinically, phages with relatively wide host ranges could be ideal candidates for phage cocktail in phage therapy. Based on the host-range analysis, three selected phages (i.e., P545, P539, and P507) can potentially cover all 54 clinical CRKP isolates, collected from various clinical sources and harboring different carbapenemase genes.

Our results also indicated that the phage lytic activity was independent of the carbapenemase genotypes. Importantly, all 54 phages showed lytic activity against some epidemic ST11 strains. The host ranges of certain phages appeared to be narrow and were specific to certain *K. pneumoniae* strains. This result was similar to the results of other studies that some phages were specific to certain capsular serotypes. For example, bacteriophage NTUH-K2044-K1-1 isolated from Taiwan exhibited specificity for capsular type K1 (Lin et al., 2014). *Klebsiella* bacteriophage K5-2 exhibited specificity for capsular types K5, K30, and K69, and bacteriophage K5-4 exhibited specificity for capsular types K8 and K5 (Hsieh et al., 2017). Three bacteriophages—KpV41, KpV475, and KpV71—had specific lytic activity against mainly K1 stains (Solovieva et al., 2018). Moreover, two phages, KpV74, and KpV763, had specific lytic activity against K2 strains, and the phage KpV767 had specific lytic activity against K57 strains (Solovieva et al., 2018).

Interestingly, we identified a phage, P545, with a relatively wide host range, that can lyse 52 of 54 (96.3%) CRKP strains from our collection. These 52 CRKP strains included 24 ST11

KL64, 22 ST11 KL47, 1 ST11 KL25, 1 ST367 KL1, 1 ST147 KL10, 1 ST656 KL14, 1 ST3155 KL139, and 1 ST230 KL136. The molecular mechanism underlying the relatively wide host range of phage P545 remains unclear. TEM of phage P545 revealed that P545 belonged to T4-like lytic phage, a member of Myoviridaes, order Caudovirales. BLASTn analysis showed that P545 was highly similar to *Klebsiella* phage vB_Kpn_F48 (MG746602) from Italy and AmPh_EK29 (MN434092) from Australia. However, both vB_Kpn_F48 and AmPh_EK29 appear to be narrow host-range phages. Phage vB_Kpn_F48 had a lytic activity specific to *K. pneumoniae* strains belonging to ST101 (K17) and its closely related strains (Ciacci et al., 2018). Similarly, AmPh_EK29 was specifically active against *K. pneumoniae* ST258 clade 1 strains (KL106). Our phage P545 had a lytic activity against ST11 strains (KL47 and KL64) and six other STs. Further studies will be performed to examine whether P545 can actively lyse other CRKP strains, especially ST258 and ST101 strains. Our genome alignment results showed that P545 harbors >2600 and >4600 core single nucleotide polymorphisms and some insertion or deletion versus vB_Kpn_F48 and AmPh_EK29, respectively. For T4-like phages, the tail fiber protein gene in general determined the specificity and host range. BLASTn analysis revealed the tail fiber protein gene sequence of P545 had only 91% query coverage and 89.4% nucleotide identity (genome level: 99% query coverage and 99% nucleotide identity) with that of *Klebsiella* phage vB_Kpn_F48. We suspected the genetic variation in tail fiber protein gene of P545, in comparison to vB_Kpn_F48 and AmPh_EK29, may contribute to the relatively wide host range observed in P545, which deserves further study.

Phage P545 had a short latent period of 20 min and a medium burst size of 82 PFU/cell and was stable at pH values (4–10) and temperatures (up to 60°C). When the MOI was 0.01 or 0.001, the titers of P545 reached the maximum value (no significant difference). Considering the input–output ratio (or growth multiple) of phage, the lower MOI (0.001) was considered the optimal MOI.

In this study, phage P545 inhibited bacterial growth within 70 min. The result of crystal violet staining assay suggested that phage P545 can not only inhibit biofilm formation but also degrade the formed mature biofilms. Many bacteriophages produced specific depolymerases, which are able to destroy the capsular polysaccharides, thereby allowing adsorption of phages to the outer membrane receptors (Pires et al., 2016) and penetration of phage DNA into the bacterial cells (Hughes et al., 1998). These phage-derived capsule depolymerases can be potentially used as therapeutic agents against capsulated bacteria, such as CRKP strains. However, the plaque morphology analysis suggested that phage P545 was a non-depolymerase-producing phage, because no clear enlarged haloes were observed (**Figure 4**). In fact, besides depolymerases, phage-encoded lysozymes (endolysins, lysins, etc.) can also digest bacterial cell wall material (Chan and Abedon, 2015; Ajuebor et al., 2016). Two tail lysozyme genes were found in the genome of P545 based on RAST predication. Therefore, we suspected that the mechanism of biofilm formation inhibition and biofilm degradation may be associated with phage-encoded tail lysozymes of phage P545. The results suggested that P545 could be an attractive candidate as an anti-CRKP agent. Moreover, in this study, P507 formed large clear and round plaques surrounded by enlarged haloes, suggesting that it most likely encodes depolymerases with polysaccharide-degrading activity (Pan et al., 2017; Wu X. et al., 2019).

One limitation of current study was that we determined the phage activities against CRKP isolates collected from only a single medical center. Nevertheless, these CRKP isolates were collected from various clinical sources and harbored a wide battery of carbapenemase genes, including the most predominant STs and capsular types of strains spreading in China. In addition, another limitation is that only one of the 54 phages (P545) was fully characterized. Further work will be conducted to characterize other phages isolated in the current study, such as P507, and to test the activities of these phages against CRKP isolates from other genetic backgrounds. Today, the sources and rapid availability of phages against clinically isolated pathogens remains the most significant challenge for phage therapy. Our study described that the 54 phages can be successfully obtained within a short period of time (1.5 months) from local sewage, especially from medical wastewater. Medical sewage in the surrounding area could serve as a rich naturally occurring phage source against clinically important pathogens. Natural phage, in combination with engineered phages and phage-encoded enzymes, may provide a more effective solution for combating epidemic CRKP infections.

DATA AVAILABILITY STATEMENT

The datasets generated for this study can be found in the annotated whole-genome sequence of phage P545 was deposited in the GenBank database under accession number: MN781108.

ETHICS STATEMENT

This study was approved by the Institutional Review Board (IRB) of The Second Affiliated Hospital of Soochow University. The clinical isolates were retrospectively collected, and patient data were not included in this study, therefore informed consent was waived by the Institutional Review Board (IRB) of The Second Affiliated Hospital of Soochow University.

AUTHOR CONTRIBUTIONS

ML, WZ, and HD conceived the study. ML, MG, LoC, PL, YX, and WZ performed the experiment and computational analysis. ML, LiC, HG, and WZ wrote the article. All authors read, revised, and approved the final manuscript.

FUNDING

This study was supported by grants from the National Key Research and Development Program of China (2018YFC1602500), the National Natural Science Foundation of China (81572032), the National Natural Science Foundation of China (U1803109), the Six Talent Peaks Project in Jiangsu Province (2016-WSN-112), the Key Research and Development Project of Jiangsu Provincial Science and Technology Department (BE2017654), the Gusu Key Health Talent of Suzhou, Jiangsu Youth Medical Talents Program (QN-867), and the Science and Technology Program of Suzhou (SZS201715).

SUPPLEMENTARY MATERIAL

The Supplementary Material for this article can be found online at: https://www.frontiersin.org/articles/10.3389/fmicb.2020.01554/full#supplementary-material

REFERENCES

Adams, M. (1959). *Bacteriophage*. New York, NY: Interscience Publishers.

Ajuebor, J., McAuliffe, O., O'Mahony, J., Ross, R. P., Hill, C., and Coffey, A. (2016). Bacteriophage endolysins and their applications. *Sci. Prog.* 99, 183–199. doi: 10.3184/003685016X14627913637705

Anand, T., Virmani, N., Kumar, S., Kumar Mohanty, A., Pavulraj, S., Ch Bera, B., et al. (2019). Phage Therapy for treatment of virulent *Klebsiella pneumoniae* infection in mouse model. *J. Glob. Antimicrob. Resist.* 21, 34–41. doi: 10.1016/j.jgar.2019.09.018

Aziz, R. K., Bartels, D., Best, A. A., DeJongh, M., Disz, T., Edwards, R. A., et al. (2008). The RAST Server: rapid annotations using subsystems technology. *BMC Genomics* 9:75. doi: 10.1186/1471-2164-9-75

Bankevich, A., Nurk, S., Antipov, D., Gurevich, A. A., Dvorkin, M., Kulikov, A. S., et al. (2012). SPAdes: a new genome assembly algorithm and its applications to single-cell sequencing. *J. Comput. Biol.* 19, 455–477. doi: 10.1089/cmb.2012.0021

Bokaeian, M., Shahraki Zahedani, S., Soltanian Bajgiran, M., and Ansari Moghaddam, A. (2015). Frequency of PER, VEB, SHV, TEM and CTX-M genes in resistant strains of *Pseudomonas aeruginosa* producing extended spectrum beta-lactamases. *Jundishapur J. Microbiol.* 8:e13783. doi: 10.5812/jjm.13783

Brisse, S., Passet, V., Haugaard, A. B., Babosan, A., Kassis-Chikhani, N., Struve, C., et al. (2013). wzi Gene sequencing, a rapid method for determination of capsular type for *Klebsiella* strains. *J. Clin. Microbiol.* 51, 4073–4078. doi: 10.1128/JCM.01924-13

Candan, E. D., and Aksoz, N. (2015). *Klebsiella pneumoniae*: characteristics of carbapenem resistance and virulence factors. *Acta Biochim. Pol.* 62, 867–874. doi: 10.18388/abp.2015_1148

Cerca, N., Martins, S., Pier, G. B., Oliveira, R., and Azeredo, J. (2005). The relationship between inhibition of bacterial adhesion to a solid surface by sub-MICs of antibiotics and subsequent development of a biofilm. *Res. Microbiol.* 156, 650–655. doi: 10.1016/j.resmic.2005.02.004

Chadha, P., Katare, O. P., and Chhibber, S. (2017). Liposome loaded phage cocktail: enhanced therapeutic potential in resolving *Klebsiella pneumoniae* mediated burn wound infections. *Burns* 43, 1532–1543. doi: 10.1016/j.burns.2017.03.029

Chan, B., and Abedon, S. (2015). Bacteriophages and their enzymes in biofilm control. *Curr. Pharm. Des.* 21, 85–99. doi: 10.2174/1381612820666140905112311

Chen, C. M., Guo, M. K., Ke, S. C., Lin, Y. P., Li, C. R., Vy Nguyen, H. T., et al. (2018). Emergence and nosocomial spread of ST11 carbapenem-resistant *Klebsiella pneumoniae* co-producing OXA-48 and KPC-2 in a regional hospital in Taiwan. *J. Med. Microbiol.* 67, 957–964. doi: 10.1099/jmm.0.000771

Chen, L., Mathema, B., Chavda, K. D., DeLeo, F. R., Bonomo, R. A., and Kreiswirth, B. N. (2014). Carbapenemase-producing *Klebsiella pneumoniae*: molecular and genetic decoding. *Trends Microbiol.* 22, 686–696. doi: 10.1016/j.tim.2014.09.003

Chen, M., Zhang, L., Abdelgader, S. A., Yu, L., Xu, J., Yao, H., et al. (2017). Alterations in gp37 expand the host range of a T4-like phage. *Appl. Environ. Microbiol.* 83:e01576-17. doi: 10.1128/AEM.01576-17

Ciacci, N., D'Andrea, M. M., Marmo, P., Dematte, E., Amisano, F., Di Pilato, V., et al. (2018). Characterization of vB_Kpn_F48, a newly discovered lytic bacteriophage for *Klebsiella pneumoniae* of sequence type 101. *Viruses* 10:482. doi: 10.3390/v10090482

Cieplak, T., Soffer, N., Sulakvelidze, A., and Nielsen, D. S. (2018). A bacteriophage cocktail targeting *Escherichia coli* reduces *E. coli* in simulated gut conditions, while preserving a non-targeted representative commensal normal microbiota. *Gut Microbes* 9, 391–399. doi: 10.1080/19490976.2018.1447291

Criscuolo, E., Spadini, S., Lamanna, J., Ferro, M., and Burioni, R. (2017). Bacteriophages and their immunological applications against infectious threats. *J. Immunol. Res.* 2017:3780697. doi: 10.1155/2017/3780697

Deng, W., Wang, Y., Liu, Z., Cheng, H., and Xue, Y. (2014). HemI: a toolkit for illustrating heatmaps. *PLoS One* 9:e111988. doi: 10.1371/journal.pone.0111988

Diancourt, L., Passet, V., Verhoef, J., Grimont, P. A., and Brisse, S. (2005). Multilocus sequence typing of *Klebsiella pneumoniae* nosocomial isolates. *J. Clin. Microbiol.* 43, 4178–4182. doi: 10.1128/JCM.43.8.4178-4182.2005

Dorp, L. V., Wang, Q., Shaw, L. P., Acman, M., Brynildsrud, O. B., Eldholm, V., et al. (2019). Rapid phenotypic evolution in multidrug-resistant *Klebsiella pneumoniae* hospital outbreak strains. *Microb. Genom.* 5:e000263. doi: 10.1099/mgen.0.000263

Gong, P., Cheng, M., Li, X., Jiang, H., Yu, C., Kahaer, N., et al. (2016). Characterization of Enterococcus faecium bacteriophage IME-EFm5 and its endolysin LysEFm5. *Virology* 492, 11–20. doi: 10.1016/j.virol.2016.02.006

Gu, J., Xu, W., Lei, L., Huang, J., Feng, X., Sun, C., et al. (2011). LysGH15, a novel bacteriophage lysin, protects a murine bacteremia model efficiently against lethal methicillin-resistant *Staphylococcus aureus* infection. *J. Clin. Microbiol.* 49, 111–117. doi: 10.1128/JCM.01144-1110

Hsieh, P. F., Lin, H. H., Lin, T. L., Chen, Y. Y., and Wang, J. T. (2017). Two T7-like bacteriophages, K5-2 and K5-4, each encodes two capsule depolymerases: isolation and functional characterization. *Sci. Rep.* 7:4624. doi: 10.1038/s41598-017-04644-2

Huang, C., Shi, J., Ma, W., Li, Z., Wang, J., Li, J., et al. (2018). Isolation, characterization, and application of a novel specific *Salmonella* bacteriophage in different food matrices. *Food Res. Int.* 111, 631–641. doi: 10.1016/j.foodres.2018.05.071

Hughes, K. A., Sutherland, I. W., and Jones, M. V. (1998). Biofilm susceptibility to bacteriophage attack: the role of phage-borne polysaccharide depolymerase. *Microbiology* 144(Pt 11), 3039–3047. doi: 10.1099/00221287-144-11-3039

Ji, Y., Cheng, M., Zhai, S., Xi, H., Cai, R., Wang, Z., et al. (2019). Preventive effect of the phage VB-SavM-JYL01 on rabbit necrotizing pneumonia caused by *Staphylococcus aureus*. *Vet. Microbiol.* 229, 72–80. doi: 10.1016/j.vetmic.2018.12.021

Kutter, E. (2009). Phage host range and efficiency of plating. *Methods Mol. Biol.* 501, 141–149. doi: 10.1007/978-1-60327-164-6_14

Kwan, T., Liu, J., DuBow, M., Gros, P., and Pelletier, J. (2005). The complete genomes and proteomes of 27 Staphylococcus aureus bacteriophages. *Proc. Natl. Acad. Sci. U.S.A.* 102, 5174–5179. doi: 10.1073/pnas.0501140102

Laemmli, U. K. (1970). Cleavage of structural proteins during the assembly of the head of bacteriophage T4. *Nature* 227, 680–685. doi: 10.1038/227680a0

Lazaro-Perona, F., Sotillo, A., Troyano-Hernaez, P., Gomez-Gil, R., de la Vega-Bueno, A., and Mingorance, J. (2018). Genomic path to pandrug resistance in a clinical isolate of *Klebsiella pneumoniae*. *Int. J. Antimicrob. Agents* 52, 713–718. doi: 10.1016/j.ijantimicag.2018.08.012

Lin, T. L., Hsieh, P. F., Huang, Y. T., Lee, W. C., Tsai, Y. T., Su, P. A., et al. (2014). Isolation of a bacteriophage and its depolymerase specific for K1 capsule of *Klebsiella pneumoniae*: implication in typing and treatment. *J. Infect. Dis.* 210, 1734–1744. doi: 10.1093/infdis/jiu332

Liu, L., Feng, Y., Tang, G., Lin, J., Huang, W., Qiao, F., et al. (2018). Carbapenem-resistant isolates of the *Klebsiella pneumoniae* complex in western china: the common ST11 and the surprising hospital-specific types. *Clin. Infect. Dis.* 67(Suppl._2), S263–S265. doi: 10.1093/cid/ciy662

Mammeri, H., Guillon, H., Eb, F., and Nordmann, P. (2010). Phenotypic and biochemical comparison of the carbapenem-hydrolyzing activities of five plasmid-borne AmpC beta-lactamases. *Antimicrob. Agents Chemother.* 54, 4556–4560. doi: 10.1128/AAC.01762-09

Morozova, V. V., Kozlova, Y. N., Ganichev, D. A., and Tikunova, N. V. (2018). Bacteriophage treatment of infected diabetic foot ulcers. *Methods Mol. Biol.* 1693, 151–158. doi: 10.1007/978-1-4939-7395-8_13

Pajunen, M., Kiljunen, S., and Skurnik, M. (2000). Bacteriophage phiYeO3-12, specific for Yersinia enterocolitica serotype O:3, is related to coliphages T3 and T7. *J. Bacteriol.* 182, 5114–5120. doi: 10.1128/jb.182.18.5114-5120.2000

Pan, Y. J., Lin, T. L., Chen, C. C., Tsai, Y. T., Cheng, Y. H., Chen, Y. Y., et al. (2017). Klebsiella phage PhiK64-1 encodes multiple depolymerases for multiple host capsular types. *J. Virol.* 91:e02457-16. doi: 10.1128/JVI.02457-16

Peng, Q., Fang, M., Liu, X., Zhang, C., Liu, Y., and Yuan, Y. (2020). Isolation and characterization of a novel phage for controlling multidrug-resistant *Klebsiella pneumoniae*. *Microorganisms* 8:542. doi: 10.3390/microorganisms8040542

Pires, D. P., Oliveira, H., Melo, L. D., Sillankorva, S., and Azeredo, J. (2016). Bacteriophage-encoded depolymerases: their diversity and biotechnological applications. *Appl. Microbiol. Biotechnol.* 100, 2141–2151. doi: 10.1007/s00253-015-7247-0

Sambrook, J., and Russell, D. W. (2006). Precipitation of bacteriophage lambda particles from large-scale lysates. *CSH Protoc.* 2006:pdb.prot3966. doi: 10.1101/pdb.prot3966

Solovieva, E. V., Myakinina, V. P., Kislichkina, A. A., Krasilnikova, V. M., Verevkin, V. V., Mochalov, V. V., et al. (2018). Comparative genome analysis of novel Podoviruses lytic for hypermucoviscous *Klebsiella pneumoniae* of K1, K2, and K57 capsular types. *Virus Res.* 243, 10–18. doi: 10.1016/j.virusres.2017.09.026

Wang, Q., Wang, X., Wang, J., Ouyang, P., Jin, C., Wang, R., et al. (2018). Phenotypic and genotypic characterization of carbapenem-resistant *Enterobacteriaceae*: data from a longitudinal large-scale CRE study in China (2012-2016). *Clin. Infect. Dis.* 67(Suppl._2), S196–S205. doi: 10.1093/cid/ciy660

Wu, X., Han, H., Chen, C., and Zheng, B. (2019). Genomic characterisation of a colistin-resistant *Klebsiella pneumoniae* ST11 strain co-producing KPC-2, FloR, CTX-M-55, SHV-12, FosA and RmtB causing a lethal infection. *J. Glob. Antimicrob. Resist.* 19, 78–80. doi: 10.1016/j.jgar.2019.08.023

Wu, Y., Wang, R., Xu, M., Liu, Y., Zhu, X., Qiu, J., et al. (2019). A novel polysaccharide depolymerase encoded by the phage SH-KP152226 confers specific activity against multidrug-resistant *Klebsiella pneumoniae* via biofilm degradation. *Front. Microbiol.* 10:2768. doi: 10.3389/fmicb.2019.02768

Yu, F., Lv, J., Niu, S., Du, H., Tang, Y. W., Pitout, J. D. D., et al. (2018). Multiplex PCR analysis for rapid detection of *Klebsiella pneumoniae* carbapenem-resistant (Sequence Type 258 [ST258] and ST11) and hypervirulent (ST23, ST65, ST86, and ST375) strains. *J. Clin. Microbiol.* 56:e00731-18. doi: 10.1128/JCM.00731-18

Zhang, R., Dong, N., Huang, Y., Zhou, H., Xie, M., Chan, E. W., et al. (2018). Evolution of tigecycline- and colistin-resistant CRKP (carbapenem-resistant *Klebsiella pneumoniae*) in vivo and its persistence in the GI tract. *Emerg. Microbes Infect.* 7:127. doi: 10.1038/s41426-018-0129-7

Zhang, X., Wang, W., Yu, H., Wang, M., Zhang, H., Lv, J., et al. (2019). New delhi metallo-beta-lactamase 5-producing *Klebsiella pneumoniae* sequence Type 258, Southwest China, 2017. *Emerg. Infect Dis.* 25, 1209–1213. doi: 10.3201/eid2506.181939

Conflict of Interest: The authors declare that the research was conducted in the absence of any commercial or financial relationships that could be construed as a potential conflict of interest.

Copyright © 2020 Li, Guo, Chen, Zhu, Xiao, Li, Guo, Chen, Zhang and Du. This is an open-access article distributed under the terms of the Creative Commons Attribution License (CC BY). The use, distribution or reproduction in other forums is permitted, provided the original author(s) and the copyright owner(s) are credited and that the original publication in this journal is cited, in accordance with accepted academic practice. No use, distribution or reproduction is permitted which does not comply with these terms.

frontiers in Microbiology

ORIGINAL RESEARCH
published: 21 July 2020
doi: 10.3389/fmicb.2020.01407

Identification of a Novel *Acinetobacter baumannii* Phage-Derived Depolymerase and Its Therapeutic Application in Mice

Can Wang[1†], Puyuan Li[2†], Yang Zhu[1], Yong Huang[3], Mingming Gao[2], Xin Yuan[2], Wenkai Niu[2], Huiying Liu[2], Hang Fan[3], Yanhong Qin[2], Yigang Tong[3], Zhiqiang Mi[3]* and Changqing Bai[2,4]**

[1] Department of Respiratory Medicine, Fuyang Hospital of Anhui Medical University, Anhui, China, [2] Department of Respiratory and Critical Care Diseases, The Fifth Medical Center of Chinese PLA General Hospital, Beijing, China, [3] State Key Laboratory of Pathogen and Biosecurity, Beijing Institute of Microbiology and Epidemiology, Beijing, China, [4] Department of Respiratory and Critical Care Diseases, General Hospital of Shenzhen University, Shenzhen, China

The rapid expansion of *Acinetobacter baumannii* clinical isolates exhibiting resistance to most or all available antibiotics is a global concern. Current treatments for infections caused by this bacterium have become less effective, and the need to explore new alternative therapies is urgent. Depolymerases derived from phages are emerging as attractive anti-virulence agents. In this study, a previously isolated *A. baumannii* phage (designated as vB_AbaM_IME285) was characterized, and genomic study was carried out using various bioinformatics tools. A gene predicted as encoding for the depolymerase was cloned and expressed, and the depolymerase activity of the recombinant enzyme (Dp49) was identified both *in vitro* and in experimental mice. The results showed that phage IME285 formed translucent halos around the plaques when inoculated onto a lawn of the host bacteria, exibiting depolymerase activity against this strain. On the basis of complete genome sequencing and bioinformatics analysis, ORF49 was speculated to be a gene encoding for the putative capsule depolymerase. The expressed recombinant Dp49 displayed an effective depolymerase activity and had a spectrum of activity similar to its parental phage IME285, which was active against 25 out of 49 *A. baumannii* strains. It was found that Dp49 greatly improved the inhibitory effect of serum on bacterial growth *in vitro*, and the administration of this enzyme significantly increased the survival rates of *A. baumannii*-infected mice in the animal experiment. In conclusion, the phage-encoded depolymerase Dp49 might be a promising alternative means of controlling infections mediated by multidrug-resistant *A. baumannii*.

Keywords: depolymerase, phage-derived, *Acinetobacter baumannii*, identification, therapeutic application

OPEN ACCESS

Edited by:
Krishna Mohan Poluri, Indian Institute of Technology Roorkee, India

Reviewed by:
Konstantin Anatolievich Miroshnikov, Institute of Bioorganic Chemistry (RAS), Russia
Vikas Jain, Indian Institute of Science Education and Research, Bhopal, India

****Correspondence:***
Yigang Tong
tong62035@gmail.com; tong.yigang@gmail.com
Zhiqiang Mi
zhiqiangmi_ime@163.com
Changqing Bai
mlp1604@sina.com

† These authors have contributed equally to this work

Specialty section:
This article was submitted to Antimicrobials, Resistance and Chemotherapy, a section of the journal Frontiers in Microbiology

Received: *19 November 2019*
Accepted: *29 May 2020*
Published: *21 July 2020*

Citation:
Wang C, Li P, Zhu Y, Huang Y, Gao M, Yuan X, Niu W, Liu H, Fan H, Qin Y, Tong Y, Mi Z and Bai C (2020) Identification of a Novel Acinetobacter baumannii Phage-Derived Depolymerase and Its Therapeutic Application in Mice. Front. Microbiol. 11:1407. doi: 10.3389/fmicb.2020.01407

INTRODUCTION

Acinetobacter baumannii (A. baumannii) is a Gram-negative bacillus and is one of the main opportunistic pathogens of hospital-acquired infections. It often causes infections such as those of the respiratory tract, blood, urinary tract, wounds, and even the central nervous system (Perez et al., 2007). With the use of broad-spectrum antibiotics, immunosuppressants, and glucocorticoids,

the multidrug-resistant *A. baumannii* (MDR-AB), pan-resistant *A. baumannii* (PDR-AB), and even carbapenem-resistant *A. baumannii* (CRAB) have emerged globally, and the treatment of infections caused by *A. baumannii* has become more difficult (Wong et al., 2017). Meanwhile, this organism is capable of continually spreading to new patients, making itself a nosocomial pathogen of particular clinical concern and a public health threat (Dijkshoorn et al., 2007). There is therefore an urgent need to develop new antimicrobial agents.

Bacteriophages, also known as phages, are viruses that could infect bacteria, and they are effective means for the treatment of drug-resistant infections (Chang et al., 2018). However, bacteria frequently live in biofilm communities surrounded by extracellular polymeric substances (EPS) that can act as a barrier to phage penetration (Azeredo and Sutherland, 2008; Pires et al., 2016a). It has been reported that EPS could protect bacteria against harsh external conditions and that they constitute an important survival strategy for bacteria (Pires et al., 2016b). For *A. baumannii*, EPS has increased the tolerance of the bacteria to antimicrobial agents due to diffusion limitations, potentially leading to severe persistent infections that are particularly difficult to treat, and this is also an important factor in resistance against phages (Hall-Stoodley et al., 2004). The thick capsular polysaccharide (CPS) surrounding Gram-negative bacteria is a crucial virulence factor in processes of infection and plays an important role in the phage-bacterium host interplay. By masking the receptors on the bacterial membrane, the potential for a phage to bind to the host cell is limited, so the infection ability of the bacteria is reduced (Samson et al., 2013). The unique ability of phage-derived depolymerases to specifically recognize and degrade CPS, EPS, and the O-antigen offers an attractive and promising tool for controlling pathogenic bacteria (Latka et al., 2017).

Our team has been working on the identification and application of phages and phage-derived proteins of Gram-negative bacteria for several years (Peng et al., 2014; Liu et al., 2016, 2019; Wang et al., 2016, 2019). In this research, a previously isolated phage was characterized, and its genome sequences were analyzed subsequently. ORF49, which was speculated as a gene encoding for the putative capsule depolymerase, was cloned and expressed *in vitro,* and its depolymerase activity against MDR-AB was testified. The enzyme greatly improved the ability of serum-mediated killing to counter bacterial growth and had promising therapeutic effects on *A. baumannii*-infected experimental mice.

MATERIALS AND METHODS

A. baumannii Strain and the Isolation of Bacteriophage

Phage vB_AbaM_IME285, shortened as phage IME285, was isolated from untreated sewage in the fifth Medical Center of Chinese PLA General Hospital (Former 307th Hospital of PLA), and its host strain was *A. baumannii* Ab387 (stored in our lab). Firstly, the sewage from this hospital was centrifuged at 12,000 g for 10 min, and the supernatant was filtered through a 0.22-μm filter. By mixing 100 μL of the mid-exponential phase strain Ab387 (OD600 = 0.8) with 2 mL of 3× Luria-Bertani (LB) medium, the mixture was then added to 4 mL of filtered sewage. After a 2-h incubation at 37°C, the mixture was centrifuged and filtered again and was mixed with logarithmic phase strain Ab387. The mixture was poured onto double-layer agar LB plates, and clear phage plaques were picked after incubation for 6 h at 37°C. This procedure was repeated three times until a single clear plaque was selected. The phage was propagated by successive extended cultivation and purified using the cesium chloride gradient centrifugation method (Bachrach and Friedmann, 1971; Peng et al., 2014). Its titer was assessed by the double-layer agar method as described (Kropinski et al., 2009). Finally, this phage was titrated and designated as vB_AbaM_IME285 (short as IME285).

Transmission Electron Microscopy and One-Step Growth Curve

A 25-μL purified phage IME285 suspension mixed with equal volumes of 4% paraformaldehyde and 0.5% glutaraldehyde was applied on carbon-coated copper grids and absorbed for 15 min. After removing the excess liquid, the phage mixture was stained with 2% phosphotungstic acid (PTA) for 30 min and subsequently dried, and then the phage particles were observed with a Philip TECNAI-10 transmission electron microscope (TEM) (Holland) (Wang et al., 2019).

Prior to one-step growth curve analysis, the multiplicity of infection (Samson et al., 2013) of phage IME285 was determined. An exponential growth phase culture of strain Ab387 was infected with 10-fold serial diluted solutions of phage IME285, and the mixtures were incubated on various LB plates for 2 hours at 37°C. The group with a rate of 10^{-3} resulted in the highest production of phage progeny (9.3×10^{11} pfu/mL), and this MOI was therefore chosen for subsequent experiments.

To assess the infection process of phage IME285, one-step growth curve experiments were performed as described previously (Wang et al., 2014). Briefly, phage IME285 was added to the strain Ab387 suspension, and then the mixture was spread on a double agar plate to determine the initial titer of the phage. Then, 100 μL phage solution (10^6 pfu/mL) was added to 1 mL (10^8 cfu/mL) bacterial suspension (at an MOI of 0.001) and was incubated at 37°C for 5 min. After brief centrifugation (12,000 × *g*, 30 s), the pellets were washed twice and then resuspended in a final volume of 10 mL pre-heated LB broth before incubation. Samples collected at a 10-min interval for 150 min were diluted immediately, and the phage titration was performed on a double-layer agar plate against time to estimate the latent period and burst size (burst size = the total number of phages liberated at the end of one cycle of growth/the number of infected bacteria) (Gadagkar and Gopinathan, 1980). Tests were conducted three times.

Whole-Genome Sequencing and Bioinformatics Analysis

The genomic DNA of phage IME285 was extracted using standard phenol/chloroform extraction protocols, as described previously, with minor modifications (Lu et al., 2013). The

phage suspension was treated with 1 μg/mL of DNase I (Takara, Dalian, China) and RNase A (Takara, Dalian, China) at 37°C overnight to remove the bacteria nucleic acids and then inactivated at 80°C for 15 min. The sample mixed with a lysis buffer (final concentration 0.5% SDS, 20 mM EDTA, and 50 μg/mL proteinase K) was then incubated at 56°C for 1 h. Then, a standard phenol/chloroform extraction protocol was performed; the genomic DNA was mixed with an equal volume of isopropanol and was incubated for at least 2 h at −20°C. The mixture was centrifuged at 12000 × *g* for 10 min at 4°C. The pellets were washed twice with 75% ethanol and dissolved in nuclease-free water. Complete genome sequencing of phage IME285 was conducted using Illumina Miseq (San Diego, CA, United States), and all data were assembled using the Newbler v2.9 software, which was annotated online by RAST (Rapid Annotation using Subsystem Technology)[1] (Margulies et al., 2005). The open reading frames (ORFs) were searched against the NCBI database[2] using BLASTN[3] and ORFfinder[4]. The sequence alignment of putative tail fiber proteins with a polysaccharide depolymerase domain, which is often located in the tail fiber or tail spike of a phage (Hernandez-Morales et al., 2018), was confirmed by using Easyfig_win_2.1 (Sullivan et al., 2011) with several related phages. The amino acid sequence alignment of the putative tail fiber proteins encoded by phage IME285 and three homologous phages was analyzed in CLC Genomics Workbench 8.0. A phylogenetic tree based on large terminal subunits with related phages from the NCBI database was generated using MEGA X software (Kumar et al., 2018).

Protein Expression and Activity Verification

The target gene ORF49, which was predicted as encoding for the depolymerase of phage IME285, was amplified with the following primers: upstream primer ORF49-F: 5′-ATGACAAATCCAACACTTATTAC-3′ and downstream primer: ORF49-R: 5′-GGTTGGATATATTTGACCAGCTA-3′. The amplified fragment was cloned into the *pEASY*®-Blunt E1 expression vector with a N-terminal His × 6 tag (Beijing Trans Gen Biotech Co., Ltd., China). By verifying using the 3730*xl* DNA Analyzer (Thermo Fisher Scientific), the recombinant plasmid was then transfected into *E. coli* BL21 (DE3) (TransGen Biotech, Beijing, China). Cells carrying recombinant plasmids were selected on LB agar plates containing 1 mg/mL Ampicillin (Sigma–Aldrich). When the recombinant isolates in the incubation were in the exponential growth phase, they were induced with 1 mM isopropyl-D-1-thiogalactopyranoside (IPTG, Sigma–Aldrich). The overnight cultured cells were centrifuged at 13,000 × *g* for 10 min at 4°C, resuspended in lysis buffer (50 mM NaH_2PO_4, 300 mM NaCl, pH 8.0), and sonicated on ice (8–10 cycles with 30-s pulse and 30-s pause). Then, the bacterial lysate was again centrifuged at 13,000 × *g* for 10 min at 4°C, and the supernatant was filtered through a 0.22-μm filter. Finally, the filtrate was purified through a Ni-NTA column (Sangon Biotech, Shanghai, China) and was eluted with five volumes of imidazole-containing buffer (50 mM NaH_2PO_4, 300 mM NaCl, 250 mM imidazole, pH 8.0) via a step gradient to renature the purified production. By dialyzing with small molecular-mass-cut off membrane (Viskase, Willowbrook, IL, United States) in pre-cooled dialyzate overnight at 4°C, the molecular weight of the recombinant enzyme was measured by sodium dodecyl sulfate polyacrylamide gel electrophoresis (SDS-PAGE, Thermo Fisher Scientific). The protein bands were visualized by staining the gels with Coomassie brilliant blue (Sigma-Aldrich). The concentration of Dp49 was quantified by using the Bradford Protein Assay Kit (Thermo Fisher Scientific).

The activity of Dp49 was determined using spot assay. Briefly, 200 μL of overnight-cultured strain Ab387 suspension was added into 4 mL of molten soft agar and was incubated for 3 h for bacterial lawn formation. A series of 2-fold dilutions of purified enzyme Dp49 (with an initial concentrate of 0.25 mg/mL) was then dropped onto the plates with bacterial lawns, and these were inoculated overnight to monitor the formation of semi-clear spots as a measure of enzymatic activity. In addition, the sensitivity of other A. baumannii isolates to Dp49 (0.25 mg/mL) was determined in single-spot assays.

Multilocus Sequence Typing of *A. baumannii* Strains and Determination of Activity Spectrum of Depolymerase and the Lytic Spectrum of Phage IME285

A total of 49 *A. baumannii* strains isolated from clinical sputum samples were used for multilocus sequence typing (MLST) typing according to the *A. baumannii* MLST database[5] (Bartual et al., 2005). They were cultured in LB broth at 37°C for 10–12 h. The seven housekeeping genes (cpn60, fsuA, gltA, pyrG, recA, rplB, and rpoB) were amplified for all the *A. baumannii* strains, and the assembled sequences were aligned by using BLAST to assign the allelic numbers and sequence types (STs). The results were then compared with the available alleles in the *A. baumannii* MLST (Pasteur) database.

The activity spectrum of depolymerase and the host range of phage IME285 was determined by double-layer agar plate assay as described previously (Kropinski et al., 2009). Plates containing mixtures of the phage and distinct A. baumannii strains were incubated for 6 h at 37°C, and plaque-forming units (PFU) were counted for each combination. Relative efficiency of plating (EOP) was calculated as the average PFU number of the phage on target bacteria divided by the average PFU number on host bacteria (Khan Mirzaei and Nilsson, 2015).

Assay of Serum Killing Contributed by the Depolymerase

Bactericidal contribution assay was performed as previously described, with some modifications (Pan et al., 2015). Briefly, 10 μL (about 10^8 cfu/mL) of overnight-cultured strain Ab387 was incubated with 180 μL of serum (inactivated or activated) from

[1]http://rast.nmpdr.org/

[2]http://www.ncbi.nlm.nih.gov/

[3]https://blast.ncbi.nlm.nih.gov/Blast.cgi

[4]https://www.ncbi.nlm.nih.gov/orffinder/

[5]http://pubmlst.org/abaumammii

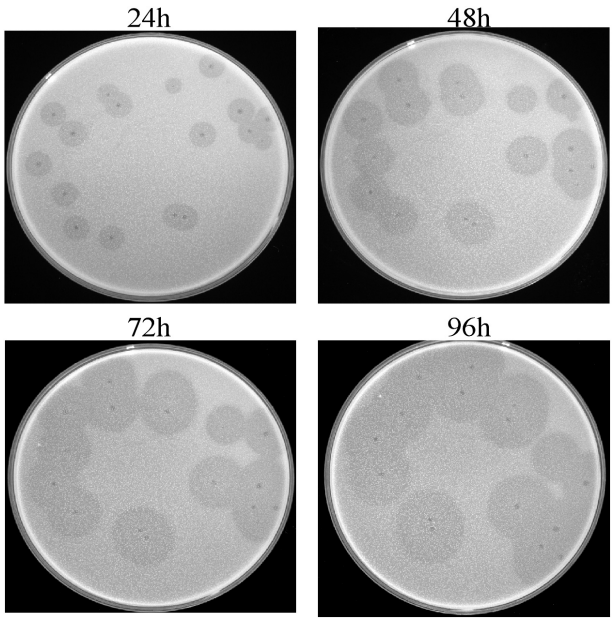

FIGURE 1 | Plaques and halos produced by phage IME285. Clear plaques surrounded by translucent halos were observed on the lawns of host strain Ab387. The plaques and halos were photographed at 24, 48, 72, and 96 h, respectively. The translucent halos emerged at 24 h, and the area of the halos expanded with prolonged incubation.

some healthy volunteers, and 10 μL (0.25 mg/mL) of purified depolymerase Dp49 was incubated with an equal volume of phosphate-buffered saline (PBS) as a control, both at 37°C for 1 h. The mixture was diluted with PBS, and 100-μL volumes of dilutions were plated on solid LB agar plates and cultured overnight; the viable bacterial counts were subsequently counted.

Depolymerase Treatment for Mouse Infections

Six groups of female BALB/c mice (12 per group, 18–20 g, specific-pathogen-free) were purchased from Beijing Vital River Laboratory Animal Technology Co., Ltd. (Beijing, China). All of the animal experiments were approved by the Institutional Animal Welfare Committee of the Beijing Institute of Microbiology and were performed in accordance with the guidelines of the Animal Welfare Agency. Mice were kept in individual cages with sufficient food and water and were euthanized by CO2 asphyxiation at the end of the experiment.

Three groups of mice were administered with 200 μL (6×10^7 cfu) of *A. baumannii* strain Ab387 suspended in PBS via intraperitoneal injection, and the rest of the groups were infected with the same dose of strain Ab220. Half an hour later, a dose of 50 μg (200 μL) Dp49 (D group), 200 μL of phage IME285 with an MOI of 10 (P group) (Wang et al., 2016), or an equal volume of PBS (Control group, also represented as the C group) was given to mice in the different groups, respectively. Survival rates over a 96-h period were analyzed using the Kaplan–Meier analysis with the log-rank test. For the bacterial counting assay, four mice infected with strain Ab387 or strain Ab220 in the control group were euthanized, and their organs, including liver, spleen, and lungs, were resected within 24 h of being in a moribund state or dead. These organs were weighed, and their tissues were homogenized in PBS, respectively. Serially diluted homogenate was coated on LB agar plates and incubated at 37°C for 24 h to determine bacterial counts. The amounts of bacteria in organs were represented as CFU/mL and CFU/g of tissue, respectively.

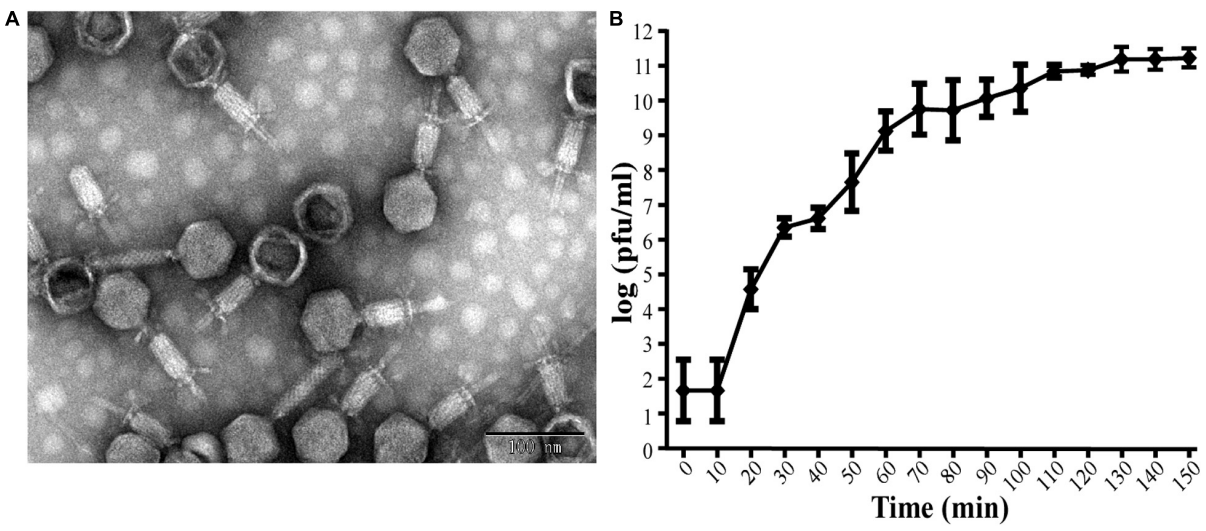

FIGURE 2 | Transmission electron microscopy of phage IME285 and the one-step growth curve. **(A)** TEM of phage IME285. Purified phage particles of IME285 exhibited icosahedral heads and contractile tails. The bar represents a length of 100 nm. **(B)** One-step growth curve of phage IME285. The *x*-axis indicates the time post-infection, and the *y*-axis indicates phage titers. Each dot on the graph represents a mean titer. Phage IME285 had a latent period of approximately 10 min, an exponential growth period of 90 min, and a final plateau phase from 100 min onward. The estimated burst size of phage IME285 was 450 pfu/cell. The experiment was repeated three times, and results are expressed as mean ± SD.

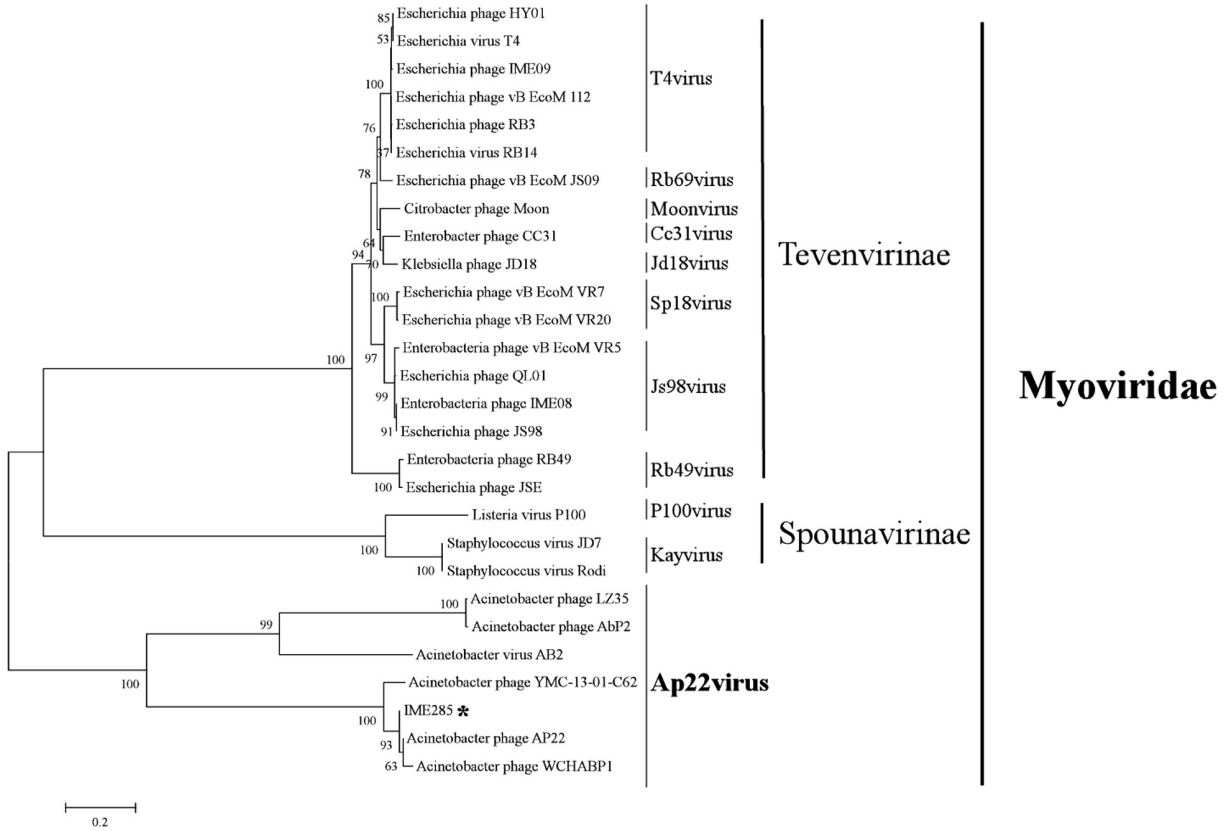

FIGURE 3 | Phylogenetic tree of phage IME285. A phylogenetic tree based on the phage large terminal subunits from the reference strains was generated by the neighbor-joining method using the program MEGA X. The numbers next to the branches are bootstrap values and represent confidence (%). Phage IME285 belongs to the *Myoviridae* family, Obolenskvirus subclass.

Four surviving mice from the depolymerase or phage groups were also euthanized, and their organ tissues were homogenized and coated on plates for bacterial colony counting, simultaneously.

Statistical Analysis

All experimental data are represented as mean ± SD. Independent Student's *t*-test was utilized to compare two groups, and two-way analysis of variance ANOVA) was used to compare multiple groups. All analyses were performed and plotted using Prism 6 software (GraphPad Software, CA, United States). A value of $P < 0.05$ was considered statistically significant.

RESULTS

Morphology and One-Step Growth Curve of Phage IME285

This isolated phage could produce clear plaques surrounded by translucent halos (**Figure 1**) when inoculated onto a lawn of strain Ab387 bacteria (the antibiotic resistance profile is presented in **Supplementary Tables S1, S2**), and the area of the halos gradually increased as incubation progressed. Transmission electron micrographs showed that this phage has an icosahedral head (about 73 nm in diameter) and a long shrinkable tail (about 92 nm), which indicates that it belongs to the *Myoviridae* family (**Figure 2A**). It was therefore designated as vB_AbaM_IME285 according to the recommendations of the International Committee on Taxonomy of Viruses (ICTV) on phage nomenclature. Phage IME285 were propagated, concentrated, and purified to a final titer of 1×10^{11} pfu/mL. For one-step growth curve analysis, strain Ab387 was infected with phage IME285 at an MOI of 0.001. As shown in **Figure 2B**, the latency of phage IME285 was about 10 min, followed by a long exponential growth period of about 90 min, and it finally became stable, plateauing, after 100 min. The estimated burst size of phage IME285 was 450 pfu/cell.

Whole-Genome Sequencing Analysis and Phylogenetic Tree

The complete genome of phage IME285 (GenBank Accession number: MH853786) consists of 45063 bp with double-stranded DNA, a low G + C content (37.9%), and a nucleotide content of 30.5% A, 31.6% T, 18.8% G, and 21% C. The annotation results of RAST indicated that the complete genome of phage IME285 contains putative 83 ORFs, predicted by NCBI BLASTP to encode four kinds of functional proteins, including the lysis model,

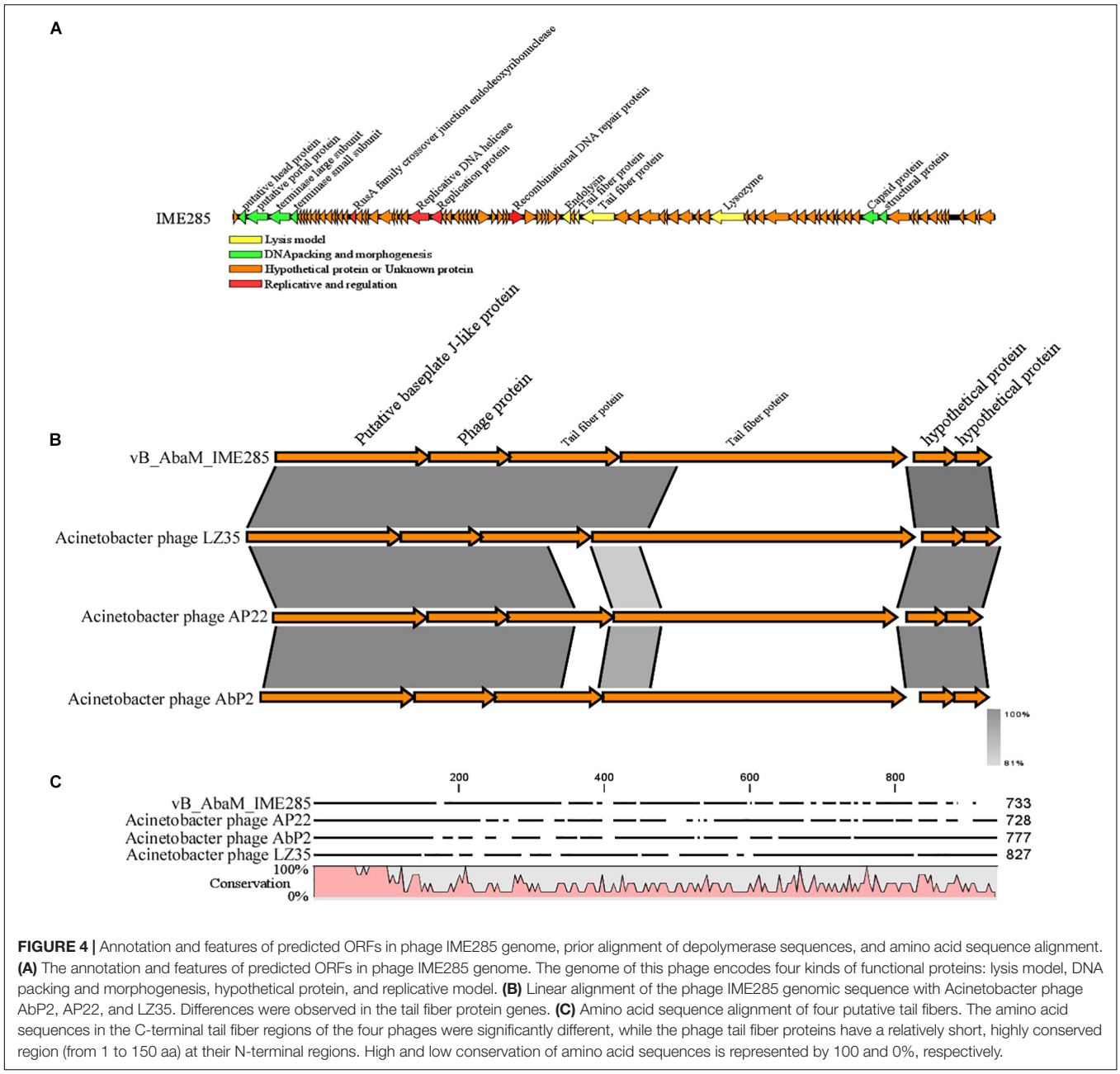

FIGURE 4 | Annotation and features of predicted ORFs in phage IME285 genome, prior alignment of depolymerase sequences, and amino acid sequence alignment. **(A)** The annotation and features of predicted ORFs in phage IME285 genome. The genome of this phage encodes four kinds of functional proteins: lysis model, DNA packing and morphogenesis, hypothetical protein, and replicative model. **(B)** Linear alignment of the phage IME285 genomic sequence with Acinetobacter phage AbP2, AP22, and LZ35. Differences were observed in the tail fiber protein genes. **(C)** Amino acid sequence alignment of four putative tail fibers. The amino acid sequences in the C-terminal tail fiber regions of the four phages were significantly different, while the phage tail fiber proteins have a relatively short, highly conserved region (from 1 to 150 aa) at their N-terminal regions. High and low conservation of amino acid sequences is represented by 100 and 0%, respectively.

DNA packing and morphogenesis, hypothetical protein, and replicative model (**Figure 4A**). A phylogenetic tree analysis based on the large terminal subunit revealed that this phage belongs to a subclass of the Obolenskvirus, which has demonstrated a very close relationship with *Acinetobacter* phage YMC-13-01-C62, *Acinetobacter* phage AP22, and *Acinetobacter* phage LZ35 from the *Myoviridae* family (**Figure 3**). BLASTp against the tail fiber amino acid sequence showed a high homology between phage IME285 and *Acinetobacter* phage AbP2 (accession number MF346584) (Query cover 16%, Ident 93.50%), *Acinetobacter* phage AP22 (accession number HE806280) (Query cover 14%, Ident 42.97%), and *Acinetobacter* phage LZ35 (accession number HE806280) (Query cover 16%, Ident 42.19%) (**Figure 4B**). Alignment based on amino acid sequence revealed that the tail fiber proteins of the four related phages shared a relatively short, highly conserved region (from 1 to 150 aa) at their N-terminal, while the C-terminal domains displayed obvious diversity, which might be a reason for the specificity of bacteriophages (**Figure 4C**).

Expression, Purification, and Identification of the Recombinant Enzyme

The target gene ORF49 encoding for the tail fiber protein was cloned into the expression vector, and the recombinant

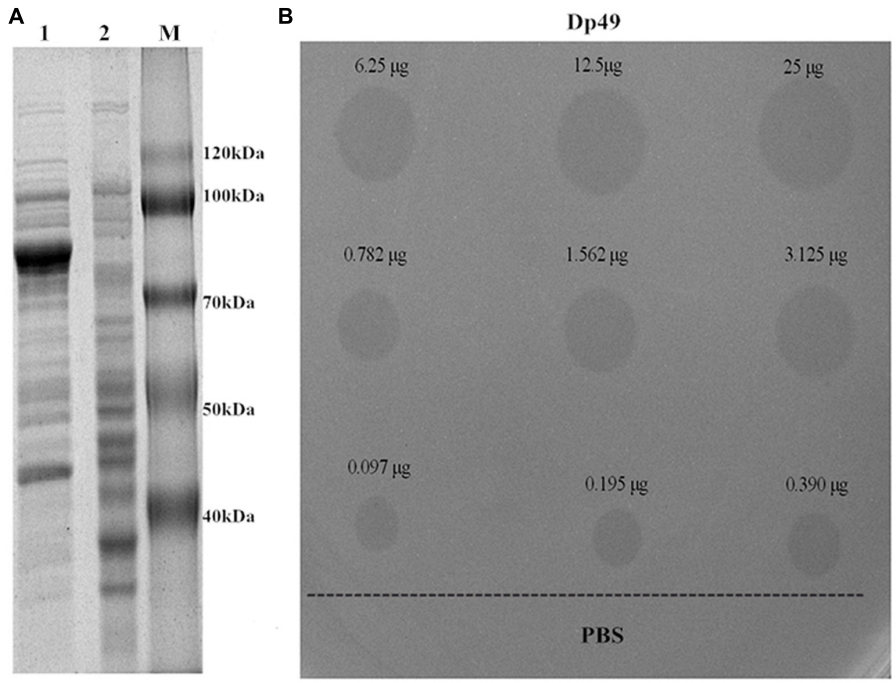

FIGURE 5 | Depolymerase expression and activity. **(A)** SDS-PAGE analysis of expressed Dp49. Lanes: 1 is the total protein of the induced *E. coli* BL21 cells containing recombinant plasmid; 2 is the empty *E. coli* BL21 cells (control); M is the protein marker. The most abundant band is the target protein Dp49, with a predicted size of 78 kDa. **(B)** The determination of depolymerase activity. Serial dilutions (25–0.097 μg) of depolymerase Dp49 were dropped on the lawn of the host bacteria strain Ab387. The area of translucent halo reduced as the concentration decreased, and the halo disappeared when the enzyme was diluted to 0.097 μg. PBS was used as a negative control.

TABLE 1 | List of *A. baumannii* strains used in this research and their ST results, including sensitivity to phage IME285 and depolymerase Dp49.

MLST type	Bacterial isolates	Sensitivity to phage	Sensitivity to depolymerase	Number of isolates
ST2	Ab14, Ab178, Ab406, Ab387, Ab7	+	+	5
	Ab2, Ab4, Ab5, Ab41, Ab1610, Ab1611, Ab1613, Ab1614, Ab2401, Ab2035, Ab2036, Ab2037, Ab2039, Ab1702, Ab1033, Ab1041, Ab1685, Ab1688, Ab1695	−	+	19
	Ab358, Ab363, Ab2529, Ab2589	+	−	4
	Ab333, Ab2712, Ab2093, Ab2099, Ab1697, Ab1706, Ab1058, Ab1689, Ab1692, Ab1694, Ab1697	−	−	11
ST36	Ab220	−	+	1
ST768	Ab 295	−	−	1
ST248	Ab 1612	−	−	1
NT[a]	Ab 2038	−	+	1
NT	Ab1704, Ab2114, Ab2116, Ab2126, Ab2129, Ab1707	−	−	6
Total				49

[a]*NT, not typeable; −, non-sensitive; +, sensitive.*

expression product was purified by the Ni-NTA column and dialysis. When analyzed with SDS-PAGE, a 78-kDa recombinant protein named Dp49 was obtained as predicted (**Figure 5A**). The activity of the purified enzyme was testified by spot assay. It showed that spotting with the purified recombinant protein could form a translucent halo on the lawn of the host bacteria strain Ab387 (**Figure 5B**). The area of the translucent halo reduced with decreasing Dp49 concentration until the enzyme was diluted to 0.097 μg, when the halo disappeared. The recombinant Dp49 exhibited good depolymerase activity.

MLST of *A. baumannii* Strains, Activity Spectrum of Dp49, and Lytic Spectrum of Phage IME285

Results of the MLST analysis revealed that 42 *A. baumannii* strains were clustered into four undivided types (ST2, ST36,

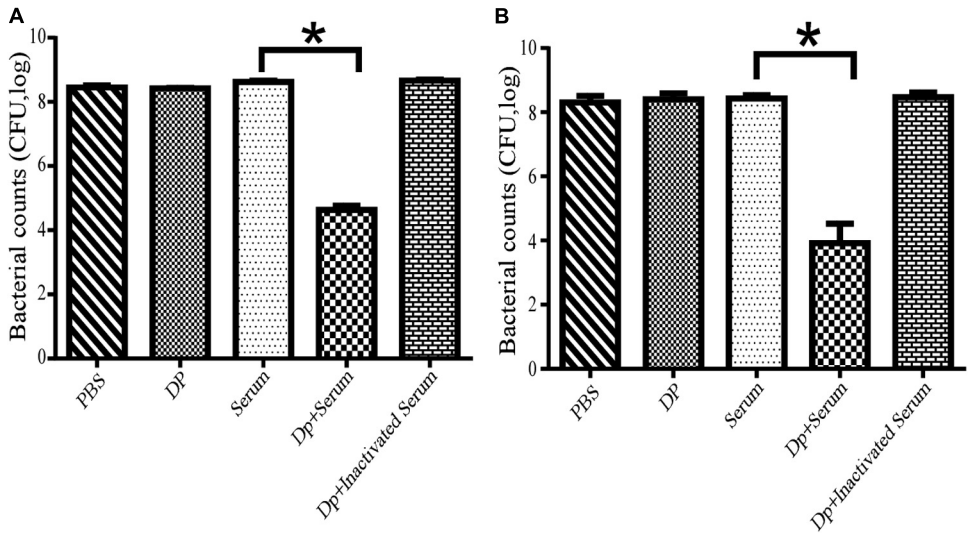

FIGURE 6 | Serum killing assay mediated by Dp49. **(A)** Dp49 enhanced serum sensitivity of strain Ab387. **(B)** Dp49 enhanced serum sensitivity of strain Ab220. In the presence of active serum, Dp49 increased serum killing to both the bacteria Ab387 and Ab220, whereas in the presence of inactivated serum, Dp49, or PBS alone, the depolymerase showed no obvious effect on bacterial count. Serum alone showed a slight effect in killing. For Ab220 bacteria, Dp49 plus serum decreased bacterial loads by at least an order of 4 (**Figure 6B**). Three independent experiments were performed, and data are expressed as the counts of bacterial reduction (mean ± SD), and the bacterial counts of the two groups (serum and enzyme with serum) were compared by Student's *t*-test (*$P < 0.01$).

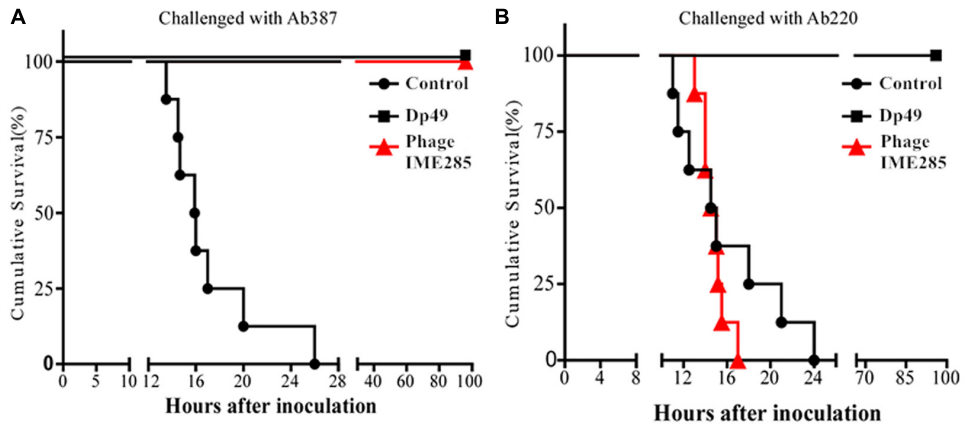

FIGURE 7 | Therapeutic efficacy of depolymerase in mice. **(A)** Survival curves of mice infected with Ab387 after treatment. **(B)** Survival curves of mice infected with Ab220 after treatment. BALB/c mice were infected with 6×10^7 cfu bacteria and treated with 50 μg (200 μL) depolymerase and an equal volume of phage IME285 or PBS half an hour later. The x-axis represents the time of infection in mice, and the y-axis represents the survival rate of mice. Statistical analysis was performed using the Kaplan-Meier method. Treatment with Dp49 ($P < 0.0001$; log–rank test) significantly increased the survival of mice infected with strain Ab387 or strain Ab220 over a 96-hour period.

ST768, and ST268), whereas seven other strains were untypeable (**Table 1**). These bacterial strains were used to determine the depolymerase ability of the expressed depolymerase Dp49, and the lytic spectrum of phage IME285 was testified simultaneously. Thirty-nine strains, including strain Ab387 infected by phage IME285, all belonged to the ST2 type, and this was the dominant *A. baumannii* bacterial population. Moreover, 23 strains of this type were also sensitive to Dp49, which had the same spectrum of activity as did phage IME285 but seemed with a high sensitivity to depolymerase than to the phage. In total, more than half of these *A. baumannii* strains (26/49, 53.1%) could be depolymerized by Dp49, while less than a quarter (9/49, 18.4%) of them could be lysed by the phage IME285.

Depolymerase Enhanced the Bactericidal Action of Serum Killing

The effects of serum killing after depolymerase treatment were evaluated *in vitro* against two *A. baumannii* strains, Ab387 and Ab220; of which the former was sensitive to both phage IME285 and the depolymerase, while the latter was only sensitive to the depolymerase. It showed that when the depolymerase or serum was applied separately, no bactericidal effect was observed in the

bacterial counts. When combined with active serum, the bacterial counts of depolymerase-treated strain Ab387 and strain Ab220 all significantly decreased ($P < 0.01$) (**Figure 6**), and a maximum of approximately 10^4 bacteria were killed (**Figure 6B**). However, when incubated with the inactivated serum, the bacterial counts scarcely reduced.

Therapeutic Effect of Depolymerase in Mice

To evaluate the therapeutic effect of depolymerase, mice were administered with 200 μL Dp49 half an hour post challenge with *A. baumannii* strain Ab387 or strain Ab220 in the experimental groups, while equal volumes of phage IME285 or PBS were administered in the rest of the groups. All mice in the control groups infected with lethal doses of bacteria died within 24–26 h, whereas mice in the experimental groups treated with Dp49 all survived. In the phage IME285-treated groups, mice infected with strain Ab387 were all rescued, but mice infected with strain Ab220 all died (**Figure 7**). The survival rate of the mice infected with strain Ab387 or strain Ab220 but treated with depolymerase was 100% within the monitored time period (0–96 h).

In a further study for bacterial enumeration, the organs of mice from the Dp49- or phage IME285-treated groups were collected and homogenized, and the organs of the control mice were also dissected in the near-death state. The results showed that the bacterial loads from organs such as liver, spleen, and lungs all significantly decreased in Dp49-treated groups (**Figure 8**). The degree of decrease in bacterial load of the different organs from mice treated with phage IME285 was more impressive compared to that of the Dp49-treated group when infected with strain Ab387 (**Figure 8A**). In contrast, phage IME285 showed little effect on bacterial elimination in mice infected with strain Ab220. Meanwhile, the bacterial count for Dp49-treated mice decreased by more than four orders of magnitude (**Figure 8B**).

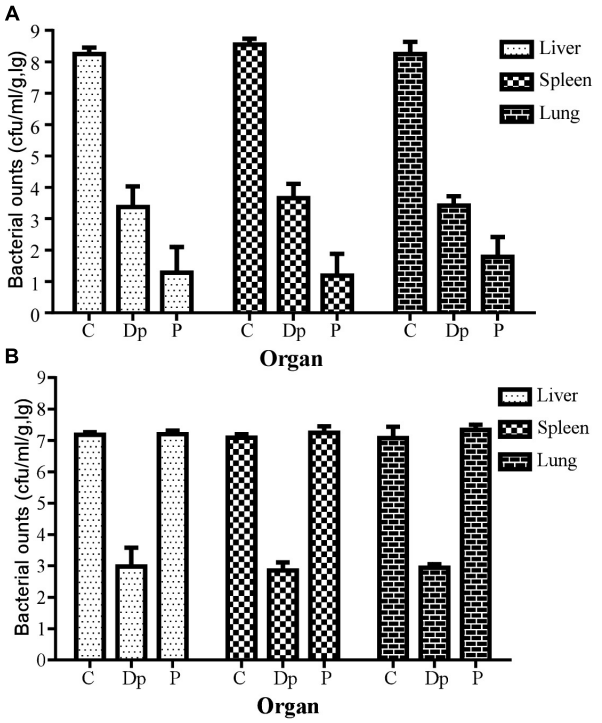

FIGURE 8 | Measurement of tissue bacterial loads in multiple organs of infected mice. **(A)** Tissue bacterial loads of strain Ab387-infected mice after treatment. **(B)** Tissue bacterial loads of strain Ab220-infected mice after treatment. Bacterial loads in liver, spleen, and lungs of different treatment groups were measured. For bacteria Ab387 infection, bacterial loads were significantly reduced in the phage IME285-treated mice, followed by the Dp49-treated group. Meanwhile, tissue bacterial loads were decreased by more than 4 magnitudes approximately in Dp49-treated mice compared to others infected with strain Ab220. Data are expressed as mean ± SD. A regular two-way ANOVA test was conducted to analyze the differences in bacterial counts between the liver, spleen, and lungs ($P < 0.05$).

DISCUSSION

Currently, antibiotic resistance in bacteria is a serious global problem, both medically and socially. Undoubtedly, antibiotics are still the most effective and reliable treatment option for bacterial infections, but the emergence of antibiotic-resistant bacteria such as MDR-AB and its rapid spread in hospitals and communities has become a serious threat to public health all over the world (Tomczyk et al., 2019). New drugs are not being developed fast enough to keep ahead of the natural ability of bacteria to evolve and defend themselves against antibiotics (Golkar et al., 2014). All of these problems indicate an urgent need to take further effective measures to control the abuse of antibiotics and to develop alternative antimicrobial agents (Brussow, 2017).

Bacteriophages (phages), which are natural enemies of bacteria, have the potential to be considered as an alternative strategy for treating infections mediated by multidrug-resistant pathogens (Kakasis and Panitsa, 2019). The main advantage of using bacteriophages as treatment options is their specificity, which can be designed to target pathogenic bacteria specifically without negatively affecting the normal microbiota and which do not cause secondary infections (Viertel et al., 2014). However, the high specificity of phages is a double-edged sword, as it means that the phage is also highly specific to its host bacteria, meaning that one single phage cannot cover the range of bacterial strains causing clinical infections. In our research, the lytic spectrum of phage IME285 was only 18.4% (9/49) against the 49 *A. baumannii* strains, which is not wide, after all.

A number of strategies have been designed to overcome this shortcoming, such as mixing several phages as a cocktail or in conjunction with antibiotics or developing a phage-derived enzyme-based complementary treatment. The fact that phage tail spikes or fibers usually exhibit depolymerase activity has been well illustrated (Pires et al., 2016b). Their great ability to degrade the thick capsule surrounding the cell wall of Gram-negative bacteria makes the depolymerases an attractive option for dealing with antibiotic-resistant bacterial infections. In this research, we identified a depolymerase, named Dp49, from a previously isolated phage, vB_AbaM_IME285. The

bioinformatics analysis data indicated that gene ORF49 of the genome was predicted as the tail fiber protein. The expressed enzyme could form a translucent halo when inoculated onto a lawn of the host bacteria strain Ab387 *in vitro* and exhibited good polysaccharide depolymerase activity in spot assay. The results regarding the activity spectrum of this depolymerase showed that more bacterial strains exhibited sensitivity to Dp49 than to phage IME285. Interestingly, the majority of these Dp49-sensitive strains were clustered into ST2 according to Pasteur's MLST. Capsular polysaccharide, also termed KL-type, is a major virulence factor for the *Acinetobacter* species. The depolymerases associated with capsular-targeting phage particles reduce the viscosity of CPS and strip it from the surface of encapsulated bacteria (Grażyna et al., 2016), and they have recently been considered as potential alternative anti-bacterial agents. Therefore, the identification of a certain KL-type-specific depolymerase makes sense. We compared the sequences of Dp49 with two KL-9-type depolymerases from phages AM24 (APD20249.1) and vB_AbaP_B5 (ASN73455.2) (Popova et al., 2019), and a high identity was recognized. The strains susceptible to Dp49 and IME285 exactly belong to the KL-9 capsular polysaccharide type. The KL type of the rest of the strains will be explored in subsequent research. Bactericidal contribution assay and a mouse therapy experiment mediated by Dp49 were performed to determine the capsule depolymerase activity of this phage-derived enzyme, and the safety of the phage-derived depolymerase was also evaluated. It was found that the phage-encoding enzyme Dp49 enhanced bacterial susceptibility to serum attack in the serum-killing experiments, leading to a 10^4 reduction in the bacterial load. When treated with Dp49, it protected the mice from dying of lethal doses of bacterial infection. These findings agreed with some current research, and our results further confirmed that Dp49 showed a broader range and was more effective in the treatments compared with phage IME285. It is speculated that the removal or modification of bacterial surface structures, which are responsible for enhancing virulence, host recognition and colonization, and biofilm formation by pathogens, leads to a reduction in pathogenicity, bacteria sensitization against some antimicrobials, or host defenses such as phagocytosis by macrophages and the bactericidal action of serum (Bansal et al., 2014; Wang et al., 2016; Liu et al., 2019).

The unique ability of phage-derived depolymerases to specifically recognize and degrade CPS and EPS offers an attractive and promising tool for controlling pathogenic bacteria (Latka et al., 2017). Compared to phages, depolymerase is more convenient and flexible in application and is believed to have a better performance against bacterial biofilms. Furthermore, its use avoids some of the disadvantages of phages, such as purification and endotoxin removal. Depolymerases derived from phages can provide a new strategy for the treatment of multidrug-resistant bacteria and have attracted increasing interest as potential antimicrobial agents, particularly in light of emerging and spreading resistance of bacteria against classical antibiotics. However, the application of depolymerases against human infections still needs to be supported by further clinical trials.

CONCLUSION

In this study, we identified a capsule depolymerase Dp49 derived from an *A. baumannii* phage. It greatly increased the inhibitory effect of serum on the growth of bacteria *in vitro* and could protect mice from dying of lethal doses of bacterial infection. This depolymerase might become a promising alternative strategy for controlling infections mediated by MDR-AB.

DATA AVAILABILITY STATEMENT

The datasets generated for this study can be found in the GenBank, Accession number: MH853786.

ETHICS STATEMENT

The studies involving human participants were reviewed and approved by the Ethics Committee of the Fifth Medical Center of Chinese PLA General Hospital (Former 307th Hospital of PLA), and an exemption of informed consent was obtained (Ethics approval No. ky-2018-10-85).

AUTHOR CONTRIBUTIONS

CW and ZM isolated the phage and characterized its biological characteristics and also identified, expressed, and evaluated the depolymerase activity. YH, HF, HL, and MG performed the genome-wide sequencing and genomic analysis. CW, XY, WN, and YQ conducted the animal experiments. PL and CW drafted the manuscript. YT, ZM, and CB conceived and designed the experiments. All authors read and agreed to the publication of the manuscript.

FUNDING

This research was supported by the National Natural Science Foundation of China (No. 81572045) and the Capital Characteristic Clinic Project of Beijing (grant no. Z161100000516181).

ACKNOWLEDGMENTS

We thank the State Key Laboratory of Pathogen and Biosecurity for scientific research. We are grateful to all the doctors of the Department of Respiratory and Critical Care Diseases at the 307th Hospital of the PLA for assistance during the course of this study.

SUPPLEMENTARY MATERIAL

The Supplementary Material for this article can be found online at: https://www.frontiersin.org/articles/10.3389/fmicb.2020.01407/full#supplementary-material

REFERENCES

Azeredo, J., and Sutherland, I. (2008). The use of phages for the removal of infectious biofilms. *Curr. Pharm. Biotechnol.* 9, 261–266. doi: 10.2174/138920108785161604

Bachrach, U., and Friedmann, A. (1971). Practical Procedures for the Purification of Bacterial Viruses. *Appl. Microbiol.* 22, 706–715. doi: 10.1128/aem.22.4.706-715.1971

Bansal, S., Harjai, K., and Chhibber, S. (2014). Depolymerase improves gentamicin efficacy during *Klebsiella pneumoniae* induced murine infection. *BMC Infect. Dis.* 14:456. doi: 10.1186/1471-2334-14-456

Bartual, S. G., Seifert, H., Hippler, C., Luzon, M. A., Wisplinghoff, H., and Francisco, R.-V. (2005). Development of a multilocus sequence typing scheme for characterization of clinical isolates of *Acinetobacter baumannii*. *Public Admin.* 43, 4382–4390. doi: 10.1128/jcm.43.9.4382-4390.2005

Brussow, H. (2017). Infection therapy: the problem of drug resistance - and possible solutions. *Microb. Biotechnol.* 10, 1041–1046. doi: 10.1111/1751-7915.12777

Chang, R. Y. K., Wallin, M., Lin, Y., Leung, S. S. Y., Wang, H., Morales, S., et al. (2018). Phage therapy for respiratory infections. *Adv. Drug Deliv. Rev.* 133, 76–86. doi: 10.1016/j.addr.2018.08.001

Dijkshoorn, L., Nemec, A., and Seifert, H. (2007). An increasing threat in hospitals: multidrug-resistant *Acinetobacter baumannii*. *Nat. Rev. Microbiol.* 5, 939–951. doi: 10.1038/nrmicro1789

Gadagkar, R., and Gopinathan, K. P. (1980). Bacteriophage burst size during multiple infections. *J. Biosci.* 2, 253–259. doi: 10.1007/bf02703251

Golkar, Z., Bagasra, O., and Pace, D. G. (2014). Bacteriophage therapy: a potential solution for the antibiotic resistance crisis. *J. Infect. Dev. Ctries* 8, 129–136. doi: 10.3855/jidc.3573

Grażyna, M. S., Agnieszka, Ł., Rita, B., Barbara, M., Flavia, S., Maria, R., et al. (2016). Capsule-Targeting Depolymerase, Derived from Klebsiella KP36 Phage, as a Tool for the Development of Anti-Virulent Strategy. *Viruses* 8:324. doi: 10.3390/v8120324

Hall-Stoodley, L., Costerton, J. W., and Stoodley, P. (2004). Bacterial biofilms: from the Natural environment to infectious diseases. *Nat. Rev. Microbiol.* 2, 95–108. doi: 10.1038/nrmicro821

Hernandez-Morales, A. C., Lessor, L. L., Wood, T. L., Migl, D., Mijalis, E. M., Cahill, J., et al. (2018). Genomic and Biochemical Characterization of Acinetobacter Podophage Petty Reveals a Novel Lysis Mechanism and Tail-Associated Depolymerase Activity. *J. Virol.* 92:e01064-17.

Kakasis, A., and Panitsa, G. (2019). Bacteriophage therapy as an alternative treatment for human infections. A comprehensive review. *Int. J. Antimicrob. Agents* 53, 16–21. doi: 10.1016/j.ijantimicag.2018.09.004

Khan Mirzaei, M., and Nilsson, A. S. (2015). Isolation of phages for phage therapy: a comparison of spot tests and efficiency of plating analyses for determination of host range and efficacy. *PLoS One* 10:e0118557. doi: 10.1371/journal.pone.0118557

Kropinski, A. M., Mazzocco, A., Waddell, T. E., Lingohr, E., and Johnson, R. P. (2009). Enumeration of Bacteriophages by Double Agar Overlay Plaque Assay. *Methods Mol. Biol.* 501, 69–76. doi: 10.1007/978-1-60327-164-6_7

Kumar, S., Stecher, G., Li, M., Knyaz, C., and Tamura, K. (2018). MEGA X: molecular evolutionary genetics analysis across computing platforms. *Mol. Biol. Evol.* 35, 1547–1549. doi: 10.1093/molbev/msy096

Latka, A., Maciejewska, B., Majkowska-Skrobek, G., Briers, Y., and Drulis-Kawa, Z. (2017). Bacteriophage-encoded virion-associated enzymes to overcome the carbohydrate barriers during the infection process. *Appl. Microbiol. Biotechnol.* 101, 3103–3119. doi: 10.1007/s00253-017-8224-6

Liu, Y., Mi, Z., Mi, L., Huang, Y., Li, P., Liu, H., et al. (2019). Identification and characterization of capsule depolymerase Dpo48 from phage IME200. *PeerJ* 7:e6173. doi: 10.7717/peerj.6173

Liu, Y., Mi, Z., Niu, W., An, X., Yuan, X., Liu, H., et al. (2016). Potential of a lytic bacteriophage to disrupt *Acinetobacter baumannii* biofilms in vitro. *Future Microbiol.* 11, 1383–1393.

Lu, S., Le, S., Tan, Y., Zhu, J., Li, M., Rao, X., et al. (2013). Genomic and proteomic analyses of the terminally redundant genome of the *Pseudomonas aeruginosa* Phage PaP1: establishment of Genus PaP1-like phages. *PLoS One* 8:e62933. doi: 10.1371/journal.pone.0062933

Margulies, M., Egholm, M., Altman, W. E., Attiya, S., Bader, J. S., Bemben, L. A., et al. (2005). Genome sequencing in microfabricated high-density picolitre reactors. *Nature* 437:376.

Pan, Y. J., Lin, T. L., Lin, Y. T., Su, P. A., Chen, C. T., Hsieh, P. F., et al. (2015). Identification of Capsular Types in Carbapenem-Resistant *Klebsiella pneumoniae* Strains by wzc sequencing and implications for capsule depolymerase treatment. *Antimicrob. Agents Chemother.* 59, 1038–1047. doi: 10.1128/aac.03560-14

Peng, F., Mi, Z., Huang, Y., Yuan, X., Niu, W., Wang, Y., et al. (2014). Characterization, sequencing and comparative genomic analysis of vB_AbaM-IME-AB2, a novel lytic bacteriophage that infects multidrug-resistant *Acinetobacter baumannii* clinical isolates. *BMC Microbiol.* 14:181. doi: 10.1186/1471-2180-14-181

Perez, F., Hujer, A. M., Hujer, K. M., Decker, B. K., Rather, P. N., and Bonomo, R. A. (2007). Global challenge of multidrug-resistant *Acinetobacter baumannii*. *Antimicrob. Agents Chemother.* 51:3471.

Pires, D. P., Cleto, S., Sillankorva, S., Azeredo, J., and Lu, T. K. (2016a). Genetically engineered phages: a review of advances over the last decade. *Microbiol. Mol. Biol. Rev.* 80, 523–543. doi: 10.1128/mmbr.00069-15

Pires, D. P., Oliveira, H., Melo, L. D., Sillankorva, S., and Azeredo, J. (2016b). Bacteriophage-encoded depolymerases: their diversity and biotechnological applications. *Appl. Microbiol. Biotechnol.* 100, 2141–2151. doi: 10.1007/s00253-015-7247-0

Popova, A. V., Shneider, M. M., Myakinina, V. P., Bannov, V. A., Edelstein, M. V., Rubalskii, E. O., et al. (2019). Characterization of myophage AM24 infecting *Acinetobacter baumannii* of the K9 capsular type. *Arch. Virol.* 164, 1493–1497. doi: 10.1007/s00705-019-04208-x

Samson, J. E., Magadán, A. H., Sabri, M., and Moineau, S. (2013). Revenge of the phages: defeating bacterial defences. *Nat. Rev. Microbiol.* 11, 675–687. doi: 10.1038/nrmicro3096

Sullivan, M. J., Petty, N. K., and Beatson, S. A. (2011). Easyfig: a genome comparison visualizer. *Bioinformatics* 27, 1009–1010. doi: 10.1093/bioinformatics/btr039

Tomczyk, S., Zanichelli, V., Grayson, M. L., Twyman, A., Abbas, M., Pires, D., et al. (2019). Control of Carbapenem-resistant *Enterobacteriaceae*, *Acinetobacter baumannii*, and *Pseudomonas aeruginosa* in healthcare facilities: a systematic review and reanalysis of quasi-experimental studies. *Clin. Infect. Dis.* 68, 873–884. doi: 10.1093/cid/ciy752

Viertel, T. M., Ritter, K., and Horz, H. P. (2014). Viruses versus bacteria-novel approaches to phage therapy as a tool against multidrug-resistant pathogens. *J. Antimicrob. Chemother.* 69, 2326–2336. doi: 10.1093/jac/dku173

Wang, C., Li, P., Niu, W., Yuan, X., Liu, H., Huang, Y., et al. (2019). Protective and therapeutic application of the depolymerase derived from a novel KN1 genotype of *Klebsiella pneumoniae* bacteriophage in mice. *Res. Microbiol.* 170, 156–164. doi: 10.1016/j.resmic.2019.01.003

Wang, Y., Mi, Z., Niu, W., An, X., Yuan, X., Liu, H., et al. (2016). Intranasal treatment with bacteriophage rescues mice from *Acinetobacter baumannii*-mediated pneumonia. *Future Microbiol.* 11, 631–641. doi: 10.2217/fmb.16.11

Wang, Y., Wang, W., Lv, Y., Zheng, W., Mi, Z., Pei, G., et al. (2014). Characterization and complete genome sequence analysis of novel bacteriophage IME-EFm1 infecting Enterococcus faecium. *J. Gen. Virol.* 95(Pt 11), 2565–2575. doi: 10.1099/vir.0.067553-0

Wong, D., Nielsen, T. B., Bonomo, R. A., Pantapalangkoor, P., Luna, B., and Spellberg, B. (2017). Clinical and pathophysiological overview of acinetobacter infections: a century of challenges. *Clin. Microbiol. Rev.* 30, 409–447. doi: 10.1128/cmr.00058-16

Conflict of Interest: The authors declare that the research was conducted in the absence of any commercial or financial relationships that could be construed as a potential conflict of interest.

Copyright © 2020 Wang, Li, Zhu, Huang, Gao, Yuan, Niu, Liu, Fan, Qin, Tong, Mi and Bai. This is an open-access article distributed under the terms of the Creative Commons Attribution License (CC BY). The use, distribution or reproduction in other forums is permitted, provided the original author(s) and the copyright owner(s) are credited and that the original publication in this journal is cited, in accordance with accepted academic practice. No use, distribution or reproduction is permitted which does not comply with these terms.

Advantages of publishing in Frontiers

OPEN ACCESS
Articles are free to read for greatest visibility and readership

FAST PUBLICATION
Around 90 days from submission to decision

HIGH QUALITY PEER-REVIEW
Rigorous, collaborative, and constructive peer-review

TRANSPARENT PEER-REVIEW
Editors and reviewers acknowledged by name on published articles

Frontiers
Avenue du Tribunal-Fédéral 34
1005 Lausanne | Switzerland

Visit us: www.frontiersin.org
Contact us: frontiersin.org/about/contact

REPRODUCIBILITY OF RESEARCH
Support open data and methods to enhance research reproducibility

DIGITAL PUBLISHING
Articles designed for optimal readership across devices

FOLLOW US
@frontiersin

IMPACT METRICS
Advanced article metrics track visibility across digital media

EXTENSIVE PROMOTION
Marketing and promotion of impactful research

LOOP RESEARCH NETWORK
Our network increases your article's readership